



National Water Infrastructure Adaptation Assessment

Part II, Smart Urban Designer (SUD) and Application Case Studies

National Water Infrastructure Adaptation Assessment

Part II, Smart Urban Designer (SUD) and Application in Case Studies

National Risk Management Laboratory
Office of Research and Development
U.S. Environmental Protection Agency
26 Martin Luther King Drive
Cincinnati, OH 45268

DISCLAIMER

The U.S. Environmental Protection Agency, through its Office of Research and Development, conducted, funded and managed the research described herein. The report “*National Water Infrastructure Adaptation Assessment: Part II – Part II, Smart Urban Designer (SUD) and Application Case Studies*”, EPA 600-R-18-275, has been subjected to the Agency’s peer and administrative review and has been approved for external publication. Any opinions expressed in this paper are those of the authors and do not necessarily reflect the views of the Agency, therefore, no official endorsement should be inferred. Any mention of trade names or commercial products does not constitute endorsement or recommendation for use.

FOREWORD

The U.S. Environmental Protection Agency (U.S. EPA) is charged by Congress with protecting the Nation's land, air, and water resources. Under a mandate of national environmental laws, the Agency strives to formulate and implement actions leading to a compatible balance between human activities and the ability of natural systems to support and nurture life. To meet this mandate, EPA's research program is providing data and technical support for solving environmental problems today and building a science knowledge base necessary to manage our ecological resources wisely, understand how pollutants affect our health, and prevent or reduce environmental risks in the future.

The National Risk Management Research Laboratory (NRMRL) is the Agency's center for investigation of technological and management approaches for preventing and reducing risks from pollution that threaten human health and the environment. The focus of the Laboratory's research program is on methods and their cost-effectiveness for prevention and control of pollution to air, land, water, and subsurface resources; protection of water quality in public water systems; remediation of contaminated sites, sediments and groundwater; prevention and control of indoor air pollution; and restoration of ecosystems. NRMRL collaborates with both public and private sector partners to foster technologies that reduce the cost of compliance and to anticipate emerging problems. NRMRL's research provides solutions to environmental problems by: developing and promoting technologies that protect and improve the environment; advancing scientific and engineering information to support regulatory and policy decisions; and providing the technical support and information transfer to ensure implementation of environmental regulations and strategies at the national, state, and community levels.

This publication has been produced as part of the EPA Office of Research and Development (ORD) research programs, conforming to the Laboratory's strategic long-term research plan. It is published and made available by EPA's Office of Research and Development to assist the user community and to link researchers with their clients.

Cynthia Sonich-Mullin, Director
National Risk Management Research Laboratory

PREFACE

Water is essential to life. Uneven distribution of population and water resources in the world results in more than 1.1 billion people with a lack of access to clean drinking water and 2.6 billion people deprived of adequate water sanitation. Today fresh water is being consumed at an alarming rate almost doubling every 20 years. Global changes further exacerbate this already stressed situation. It can be said that water availability is not only a problem for developing countries, but one facing developed nations that are saddled with an aging water infrastructure. Pressed by challenges, however, civilizations have always found innovative solutions to meet water resource needs and adapt to evolving social and environmental conditions. This spirit of adaptation continues to this very date and will continue.

Today one of the most complex challenges facing our nation revolves around water supply sustainability, often framed in name of water-environment-energy nexus. The challenge is acute in light of occurring and future changes in land use and hydroclimatic conditions, and thus require a holistic water management approach. For the purpose, interdisciplinary research and developments are often a first step in order to supplement and improve current water management and engineering practice.

The national adaptation assessment report synthesizes the results of multidisciplinary research and development in the last eight years. It presents an assessment of our nation's water resource infrastructure, characterizes hydroclimatic provinces and future hydroclimatic and land use conditions. It further introduces planning and engineering means to develop quantitative scientific basis for adapting water infrastructure and, in general, for urban development. The systematic adaptation approach is structured at multiple levels from integrated watershed management, urban-scale planning, to individual water system engineering.

In considering the water infrastructure adaptation needs, a suite of tools ranging from those in strategic planning, master planning and engineering, to those in watershed modeling and drinking water plant simulations, have been developed or adopted. These adaptation techniques for different levels of purposes are described in this report and other accompanying publications with illustration of case studies. The focus is to develop actionable science and engineering basis for adapting to the likely future environmental stressors at local scales, and by doing so, to support water resource managers and technical stakeholders who face the technical complexity. While this report provides a wealth of technical data and information, it only marks the beginning of a long march toward the goal of sustainable water resource and resilient infrastructure in the time of accelerating global changes.

ACKNOWLEDGEMENT

The U.S. Environmental Protection Agency (EPA), through its Office of Research and Development (ORD), funded and managed, and conducted the intramural and extramural research described herein. The research was a part of the ORD Air and Energy (A-E) research program. It was implemented by the U.S. EPA Water Resources Adaptation Program (WRAP) in the ORD's Water Systems Division (WSD), by Pegasus Technical Services, Inc. through EPA Contract EP-C-05-056, and by Cadmus Inc. through the contract EP-C-06-100.

Programmatic guidance from ORD's former Aging Water Infrastructure (AWI) program and now from the A-E and SSWR research programs is acknowledged. Special thanks are due to Jeff Peterson, Karen Metchis, Elizabeth Corr, Robert Cantilli, Rachael Novak, Elana Goldstein, and Curt Baranowski of the EPA Office of Water for their efforts to bring together experts and practitioners from around the country, and for their involvement in this research. Additionally, the Office of Air and Radiation (OAR) Climate Division and the Office of Transportation Air Quality (OTAQ) engaged with interests in this research through the A-E research programs.

The project and writing team would like to acknowledge numerous technical staff and participants from EPA and contracting research organizations. This investigation of both a wide breadth and a substantial depth was accomplished only with their participation and contribution, including the administrative and contract supports from Dr. Michael Moeykens, Michelle Latham, Steve Harmon, and Stephen Wright. Finally, technical data and collaboration efforts by the Manatee County Water Department, the Great Cincinnati Water Works, the Las Vegas Valley Water District, and the local governments from Massachusetts coast are acknowledged.

The national adaptation assessment report was a result of continuing research efforts in the past several years. The report was initially prepared in 2011 and reviewed by individuals inside and outside of the U.S. EPA. Upon the review comments, additional technical contents were added with new research, especially in the area of adaptation tools and methods. This development led to rewriting and reorganization of the entire reports. In the process, three rounds of internal and external peer reviews were conducted. After these peer-reviews, Part I of the national water infrastructure assessment report was published in 2015. This current Part II report has also been subjected to administrative review and is now approved for publication. The contributing teams to this volume include:

Principal Investigator and Lead Author

Dr. Y. Jeffrey Yang, P.E., D.WRE, ORD/NRMRL

EPA project and writing team

Jill Neal, ORD/NRMRL

Dr. Chelsea Neal, ORD/NRMRL ORISE Participant, now at Los Alamos National Laboratory

Dr. Marissa Liang, ORD/NCEA ORISE Participant

Dr. Britta Bierwagen, ORD/NCEA

Susan Julius, ORD/NCEA

Karen Metchis, Office of Water
Jeri Weiss, EPA Region 1

Principal Authors and Contributors from Contracting Organizations:

Dr. Steven Buchberger, P.E., University of Cincinnati
Dr. Zhiwei Li, Carbon Capture Scientific, LLC.
Dr. Heng Wei, University of Cincinnati
Dr. Xinhao Wang, University of Cincinnati
Late Dr. Timothy C. Keener, P.E., University of Cincinnati
Dr. Robert C. Clark, P.E., Environmental Consultant
Dr. Dominic L. Boccelli, University of Cincinnati
Dr. Walter Grayman, P.E., W.M. Grayman Consulting Engineers
Dr. Ni-Bin Chang, P.E., D.WRE, University of Central Florida
Mr. Hou Liu, University of Cincinnati

Other Research Organizations and Individuals:

Pegasus Technical Services

Dr. Karen Koran,
University of Cincinnati

Hao Liu, Zhuo Yao, Ting Zuo, Dr. Yu Sun, Amy Burgess, Heng Yang, Jie He,
Patcha Huntra, Dr. Pamela Heckle, P.E., Dr. Thushara Ranatunga
University of Central Florida

Dr. Ammarin Makkeasorn, Dr. Sanez Imen, Lee Mullon,
Cadmus Inc.

Chi Ho Sham, Jaime Rooke, Brent Ranalli, Laurie Potter, Laura Blake, Julie Blue,
Donna Jensen, Patricia Hertzler

This report has been peer-reviewed, for which the following reviewers are acknowledged:

(First Round)

Dr. Vahid Alavian, World Bank
Mr. Jeff Adams, U.S. EPA, ORD
Dr. Nancy Beller-Simms, NOAA
Dr. E.P.H. Best, U.S. EPA, ORD
Dr. Pratim Biswas, P.E, Washington University
Dr. Levi Brekke, Bureau of Reclamation
Mr. Mao Fang, P.E., Las Vegas Valley Water District
Mr. Gary Hudiburgh, Office of Water, AIEO
Dr. Timothy C. Keener, P.E., University of Cincinnati
Dr. Paul Kirshen, University of New Hampshire
Dr. Julie King, U.S. Geological Survey
Dr. Thomas Johnson, U.S. EPA, ORD
Mr. Craig Patterson, P.E., U.S. EPA, ORD
Dr. Joo-Youp Lee, University of Cincinnati
Dr. Steven McCutcheon, P.E., D.WRE., U.S. EPA, ORD

Mr. Ken Moraff, U.S. EPA, Region 1
Ms. Angela Restivo, U.S. EPA, Region 6
Dr. Neil Stiber, EPA, OSA
Mr. Michael J. Wallis, East Bay Municipal Utility District, CA
Dr. Xinhao Wang, University of Cincinnati
Cadmus, Inc.: Glen Boyd, Dr. Rudd Coffey, Laura Dufresne, Carles A. Hernick, Ken
Klewicki, Dr. Janathan Koplos, William M. Jones, Frank Letkiewicz, Richard
Kro, Vanessa M. Leiby, Jeff Maxted, G. Tracy Mehan III, Tom Mulcahy,
Karen Sklenar, Mary Ellen Tuccillo.

(Second round)

Dr. Audrey Levine, formally at the National Science Foundation
Dr. Frederick Bloetscher, Florida Atlantic University

(Final round)

Dr. Frederick Bloetscher, Florida Atlantic University
Dr. Weiwei Mo, University of New Hampshire
Dr. James Goodrich, ORD/NHSRC
Karen Kleier Schrantz, ORD/NRMRL
Dr. Mark Rodgers, ORD/NRMRL
Laura Bachle, EPA/OWOW/WRAPD

ABSTRACT

This report “National Water Infrastructure Adaptation Assessment: Part II, Smart Urban Designer (SUD) and Case Studies” is a part of the research effort undertaken by the EPA Office of Research and Development (ORD) Water Systems Division (WSD) on national water infrastructure assessment. The multi-year research has generated data, models and methods to assess the water infrastructure vulnerability and develop sustainable planning and designs for infrastructure improvement. This research, organized by ORD’s Air and Energy (A-E) program in collaboration with EPA’s Office of Water (OW), is summarized into four documents. The first document published in 2015 contains a preliminary regulatory and technical analysis of the United States water infrastructure, and its relationship to hydroclimatic and socioeconomic changes.

The Part II report is focused on the SUD tools and methods for urban planning and infrastructure adaptation design. The content aims to assist water practitioners and urban planners in developing resilient, efficient and economic water supply systems and water management programs. At the same time, the tools and methods can help practitioners with understanding the interconnectedness of urban growth, transportation and pollution to the water infrastructure system. In sequence, the report first outlines adaptation objectives and the SUD framework in three spatial scales. Next, it describes unique environmental properties associated with urban growth and current planning practices to facilitate urban growth. In Sections 3.0-7.0, the core SUD components in urban planning and water system engineering are described. Case studies are provided for further insights on the utilities and function of SUD tools and methods. In Section 8.0, the SUD application in coastal areas illustrates the complex factors of the hydroclimatic impacts in adaptation planning.

It is noteworthy that water infrastructure adaptation can take place at different scales: regional urban-wide planning, water system optimization for master planning, and adaptive engineering and design for local water infrastructure components. The adaptive urban planning concept consists of an integrated analysis and scenario-based simulation of future land use, transportation and water infrastructure. The actions aim to improve urban efficiency and achieve adaptation co-benefits in infrastructure economics and resilience. The resulting urban form sets up the framework to which water infrastructure services can be adopted. At the water-system level, the SUD adaptation tools include those for trade-off analysis in evaluating infrastructure master planning options. At the local level, the SUD tools and methods include those newly developed for modeling water treatment, distribution, water storage and conservation. Together with real-time water monitoring and forecasting techniques that will be described in other Adaptation Assessment documents, a suite of techniques has become available for water managers in assisting water supply system planning and improvement.

These developed adaptation methods were examined in adaptation case studies on urban water supplies in both the U.S. inland and coastal regions. The applications include adaptation studies for urban infrastructure and water systems in Cincinnati, Ohio; Manatee County, Florida; Las Vegas Valley Water District, Nevada; and Mattapoisett, Massachusetts. It is noted that the technical national adaptation assessment report covers a wide range of technical subjects and is

developed for technical professionals. A companion synopsis report is prepared and will be published separately to disseminate the highly technical information to managers, policy-makers and a broader audience.

Table of Contents

Disclaimer	ii
Forward	iii
Preface	iv
Acknowledgement	v
Abstract	vii
Abbreviations and Notations	xx
 Part Two: Smart Urban Designer (SUD) and Application Case Studies	 1
1. Sustainable Development of Urban Water Systems.....	2
1.1. Adaptation considerations.....	2
1.1.1. Defining adaptation objective	4
1.1.2. Understanding adaptation constraints	6
1.1.3. Revising or redefining planning and engineering focus	11
1.1.4. Selecting adaptation evaluation matrix	13
1.2. Three levels of water infrastructure adaptation	15
1.3. Smart Urban Designer (SUD) for systems analysis.....	15
1.3.1 The Integrated Watershed Modeling (IWM) tool	15
1.3.2 Adaptive Urban Planning and Engineering Tool (AUP&ET)	20
1.3.3 SmartWater for water supply	22
1.3.4. Source-to-tap water supply in system approach	23
2. Adaptive Urban Planning in Urban Scales.....	24
2.1 Physical infrastructure and urban forms in current practice	24
2.1.1. Land use encouraging urban sprawl	26
2.1.2. Transportation and energy performance	27
2.1.3. Water planning and engineering	29
2.2 Transformation toward smart growth.....	30
2.3. Monitoring and re-evaluation	31
3. SUD Methods and Tool in Adaptive Urban Planning.....	32
3.1. AUP&ET principles and utilities	33
3.1.1. Land use projection – CA-Markov model and iCLUS	33
3.1.2. Calibration and validation of the land use simulation model	35
3.1.3. AIR-SUSTAIN system for transportation simulation.....	36
3.1.4. The linkage to water infrastructure simulations.....	37
3.2. The AIR-SUSTAIN simulation tool for transportation	37

3.2.1.	Basic functions and interfaces of AIR-SUSTAIN	38
3.2.2.	Travel demand forecasting – VISUM	40
3.2.2.1.	Modeling	40
3.2.2.2.	Model calibration and validation	41
3.2.3.	Hotspot identification	42
3.2.4.	Microscopic simulation using VISSIM	42
3.2.5.	Emission estimation using MOVES	44
4.	Adaptive Urban Planning in SUD Case Studies	46
4.1	Urban form and urban infrastructure	46
4.1.1.	Urban form and land use patterns	46
4.1.2.	Transportation and traffic distribution	50
4.1.3.	Urban form and air quality	53
4.1.4.	Thermal inversion and mixing height	54
4.1.5.	Urban and exurban differences	56
4.1.6.	Urban form effects on urban heat island and air quality	56
4.1.6.1	Long-term changes in the urban center	56
4.1.6.2	Urban-wide co-variations in temperature and PM _{2.5}	56
4.1.6.3.	Thermal inversion and wind conditions	61
4.1.6.4.	UHI formation and spatial variations	62
4.1.6.5.	Adaptation and potential effects	63
4.2.	Adaptive urban planning modeling and analysis in Cincinnati	64
4.2.1	Three development scenarios	64
4.2.2	Transportation and emission analysis using AIR-SUSTAIN tool	65
4.2.2.1	The modeling processes	67
4.2.2.2	Comparison of future developmental scenarios	70
4.2.2.3	Implications on adaptation co-benefits	74
4.3	Adaptation analysis for water master planning in Manatee County, Florida	75
4.3.1	Water supply assessment	76
4.3.1.1	Water supplies	76
4.3.1.2	Water demand	77
4.3.1.3	Future water supply alternatives	78
4.3.2	Expansion scenario analysis	82
4.3.2.1.	Carbon footprint estimates	82
4.3.2.2.	Multi-objective evaluation	83
4.3.3.	Quantitative modeling and systems analysis	84
4.3.4.	Adaptation analysis on cost and carbon/energy footprint	88
4.3.3.1.	Carbon/energy footprint and cost optimization	88

4.3.3.2. Optimal expansion solutions and construction sequence	89
5. System-Scale Adaptation for Existing Urban Water Infrastructure	94
5.1. Basic considerations in adaptation engineering	94
5.1.1. Adaptation engineering for water infrastructure	94
5.1.2. Adaptation attributes of three types of water infrastructure	96
5.1.3. The capacity reserve concept and climate resilience	98
5.1.4. CR and engineering practice	100
5.2. Water infrastructure capacity reserve and resilience	101
5.2.1. Storm water infrastructure functions and design tolerances	101
5.2.1.1. Realized hydraulic capacity reserve	101
5.2.1.2. Water quality limitations	106
5.2.2. Drinking water infrastructure functions and design tolerances	107
5.2.2.1. Engineering resilience in a distribution network	107
5.2.2.2. Realized capacity reserve in drinking water treatment	107
5.2.3. Wastewater infrastructure functions and design tolerances	110
5.2.3.1. Realized capacity reserve in hydraulic loading	110
5.2.3.2. Realized capacity reserve in biological systems	110
5.2.3.3. The CR efficacy in current system design	113
5.3. Water infrastructure vulnerability analysis for adaptation	115
5.3.1. The resilience assessment and two approaches	115
5.3.2. Water resilience evaluation and resilience tool – CREAT	117
5.3.3. From vulnerability analysis to adaptation engineering	119
6. SUD Methods and Tools for Drinking Water Treatment	120
6.1. Water Treatment Plant – Climate Adaptation Model (WTP-cam)	120
6.1.1. WTP-cam functionality and approaches	121
6.1.1.1. Treatment processes in simulation	121
6.1.1.2. Incorporation of hydroclimate uncertainties	122
6.1.1.3. Source of influent water quality statistics/correlation	125
6.1.1.4. Customization of GAC unit process model	125
6.1.2. WPT-cam program and model simulations	126
6.2. Principles, models and algorithms in WTP-cam	126
6.2.1. Monte Carlo methods in modeling source water variability	126
6.2.1.1. Seasonal multivariate analysis	127
6.2.1.2. TOC compliance simulation	128
6.2.1.3. GAC unit adaptation analysis	128
6.2.1.4. Unit Process Engineering Analysis	129
6.2.1.5. Adaptation cost and economics	131

6.3. GCWW Miller plant case study using WTP-cam	132
6.3.1. Miller plant operation and performance	133
6.3.1.1. Treatment process and modeling.....	133
6.3.1.2. GAC absorption and TOC removal.....	134
6.3.2. WTP-cam simulation of hydroclimatic change impacts.....	136
6.3.2.1 Simulation and model assumptions.....	136
6.3.2.2 Source water characterization	137
6.3.2.3 Projecting raw water quality in 2050	138
6.3.2.4 WTP-cam model calibration and validation.....	140
6.3.3. Engineering analysis for water treatment adaptation.....	141
6.3.3.1. Adaptation feasibility evaluation.....	141
6.3.3.2. Adaptation economics in TOC treatment.....	144
6.3.3.3. Implication for engineering practice	145
7. Adaptation Engineering for Drinking Water Distribution	145
7.1. Water age and water quality changes in distribution: Need for adaptation.....	147
7.1.1. EPANET-based risk assessment on DBP formation	147
7.1.2. Water age variations, modeling and adaptive control.....	150
7.2. In-network water treatment as adaptation measure.....	150
7.3. Water conservation, storage and reuse through adaptive planning.....	154
8. SUD Applications in Coastal Regions: Water Infrastructure and Emergency Planning .	155
8.1. Water infrastructure vulnerability in coastal regions	155
8.2. Wastewater vulnerability and adaptation in storm surge	158
8.3. Emergency evacuation and water supplies.....	161
9. Summary and Recommendations.....	162
10. References	164
 Appendix A AIR-SUSTAIN program input and output structures	 162
Appendix B WTP-CAM User's Manual	247

List of Tables

Table 2-1	Adaptation attributes for common objectives	14
Table 2-2	General advantage and challenges of three-level adaptation actions.....	17
Table 2-3	Selected urban functions impacted by hydroclimatic factors	25
Table 2-4	Four daily periods of traffic compositions on the highway in Cincinnati	50
Table 2-5	Locations and traffic flow in 2009 for selected locations in the Cincinnati road network	52
Table 2-6	Statistics of daily temperature measurements at NQAAS Station 17-061-00040	53
Table 2-7	Temperature differences between the reference station and other stations abstracted from the >10-year daily temperature measurements	59
Table 2-8	Trip generation results in number of trips per day	72
Table 2-9	Trip Distribution results for number of trips per day originated from and attracted to centers	72
Table 2-10	Average queue length, average wait time, total delay and average delay during morning peak hours (7:00 ~9:00 am).....	73
Table 2-11	Water demand in 2006 and projections for wholesale customers in annual average (Board of County Commissioners, 2008).	77
Table 2-12	Water demand projections for retail and significant users in terms of annual 1535 average flows (Board of County Commissioners, 2008).....	78
Table 2-13	Twenty alternatives for water supply expansion in the county master planning..	78
Table 2-14	Maximum water credit and unit cost of the twenty water supply alternatives	81
Table 2-15	LCA of carbon footprint of twenty water supply alternatives	84
Table 2-16	Ideal solution of the multi-objective model	89
Table 2-17	The Pareto optimal expansion strategies (n = 1).....	89
Table 2-18	The Pareto optimal expansion strategies for the best and worst cases (n = 1).....	90
Table 2-19	Water infrastructure design and engineering domains, and their attributes.....	102
Table 2-20	Important engineering attributes for storm water infrastructure adaptation	104
Table 2-21	Important engineering attributes and likely vulnerability in drinking water treatment and distribution systems for community water supplies.....	108
Table 2-22	Important engineering attributes and potential vulnerability of wastewater infrastructure	111
Table 2-23	Types and approaches of eight water utilities in climate vulnerability assessment	116

Table 2-24	Options for Monte Carlo analysis	124
Table 2-25	Illustration of calculating running annual average for finished water TOC	128
Table 2-26	GAC contactor cost.....	131
Table 2-27	GAC reactivation cost.....	132
Table 2-28	Miller WTP Unit Process Design Parameters.....	133
Table 2-29	Inflow and chemical feed levels for the Miller WTP	134
Table 2-30	Statistics of full-scale field measurements.....	134
Table 2-31	Source water inputs for the Miller water treatment plant in 1998 (Baseline).....	138
Table 2-32	Correlation matrix for source water quality parameters (for Ohio River during July 1997 to December 1998).....	139
Table 2-33	Projected raw water quality parameters for the Miller WTP in 2050.....	141
Table 2-34	Comparison of sampled and modeled water quality results	142
Table 2-35	Selected hydrological impacts and adaptation variables in coastal area.....	157
Table 2-36	SLOSH modeling parameters for storm surge modeling at Mattapoisett, MA.....	159
Table 2-37	Population affected for evacuation under four categories of hurricane	161

List of Figures

Figure 2-1	Schematic process diagram of iterative monitoring-adaptation framework for water infrastructure adaptation	3
Figure 2-2	Typical spatial relationships of water infrastructure in an urban environmental with illustration of infrastructure adaptation scales and general process	5
Figure 2-3	Schematic diagram showing three major types of urban forms and their typical properties.	7
Figure 2-4	General process of current urban master planning and its relations to transportation and water infrastructure engineering.	9
Figure 2-5	Three major types of urban sprawl expanding the urban footprints into exurban areas	10
Figure 2-6	General process of adaptive urban planning and engineering.	12
Figure 2-7	Schematic of the SUD structure for scenario-based urban development planning and engineering.	16
Figure 2-8a	Program flow diagram of the Integrated Water Management (IWM) program for watershed simulations	18
Figure 2-8b	Program flow diagram of the Integrated Water Management (IWM) modeling for urban catchment using EPA's National Stormwater Calculator (U.S. EPA, 2014).	19
Figure 2-9	Process flow block diagram of the scenario-based AUP&ET for urban planning and engineering	21
Figure 2-10	Schematic diagram showing basic modeling framework for WTP3.0 as a major SUD element	22
Figure 2-11	Schematic diagram of water supply in a municipality and major system variables	23
Figure 2-12	Examples of urban expansion and urban form transformation for Atlanta (upper) and Phoenix (lower) metropolitan regions between 1970 and 1992.	27
Figure 2-13	Transportation efficiency (annual delay, travel index, excess fuel use, and annual cost) in year 2007 as a function of urban population in the U.S. urban centers... ..	28
Figure 2-14	Simulation block diagram for CA-Markov based urban land projections	34
Figure 2-15	AIR-SUSTAIN modeling framework for transportation analysis of efficiency and CO ₂ emission in urban infrastructure adaptation	36
Figure 2-16	AIR-SUSTAIN graphic interface for scenario modeling and analysis	38
Figure 2-17	Results Comparison interface in the AIR-SUSTAIN tool	40
Figure 2-18	PM _{2.5} hotspot identification process	43
Figure 2-19	Accuracy and data requirements for three types of vehicle activity inputs	44

Figure 2-20	Modeling framework for emission estimation using both the macroscale VISUM and microscopic VISSUM traffic simulation models	45
Figure 2-21	Major transportation traffic routes and the urban physical footprints of the Cincinnati metropolitan region	47
Figure 2-22	Land use patterns differing among 12 NAAQS monitoring stations	48
Figure 2-23	A schematic diagram of three-dimensional model illustrating the urban formation, traffic and atmospheric structure in the Cincinnati metropolitan area.....	49
Figure 2-24	Truck and passenger car traffic volume distribution in the Cincinnati metropolitan region.....	51
Figure 2-25	Representative temperature profiles showing the boundary inversion and capping inversion	54
Figure 2-26	Temporal L_R and H_{inv} variations showing diurnal thermal inversion in the urban boundary layer in October 2011	55
Figure 2-27	T_{min} , ΔT , and $PM_{2.5}$ variations with time at NAAQS monitoring station 061-0040.	57
Figure 2-28	Change of ambient temperature T_{min} and ΔT at station 061-0040 in the central urban interior. The regression slopes are statistically significant with $p < 0.0001$	58
Figure 2-29	T_{min} at 17-061-0040 station is linearly correlated with those of other stations in the 2005 measurements	58
Figure 2-30	Spatial variations of temperature difference for mean and maximum T_{avg} and $PM_{2.5}$ in cross section O-O'	60
Figure 2-31	Co-variation of minutely average wind speed at the I-75 site with the lapse rate in the boundary layer during the roadside black carbon dispersion experiments ...	61
Figure 2-32	Schematic diagram showing major types of microclimate conditions in the surface roughness layer (SRL) equivalent to the urban canopy layer (UCL)	63
Figure 2-33	The base-year distribution of population, household and employment in the Cincinnati metropolitan area.	65
Figure 2-34	Three development scenarios for the Cincinnati metropolitan area in target year 2030. A) monocenter of development in downtown; B) two-center configuration in downtown and Mason area; and C) two-center configuration with mass transit between the centers	66
Figure 2-35	Setup of a new scenario in AIR-SUSTAIN	67
Figure 2-36	Program interface for A) importing the Base Year data; B) assigning population change; and C) assigning employment changes at TAZ levels	67
Figure 2-37	Simulation module of demographic analysis for a development scenario. High population density is specified for analysis of the urban adaptation option	68

Figure 2-38	Hotspots identified for typical peak-hour traffic for 2009 in Hamilton County, showing concentrations along I-71, I-75, I-275N, and Ronald Reagan highway	69
Figure 2-39	Population changes by 2030 for the three developmental scenarios (S1, S2, and S3 in the inserts) in comparison to the distribution of base year 2010 (background) ...	70
Figure 2-40	Changes in number of household by 2030 for the three developmental scenarios (S1, S2, and S3 in the inserts) in comparison to the distribution of base year 2010 (background).....	71
Figure 2-41	Employment changes by 2030 for the three developmental scenarios (S1, S2, and S3 in the inserts) in comparison to the distribution of base year 2010 (background).....	71
Figure 2-42	Peak hour (7:00-9:00 am) traffic volume distribution over the Cincinnati road network for the base year (2010) and under three target-year (2030) development scenarios.....	73
Figure 2-43	Comparison of three development scenarios (S1, S2, and S3) in peak hour (7:00-9:00) vehicular CO ₂ emission and energy (fuel) consumptions	74
Figure 2-44	Location of the Manatee County water supply system along the upper Manatee River in Florida	75
Figure 2-45	Locations of WTP, ASR, well fields (ECWF-1, MPWF), and the twenty potential water supply alternatives A1-A20.	76
Figure 2-46	The life-cycle system analysis flow diagram for determining carbon footprint in water infrastructure expansion alternative evaluations.	83
Figure 2-47	Pareto solution fronts for the best compromised solutions for projected future water demand (base case) and the demand with 10% uncertainties (best case and worst case).	91
Figure 2-48	Suggested optimal facility expansion strategies in each of five-year periods based on the optimization modeling of water infrastructure expansion options for Manatee County, Florida	93
Figure 2-49	Assessment-adaptation framework for water infrastructure planning and engineering. The box in dashed line contains the elements of climate and land use projections for infrastructure master planning.	95
Figure 2-50	Process schematic diagrams for typical centralized drinking water, wastewater, and storm water infrastructure in an urban watershed.	97
Figure 2-51	Four types of infrastructure vulnerability under the threat of external impact event (e.g., storm surge).	98
Figure 2-52	Maximum percentage increase ($\Delta Q\%$) in hydraulic capacity of stormwater conveyance using commercial concrete pipes of discrete nominal diameters (D)	105

Figure 2-53	BOD removal efficiency of a wastewater activated aeration tank as a function of flow, BOD mass loading, and aeration capacity	112
Figure 2-54	Relative magnitude of infrastructure <i>CR</i> installed in current engineering practice (left) in comparison with the relative precipitation change (solid bar) and uncertainty (pattern and solid line with whisker) by 2060.	114
Figure 2-55	The process of climate vulnerability analysis using EPA tool CREAT	117
Figure 2-56	Schematic diagram for (A) treatment unit process at the GCWW Richard Miller water treatment plant, and (B) TWP-ccam program flow in the example simulation.....	121
Figure 2-57	Original input data for the Miller example processing train.....	122
Figure 2-58	Program logic sequences in Monte Carlo simulation of future source water quality variations using the correlation matrix method (Li et al., 2014)	123
Figure 2-59	Graphic user interface for inputs in Monte Carlo simulations of future water qualities	125
Figure 2-60	Manual input window for influent water quality statistics	126
Figure 2-61	Cost curve for annual cost of GAC unit.....	132
Figure 2-62	Temporal variations of influent and blended effluent TOC in the GAC unit.....	135
Figure 2-63	Temporal variations of inflow, mass inflow and active number of GAC contactors.	135
Figure 2-64	Temporal variations of active contactors and blended effluent TOC concentration	136
Figure 2-65	Time series of plant inflow and EBCT variations..	136
Figure 2-66	Normal probability plots for source water pH (107 samples) and TOC (93 samples) for Ohio River from the ICR database (July 1997-December 1998)...	137
Figure 2-67	Modeled treatment performance of the Miller water plant in baseline (1998) and future (2050) scenarios. (A) TOC running average at finished water; (b) TTHM after 3 days residence in distribution system.....	143
Figure 2-68	Cost curve for the GAC reactor at the Miller water treatment plant.	144
Figure 2-69	The probability distribution for net annual adaptation cost against the source water change scenario in year 2050	145
Figure 2-70	Schematic diagram showing the simultaneously occurring chlorine reactions with bulk and wall demands, mass exchange between the bulk water and pipe wall, and the relationship between reaction kinetics for bulk decay (k_b), DBP formation (k_D), and wall decay (k_w)	148
Figure 2-71	Water demand and computed Re variations in a two-week period for a single home, 31 and 114 homes of a pipe dead-end section showing significant	

	differences between the APAD model and the generalized water demand pattern	151
Figure 2-72	Probability distribution and corresponding CDF of simulated water age for the network	152
Figure 2-73	Schematic views of in-network aeration in LVVWD water distribution to remove volatile THM from drinking water in the alphas tank reservoir	153
Figure 2-74	EPANET simulation of flow and THM distribution in the Western Hill portion of the LVVWD water distribution system.	154
Figure 2-75	Schematic illustration of long-term climate and short-term meteorological and disruptive storm surge events in a typical coastal zone... ..	156
Figure 2-76	Schematic diagram showing wave action and storm surge height as a function of storm surge, tidal cycle, and sea level rise.....	158
Figure 2-77	Location of the water infrastructure at the Town of Mattapoisett aside of the Mattapoisett Harbor... ..	159
Figure 2-78	A cartoon illustration of SLOSH modeling results for likely inundation risk for the wastewater transfer station	160
Figure 2-79	Hourly traffic map in the Mattapoisett region after evacuation order activated at noon time.. ..	162

ABBREVIATIONS AND NOTATIONS

Definitions and Abbreviations

AADT	annual average daily traffic
AERMOD	American Meteorological Society and U.S. Environmental Protection Agency Regulatory Model
AIR-SUSTAIN	Air Impact Relating Scenario-Based Urban Setting and Transportation Asset in Network
AMO	Atlantic Meridian Oscillation
APAD	all-pipe and all demand
ASR	aquifer storage and Recovery
AUP&ET	Adaptive Urban Planning and Engineering Tool
AwwaRF	Water Research Foundation
BASINS	U.S. EPA's Better Assessment Science Integrating Point and Non-Point Sources model
BMP	better management practices
BOD	biological oxygen demand
CA	cellular automata
CAA	Clean Air Act
CAL3QHC	CALINE3-based CO model with queuing and hot spot calculations and with a traffic model to calculate delays and queues
CBD	central business district
CDF	cumulative density function
CR	capacity reserve
CSO	combined sewer overflow
CSS	combined sewer system
CWA	Clean Water Act
CWT	continuous wavelet transformation
CWS	community water systems
D/DBP	disinfectant/disinfection byproduct
DALR	dry adiabatic lapse rate
DBP	disinfection by-products
DOC	dissolved organ carbon
DOT	U.S. Department of Transportation
DW	drinking water
EBMUD	East Bay Municipal Utility District
EC	elemental carbon in air emission
GAC	granular activated carbon
GCWW	Greater Cincinnati Water Works
GHG	greenhouse gas
GIS	geographical information system

GUI	graphic user interface
HAAs	haloacetic acids (nine individual species and the total of five (HAA ₅), six (HAA ₆) and nine (HAA ₉) species)
HDVC	hourly demand variation curve
iCLUS	U.S. EPA's Integrated Climate and Land Use Scenarios
ICR	information collection rule
IDF	precipitation intensity – duration – frequency
IPCC	United Nation's Intergovernmental Panel on Climate Change
IWM	integrated watershed modeling
LANDSAT	land remote-sensing satellite (system)
LCA	life cycle analysis
LID	low-impact development
LVVWD	Las Vegas Valley Water District
MARS	Manatee agricultural reuse supply
MCE	multiple criteria evaluation
MCL	maximum contaminant level
MCLG	maximum contaminant level goal
MGD	million gallons per day
MIA	most impacted area
MSX	EPANET Multi Species Extension
NOAA	National Oceanic and Atmospheric Administration
MODIS	moderate resolution imaging spectroradiometer (for satellite)
NOM	natural organic matter
MOVES	U.S. EPA's Motor Vehicle Emission Simulator model
NAAQS	U.S. EPA's National Ambient Air Quality Standards
NPDES	National Pollution Discharge Elimination Systems
NRMRL	U.S. EPA National Risk Management Research Laboratory
NSC	U.S. EPA's National Stormwater Calculator
NTU	nephelometric turbidity unit
NYCDEP	New York City Department of Environmental Protection
O&M	operation and maintenance
OC	organic carbon in air emission
OKI	Ohio-Kentucky-Indiana Regional Council of Governments
ORD	U.S. EPA Office of Research and Development
OTAQ	U.S. EPA Office of Transportation Air Quality
OW	U.S. EPA Office of Water
POU	point-of-use
PR/MRWSA	Peace River Manasota Regional Water Supply Authority
PVC	polyvinyl chloride
R&D	research and development
RO	reverse osmosis
RSSCT	rapid small-scale column test
SAWS	San Antonio Water System
SBL	stable boundary layer
SDWA	Safe Drinking Water Act

SLOSH	sea land overland surge height, NOAA's computer program
SLR	sea level rise
SRES	Special Report on Emissions Scenarios
SUD	Smart Urban Designer
SWFWMD	Southwest Florida Water Management District
SWMM	surface water management model
SWAT	Soil and water assessment tool
TAZ	traffic analysis zone
TDF	travel demand forecasting
THM	trihalomethane
TTHM	sum of four individual species of trihalomethanes
UHI	urban heat island
U.S. EPA	U.S. Environmental Protection Agency
USGS	U.S. Geological Service
UVA	ultraviolet absorbance at 254 nm
VISUM	a macroscopic traffic model after "Verkehr In Städten - SIMulationsmodell"
VISSIM	a microscopic traffic model after "Verkehr In Städten - SIMulationsmodell"
VSP	vehicle specific power
WHO	World Health Organization
WRAP	U.S. EPA Water Resources Adaptation Program
WTP	water treatment plant
WTP-cam	water treatment-climate adaptation model
WUCA	water use caution area
WUP	water use permits
WW	wastewater

Notation and Symbols in Equations

α	level of significance
η_{BOD}	BOD removal rate
ε_t	a vector of independent, normally distributed random variables with mean zero and variance one
θ	hydraulic residence time
θ_c	biomass cell age in the aeration tank
ϑ	defined by $\vartheta = (1 + k_d \theta_c) / \theta_c$
μ_0	average of water quality for baseline scenario
μ_1	average of water quality for future scenario in 2050
ρ	correlation coefficient
σ_0	standard deviation of water quality for baseline scenario
σ_1	standard deviation of water quality for future scenario in 2050

$\sigma_{Q_{1ij}}$	standard deviation of Q_{1ijk}
$\sigma_{Q_{2ij}}$	standard deviation of Q_{2ijk}
Ψ	defined by $\Psi = X/Y_o$
a	a parameter for TOC removal, defined by $a = 0.682 \cdot TOC_{in}$ or an empirical parameter for GAC cost estimation
b	a parameter for TOC removal, defined by $b = 0.167 pH^2 - 0.808 pH + 19.086$ or an empirical parameter for GAC cost estimation
c	BOD concentration in discharge or an empirical parameter for GAC cost estimation
c_o	initial BOD concentration
D	GAC reactivation period
D_o	a known correlation matrix for the nine raw water quality parameters
$EBCT$	empty bed contact time
i	sequence number of pixel of a quantitative component
j	sequence number of time period
k_d	BOD degradation constant
m_o	mass loading
Q	flow rate
TOC_{eff}	effluent TOC concentration from GAC processing
TOC_{in}	input TOC concentration to GAC unit
$USRT$	process design or operating variable
V	aeration tank volume
w	weighing factor
X	microorganism concentration in the aeration tank in mg/L; and TOC increment over the compliance criterion, 2 mg/L
y	capital of operation and maintenance cost for GAC processing
Y	maximum yield coefficient in mg/mg for an aeration tank; and net annual cost of GAC processing
z	either 0 or 1 for adjusting the cost functions for a range of USRT values
Z_t	vector of nine raw water quality parameters used in WTP/WTP-cam modeling

Part Two: Smart Urban Designer (SUD) and Application Case Studies

Y. Jeffrey Yang¹, Heng Wei², Xinhao Wang, Steven Buchberger², Marissa S. Liang³, Ni-bin Chang⁴, Britta Bierwagen⁵, Susan Julius⁵, Zhiwei Li⁶, Dominic L. Boccelli², Robert M. Clark⁷, Hou Liu², and Jill Neal¹

The national adaptation report Part I (U.S. EPA, 2015a) described multiple environmental and economic stressors facing our nation's water infrastructure. It further discussed the need for adaptation of the infrastructure resilience and sustainability. This Part II report investigates the relationship through scenario-based adaptation among the factors of climate factors, land use changes, urban growth, population shifts, transportation, energy, air and water pollution, and water management. These factors can be shown to interact at the watershed, urban, and system-specific local levels. For example, development can lead to an urban heat island (UHI) occurrence, which increases energy use and water consumption, but may reduce overall energy needs when smart growth policies are devised. Low density development leads to a lesser UHI effect, but higher use for energy in transportation, which adds to air pollution. Development can also alter rainfall and runoff characteristics, which have subsequent impacts on water supplies and water quality. The latter changes may require water plant processes to be altered, thereby increasing energy needs. Poorly planned development patterns also impact water demand distribution and sewer system operations with respect to pipe condition, water age and power usage. The current situation is not sustainable. Obviously, water infrastructure sustainability is a multi-dimensional issue intrinsically related to watershed management, urban development pathways, and individual water system engineering.

As a result, the Part II report presented here is focused on Smart Urban Design (SUD) tools and methods, their principles for urban planning and infrastructure adaptation design. Thus the report aims at assisting water practitioners and urban planners in developing resilient, efficient and economical water supply, wastewater disposal, stormwater management and transportation systems. In sequence, the report first outlines adaptation objectives and the SUD framework at three spatial scales. Next, it describes unique environmental properties associated with urban growth and current planning practices to facilitate the growth. In Sections 3.0-7.0, the core SUD components in urban planning and water system engineering are described. The case studies provide further insight on the function and utility of SUD tools and methods. In Section 8.0, the SUD application in coastal areas briefly illustrates the complex factors of the hydroclimatic impacts in adaptation planning. Finally, the summary and recommendations are presented in Section 9.0.

¹ U.S. EPA, Office of Research and Development, Cincinnati, Ohio

² University of Cincinnati, Cincinnati, Ohio

³ U.S. EPA, Office of Research and Development, ORISE participant, Cincinnati, Ohio

⁴ University of Central Florida, Orlando, Florida

⁵ U.S. EPA, Office of Research and Development, Washington, District of Columbia.

⁶ Carbon Sequestration Technologies, LLC., Pittsburgh, Pennsylvania

⁷ Environmental and Health Consultant, Cincinnati, Ohio

1. Sustainable Development of Urban Water Systems

Hydrological impacts from climate and land use changes are often not well characterized or understood by local agencies charged urban infrastructure planning and engineering. Given that the practitioners and water managers are risk-averse, a properly defined design basis is the first and fundamental step. How to developing the design basis can directly affect the infrastructure management objectives in years to come. Because much of this infrastructure will remain in place for 50 to 100 years, there is significant uncertainty on how it relates to planning today, and on the potential for stranded capacity in the future, which is costly to rate and tax payers. Failure to provide adequate infrastructure has serious economic consequences. Similarly, the uncertainty resulting from the capacity excess or deficit creates significant concern for local officials charged with infrastructure management. Providing a means to help reduce these uncertainties with methods and tools for local officials to construct a more resilient future is the focus of this research report.

1.1. Adaptation considerations

The projections of future hydroclimatic and land use conditions often have too much uncertainty for widely practiced planning and engineering of capital-intensive water infrastructure and urban development. Thus, it is essential to incorporate them into planning and design process. The adaptation process defined by this report is intended to manage the uncertainties of the hydrological and land use projections. For this reason, an iterative modeling-monitoring approach in Figure 2-1 is developed. It aims at reducing the uncertainty to the degree that is appropriate for infrastructure projects. It also incorporates a process of re-evaluating the adaptation design and objectives to permit ongoing changes with the ability to further adapt to the changing circumstances. This adaptive practice is pertinent when significant hydroclimatic impacts may be realized in a local watershed.

Because of the uncertainty on future projections, water managers need to manage the risk of consequences from inadequate, poorly planned or delayed adaptation efforts. The consequences of inadequate adaptation and adaptation limitations has been described in literature (e.g., Felgenhauer and Bruin, 2009; Felgenhauer and Webster, 2013). SUD tools and methods are described here for infrastructure planners and engineers to use when developing appropriate investments that will have long life and utility, minimize contributions to global impacts (reduced emission, for example), provide for added economic efficiency (e.g., improved transportation and water service), and protect public and private infrastructure investments, while minimizing the need for future costly investments.

Hydrological responses from climate and land use changes are realized in long durations, while short-term disruptive climate events or climate impacts of large magnitudes can be explicit and quantifiable. Examples of disruptive events include storm surge, urban flooding and salt water intrusion, all of which are commonly found in coastal areas. Actionable technical information is usually available for design and implementation of adaptation actions. This scenario is marked as Step (1) in Figure 2-1. For long-term hydrological impacts, model simulations of land use and future climate are frequently used to project the hydroclimatic impact on watershed hydrology. This is marked as the first tier of actions in Figure 2-1. The integrated model simulation and monitoring framework to quantify the combined hydrological effects of climate, land use and population changes, will be presented in subsequent publications.

The Processes A and B (Figure 2-1) involve real-time or near real-time monitoring and data development as tools to validate and further refine climate and land use projections. The land use and climate modeling updates, marked as Actions (a) and (b) in Figure 2-1, may yield projections with less uncertainty. The outputs and subsequent integrated hydrological modeling should be helpful toward developing the technical basis for adaptation planning and engineering design. This step is marked as Step (2) in Figure 2-1. In case the results remain inadequate in the degree of certainty for engineering standards and adaptation option evaluation, the iterative process continues in Steps (3) and (4). For this objective-oriented monitoring-to-adaptation process, the tools for integrated hydrological modeling and the near real-time monitoring are available. Examples include the framework using MODIS and LANDSAT satellite imagery (e.g., Chang et al., 2006). A future publication will describe the monitoring framework and its application examples.

Water infrastructure and transportation infrastructure are two fundamental elements in urban developments that provide vital urban services and closely relates to land use and urban economic activities. Several considerations in framing the infrastructure adaptation are important, including objective definition, constraint assessment, adaptation feasibility analysis, adaptation option comparison and evaluation, and finally adaptation effectiveness evaluation. These considerations are specific to the physical boundary of the service area, or projected service area, under consideration (Figure 2-2), whether the adaptation is on the scale of a

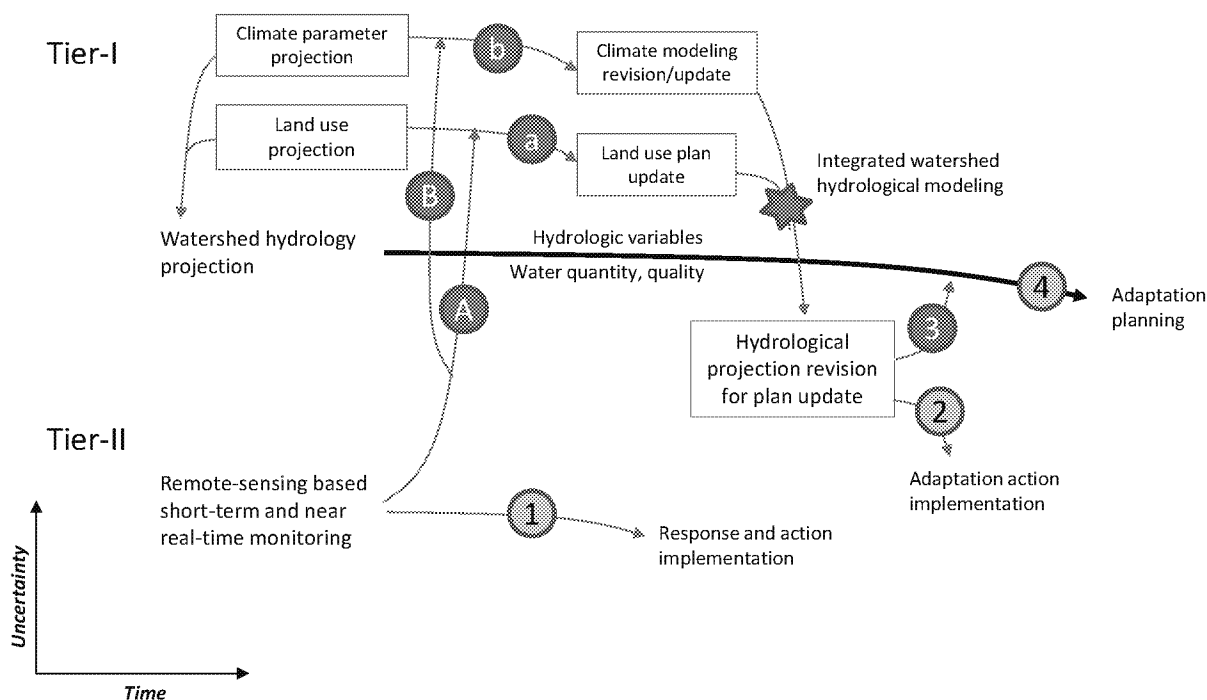


Figure 2-1 Schematic process diagram of iterative monitoring-adaptation framework for water infrastructure adaptation. Symbols show steps in design basis development (See text for details).

watershed, urban water systems, or unit operations (e.g., techniques). The adaptation effectiveness evaluation may further warrant urban adaptation and/or adjustment to the regional economic and land use policies. This systematic approach serves as a venue to better communicate the adaptation options and their tradeoffs to stakeholders.

1.1.1. Defining adaptation objective

Water infrastructure adaptation to future conditions of hydroclimate and land use is effective only when taken in context of sustainable urban and socioeconomic development, a central objective of many stakeholders. This emphasis agrees with the objective “downscaling” concept described by Brown et al (2012). Although specific goals of adaptation may vary among stakeholders and local conditions, an over-reaching and commonly shared objective can be defined as:

- To enhance water infrastructure resilience. The ultimate purpose is to provide uninterrupted water supply and wastewater services, and to provide the required amount of storm water management and urban drainage, for a projected socioeconomic growth under both current and future climate conditions.
- To increase the ability to comply with the existing regulations and help the implementation of urban development policies. The environmental regulations related to hydrological impacts were reviewed in the National Water Infrastructure Adaptation Assessment Part I (U.S. EPA, 2015a). For example, in the case study described later in Section 6.0, high total organic carbon (TOC) content, increased water age in underutilized sections of drinking water distribution systems and increased disinfection by-product (DBP) formation under future climate conditions can be a principal concern for water managers.
- To achieve co-benefits in water infrastructure adaptation and environmental resilience in urban development. Water infrastructure construction and operation consume a significant amount of energy and consequently yield air emissions, water pollution, and negative ecological impacts. Thus, the co-benefit in conjunction with transportation and building design, water infrastructure development and operation, is important to the effectiveness of water adaptation planning and design. This is particularly pertinent in the view of urban growth and future energy needs (Yang and Goodrich, 2014; Yang, 2010; Dodder, 2014; Dodder et al., 2010).
- And to minimize the systems’ adaptation cost.

There is a need to analyze water and transportation infrastructure because both are traditional and fundamental focus of urban planning and development. Transportation and environmental impacts will be analyzed in Section 3.0. The engineering components and functions of each of storm water, wastewater, and drinking water infrastructure will be analyzed in Section 4.0. In addition to the traditional water management functions, attention has been galvanized recently on water availability on the supply side and water footprints on consumption side. For water infrastructure, these fundamental concepts can be expressed as water reuse or

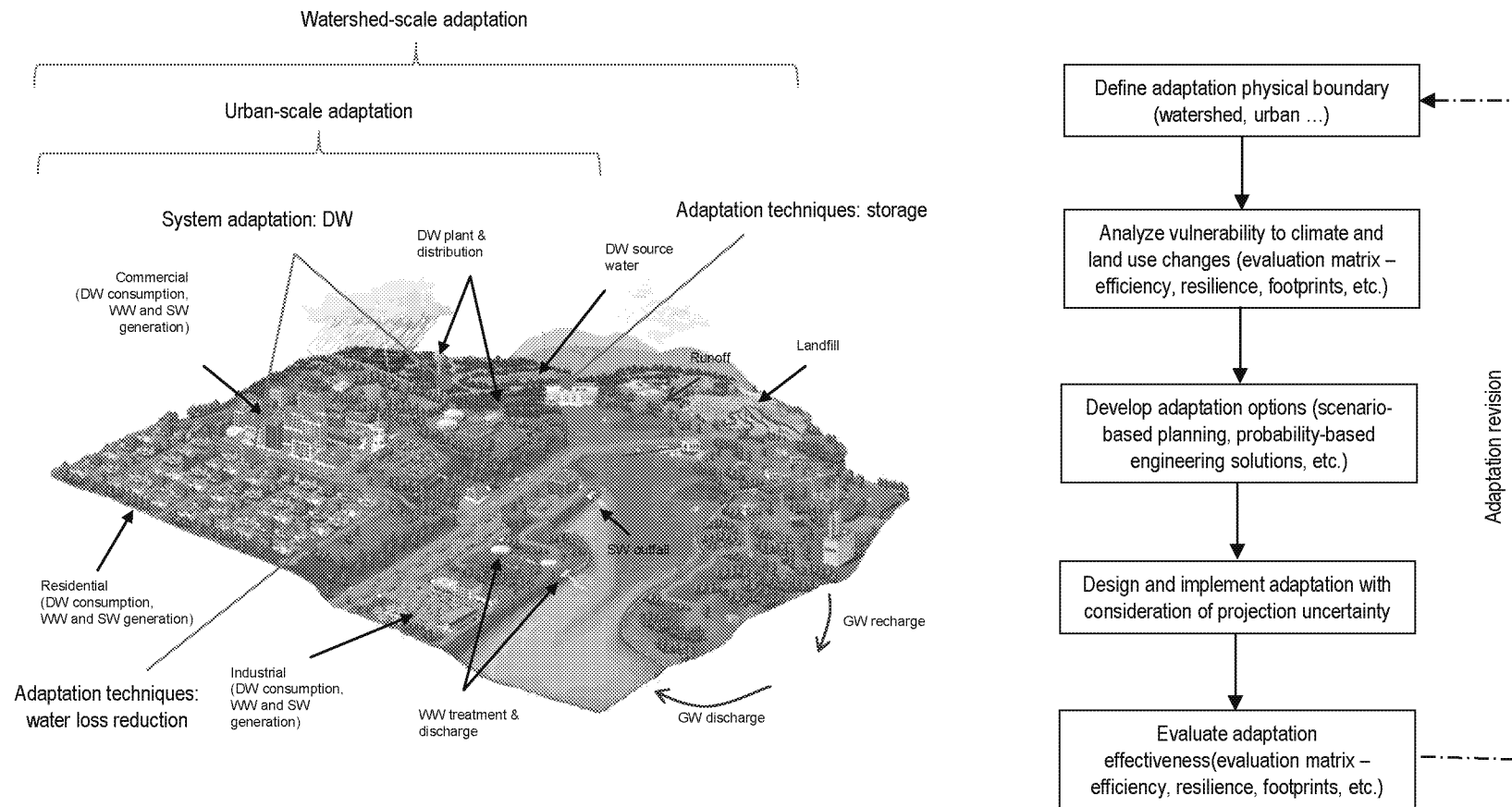


Figure 2-2 Typical spatial relationships of water infrastructure in an urban environment with illustration of infrastructure adaptation scales and general process. SW- surface water; DW – drinking water; GW – groundwater; WW – wastewater.

reclamation, water storage, water loss prevention, water conservation, and more importantly in water-energy nexus (PNNL, 2012; Yang and Goodrich, 2014, and references therein).

One important attribute for consideration is the time and planning horizon for infrastructure systems, and urban development in general. In many parts of the contiguous U.S., rapid urbanization and newly improved and/or constructed infrastructure services are projected to occur, concurrently, with significant changes in hydroclimatic and land use conditions. In the global scale, urban centers only occupy ~2% of land area on Earth, but account for 70% of global energy consumption and air emissions (e.g., Parshall et al., 2010, ADB, 2012; IEA 2013a,b). Urban population will further increase, reaching 6.3 billion by 2050, from 3.4 billion in 2009 (IPCC, 2014). In the future, urban change will likely lead to an even greater contribution to global energy, water, and food consumption, as well as air emissions unless adaptation action is taken to improve the sustainability. Surprisingly, because of the higher population density in urban centers, emission intensity and water consumption rates on a per capita basis are mostly lower than national averages (Dodman, 2009; ADB, 2012). Therefore, the shifting of energy and water consumption into high-density urban centers creates location-specific socioeconomic dynamics that adaptation needs to address. The conditions in the U.S. are similar. It is worthy to note that this adaptation need offers opportunities to reduce per capita emissions and water consumption, allowing meaningful changes in global energy consumption growth (Dodman, 2009). The urban infrastructure development and redevelopment have a significant potential for these co-benefits (Yang and Goodrich, 2014). Further decreases in per capita emissions and water intensity are possible, depending on the design and implementation of effective urban planning and adaptation actions.

Apparently, effective infrastructure adaptation demands for a systems approach as the means to increase urban sustainability. Many urban sustainability issues and assessment matrix are described in relevant EPA publications (e.g., U.S. EPA, 2007a,b; 2009; 2012a). For example, high-density developments, mixed use zoning, walkable communities, and green development all are specific sustainability measures. These measures aim to eliminate unnecessary urban sprawl, thereby effectively adapting water and transportation infrastructure to a changing environment. The developments are all focused on urban performance and efficiency. One of these matrices includes the energy and water footprint, and their combination with economic analysis (e.g., Chang et al., 2012; Yao et al., 2014). These considerations will be further discussed in Sections 2-4.

1.1.2. Understanding adaptation constraints

The National Water Infrastructure Adaptation Assessment Part I (U.S. EPA, 2015a) described the vast water infrastructure built in the nation over the past century, discussed the stressors on these water infrastructure systems (e.g., aging infrastructure, increasing demand) and the implications on their ability to be adaptable to future changes while complying with the water and air regulations. In the past, a significant national investment has been made to create this vast physical urban infrastructure and is being continuously made to improve the infrastructure reliability, resilience, and service. Thus, the physical footprints, planning guidelines, and engineering practices, all define the premise upon which the constraints must be understood and managed for adaptation.

In urban development, water infrastructure is spatially associated with roads and mass transit. Together both types of the urban infrastructure form the structural building blocks of urban communities. The resulting urban form defines the social structure, population and business distribution, which is enforced by local zoning laws and local ordinances. Common types of urban forms are monocentric, polycentric, and those in between (Figure 2-3). Each of the urban forms defines how urban population and economic activity are distributed in space. The result is the so-called infrastructure “locked-in condition”, limiting the optimization potential for water infrastructure. Consequently, fundamental change to how urban systems are planned requires the ability to overcome the physical as well as socioeconomic barriers associated with these “locked-in” infrastructure systems.

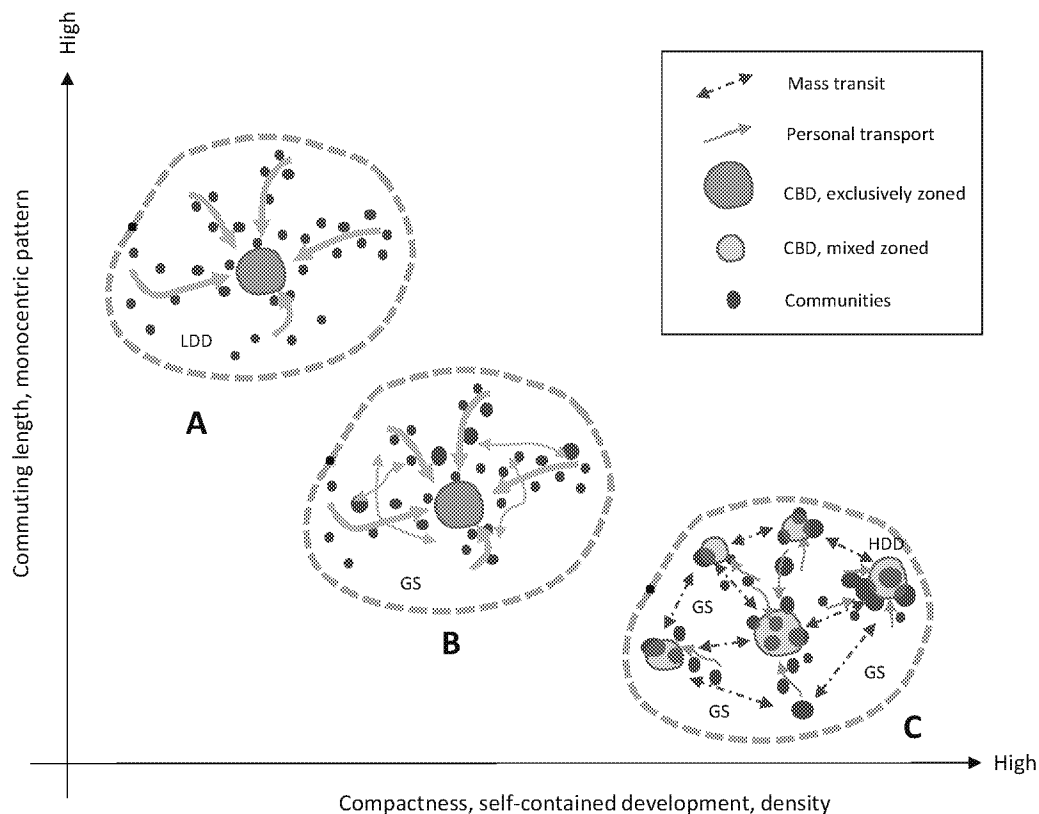


Figure 2-3 Schematic diagram showing three major types of urban forms and their typical properties. A – monocentric; B – mixed development with high reliance on personal transport; and C – polycentric developments with mass transit. Other symbols: GS – green space; LDD – low density development area; HDD – high-density development area; and CBD – central business district. Modified from Zhao et al. (2010).

The current urban development is oriented toward protecting public health and meeting service demands, while being limited by economic considerations. This development mode has resulted in unprecedented urban sprawl that expands the urban footprints into exurban areas. Figure 2-4 shows the steps utilized in the current practice of urban infrastructure planning and engineering. It starts with stakeholder engagement to determine urban socioeconomic goals, the projected or anticipated growth factors, and related socio-physical conditions. The subsequent

master urban planning guides the type and spatial distribution of urban land use, economic activities, residential distribution, as well as environmental assets including water resources, parks, green space and reservation of environmental sensitive areas. The guidelines can be implemented and enforced through use of zoning ordinances and other regulations. This traditional practice in urban planning leads to a final urban form, in which population and urban activities are distributed in the monocentric, polycentric forms, and those in between.

To the extent to which a specific urban form conforms to topography and natural environments, planning policies also play a significant role. They either reinforce the monocentric form or change it to a multi-center polycentric configuration. As shown in Figure 2-4, each of these urban forms has distinct composition and configuration of land use patterns, population distribution, and thus different characteristics of transportation and water infrastructure. The subsequent phase of infrastructure planning and design follows various guidelines and economic considerations.

For example, the Department of Transportation (DOT) has published a series of guidelines on transportation mobility and infrastructure improvements (e.g., FHWA, 2002, 2012a, b). The EPA Office of Transportation Air Quality (OTAQ) has issued guidelines on the emissions criteria, fuel standards and transportation vehicle technologies that affect urban air quality (e.g., U.S. EPA, 2012a; 2011). Other technical models and tools are widely used to evaluate and simulate the transportation needs, travel demand simulation (e.g., VISUM and VISSIM), and air quality impacts (e.g., MOVES, AERMOD, and CAL3QHC). These topics are discussed later in Section 3.0.

Water infrastructure is one principal element of urban infrastructure supporting and also shaping the urban form. The water services start with potable water supplies, distribution of drinking water to customers, followed by the collection of sewage and storm water and the subsequent management of same to protect public health and property. Master plans are developed for a given set of land use and economic projections with the purpose to satisfy the current and future water supply and water sanitation expectations. Many municipalities follow a well-defined process in developing planning objectives and determining planning variables. Planning and engineering tools are widely available, including EPANET and its commercial derivatives (e.g., WaterCAD, H2Omap) for drinking water supply, EPA's SWMM and related storm water packages for storm water management and urban drainage, and engineering software platforms (e.g., SewerGems, H2OMap/Sewer, HydraSewer). Overall, most municipalities pay attention to the operation and management of existing infrastructure, which is aging across the U.S. Some communities and researchers have expended efforts focused on component optimization, system improvement and capacity expansion, but system-wide re-planning and re-design rarely happens. These focus areas, for example, are identified in the nation-wide assessment as described in Section 7.0 of the National Water Infrastructure Adaptation Assessment Part I (U.S. EPA, 2015a). Apparently, the current practice promotes expansion of existing water system infrastructure and their physical footprints.

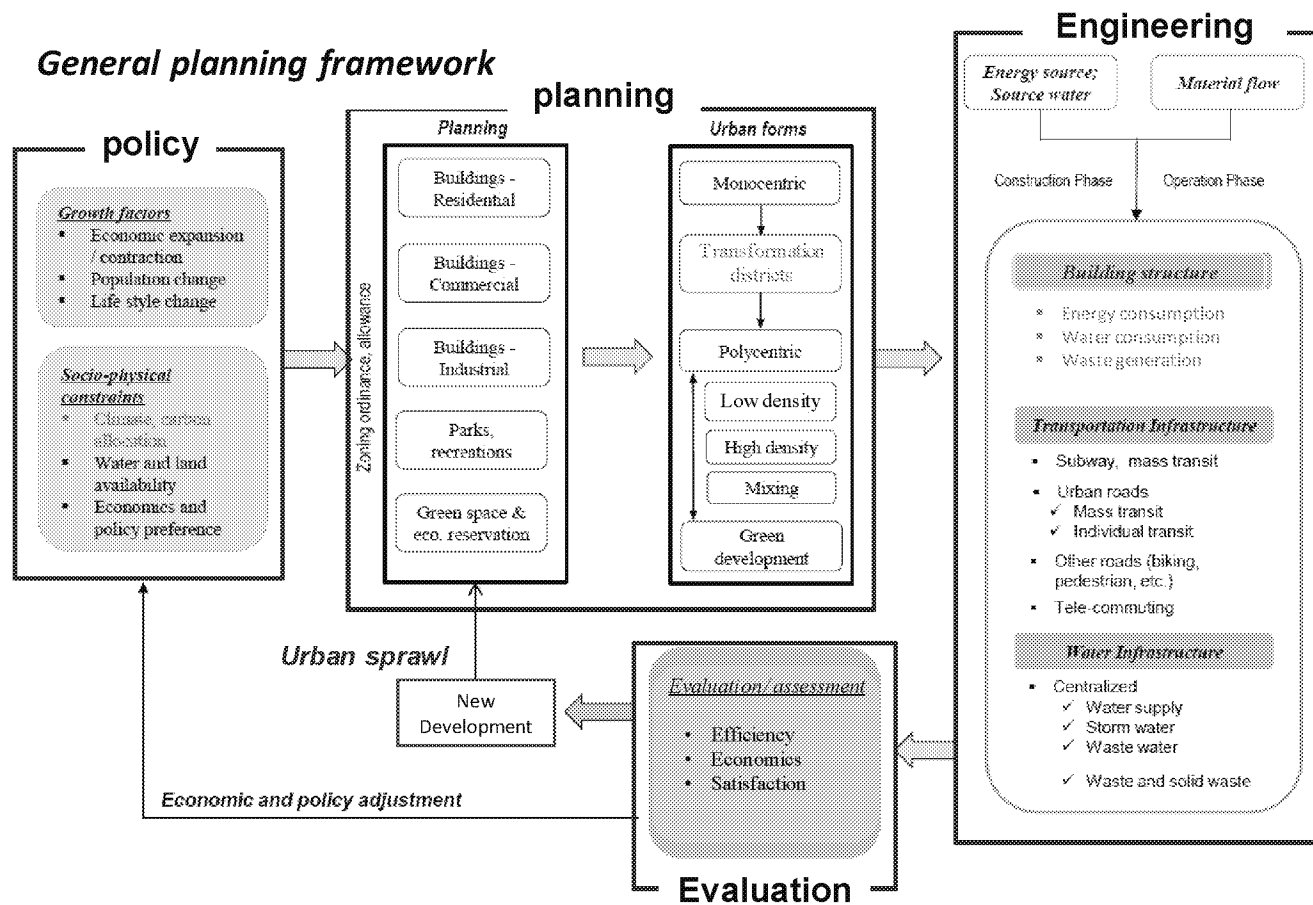


Figure 2-4 General process of the current urban master planning and its relations to transportation and water infrastructure engineering. Less emphasis on urban form transformation and the evaluation criteria often result in urban sprawl. The element in gray text in Planning step is not applicable; those in the Engineering step are not discussed in this report.

Municipalities and stakeholders periodically assess urban infrastructure performance after construction and a period of operations to compare its performance against the intent of the original master plans or new urban growth objectives. The performance evaluation serves as the basis for master planning revision and modifications of existing urban infrastructure. This master plan revision reoccurs periodically. Many county or municipal master-planning time horizons are 5-30 years depending on the infrastructure types, and a revision frequency every approximately 5 years is common in practice. Whether 5 to 30 years is sufficient has more to do with dealing with uncertainty than other factors. Public officials are reluctant to invest too far ahead, yet adaptation needs ultimately require them to do so. The current planning, engineering and political process supports continuous urban sprawl into the exurban areas as opposed to reevaluating the underlying framework of urban systems. Flanders et al. (2014) described this type of urban sprawl in an EPA internal report for the sustainable health community research, and analyzed its implications on urban infrastructure.

Three common types of urban sprawl are radial sprawl, ribbon sprawl, and leapfrog sprawl, as shown schematically in Figure 2-5. Their occurrence is often a result of unplanned or uncontrolled development. For example, general planning and engineering for water infrastructure consists of three major steps: 1) land use and economic projection, 2) analysis of spatial population distribution, and 3) projection of water demand and wastewater generation in a planning timeframe. Economy-of-scale for operations favors a centralized water supply system, which results from the initial monocentric urban form. The result is the single water, wastewater and storm water management network, if the hydrographic conditions permit, as commonly found in most large U.S. cities. In principle, a centralized water supply system delivers water from a central treatment plant through a vast distribution network at a lower treatment cost than a decentralized system, but may do so at the expense of increased energy consumption and greater risk of water quality changes in downstream use areas. Sewer systems collect wastewater from individual users and carry it to a central location for treatment before discharge. The same economy-of-scale/energy expense trade-off occurs. Storm water sewers drain an urban area and discharge overland runoff into a natural way under a NPDES permit. This arrangement is the most energy-efficient service within a mono-centrally distributed population.

Compounding the current planning and engineering practice is that all design guidelines are based on the assumed climate stationarity. This assumption and implication on water infrastructure were described in the adaptation report Part I (U.S. EPA, 2015a) and in the early EPA's adaptation conference proceeding (U.S. EPA, 2009c). The stationarity issue is embedded

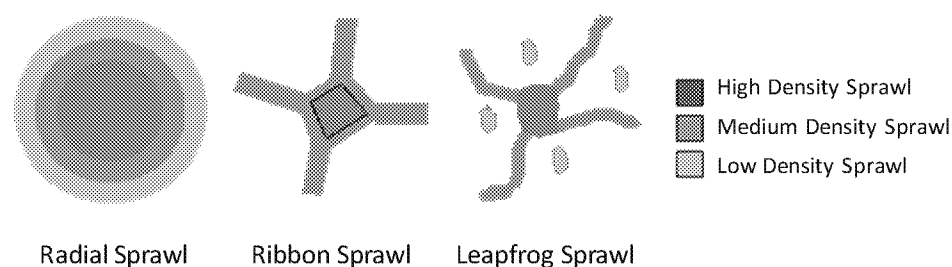


Figure 2-5 Three major types of urban sprawl expanding the urban footprints into exurban areas. Reproduced from Sudhira et al. (2005).

in planning guidelines and engineering codes, although recent revisions to the American Society of Civil Engineers' code of ethics includes language on the need to "*comply with the principles of sustainable development in the performance of their professional duties.*"

1.1.3. Revising or redefining planning and engineering focus

There is a critical need for a significant national investment to improve and renovate the nation's water infrastructure. The new investment provides a rare opportunity to re-evaluate the current urban development framework, and if needed, to break up the current urban sprawl cycle and re-orient the growth pathways toward sustainability. Among many technical pathways, the master planning process and plan revision process is the most practical opportunity to reduce unnecessary urban expansion and increase the urban efficiency. This point in the process also allows initiating and developing effective water infrastructure adaptation to hydrologic change, in addition to the traditional land use considerations.

Figure 2-6 shows a change in the master planning process for urban adaptation that complies with the principles of SUD. How the change for hydrologic change adaptation can take place in planning process is schematically illustrated. The revised process, called adaptive urban planning, contains two sets of adjustments to overcome deficiencies of the current practice exposed in urban performance evaluation. The first pathway revolves around the urban and infrastructure adaptation through adaptively re-aligning of the urban layouts and basic functions. These pre-planned and adaptive actions induce changes to urban forms for better sustainability attributes in developmental scenarios. Through adaptive planning, for example, transformation districts and corresponding infrastructure (e.g., smart transportation and water supply and management) may be able to induce urban transform into multi-center high-density configurations (Figure 2-6). The principles along with an example of urban transformation will be illustrated in subsequent Section 4.1 by analyzing the potential development scenarios for the Cincinnati metropolitan area.

Such scenario development in urban adaptation is essential to evaluate the cost and benefits in developing adaptation alternatives. The results provide a technical basis to inform decision makers on the limitation of physical adaptation approaches and the likelihood of successful adaptation of water and other urban infrastructure systems. A careful assessment of the future changes in hydroclimate and land use conditions allows better engineering evaluation and planning. This is important to develop a better technical basis for infrastructure planning and design. The results may help inform decision makers about the limitations of adaptation, leading to other options such as an infrastructure rebuild (Felgenhauer and Webster, 2013).

The second potential adaptive path is to change the developmental objectives in the evaluation/assessment phase through inclusion of sustainability of the future urban performance as measured against the adaptation objectives. This adjustment to the developmental objectives can be viewed as a way to change the growth factors and socio-physical constraints, i.e. the basic planning variables (Figure 2-6). The process and its attributes in urban development policy setting such as environmental justice, capital flows, centralized versus decentralized management, have been discussed extensively in literature (Small and Song 1994; Ewing 2008; Heikkila et al. 1989; U.S. EPA 2006, 2007b; Baynes 2009; Ostrom 2010).

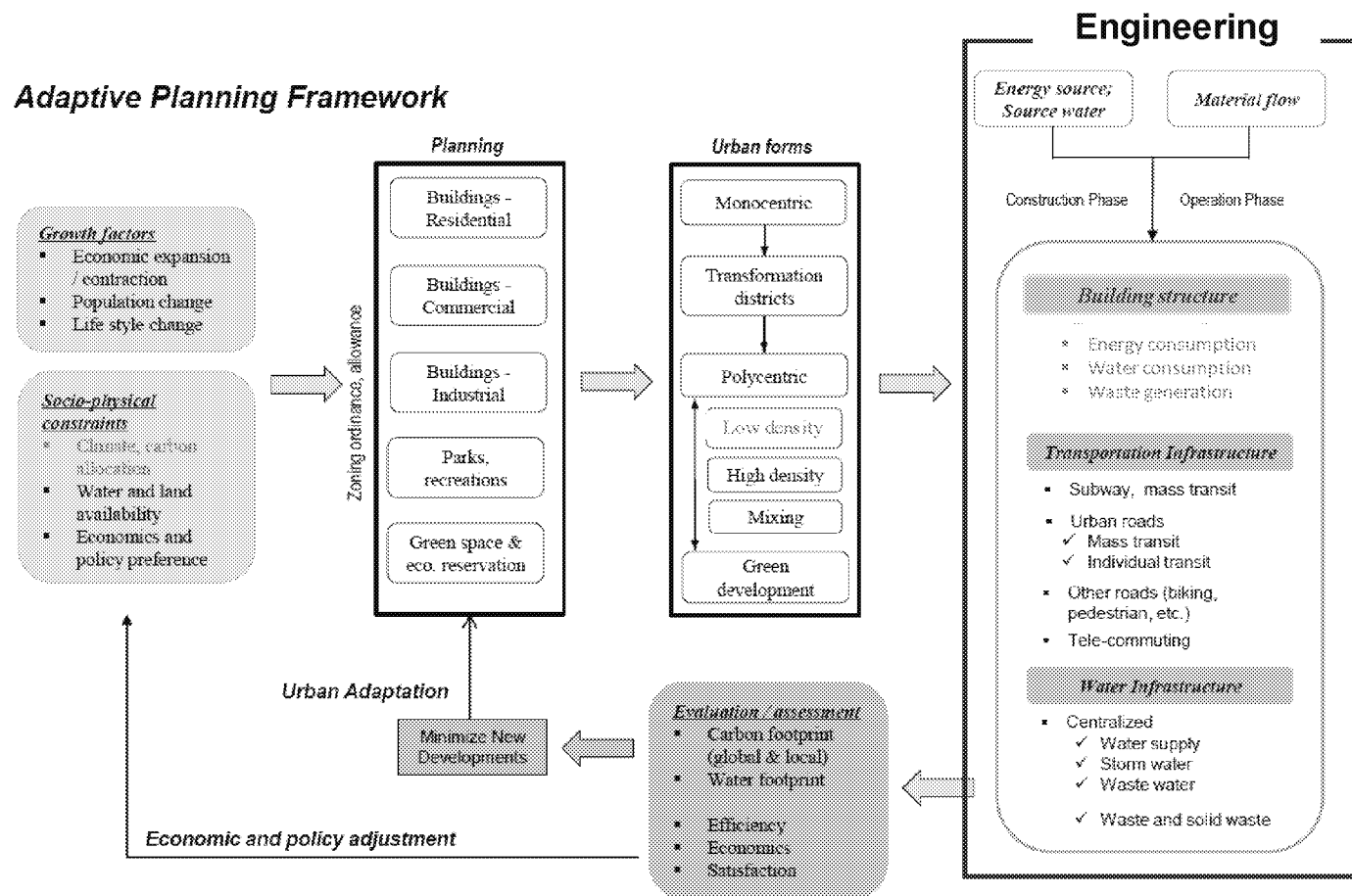


Figure 2-6 General process of adaptive urban planning and engineering. Compared to traditional master planning in Figure 2-4, adaptive planning promotes economic and policy adjustment on urban development goals and urban adaptation for high-density, polycentric form through transformation and proper transportation and water infrastructure adjustment. The element in gray text in Planning step is not applicable; those in the Engineering step are not discussed in this report.

It is worthwhile to note that the evaluation results depend on how the impacts of hydroclimatic and land use changes are projected and characterized at the scale of interest. The results also depend on the degree to which the projected impacts are compared to those originally assumed in the existing master planning. This important hydrological evaluation can encompass several key elements including:

- The degree of hydroclimatic change that affects the precipitation intensity-depth-frequency (IDF) relationship in the watershed of interest. Because of its impacts on infrastructure's hydrological design basis, the long-term hydrological effects deserve careful re-evaluation (Mailhot et al., 2007). This fundamentally important hydrological impact has been extensively discussed in literature (e.g., Wilby, 2007; Beck, 2005; Semadeni-Davies et al., 2008; Ashley et al., 2007; Pielke Sr. et al., 2007), and will be described in the subsequent adaptation reports.
- The degree of infrastructure capacity reserve incorporated into the current planning and engineering practices such as the use of safety factors in design basis. A quantitative evaluation of the capacity reserve (See Section 5.2) helps identify the vulnerability under future conditions. The results inform decision-makers on the need of economic and policy adjustment. This type of "bottom-up" assessment is facilitated by the Climate Resilience Evaluation and Awareness Tool (CREAT) available from EPA Office of Water⁸ which assesses direct and indirect hydrological impacts, as well as the atmospheric feedback of large-scale adaptation efforts. It is generally accepted that the precipitation and temperature changes in the future can directly affect hydraulic and water quality engineering. The impact can be exacerbated through a complex interaction among the changes in hydrology, land use and population growth in an urban catchment. On the other hand, atmospheric feedback of land use change can be significant. Effect on mass conservation and energy momentum in the planetary boundary layer is known to create precipitation variations in local and regional scales (Adegoke et al., 2007; Pielke Sr. et al., 2007), and in changes of soil erosion and soil moisture (O'Neal et al., 2005; Miller et al., 2007). For simplicity, this type of feedback-loop interaction is often neglected in adaptation analysis.
- The adaptation co-benefits derived from energy efficiency when developing and evaluating the adaptation options for urban planning as they may relate to atmospheric pollution and impacts of energy savings on precipitation patterns. In evaluating urban infrastructure performance, such co-benefits are often neglected in current planning and engineering practice causing a major unrealized benefit to remain unassessed. However, this concept deserves attention in adaptive urban planning as shown in Figure 2-6.

1.1.4. Selecting adaptation evaluation matrix

In adaptive urban planning, the urban performance evaluation and assessment step (See Figures 2-2 and 2-6) requires a selection of the appropriate evaluation matrix. The matrix should include criteria that directly and indirectly related to hydrologic adaptation impacts, dependence

⁸ <http://water.epa.gov/infrastructure/watersecurity/climate/creat.cfm>

Table 2-1 Adaptation attributes for common objectives

Attribute	Objective
<i>Adaptive urban planning</i>	
Urban form	More sustainable land use and resilient infrastructure
Urban sprawl index	Reducing exurban development
Population density	Compact development
Housing density	Achieving compact development
Transforming district	Transitioning to polycentric form
Zoning	Land use change for planned developments
<i>2. Urban transportation</i>	
Traffic delay	Increasing transportation efficiency
Trip generation	Promoting walkable community and mass transit
Fuel consumption	Reducing fuel use in urban activities
Emissions	Increasing mitigation co-benefit
<i>Urban water systems</i>	
Water availability	Adequate supply to meet demand
Water quality	Compliance to SDWA and CWA regulations
Energy use	Reducing energy cost in managing water systems
Energy and emission	Reducing life-cycle emission and improving overall energy efficiency for the mitigation co-benefit
Resilience	Ability to provide service function under natural and man-made emergency and disruptive events

between water and carbon footprints, time of adaptation in considering the capital flow and a trade-off analysis, as well as defining the limitations of the adaptation analysis. Some attributes in adaptation evaluation are listed in Table 2-1.

The adaptation co-benefits in energy and air emissions are very important. This is the basic attribute in urban infrastructure adaptation (Yang and Goodrich, 2014). Water infrastructure contains significant energy footprints – up to 4% of total energy for a community and the largest energy user in most communities, and may produce significant air emissions both during construction and thereafter operations. An example is described in subsequent Section

4.0. To evaluate the co-benefits and tradeoffs, one method relies on a conjugate water and energy/carbon footprints (PNNL, 2012). These two sustainability indices unlock the dependence between energy usage and water availability, and therefore can provide a useful criterion to find compromised solutions in the adaptation option analyses. For example, adaptation solutions for water availability in water-stressed regions often include water reclamation, reuse of treated wastewater for non-portable and even potable purposes, desalination, and water storage (Oron et al., 2007; Yang et al., 2007, 2010). These water availability adaptation options have high energy intensities and generate air emissions when producing the new “virgin water.” Similarly, compromised solutions between energy/carbon footprint and economic cost are relevant to water infrastructure planning (Chang et al., 2013). This is illustrated in the Manatee County, Florida case study described later in Section 4.2).

Obviously, an evaluation matrix is always objective-dependent. Some commonly investigated pairs include water and energy/carbon footprints, water availability and cost analysis, and water and ecological footprints (see Table 2-1). Therefore, selection and specification of a particular evaluation matrix need to be clearly described in urban performance evaluation and may be highly location-specific. Defining the evaluation matrix is the first step in the adaptation process (Figure 2-1) as it can affect the adaptation pathways and the outcome.

1.2. Three levels of water infrastructure adaptation

The physical adaptation to urban infrastructure can take place at three levels of spatial scales (Figure 2-2). Referring to Figure 2-6, adaptation may also occur at the different stages of planning-engineering-evaluation process, such as in the planning phase, or engineering of specific adaptation measures against specific hydroclimatic impacts (e.g., floods and chronic droughts). As the adaptation level changes from systems adaptation (e.g., storage, water conservation, and water loss prevention) to urban-scale and watershed-scale adaptation, the complexity increases with respect to the system analysis, adaptation planning and engineering design. For the remainder of this report, the technical approach for adaptation in these three levels are discussed and illustrated in selected case studies.

1.3. Smart Urban Designer (SUD) for systems analysis

Water infrastructure adaptation in watershed scale, the urban scale, and the water system scale has own advantages and challenges (Table 2-2). To quantify specific adaptation actions, one integrated modeling tool “Smart Urban Designer (SUD)” was developed. It consists of scenario-based modeling tools integrated as a platform for design of adaptation actions (Figure 2-7). The main SUD components are described below.

1.3.1 The Integrated Watershed Modeling (IWM) tool

The IWM tool is built upon EPA’s Better Assessment Science Integrating Point and Non-Point Sources (BASINS) program (U.S. EPA, 2015b) with an integration of a land use model under the future climate conditions (Figure 2-8a,b).

One land use model is EPA’s Integrated Climate and Land Use Scenarios (iCLUS) that provides explicit projection of population, housing and land use under the future climate as specified in Intergovernmental Panel on Climate Change’s (IPCC) Special Report on Emissions Scenarios (SRES). At present, the iCLUS projections are at the county-scale spatial resolution through 2100. This large development scenario tool is based on a pair of models: a demographic model for population projection, and a spatial allocation model to distribute the projected

Table 2-2 General advantage and challenges of three-level adaptation actions

Adaptation level	Advantage	Challenges
<i>Integrated Watershed Management (e.g., iCLUS, CA-Markov, HSPF)</i>	<ul style="list-style-type: none"> • Ability to protect source water quality and water availability • High feasibility via CWA and SDWA regulatory framework 	<ul style="list-style-type: none"> • Data requirements for watershed process understanding • Land use planning and action often difficult to implement • Close interactions with urban-scale adaptation
<i>Adaptive urban planning tools (e.g., AUP&ET)</i>	<ul style="list-style-type: none"> • Large emission mitigation potential • Greater changes amenable to urban development goals • Increasing urban resilience • Potential to accommodate multiple objectives (e.g., economic, etc.) 	<ul style="list-style-type: none"> • Complex requiring integrated planning • Transformation required in urban development • Cost and time for capital investment payoff • Public acceptance
<i>Infrastructure systems adaptation (e.g., WTP-cam, EPANET)</i>	<ul style="list-style-type: none"> • Taken as a part of capital improvement • Well-defined actions for decision making • Increase infrastructure capacity for specific needs • Independent for quick actions at relatively small capital cost 	<ul style="list-style-type: none"> • Difficult to resolve urban-wide performance issues • Limited adaptation potentials after years of improvement • Difficult to resolve urban-wide performance issues

population into housing units at a 1-ha pixel resolution. Population allocation from a county scale to census tract resolution is technically challenging, because of uncertain model assumptions for present, near-term and distant economic growth. For example, the spatially explicit regional growth model (SERGoM) is used in population allocation to generate the projections at a spatiotemporal resolution of 10 years for one (1) hectare. The uncertainty associated with high-resolution population projection may be excessive for infrastructure planning. However, this potential risk has not been assessed fully. More details on the methodology can be found in U.S. EPA (2009b, 2010b). Projections covering the contiguous U.S. can be accessed at <https://www.epa.gov/iclus/iclus-downloads#tab-1>.

Urban land use changes are dynamic. They occur at a spatial resolution much finer than the county level resolution used in iCLUS. For applications in urban areas, the cellular-automaton Markov (CA-Markov) land use model can be used instead (Figure 2-8a,b). The CA-Markov method for land use projection combines the stochastic probability of future evolution that builds on the current situation (namely, the statistical state), and the geographic association with current and projected land use. The latter is captured by cellular automaton that depicts the probability of spatial association in state changes. In combination, the CA-Markov modeling is

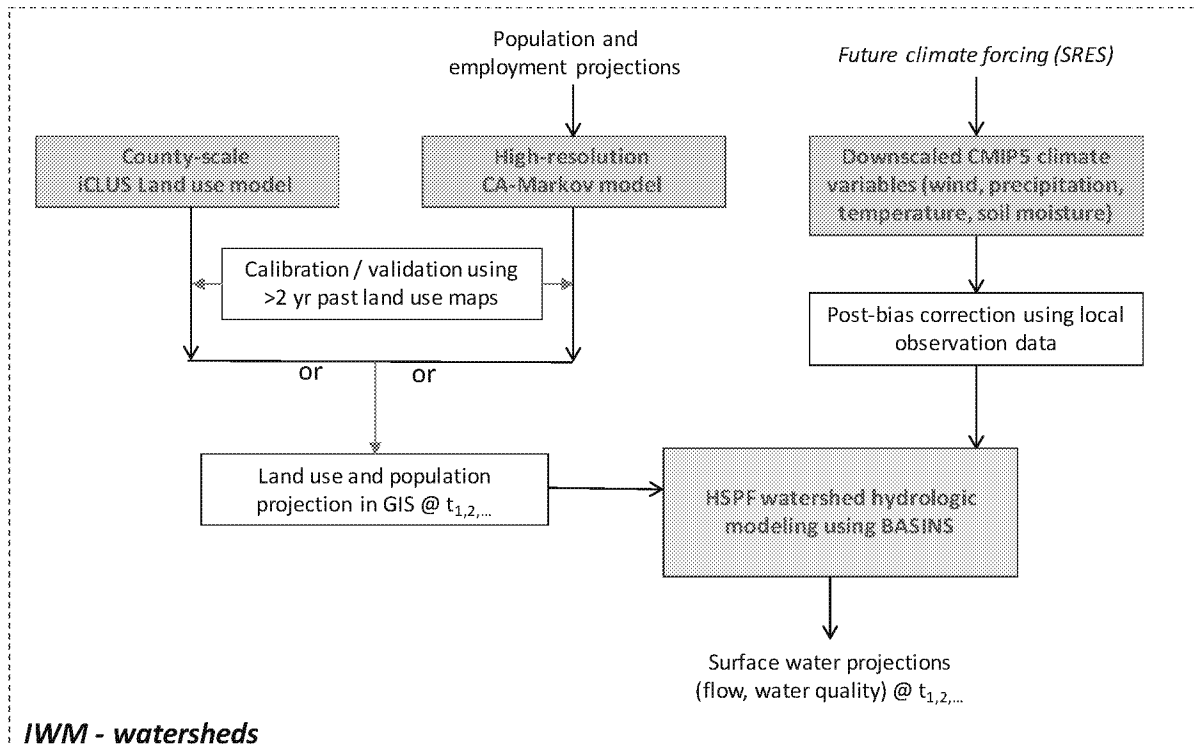


Figure 2-8a Program flow diagram of the Integrated Water Management (IWM) program for watershed simulations. It consists of the climate-influenced hydrological model HSPF and land use models either by iCLUS or high-resolution CA-Markov modeling. The program resides in the EPA's BASINS framework. Colors indicate different blocks in the integrated simulation process.

capable of predicting probable land changes in spatial aggregation using the geographical information system (GIS) modeling capabilities (See Tong et al., 2012; Sun et al., 2013). However, population and land use projections in planning scenarios are the most difficult and least quantifiable for urban areas, especially as they may relate to impacts like sea level rise which will alter the current land form. The problem is confounded for projections requiring high spatial resolutions, such as in the census tract levels. Disruptive urban development policy and events can also make model projections less accurate and not useful. Policy-driven changes can lead to violate spatial continuum assumptions embedded in the semi-empirical CA-Markov method. This potential problem cannot be under-estimated.

Figure 2-8a shows a general modeling framework for suburban and rural watersheds. For urban catchments with unique land use and hydrological changes, the modeling framework is shown in Figure 2-8b. In Figure 2-8a, the hydrological parameters (e.g., stream flow and water quality) are modeled for future time frames of interest (e.g., t_1 , t_2 , etc.) using BASINS program. BASINS for assessment of water quality and flow variations in watershed runoff and surface streams is documented in U.S. EPA (2015b) and in application studies (Tong et al., 2012; Sun et al., 2014). The newly released BASINS4.1 is a comprehensive platform, providing a choice of multiple hydrological simulation engines. Available models include HSPF, the Soil and Water Assessment Tool (SWAT), the EPA Storm Water Management Model (SWMM), Generalized

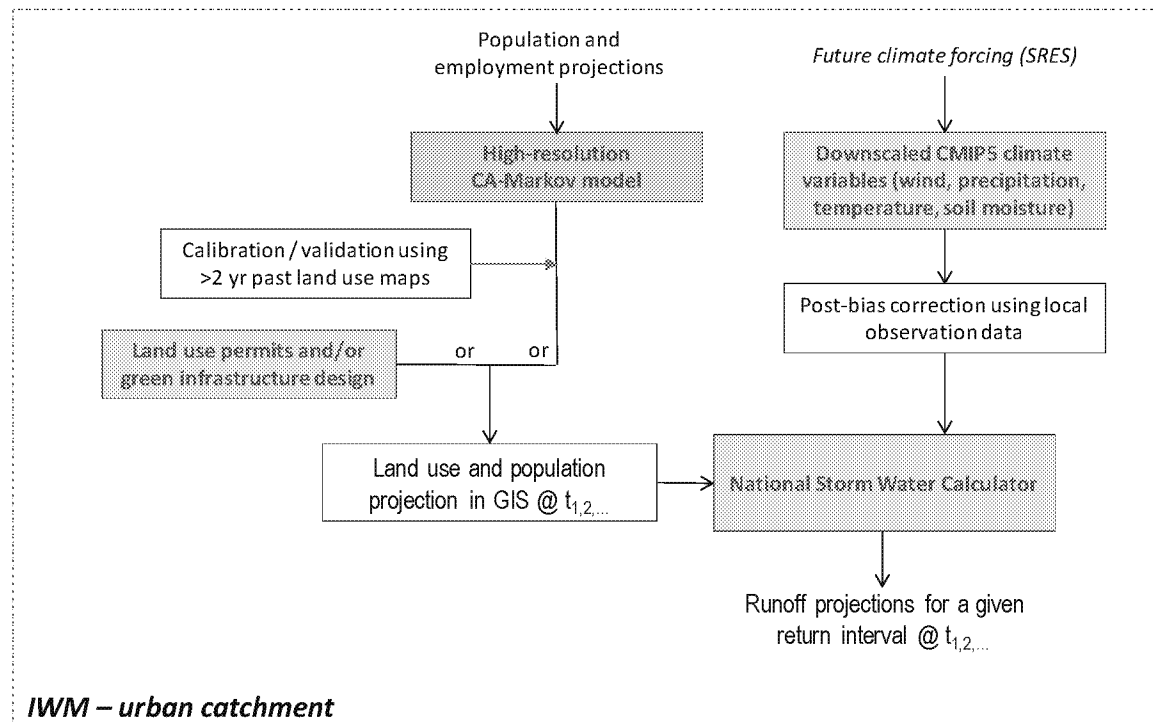


Figure 2-8b Program flow diagram of the IWM modeling for urban catchment using EPA's National Stormwater Calculator (U.S. EPA, 2014). Modeling functions in light blue box exist in the National Stormwater Calculator. Colors indicate different blocks in the integrated simulation process.

Watershed Loading Function model extension (GWLF-E) MapShed, and the simple watershed model Pollutant Loading Estimator (PLOAD), as well as two instream water quality models AQUATOX and the Water Quality Analysis Program (WASP).

There are some generalities with model inputs for the IWM tool. The parameters for hydrological and land use modeling are of greatest interest. First, land use projections can be made for a desired future period, using past land use in digital format for model calibration and validation. Additional land use constraints including nature preservations, water bodies, historical preservations, are specified as the GIS land use model constraints. Examples can be found in Sun et al. (2014). Separate anticipated population changes can be directly downloaded from the iCLUS model outputs. When higher spatial resolution than the county-scale is needed, population change is often available from master plans created by local governments. The model outputs of land use types and population distributions are used as inputs for subsequent BASINS hydrological modeling (Figure 2-8a).

Future climate parameters (i.e., precipitation, temperature, dew point, wind) are another set of input parameters for hydrological modeling in BASINS. The IWM module obtains these parameters from climate models. The model projections are further revised for post-bias corrections using the techniques from Liang and Julius (2017) and Yang et al (2017). The projected precipitation for given return intervals is used as one HSPF parameter in BASINS

simulations Urban catchment is smaller in size than a rural watershed, but may contains more dynamics changes in land use and infrastructure. EPA's National Storm Water Calculator (U.S. EPA, 2014) is the main simulation engine (Figure 2-8b); it is a simplified model based on EPA SWMM on a GIS platform. In a IWM simulation, the Storm Water Calculator accepts future land use either by green infrastructure design (e.g., detention and retention ponds, swales and other catchment areas) or directly from CA-Markov modeling of land use at census tract resolutions. The land use modeling techniques are described in Tong et al. (2012), Sun et al. (2014), and Fu et al. (2018). More details will be described in a separate adaptation report.

Precipitation is the other modeling input for IWM-urban catchment. For this purpose, downscaled climate modeling outputs are not suitable for infrastructure design or planning because of their uncertainty. One principle reason is that microclimate in urban centers can be significantly different than the regional climate of natural land cover. One example is the UHI effect often discussed in literature. The unique nature of the urban microclimate is illustrated in a case study described here in Section 4.1.

For both watershed and urban catchment areas, the IWM modeling projects key hydrological parameters at a future time for subsequent analysis in the Adaptive Urban Planning and Engineering Tool (AUP&ET) discussed in the next. These projections include:

- Unit hydrographs for storms of a given return interval. Both peak flow and time of concentration are specified. Often these parameters are given in form of storm return intervals.
- Stream base flow. The model outputs can be analyzed for changes in stream base flow under the future land use and climate conditions. An application example can be found in Johnson et al. (2015) and U.S. EPA (2013).
- Surface water quality parameters such as total nitrogen (TN), total phosphorus (TP), turbidity, and organic pollutants (e.g., Tong et al., 2012).

1.3.2 Adaptive Urban Planning and Engineering Tool (AUP&ET)

The schematic diagram in Figure 2-9 shows major model components and data flows for the scenario-based Adaptive Urban Planning and Engineering Tool (AUP&ET). The tool considers urban development scenarios for major infrastructure systems, including transportation, water supply, wastewater and storm water systems. These infrastructure systems are the controlling factors for the basic urban form, employment and economic activity and population distributions.

Urban infrastructure has a large physical footprint; one that is difficult to change significantly after it has been built, and is highly capital-intensive. Because of the nature of large urban infrastructure systems, it precludes the ability to perform real-world experiments for optimal planning and design solutions. Thus AUP&ET takes the technical approach of scenario-based computer simulations. The tool relies on two major inputs. First, the development objectives are defined, for which a set of development options can be created for a given physical and environmental setting. Second, for water infrastructure adaptation, water availability and hydrological parameters of surface streams (e.g., peak and base flows, water quality) are fundamental variables to be considered in developing the urban scenarios (Figure 2-9). For a given urban scenario, one can quantitatively examine the future land use outputs and

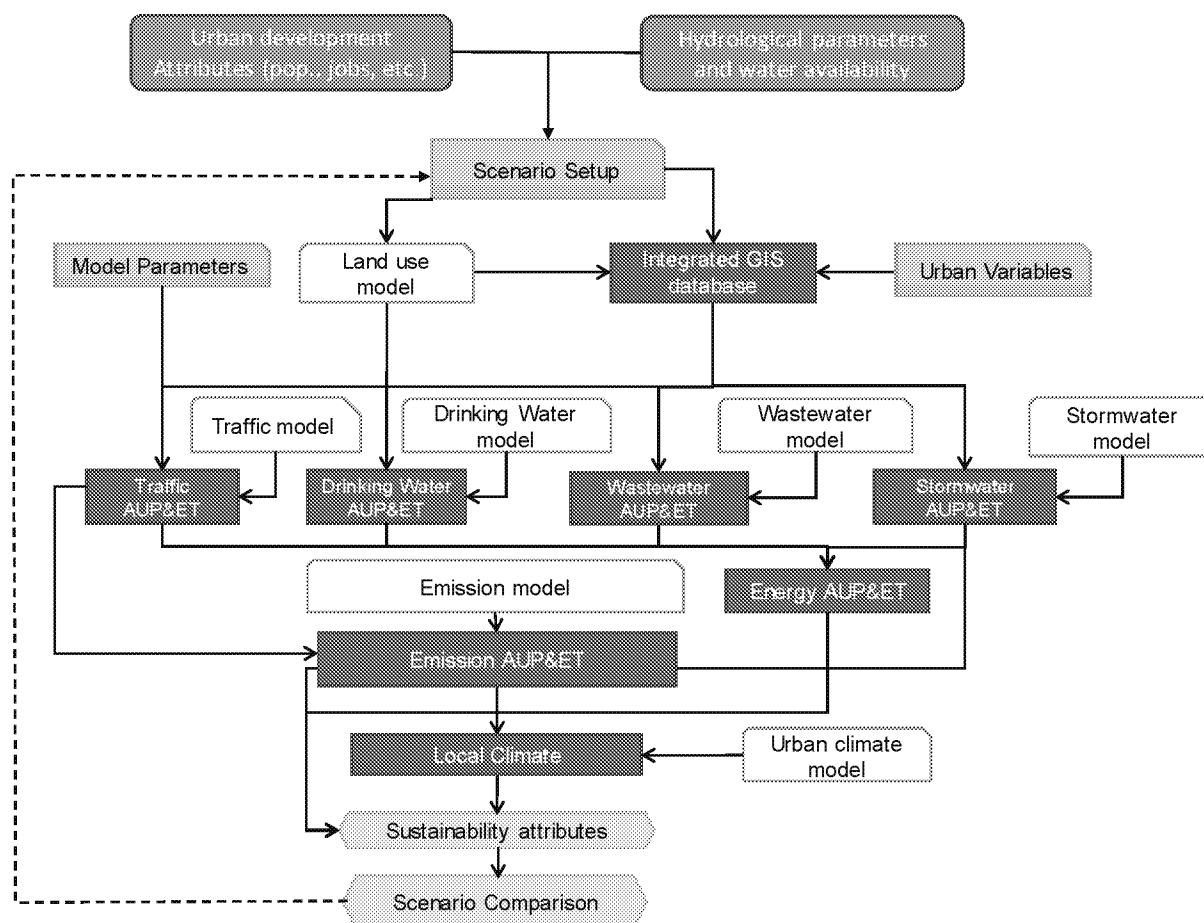


Figure 2-9. Process flow block diagram of the scenario-based AUP&ET for urban planning and engineering. Each of the four program modules – traffic, drinking water, wastewater and storm water, is discussed separately in Sections 3.1 and 5.0. Colors indicate different blocks in the integrated simulation process.

urban parameters including urban form, community functions such as literacy, convenience, health care, and the need for transportation infrastructure. These model variables are then incorporated into the land use modeling and imported into GIS for spatial analysis (Figure 2-9).

In an EPA internal report, Flander et al. (2014) analyzed the roles and inter-dependency of transportation and water infrastructure in determining physical form and efficiency of urban systems. Here the use of AUP&ET is intended to quantify environmental attributes on urban-scale considering the interactions in development scenarios. An application example will be described in Section 4.1. Potential analysis outcomes may include:

- Population distribution for specified development goals;
- Daily and peak traffic flow at road link levels;
- Urban-wide emissions, traffic hot-spot identification, and regional conformity analysis;
- Drinking water supply needs and their spatial variations;

- Storm water and wastewater generation rates and spatial variations;
- Energy consumption and cost comparisons in the transportation and water sector.

1.3.3 SmartWater for water supply

Within AUP&ET, one engineering tool is the SmartWater module for water treatment and distribution. Different from the other planning-centric AUP&ET modules, the SmartWater tool is developed for system engineering and for detailed unit process analysis. It consists of an updated Water Treatment Plant (WTP) model for water treatment process engineering, and a sensor-based data-driven EPANET for water distribution (Figure 2-10).

For WTP modeling and design, specifically, the SmartWater WTP3.0 consists of two separate modules that are linked by an overall graphic user interface (GUI) (Figure 2-10). WTP2.0/2.2, originally developed in 1994 and updated in 2004 (U.S. EPA, 1994; 2004), was intended for national evaluation of water treatment plant performance to support the promulgation of the Safe Drinking Water Act (SDWA) DBP Stage II regulations. In the SUD, the water treatment plant – climate adaptation model (WTP-cam) is developed for plant-specific adaptation analysis. Its application in a case study at the Greater Cincinnati Water Works (GCWW) Richard Miller plant is described later in Section 6.3.

The SmartWater module in SUD treats the two processes in water treatment and distribution as a single system (Figure 2-11). This approach aligns well with U.S. water utilities having water treatment and distribution under the same management, or those distributors with

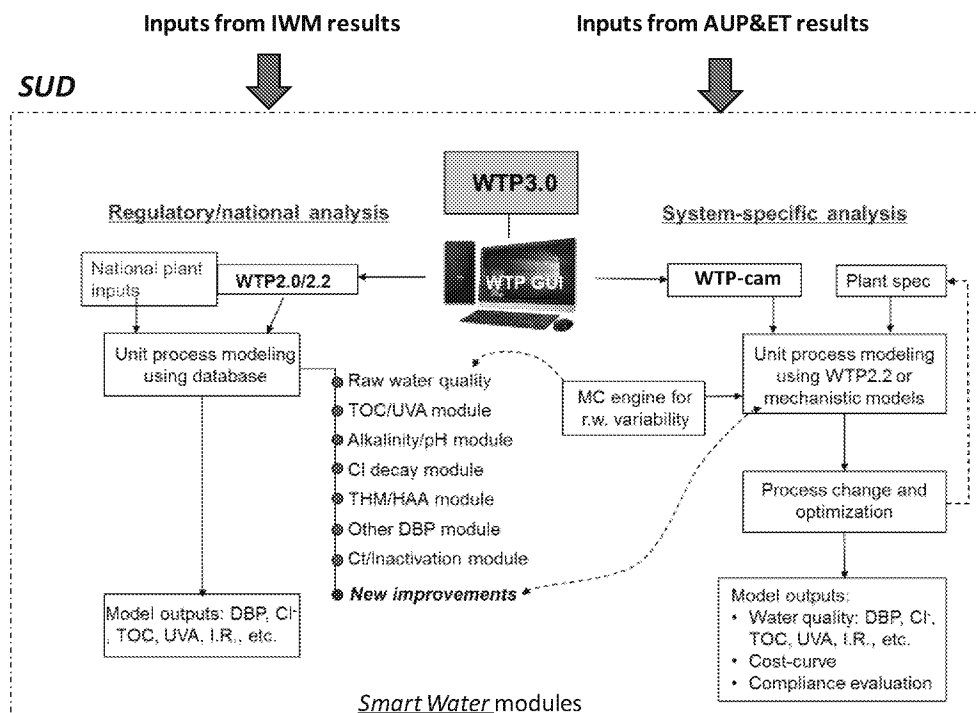


Figure 2-10. Schematic diagram showing basic modeling framework for WTP3.0 as a major SUD element. It consists of the system-specific analysis using WTP-cam (Water treatment plant – Climate Adaptation Model) and the regional analysis in WTP2.0/2.2.

real-time data exchange with water producers. As shown in Figure 2-11, this integrated approach in SmartWater allows one to manage and optimize the engineered treatment and distribution infrastructure in a timely manner to address changes in source water quality and supply to meet changing water demands. This communication exchange has become feasible because of recent technical advances in sensor-based monitoring, real-time data communication, and algorithms for systems optimization. More technical details will be presented in Section 6.0.

1.3.4. Source-to-tap water supply in system approach

The SUD methodology takes a systems approach toward efficient and resilience infrastructure. The common line process diagrams in infrastructure analysis usually describe the water systems and unit processes with simplistic consideration of the spatial interactions with other urban components and surrounding watersheds. It is convenient. However, the traditional approach may discount interactions between the highly dense socioeconomic activities and required water infrastructure in the urban footprint.

Taking water supply as an example, the “source to tap” systems approach (Figure 2-11) is the basis of SUD. Currently, the SUD tool only has surface water as the source water for drinking water production; groundwater and reclaimed water will be considered for addition in a later time. The rest of this Part II report discusses the four basic steps in the systems approach, the tools, methods, and application examples:

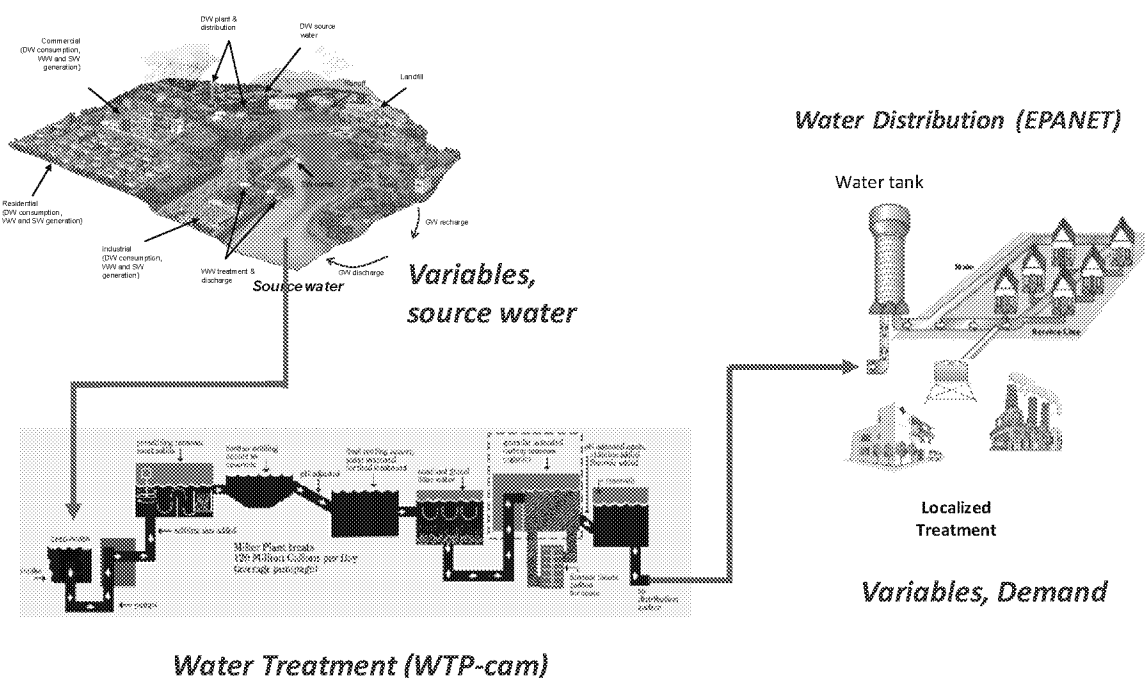


Figure 2-11. Schematic diagram of water supply in a municipality and major system variables. Water treatment and distribution are two engineered systems to meet variations in source water and demand. The consideration of disinfection by-products (DBPs) is cited for specific management and technical considerations.

- IWM modeling and analysis for water quantity and quality variations in watersheds;
- AUP&ET modeling and analysis for urban development scenarios. The objective is to define the water demand and its distribution at present and in the future. Energy and economic efficiency of the urban scenarios for decision-making is also analyzed;
- SmartWater modeling and analysis to optimize water supply efficiency. First, the system capacity and capacity reserve are defined for the water supply objectives. Second, for a changing source water or water demand, the potential system alteration / expansion / addition is evaluated;
- Upon evaluation of the water infrastructure performance, a new round of system evaluations may take place to improve infrastructure's resilience and sustainability. This iterative re-evaluation and adaptation process, as commonly practiced in periodic master planning, is shown in Figure 2-2.

2. Adaptive Urban Planning in Urban Scales

In the recent fifth IPCC climate assessment report (IPCC, 2014), the 3rd Work Group investigated mitigation and adaptation in urban environment. They concluded that urban form transformation has by far, the single largest potential to achieve meaningful carbon emission reductions while improving urban efficiency. Many publications (e.g., U.S. EPA, 2006, 2009b, and references therein) identified several common planning options including infill, interior redevelopment, mixed land use, and employment centers. They can introduce urban transformation to more desired configurations.

These smart growth practices and transformation measures have been applied in a number of U.S. cities (U.S. EPA, 2007b, 2013b). They are designed to slow urban sprawl and achieve adaptation-mitigation co-benefits, but often require changes in the metropolitan transportation and water services. Other urban forms alternative to the traditional monocentric configuration may offer a smaller urban physical footprint with a higher population and housing density. However, this change is accompanied with more complicated transportation and water infrastructure, and thus greater difficulties with planning to incorporate existing infrastructure assets. To overcome these planning and engineering challenges, new approaches are essential to achieve smart growth through urban form transformation. Attention in this report is given to the methods and tools in water infrastructure planning.

Because of the high population density and integrated urban infrastructure, the urban centers also are vulnerable to natural and man-made disruptions including significant hydroclimate changes in the future. Three major climate effects on urban functions are shown in Table 2-3.

2.1 Physical infrastructure and urban forms in current practice

Monocentric urban formation is common in the U.S., where urban population is distributed around a single central business district (CBD) of concentrated economic activities. In this urban form, automobile-based mobility is a precondition to facilitate the urban-suburban-exurban arrangement. Typical geometry of the urban form is schematically shown as the radial sprawl in Figure 2-5. Examples include numerous, mostly middle-to-large sized, urban centers

such as Las Vegas, Cincinnati, Houston and most urban centers of the Northeast and the Midwest.

As a city grows into a very large metropolitan center, the population becomes more dispersed and the monocentric form evolves into a polycentric arrangement of connected satellite cities. This urban form is now characteristic of very large metropolitan areas, such as the New York City, Washington DC, San Francisco, and Los Angeles metropolitan regions. The urban form transformation, and its implications to the CBD formation, population distribution, and transportation service, have been investigated in literature (e.g., Gordon et al., 1986; Small and Song, 1994; Heikkila et al., 1989; Larson et al., 2012, Garcia-Lopez, 2012, and Zhou et al., 2013). The nature and process of the transformation has significant implications for the feasibility of development and implementation of the adaptation options.

Table 2-3 Selected urban functions impacted by hydroclimatic conditions

Hydroclimate Factors	Urban Functions
Long-term drought and large swings in precipitation variation	<ul style="list-style-type: none"> • Water supply, landscape, local agriculture • Wastewater and storm water NPDES discharge to streams • Urban heat island effects and heat spells on population health • Example: U.S. southwest, southeast, Rocky Mountains
Heavy downpour, disruptive climate/meteorological events (e.g., tornados damaging winds, etc.)	<ul style="list-style-type: none"> • Transportation management and roads operations • Urban flooding and water service systems operation • Water pollution management from non-point source • Sewer and storm water pipe I/O flows, and CSO occurrence
Storm surge and sea level rise	<ul style="list-style-type: none"> • Disruption to water supplies; changes to hydraulic gradients affecting storm water drainage and wastewater collection • Disruption to transportation systems • Inundations of roads and pipe systems

Polycentric urban form is marked by a multi-center urban configuration, shown as leapfrog sprawl in Figure 2-5. The transition toward polycentric form may take different pathways. On the one hand, continuous urban expansion toward more dispersed polycentric form is a persistent trend leading to unplanned uncontrolled urban sprawl. In contrary, the transition can permit high-density development, less personal travel, better use of mass transit and green space, but requires a different configuration for fixed urban infrastructure assets. As population and urban activities are redistributed, water infrastructure is accordingly transitioned in space for a new set of operation requirements because of the need to meet new water service and management needs. The three typical urban expansion configurations in Figure 2-5 are all

linked to the transportation routes and other infrastructure services, forming the mode of radial, ribbon and leapfrog sprawls (Sudhira et al., 2005). The trade-off in urban efficiency and infrastructure sustainability is under debate on subjects ranging from resource allocation and urban ecology, to engineering and operations (Small and Song, 1994; Ewing, 2008; Heikkila et al., 1989; U.S. EPA, 2006; Bayes, 2009; Ostrom, 2010).

Nevertheless, the developmental effects have been widely recognized on water infrastructure. For example, the centralized operation and management in water services have allowed for better control of water pollution and management toward meeting water regulations. It benefits from the economy-of-scale. However, negative environmental consequences of centralized water infrastructure framework are found in energy use and thus potential higher indirect emissions, barriers to resource recovery, water age in distribution systems and vulnerability to the impact of natural and man-made incidences. The alternative form of urban development promotes more decentralized water systems. As urban transforms into polycentric form, the centralized water system may become decentralized. This can result in better service to localized, high-density population centers. Yet the infrastructure transformation can be a difficult technical and engineering challenge, and may require a coordinated urban planning among transportation and water services.

2.1.1 Land use encouraging urban sprawl

The three types of sprawl modes (Figure 2-5) are found in the historical developments of U.S. cities. In Figure 2-12, the old urban centers of Atlanta and Phoenix expanded radially toward exurban at a rapid rate in merely 22 years from 1970 to 1992. The older urban centers, such as DeKalb County in Atlanta, further evolved into spatially continuous high-density development. At the same time, smaller development centers in exurban perimeters in 1970 were later expanded in size, linking to the major urban centers through fill-in development. This leapfrog pattern is very common; for example, in development in the Norcross, Marietta, and Douglas communities of the Atlanta metropolitan area, and in the communities of Sun City, Mesa, and Chandler in the greater Phoenix area (Figure 2-12). Furthermore, the ribbon sprawl (Figure 2-5) can be observed along transportation roads, forming linear spreading of urbanized lands. This urban development is obvious along the roads of regular shapes around the Luke Air Force Base (AFB) west of Phoenix (See 1992 map in Figure 2-12).

Urban population and land use are difficult to project. Future population and land use are a function of urban economic conditions, political motives, development pressures and economic policy initiatives; the latter can introduce sudden changes in spatial continuity of land use development patterns, and thus poses a modeling challenge in mathematic formulations. As an approximation, the CA-Markov simulation in GIS can be used with model boundary conditions representing urban land policy restrictions. Wei et al (2012, 2018), Tong et al (2012) and Sun et al. (2013) successfully projected future land use changes in the urban distribute, suburban watersheds of the Cincinnati and Las Vegas suburbs. Their modeling methodologies incorporated population and land use variables as a GIS model filter in the CA-Markov simulations. The iCLUS tool and projections (U.S. EPA, 2010b) is the alternative tool to project housing density and land use categories. See associated discussions in Section 1.3.1.

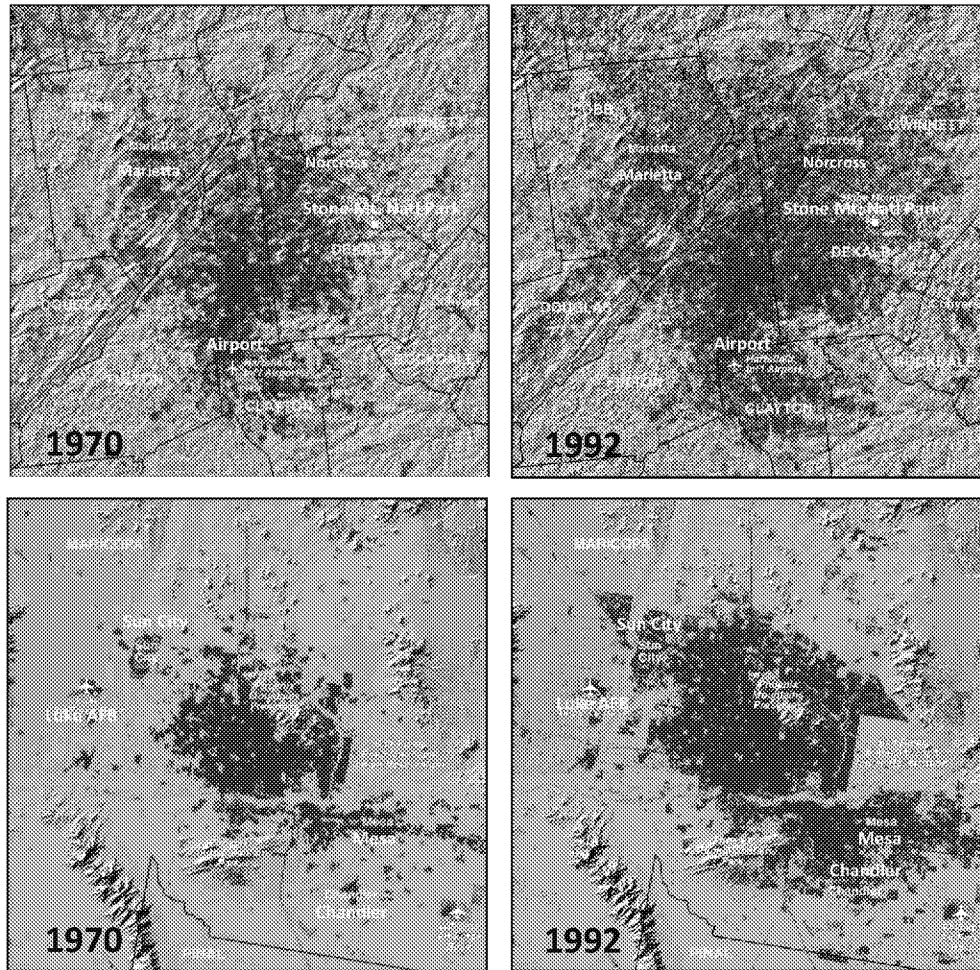


Figure 2-12 Examples of urban expansion and urban form transformation for Atlanta (upper) and Phoenix (lower) metropolitan regions between 1970 and 1992. Red color indicates developed urban land use. Images obtained and modified from Auch et al. (2004).

2.1.2 *Transportation and energy performance*

The concept of urbanization along transportation routes is shared by most U.S. cities. Such urban expansion, facilitated by current urban planning practices, has a set of characteristic physical layouts for water and transportation infrastructure, which in turn defines urban functions and affects infrastructure efficiency and adaptability.

Figure 2-13 shows the evolutionary trajectory of urban transportation efficiency as the U.S. cities grow in size from medium to very large metropolitan areas. Plotted statistical data were obtained from Department of Transportation (DOT) annual urban mobility reports prepared by the University of Texas (Schrank and Lomax, 2009). In these plots, the efficiency variables (annual delay, excess fuel usage, travel index, and annual cost) in 2007 are all based on a comparison between peak hour traffic and free flow conditions in principal freeway and arterials. Travel index is a ratio between time used in peak hour versus free flow at 60 and 35 miles per hour (mph) on the freeway and arterials, respectively. The excess fuel usage is defined as fuel

wasted at vehicles moving at a slower speed than at free flow conditions. These measures quantify the consequences of urban traffic, indicative of the urban transportation efficiency.

The urban transportation efficiency is correlated to urban population size. The correlation is the strongest ($R^2=0.84$) with respect to excess fuel use. The correlation slope indicates the change of transportation performance (e.g., delay or excess fuel use) as population grows. The bended excess fuel and cost curves indicate that as cities grow into very large metropolitan centers, the slope becomes smaller and nearly a constant. For cities of population <3 million, they tend to plot to the left side of the regression line indicating greater excess fuel consumption (Figure 2-13). The efficiency appears to be attributable to the effect of mass transport and high-density development in these cities (Schrank and Lomax, 2009).

The similarities and differences show underlying principles that govern the efficiency of urban transportation systems. In all cases, the limitation in infrastructure adaptation under the current decades-long urban planning practice is important. More meaningful improvement may come from the change in urban form from the traditional monocentric to polycentric urban

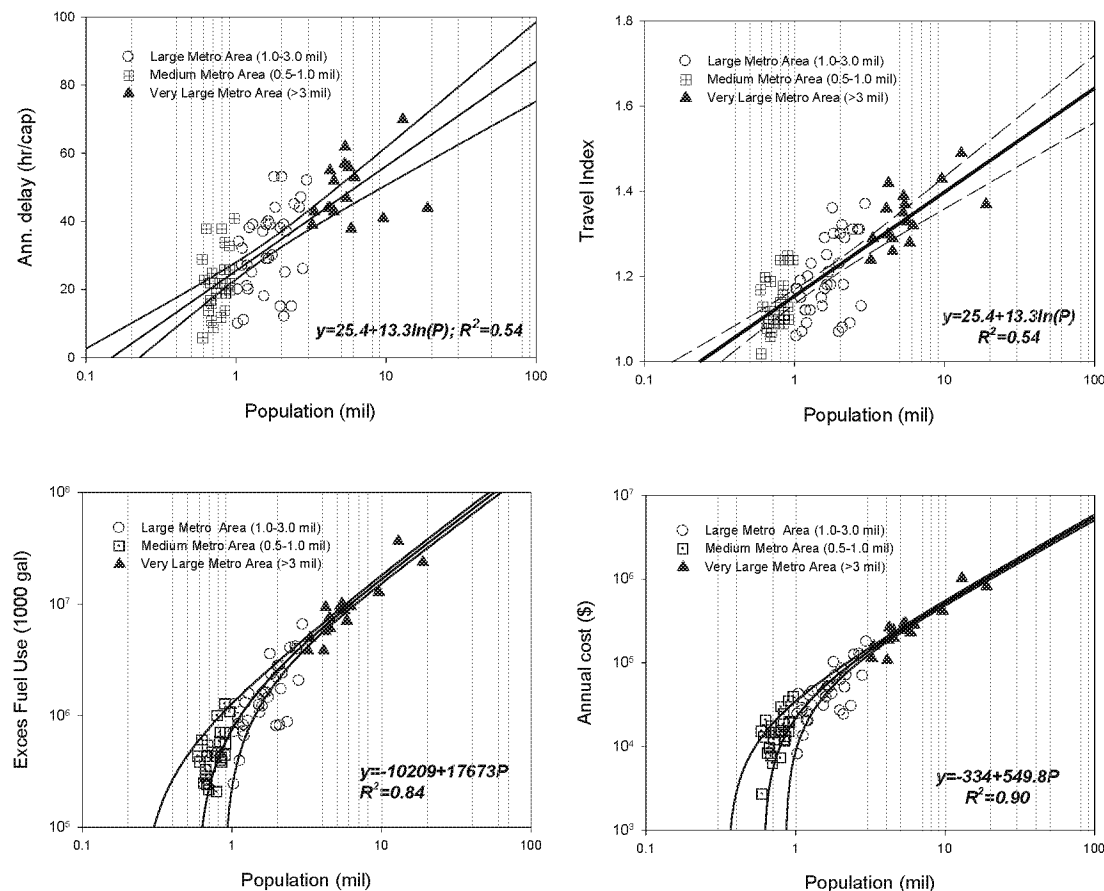


Figure 2-13. Transportation efficiency (annual delay, travel index, excess fuel use, and annual cost) in year 2007 as a function of urban population in the U.S. urban centers. Data from the 2009 urban mobility report (Schrank and Lomax, 2009). The blue dashed lines are 95% upper and lower bounds of the regression of all data.

arrangements. Such change is conceptually illustrated in Figure 2-5. How to facilitate the urban form transformation from monocentric to polycentric form for improved urban efficiency is a challenge to urban planners and infrastructure engineers. An example of this transition has been examined in a detailed mechanistic study of the transportation system in Cincinnati metropolitan area. The results are described in the subsequent sections to illustrate the likely benefits from urban transformation using computer simulation of urban planning scenarios.

2.1.3 Water planning and engineering

The water infrastructure planning and design follows the guidelines for urban development master planning, and further details the needed assets and management required to provide services to the existing and new urban developments (See Figure 2-4 or 2-6). In general, the water infrastructure is often scoped during or after transportation planning according to master plans or development policies.

In expansion, an urban form evolves and, sometimes, develops into polycentric configurations. Transportation structure reinforces the changes. Thus, the infrastructure-facilitated change alters the spatial distribution of population and urban activity, and in return generates new water service needs. Often passively, the water service is compelled to adapt and expand to meet the new water service demands (Figure 2-4). It is not uncommon that the legacy of the centralized water system configuration remains intact even after cities are transformed into a polycentric formation. Practical examples are numerous, such as the vast centralized water service infrastructure in Detroit, Cleveland, Los Angeles and New York City.

Existing water systems are mostly monocentric in the U.S.: centralized water treatment and water distribution, centralized wastewater collection and discharge treatment and, to a lesser extent, centralized storm water systems (mainly gravity-driven) with discharges to available water ways. Specific engineering of the water supply and water sanitation infrastructure is described later in Section 5.0. Additionally, current water infrastructure planning and design are commonly focused on component optimization, system improvement and capacity expansion. This tendency conforms to several notable attributes as follows:

- Water infrastructure, most of which is buried, is planned and designed to meet water and wastewater demands as defined by urban master plans. Once designed and built, the water infrastructure and their functions create a “locked-in” condition whereby the infrastructure framework can be difficult to modify in the future.
- For the most part, the treatment plants characteristic of centralized water and wastewater systems are located away from urban centers. This was done to protect water supplies to the degree possible from contamination, and to discharge waste downstream of the population to limit the potential for waterborne disease. In addition, few people desire to be located in the vicinity of these plants. Compounding the issue, many older central cities have lost population and industry to the extent to which having excess capacity to “sell.” This current practice in development cycle results in natural tendency to expand distribution and collection pipe networks into the new areas of development because of relatively small capital cost and leverage over the utilization efficiency of the centralized system. However, this sprawling expansion occurs at a price of potential increase in energy usage and decrease in environmental qualities. There is a limit to this expansion

before the basic system configuration and operational parameters require changes, often at a substantial economic cost.

- Water infrastructure has as its primary service function to ensure compliance with applicable SDWA and Clean Water Act (CWA) regulations. “Secondary” requirements include providing adequate capacity and reliability to meet the urban service needs, providing fire service, and controlling rates through managing capital and operational costs. The system efficiency, energy consumption and emissions are often lesser priorities in master planning.
- Although subject to the master development plans, urban water infrastructure is often engineered independently from transportation infrastructure. The two may become decoupled and uncoordinated. As a result, water infrastructure may not be sufficient to meet the service needs when transportation infrastructure and associated land use induce further spatial shifts in population and business activities (Flanders et al., 2014). This nature in planning may not only create conflicts with construction and service timing for the two types of urban infrastructure, but also add greater complexity when changes and adaption become necessary to support new urban functionalities in the future.

2.2 Transformation toward smart growth

Smart growth aims to achieve low-carbon development through adaptive planning. Urban transformation is one approach to change existing urban form to a configuration of high urban density, walkable and livable environments (U.S. EPA, 2013b). This smart growth concept is now being incorporated by many municipalities. In the national trends, smart growth often entails techniques such as infill, green planning, and high-density residential developments, which has been increasingly applied throughout the US. (U.S. EPA, 2013b, 2009). The infill development and mixed transportation mode are demonstrated to improve system efficiencies and reduce transportation emissions. A series of EPA reports have been published on smart growth applied to residential development and its pertinent transportation and water infrastructure (e.g., U.S. EPA, 2006, 2009, 2011, 2013b, and 2012a).

Transformation districts as a smart growth measure (Figure 2-6) can induce a transition from a monocentric to a polycentric urban form that has higher efficiency. These districts are planned with some degrees of flexibility to evolve into polycentric, high-density, walkable communities with ready access to mass transit, and thus have the least environmental impacts. This planning process rests on the ability to plan infrastructure to accommodate urban growth and population increase with the minimum environmental impacts and the economy-of-scales. For this purpose, the transformation districts are the necessary links for the natural evolution toward very large polycentric urban centers. For example, multi-mode transportation systems and multiple water supply or wastewater management districts are common examples for very large urban centers. These urban features are characteristic of smart urban growth principles. These districts can be initiated by adaptive urban planning as a part of long-term master planning. Techniques for such adaptive planning are described in subsequent sections with a planning example in Cincinnati.

The transition from monocentric to polycentric forms, when realized in practice, has significant implications for water infrastructure planning, engineering and operation. Currently the infill and green infrastructure are designed around water availability and the cost for

providing reliable water services (U.S. EPA, 2006). The use of green infrastructure is emphasized in the management of combined sewer overflows (CSO) for many cities in the U.S. Midwest, East, and Northeast. Less often they are considered in coordination with transportation and other types of urban infrastructure to achieve smart urban growth. With adaptive planning, several possibilities are potentially achieved through design and implementation of a polycentric urban form. For example, polycentric distribution of urban populations and activities may allow for developing the decentralized or satellite systems for water supply and wastewater management. The decentralized management shortens the urban water cycle, making it possible to increase wastewater reclamation, nutrient recovery, and potential energy harvesting (See Luther, 2013; Lee et al., 2013). In addition, the high-density housing development in the multiple centers yields a smaller carbon footprint per capita (ADB, 2012), and may facilitate the development of mass transit systems to connect the new urban centers. Examples include Washington DC and New York City. For these urban centers, the higher energy efficiency and lower carbon footprint per capita can be observed from Figure 2-13.

2.3. Monitoring and re-evaluation

Adaptive planning examines possible urban development options against a set of adaptation objectives. Such analysis aims to evaluate capacity and efficiency of existing transportation and water infrastructure, identify future improvement options, and compare their benefits against a set of planning objectives, mostly through model simulations. Major planning activities may include:

- Population and land use planning and future projections
- Transportation analysis and planning, including assessing the potential to further the goals of the Clean Air Act (CAA), state implementation plans and air quality conformity analyses
- Water infrastructure analysis and planning to either assist or limit transportation development and urban development scenarios

Adaptive urban planning can be incorporated in the conventional master planning process. The current urban planning (Figure 2-4) evaluates water and transportation infrastructure conditions, and defines infrastructure improvements, mostly through increments, between two adjacent master planning periods. Often infrastructure development is uncoordinated, producing a condition that hampers future water service optimization. To avoid this undesired consequence, adaptive planning uses an iterative process and integrates the planning, engineering, outcome assessment, and re-planning (See Figure 2-6). It first evaluates urban efficiency against the evaluation criteria, such as energy consumption and emissions. Then it gradually, and systematically, shifts the development paradigm toward smart growth.

The change in development path by adaptation takes place in two levels. At one end, the adaptation weighs into the readjustment of developmental goals, and water and land use policies. This adjustment varies among locations and individual cities, because of different constraints in the natural environment, and the local socioeconomic conditions. At the second level, adaptive planning is focused on urban form and infrastructure. Urban growth is adaptively planned to change the paradigm from urban sprawl to the high-density, low-carbon, and high-efficiency urban form (Figure 2-6). Such adaptive planning expands wastewater management options through a combination of gray and green water infrastructure. This report does not cover the

adaptation approach through development policy adjustment, but instead focuses on adaptive planning for physical systems.

In addition to the mandatory environmental standards, water and energy/carbon footprints are two indices of urban efficiency. The two non-parameterized indices are orthogonal, quantifying the water and energy tradeoffs at a systems scale. This evaluation matrix is one basis to compare developmental options. Published studies are mostly based on simple water or energy usage, and for analysis of a single industry or single service sector such as a municipal drinking water supply or a transportation system. These previous studies provided insight into the water-energy interactions in energy production (Cooley et al., 2011; Rothausen and Conway, 2011; Zhou et al., 2013; Azadi et al., 2013; Dodder et al., 2011; Webster et al., 2013; Chang et al., 2012; and Ibrahim et al., 2008) and in urban planning and operation (Hering et al., 2013; Yang et al., 2013; Wang et al., 2013; Kenworthy, 2006; Novotny, 2013; Lee et al., 2013). In recent decades, more attention has been toward both indices and their relative importance for a given system, infrastructure asset or sector; for example, to the planning of energy biomass and hydropower production in the water-stressed U.S. west (PNNL, 2012).

3. SUD Methods and Tool in Adaptive Urban Planning

Much of the discussion to this point has been centered on the water sector and how the change in urban form might impact it. Minor discussion has concerned the fact that in urban planning, energy and air emissions are also related to construction and operation of water infrastructure. This interrelationship can be dissected in many ways. For example, as noted in Section 1.1 (especially 1.1.2), transportation and water infrastructure relate to the urban form and the potential development mode. Conversely, an urban form defines population and economic activities, and thus can significantly affect the energy use of water supply – both in form of energy involved in infrastructure construction and operation, and also due to spatiotemporal variations in water demand because of the demand distribution and the unique urban heat island (UHI) effect.

The concept of the UHI is that urban gray infrastructure tends to create a greater amount of reflective heat than green infrastructure. Hence as an area develops, the man-made structure absorbs and emits heat in a day cycle, causing higher ambient temperature especially during night time. However, the UHI effect and temperature variation are not uniform across a metropolitan area. The variations depend on land use and land covers, and ultimately, the urban form. Such conclusions were made by several studies on detailed thermal mapping of the UHI effects (e.g., Liu et al., 2012; Buyadi et al., 2013). In later Section 2.2, a case study in the Cincinnati metropolitan region shows how the urban form, defined by transportation roads, can lead to the occurrence of UHI, its degrees and spatial distributions. It is also known that the urban form has impact on emission/ambient air quality, the distribution of population and business activities, and thus the water demand and services. Their combined effects are the basis for adaptive urban planning.

To assist the analysis of energy and emissions in urban development, U.S. EPA has conducted research to develop an adaptive urban planning and engineering tool (AUP&ET). The tool can be used for quantitative analysis of water and carbon footprints as well as other performance criteria (e.g., travel delay, air emission) of the infrastructure in adaptation scenarios.

This section describes the tool's structures, functionality and its application in the Cincinnati metropolitan area.

3.1 AUP&ET principles and utilities

The integrated modeling framework for the Adaptive Urban Planning and Engineering Tool (AUP&ET) is shown in Figure 2-9. Hydroclimatic conditions and land use changes are the two principle variables affecting the adaptation options. Land use change reflects urban development under a set of policies. By using this tool, a climate adaptation co-benefit is assessed in form of energy usage and air emissions.

Overall the AUP&ET program consists of three major modules: land use projections, urban-scale transportation modeling, and water infrastructure modeling as discussed in the prior sections. In this framework, the urban variables refer to the physical attributes such as topography, environmental conditions, and natural resources. The urban developmental policy and growth factors, along with the impacts of climate variations, are collectively represented in the scenario attributes covering the range of probabilistic occurrence of future developmental and environmental conditions. In this section, the models and analysis methods are described for the AUP&ET modules for transportation infrastructure.

3.1.1 Land use projection – CA-Markov model and iCLUS

Land use projection is the basis for scenario-based planning (Figure 2-14). In subsequent adaptation reports, methods and examples of future land use projections will be discussed for rural, suburban and urban watersheds. As discussed in Section 1.3.1., iCLUS land use database can be used when the analysis is based on county-level resolutions. For many urban adaptive planning exercises, land use and employment projections are conducted in finer spatial resolutions, typically at census block levels. CA-Markov modeling is incorporated as the default in AUP&ET module.

A land use model predicts target year land use according to the base year data (land use, demographic, and socioeconomic factors) using a series of scenarios involving demographic and socioeconomic changes anticipated for the target year. In the Cellular Automata (CA) - Markov analysis, the CA model is combined with Markov Chain analysis and Multiple Criteria evaluation. The Markov model is based on the formation of Markov random process for the prediction and optimal control theory (Jiang et al., 2009). The calculation is a multifaceted cross-tabulation between a pair of land use images from two years of different historical observations. Future change probabilities are derived from observed change patterns (Eastman, 2009). Markov modeling predicts each land use transition area objective for future year that is based on transition probability derived from two different historical observed land use data sets (Sang et al., 2011; Eastman, 2009). Therefore, in order to project target year land use, an initial year condition should be provided.

Geographic proximity, also known as spatial autocorrelation, assumes that adjacent areas tend to be similar in land use and that changes occur gradually. In a natural environment, for instance, similar soil characteristics, terrain, weather, and vegetation are usually found within a defined region. The impacts of all these factors are evaluated according to the factor's relative importance or weights (Rao, 2005) by using the Multiple Criteria Evaluation (MCE) as a multi-attribute decision making tool. MCE can be incorporated in CA-Markov modeling to provide

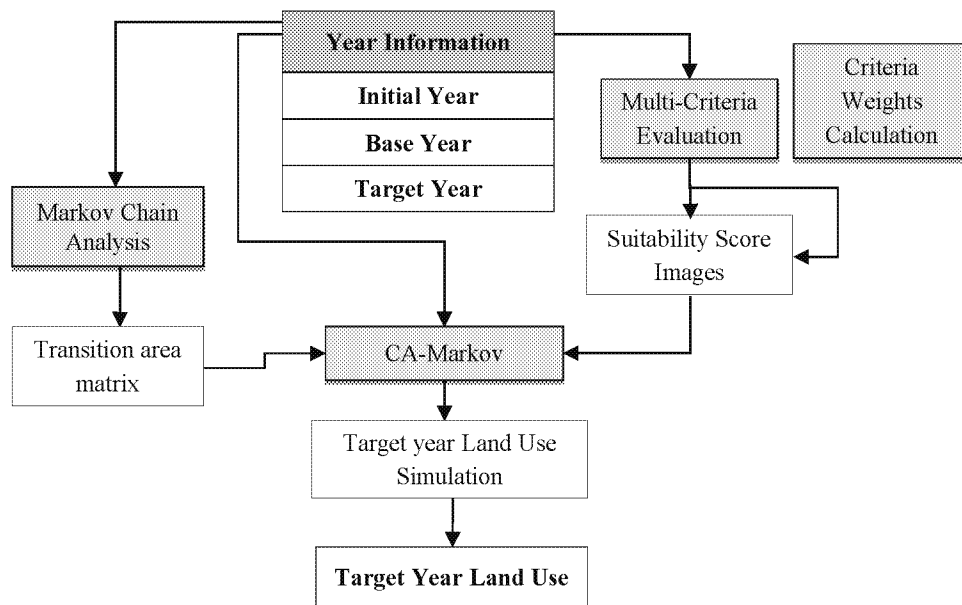


Figure 2-14. Simulation block diagram for CA-Markov based urban land projections.

land suitability analysis with the support of GIS. Overall, the CA-Markov model allocates land use under the objective that was produced by Markov Chain Analysis based on terrestrial suitability produced by Multiple Criteria Evaluation. It takes original land use and its neighborhood land suitability into consideration (Feng et al., 2011; Eastman, 2009). These basic principles and applications can be found in land use projection literature (Tong et al., 2012; Sun et al., 2013; U.S. EPA, 2010b and references therein).

Figure 2-14 shows a framework of urban land use projection used in AUP&ET. There are three properties essential to calculate the transition probability: past trends, geographic proximity, and spatial dependency. Past trends are land use changes observed during a previous period. They can be measured by comparing land uses at the initial year and the base year. The elements of multi-criteria evaluation using differential criteria weights, is converted numerically into sustainability score (Figure 2-14) that can be analyzed spatially. For example, population density and land value are similar within a defined geographic unit (i.e. neighborhoods, cities), but significantly differ among such units. Such geographic proximity and policy drivers are necessary considerations in any land use analysis. Spatial dependency may restrict or promote future changes. While spatial dependency factors may vary by location and types of land use, they are derived from four major categories: population density, accessibility, administrative restrictions, and physical limitations.

The land use projection in AUP&ET in ArcGIS consists of three major steps (Figure 2-14) and uses four major modules: Markov Chain Analysis, Criteria Weights Calculation, Multi-Criteria Evaluation, and Cellular Automata Markov simulation.

In CA-Markov modeling, the base year land use image is taken as the model input, from which changes are projected. The modeling further considers transition areas objective as produced by Markov analysis, and a collection of suitability images that express the suitability of

a pixel for each of the land use type from MCE criteria. Then the modeling begins an iterative process of reallocating land use until it meets the area totals predicted by the Markov analysis. The modeling process and underlying principles are as follows (Eastman, 2009):

- The total number of iterations is based on the number of time steps, namely the projection time frame. For example, if the projection is for 10 years into the future, the time steps might be chosen to complete the model simulation in 10 steps. The time step is chosen to strike a balance between the model precision and computation time. It also needs to be appropriate for the rate of urban development in the past and potentially in the future.
- Every land use type in the model iteration will typically lose some of its land to one or more of the other classes (and it may also gain land area from others). For each modeling iteration, claimant classes select land from the host according to the suitability map for the claimant class.
- The CA component arises in part from the iterative process of land allocation. It also results in part from a filtering stage with each iteration that reduces the possibility of unsuitable changes. The net result of this iterative process is that the land use changes occur in response to growth in areas of high suitability proximate to existing areas.

3.1.2. Calibration and validation of the land use simulation model

The land use model calibration is particularly important for urban land use because of its dynamic nature in evolution. Calibration aims at obtaining values of the transition rule parameters that allow for the most accurate reproduction of the past evolution of land uses. There are two traditional methods to calibrate CA-based models: methods based on trial and error, and methods based on statistical techniques.

The first category does not require a set of strict mathematical formula. It assesses the results obtained from alternative combinations of parameter values (Ward et al., 2000) and the sequential multistage optimization by automated exploration of combinations of parameters (Silva and Clarke, 2002). For the second category, the most frequent statistical method is logistic regression which provides the weights of the variables involved. However, the statistical equations might not reflect the actual relationships or explain the underlying mechanisms (Inés et al., 2012). The first method is used in the case study in Cincinnati (See Section 4.2 later).

The general validation method consists of the visual comparison of model results and observed data in a historical period/point of time. The method is usually complemented by quantitative methods that evaluate overall accuracy. For accuracy measurement purposes, the most frequent metrics in increasing order of complexity are (i) ratio of simulated to real number of cells (or clusters) for a given land use, (ii) overall accuracy measured by the percentage of correctly classified pixels, (iii) regression analysis between simulation results and real data, and (iv) a coincidence matrix and the Kappa index (Santé et al., 2012, and references therein). Because method based on trial and error is applied in calibration process, overall accuracy and the Kappa index are popular measurements in comparing simulated land use with reference land use. Therefore, the overall accuracy and the Kappa index were adopted for land use calibration and validation in the AUP&ET simulations.

3.1.3 AIR-SUSTAIN system for transportation simulation

The other major AUP&ET component is urban transportation planning (Figure 2-15). The scenario-based adaptive planning has basic objectives for high transportation efficiency and reduced air emissions, energy usage and carbon footprints for the current and future land use scenarios. The land use types and spatial relations are the basis for defining population, employment, and urban activity distributions in the transportation modeling (See Section 3.1.1 above).

The scenario analysis for transportation planning is hosted within a newly developed simulation tool “Air Impact Relating Scenario-Based Urban Setting and Transportation Asset in Network” or AIR-SUSTAIN (Yao et al., 2014). Figure 2-15 shows its architectural structure. The current version consists of three application modules: the scenario development, regional level analysis, and project level analysis. The scenario development module is built upon the base-year land use, demographic and socio-economic factors, and transportation infrastructure data. It further considers the assumed changes in the demographic and socio-economic factors

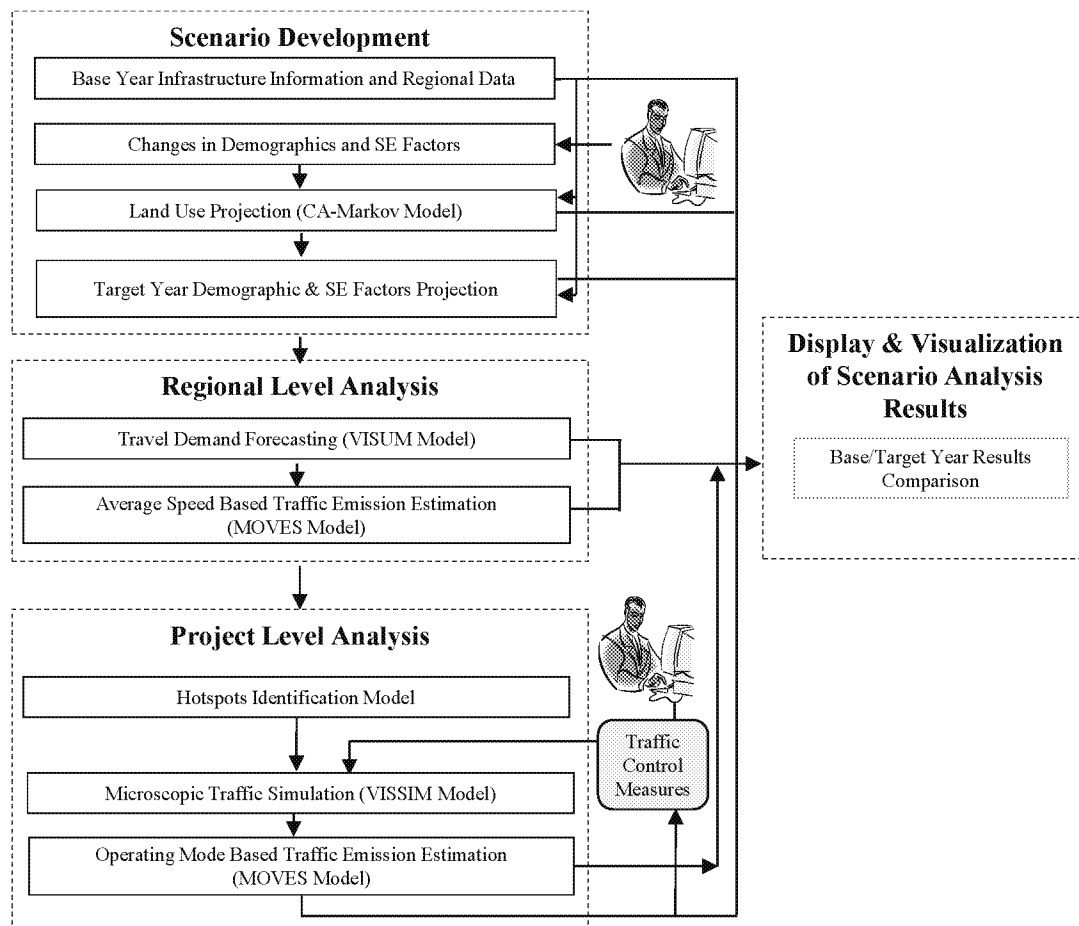


Figure 2-15 AIR-SUSTAIN modeling framework for transportation analysis of efficiency and CO₂ emission in urban infrastructure adaptation.

for a target year. The target-year land use is projected by the CA-Markov land use model. For regional analysis at county-resolution, the iCLUS model (U.S. EPA, 2010b) can also be used.

In general sequence, the AIR-SUSTAIN regional analysis can be used to assess the impacts of a growth scenario on urban transportation system performance (Figure 2-9). Then the results are used to identify emission hotspots where the transportation efficiency deteriorates and air emissions increase beyond a threshold defined in policies and regulations. The U.S. DOT defines a hotspot using a systematic evaluation and judging criteria. For the identified hotspots, a project level analysis is then conducted to identify most appropriate traffic control measures and other engineering solutions (Figure 2-15). The analysis is centered on engineering and management options to improve the transportation performance and reduce on-road traffic emissions. Together, the regional level and project level analysis provides a complete AUP&ET analysis of transportation performance in each planning scenario.

The AIR-SUSTAIN modeling and analysis starts with computation of target-year demographic and socio-economic distributions on the basis of projected land use. A linkage model using the user-specified growth rates populates the spatial distribution of the future changes within an urban area of analysis. The linkage model projection includes future population, employment, university enrollment and high school enrollment in each traffic analysis zone (TAZ) in a target year. The principal variables in the regional level analysis of travel demand forecasting include employment, student enrollment, etc. Subsequently, traffic emissions based on the travel demand forecasting (TDF) outputs are estimated. Subsequent Section 3.2 further describes data flows and model simulation using the AIR-SUSTAIN tool. Section 4.1 presents a real-world case study in the Cincinnati metropolitan region for illustration.

3.1.4. The linkage to water infrastructure simulations

The adaptive planning framework within SUD also contains three water infrastructure modules for drinking water supply, wastewater and storm water management, respectively (See Figure 2-9). Because water infrastructure normally follows the population and land use changes, its planning and design are assumed to be passive in nature after transportation.

3.2. The AIR-SUSTAIN simulation tool for transportation

Inside the SUD, AIR-SUSTAIN is a software interface developed in the research reported here. It integrates land use projection, traffic simulations and optimization. The purpose is to evaluate land use and transportation development scenarios by modeling and analyzing emissions over the urban transportation network, fuel usage and transportation performance parameters such as excess travel time, air emission hotspots, regional conformity evaluation, etc. The tool utilizes a GIS platform in order to provide the urban-wide spatial information for model projections of land use, employment, residential development, travel demand, and automobile-based travel conditions. Other modeled environmental performance criteria include fuel consumption and total carbon emissions.

The basic features of the AIR-SUSTAIN system, when the integrated SUD tool is used in scenario-based urban adaptation analysis, include data flows and linkages among the model components. The modeling process is shown in Figure 2-15, and are described below. In Appendix A, the program structure and model input and output are described in detail. The major model components include:

- Linkage model. The linkage model combines the land use model output, the target year population and employment projections, and base year population and employment data. This prepares target year population and employment for each TAZ as the model inputs for traffic simulation.
- Travel demand forecasting (TDF) model using VISUM software. VISUM is comprehensive flexible software widely used worldwide for metropolitan, regional, state and national planning applications. The TDF model simulates link (i.e., roadway segment) traffic volume and speed. The results are used as inputs for the traffic-related emissions estimation in AIR-SUSTAIN.
- Microscopic traffic simulation model using VISSIM software. The commercial traffic analysis software allows for the analysis of traffic measures designed to improve traffic capacity. It is also used with AIR-SUSTAIN to evaluate engineering options to reduce CO₂ and pollutant emissions.
- Automobile vehicular emissions calculation using EPA's regulatory model MOVES (U.S. EPA, 2010) for adaptation analysis of urban-wide transportation or specific traffic measures.

3.2.1. Basic functions and interfaces of AIR-SUSTAIN

The AIR-SUSTAIN software interface integrates transportation and land use models in scenario analysis. The scenario analysis aims to measure and assess the effects of urban infrastructure adaptation for projected demographic and socioeconomic changes. In adaptive planning, this analysis helps evaluate planning options according to development policies (Figure 2-6) given location-specific natural resource and climate constraints. Through scenario-based planning analysis, sensitive interactions among travel demand, the impact of transportation activities on road emissions, and urban development policies can be quantitatively assessed in scenario comparisons.

The quantitative analysis is executed in the AIR-SUSTAIN through interfaces embedded in a GIS environment (Figure 2-16). Main functions and interfaces of the AIR-SUSTAIN include: 1) Scenario Information Specification; 2) Scenario Development; 3) Regional Level Analysis; 4) Project Level Analysis; and 5) Results Comparison.

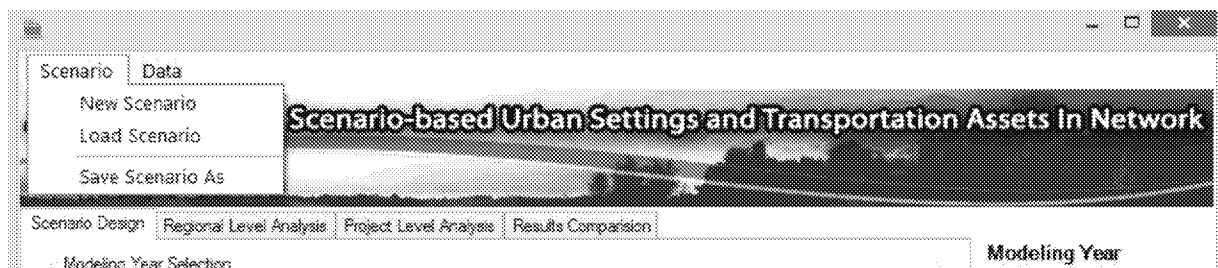


Figure 2-16. AIR-SUSTAIN graphic interface for scenario modeling and analysis

- ***Scenario Development***

Scenario development for transportation adaptation is set by importing base year data and developing demographic and socioeconomic attributes of a scenario. In particular, base year demographic and socio-economic data are imported with the feature class *TAZ*. The target year demographic and socioeconomic data are contained in the feature class *TargetYearTAZ* of the computer program (its format is shown in Tables A1-1 to 1-4 of Appendix A). It is computed based on the assumed demographic and socio-economic changes, target year land use projection, and base year demographic and socioeconomic data.

Among those datasets, the assumed demographic and socio-economic changes in the future scenario depend on urban development policies or objectives. This group of data are specified by the user through the functions provided by the *Scenario Development* module. The target year land use data are projected by the land use model embedded in the AIR-SUSTAIN system. The data inputs, demographic and socioeconomic factor specification and model execution, are implemented by different parts of the Scenario Development module.

- ***Regional Level Analysis***

The *Regional Level Analysis* module is used to estimate travel demand and on-road emissions for the base and target year in a project area. It consists of two major elements: *Travel Demand Forecasting* and *Emission Estimation*. When performing the regional level analysis, a TDF model first simulates trips on roadway links for the entire area based on demographic and social economic data, as well as transportation infrastructure; for example, road network, parks, water bodies, TAZs, etc. Subsequently, the forecasted traffic data is utilized to generate inputs for a traffic emissions model to estimate vehicle emissions for each road link. In the emission analysis, CO₂ equivalent ($CO_{2,T}$), other criteria pollutants, and energy consumption are estimated by using the EPA's MOVES model.

- ***Project Level Analysis***

In the *project level analysis*, hotspot links are identified based on the regional level analysis results. A microscopic traffic simulation model such as VISSUM is used to estimate the traffic flow operations on the hotspot links under alternative traffic control measures. The assumed traffic control measures are assessed in terms of traffic operation performance and their influence on the on-road traffic emission rates. Emission rates of each hotspot link are also calculated using the MOVES model in the project-level analysis module.

- ***Results Comparison***

After performing the scenario design, regional level analysis and project level analysis, results from the base year and target year can be compared and visualized in ArcGIS by the Results Comparison tab (Figure 2-17). In the subsequent sections, the AIR-SUSTAIN tool is described. Particular attention is focused on the data structure, model linkage, travel demand, hotspot identification, the microscopic simulation of adaptation options, and lastly the emissions and energy consumption estimation.

3.2.2. Travel demand forecasting – VISUM

Travel demand forecasting (TDF) is an essential component of the traffic impact analysis that links transportation to land use and socio-economic factors at a regional level. In the AIR-SUSTAIN tool, the TDF model is used to forecast travel demand for both base year and target year. This projection is primarily dependent upon the settings of land use based on the socioeconomic datasets. TDF model outputs include the link (i.e., roadway segment) traffic volume and speed, which can be further used as inputs for the traffic-related emission estimation.

3.2.2.1. Modeling

Travel demand analysis was first developed in the late 1950s for highway planning using a four-step model. This four-step model, in the conventional trip-based approach, is a primary tool in forecasting future demand and performance of regional transportation system. The AIR-SUSTAIN tool adopts this traditional four-step model for the travel demand forecasting. The demand forecasting involves four basic steps:

Scenario Data

Air Impact Relating Scenario-based Urban Settings and Transportation Assets In Network

Scenario Development Regional Level Analysis Project Level Analysis Results Comparison

Land Use

Land Use View Res

Demographic and Socioeconomic Results

Demographic and Socioeconomic Data View

Travel Demand Forecasting Results

Travel Demand Forecasting Data View

Emission Estimation Results

Emission Estimation View

Modeling Year

yyyy

Process Status

Project Information

Modeling Year Selection

Base Year Data

Target Year Scenario Design

Travel Demand Forecasting

Emission Estimation

Hotspots Identification

Microscopic Simulation Result

Hotspots Emission Estimation

Regional Emissions Update

Figure 2-17 Results Comparison interface in the AIR-SUSTAIN tool.

- *Trip generation.* This is the process in estimating the number of person-trips that will begin from or end in each TAZ within the region on a typical day. The traditional trip-based approach considers each trip as the unit of analysis. Where an individual makes a series of trips, each trip is treated as a separate, independent trip (McNally, 1996, 2007).
- *Trip distribution.* This process allocates the trips generated in one zone to other zones.
- *Mode split.* It estimates modal percentages of the travel according to the time and cost characteristics of the various competing modes based on the demographic and socioeconomic characteristics of the urban residents.
- *Traffic assignment.* This last step in travel demand forecasting assigns trips to the transportation network.

Notably, the four-step models rely on average transportation behavior between and within zones, whereas more sophisticated activity-based models attempt to represent focus groups of populations. This creates an alternative whereby the activity-based approach explicitly recognizes and addresses the limitations of the conventional trip-based approach by considering the underlying human behavior in general and travel behavior in particular (Jones et al., 1990). For this reason, the unit of analysis is shifted from rough aggregates to the level of the individual traveler (Zmud et al., 2014). This development makes it possible to incorporate detailed demographic data.

Several travel demand modeling software packages are commercially available for this type of application; they all are based on the four-step model. Those widely used by practitioners and researchers include VISUM, Cube, and TransCAD. The current version of the AIR-SUSTAIN system utilizes VISUM software.

3.2.2.2. *Model calibration and validation*

Model calibration and validation is fundamental to travel demand forecasting. Model calibration and validation data may include:

- Reliable estimates of base year TAZ household characteristics and employment information.
- An accurate representation of the base year highway (and transit, if any) network.
- A reliable base-year travel survey or monitored traffic data based on main permanent stations.

Model calibration and validation can proceed after the model parameters are estimated in the AIR-SUSTAIN simulation. Model calibration allows model parameters to be adjusted until the predicted travel matches the surveyed travel (e.g., O-D survey data) across the region for the base year. As the calibrated model is applied for the purpose of forecasting, it is assumed that these calibrated parameters will remain constant over time (Pedersen and Sandahl, 1982). On the other hand, model validation tests the model predictability of the future. In many areas, traffic counts are commonly used for model validation. Validation requires comparing the TDF model predictions on specific roadways with the traffic counts data (e.g., Annual Average Daily Traffic – AADT) that occurred on the same roadways.

TDF calibration and validation is based on the Mean Absolute Percentage Error (MAPE) in Eq. 2.2. In the travel demand model, parameters such as the utility functions' parameters and network capacity are adjusted to calibrate the model.

$$MAPE = \frac{1}{T} \sum_{t=1}^T \left| \frac{M_{abs}(t) - M_{stin}(t)}{M_{abs}(t)} \right| \quad (2.2)$$

where, $MAPE$ is the Mean Absolute Percentage Error; $M_{abs}(t)$ is field measured time-series values during a period of time t ; and $M_{stin}(t)$ is the simulated time-series values during a period of time t . In AIR-SUSTAIN, MAPE is calculated for the measured and simulated traffic count and model volume. The MAPE ranges for total error by functional classification (type of road) are set by FHWA (1990):

Freeway	<7%
Expressway	<10%
Arterial	<15%
Collector	<25%
Frontage/Ramps	<25%

3.2.3. Hotspot identification

The Federal Highway Administration (FHWA) standard for hotspot identification is followed in AIR-SUSTAIN. A $PM_{2.5}$ hotspot analysis is required when a non-exempt project is located in a $PM_{2.5}$ nonattainment or maintenance area, and when the project's design year Annual Average Daily Traffic (AADT) $\geq 125,000$ and the design year diesel truck volume $\geq 10,000$. For a project in a $PM_{2.5}$ nonattainment or maintenance area, but where a $PM_{2.5}$ hotspot analysis is not required based on AADT and diesel truck volume, then the project is either exempt from air quality conformity requirement for $PM_{2.5}$ according to the 40CFR93.126 regulation (FHWA, 2012). The determination process is shown in Figure 2-18. The hotspot identification criteria include:

- Project is located in $PM_{2.5}$ nonattainment or maintenance area;
- Project does not exempt from air quality conformity per 40CFR93.126 or per 40CFR93.128;
- Design year link-based AADT is $\geq 125,000$ and diesel truck volume $\geq 10,000$.

In the AIR-SUSTAIN simulation program, all corridors necessary for hotspot analysis are identified according to the regional level analysis results. Their link information is saved in the AIR-SUSATIN database and marked in ArcGIS for the microscopic analysis in the subsequent step.

3.2.4. Microscopic simulation using VISSIM

In the AIR-SUSTAIN simulation package, hotspot links identified from the regional level analysis results can be further modeled using VISSIM software. VISSIM was developed at University of Karlsruhe in Germany and is distributed by PTV, for microscopic simulation at a

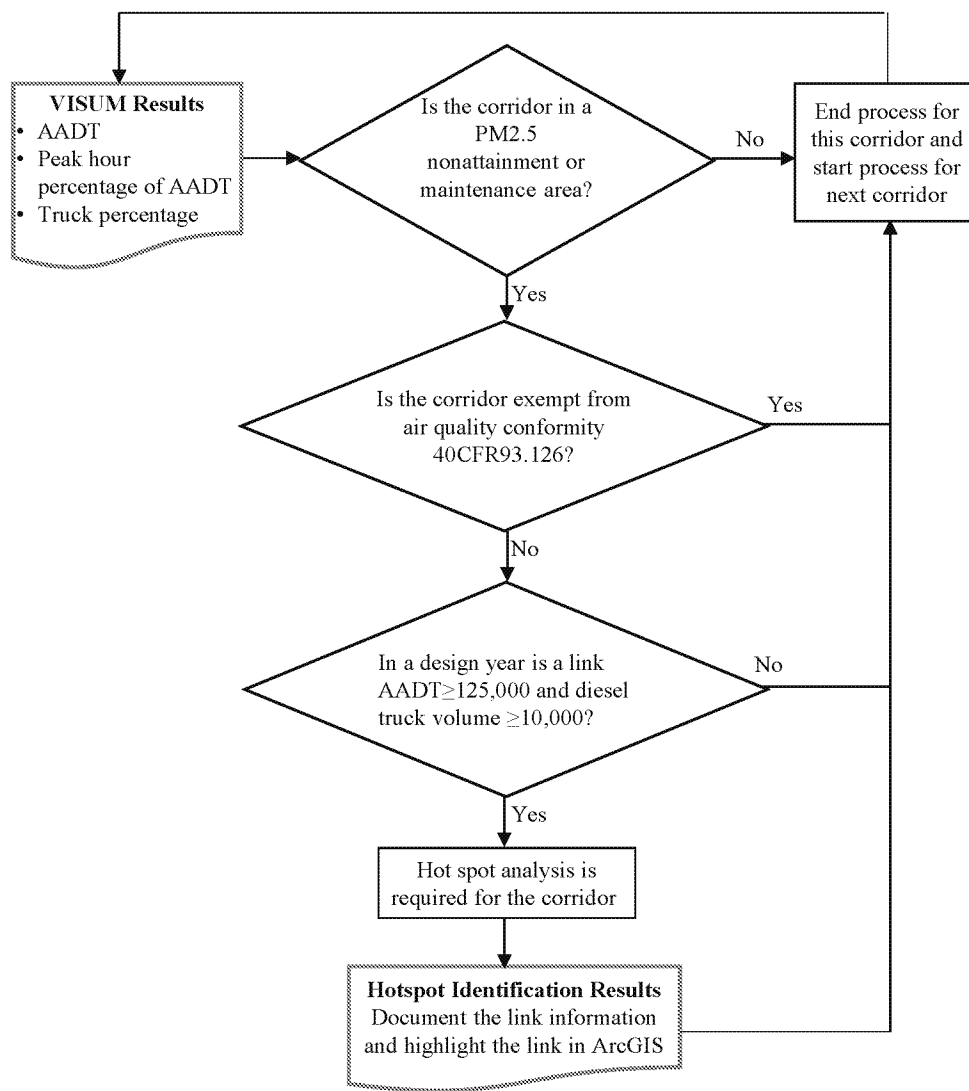


Figure 2-18 PM_{2.5} hotspot identification process

higher spatial resolution. The model attempts to analyze the traffic flow by modeling each entity (car, train, or person) within a traffic stream and studying the interaction between drivers (Barceló et al., 2005). This modeling capability allows one to simulate the traffic control and management systems on all levels, from the traffic control platform to individual traffic controllers (Gettman and Head, 2003). It is applicable for highway corridors, local arterial roads and other simulations. Thus, the analysis of traffic operations and emissions in hotspots allows one to design and evaluate traffic control measures and/or transportation control strategies that improve the use of transportation facilities, roadway operations, and to reduce air emission and fuel consumption (U.S. EPA, 2011). This type of analysis facilitates urban adaptation down to a local project level analysis. The current version of the AIR-SUSTAIN tool has the microscopic

simulation model with the microscopic simulation capability. More functions can be added in the future.

By using AIR-SUSTAIN, TDF analysis in the regional level analysis can yield estimates for AADT, peak hour percentage of AADT, and truck percentage. Those results are then imported into the VISSIM for local traffic modeling. Other inputs for VISSIM network include link geometry attributes and the observed traffic data for model calibration and validation. A validated simulation can predict and compare the average speed, delay and queue length for different scenarios by using, or without using, transportation control measures. Figure 2-18 shows the process of microscopic simulation analysis. Appendix A provides the details of principles and modeling steps for VISSIM microscopic analysis, including input data structure, scenario determination, model calibration and validation. Both high resolution traffic results and evaluation results can be input values in MySQL and Geodatabase available in AIR-SUSTAIN. Simulation results include:

- High-resolution traffic condition at the link, including second-by-second speed and acceleration. Such results can be used as the inputs for emission calculation in MOVES at the project level.
- Evaluation results on average speed, delay and queue length of each link. This modeling output can be used to compare the differences of scenarios in different transportation control measures.

3.2.5. *Emission estimation using MOVES*

AIR-SUSTAIN incorporates EPA's Motor Vehicle Emission Simulator (MOVES) program as the energy and emission analysis tool. In 2010, the MOVES model and software were released by the U.S. EPA (U.S. EPA, 2010) for estimating air pollution emissions from on-road mobile sources (FHWA, 2012). The regional level and project-level simulation in AIR-SUSTAIN provides traffic data to estimate the emissions factors used in MOVES. This model integration enables users to evaluate air quality, carbon emission and energy consumption for competing adaptive urban scenarios.

The MOVES model has options for three levels of vehicle activity inputs. They are average speed, drive cycle and operating mode distribution; each is associated with different levels of model accuracy and data requirement (Figure 2-19). Average speed is a basic parameter in traffic operation. It can be conveniently obtained from the AIR-SUSTAIN's TDF models. For the average speed as the traffic input, MOVES uses the default operating mode distribution associated with different speed ranges (bins). It should be noted, however, that this method

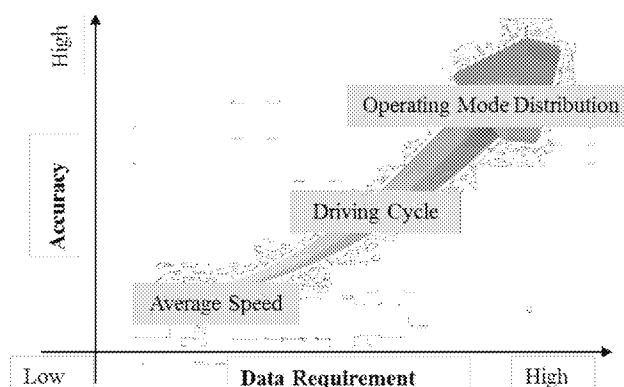


Figure 2-19 Accuracy and data requirements for three types of vehicle activity inputs

may not accurately represent the field traffic operation varying with time and locations. The second option Drive Cycle is a second-by-second description of vehicle activity over time. Such data are usually collected by using a GPS-equipped probe car. It is assumed that every vehicle on road is following the same trajectory of the probe car. This option can accurately represent the traffic operation. However, the data collection can be burdensome. This option has not been incorporated in AIR-SUSTAIN for scenario analysis.

At the highest level, the operating mode distribution method takes a different approach. It assumes a fraction of vehicle operation mode bins on the basis of its instantaneous operating mode distribution; the latter is determined by vehicle specific power (VSP) and speed. This method describes the entire vehicle population's operation of a study area and provides the highest individual vehicle level of resolution data. It is worth noting that MOVES program internally converts all the average speed and drive cycle inputs into operating mode distribution, and then relates them using the MOVES emission rate database. A comparison of the relative accuracy and data requirement for the three methods are illustrated in Figure 2-19.

Considering traffic data availability, the AIR-SUSTAIN tool uses the average speed option for regional level analysis, and the operating mode distribution for project level analysis. This modeling approach is illustrated in Figure 2-20. Traffic inputs for the regional level analysis are extracted from TDF model outputs. In addition to the average speed, other traffic inputs include link traffic volume and vehicle composition. Traffic inputs for the project-level analysis are generated by the microscopic simulation model. They consist of traffic volumes, link average speed, operating mode distribution and vehicle composition.

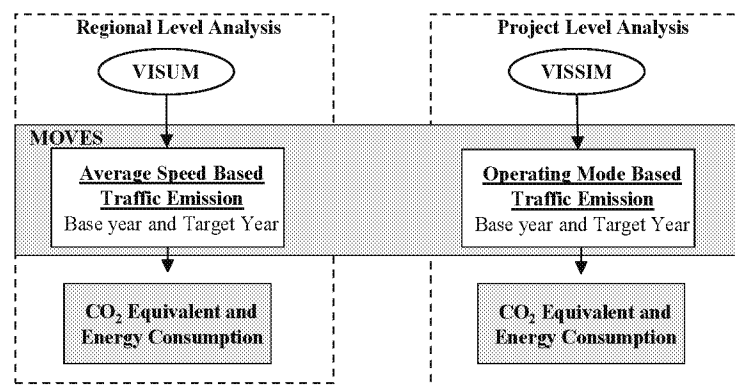


Figure 2-20 Modeling framework for emission estimation using both the macroscale VISUM and microscopic VISSIM traffic simulation models.

Both average speed-based and operating mode-based approaches apply similar procedure to estimate the emission rate. Details of model inputs, governing equations, and model simulations for traffic flow, vehicle compositions and operating modes are contained in Appendix A. Common parameters for model inputs include:

Emission Source Type

The MOVES source type is a combination of vehicle type and how the vehicle is used. For example, long haul and short haul trucks tend to be very similar in size and design, but the way they are used defines their source use type in the emission category. Table A2-5 in Appendix A shows the source types, their descriptions, and their equivalents as defined by the Highway Performance Monitoring System (HPMS).

Road Type

The list of Road Types is contained in the underlying MOVES database. The default database has Road Types that represent urban and rural driving on roads with restricted and unrestricted vehicle access. Restricted access road types are usually used to model freeways and interstates; ramps are considered part of restricted access road types. In the modeling program, the Ramp Fraction tab of the County Data Manager will only become available if an unrestricted road type (i.e. 2 or 4) is selected. Table A2-6 in Appendix A shows the MOVES road type.

Vehicle Age Distribution

The MOVES model use vehicle age information and group the vehicle specific power (VSP) for light-duty vehicles and scaled tractive power (STP) for heavy-duty vehicles into the age groups. Table A2-7 in Appendix A shows the age categories used in MOVES model.

Operating Mode

The operating mode bins are predefined in the MOVES model, as shown in Table A2-8 in Appendix A. Each operating mode categorized by vehicle source type, road type and age group corresponding to an emission rate that is previously determined in the MOVES database.

4. Adaptive Urban Planning in SUD Case Studies

Urban-scale adaptation, as described in Section 2.0, is essential to the development of sustainable infrastructure under current and future climate and land use changes. Adaptation co-benefits can be achieved for increased water infrastructure resilience and CO₂ reduction simultaneously as described in 3.0. The two benefits do not conflict, and are achievable through adaptive planning. The sequence for such planning analysis is shown earlier in Figure 2-6.

In this section, two SUD application case studies in Cincinnati of Ohio and in Manatee County of Florida are described for illustration. The case study in Cincinnati aimed to characterize the relationships between land use, population, transportation under present and possible development scenarios. The scenarios were compared using urban efficiency parameters including fuel and energy consumption, emission and air quality, the UHI effects, and commuting times. For water, this type of scenario analysis in adaptive planning is illustrated by a case study for water supply master planning in Manatee County, Florida.

4.1 Urban form and urban infrastructure

4.1.1. Urban form and land use patterns

Cincinnati metropolitan area hosts approximately 2.1 million people in 10 counties over 7350 km² of the land on the banks of Ohio River (Figure 2-21). Traffic patterns in the region are characteristic of a monocentric urban framework centered around downtown Cincinnati. Rolling hills with limited topographic relief follow the Ohio River and the NNE-SSW oriented Mill Creek, surrounded by flat to moderately hilly farm lands and forest to the east and south. Valleys along the Ohio River and the Mill Creek are about 100 m lower in elevation than the other areas.

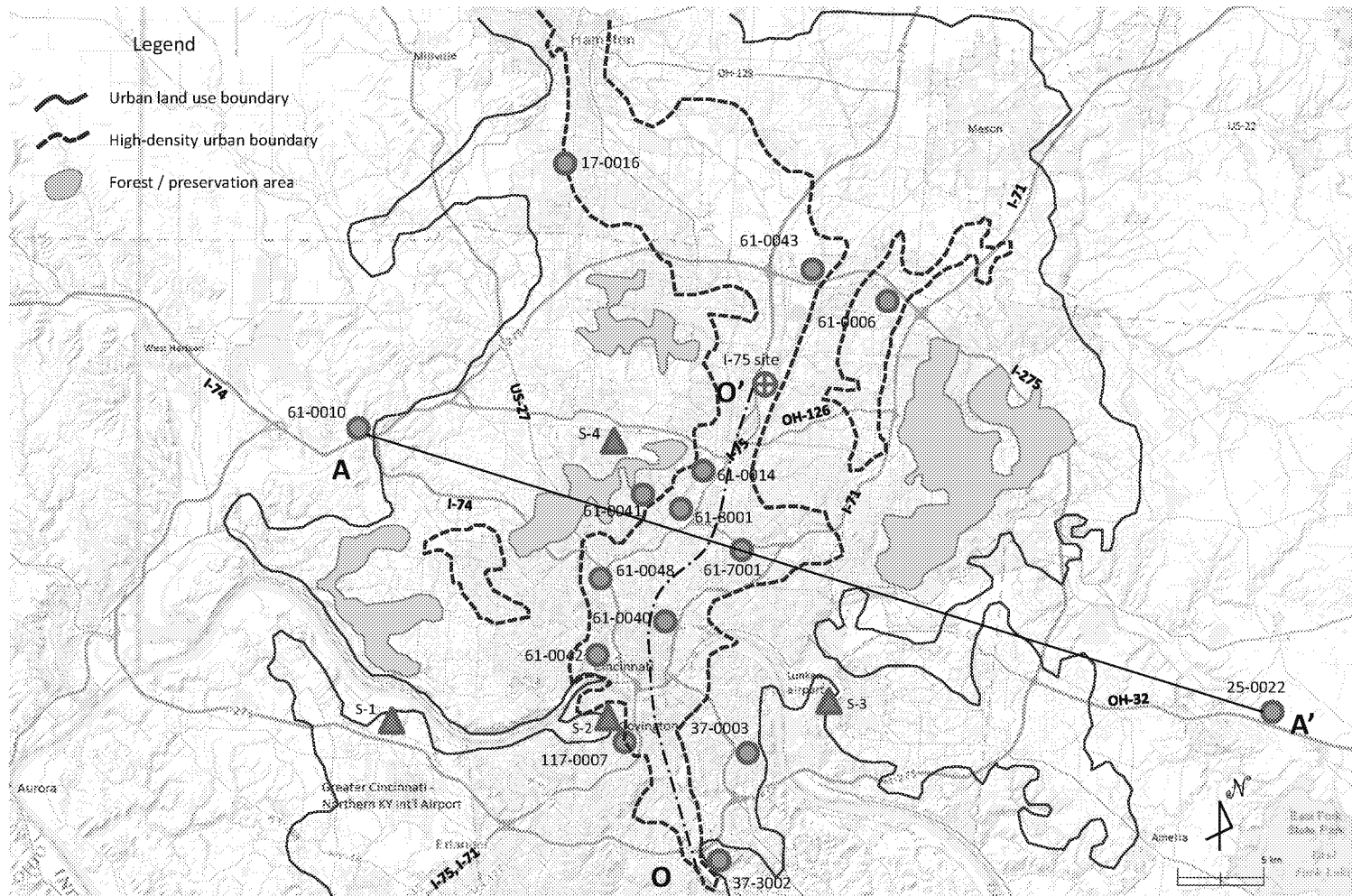


Figure 2-21 Major transportation traffic routes and the urban physical footprints of the Cincinnati metropolitan region. Also shown are the locations of four radio sounding locations (S-1 to S-4) and 15 EPA's NAAQS air quality monitoring stations in filled circles. The I-75 site location refers to the study area by Liang et al (2013). Urban footprint and high-density pavement areas are delineated from the 2007 USGS land use maps.

The north-south trending and narrow high-density urbanized zone with heavy surface pavement is delineated from a U.S. Geological Survey urban land use map and by interpretation of a Google® satellite map dated 2013. The high-density zone is shown in Figure 2-21; O-O' marks its long axis. Inside the zone it is characterized by a large fraction of surface pavements and roofs (Figure 2-22a,b). Small paths of green lands and lawns are interspersed among the man-made structures. Besides the continuous large area of the heavy urbanized Mill Creek corridor, two small areas of high-density development appear in the Western Hills area west of I-75, and in the Blue Ash-Mason area along I-71. These small and isolated patches of high-density development are surrounded by residential development of single houses and forest reserves.

Beyond the high-density urbanized zone is a mixed zone of dispersed low-density developments that are dominated by detached residential houses and commercial areas separated by lawns and tree zones. Typical formation is shown in Figures 2-22c,d. Figure 2-23 schematically shows the spatial transition from the internal high-density core, to the mixed zone, and ultimately to the exurban farm lands. In recent decades, the urban development in the Cincinnati metropolitan area has been concentrated in several areas leading in the direction of a polycentric urban form:

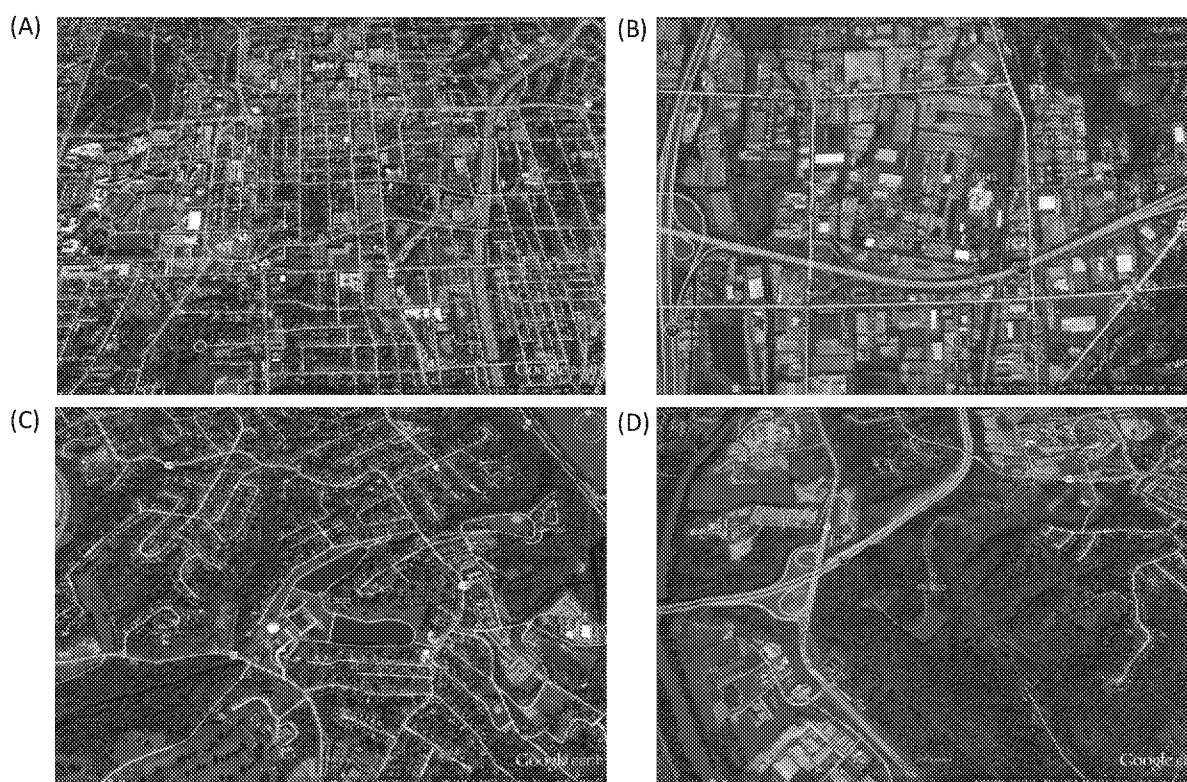


Figure 2-22 Land use patterns differing among 12 EPA's NAAQS monitoring stations. (A) high-density urban core of residual/commercial area at NAAQS station 061-0040; (B) urban core of industrial/commercial area at station 061-0043; (C) low-density residual area at station 037-0003; (D) greenness in urban perimeter at station 037-3002. Each long photo side is ~2.0 km. Maps obtained from GoogleMap™.

- Significant urban development has occurred in the West Chester area and Mason area along north I-75 and north I-71, respectively. These developments sprouted from significant establishment of commercial activities, introducing satellite urban centers through the process of ribbon and leapfrog sprawls in Figure 2-5.
- Cincinnati downtown has been redeveloped over the past decades, with increasing development of high-density residential communities. The ongoing development of street car system solidifies the current development further into a walkable urban center.
- The city's policy on infill development along I-75 and I-71, and continued development in the northern Kentucky region, have led to large transformation of the commercial activities in the region. These developments further lead to a formation of polycentric form with implications in both transportation and water management.

In the following sections, the urban form and land use types are related to the urban climate, transportation demands and atmospheric structure above an urban center. The most important properties include urban heat island shown in ambient temperature (T_a) and thermal inversion in the urban boundary layer (UBL) (Figure 2-23); both affect the air quality as well as water consumption and hydrology in the urban environment.

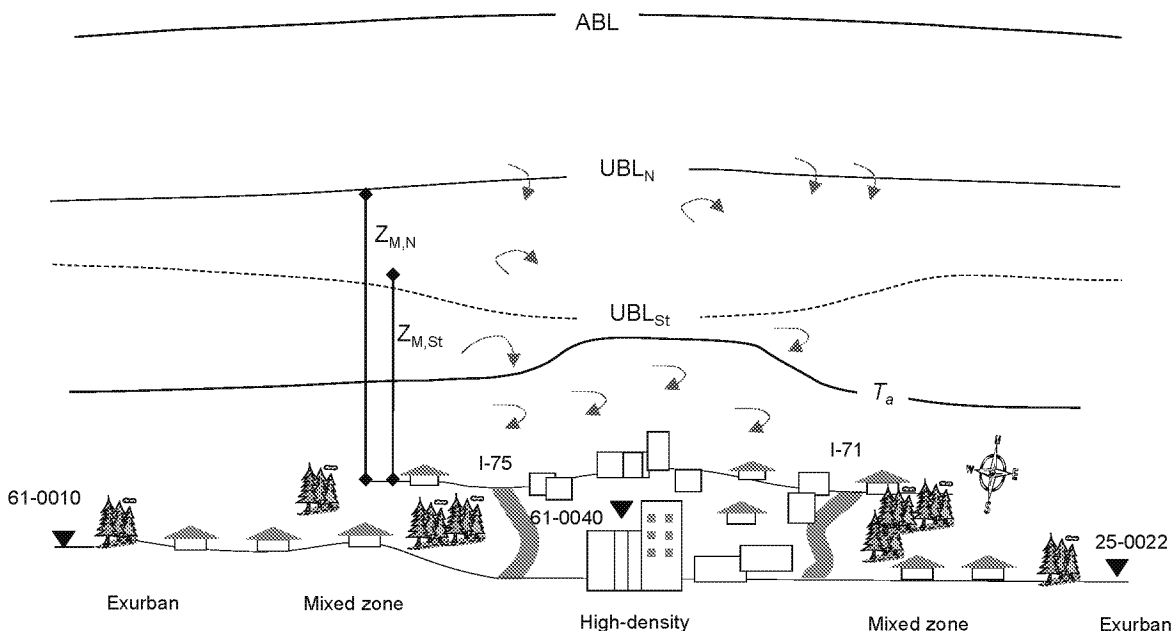


Figure 2-23 A schematic diagram of three-dimensional model illustrating the urban formation, traffic and atmospheric structure in the Cincinnati metropolitan area. T_a – ambient temperature; ABL – Atmospheric boundary layer; UBL – urban boundary layer; subscripts N and St for neutral and very stable atmosphere, respectively, and Z is height. NAAQS stations are indicated for their relative locations. From Liang (2014).

4.1.2. Transportation and traffic distribution

Current transportation in the Cincinnati metropolitan area mostly relies on automobile with limited bus-based mass transit. The road network in the metropolitan region consists of interstate freeways and arterials (I-71, I-75, I-74, and I-275), collectors (SR-126, SR-129), and local roads. The road network connects the north-south high-density industrial-commercial zone to the low-density residential and commercial districts in the urban perimeters and exurban area. The high-density zone is extended along the Mill Creek valley with automobile as the primary transportation means. The Ohio-Kentucky-Indiana Regional Council of Governments (OKI) collected the 2009 traffic data and provided traffic counts and composition of 20 traffic stations for this research.

Analysis of the year-2009 traffic data indicates strong diurnal and spatial variations from daily traffic counts and traffic composition at interstate freeways and arterials (I-71, I-75, I-74 and I-275), collectors (SR-126, SR-129) and local roads. The traffic is generalized into the five time periods of different traffic compositions in Table 2-4. Similar traffic diurnal variability and spatial distributions were reproduced by Yao et al. (2014) in a detailed area-wide trip generation and traffic volume modeling. In the analysis here, hourly traffic profiles during weekdays were constructed for each of the stations.

Table 2-4 Four daily periods of traffic compositions on the highway in Cincinnati.

Period	Time	Traffic Composition
Night period	11 pm – 6 am	Diesel truck dominant
Morning rushing hours	6 am – 8 am	Gasoline car dominant
Daytime period	8 am – 3 pm	Mixture
Afternoon rushing hours	3 pm – 5 pm	Gasoline car dominant
Evening period	5 pm – 11 pm	Increasing diesel truck

Figure 2-24 shows the 2009 yearly averaged traffic volume for passenger cars in automobile class C1-C3, diesel trucks including single-unit truck (C4-C7) and multi-unit trucks (C8-C13) on the highways and local roads. Average weekly traffic compositions for selected major monitoring stations are listed in Table 2-5. The highest traffic volume and large variations occur along I-71 and I-75. The average and standard deviation of weekday total traffic volumes are 69485 ± 26590 vehicles/day (N=13 stations), 34770 ± 14180 vehicles /day (N=3 stations), and 43452 ± 22661 vehicles /day (N=3 stations), for the interstate freeways, collectors, and local roads, respectively. The level of service is consistent with the field traffic measurements Liang et al. (2013) reported for October 2010 during the I-75 black carbon dispersion studies.

In the Cincinnati area, most of multi-unit truck traffic is concentrated along the interstate freeways with a traffic volume of 8159 ± 4339 vehicles /day, or approximately 10 times more than in the collector and local roads. Truck volume above 13300 vehicles /day was measured at north I-75 serving the industries and in I-75/I-71 after merger leaving Ohio into Kentucky developments and mixed land use in perimeter and exurban. Representative examples are shown in Figure 2-22.

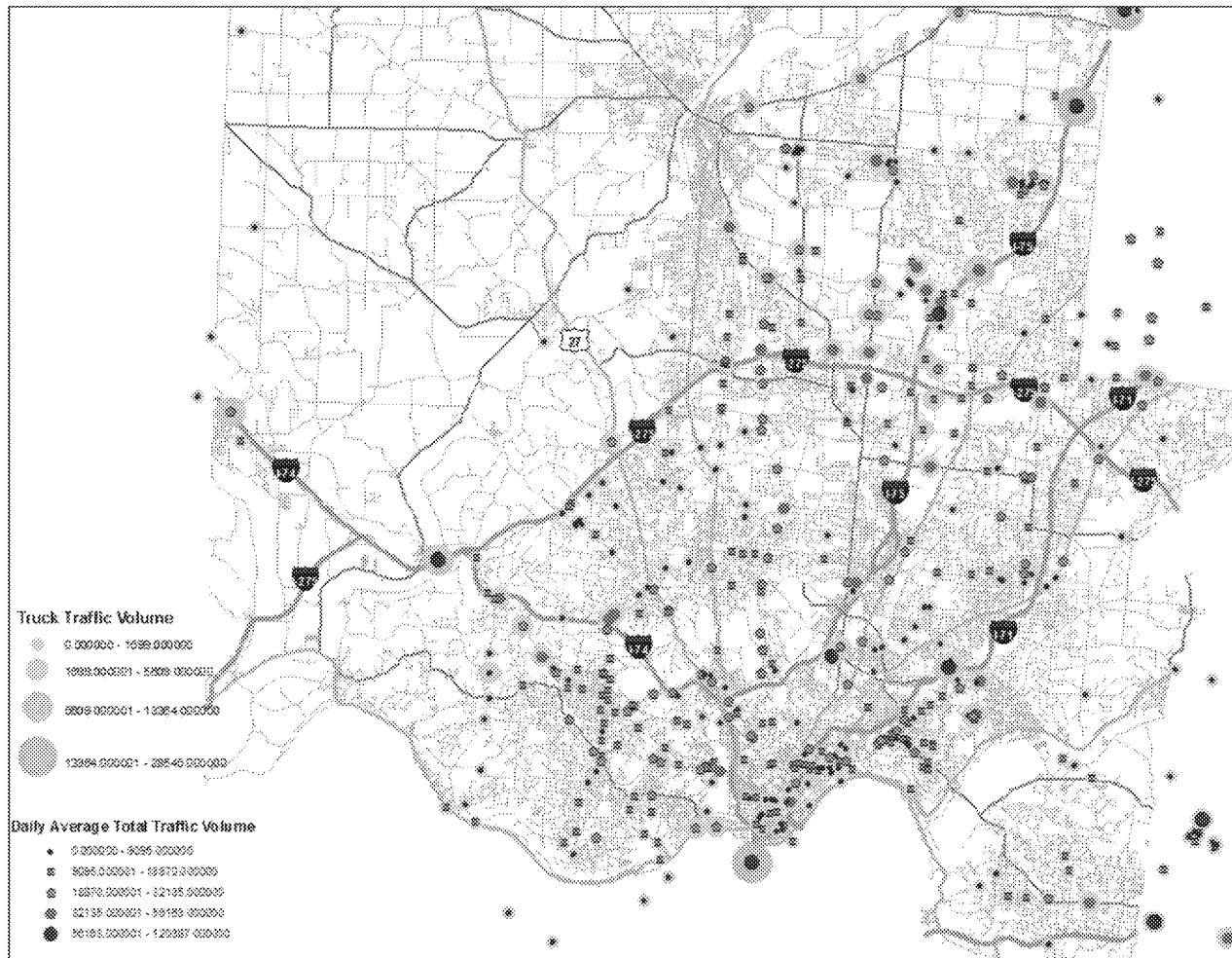


Figure 2-24

Truck and passenger car traffic volume distribution in the Cincinnati metropolitan region. Heavy truck traffic concentrated in I-75, I-74 and the confluence of I-75/I-71 leading to Kentucky in the south. Relatively, I-71 has greater car traffic. From Liang (2014).

Table 2-5 Locations and traffic flow in 2009 for selected locations in the Cincinnati road network.

OKI Station	Traffic Roads		Average Weekday Traffic**				Location
	Target	Cross-by	Auto	SU Truck	MU Truck	Total	
HAM3343	I-71 (E)	Kennedy Ave	96907	6371	6791	110039	1
WAR0422	I-71 (E)	SR-48	25164	3376	9989	38528	2
WAR0509	I-71 (E)	SR-123	32617	3833	9048	45498	3
WAR0471	I-75 (N)	Central Ave	62956	11445	13943	88344	4
WAR0548	I-75 (N)	SR-63	54975	7265	11432	73671	5
BUT0475	I-75 (S)	Kyles Station Rd	61260	5878	11664	78802	6
BUT0670	I-75 (S)	Union Center Blvd	53124	4347	6245	63715	7
BUT0701	I-75(S)	Cincinnati-Dayton Rd	47391	2996	5776	56164	8
KEN0458	I-71/75(S)	Fifth St	91842	12444	16101	120386	9
HAM2246	I-74-275(W)	I-74	62234	4797	5303	72334	10
CLE0180	I-275(N)	SR-32	66355	2885	1964	71204	11
CLE0211	I-275(S)	SR-125	54706	2412	1868	58987	12
HAM3383	I-74(W)	New Haven Rd	18106	1576	5948	25631	13
HAM0970	SR-126(W)	I-75	51627	2386	580	54593	14
BUT0437	SR-129(W)	SR-747	32603	1901	876	35380	15
BUT0842	SR-129(W)	SR-4 Bypass	22117	1204	469	23790	16
BUT0479	SR-129(W)	I-75	23310	1237	771	25318	17
HAM2022	Norwood Lateral (E)	I-75	63692	4099	1510	69301	18
HAM3818	Lebanon Rd (US-42) (S)	Cottingham Dr	25565	1110	331	27006	19
HAM3408	Winton Rd (S)	Fleming Rd	32653	1115	279	34048	20

Note: * - Data from OKI.

** - Vehicle types following ODOT: Auto - 4-axial passenger cars; SU Truck - Single unit truck; and MU truck - multi-unit truck.

4.1.3. Urban form and air quality

The monocentric urban form in Cincinnati is facilitated by the transportation system and water services. This urban form and its environmental impacts are shown by ambient air quality variations within the urban area and in the exurban regions. From Liang (2014), the spatial correlation and inferred role of the urban form are evident:

- from the analysis of the decade-long measurements of particulate matter with aerodynamic diameter $<2.5 \mu\text{m}$ ($\text{PM}_{2.5}$) for 13 U.S. EPA National Ambient Air Quality Standards (NAAQS) monitoring stations, and
- from quantitative modeling of black carbon dispersion experiment for 10 days (October 6 to October 15, 2010) at the road site of northern highway I-75.

Figure 2-21 shows locations of the 10-day experimental study and the 15 NAAQS stations in areas of distinct land use types. Station 17-061-0040 in the high-density urbanized zone at the center of the Cincinnati metropolitan area is the reference station for analysis of spatial relationships between the urban heat island, ambient air temperature and quality variations. Table 2-6 lists the statistics of ambient temperature and $\text{PM}_{2.5}$ measurements at the reference station 17-061-0040 for 10.5 years. The yearly temperature and $\text{PM}_{2.5}$ mean have a large standard deviation and a large range. The yearly minimum to maximum occurred in the winter and summer season, respectively. Frequency distribution of $\text{PM}_{2.5}$ concentration measurements are asymmetric, with a bias toward small concentrations (Kurtosis = 2.21 and Skewness > 1; see Table 2-6). Ambient temperature is evenly distributed across the date range.

Table 2-6 Statistics of daily temperature measurements at NQAAS Station 17-061-00040.

Statistics	T_{AVG} (°C)	T_{MIN} (°C)	T_{MAX} (°C)	ΔT (°C)	$\text{PM}_{2.5}$ (mg/m ³)
Mean	14.22	9.20	20.09	10.88	13.89
Standard Deviation	10.17	9.66	11.14	3.83	7.27
Kurtosis	-0.91	-0.84	-0.90	-0.51	2.21
Skewness	-0.35	-0.32	-0.35	-0.03	1.25
Minimum	-15.2	-20.4	-10.2	1.1	1.2
Maximum	34.3	27.4	42.1	22.8	52.1
Count	1661	1458	1458	1457	1717

Note: Raw data obtained from EPA NAAQS monitoring network.

Temperature and $\text{PM}_{2.5}$ measurement data for the period 1999-2014 were analyzed using ordinary linear regression between a station (C_i) and the reference station 17-061-0040 (C_{ref}):

$$C_i = \alpha_i C_{\text{ref}} + \epsilon_i \quad (2.1)$$

Despite the large seasonal variations, the daily temperatures and PM_{2.5} concentrations are correlated among the 15 NAAQS stations. Based on Eq.2.1, the correlations between the reference station and all others in the area are obtained from regression for four temperature parameters (daily maximum, daily minimum, daily average, and diurnal temperature range) and PM_{2.5} concentrations. The obtained slope (α_i) and intercept (ϵ_i) from the highly correlated variations ($R^2 \sim 0.99$) are statistically significant (See Liang, 2014). Departure from 1:1 relationship indicate atmospheric differences among stations rather than measurement errors.

4.1.4. Thermal inversion and mixing height

Liang and Keener (2015) analyzed atmospheric sounding data from NOAA/NESDIS⁹, and constructed atmospheric temperature profiles using the method by Ma et al. (1999). Two satellites, GOES-8 and GOES-9, equipped with filter wheel radiometers, were collecting measurements of radiance from the on-board thermal infrared channels, while allowing retrieval of the atmospheric temperature and moisture profiles. The data were retrieved at a 10-km spatial grid and at hourly intervals for sounding data locations S-1 to S-4 shown in Figure 2-21.

Figure 2-25 shows a typical diurnal atmospheric profile in the Cincinnati metropolitan region. The tropopause layer separates the turbulent troposphere from the temperature-inverted laminar stratosphere above. It is important to note the urban boundary layer, where a nocturnal temperature inversion is evident¹⁰. At this location (39°14'43", -84°26'46"), thermal inversion in the surface boundary layer reached its maximum in early morning, followed by inversion destruction and then the recovery to normal lapse rate at a slightly stable boundary layer (SBL) in the early afternoon. The daytime lapse rate returned to a level of neutral stability close to the dry adiabatic lapse rate (DALR) at 9.8 °C/km (Figure 2-25). The nocturnal

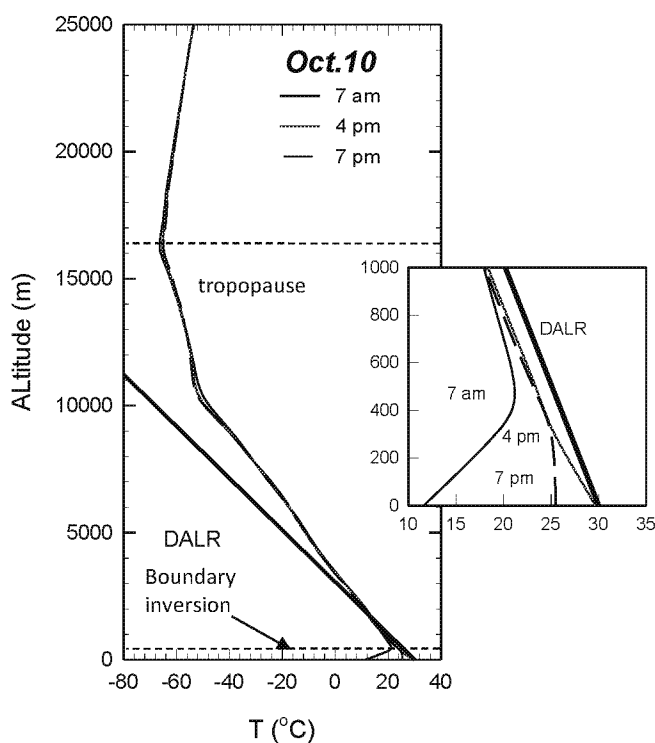


Figure 2-25 Representative temperature profiles showing the boundary inversion and capping inversion. Temperature data were obtained from NOAA for the northern Cincinnati site. Altitude 0 is set at surface elevation. DALR is the atmospheric dry adiabatic lapse rate. From Liang and Keener (2015).

⁹ <http://www.star.nesdis.noaa.gov/smcd/opdb/goes/soundings/skewt23L/html/skewhome.html>

¹⁰ Lapse rate is defined as the gradient of temperature change per unit distance from ground surface.

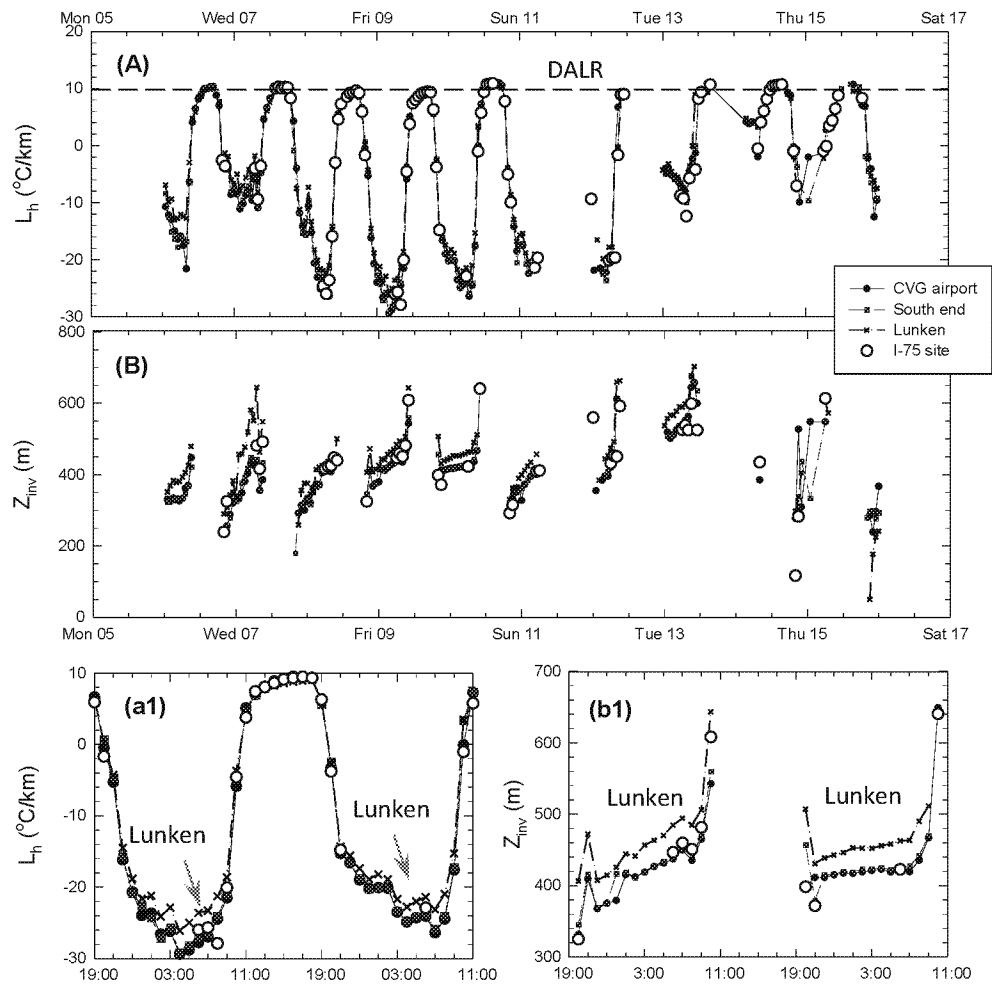


Figure 2-26 Temporal L_R and H_{inv} variations showing diurnal thermal inversion in the urban boundary layer in October 2011. The inserts (a1) and (b1) show the observed difference of hourly variation among the sounding sites in the period of October 9-10. From Liang (2014).

temperature inversion was re-established by the late evening. This diurnal variation is evident for all radio sounding locations S-1 to S-4. From the temperature profiles, the lapse rate (L_h) and mixing height (Z_{inv}) were determined for each day.

The determined L_h and Z_{inv} values in a 10-day period of October 2010 are shown in Figure 2-26. It is clear that a sequential occurrence of nocturnal thermal inversion with the strongest phase in days of October 7-12. Changes in temperature gradients in altitude became gradual in the tropopause. The lapse rate in daytime returned to a level of neutral stability close to neutral DALR of 9.8 °C/km. In all cases, the near-surface boundary layer above the urban canopy marks the extent to which thermal and mechanical mixing occurs. The near-surface boundary layer had a thickness of 421-607 m and the thermal inversion reached a maximum strength with a lapse rate of -29.2 °C/km at 4 am on October 9.

The difference in the slope is statistically significant, reflecting the inversion strength in the peak inversion phase. This physical interpretation implies weaker thermal inversion at

Lunken airport as shown in the temporal profiles. The Lunken airport is located outside of the high-density urban interior in the exurban region.

4.1.5. Urban and exurban differences

Thermal inversion development in the region had similar overall diurnal L_h and Z_{inv} variability across the urban scale. However, a small difference exists, reflecting the effects of urban land uses. In Figure 2-26, the measured inverse lapse rates are lower at Lunken airport compared to the other locations inside of the high-density urbanized area. Liang (2014) further showed the difference was persistent based on linear correlations of L_h values at different locations. The S-2 station at the southern end of the high-density urbanized zone is highly correlated in lapse rate with other stations (S-1, S-3 and S-4). The correlation slope is around 1.0 with $p < 0.0001$, and is < 1 at 0.910 ± 0.009 for the Lunken airport.

4.1.6. Urban form effects on urban heat island and air quality

4.1.6.1 Long-term changes in the urban center

The unique structure of urban boundary layer has been related to urban heat island effect and air quality (Rotach et al., 2005; Liang et al., 2013; Trompetter et al., 2013; Wang et al., 2012). This relationship is evident in the long-term ambient temperature and $PM_{2.5}$ concentration from 1999 to 2013 for the reference station 17-061-0040 in urban center of the Cincinnati metropolitan area.

For the 1457 daily measurements collected in the reference station, the daily T_{max} and T_{avg} values show no statistically significant change over time, while long-term changes in T_{min} and ΔT can be evidently identified amid the noise of seasonal variations using the so-called continued wavelet transformation (CWT) techniques. At a data noise threshold $db=0.80$, wavelet-denoising (Torre and Compo, 1998; Farge, 1992) to T_{min} and ΔT raw data captured nearly 80% of the variation in Figure 2-27. Wavelet-transformed T_{min} and ΔT maxima occurred in May-June of each year, and the minima in the winter period. The seasonal cyclic variation is the most prominent.

These temperature highs and lows after denoise shows an increase of ~ 1.6 and ~ 2.1 °C over 10 years, respectively, by linear regression (Figure 2-28). These long-term changes correspond to night-time maximum and minimum temperature, respectively, in the summer and winter seasons. Because of the increase in night-time temperature, diurnal temperature range ΔT decreased by 1.2 °C over a decade (Figure 2-28). These long-term changes are consistent with the other publications on urban microclimate (Rebtez, 2001; Wang et al., 2012; Braganza et al., 2004).

4.1.6.2 Urban-wide co-variations in temperature and $PM_{2.5}$

- **Ambient temperature**

The urban heat island (UHI) effect in the greater Cincinnati area is shown by ambient temperature measurements. Ambient temperatures measurements for each year are correlated among stations, and the slope of correlation shows quantitatively the difference in temperature across the region.

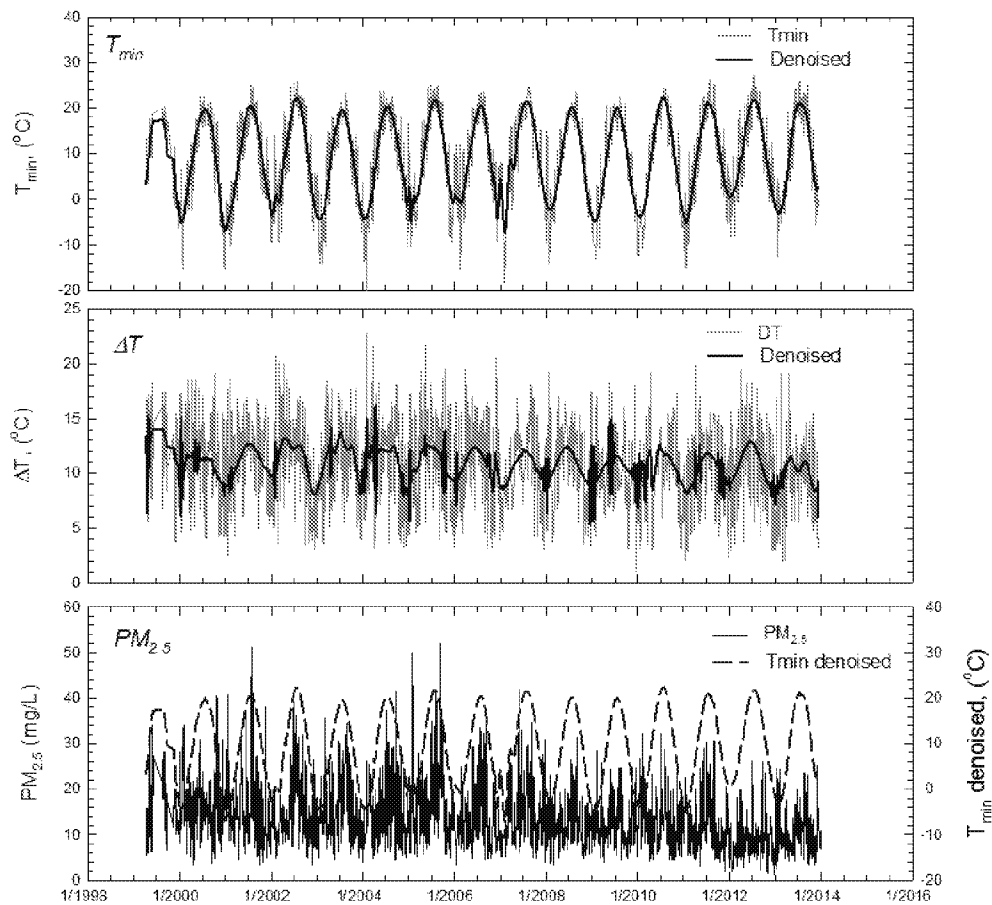


Figure 2-27 T_{min} , ΔT , and $PM_{2.5}$ variations with time at NAAQS monitoring station 061-0040. After wavelet denoise, the seasonal variations are shown in heavy lines.

Figure 2-29 shows the strong linear correlation between the reference station 17-061-0040 at the urban core and other stations. Average value of square coefficient of correlation (R^2) for the 91 to 116 station-year correlations is >0.993 (0.941-0.999). Because the data covers a 10.4-year long period and for all seasons, the strong linear correlation indicates an effective and time-persistent urban-scale heat flux and air circulation above the canopy layer.

Based on the correlation, the temperature difference at the site station and the reference station in the urban core can be calculated for the decade-long measurements. The results are presented in Table 2-7. Apparently, the calculated T' values are correlated to the delineated urban land use, showing quantifiable and statistically significant UHI effects coincide with high-density urbanized zones.

In cross-section A-A' (Figure 2-21), annual mean T'_{avg} and the summer T'_{avg} are plotted in distance across the high-density zone (Figure 2-30). Also plotted for comparison are the relative differences of $PM_{2.5}$ concentrations. It is obvious that ambient temperatures above the urban canopy layer are consistently higher inside the high-density zone than in the surrounding areas (Figure 2-30). For three stations outside of the zone, annual mean T'_{avg} and

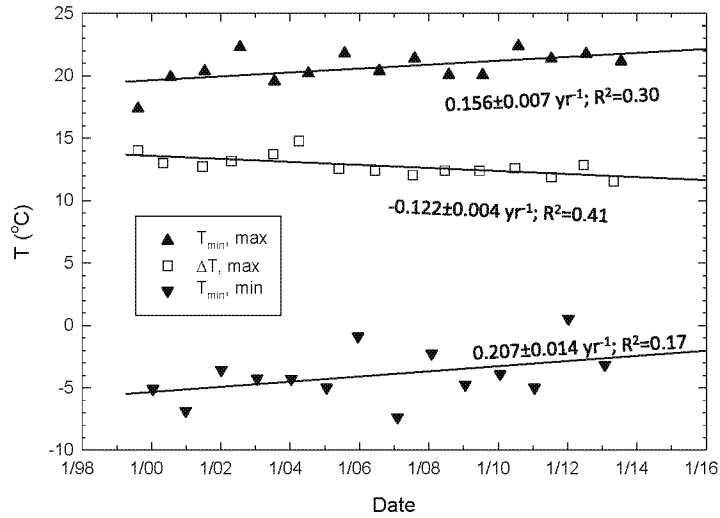


Figure 2-28 Change of ambient temperature T_{min} and ΔT at station 061-0040 in the central urban interior. The regression slopes are statistically significant with $p < 0.0001$. Adopted from Liang (2014).

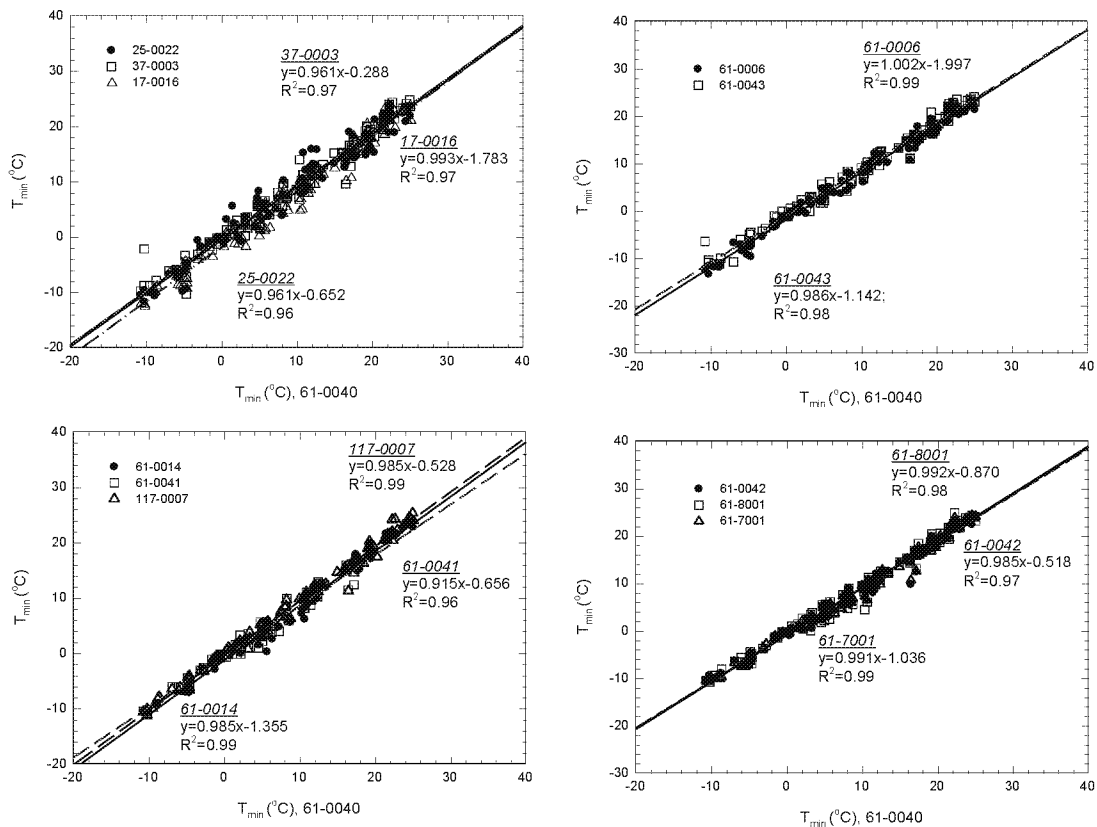


Figure 2-29 T_{min} at 17-061-0040 station is linearly correlated with those of other stations in the 2005 measurements.

Table 2-7 Temperature differences between the reference station and other stations abstracted from the >10-year daily temperature measurements.

Station	Annual Mean			Winter			Summer		
	T' _{AVG} (°C) 14.22	T' _{min} (°C) 9.30	T' _{max} (°C) 20.09	T' _{AVG} (°C) -15.20	T' _{min} (°C) -20.40	T' _{max} (°C) -10.20	T' _{AVG} (°C) 34.3	T' _{min} (°C) 27.4	T' _{max} (°C) 42.1
39-061-0006	-0.79 ± 0.45	-1.82 ± 0.20	-1.52 ± 0.19	-1.17 ± 0.93	-2.50 ± 0.65	-1.19 ± 0.87	-0.53 ± 0.82	-1.40 ± 0.72	-1.76 ± 0.96
39-061-0010*	-1.05 ± 0.22	NA	NA	-0.67 ± 0.74	NA	NA	-1.31 ± 0.78	NA	NA
21-037-3002 [#]	-0.58 ± 0.48	-1.18 ± 0.82	-0.34 ± 0.54	0.06 ± 0.90	-1.15 ± 1.06	0.64 ± 1.11	-1.03 ± 0.91	-1.19 ± 1.07	-1.05 ± 1.09
21-117-0007	-0.25 ± 0.38	-0.33 ± 0.42	-0.58 ± 0.54	0.08 ± 0.47	-0.33 ± 0.63	0.48 ± 0.75	-0.48 ± 0.74	-0.32 ± 0.91	-1.34 ± 0.99
39-025-0022*	-0.82 ± 0.65	-1.40 ± 0.51	-0.37 ± 0.36	0.11 ± 0.85	-0.50 ± 1.05	0.80 ± 1.65	-1.46 ± 0.86	-1.95 ± 0.19	-1.22 ± 0.57
39-017-0016	0.39 ± 0.54	0.91 ± 0.64	-0.61 ± 0.87	-0.16 ± 0.88	0.22 ± 1.27	-0.90 ± 0.86	0.77 ± 0.60	1.33 ± 0.81	-0.40 ± 1.02
39-061-0014	-0.28 ± 0.58	-0.69 ± 0.65	0.02 ± 0.69	0.17 ± 0.87	0.16 ± 1.34	1.13 ± 2.19	-0.58 ± 0.77	-1.21 ± 0.74	-0.78 ± 0.94
39-061-8001	-0.05 ± 0.31	-0.31 ± 0.43	-0.18 ± 0.51	0.18 ± 0.61	-0.12 ± 0.53	0.51 ± 0.46	-0.21 ± 0.64	-0.43 ± 0.69	-0.68 ± 0.75
39-061-7001	-0.22 ± 0.52	-0.39 ± 0.41	-0.36 ± 0.70	0.29 ± 0.71	0.25 ± 0.86	1.54 ± 3.29	-0.57 ± 0.77	-0.78 ± 0.49	-1.73 ± 1.55
39-061-0041 [#]	-0.48 ± 0.38	-1.04 ± 0.41	-0.38 ± 0.41	0.38 ± 0.46	-0.24 ± 0.84	0.41 ± 0.49	-1.07 ± 0.80	-1.52 ± 1.12	-0.95 ± 0.63
39-061-0043	-0.36 ± 0.42	-0.60 ± 0.46	-0.14 ± 0.58	0.05 ± 0.69	-0.32 ± 0.91	0.26 ± 0.62	-0.63 ± 0.65	-0.77 ± 0.65	-0.43 ± 0.82
21-037-0003*	-0.79 ± 0.93	-0.86 ± 1.08	-0.77 ± 0.60	0.81 ± 0.71	0.08 ± 0.82	1.20 ± 0.53	-1.88 ± 1.18	-1.43 ± 1.36	-2.20 ± 0.92
39-061-0042	0.11 ± 0.57	-0.03 ± 0.71	-0.11 ± 0.79	0.84 ± 0.88	0.95 ± 1.49	0.98 ± 0.76	-0.39 ± 0.79	-0.63 ± 0.70	-0.90 ± 0.94

Note: * Stations are outside of the high-density urban area.

Stations are outside but near the high-density urban area.

NA - Data not available.

the largest T'_{avg} in summer are lower by 0.89 ± 0.14 °C and 1.55 ± 0.30 °C, respectively. The largest $\Delta T'$ also occurred in summer when highest night-time $T_{min}=27.4$ °C and highest day-time $T_{max}=42.1$ °C were measured in 17-061-0040 station. The average $\Delta T'_{min}$ and $\Delta T'_{max}$ were -1.69 °C and -1.71 °C. In contrast, temperatures are relatively uniform inside of the high-density zone. The mean T'_{avg} is $-0.09(\pm 0.27)$ °C. From its southern tip at station 037-3002 (See Figure 2-21), the annual mean T'_{avg} increases slightly toward station 061-0040 in the urban core. The difference in summer T'_{avg} is greater for a two-fold increase to -1.03 °C.

- *PM_{2.5} variability*

Like ambient temperature, the observed PM_{2.5} concentrations are linearly correlated between the reference station 39-061-0040 and all other stations (Liang, 2014). The correlation is persistent for all years of measurements at sampling height above the urban canopy layer. This correlation covers all PM_{2.5} concentration range of 1.2-52.1 mg/m³

($\bar{m}=13.89$, N=1717) (See Table 2-6). The high degree of linear correlation among the stations is significant for the long duration of monitoring. The correlation coefficient (R^2) for the 130 station-year correlations ranges 0.53-0.99 with an average of 0.92. Almost 92% PM_{2.5} variability can be explained by urban-wide correlation. Similar conclusions on small area-wide PM_{2.5} variations were made by Martuzevicius et al. (2005) using hourly monitoring data, instead of daily, of the 13 NAAQS network stations in the Cincinnati area.

These intra-station correlations, both in temperature and PM_{2.5}, strongly suggest atmospheric mixing and mass communication at station's sampling height above the roughness boundary layer. Below the layer, the urban heat island effect is evident at the urban core along with the air quality variations.

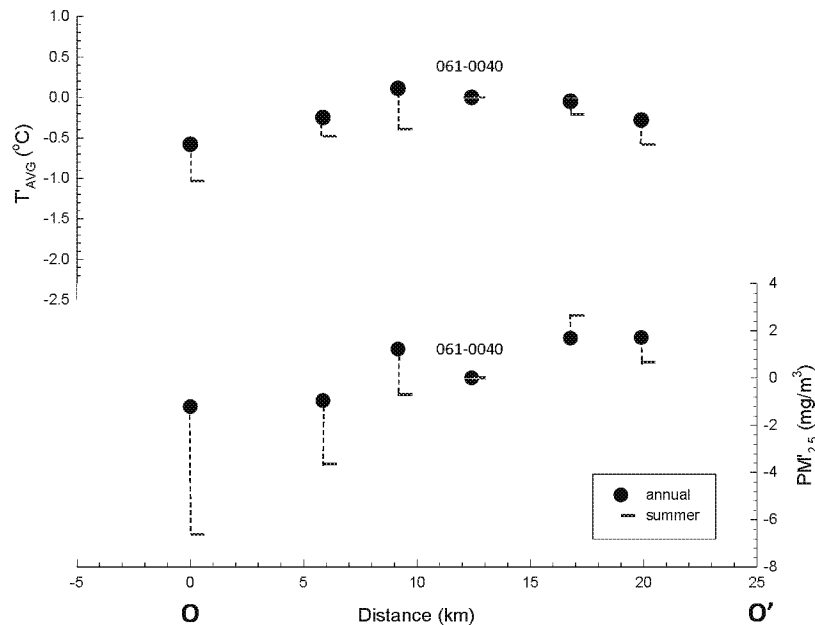


Figure 2-30 Spatial variations of temperature difference for mean and maximum T_{avg} and PM_{2.5} in cross section O-O'. The profile starting point a is station 037-3002 at southern tip of the high-density zone. See Figure 2-21 for the cross-section locations.

4.1.6.3. Thermal inversion and wind conditions

The frequent and high-strength thermal inversion in the Cincinnati metropolitan area is linked to the weakened wind field and air qualities. Liang et al (2013) reported the weak to stagnant wind conditions in early morning hours, and an associated high black carbon concentration, high ratio of organic carbon (OC) over elemental carbon (EC) concentration, at near-ground levels at the I-75 highway in the high-density urbanized zone in northern Cincinnati. The location of the study is shown in Figure 2-21.

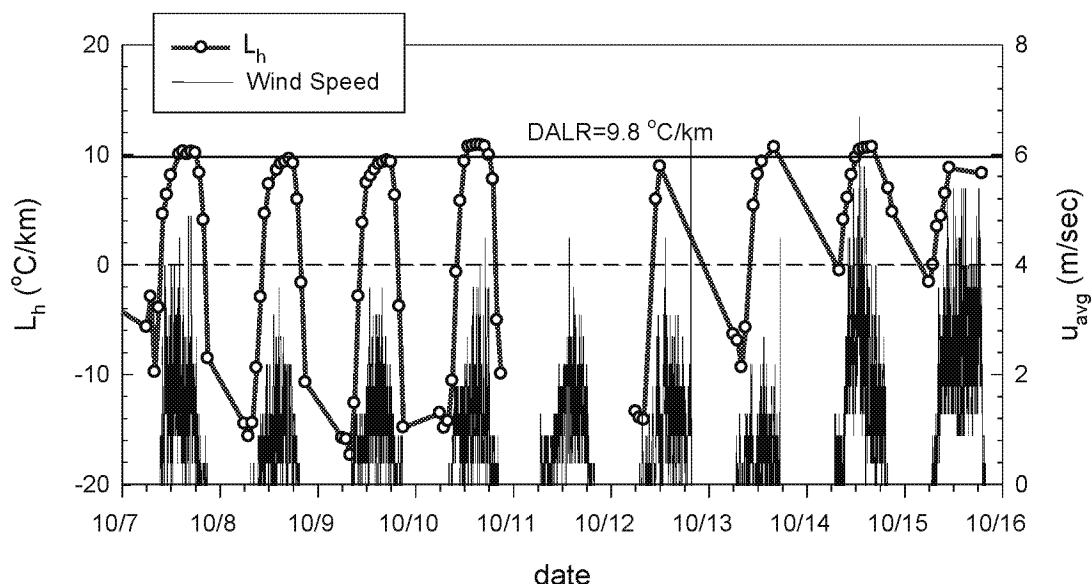


Figure 2-31 Co-variation of minutely average wind speed at the I-75 site with the lapse rate in the boundary layer during the roadside black carbon dispersion experiments. U_{avg} is the hourly average wind speed.

The co-variation between field-observed wind speed and the determined temperature lapse rate (L_h) is shown in Figure 2-31. Here L_h quantitatively measures the inversion strength; the SBL, weak SBL, and very weak SBL correspond to L_h of 5 to -15, 5-10 °C/km, and <15 °C/km, respectively. Clearly, the weak SBL in October 14-15 corresponds to the highest wind speed at 1.47-2.6 m/s measured in the field study of Liang et al. (2013). The high winds and convection lead to low OC and EC concentrations, a low OC/EC ratio around 1.272.

The very weak SBL, with $L_h < -15$ °C/km, was pronounced at the beginning of the experimental period, notably in the early morning of October 7-13 before 8:28-9:10 am. The lapse rate L_h was < -10 °C/km, and the inversion reached a maximum strength at -29.2 °C/km at 4 am on October 9. Strong thermal inversion in this phase was non-stationary and induced downward thermal flux due to radiative urban cooling (Martilli et al., 2002; Uno et al., 1988, 1989; Iziomon et al., 2003). As a result, a near-surface non-Gaussian transport mechanism such as meandering (Cooper et al., 2006; Guzman-Torres et al., 2009) could have happened for which the similarity theory cannot be applied (Uno et al., 1989). This relationship among black carbon (and other pollutants) concentrations, weak wind speed, and the thermal inversion has been observed in numerous field studies worldwide (Trompetter et al., 2013; Uno et al., 1988; Guzman-Torres et al., 2009; Kumar et al., 2012).

4.1.6.4. UHI formation and spatial variations

The weak wind condition is associated with weak atmospheric circulation in the urban area, a condition that is marked by high nighttime temperature or greater degree of UHI effects. The hilly topography in Cincinnati metropolitan area has a small relief $< \sim 50\text{m}$ except for along the Ohio River banks and Mill Creek valley (See Figure 2-21). Such general geographic feature may permit the occurrence of thermal inversion that Clarke (1969) proposed for the Mill Creek valley west of the downtown. Similar topography-induced inversion was characterized in later studies, notably by Fernando (2010) who noted that the thermal and gravity-induced upslope and downslope flow are needed to produce nocturnal inversion in a complex terrain. For areas with a gentler topographic slope, other possible mechanism is more likely. It involves of UHI-induced thermal flux and horizontal air movement. Upward sensible heat flux and air aloof from warmer urban interior may induce movement of colder air masses from surrounding rural areas, leading to evening urban breeze, colder air at ground surface, and hence the concurrence of UHI and thermal inversion (Rotach et al., 2005; Rendón et al., 2014; Hidalgo et al., 2010). Temperature condition for this UHI formation was observed in the higher night-time temperature T'_{min} , in the high-density urban zone (See Table 2-7).

The UHI effect and temperature variation are not uniform across the metropolitan area. They depend on land use and land covers, and ultimately, the urban form. Similar conclusions were made by several studies on detailed thermal mapping of the UHI effects (e.g., Liu et al., 2012; Buyadi et al., 2013). As shown in this case study, the high-density urbanized zone is accompanied by a rise of ambient daily temperature by $0.89\text{--}1.55\text{ }^{\circ}\text{C}$. Night-time temperature increase is larger at $\sim 1.7\text{ }^{\circ}\text{C}$. While the increase closely follows high-density zone boundary in cross section A-A', the N-S elongated high-density zone has a varying width and is found having different degree of UHI effects. Temperature increase is the largest in the Cincinnati downtown area, around stations 37-061-0040 and 37-061-0042. The increases reduce in the north, where the high-density zone narrows, and nearly disappear in the southern tip at station 21-037-3002.

The trend is further testified by a negligible small temperature increase in three stations in residential area outside of the high-density zone but within the perimeters of Cincinnati metropolitan area. Daily average T'_{avg} is much lower than in the high-density zone. Similarly, station 37-061-0006 located in a small and isolated high-density urban area along I-71 has temperatures close to that of three exurban stations. As shown in Figure 2-23, these residential areas are characteristic of detached single house with large trees, a large yard and acres of natural area in between. This type of suburban region with less UHI effect was common for over 38 U.S. urban centers that Imhoff et al (2010) studied using LANDSAT satellite imagery data.

It is worthy to note that UHI effects measured by this study are much smaller than one derived using the empirical formulation of Oke (1976 and references therein). Based on the formula, the Cincinnati metropolitan area of ~ 2.1 million population would yield a $4.91\text{ }^{\circ}\text{C}$ temperature increase. It is likely that the majority of the Cincinnati area is typical of the medium to low density suburban areas in the new urban climate zone classification of Oke (2006). The urban formation, use of green space, and the elongated narrow shape of the high-density zone may contribute to the less UHI effect. Thus, the UHI effects and spatial variations are closely related to urban form and can respond to urban adaptation measures.

4.1.6.5. Adaptation and potential effects

Urban-scale occurrence of UHI phenomenon affects both air pollutant transport and water demand. The planning of high-density urbanized area and green spaces can result in different degrees of UHI and atmospheric circulation in the boundary layer. Such analysis is location-specific, but the studies in the Cincinnati metropolitan area indicate the potential of adaptation co-benefit effects in the following two areas.

- *Air pollutant transport*

The meso-scale UHI and thermal inversion occurrence, as discussed in this case study, are the causes for diurnal and seasonal variations in urban-wide temperature and PM_{2.5} concentrations above the urban canopy layer. These factors also affect daily variability of pollutants within the urban canopy layer. For the latter, U.S. EPA has published a series of guidelines on such assessments (U.S. EPA, 2013a, 2004). Investigations reported in literature call for a range of adaptation actions such as the use of tree barriers (e.g., Baldauf et al., 2008).

On the micro-scale, the Cincinnati case study shows that the urban form and its physical structure configurations can affect urban climate conditions and, thus, the air pollutant transport. Figure 2-32 illustrates three typical types of canopy layer settings that affect near-ground pollutant distribution. These include the open-field setting at the highway I-75 site, the street canyons among the low- and high-rise buildings of urban interior, and lastly, residential areas with significant tree canopy effects. Among the three types, highway roads in open fields are most common in the Cincinnati metropolitan area. Both the UHI and particulate pollution are impacted by the canopy, transportation infrastructure, vehicle numbers and emission rates.

- *The UHI and controlling factors*

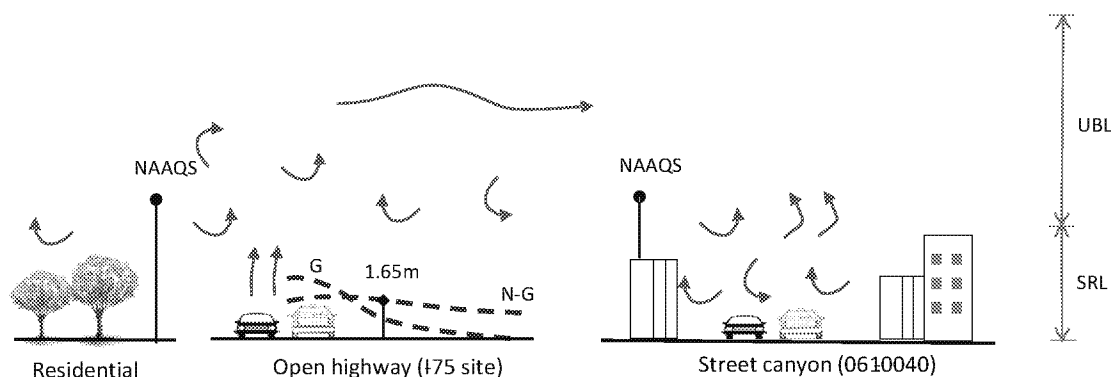


Figure 2-32 Schematic diagram showing major types of microclimate conditions in the surface roughness layer (SRL) equivalent to the urban canopy layer (UCL). The NAAQS stations above the UCL are affected by urban boundary layer (UBL) circulations. Other symbols: G – Gaussian dispersion, NG – Non-Gaussian dispersion. Modified from Liang and Keener (2015).

The high-density urbanized zone along the I-75 and Mill Creek has many properties of UHI effects: night-time temperature increased by ~1.7 °C compared to exurban areas; a long-term night temperature increased by 2.0 °C over a decade; and a higher PM_{2.5} concentration occurred above the urban canopy layer. The UHI effect is much less in the low density suburban residential area and apparently reduced by the presence of forested natural areas. In addition, the

UHI formation enhances thermal inversions through the urban-rural air flows and reduces urban-wide circulations.

The city-wide thermal effects of UHI occurrence can also affect water consumption, and thus water demand variations in space and seasons. The exact dependence on water consumption in the urban area is not quantified in the case study. It is generally understood that the higher daily temperature and smaller diurnal temperature ΔT result in changes in evapotranspiration in lawns and vegetation along with the increase of residential water usage, particularly in the summer season. In the literature (e.g., Guhathakurta and Gober, 2007), the thermal inversion, weak winds, and associated UHI formation have been reported to cause greater water consumption per capita.

Nevertheless, this case study shows the impacts of urban form on UHI and related atmospheric conditions. Major factors in urban transformation include spatial continuity of high-density areas with gray infrastructure (e.g., concrete pavements), green space, forest and native land coverage, non-continuous multi-centers, even tree canopy barrier that help modify the interactions between the urban canopy and the overlying urban boundary layer.

4.2. Adaptive urban planning modeling and analysis in Cincinnati

Based on actual measurements, the preceding section 4.1 on the Cincinnati case study shows the urban form, its effects on air quality, UHI formation, and population distributions. On this basis, the goal of this section is to outline how adaptive urban planning can be applied for the future development scenarios. The Cincinnati metropolitan area appears to be following other U.S. very large metropolitan areas with its development trajectories, including downtown revitalization, infill developments, Ohio River bank development, and a series of land use policies to improve the urban efficiency including transportation and initiatives like the street car system. These policy initiatives have changed the population and urban activity distribution, a change that, when coordinated in planning, can positively affect the water and transportation infrastructure planning and operation.

4.2.1 Three development scenarios

This scenario-based adaptive planning for the Cincinnati metropolitan area was conducted to assess development options in the form of land use changes, and the downstream effects on transportation performance and benefits in carbon emissions. Through this example, the step-by-step process will be illustrated for using the AIR-SUSTAIN tool in adaptation planning.

Figure 2-33 shows the distribution of population, household, and employment in the metropolitan area. It is noteworthy that the classic monocentric urban form is starting to evolve into multi-centers of employment, with the population and households scattered and distributed across the region. The populations distributing along the north-south trending I-71 and I-75 corridors are required to travel toward the employment centers.

To explore the potential future developmental scenarios, three options are explored and analyzed using AIR-SUSTAIN for the Hamilton County, Ohio. The year 2010 is chosen as the base year, and the year 2030 is set as the target year. The three scenarios are:

- The Scenario 1 (S1) is referred to the single center development pattern. The single center is taken to occur in the Downtown and Uptown Cincinnati areas, as shown by Figure 2-34a.
- The Scenario 2 (S2) is referred to the multiple-center development pattern. Two-center development is assumed in this scenario. They are located in the Downtown Cincinnati and Mason area which is located north of the Hamilton County, as shown by Figure 2-34b.
- The scenario 3 (S3) adopts the same development pattern as S2. However, it differs by having two Rapid Bus Transit lines connecting these two centers, as shown in Figure 2-34c.

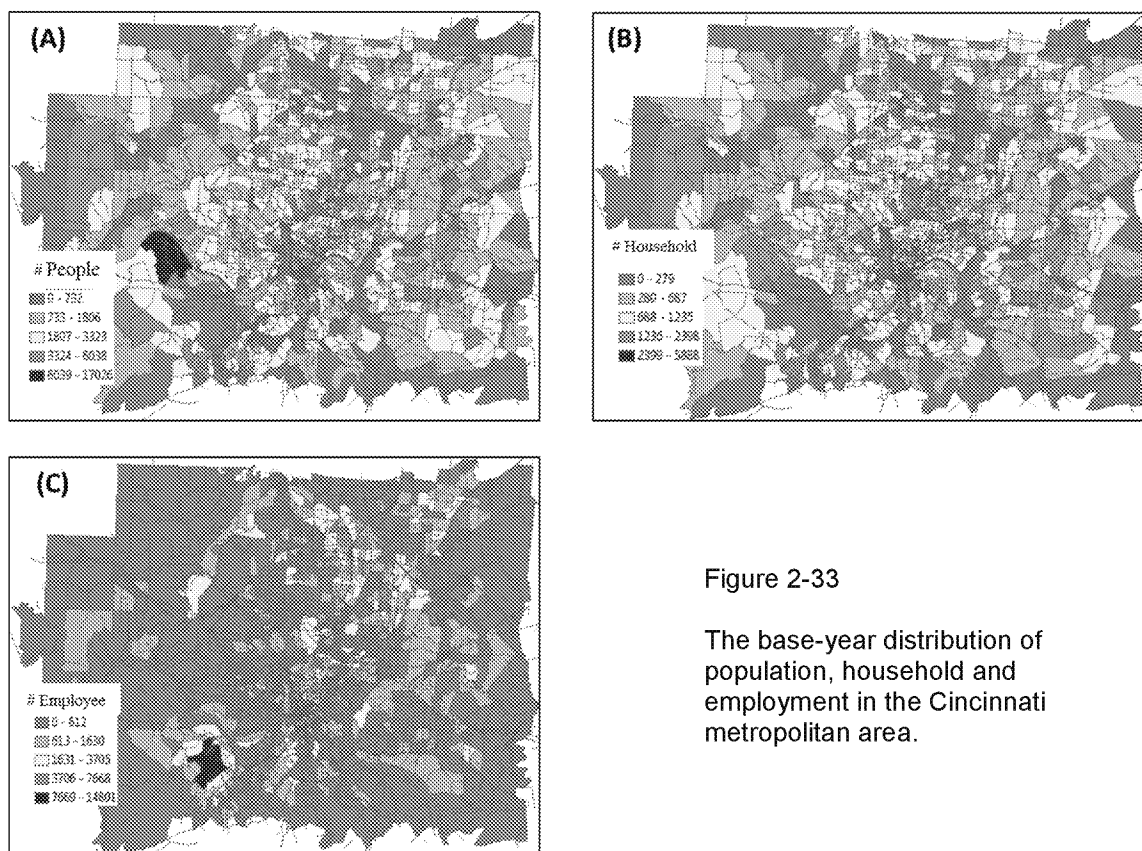


Figure 2-33

The base-year distribution of population, household and employment in the Cincinnati metropolitan area.

4.2.2 *Transportation and emission analysis using AIR-SUSTAIN tool*

The three developmental scenarios in Figure 2-34 were analyzed using AIR-SUSTAIN tool on transportation first; the results can be used later for water infrastructure planning and adaptation. Generally, this type of planning and engineering analysis requires extensive stakeholder engagement, economic analysis, and engineering evaluation. The analysis presented here is intended to show how the AIR-SUSTAIN tool can be used in the scenario-based adaptive planning.

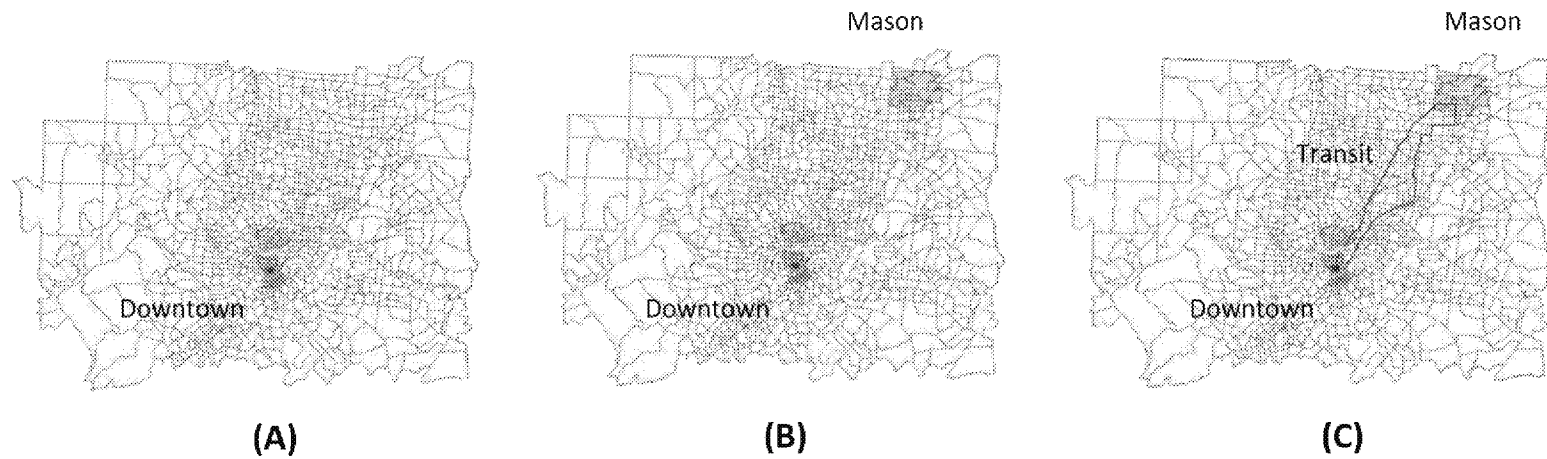


Figure 2-34

Three development scenarios for the Cincinnati metropolitan area in target year 2030. A) monocentric development around the downtown; B) two-center configuration in downtown and Mason area; and C) two-center configuration with mass transit between the centers.

4.2.2.1 The modeling processes

All three competing scenarios assume the same 15% increase of population and employment to occur from the base year to the target year 2030. The increases in population and employment are allocated and distributed around the activity center(s). The process for a scenario analysis was developed through 19 steps from scenario setup (Figure 2-35), regional and project level traffic analysis, to emissions modeling using MOVES to obtain the final simulation results. Details of these simulation steps are contained in Appendix A. Several important modeling steps are discussed in the following paragraphs

After setting up the adaptive planning project, a new scenario is created and saved with specified AIR-SUSTAIN database in MySQL and ArcGIS. Figure 2-36 shows a graphic user interface for the project scenario setup. The subsequent Steps 2-4 specify the existing TAZ, road network, as well as boundaries of the activity centers. The latter is an important element in adaptive urban planning. Activity centers or incentive districts function as the transformation districts important to urban adaptation (Figure 2-6), and by design, introduce changes to the urban form and

Figure 2-35 Setup of a new scenario in AIR-SUSTAIN

Figure 2-36 Program interface for A) importing the Base Year data; B) assigning population change; and C) assigning employment changes at TAZ levels.

associated changes in population and urban activities. The tool has the capability of specifying the changes of population and employment from the base year at the TAZ level. Population Change and Employment Change can be specified for regions inside and outside of the incentive boundaries separately.



scenario, the adaptive planning process is conducted to understand the adaptation needs including:

- Projecting the future trip generation or the “travel need” (Steps 7-10). This analysis is based on scenarios of growth policies in anticipation of future economic status and the conditions specified in the beginning of an urban planning cycle (Figure 2-6).
- Analyzing the transportation consequences with respect to air emissions (Steps in 11-13) and in hotspot occurrence (Step 14). The simulation provides technical information on traffic vehicle-to-capacity ratio (V/C), occurrence of hotspots, and permits exploration of adaptation solutions. An example of the hotspot analysis in the Cincinnati metropolitan area is shown in Figure 2-38.
- Developing traffic management solutions and estimating the limits of adaptation measures relying on traffic management and limited improvement of existing transportation network. This adaptation analysis (Steps 15-16) relies on the evaluation of infrastructural optimization using the microscopic simulation model VISSUM.
- Evaluating environmental and economic consequences of urban planning scenarios (Steps 17-19). In these steps, the adaptive urban planning is focused on quantitative analysis of carbon emission emissions, transportation performance (traffic delay, fuel consumption, etc.), and economic analysis of adaptive measures.

Hotspots

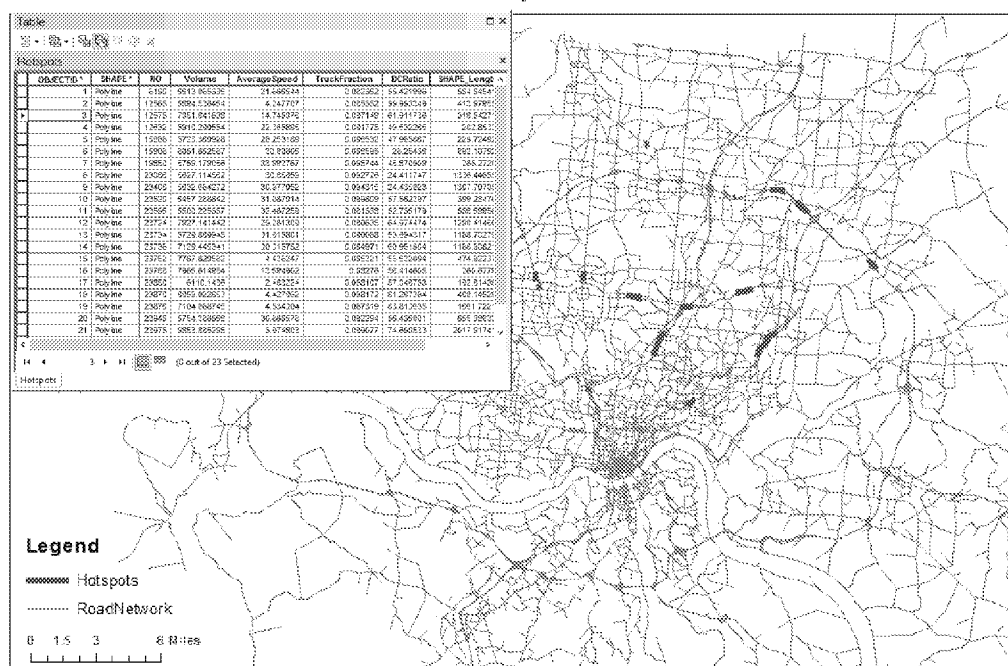


Figure 2-38 Hotspots identified for typical peak-hour traffic for 2009 in Hamilton County, showing concentrations along I-71, I-75, I-275N, and Ronald Reagan highway. Annual traffic data from Ohio-Kentucky-Indiana Council of Governments.

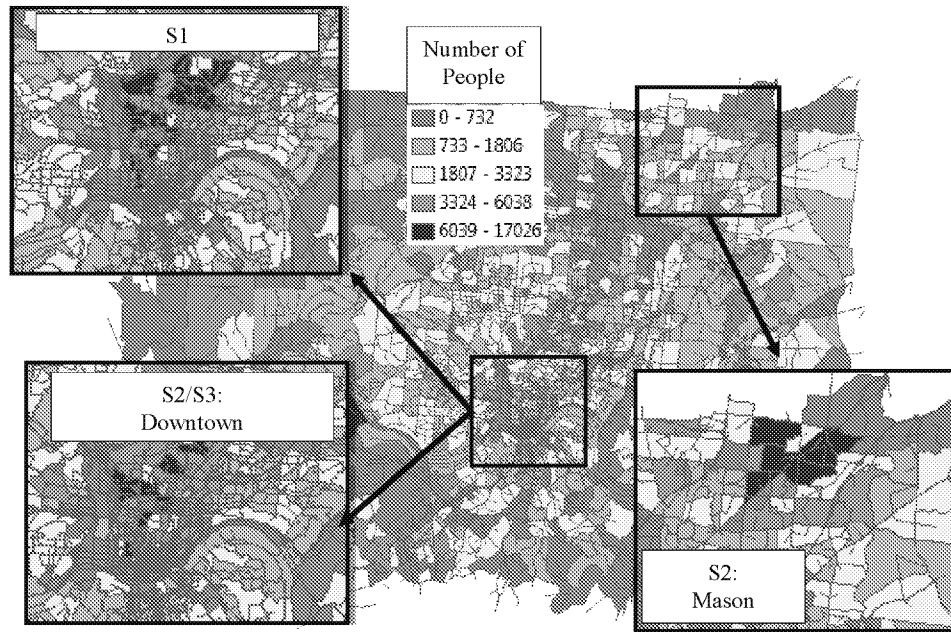


Figure 2-39 Population changes by 2030 for the three developmental scenarios (S1, S2, and S3 in the inserts) in comparison to the distribution of base year 2010 (background). Land boundaries indicate census blocks.

In the last step, the transportation performance is reviewed and evaluated against the master planning or adaptation objectives. The selected developmental scenario is then examined in analysis of the infrastructure adaptation for water supply, wastewater and storm water managements. See AUP&ET process diagram in Figure 2-9.

4.2.2.2 Comparison of future developmental scenarios

The scenario analysis for the Cincinnati metropolitan area forms a quantitative basis to compare the three development scenarios for target year 2030.

1) Demographic and socioeconomic changes

The changes in population, household, and employment from 2010 base year to 2030 target year are illustrated in Figures 2-39, 2-40, and 2-41, respectively. The future population distribution depends on the developmental scenario. For the S1 developmental scenario, all anticipated population growth is allocated in the downtown area. The increase is mostly likely to occur throughout downtown, particularly in the Over-the-Rhine area to the north. In comparison, the changes in downtown are less prominent in S2 and S3 scenarios, because of significant change in the Mason-West Chester region along the northern I-75 and I-71 highways and their connectors (Figure 2-39).

Changes in future household numbers in 2030 are similar to those in population (Figure 2-40). The household number is projected for a largest increase in a number of small downtown TAZs, where only a moderate-high rate of population increase is anticipated. This disparity is found to be related to the smaller households in the downtown area. The intercity re-development policy of the city may also play a role in these changing trends.

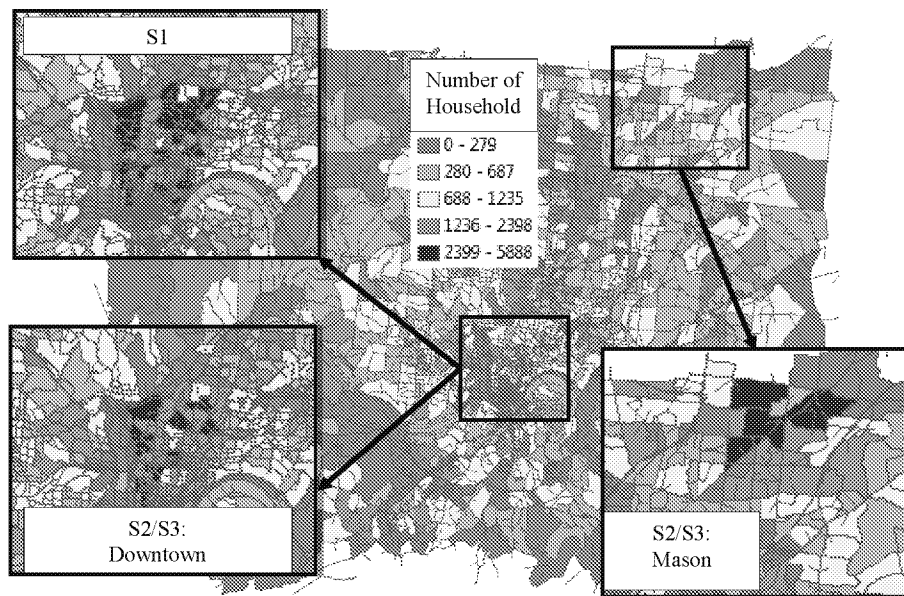


Figure 2-40 Changes in number of household by 2030 for the three developmental scenarios (S1, S2, and S3 in the inserts) in comparison to the distribution of base year 2010 (background). Land boundaries indicate census blocks.

Figure 2-41 shows the employment changes at TAZs. The change shows a large increase in northern Cincinnati (West Chester – Springdale – Mason area), the downtown (river bank, and university hospital area), and in northern Kentucky. These increases are considered reasonable based on the current developmental trends; for example, there are projected increases of

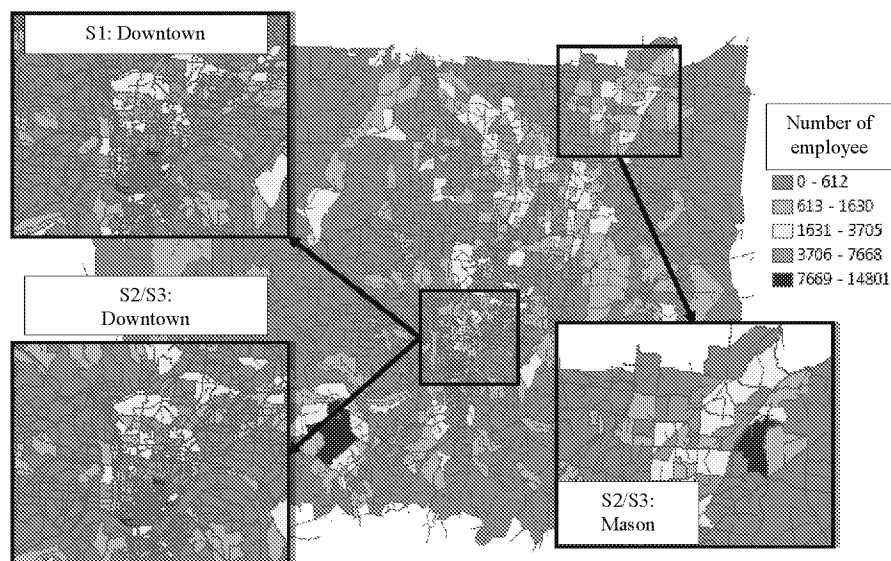


Figure 2-41 Employment changes by 2030 for the three developmental scenarios (S1, S2, and S3 in the inserts) in comparison to the distribution of base year 2010 (background). Land boundaries indicate census blocks.

employment in the River Bank area that has been redeveloped in the past two decades and continues to experience relocation of business operations into the area – an example is the future GE headquarters. It is important, however, that in S2 and S3 developmental scenarios, a large increase in employment is predicted in the Mason area (Figure 2-41).

2) Travel demand forecasting results

The travel demand forecasting results of the three scenarios are illustrated by trip generation (Table 2-8) and trip distribution (Table 2-9). Based on the AIR-SUSTAIN modeling results, there is a ~20% increase in trip generation from the base year (2010) to the target year (2030). This increase is largely due to the assumed population increase of 15%. The trip generation is around 6 million per day for the S1 and S2/S3 scenarios. However, the model projection shows the nature of the trips will change. Comparing the two sets of scenarios, the multi-center configuration in S2/S3 favors HBW with trips within the home TAZs, while the monocentric S1 scenario has a greater number of non-home-based (NHB) trips (Table 2-8).

Table 2-8 Trip generation results in number of trips per day

Daily Trips-	Base Year	S1	S2/S3
HBO	2,237,609	2,795,451	2,802,678
HBSC&HBU	66,635	93,287	93,553
HBW	1,127,146	1,347,873	1,359,091
NHB	1,541,498	1,794,372	1,780,907
Total Trips	4,972,888	6,030,983	6,036,229

Note: HBO – home-based-other trips; HBW – home-based-work trips; NHB – non-home-based trips; HBSC – home-based school trips; HBU – home-based university trips

Table 2-10 summarizes the traffic performance for the three developmental scenarios simulated for year 2030. Average queue length and wait time increases because no expansion of transportation network was assumed for the modeling period (2010-2030). This assumption was used to evaluate the potential roadway infrastructure capacity reserve. The analysis results provide the potential capacity of the existing network as adapted through traffic management tools. For example, for the same queue length, the S3 scenario with mass transit between two future centers reduces the average time by 27.5% or $2.87 - 2.08 = 0.79$ min/link. The average total delay is reduced from 16.1 to 12.0 min/veh/mile for a 25.4% reduction (Table 2-10).

Table 2-9 Trip Distribution results for number of trips per day originated from and attracted to centers*

Daily Trips	Base Year	S1	S2/S3
Intra-center	181,232	398,746	422,073
External	432,667	425,816	435,525
Total	613,899	824,562	857,598

Note: * - Centers are future incentive areas as shown in Figure 2-34.

Table 2-10 Average queue length, average wait time, total delay and average delay during Morning Peak Hours (7:00 ~9:00 am)

Scenario	Base Year	S1	S2	S3
Average queue length (veh per link)	9	12	12	12
Average wait time (min per link)	2.03	2.87	2.56	2.08
Total Delay (veh·h)	113456.4	205121.3	179796.6	153018.4
Average Delay (min/veh)	10.8	16.1	14.1	12.0

Note: Link refers to model road segment in model space.

The improvement by use of the mass transit in the two-center configuration is graphically shown in the traffic volume distribution over the metropolitan's road network (Figure 2-42). Compared to the current condition, the 2030 traffic pattern is characterized by increased traffic along the I-75 and I-71 highways. The traffic around Cincinnati downtown area (I-71, I-75, I-562, and connectors) becomes increasingly heavy in S1 - the concentrated downtown development. The condition improves for the two-center configuration particularly with the development of mass transit.

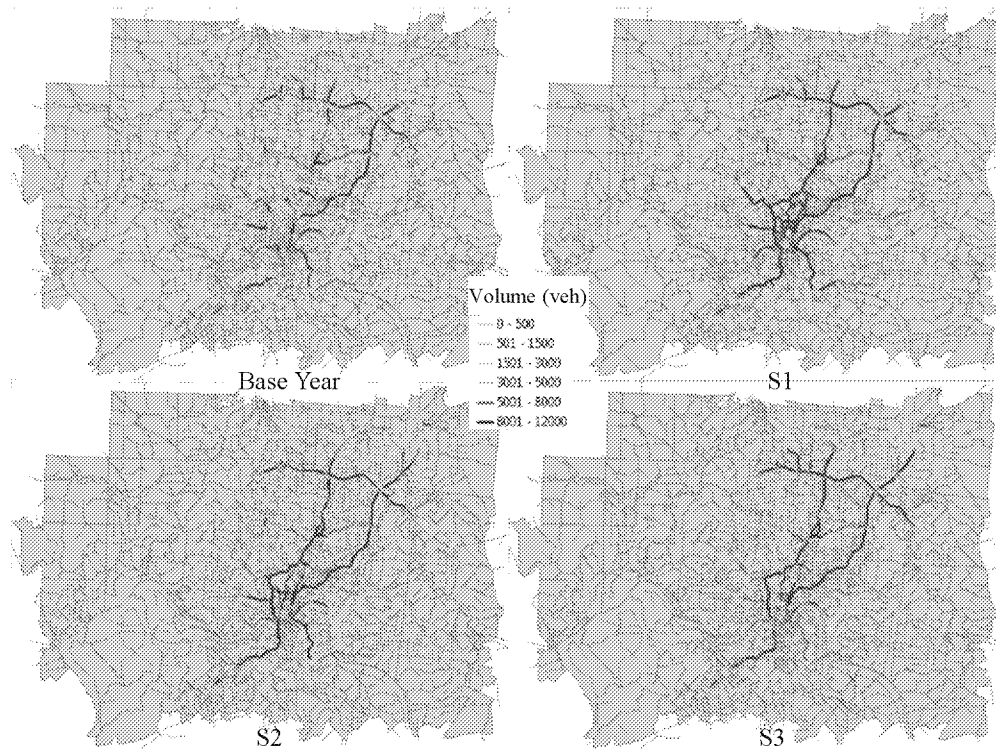


Figure 2-42 Peak hour (7:00-9:00 am) traffic volume distribution over the Cincinnati road network for the base year (2010) and under three target-year (2030) development scenarios.

3) Energy and emission reduction as adaptation co-benefits

The computer-simulated city-wide CO₂ emissions and energy consumption (per day) from transportation are shown in Figure 2-43 for comparison of development scenarios. From the 2010 to 2030, the S1 developmental scenario is projected to have the largest increase in CO₂ emissions and energy or gallons of fuel consumed. These two variables (energy/fuel and emissions) are internally related to each other. The CO₂ emissions would increase by 13.6%. This degree of increase is comparable to and slightly less than 17.5% increase in trip generation (See Table 2-10), mostly due to the higher population and employment in the downtown area. The improvement is attributed to use of the high-density/ “walkable” community development.

Significant improvement in CO₂ emission reductions and energy savings is predicted for the S3 development scenario with two centers and mass transit. The emissions are 15.6% less compared to that in S1 scenario with the monocentric development (Figure 2-43). Transportation efficiency also increases. The average traffic delay per person is 25% less than in the S1 scenario, and only slightly higher than the base year in 2010 (See Table 2-10).

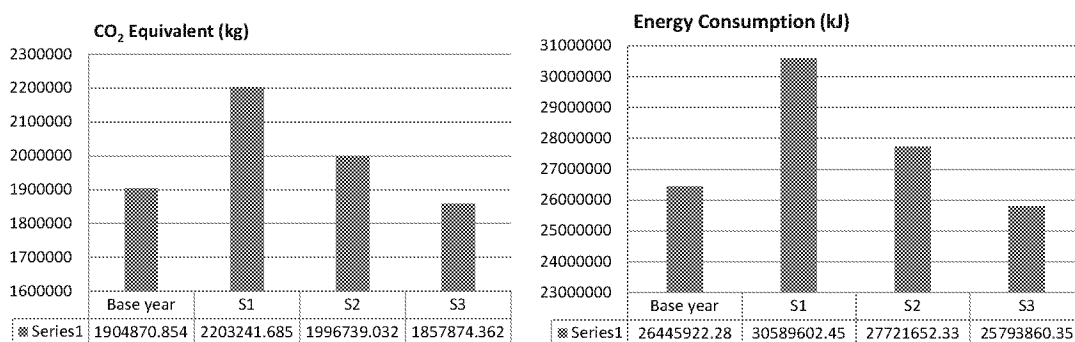


Figure 2-43 Comparison of three development scenarios (S1, S2, and S3) in peak hour (7:00-9:00) vehicular CO₂ emission and energy (fuel) consumptions.

4.2.2.3 Implications on adaptation co-benefits

The case study in the Cincinnati metropolitan area shows the utility of an integrated analysis tool AIR-SUSTAIN for the analysis of urban-scale development scenarios. The holistic interactions among travel demand from population and land use change, demographic and socioeconomic distributions, as well as the transportation activities on road emissions can be quantified to assess the effects of urban infrastructure adaptation policies.

The scenario-based analysis points to the co-benefit of urban adaptation. Adaptive planning for transportation optimization is projected to reduce emissions and, at the same time, improve the urban efficiency. Transportation measures such as mass transit can facilitate the urban form transformation from the current monocentric form to polycentric development. It should be noted, however, that such urban scale adaptation was only analyzed considering land use and transportation. The impacts on water infrastructure and service functions also need a thorough evaluation by which the results may lead to further refinement of the developmental scenarios. This adaptive process is illustrated in the framework in Figure 2-6.

4.3 Adaptation analysis for water master planning in Manatee County, Florida

Following the prior example for adaptive urban planning with a focus on transportation and urban growth, this case study illustrates the use of county/urban-scale water supply adaptation through master planning. The case study was conducted in 2009-2011 for Manatee County in Florida (Figure 2-44). A large growth in population, tourism, and economic development occurred in the past two decades preceding this study. This trend is expected to continue in the future. The combination of increasing water demand, climate-related chronic droughts, and depletion of the Upper Floridian Aquifer as the main source water was the central concerns to local water resource managers who need to provide adequate and sustainable water supplies for the future.

In response to the chronic drought conditions in recent decades, the Southwest Florida Water Management District (SWFWMD) designated the entire western portion of Manatee County as the Most Impacted Area (MIA) and managed it as a part of the Eastern Tampa Bay Water Use Caution Area (WUCA). In May 2008, the Manatee County Board of County Commissioners adopted the Water Supply Facilities Work Plan (Master Plan hereafter) that describes alternative capital improvement options for water resource development. The long-term strategies are documented in the County's master plan.

The adaptation study documented here was designed to analyze the Master Plan options for water supply expansion, and to identify the most feasible and effective adaptation solutions. Life-cycle analysis (LCA) was used to analyze carbon emissions, energy consumption, and cost/cash flows by systematically considering each phase of planning, design, construction and operation. Both the existing and planned new water infrastructure facilities were considered.

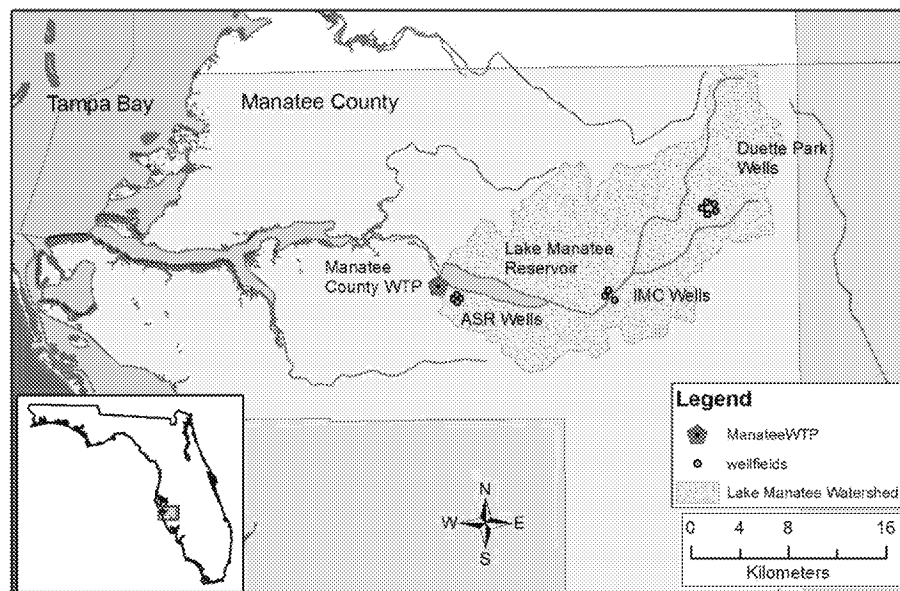


Figure 2-44 Location of the Manatee County water supply system along the upper Manatee River in Florida.

The focus was to reduce CO₂ emissions and at the same time, achieve socioeconomic objectives. Details of the analysis can be found in Chang et al. (2012). By implementation of the Master Plan and other adaptation measures, the County successfully provided uninterrupted water supply in recent years, even during the severe drought of 2017¹¹.

4.3.1 Water supply assessment

4.3.1.1 Water supplies

Water supply for the county is sourced from surface water and groundwater. Surface water from Lake Manatee, a man-made reservoir on the Manatee River, provides an average of 132,110.9 m³d⁻¹ (34.9 million gallons per day). The permit for withdrawal is governed by permits issued by the Southwest Florida Water Management District according to Florida water law (Chapter 373 FS).

Groundwater for water treatment is derived from two local wellfields: East County Wellfield I (ECWF-1) and the Mosaic Phosphate Wellfield (MPWF). Their relative locations are schematically shown in Figure 2-45. The ECWF-1 wellfield is permitted for 60,513.6 m³d⁻¹ (15.986 million gallons per day) average annual withdrawals, while MPWF is permitted for 7,419.4 m³d⁻¹ (1.96 million gallons per day). The Lake Manatee Water Treatment Plant (WTP) located in the southwest of the Lake Manatee is the only WTP in the Manatee County, providing all potable water supplies from the Manatee County Utility Department (MCUD). The treatment plant has a maximum operating capacity of 317,974.6 m³d⁻¹ (or 84 million gallons per day); 204,412.2 m³d⁻¹ (or 54 million gallons per day) is for surface water treatment and 113,562.4 m³d⁻¹ (or 30 million gallons per day) is for groundwater treatment.

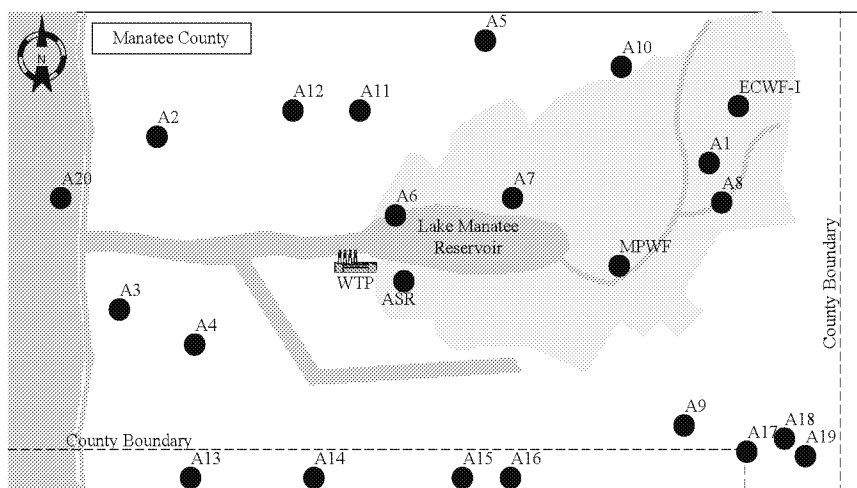


Figure 2-45 Locations of WTP, ASR, well fields (ECWF-1, MPWF), and the twenty potential water supply alternatives A1-A20. Not drawn to scale.

¹¹ <http://www.bradenton.com/news/local/article145043929.html>

A total of six (6) Aquifer Storage and Recovery (ASR) wells are located next to the Lake Manatee WTP. The ASR wells were used to store treated potable water in the Floridian Aquifer and for withdrawal to augment water supply during drought season. These ASR wells have been in operation since 1986. This operation was permitted to provide up to 11,356,235.3 m³ (3 billion gallons) of storage with a combined capacity of 37,854.1 m³d⁻¹ (10 million gallons per day).

Figure 2-45 schematically shows the locations of water supply system components, including Lake Manatee WTP, the ASR Wells, Lake Manatee surface water system, and the two groundwater wellfields. Manatee County also connects three (3) regional wastewater treatment plants to a 32-mile regional distribution system called Manatee Agricultural Reuse Supply (MARS) for customers to use reclaimed wastewater for agricultural irrigation. The use of reclaimed water saves groundwater from the Florida Aquifer that would otherwise be used for irrigation. The saved credits from reduced groundwater use become the net benefits that can be used as future potable water sources.

4.3.1.2 Water demand

MCUD provides water to retail customers, significant users, and wholesale customers. Retail customers distribute in both incorporated (e.g., administrative) areas and unincorporated areas of the County. Significant users refer to those with demands over 94,635 m³d⁻¹ (or 25,000 gallons per day). In 2006, this category of customer accounted for approximately 8782.2 m³d⁻¹ (or 2.32 million gallons per day). Wholesale customers include the cities of Bradenton, Palmetto, Longboat Key, and some regions in Sarasota County south of the Manatee County. Detailed water demand for wholesale customers is listed in Table 2-11. Reserve capacities available to the wholesale users remained constant over time as defined in the fixed water supply agreements.

Table 2-11 Water demand in 2006 and projections for wholesale customers in annual average (Board of County Commissioner, 2008)

Wholesale Customers	Water Demand (m ³ /day)					
	2006	2010	2015	2020	2025	2030
City of Bradenton	1,892.7	1,892.7	1,892.7	1,892.7	1,892.7	1,892.7
City of Palmetto	7,570.8	7,570.8	9,463.5	10,409.9	11,356.2	12,113.3
Town of Longboat Key	9,463.5	9,463.5	9,463.5	9,463.5	9,463.5	9,463.5
Sarasota County	37,854.1	30,283.3	22,712.5	18,927.1	NA	NA

Note: NA – Not available

Future water demands for retail customers and significant users is generally unknown because of the uncertainty in socioeconomic development. Detailed population projections using historical population trends (Board of County Commissioners, 2008) are the basis to calculate future water supply needs. A constant water usage rate per capita, according to the Master Plan, is assumed for the period of analysis. The water usage per capita in the MCUD service area is set by permitting and planning. The total municipal water demand estimated for MCUD corresponding to the population growth is listed in Table 2-12.

The historical data indicate an average daily demand of 181,018.4-m³ (or 47.8 million gallons) in 2006. The demand total includes 115,455.1 m³d⁻¹ (or 30.5 million gallons per day) for domestic water usage, 65,563.3 m³d⁻¹ (or 17.3 million gallons per day) for wholesale customers and significant users. With the projected population growth, annual average potable water demand will increase to 234,317 m³d⁻¹ (or 61.9 million gallons per day) by 2030 as specified in the Master Plan (Board County Commissioners, 2008). MCUD currently has an annual average of permitted water supply of 200,059.0 m³d⁻¹ or 52.9 million gallons per day. According to the Master Plan, a total of 34,447.2 m³d⁻¹ (or 9.1 million gallons per day) of additional water supply is required by the year 2030.

Table 2-12 Water demand projections for retail and significant users in annual average (Board of County Commissioner, 2008)

Customers	Water Demand (m ³ /day)					
	2006	2010	2015	2020	2025	2030
Retail customers	115,455.1	115,303.6	132,186.6	149,864.5	168,299.4	187,605.0
Significant customers	8,782.2	14,346.7	16,466.5	18,662.1	20,933.3	23,356.0

4.3.1.3 Future water supply alternatives

MCUD identified twenty potential water supply alternatives to meet the increased water demands in the future. The master planning called for a combination of surface water and groundwater sources grouped into five categories: groundwater options, surface water options, water permit transfer options, regional water options, and other options. Table 2-13 lists the twenty competing water supply alternatives. Groundwater options include building new wellfields in various locations of Manatee County. By operating the MARS system with less groundwater for irrigation, MCUD can increase the permitted groundwater pumping for potable water supply. Overall, the MARS projects consist of four phases: MARS-I, MARS-II, MARS-III, and MARS-IV; MARS-I and MARS-II projects have been implemented as of 2012 (Chang et al., 2012).

Table 2-13 Twenty alternatives for water supply expansion in the county master planning.

Alternative	No.	Brief Description
Groundwater Options		
MARS-I	1	This option is to supply new groundwater by developing a new wellfield in central Duette Park area near the existing ECWF-1.
MARS-II	2	This option is to supply new groundwater by developing a new wellfield in Erle Road Tank site.
MARS-III	3	

Alternative	No.	Brief Description
MARS-IV	4	These options are to supply new groundwater by developing a new wellfield. The location of the new wellfield has not yet been decided.
Surface Water Options		
Lake Parrish Reservoir	5	This option is to divert more surface water from the Little Manatee River in to the existing Lake Parrish Reservoir located in the northern part of Manatee County as a cooling pond for a power plant. The increased water storage in the Lake Parrish Reservoir is used for irrigation purpose to obtain well credits. Improvements on the existing systems include upgrading diversion pumps and distribution pumping and piping facilities.
Dredging of Lake Manatee	6	This option is in an attempt to increase the storage of the Lake Manatee Reservoir so as to increase the surface water annual yield from Lake Manatee. The capital investment includes creation and maintenance of new reservoir and dam, wetlands mitigation costs, and water transmission and treatment at the existing water treatment plant. This alternative may or may not be funded by Southwest Florida Water Management District (SWFWMD).
Gilley Creek reservoir	7	This option is to build a new reservoir upstream of Lake Manatee at the Gilley Creek location so as to yield more annual surface water. This alternative may or may not be funded by SWFWMD.
North and East Fork Reservoir	8	This option is to create an upstream impoundment at the North and East Fork locations to increase storage and yield available at the Lake Manatee intake. The capital investment includes creation and maintenance of a new reservoir and dam, wetlands mitigation costs, and water transmission and treatment at the existing water treatment plant. This alternative may or may not be funded by SWFWMD.
Tatum Reservoir – Lake Manatee WTP	9	This option is to develop a reservoir to store surface water diverted from the Myakka River located in the southeastern portion of Manatee County. The stored surface water due to the Tatum Reservoir is used for irrigation purposes so that the well credits that are originally used for irrigation can be transferred for potable water supply. The facilities to be built include an impoundment structure and distribution pumping and piping.
Transferred Water Use Permit Options		
Well Credit from Current Reuse Customers	10	This option is to renegotiate with the current reclaimed water customers for increased reclaimed water flows in the new agreement term. The cost associated with this alternative is for pumping to and treatment at the existing water treatment plant.
Developer Provided Water Use Permits (WUP) Transfer	11	This option is to implement a policy that will require new farmland developers to obtain the previous landowner's water use permit as a part of a land purchase. In this way, Manatee County Utility Department (MCUD) can take off the burden of increasing the water supply to the new potable water demand of new developers.
Direct Purchased of WUP	12	This option is to buy water use permits from permittees who are discontinuing farming operations instead of making new developers purchase the water use permit. This alternative is in conflict with

Alternative	No.	Brief Description
		option #11 and Manatee County wishes to forego the option if option #11 can be implemented.
Regional Water Options		
Peace River Water Treatment Facility Expansion	13	This option is to improve the existing Pease River water treatment facility in Desoto County by construction of a new 6.0-billion-gallon reservoir and expansion water treatment facility's production capacity from 12 to 24 and finally to 48 million gallons per day.
Shell Creek Restoration	14	This option is based on improvements on the existing Shell Creek water system by restoration and enhancement of natural water storage areas. This alternative is for potable water supply to the City of Punta Gorda and the region. An environmental benefit is identified for this alternative due to restoration of natural conditions.
Dona Bay/Cow Pen Slough Restoration (Option A)	15	This option is to build a surface new water supply system located within Sarasota County. Dona Bay Option A is a two-phase project. The first phase is to build a new reservoir and a new water treatment plant at the Dona Bay site and the second phase is to expand the size and capacity of the reservoir and the water treatment plant.
Dona Bay/Cow Pen Slough Restoration (Option B)	16	This option is to build a new surface water supply system located within Sarasota County. Dona Bay Option B is a single phase project. This alternative is in conflict with option #15.
Flatford Swamp Restoration	17	This option is to build a new water supply system at Flatford Swamp area located in the southeastern portion of Manatee County. The water source comes from the excess irrigation run-off in Flatford Swamp which causes widespread tree mortality. This alternative is in conflict with options #18 and #19.
Other Options		
Flatford Swamp – Stored and Treated at Tatum Reservoir	18	This option is to pump the surplus water stored in the Flatford Swamp which is located in southeastern portion of Manatee County immediately north of Myakka City to the Tatum Reservoir for storage and to build a new water treatment plant to treat the water to potable water standards at the Tatum Reservoir site. This alternative is in conflict with options #9, #17 and #19. This alternative may or may not be funded by SWFWMD.
Flatford Swamp supplemented with Diversion from the Myakka River – Stored and Treated at Tatum Reservoir	19	This option is similar to option #18. The difference is that this option will divert seasonal surface water from the Myakka River to supplement the Flatford Swamp irrigation runoff. Diversion structure, pumping facilities and additional capacity of the new water treatment plant will be needed. This alternative is in conflict with option #9, #17 and #18. This alternative may or may not be funded by SWFWMD.
Seawater Desalination	20	This option is to treat seawater to potable water standards. New seawater desalination facilities at the Port Manatee site need to be built. High operation and maintenance costs may be experienced. But potential price reduction equipment and funding from SWFWMD may make this alternative a competitive one.

Surface water options refer to those alternatives that involve new or expansion of existing reservoirs, by which additional surface water can be diverted from rivers into the reservoirs during the wet season. Some of the surface water may be used for irrigation purposes without treatment at Manatee WTP. This amount is then counted as groundwater credits for MARS-I expansion. The expansion timing for MARS-III and IV are unknown. Groundwater credits may be reserved for the MARS-I expansion if it can be replaced with surface water sources. Water permit transfer options are possible where a water use permit holder no longer needs the water or reclaimed water becomes available.

A regional water supply is another option. The Peace River Manasota Regional Water Supply Authority (PR/MRWSA) aims to integrate and improve water resource management in Charlotte County, DeSoto County, Manatee County and Sarasota County in order to provide the region with an adequate, reliable, and sustainable water supply into the future. Starting in 2014, the PR/MRWSA has begun providing water to the Manatee County. Other water options considered in the master planning process include seawater desalination, and swamp restoration at the Flatford Swamp in southeastern Manatee County. The Flatford Swamp receives a significant amount of irrigation runoff. Reducing the irrigation runoff flow into the swamp was predicted to help re-establish hardwood trees in the swamp and reduce environmental impact. Seawater desalination involves building a seawater treatment plant at the Tampa Bay.

Figure 2-45 schematically illustrates the relative locations of all twenty potential water supply alternatives. Among them, locations of alternatives #10, #11 and #12 are shown only for the purposes of illustration; these three alternatives require no physical facilities. Some of the twenty alternatives may be eligible for SWFWMD funding, thus decreasing the county's capital investment and thereby unit cost of potable water. It was noted, however, that the SWFWMD funding was not guaranteed even if all required criteria were met. In the comparative analysis, the highest (conservative) unit cost was used for the alternative following the common practice of engineering feasibility analysis.

Table 2-14 summarizes the maximal water credit and unit cost for each of the 20 water supply alternatives. The maximum water credit is defined as the maximum permitted water withdrawal. Unit cost was calculated as the present value for a cubic meter in U.S. dollars based on the 2007 value. It includes the amortization of the estimated initial capital investments and the operation and maintenance (O&M) costs.

Table 2-14 Maximum water credit and unit cost of the twenty water supply alternatives[#]

	1	2	3	4	5	6	7	8	9	10
Max Water Credit	8.21	11.36	7.57	18.93	15.52	44.29	34.83	40.13	17.79	17.03
Unit Cost (\$/m ³)	0.34	0.53	0.31	0.50	0.51	1.09	0.67	0.74	1.08	0.50
	11	12	13	14	15	16	17	18	19	20
Max Water Credit	0*	0*	45.42	75.71	75.71	75.71	56.78	30.28	43.15	37.85
Unit Cost (\$/m ³)	0.53	0.60	0.30	0.51	0.76	0.62	0.72	0.61	0.55	1.07

Note: * - The max water credits for alternative #10 and #11 are not available and the value of zero was assigned as default. Maximum water credit is 1,000 m³/d

- Adopted from the 2008 Manatee County Water Supply Facilities Work Plan (Board of County Commissioner, 2008)

4.3.2 Expansion scenario analysis

Most current decision-making systems rely on a single attribute; for example, economic cost or water supply capacity. However, the cost saving money alone does not reflect all sustainability attributes in evaluating the adequacy of the competing water supply expansion options. In the Manatee County case study, a decision-making framework included both savings in the carbon footprint and economic cost based on LCA to achieve optimal expansion planning.

Two approaches in a systems evaluation are common in finding the global optimal solution among competing alternatives. One is a top-down modeling assessment; the other is bottom-up threshold analysis. Optimization models for the top-down water supply system planning have been developed to address multiple planning goals (Harrington and Gidley, 1985; Yamout and Ef-fadel, 2005). Traditional decision-making mostly relies on the outcome of a cost and benefit analysis in the context of single objective optimization, which was of particular interest to both water supply (Urbaniak, 1988; Slowinski et al., 1995) and wastewater treatment (Ong and Adams, 1990). Various analysis techniques have been used including nonlinear programming models (Mulvihill and Dracup, 1974) and multicriteria decision analyses (Slowinski et al., 1995).

LCA is a well-established and standardized method of analysis for cost comparisons and can be applied to evaluate and reduce possible environmental impacts as a part of a sustainability analysis. For example, some LCA investigations have introduced greenhouse gas (GHG) emissions, namely the carbon footprint, as one of the categories when evaluating multiple technical solutions or alternatives for municipal wastewater treatment systems (Tillman et al., 1998; Dennison et al., 1998; Lundin et al., 2000; Peters and Lundie, 2001) and for water supply assessment (Voivontas et al., 2003; Lundie et al., 2004).

Evaluation of the expansion alternatives in Manatee County followed the LCA principles in an analysis of the cost and life-cycle GHG emissions. Based on these determined parameters, a multi-objective optimization scheme was developed to identify the global optimal planning solutions.

4.3.2.1. Carbon footprint estimates

The carbon footprint is a sum of CO₂ equivalents in all phases of each expansion alternative. Time duration for this analysis was twenty years (from 2011 to 2030) during which the construction, production, use, and recycle phases were analyzed sequentially as shown in Figure 2-46. The system diagram shows material and energy flows, where each block represents materials stocks and is connected by arrows with surrounding blocks to indicate critical material flows. Materials, or raw water in this analysis, is extracted at the beginning of a life cycle, passes through intermediate phases, and finally returns to the environment in the end of the life cycle. In this analysis, the end-of-life phase of water facilities was not included because water facilities usually have a service life far beyond our focused time period.

Qi et al (2010) analyzed carbon footprint for all twenty water supply alternatives. Their results were used in this LCA analysis. The emissions in construction and operation phases were calculated in the 20-year time period. The total CO₂ equivalent emissions in a 20-year time period was the sum of CO₂ equivalent emissions for construction and operations. As shown in Figure 2-46, construction phase includes the processes ① and ②. Their CO₂ equivalent emissions were independent of the amount of water supplied. When a potential water supply

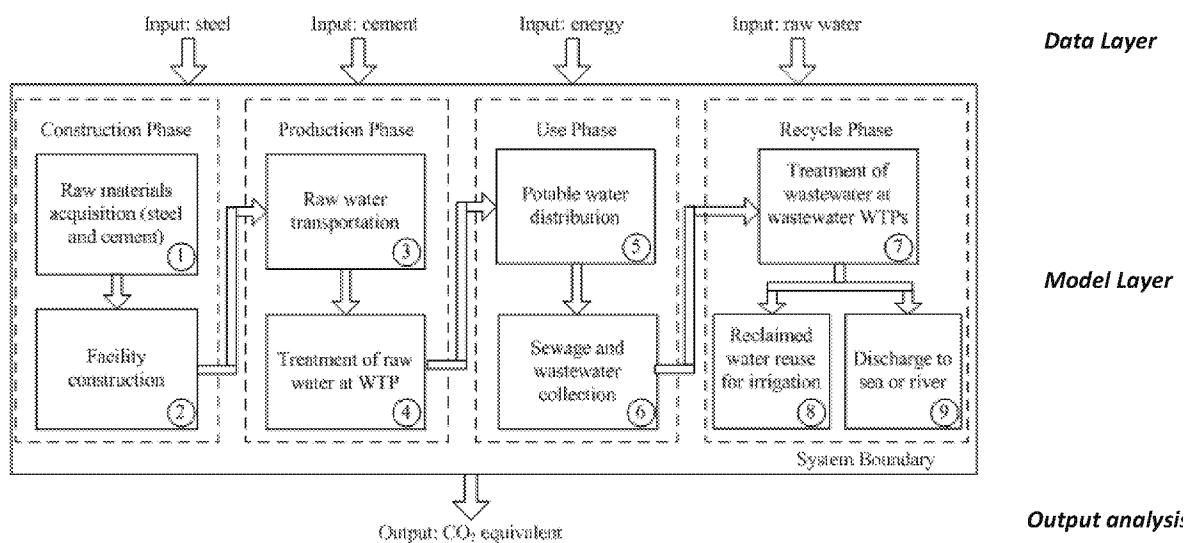


Figure 2-46 The life-cycle system analysis flow diagram for determining carbon footprint in water infrastructure expansion alternative evaluations. Process is divided into three layers. Adopted from Qi et al. (2010) and Chang et al. (2012).

alternative was selected and implemented, the CO₂ equivalent emissions were determined for both facility construction and operation. The operation phase included processes ③, ④, ⑤, ⑥, ⑦, ⑧, and ⑨. The LCA results are listed in Table 2-15.

In this analysis, the CO₂ equivalent emissions were proportional to the amount of water supplied, but the total energy usage in the water infrastructure life-cycle varied significantly among the expansion options (Table 2-15).

4.3.2.2. Multi-objective evaluation

A multi-objective mixed integer programming model was developed to assess these multi-stage expansion strategies based upon the LCA and cost evaluation results. The analysis of future water supply scenarios covered a 20-year timeframe from 2011 to 2030. The trade-off analysis for a compromised solution was based on two objectives. One was to minimize the total system costs required for the water supply expansion. The other was to minimize the total GHG emissions expressed as CO₂ equivalent. Both objectives were applied through modeling to screen and order the relevant water supply alternatives.

A compromise programming model simulation produced the best Pareto frontier solutions for the alternative expansion options. The model computation is a function of the total number of planning periods in the multi-stage framework of infrastructure planning, construction, operation and disposal (See Figure 2-46). The time interval depends on location-specific conditions and local decision-making requirements. More stages of greater implementation details lead to more decision variables and parameters that require greater computation time. For the purpose of this illustration, a 5-year time span was assumed for the construction phase in the decision analysis. The five-year duration is generally in agreement with the capital expenditure process.

Table 2-15. LCA of carbon footprint of twenty water supply alternatives (modified from Qi et al., 2010)

Alternative		CO ₂ equivalent emissions in constructional phase Process ① + ② (kg)	CO ₂ equivalent emissions in operational phase. Process ③+④+⑤+⑥+⑦+⑧+⑨ (kg·m ⁻³)
Groundwater	1	1.96×10^{10}	2.35
	2	2.85×10^{10}	2.68
	3	2.08×10^{10}	2.48
	4	4.11×10^{10}	2.87
Surface water	5	3.40×10^{10}	2.71
	6	1.88×10^{10}	1.16
	7	2.67×10^{10}	1.99
	8	8.91×10^{10}	3.75
	9	4.63×10^{10}	3.13
Water use permit transfer	10	Negligible*	1.16
	11	Negligible*	1.16
	12	Negligible*	1.16
Regional water	13	1.81×10^{11}	5.89
	14	2.72×10^{11}	6.85
	15	1.07×10^{11}	3.35
	16	1.07×10^{11}	3.35
	17	6.56×10^{10}	2.71
Others	18	4.88×10^{10}	2.71
	19	5.75×10^{10}	2.71
	20	6.28×10^{10}	3.28

Note: * - Water permit transfer is simply an administrative action with almost no obvious carbon footprint relative to other options.

4.3.3. Quantitative modeling and systems analysis

In quantitative analysis, the multistage planning horizon was divided into the four time periods with each having a 5-year time span. Decisions in each period of expansion decisions for the growing water demand can be evaluated in a trade-off analysis between the two

objectives. The Multi-objective and Multistage Mixed Integer Programming model used in the Manatee County evaluation is described below.

Objective Functions

Two governing objective functions were implemented at 5-year interval. The CO_{2,eq} total was calculated using the LCA procedures shown in Figure 2-46. Monetary values of cost are discounted to the year 2007. According to Chang et al. (2012),

Objective function 1:

$$\text{Minimize } Z_1 = \text{total CO}_2 \text{ equivalent emissions (unit: g)} = \sum_{i=1}^{20} (1000A_{i1}CO_{2,eqi} \times 1825 + Y_{i1}CO_{2,eci}) + \sum_{t=2}^4 \sum_{i=1}^{20} [1000A_{it}CO_{2,eci} \times 1825 + (Y_{it} - Y_{i(t-1)})CO_{2,eci}]$$

Objective function 2: Minimize $Z_2 = \text{total cost (unit: \$)} =$

$$\sum_{i=1}^{20} (1000A_{i1}C_i \times 1825 + Y_{i1}F_i) + \sum_{t=2}^4 \sum_{i=1}^{20} [1000A_{it}C_i \times 1825 + (Y_{it} - Y_{i(t-1)})F_i]$$

where Y_{it} is 1 if the alternative i is implemented in and after time stage t ; otherwise $Y_{it} = 0$, $i = 1, 2, \dots, 20$; $t = 1, 2, 3, 4$ for the period of 5-year implementation interval. CO_{2,eci} is the amount of CO₂ equivalent emissions in the construction phase of alternative i in unit of g, and CO_{2,eqi} is the amount of CO₂ equivalent emissions in the operational phase of alternative i in unit of g·m⁻³, $i = 1, 2, \dots, 20$. A_{it} is actual water withdrawn (10³m³d⁻¹) from alternative i ($i = 1, 2, \dots, 20$), and $t = 1, 2, 3, 4$. C_i is unit water cost of the alternative solution i in \$·m⁻³ ($i = 1, 2, \dots, 20$). F_i is the fixed capital investment for the alternative solution i ($i = 1, 2, \dots, 20$).

Model Constraint Setting

Constraints setting in the compromise programming model included definitional constraints, water demand constraints, capacity limitation constraints, availability constraints, sequencing constraints, mutually exclusive constraints, irreversible constraints, screening constraints, and non-negative and binary constraints. These constraints provided different functionalities in an intertwined solution space that narrowed down the dynamic selection and ranking based on streamlined logic described by the coupled objective functions and constraints over the planning horizon.

The set of model constraints below defined the current maximum water supply and projected water demand in the unit of 10³ m³/day in each time period:

$$S = 200.04 \quad 10^3 \text{m}^3 \text{d}^{-1} \quad (2.3)$$

$$D_1 = 192.19 \quad 10^3 \text{m}^3 \text{d}^{-1} \quad (2.4)$$

$$D_2 = 209.14 \quad 10^3 \text{m}^3 \text{d}^{-1} \quad (2.5)$$

$$D_3 = 211.83 \quad 10^3 \text{m}^3 \text{d}^{-1} \quad (2.6)$$

$$D_4 = 234.43 \quad 10^3 \text{m}^3 \text{d}^{-1} \quad (2.7)$$

$$F_i = 0.001 \text{ \$} \quad (2.8)$$

$$G = \text{a large dumb number (e.g., 999999999)} \quad (2.9)$$

where S is the current water supply upper limit; D_t is water demand in time period t ($= 1, 2, 3, 4$); F_i is the virtual fixed cost, an artificially assigned small number relative to all cost parameters to support screening logic in the cost-effectiveness objective and associated constraints. The use of dumb number G in programming is to assure computing stability for the If-Then logic screening in constraints by Eqs.(2.10)-(2.12). The settings of F_i and G also help avoid the selection of an alternative with no additional water supply over the planning horizon. In the modeling, the following constraints were applied:

- The constraints between demand (D) and supply (S) were applied to the entire 20-year period in the modeling space:

$$\sum_{i=1}^{20} A_{it} \geq D_t - S \quad \text{for all } t \quad (2.10)$$

- The water amount supplied by each future water source would not exceed its predetermined supply limit:

$$A_{it} \leq A_i^{\max} Y_{it} \quad \text{for all } t \text{ and all } i \quad (2.11)$$

in which A_i^{\max} is the maximum water credit ($10^3 \text{m}^3 \text{d}^{-1}$) for A_i , $i = 1, 2, \dots, 20$.

- Only MARS-I and MARS-II were available in time period 1 and the rest of future water supply alternatives may be available only after time period 1 because of the original setting in the work plan

$$Y_{it} = \begin{cases} 1 & i = 1, 2 \\ 0 & i = 3, 4, \dots, 20 \end{cases} \quad (2.12)$$

Construction sequencing constraints

This set of constraints assured that the MARS-II project could not be implemented until the completion of the MARS-I project as specified in the infrastructure expansion work plan. Similarly, the MARS-II project implementation could only occur before the MARS-III project. This forward-looking sequence applies to MARS-III project as it might be implemented ahead of MRAS-IV project. Mathematically,

$$\begin{aligned} Y_{1t} &\geq Y_{2t} \\ Y_{2t} &\geq Y_{3t} \\ Y_{3t} &\geq Y_{4t} \end{aligned} \quad \text{for all } t \quad (2.13)$$

Mutually exclusive constraints:

Some future water supply alternatives were mutually exclusive as specified in the original work plan. This set of constraints assured that only one of the exclusive future water supply alternatives could be implemented in any time period. For example, Alternatives 11 and 12 are mutually exclusive because the water use permit allocation is either transferred from developers

to the County or otherwise acquired by Manatee County through other means; an example was to exchange the County's reclaimed water for groundwater currently used for agricultural irrigation. The MARS-III project conflicts with the other regional water supply alternatives because any one of the regional water supply sources or completed implementation of MARS projects can provide adequate water supply (Board of County Commissioners, 2008). Alternatives 15 and 16 are mutually exclusive because both alternatives use the same water supply sources with different implementation schedules. Similarly, alternatives 17, 18 and 19 are mutually exclusive because all three alternatives rely on Flatford Swamp as a water source. The differences among the three alternatives depend on the construction of a new WTP as a part of the regional water supply option. Alternatives 9, 18 and 19 are mutually exclusive because all three are related to a new reservoir site at Tatum. The difference is whether the new reservoir site will be used to store water pumped from Myakka River or from Flatford Swamp.

Furthermore, Eqs.2.19-2.22 define the need for MARS-I implementation before considering relevant alternatives #5, #9, #10, and #11, because of the constraints derived from sequential water credit transfer. Mathematically, these constraints are:

$$Y_{11t} + Y_{12t} \leq 1 \quad \text{for all } t \quad (2.14)$$

$$Y_{3t} + Y_{13t} + Y_{14t} + Y_{15t} + Y_{16t} + Y_{17t} \leq 1 \quad \text{for all } t \quad (2.15)$$

$$Y_{15t} + Y_{16t} \leq 1 \quad \text{for all } t \quad (2.16)$$

$$Y_{17t} + Y_{18t} + Y_{19t} \leq 1 \quad \text{for all } t \quad (2.17)$$

$$Y_{9t} + Y_{18t} + Y_{19t} \leq 1 \quad \text{for all } t \quad (2.18)$$

$$Y_{5t} \leq Y_{1t} \quad \text{for all } t \quad (2.19)$$

$$Y_{9t} \leq Y_{1t} \quad \text{for all } t \quad (2.20)$$

$$Y_{10t} \leq Y_{1t} \quad \text{for all } t \quad (2.21)$$

$$Y_{11t} \leq Y_{1t} \quad \text{for all } t \quad (2.22)$$

Irreversible constraints:

This set of constraints assures that the implemented water supply alternatives in one time period will be available in and after that time period.

$$Y_{it} \leq Y_{i(t+1)} \quad i = 1, 2, \dots, 20, t = 1, 2, 3 \quad (2.23)$$

Screening constraints:

This set of constraints defines the sequence by which alternatives for meeting water demands will be considered. A new water supply alternative is screened when the maximum capacity of the current water supply in given time period is incapable of meeting the projected water demand in the next time period. Otherwise, there is no need to implement any new water supply alternative. In Eqs. 2.24-2.26, the formulation would allow n number of water supply alternatives to be included in each time period for capacity expansion, in which n is a positive integer. If $n=1$, it implies the model would only pick up one alternative at a time for ranking in

sequence. Three different scenarios were analyzed at $n=1$, $n=2$ and $n=3$, respectively, or the number of alternatives that is allowed to be selected at a time ranges from 1 to 3.

$$\sum_{i=1}^{20} Y_{i1} A_i^{\max} - (D_2 - S) < GY_1 \quad (2.24)$$

$$\sum_{i=1}^{20} Y_{i2} - \sum_{i=1}^{20} Y_{i1} \leq n(1 - Y_1)$$

$$\sum_{i=1}^{20} Y_{i2} A_i^{\max} - (D_3 - S) < GY_2 \quad (2.25)$$

$$\sum_{i=1}^{20} Y_{i3} - \sum_{i=1}^{20} Y_{i2} \leq n(1 - Y_2)$$

$$\sum_{i=1}^{20} Y_{i3} A_i^{\max} - (D_3 - S) < GY_3 \quad (2.26)$$

$$\sum_{i=1}^{20} Y_{i4} - \sum_{i=1}^{20} Y_{i3} \leq n(1 - Y_3)$$

where Y_1 , Y_2 , and Y_3 are binary integer variables for screening multiple alternatives associated with differing scenarios in the optimization context.

Non-negative and binary constraints:

This set of constraints assures that the amount of water assigned to each water supply alternative is non-negative and the binary decision variables are dichotomous.

$$A_{it} \geq 0 \quad (2.27)$$

$$Y_{it} = 0, 1 \quad i = 1, 2, \dots, 20, \quad t = 1, 2, 3, 4 \quad (2.28)$$

$$Y_1, Y_2, Y_3 = 0, 1 \quad (2.29)$$

4.3.4. Adaptation analysis on cost and carbon/energy footprint

4.3.3.1. Carbon/energy footprint and cost optimization

Ideal solutions were identified using the multi-objective model simulation by solving each of the individual objective equations sequentially. The solution (shown in Table 2-16) was considered optimal when each objective is optimized individually and achieved together. However, the ideal solution may not be feasible or practical because the objectives may be competing, even conflicting in the decision space. In this type of application, the “Pareto Optima” solution set is commonly used. The solution optimization can be found the Pareto Optima frontier in the solution space of the compromise programming model. Alternatively, the compromised solution can also be obtained by applying the distance-based metrics defined in a compromise programming model (Zeleny, 1973).

For the two objective functions, the solution space is a two-dimensional objective space. The x-axis was selected for CO₂ equivalent emissions (Z_1) and the y-axis for total system cost (Z_2). In all cases, a Pareto Optimal solution in global optimization space represents the best alternative that may perform better simultaneously in both objectives. For exclusive

optimization decision ($n = 1$), five sets of solutions are found Table 2-17. Solution #1 is the GHG effective solution; Solution #5 is the most cost effective; and the other three are compromised solutions. For alternative management decisions at $n = 2$ and $n = 3$, the Pareto Optimal solutions were found and described in Chang et al. (2012).

Table 2-16 Ideal solution of the multi-objective model

	Minimize Z_1 (kg)	Minimize Z_2 (\$million)
$n = 1$	1.15×10^{11}	223
$n = 2$	7.55×10^{10}	172
$n = 3$	7.54×10^{10}	172

Note: n is a number of alternatives allowed in one set of ideal solution.

A sensitivity testing for the optimal solution was conducted at assumed 10% uncertainty in the estimates of future water demand change at all four stages. For water managers, the future prediction is the basis for decision making. The results are shown in Table 2-18. The best case is that future water demand is 10% less than the prediction; conversely the future water demand of more than 10% than predicted is the worst-case scenario in planning.

Table 2-17 The Pareto optimal expansion strategies ($n = 1$)

Solution Number	Z_1 (kg)	Z_2 (\$million)	Expansion Strategies			
			Period 1	Period 2	Period 3	Period 4
1	1.15×10^{11}	313	1, 2	17	-	6
2	1.42×10^{11}	295	1, 2	17	-	7
3	<i>1.56×10^{11}</i>	260	<i>1, 2</i>	16	-	10
4	2.14×10^{11}	258	1, 2	16	-	19
5	3.22×10^{11}	223	1, 2	14	-	10

Note: Best compromised solution #3 is in bold and italic.

For $n = 1$, the Pareto Optimal solution sets were examined for the best case $0.9D_i$ ($D_1 = 172.97$, $D_2 = 188.23$, $D_3 = 190.65$, and $D_4 = 210.99$) and the worst case of $1.1D_i$ ($D_1 = 211.41$, $D_2 = 230.05$, $D_3 = 233.01$, and $D_4 = 257.87$). Solutions marked by “-” or “+” represents 10% lower or higher water demand than the predicted level in the Master Plan, respectively. A comparison indicates that the Pareto Optimal frontier remains unchanged in shape.

4.3.3.2. Optimal expansion solutions and construction sequence

Water supply system expansion normally takes place in phases with an ultimate goal to satisfy water service needs and accommodate economic considerations such as capital flow and construction cost. The preceding analysis for the Manatee County water infrastructure expansion showed multiple compromised solutions in trade-off between the system’s cost and life-cycle carbon footprints. It is worth noting that practical master planning of water infrastructure

improvement involves many other considerations such as land availability, engineering feasibility, capital expenditure and cash flow, among the others. For the Manatee County case

Table 2-18 The Pareto optimal expansion strategies for the best and worst cases ($n = 1$)

Solution Number	Z_1 (kg)	Z_2 (\$million)	Optimal Expansion Strategies			
			Period 1	Period 2	Period 3	Period 4
1–	4.87×10^{10}	2.77	1, 2	6	-	10
2–	7.54×10^{10}	193	1, 2	7	10	6
3–	9.63×10^{10}	185	1, 2	7	10	3
4–	<i>1.06×10^{11}</i>	<i>172</i>	<i>1, 2</i>	<i>19</i>	-	<i>10</i>
5–	2.31×10^{11}	111	1, 2	13	-	10
1+	1.57×10^{11}	347	1, 2	16	10	6
2+	1.84×10^{11}	339	1, 2	16	10	7
3+	1.91×10^{11}	335	1, 2	16	10	5
4+	<i>2.14×10^{11}</i>	<i>333</i>	<i>1, 2</i>	<i>16</i>	<i>10</i>	<i>19</i>
5+	3.23×10^{11}	303	1, 2	14	10	6
6+	3.50×10^{11}	296	1, 2	14	10	7
7+	3.57×10^{11}	293	1, 2	14	10	5

Note: Best compromised solutions #4– and #4+ are in bold and italic.

study, however, one can further assess the best options for further engineering analysis and evaluate the optimal management options. These two subjects are discussed below.

Best Compromised Solution

The optimal solutions in Tables 2-19 and 2-20 represent the best combination of systems' cost and carbon footprints for the anticipated future water demand and the demands at the 10% uncertainty bounds. To find the best compromised solutions for all three sets of future water demands, the two objective functions are normalized for Z_1 and Z_2 in the same scale between 0 and 1. The normalized objective functions (NZ_1 and NZ_2) are given by:

$$NZ_1 = \frac{Z_1 - Z_1^{\min}}{Z_1^{\max} - Z_1^{\min}} \quad (2.30)$$

$$NZ_2 = \frac{Z_2 - Z_2^{\min}}{Z_2^{\max} - Z_2^{\min}} \quad (2.31)$$

The normalized solution space for the optimal water infrastructure solutions is shown in Figure 2-47. By the normalization, the best solution can be found by the distance to imaginable solution of zero cost and zero carbon emission or the origin (0,0) of the plot in Figure 2-47. A

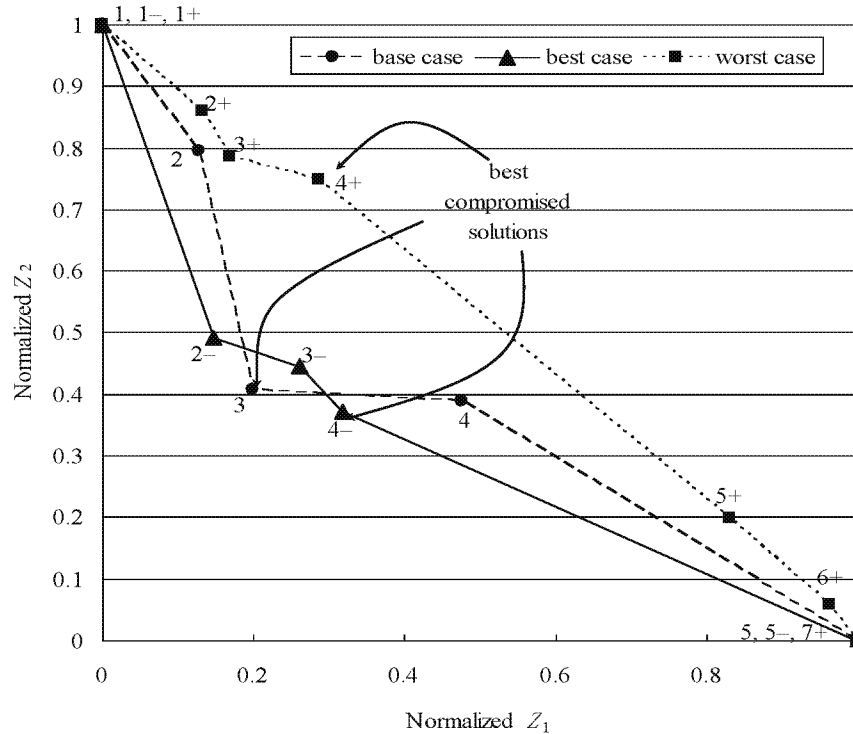


Figure 2-47 Pareto solution fronts for the best compromised solutions for projected future water demand (base case) and the demand with 10% uncertainties (best case and worst case).

widely accepted definition of such distance is based on Minkowski's L_a metrics (Zeleny, 1973), where $1 \leq a \leq \infty$.

$$L_a = \left[\sum_{i=1}^2 w_i (NZ_i)^a \right]^{1/a} \quad (2.32)$$

For water managers, $a = 1$ means equal weighing for both objectives; $a = 2$ implies weighted geometric distance between the solution (NZ_1, NZ_2) to the ideal solution $(0, 0)$; and $a = \infty$ implies minimization of the maximum NZ_i when L_a is to be minimized. The parameters were set at $a = 2$ and $w_1 = w_2 = 1$, for the Manatee County case study as an illustration. Using these assumptions, the best compromised solutions for the three cases are:

- For the projected water demand, the best compromised solution #3 would cost \$2 million or 0.8% more than the next less expensive option. The $\text{CO}_{2,\text{eq}}$ emissions would decrease by 27.1%.
- For the best case with lower future water demand, the best solution #4+ would cost more by 55% or \$61 million than the next less expensive option. It would result in a 54% reduction in $\text{CO}_{2,\text{eq}}$ emissions.
- For the worst case with higher future water demand, the best solution #4- would increase the cost by \$30 million or 9.9% more than the next less expensive option. The carbon emissions reduction would be 33.9%.

Decision support in master planning

It is noteworthy that the Pareto front is not continuous because practical water engineering solutions are discrete. The trade-offs of the best discrete alternatives, as described above and described in Tables 2-20 and 2-21, present a quantitative basis for managers to use in the decision-making process. The co-benefits in emissions savings, cost, and engineering feasibility are obvious when adaptive planning is considered for the water infrastructure expansion.

Based on the optimization results, Figure 2-48 shows the optimal facility expansion strategies in each of the five-year implementation periods, including the cost and carbon emissions. The following conclusions can be drawn from this example exercise:

- In the base case and the best case, the current water supply would be self-sufficient in the first five-year period. The modeling results indicate that if the forecasted water demand is underestimated, extra water resources would become necessary. Then the MARS-I and MARS-II projects could provide sufficient water supplies to meet the demand until 2025.
- According to Chang et al. (2012), the need for and the nature of optimal expansion strategies in this time period are highly dependent upon the level of forecasted water demand. The regional water option offers larger water supply capacity at relatively lower unit costs than other alternatives. It would be needed in the worst case. In the best case, however, regional water supply options are avoided due to their relatively larger carbon footprints, primarily because of long distance water transfer. Other alternatives available inside the Manatee County would provide better performance for both objectives.
- More water demand is anticipated starting from 2026. The modeling results indicate that a variety of expansion strategies are available for selection in the decision-making process. In all cases, the WUP alternative (e.g. alternative #10) is always preferred due to its zero carbon footprint, or energy neutral, and low unit cost. In fact, was considered as a priority in the County's master planning.
- The County's Master Plan suggests that the MARS-I and MARS-II projects be adopted by 2014, some regional water alternatives by 2017, and possibly another regional alternative or MARS-IV by 2024. This case study on carbon footprint and cost suggested that MARS-I, MARS-II and WUP alternatives would be the optimal alternatives in the near future.
- For the worst case in future water demand, MARS-I and MARS-II are still the most desirable alternatives by 2016 (Figure 2-48). Regional supply alternatives would be cost effective compared to other alternatives except the MARS projects. They may not represent the most favorable solution in carbon emissions, because of necessary facility expansion/construction and long-distance water transfer. As a compromised solution, Dona Bay/Cow Pen Slough Restoration Option B (alternative #16) could be selected. It has the lowest GWP impacts among all the regional alternatives.

There are several limitations in this analysis. These include uncertainties surrounding water price, discount of the potential to receive SWFWMD funding and thus arbitrarily higher unit costs, among the others. Their impacts on the determined optimal solutions are not evaluated.

5. System-Scale Adaptation for Existing Urban Water Infrastructure

5.1. Basic considerations in adaptation engineering

Shown in Figure 2-6, urban planning is one major element with opportunity for infrastructure adaptation. Urban-scale adaptive planning of water and transportation infrastructure has the potential to generate adaptation co-benefits and improve the urban performance and resilience with changes in climate and land use. Examples of co-benefit potential were examined in preceding Section 4.0. The local-scale adaptation is focused on the water infrastructure components. This type of adaptation is proceeded at the system-scale (Figure 2-2) in the engineering steps (construction and operation) (Figure 2-6).

One key requirement in adaptation is to define the limit of adaptation actions. Felgenhauer (2013) defines the adaptation limit as the point beyond which adaptation's economic return is diminished and a paradigm shift is necessary. To determine the threshold, engineering assessments need to develop the technical basis necessary for evaluating adaptation potential and feasibility. When necessary, additional rounds of planning-engineering-adaptation can be conducted as illustrated in Figure 2-6.

Here in Section 5.0, these themes and basic considerations for adaptation are detailed from an engineering approach. The concept of capacity reserve (*CR*) is introduced in the analysis of the threshold in order to define the need for adaptation engineering and evaluate the adaptation limitation. In the subsequent Sections 6.0 and 7.0, case studies will be used to illustrate the adaptation engineering approaches for *CR* improvement in drinking water treatment and distribution. Associated adaptation tools will be described.

5.1.1. Adaptation engineering for water infrastructure

Engineering design and implementation for adaptation of existing infrastructure can be broken down into two stages: 1) system assessment of adaptation feasibility, 2) adaptation design and implementation, and 3) effectiveness monitoring and adaptation update. These adaptation elements are shown in Figure 2-49 in the context of existing water planning-engineering processes.

The first step is to know the resilience of existing water infrastructure against the projected hydroclimatic impacts. The process marked as Stage “1” in Figure 2-49 follows the traditional water infrastructure planning for future land use and economic projections; the planning and projections are the basis for planning and designing the existing infrastructure (See Stage “0” in Figure 2-49). The capacity assessment of existing structure is commonly known as the “bottom-up” approach. It is intended to evaluate the water infrastructure capacity and capacity reserve, and then determine the threshold beyond which the water infrastructure would lose its service functionality or said functionality is compromised. An example of “bottom-up” approach is the EPA Climate Resilience Evaluation and Assessment Tool (CREAT)¹². In Section 5.3.2, the CREAT tool and its applications will be discussed.

¹² <http://water.epa.gov/infrastructure/watersecurity/climate/creat.cfm>

Adaptation engineering can take place in Stage “2” of the planning and engineering process in Figure 2-49. This second stage is focused on improvement of system’s *CR* by adaptation and improvement of the existing water infrastructure. Because new infrastructure or system revitalization requires an initial capital investment, a common management practice is to first improve resilience through capacity improvement. This management consideration is also shared in developing urban transportation infrastructure. As described in Sections 3.0 and 4.0, scenario analysis for transportation and water infrastructure is often used to identify the most cost-effective approaches, which primarily rely on capacity improvement as opposed to new construction.

It is worth noting that the adaptive planning and engineering approach differs from the traditional water infrastructure practice by considering climate as a variable (Figure 2-49). Water infrastructure and land use planning time horizons can be as long as 30-50 years. This time frame is comparable to the time in which change in hydroclimatic conditions can occur. However, current model projections of future climate and hydrological conditions have a substantial degree of uncertainty (Miller and Yates, 2008; IPCC, 2014, 2007), which means developing an actionable and reliable technical and engineering design basis is often unavailable. It should be

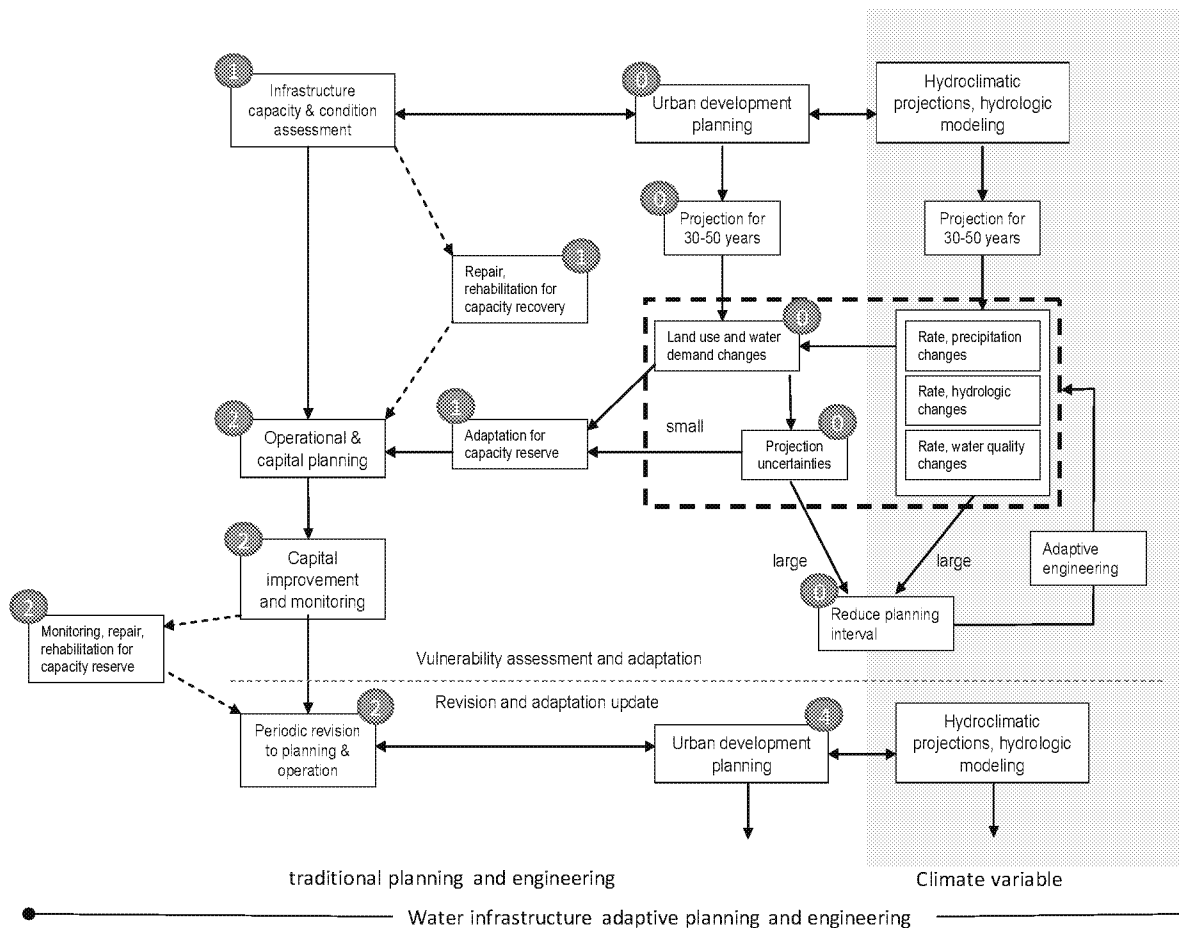


Figure 2-49 Assessment-adaptation process for water infrastructure planning and engineering. The box in dashed line contains the elements of climate and land use projections in infrastructure master planning. Arrows indicate process direction. Numbered labels indicate the stages of engineering analysis (See text for explanation).

noted that this uncertainty is likely to decrease as more comprehensive and accurate model projections become available, but to overcome this current difficulty, an overall iterative adaptive approach was outlined earlier in Figure 2-1 of this report. The iterative process and planning/engineering elements from modeling, to adaptation design, to implementation and monitoring are illustrated in the flow diagram in Figure 2-49.

Hydroclimatic variables important to water infrastructure services include the rate of precipitation change, changes in watershed hydrologic variables such as runoff characteristics, and water quality changes. Precipitation intensity, total precipitation, precipitation return frequency and temperature are the most fundamental hydrologic parameters. All are currently assumed to be constant in hydrological design guidelines such as the Atlas-14 precipitation intensity-depth-frequency design charts (Bonnin et al., 2006, 2011). These parameters are not static. Small rates of change and hydrological uncertainties can be managed through the use of engineering safety factors. However, when the rate is excessive under a non-stationary climate conditions, the current engineering design principles and technical basis may become inappropriate (Yang and Goodrich, 2014). An adaptive modeling-monitoring approach is necessary to successively refine the design basis (See Figures 2-1 and 2-49). This can lead to better management of the climate risk and adaptation economics. Case studies are provided for illustration in subsequent Section 6.0-7.0.

5.1.2. Adaptation attributes of three types of water infrastructure

Existing water infrastructure has a large physical footprint that is difficult to change quickly, without large capital investment, when responding to new hydroclimatic conditions. Over the past century, water infrastructure was designed and constructed underground based on anticipated population increases and land use projections to meet the water needs, while climate and precipitation regimes were assumed to be stationary (See Figure 2-49). The properties of this infrastructure and its urban service functions developed so far under the stationarity assumption can limit adaptation approaches.

Currently, the U.S. urban water supply and sanitation are carried out by three principal types of water infrastructure: wastewater collection and treatment, drinking water treatment and distribution, storm water collection and management (Figure 2-50). While the service function varies geographically and differs among types of water infrastructure, general engineering and management principles follow a triple bottom line of management objectives: protection of public health, safety and welfare while maintaining environmental sustainability and stewardship, system reliability, and engineering economics.

In this specific context the drinking water treatment and distribution in the U.S. are designed for regulatory compliance with drinking water quality standards and for uninterrupted water supply. Centralized wastewater systems serve to collect wastewater from individual users, transfer it to a location for treatment and subsequent discharge into a water body under a regulatory permit while minimizing public health risks and exposure. Onsite small wastewater systems and decentralized wastewater management are the alternative systems serving small communities and individual households (U.S. EPA, 2002), but are not discussed here because by the very nature, they cannot be used in dense urban communities. Additionally, storm water infrastructure has been constructed on a massive scale to provide drainage, sanitation and flood control in an urban catchment area, primarily as a means to protect public infrastructure and private property. In the U.S. Northeast and the Great Lakes region, storm water and wastewater

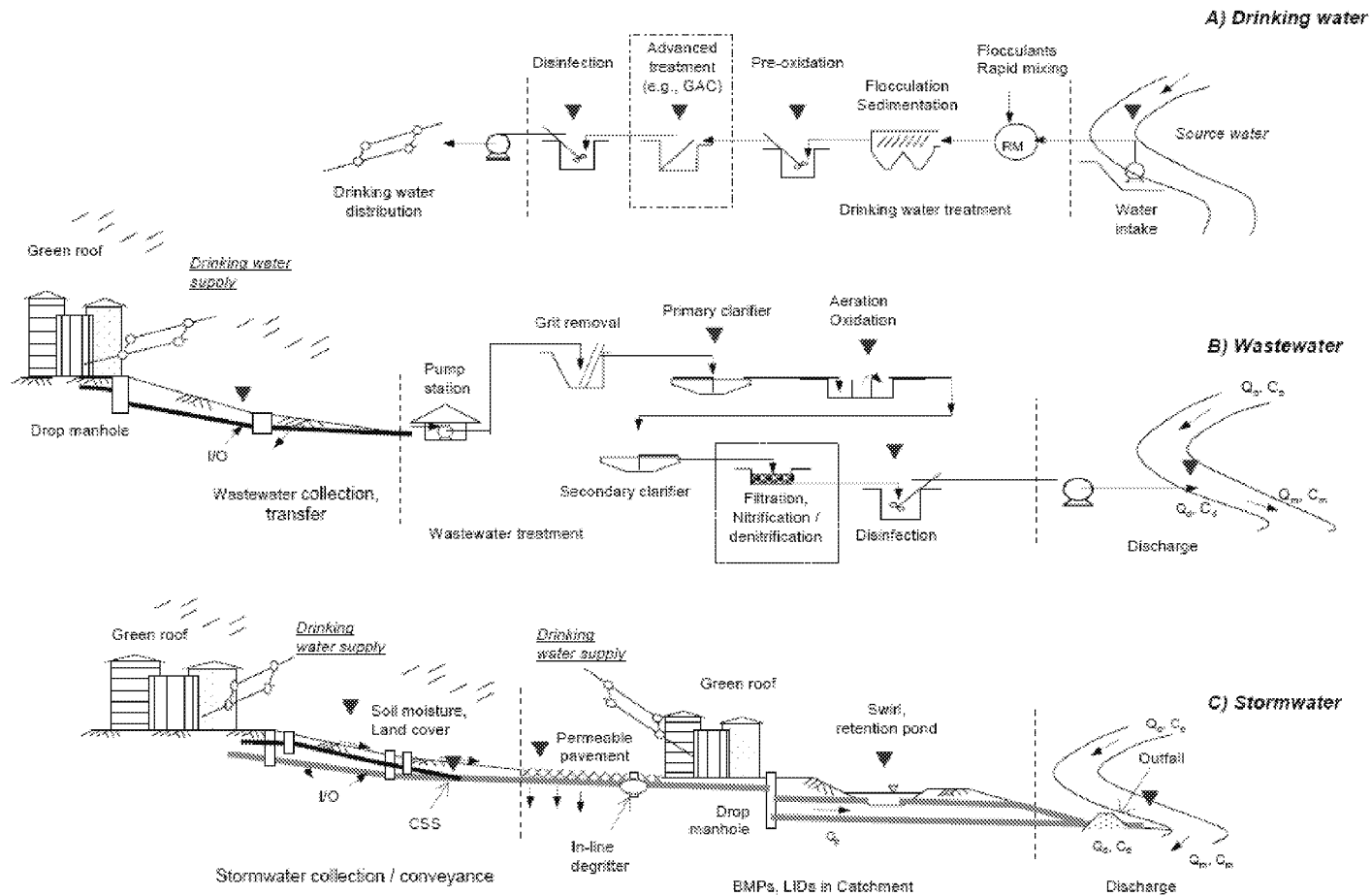


Figure 2-50 Process schematic diagrams for typical centralized drinking water, wastewater, and storm water infrastructure in an urban watershed. Combined sewer system (CSS), storm water, and wastewater treatment effluent discharges (Q_d , C_d) are regulated for stream flow (Q_o) and pollutant concentration before and after the discharge point (C_o and C_m). Solid arrow indicates water flow directions. I/O is water inflow and outflow in the buried pipes through infiltration and exfiltration. Solid triangle indicates process unit potentially vulnerable to future precipitation changes.

networks often share pipes in a combined sewer system (CSS). Combined sewer overflows (CSOs) occur during high-intensity precipitation, causing untreated or minimally treated, but highly diluted wastewater to be by-passed at treatment plants due to hydraulic limitations of the plants. The result is pollution in the receiving water bodies (U.S. EPA, 2001, 2008, 2009; Weinstein, 2009; Capodaglio, 2004).

In the urban water cycle of water-wastewater-storm water, extreme precipitation impacts on surface urban watersheds can potentially make several infrastructure components vulnerable to providing desired service functions. These vulnerable locations are shown in Figure 2-50. The nature of vulnerability is explained in Tables 2-22 and 2-23. Further technical discussions for each are presented subsequently in the aspect of infrastructure *CR*.

5.1.3. The capacity reserve concept and climate resilience

The sustainability of water infrastructure is shown in its resilience and adaptability to a changing environment. Resilience is defined here as the ability for a system to recover its physical state and service functions after an external impact (Milman and Short, 2008; McDaniels et al., 2008). Capacity reserve (*CR*) is an important physical attribute that quantifies the resilience as discussed extensively in sustainability science literature (Tillman et al., 2005, 1998; Dominguez and Gujer, 2006). Some (e.g., Oh et al., 2005; Chen et al., 2008) have discussed *CR* in the context of urban carrying capacity.

The *CR* concept is a traditional concept in civil, structural and process engineering, referring to extra capacity for assurance of desired structural integrity or performance (e.g., Tillman et al., 2005; Matos et al., 2013). A commonly used term is the margin of safety, or safety

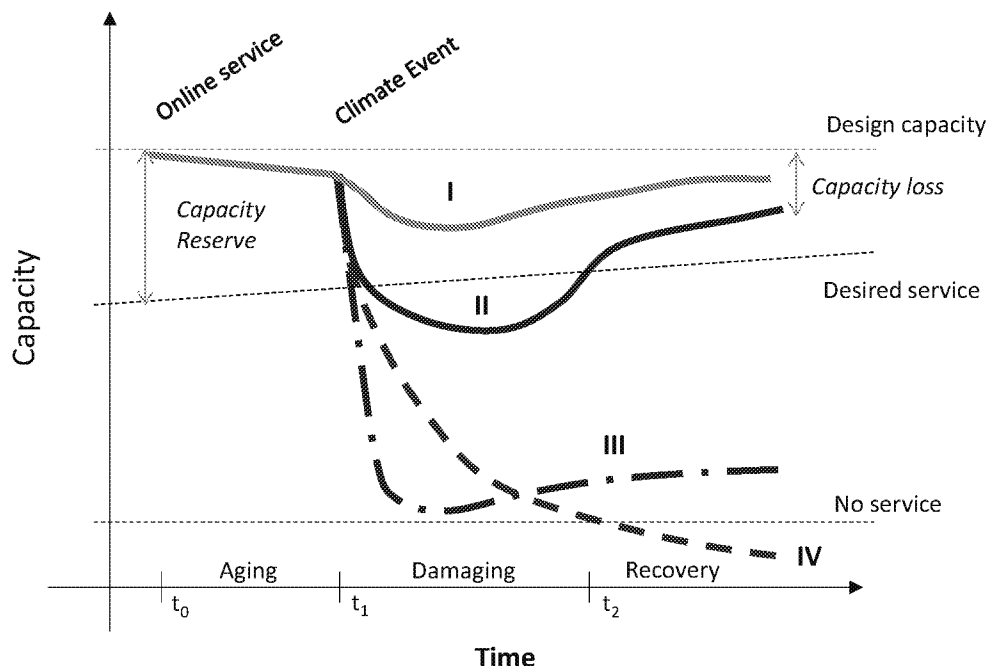


Figure 2-51 Four types of infrastructure vulnerability under the threat of external impact event (e.g., storm surge). In all cases, capacity reserve is the capacity difference between the minimum service required and the design capacity. See text for more explanations.

factor in design. The system resilience in *CR* is measured by the ability of a water system to provide a service level above the desired sustained level of service. One ultimate goal is to balance *CR*, the risk of failure, and adaptation cost. Note that the risk of failure of water infrastructure is the overarching concern, and it why significant redundancy or *CR* is built into these systems. Similar social, environmental and economic objectives, known as the “triple-bottom line,” apply to hydroclimatic adaptation in general (Cromwell III et al., 2007).

Figure 2-51 shows the *CR* concept and its relationship with infrastructure resilience. The installed *CR* is a parameter to quantitatively measure the vulnerability threshold from which the ecological system resilience concept of Marshall and Toffel (2005) is modified for infrastructure adaptation analysis (Figure 2-51). For capital-intensive water infrastructure, at the core of adaptation is the ability to increase its resilience for unanticipated changes and to build-in adequate flexibility for control of the uncertainty-related risk. This capacity is shown for scenario I and II in the case of an external impact from hydroclimatic or other environmental change. The scenario II represents temperature vulnerability of the infrastructure “out-of-service” below the desired capacity. This condition in urban water supply and sanitation has happened with an increasing frequency in the past decade; examples include the recent Hurricane Sandy in the New York City and the adjacent coastal states, the droughts in Florida during the 2000s, flooding in Houston in 2017 from Hurricane Harvey, and the ongoing droughts and fires in California. After such hydroclimatic disruptions, some urban water infrastructure may not recover to the original design capacity. The difference is capacity loss (Figure 2-51), often because of aging infrastructure and damages from external climate impacts.

In contrast, the Types III and IV changes in infrastructure service are not recoverable (Figure 2-51). The impact at t_I results in permanent impairment of the infrastructure service functions, while the Type IV results in the failure of water services, a condition that water managers strive to avoid at all costs. In both cases, the infrastructure service functions are significantly impaired to the extent to which it cannot provide the desired service level (Figure 2-51). A service recovery requires capital investment for rebuilding at a significant cost or paradigm shifts to avoid future recurrence of the service disruptions. Examples of these potential scenarios include the damage by coastal hurricanes, storm surge, sea level rise and periodic inundation (Comfort, 2006; Turnipseed et al., 2007; Gesch, 2005; Wing et al., 2002), impacts from water pollution resulting from a climate event (e.g., Wing et al., 2002; Cann et al., 2012), as well as preventative measures taken for adaptation and mitigation (e.g., Rosenzweig et al., 2007). During the 2012 Hurricane Sandy, boil water advisories were issued to a large number of customers and local health agencies, during and after the disruptive events¹³.

As shown in Figure 2-51, adequate *CR* at the time of design and construction (t_0) is needed to account for the *CR* reduction due to infrastructure aging. Effective *CR* at the time of the global impact t_I that is sufficiently large to avoid service disruption allows for timely recovery in the recovery phase (Type I). Compared to this sustainable water infrastructure condition, the Type II change makes the water service temporarily unavailable during the damage phase, a condition that will require adaptation measures and engineering solutions.

Significant functional damage to water infrastructure in Type III and IV situations require attention because of their long-lasting effects. While conventional rebuilding and reconstruction are often the water resource measure, long-term sustainability has been discussed. Examples

¹³ <https://www.health.ny.gov/environmental/emergency/weather/hurricane/>

include water supply and sanitation paradigm changes (Gleick, 2000; Pahl-Wostl, 2007), urban system re-planning and avoidance of disaster areas (Bull-Kamanga, et al., 2003; Godschalk, 2003; Comfort, 2006), and urban-scale or region-scale water management. Urban-scale adaptive planning is another approach in that the urban resiliency that has been analyzed and improved through a systematic analysis of land use, population distribution, and transportation-water infrastructure. This method and application example in Cincinnati, Ohio will be described subsequently in Section 5.3 and 6.0

One further complication in the systems analysis is the evolving urban management objectives evolve with time. Thus the required service capacity $f(t)$ is time-dependent. The $f(t)$ increases with urban population and economic activities, while decreasing as water conservation takes place. Thus, the resilience CR varies with time as either change in the required $f(t)$ or deterioration of infrastructure's service capacity with time (e.g., aging water infrastructure). When the CR limit is exceeded, the water structure functions are compromised (Figure 2-51) with partial or complete loss of service capacity (Type III and IV). For many water managers, the central question is how to avoid the hydroclimatic impacts that lead to the Type II, III and IV changes, by taking necessary and proactive adaptation measures.

5.1.4. *CR and engineering practice*

Engineering practices take different approaches to define and use CR for various water infrastructure (more details will be provided in Section 5.2). The current practice emphasizes accurate determination of the design variables to minimize the uncertainty and ensures a system capacity adequate to provide a margin of safety or safety factor. The purpose is to minimize the excessive capacity that could later become stranded (unused) capacity for economic considerations, or on the opposite side to avoid the lack of capacity for intended services. Making such design decisions occurs within a decision space that has a host of uncertain variables (population changes, land use changes, economic uncertainty, climate, etc.). To partially address the problem, some technical basis for design is incorporated. To wit, engineering such systems commonly assumes a stationarity whereby the climate and hydrological design parameters can be specified with appreciable degrees of "perceived" certainty; for example, by using the Atlas-14 precipitation design charts.

In deterministic engineering, progressive refinement of design basis and engineering objective is widely used to minimize uncertainty and thus the system costs. A small design uncertainty, under the assumed stationary precipitation, allows the use of simple engineering techniques such as a safety factor for key design parameters. However, this traditional engineering practice is challenged by the recognition of a non-stationary climate and hydrological variables. Because failure is so judiciously avoided, excess capacity is common in the water industry, in the form of redundant systems. The large uncertainties in consideration of a non-stationary climate would ensure excessive, if not prohibitive, capital and operational cost. The alternative is to use adaptive engineering, by which the modification of water infrastructure CR is planned, but not installed until the uncertainty is adequately reduced. One pre-requisite for this adaptive approach is the modeling-monitoring framework shown earlier in Figure 2-1.

The engineering approach for adaptation differs from the current in how the required CR is defined installed. The CR contingency can be designed into the system. It is constructed and operated later only when the engineering basis is adequately defined at a given level of managed engineering risk. Several widely used engineering practices have a potential for adaptive

engineering, such as modular design and phased construction (Girard and Mortimer, 2006; Chung et al., 2009), decentralized water supply, wastewater and storm water management (Weinstein, 2009; Gikas and Tchobanoglous, 2009), as well as model-driven water reservoir operations for river flow management under changing hydroclimatic conditions.

For existing water infrastructure, adaptation potential can be pre-installed during retrofitting and process optimization, realignment and expansion of existing infrastructure assets, as well as operational changes; all may require substantial physical asset alteration which may be surprisingly easy to accomplish as a part of renovation and replacement of aging infrastructure. It requires water managers to consider adaptation at the time of conceptual engineering. The consideration of the adaptation is considered necessary under following three conditions:

- Infrastructure planning horizon is long, for which future precipitation, land use and population changes are not precisely determined. Only using this timeline can one evaluate whether the rate of hydroclimatic change is too small to be “tangible” for adaptation, or too excessive for the infrastructure to adapt at a reasonable cost. In this report, the adaptation need analysis is set for the next 30-50 years or by year 2040-2060;
- The rate of precipitation change is larger than assumed in the original engineering design, or the rate is comparable to those of the other two non-stationary variables – population and land use changes;
- Large uncertainty in precipitation projection is translated and further propagated into infrastructure engineering parameters, affecting the *CR* determination. The uncertainty is also time-dependent, decreasing over time as the climate (precipitation) projection improves.

The similarity and differences among the three engineering approaches to improve the infrastructure *CR* and performance are summarized in Table 2-19. Note that the engineering methods and techniques are different for the existing and new water infrastructure.

5.2. Water infrastructure capacity reserve and resilience

5.2.1. Storm water infrastructure functions and design tolerances

Storm water, drinking water and wastewater infrastructure in an urban catchment are schematically shown in Figure 2-50. Storm water infrastructure manages overland runoff and channel flows. Its major components, service functions, and likely vulnerability to precipitation change are listed in Table 2-20. In a non-stationary climate, future runoff time-flow (t - Q) variations can significantly differ from that of the original engineering basis of design. This difference affects the designed hydraulic conveyance capacity of a built storm water network. The difference can also adversely affect the hydraulic and water quality design functions of low-impact-development (LID) measures and storm water best management practices (BMPs).

5.2.1.1. Realized hydraulic capacity reserve

Carrying capacity and hydraulic profiles of a storm water network are designed to limit the nominal pipe flow to a range of 0.6-4.6 m/sec. This design criterion is intended to prevent excessive sedimentation in or erosive damage to the conveyance piping and the receiving water. For a fixed topography, the runoff t - Q profile in a storm water pipe depends on the precipitation intensity, pre-storm soil moisture content, vegetation cover and land use patterns. Among the

Table 2-19. Water infrastructure design and engineering domains, and their attributes.

	Deterministic Engineering Domain (1)		Adaptation Engineering Domain (2)		Re-design & Re-construction Domain (3)	
	Attribute	Potential action*	Attribute	Potential action*	Attribute	Potential action*
<u>New Infrastructure</u>						
Hydraulic capacity	Specific value	Process adjustment and retrofitting; No large-scale asset modification; Go to Domain (2) or (3) in severe CR limitation	Range; capacity adaptively installed	Assessment-adaptation-monitoring for optimal cost-benefit balance; Go to Option (3) for severe CR limitation	Specific value	Optimization, retrofitting; Management and objective re-evaluation
Engineering flexibility	Limited in quantity. Realized at construction		Flexible timing for extra capacity installation		Large CR expansion after re-construction	
Water quality capacity**	Specified value		Range; capacity adaptively installed		Specified value	
Engineering flexibility	Limited in quantity. Realized at construction		Flexible timing for extra capacity installation		Large CR expansion after re-construction	
<u>Techniques and examples</u>						
Stormwater infrastructure	Hydraulic design using runoff rational methods for facilities (e.g., retention ponds and storm sewer)	Satellite retention facilities; Slice gate automation; Go to Domain (2) or (3) in severe CR limitation	Structure, LIDs / BMPs design for non-stationary precipitations; Module design, phased installation; System monitoring and forecasting	Adaptive capacity installation; Go to Domain (3) for severe CR limitation	New infrastructure network with or without use of existing assets	Optimization, retrofitting; Management and objective re-evaluation.
Wastewater infrastructure	Ten-State design standards, other design protocols	Process automation; Flow detention facility; Go to Domain (2) or (3) in severe CR limitation.	Module design, phased installation; Decentralized wastewater system; Onsite wastewater reuse; System monitoring and forecasting.	Adaptive capacity installation; Go to Domain (3) for severe CR limitation	New designs and use of revolutionary technologies and concepts	
Drinking water infrastructure	Unit process and system modeling and specifications (e.g., disinfection chamber)	Disinfectant, dosage change; Go to Domain (2) or (3) in severe CR limitation	System optimization, retrofitting; Module design, phased installation; System monitoring and forecasting.	Network expansion; Adaptive capacity installation; Go to Domain (3) for severe CR limitation	New designs and use of revolutionary technologies	
References	ASCE (2004), Lin (2001), USEPA (1994; 2002a; 2008), Salvato et al. (2008), engineering codes and guidelines		Carter and Jackson (2007); Chung et al. (2009); Semadeni-Davies et al. (2008); Gikas and Tchobanoglous, 2009; Oron et al., (2007), Gupta and Shrivastava (2006), and USEPA (2009b)		Chang et al., 2006; Neuman (2009).	

Table 2-19 continued.

	Deterministic Engineering Domain (1)		Adaptation Engineering Domain (2)		Re-design & Re-construction Domain (3)	
	Attribute	Potential action*	Attribute	Potential action*	Attribute	Potential action*
<u>Existing Infrastructure</u>						
Hydraulic capacity	Fixed	Infrastructure optimization, retrofitting; Go to Domain (2) or (3) for severe CR limitation	Range of values	Iterative assessment- adaptation-monitoring for optimal cost-benefit ratio; Go to Domain (3) for severe CR limitation	Specific value	Optimization, retrofitting; Management and objective re-evaluation
Engineering flexibility	Limited, and deteriorated after construction		Large, adaptively installed		Large CR expansion after re-construction	
Water quality capacity**	Fixed		Range of values		Specified value	
Engineering flexibility	Limited and deteriorated after construction		Large, adaptively installed		Large CR expansion after re-construction	
<u>Techniques and examples</u>						
Stormwater infrastructure	Operation and maintenance	CSO division adjustment; Go to Domain (2) or (3) for CR expansion	Urban LIDs, BMPs designed for non-stationary precipitation; Structure retrofitting; Recursive monitoring- adaptation-assessment	Adaptive CR installation (new infrastructure); Go to Doman (3) for severe CR limitation	New infrastructure network with or without use of existing assets	Optimization, retrofitting; Management and objective re-evaluation.
Wastewater infrastructure		Operational adjustment for CR increase; Process optimization without large asset change; Go to Domain (2) or (3) for severe CR limitation	Model-based system design and upgrading; Adaptive system retrofitting and improvement; Recursive monitoring- adaptation-assessment	Adaptive CR installation (new infrastructure); Go to Doman (3) for severe CR limitation	Application of new and revolutionary technologies	
Drinking water infrastructure		Operational adjustment for CR increase; Process optimization without large asset change; Go to Domain (2) or (3) for severe CR limitation	System optimization; Process retrofitting without large asset alteration; Recursive monitoring- adaptation-assessment	Adaptive CR installation; Network expansion; Go to Doman (3) for severe CR limitation.	Application of new and revolutionary technology; New infrastructure expansion for CR	
References	ASCE/AWWA (2004), USEPA (2004), engineering codes and guidelines		Chung et al. (2009), Gikas and Tchobanoglous (2009), Montalto et al. (2007); and Donofrio et al. (2009).		Chang et al. (2006); Neuman (2009).	

Note: * - Potential actions at the upper limits of infrastructure CR and flexibility.

** - Refers to the capacity of a water infrastructure in maintaining performance on specific water quality criteria.

Table 2-20. Important engineering attributes for stormwater infrastructure adaptation

Unit Operation	Function	Major Design Criteria*		Vulnerability **			Adaptation	
		Physical	Chemical, biological	Physical damage	Hydraulic Function	Water Quality Function	Function	Example
<u>Stormwater collection</u>								
Stormwater collection	Stormwater runoff collection in urban area for reliable drainage and sanitation	Drain inlet spacing <183 m; Manhole spacing: 122-183 m (varied with pipe diameter); 25-year design storm (varied)	Prevent methane and sewer gas generation; Remove oil and grease, debris and large objects.	Likely medium	Likely high	Likely low	Stormwater ponding, urban flooding, and drainage management	Stormwater inlet design for non-stationary precipitation.
Stormwater gravity drain and conveyance	Stormwater transfer by pipe network to discharge locations or retention facilities	I/O design limit in per day -km-cm; Flow velocity: 0.6-4.6 m/s for gravity sewer	Prevent methane and sewer gas generation	Likely medium	Likely high	Likely low	Infiltration / exfiltration (I/O) management; Pipe flow velocity control	Pipe repair, I/O management; Drop manhole alignment for new Q-t profiles; In-line degritter for debris
<u>Stormwater BMPs and LIDs</u> #								
Hydraulic retention	Increased water retention in urban catchment basin for reduced peak flows	Varies, based on assumed precipitation stationarity		Varied	Likely high	Varied	Increased retention function for non-stationary precipitation	Detention pond, stormwater swirl, and permeable pavements
Stormwater treatment ponds and bioretention facilities	Enhanced water quality improvement within an urban catchment		Performance design for target pollutant removal.	Varied	Varied	Likely high	Enhanced water quality improvement within an urban catchment	Distributed stormwater retention and treatment ponds
Groundwater recharge or evapotranspiration	Diverting water from the urban catchment and channel flows			Varied	Likely low	Likely low	Reduced stormwater channel flow and discharge	Permeable pavement, green roof, recharge sewer.
Stormwater reclamation	Reclamation and reuse of storm water diverted from channel flows		Contaminant prevention for source water in reclamation	Varied	Likely high	Likely high	Collection and treatment of stormwater for beneficial reuse	Cisterns, rain barrels, rain gardens
<u>CSS and CSO control</u>								
Stormwater diversion	Prevent hydraulic overloading of wastewater treatment plant in high-intensity precipitations	Flow rate and water level for diversion valves in CSS; Water level control in CSO retention facilities.		Likely low	Likely high	Likely high	Reduce CSO impacts to both wastewater treatment plants and discharge receiving water	System engineering of retention and CSO treatment facilities; Extreme precipitation forecasting and emergency responses.
<u>Stormwater discharge</u>								
Stormwater discharge at constructed outfalls	Discharge treatment effluent into a water body under a NPDES permit	Flow rate and discharge velocity	Varied in water quality parameters	Likely low	Likely medium	Likely medium	Reduce discharge impacts on receiving water in erosion, temperature, turbidity and nutrients.	Discharge swirl and detention; Sensor-based monitoring-controlled discharge

Note: * Summarized from civil engineering manuals and U.S. engineering codes and guidelines. These design criteria are for general guidance.

** - Qualitative rating for anticipated major changes in precipitation and hydrology, excluding the extreme meteorological events.

- Stormwater BMPs and LIDs are organized in the four groups.

factors, precipitation intensity and soil moisture are climate-dependent. Design precipitation intensity at a given return interval (e.g., 10-year design storm) is commonly determined from categorized precipitation charts such as NOAA precipitation Atlas 14 (NOAA, 2007), National Weather Bureau Technical Paper 40 (Hershfield, 1961), and the SCS 24-hour rainfall curves (Guo and Hargadin, 2009). These current methods are all based on assumed precipitation stationarity.

Hydraulic *CR* of a storm water pipe is realized from two primary sources. Because of the stochastic hydrologic process and the uncertainties in hydrologic parameters, a large empirical safety factor around 1.5–2.0 is often used in hydraulic design. For example, Schaad et al. (2009) described an approach of using large safety factors in hydraulic engineering of a holistically managed storm water system. The other primary source of hydraulic *CR* comes from the fact that

storm water pipes are available only at fixed nominal diameters, and minimum diameter (typically 15 inches) are often specific. This means that the hydraulic carrying capacity (Q_2) of installed pipe with a diameter (d_2) is greater than the design peak flows (Q_1) carried by a pipe diameter (d_{min}). The maximum increase for the installed carrying capacity $\left(\frac{Q_2 - Q_1}{Q_1}\right)$ is:

$$\frac{Q_2 - Q_1}{Q_1} = \left(\frac{d_{min}}{d_2}\right)^{\frac{2}{3}} - 1 \quad (2.33)$$

For storm pipe mains larger than 0.60 m (24 in) in diameter, this engineering practice potentially offers a hydraulic *CR* of 31% on average while satisfying the design criteria on pipe flow velocity selections (Figure 2-52). In this simple envelope calculation, $\Delta Q\%$ is calculated using Eq. 2.33 for pipes at a hydraulic slope (S) of 0.2% and 0.5%. Pipe flow velocity (V) in a range of 0.6–4.6 m/sec by engineering standards, is calculated using Manning's equation. The

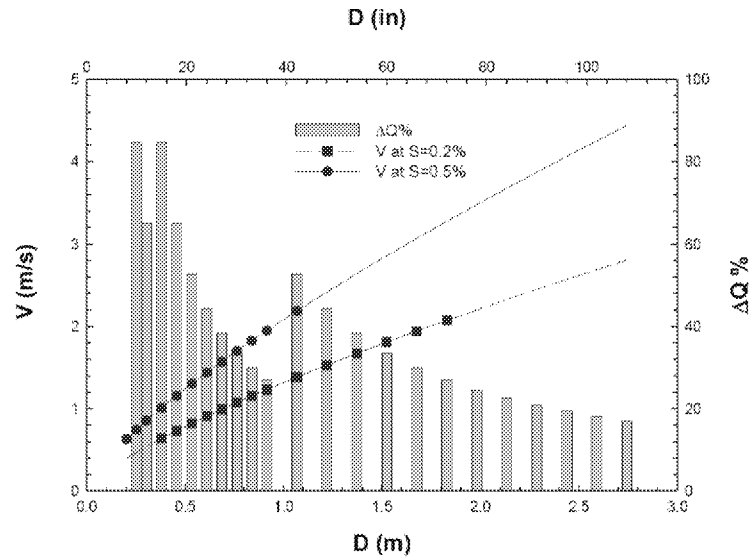


Figure 2-52 Maximum percentage increase ($\Delta Q\%$) in hydraulic capacity of storm water conveyance using commercial concrete pipes of discrete nominal diameters (D). Eq. 2.33 is used for the calculations.

maximum capacity increase is approximately 60% for lateral pipes of diameter <0.61 m (24-in). Therefore, combining with a safety factor of 1.5-2.0, the pipe engineering practice could have installed a maximum hydraulic capacity up to 230% of the design value. Of course, one reason for doing this is that the stormwater pipes get sand and other material building up on the bottom since the flows are often not continuous, which reduces the capacity of the pipe and the available *CR*.

5.2.1.2. *Water quality limitations*

Climate-driven water quality changes can significantly limit the infrastructure *CR* in storm water adaptation. Studies (e.g., Horowitz, 2009; Whitehead et al., 2009; Yang et al., 2002) have linked the intensity of peak runoff to the increased turbidity, and higher metals, chemical, and dissolved organic carbon loading in urban streams. Peak pipe flow and high discharge velocities are also found to be responsible for soil erosion, water quality degradation and ecological deterioration at outfalls and their immediate downstream segments (See McCorquodale, 2007; Novotny and Witte, 1997). These hydrologic and water quality changes can be attenuated or amplified within an urban catchment (Table 2-20).

CSO events during intense precipitation are a major factor limiting infrastructure *CR* otherwise available for adaptation. Storm water runoff and untreated, but diluted, sewage is diverted for discharge when storm water peak flows exceed hydraulic capacity of the wastewater treatment plants and the available retention facilities. The peak flow, on the other hand, is a function of the precipitation duration and intensity, the catchment basin hydrograph, and the groundwater infiltration rate into the pipes (Black and Endreny, 2006; Lai, 2008; and Diaz-Fierros et al., 2002). More intense precipitation events projected as future climate conditions will likely yield greater peak flows and more frequent CSO events unless efforts are undertaken to separate flows (U.S. EPA, 2009a; Capodaglio, 2004; Alp and Melching, 2009). The U.S. EPA (2013c) 20-watershed study showed significant hydrological flow modifications that can worsen the CSO situations (Johnson et al., 2015).

Furthermore, the national adaptation reports on watershed hydrological responses (U.S. EPA, 2014) demonstrated different responses in watersheds to different hydroclimatic provinces. Land use and the degree of impervious surface in the urban watersheds can lead to varying responses to future climate-related precipitation changes, often increasing peak flows and runoff.

Storm water BMPs and LIDs are widely used for enhanced storm water retention and reduced peak runoff. They are also currently engineered assuming a precipitation stationarity (e.g., Lai, 2008; Montalto et al., 2007; U.S. EPA, 2004; Marsalek and Chocat, 2002; Dietz, 2007; Carter and Jackson, 2007; and Gilroy and McCuen, 29). Thus, they are also vulnerable to reduced performance and effectiveness under a non-stationary climate (Table 2-20). Semadeni-Davies et al. (2008) further suggested the need to consider climate and precipitation changes in storm water BMPs designs.

The U.S. EPA's National Stormwater Calculator (NSC) estimates and evaluates BMP and LID applicability in reducing storm water runoff (U.S. EPA, 2014). While the tool includes precipitation projections under future climate scenarios, a comprehensive nationwide evaluation has not been conducted. With this data not yet available, the maximum *CR* of 230% of the design value was taken as the upper limit.

5.2.2. Drinking water infrastructure functions and design tolerances

5.2.2.1. Engineering resilience in a distribution network

Community water systems (CWS) in the U.S. provided water supplies to over 292 million people in 2008. Engineering attributes of major CWS components and their potential vulnerability to precipitation changes are shown in Table 2-21. Drinking water distribution following the treatment (Figure 2-50) is engineered to meet water demand for both domestic consumption and firefighting throughout a service area. Long-term water demand variations, a prime engineering factor in water distribution design and operation, is linked to demographic and land use changes and to the transformation of water-intensive industries (Levin et al., 2002; Pires, 2003; Hummel and Lux, 2006). It is commonly captured in urban development master plans and prime engineering factor in water distribution design and operations, is linked to demographic and land use changes and to the changes with water-intensive industries (Levin et al., 2002; Pires, 2003; Hummel and Lux, 2006). Long-term water demand variations are commonly captured in urban development master plans and regional economic development projections (See Figure 2-49) that may have intrinsically included adequate hydraulic capacity for adaptation.

Water quality changes within a distribution system have been extensively studied. However, little is directly related to future climate and hydrological conditions. In a study of climate adaptation for a large U.S. Midwest utility, Li et al. (2009, 2014) and Clark et al. (2009) reported that an increased total organic carbon (TOC) level in (surface) source waters under future climate scenarios could lead to higher TOC concentrations in produced water and subsequently greater disinfection by-product (DBP) formation, potentially at levels in violation of the U.S. drinking water standards. This water quality effect can significantly reduce the available infrastructure *CR*, making adaptation necessary. Table 2-20 lists a variety of adaptation options in unit process engineering, such as enhanced TOC removal using GAC or chemical flocculation (e.g., Järvinen et al., 1991; Crozes et al., 1995; Li et al., 2009; and Clark et al., 2009), water age reduction and chlorine addition optimization for DBP control (Carrico and Singer, 2009; Prasad et al., 2004; Boccelli et al., 2003). In addition, higher surface water and associated drinking water temperatures in future climate scenarios will very likely change the disinfection kinetics, DBP formation rates and biological stability in a distribution system. These areas of indirect hydroclimatic impacts are worthy of further investigations.

5.2.2.2. Realized capacity reserve in drinking water treatment

Water intake and water treatment are vulnerable to the direct impacts of precipitation changes (Table 2-21). Detailed modeling-monitoring studies have shown the degree of these impacts in surface water bodies of different sizes across the U.S. (See U.S. EPA, 2013b). These impacts vary among watershed, different types of land use and land cover, as well as the nature of precipitation and temperature changes. Overall, a water treatment process is required to accommodate these source water variations and to provide finished drinking water in compliance to the SDWA regulations.

As shown in Figure 2-50, a typical surface water treatment process in the U.S. consists of pre-oxidation, rapid mixing, flocculation and sedimentation, granular filtration, advanced treatment if necessary [e.g., GAC filtration, membrane separation], and finally disinfection in

Table 2-21. Important engineering attributes and likely vulnerability in drinking water treatment and distribution systems for community water supplies.

Unit Operation	Function	Major Design Criteria*		Vulnerability **			Adaptation	
		Physical	Chemical, biological	Physical	Hydraulic Function	Water Quality Function	Function	Example
<u>Source water protection</u>								
Source water intake	Protect source water quality at water intake Assure water availability for drinking water production	Water level at water intake	Minimize daily and seasonal water quality variations; Minimize biological growth at intake (e.g., mussel).	Likely High	Likely Medium	Likely Medium	Adaptive change of intake elevation and location;	Multi-elevation intake aprons
		Intake security against physical damage					Physical damage protections	Enhanced structure supports
<u>Drinking water treatment</u>								
Rapid mixing	Rapid dispersion of coagulants in water	<1 min retention time		Likely Low	Likely Low	Likely Low		
Coagulation & Flocculation	TOC and particulate removal	15-20 min and 18-25 min residence time for high-energy and low-energy flocculation.	Varied dosage among coagulants: alum, chlorine, polymer, and potassium permanganate	Likely Low	Likely Low	Likely High	Inflow TOC variations monitoring and chemical dosing control.	Sensor-based TOC monitoring and process adaptive control
Clarification	Remove settleable solids after flocculation. Alternative unit processing by membrane and particulate filtrations	32.6-48.9 m ³ /d/m ² for turbidity removal 20.4-32.6 m ³ /d/m ² for algae removal		Likely Low	Likely Medium	Likely Medium	Reduce high-turbidity effect on downstream units; Remove excessive algae present in raw water.	Process monitoring and control; Unit process optimization
Dissolved air floatation (DFA)	Remove solids and odor with ascending fine bubbles	10-12 m/h air flow; 5-10% recycle flow.	Follow coagulation / flocculation unit process	Likely Low	Likely Low	Likely Low	Adjust particle surface charge for enhanced DFA	Unit process optimization
High rate filtration	Remove various constituents, including turbidity, coliform, color, taste, metals, and toxic chemicals	hydraulic loading: 83 L/m ² /min (rapid sand) Backwash monitoring and operation.		Likely Low	Likely Medium	Likely Medium	Reduce shock loading of high turbidity; Optimize backwash scheduling, operation.	Process monitoring and control
Oxidation and disinfection	Biological inactivation and oxidation of organic matters		Disinfectant concentration limit: 1.0 mg/L Cl ⁻ ; Contact time	Likely Low	Likely Low	Likely High	Reduce TOC concentration and variations; Unit process optimization.	Retrofitting for higher contact efficiency; Change of oxidants.
Ion exchange	Cation or anion exchange to remove nitrate, Fe, Mn, and hardness	Service flow rate: <668 L/m ³ for N ⁺² removal; Backwash rate: 81-122 L/m ² for N ⁺² removal.		Likely Low	Likely Low	Likely Medium	Remove excess turbidity in pretreatment; Process unit arrangement, optimization, retrofitting.	Process adjustment; Enhanced water pretreatment; Process monitoring
Membrane filtration	Remove organic and inorganic contaminants by using membranes	Hydraulic loading rate; Temperature; Suspended solids.	Inflow pH range; Membrane anti-degradation; Biological growth.	Likely Low	Likely Low	Likely Low	Pretreatment to remove excessive turbidity; Backwash operations.	Pretreatment with coarse membrane filter; Back-wash automation
GAC adsorption	Absorb chemicals onto absorbent media	10-12 m/h loading; Bed depth and volume.	Regeneration time; DOC, odor, and other contaminant removal.	Likely Low	Likely Low	Likely High	Increase GAC adsorption efficiency and prevent break-through	Adjust GAC regeneration cycle; Operation optimization.

Table 2-21 continued.

Major Operation Unit	Function	Design Criteria*		Vulnerability **			Adaptive Engineering and Management	
		Physical	Chemical, biological	Physical	Hydraulic Function	Water Quality Function	Functions	Example
Treatment process	Overall specification of each process unit for treatment objectives	Process flow rate; Flow variations.	Drinking water treatment guidelines Drinking water quality standards.	Likely Low	Likely Medium	Likely High	Increase treatment capacity reserve for new source water variations and water demand changes	Process optimization, retrofitting, or change and expansion
<u>Drinking water distribution</u>								
Water demand	Spatial and temporal demand variation affect network operation and water age	Not applicable	Not applicable	Not Applicable	Likely High	Likely High	Water demand management under high temperature and heat stress of future climate	Water pricing, lawn irrigation timing and management
Pipe network	A network of pipes in different diameters and materials to deliver water from treatment plant to consumer's tap	Pressure management: 413 kpa (241-689 kpa) Flow velocity: 1.2-1.8 m/s in mains.	Corrosion protection; Water age management; Water quality standard compliance at user's tap.	Likely High	Likely Low	Likely High	Prevent pipe corrosion and leaks under future climate; Water quality management;	In-network water treatment such as chlorine addition and THM stripping.

Note: * Summarized from ASCE/AWWA (2004), Lin (2001), Salvato et al. (2008).

** - Qualitative rating given for major changes in precipitation and hydrology, excluding the extreme meteorological events.

clear wells before distribution. In the design of these treatment process units, a simple empirical safety factor of 1.2-1.5 is often used; some larger values are possible. For example, Kim and Bae (2007) proposed a safety factor of 2.0 in hydraulic design of a baffled GAC contactor for odor control. More advanced probability-based methods are developed for systematic reliability-cost tradeoff evaluation. Boccelli et al (2007) described process optimization guided by a cost-performance ratio to determine safety factors in the flow rate design of an infiltration-based surface water treatment plant. Gupta and Shrivastava (2006) introduced a water treatment design method based on Monte-Carlo simulation to quantify performance uncertainties in suspended solids removal.

Li et al. (2009) developed a Monte Carlo methodology to simulate the cost-probability curves in GAC contactor process modification. While these advanced design methods better quantify the capacity and cost CDF curves, they require extensive input data and computation. Instead, the traditional safety factor method is widely used in field engineering of the deterministic domain. This practice alone yields a maximum treatment capacity at 150% of the design value to permit redundancy when units are out of service. For impacts exceeding the *CR* limits, adaptation is needed to increase infrastructure *CR*, mostly through treatment plant retrofitting, process modification, or change of unit operations (Table 2-21).

An engineering adaptation example is given by Li et al. (2014; 2009) and Clark et al. (2009). In the Section 6.0, the adaptation engineering model “Water Treatment Plant – Climate Adaptation Model” will be described. Its application at the Greater Cincinnati Water Work’s Richard Miller treatment plant will be described in a later section.

5.2.3. Wastewater infrastructure functions and design tolerances

5.2.3.1. Realized capacity reserve in hydraulic loading

Important engineering functions and physical attributes for wastewater infrastructure are shown in Table 2-22. A general wastewater treatment process in the U.S. includes physiochemical pretreatment, biological oxidation of macronutrients (primarily BOD), possible filtration to reduce suspended solids, optional tertiary treatment (N and P removal), and finally effluent disinfection before discharge (See Figure 2-50). Hydraulic loading capacity is often specified for future wastewater generation within a service area and to account for groundwater infiltration into wastewater collection pipes (Lai, 2008; Lin, 2001). These variables are lumped into a single parameter – wastewater generation rate per capita in engineering designs (for example, 1900-4550 lpd/person (500-1200 gpd/person)). In addition, an empirical safety factor of 1.2-4 is used to accommodate unexpected hydraulic variations (peak hours). Values up to 4.0 are justified for special engineering conditions, such as complex hydrogeological regions, aged water collection networks with extensive infiltration and exfiltration, very small service areas, or service areas of large variation in wastewater generation rates.

5.2.3.2. Realized capacity reserve in biological systems

Space-demanding aerobic and anaerobic biological treatment is a limiting unit process that frequently determines available *CR* at a wastewater treatment plant. All wastewater plants have significant *CR* to permit unit operations being taken out of service for maintenance due to the corrosive environment in which they operate. The limitation and vulnerability are illustrated in the design or retrofitting of an aeration tank, a principal unit in the activated sludge

Table 2-22. Important engineering attributes and potential vulnerability of wastewater infrastructure

Major Operation Unit	Function	Major Design Criteria*		Vulnerability**			Adaptation	
		Physical	Chemical, biological	Physical	Hydraulic Function	Water Quality Function	Function	Example
<u>Wastewater collection</u>								
Wastewater collection	Wastewater collection from all users in a service area	WW yield: 0.38 m ³ /person-day; Flow velocity: 0.6-4.6 m/s; Flow rate: 1.5 m ³ /person-day (laterals and branches)	Sulfur and methane gases generation	Likely High	Likely High	Likely Low	Pipe I/O flow management; Wastewater reuse and separation.	Pipe leak detection; Dual pipe system; Onsite wastewater treatment
Wastewater pumping and conveyance	Wastewater transfer to a central location(s) for treatment	I/O rate: < 0.45 m ³ /day-km-cm; Flow: 0.95 m ³ /ca-day (main); Flow velocity: 0.6-4.6 m/s	Sulfur and methane sewer gas management; Fire hazard prevention.	Likely High	Likely High	Likely Low	I/O management; Flow velocity & abrasive damage control.	Pipe leak detection Drop manholes; In-line degritter
<u>Wastewater treatment</u>								
Preliminary treatment (screening, degritting)	Solids and debris removal in headworks	Screen debris removal: >5.1-cm Flow (grit chamber): ~0.328 m/s; Aerated grit chamber: 2-5 min residence time	Not applicable	Likely Low	Likely Low	Likely Low		
Primary treatment - Sedimentation tank	Removal of settleable solids and 25-35% BOD	Peak flow <0.71 lps/m ² ; Maximum weir load: 2.16 lps/m; Water depth: >2.1m.	Target removal rates: BOD: 20-40%, TSS: 35-65%; Settleable biosolids: 50-75%.	Likely Low	Likely Medium	Likely Medium	Flow equalization facilities to smooth flow variations; Process monitoring	Monitoring and increased maintenance
Secondary treatment - Trickling filters	Biological treatment to remove BOD and macronutrients	Filter depth: 1.5 - 3.0 m; Hydraulic loading: 0.012 - 0.047 lps/m ² , or 0.047- 0.47 lps/m ² (high rate).	Normal: 0.08 - 0.40 kg BOD/m ³ -day; High-rate: 0.48 - 1.44 kg BOD/m ³ -day.	Likely Low	Likely High	Likely High	Process control for resilience in shock loading Process flow stabilization	Trickling filter retrofitting; Change recirculation ratios; Process monitoring and control for weir loading.
Secondary treatment - Activated sludge process	High efficiency of BOD and nutrient removal	Weir loading: 1.44 lps/m; Hydraulic loading: 0.47-0.57 lps/m ² 0.38 lps/m ² with nitrification	Maximum BOD loading: 0.24-0.64 kg/day/m ³ ; Aeration rate: 93.5-125 m ³ oxygen / kg BOD	Likely Low	Likely High	Likely High	Process control for resilience in shock loading Increase treatment capacity reserve.	Modify cell age and sludge return rate; Improve aeration efficiency; Increase aeration capacity.
Secondary and final clarifier	Settleable biosolid removal	Surface settling rate: 50-62 lps/m ²	Not applicable	Likely Low	Likely Low	Likely Low	Enhance biomass setting	Operational adjustment
Nitrogen removal	Successive nitrification and denitrification	Varies. See U.S. EPA (2009b).	Varies. See U.S. EPA (2009b).	Likely Low	Likely Low	Likely High		
Chlorination	Treatment effluent disinfection	>15 min contact time in chlorination contact basin	<200 fecal coliform / 100 ml	Likely Low	Likely Low	Likely Low		
Treatment process	Overall specifications of each process unit for treatment objectives	Process flow rate; Flow rate variance.	Surface water quality standards for discharge control	Likely Low	Likely Medium	Likely High	Increase treatment capacity reserve to against source water variations and water demand changes	Process optimization, retrofitting, or change and expansion
<u>Wastewater effluent discharge</u>								
Treatment effluent discharge	Treatment effluent discharge under a permit	Varies depending on discharge regulations	Varies depending on discharge regulations	Likely Low	Likely Medium	Likely High	Discharge limits sensitive to the impacts on receiving streams; Compliance to discharge limits.	Adjust treatment process for likely to-be-revised discharge limits.

Note: * Summarized from "10-state" wastewater treatment standards and Lin (2001). These design criteria are for general guidance.

** - Qualitative rating given for major changes in precipitation and hydrology, excluding the extreme meteorological events.

I/O - wastewater inflow and outflow by infiltration and exfiltration; WW - wastewater.

wastewater treatment process. The BOD removal rate (η_{BOD}) in an aeration basin/clarifier combination, represented as tank influent (c_o) and effluent (c) is a function of flow rate (Q), tank volume (V), BOD oxidation rate (k_d), biomass cell age (θ_c), microorganism concentration in the tank (X), waste rate, and maximum yield coefficient (Y). Following Lin (2001), the removal rate can be written as:

$$\eta_{BOD} = \frac{c_o - c}{c_o} = \frac{\theta_c X V}{(1 + k_d \theta_c) Y c_o} \frac{1}{Q} \quad (2.34)$$

An increase in wastewater flow rate reduces hydraulic retention time and decreases BOD removal rate (Figure 2-53). Such an occurrence under future climate conditions may occur due to more frequent hydraulic overloading resulting from increased variability of precipitation. An increase in CSOs are a likely sign of such overloads. These events are responsible to treatment process upsets and discharge violations (e.g., Tafuri and Selvakumar, 2002; Diaz-Fierros et al., 2002; Capodaglio, 2004). Efforts to split combined systems and seal the piping at the surface are appropriate measures to address this problem.

Capacity reserve in biological treatment is recognized by using an empirical design safety factor commonly 1.2–1.3, and by modifying unit operations without large physical asset alteration (Table 2-22). In addition, the treatment *CR* is also made available through optimization of the biological process. One operational adjustment, for example, increases the

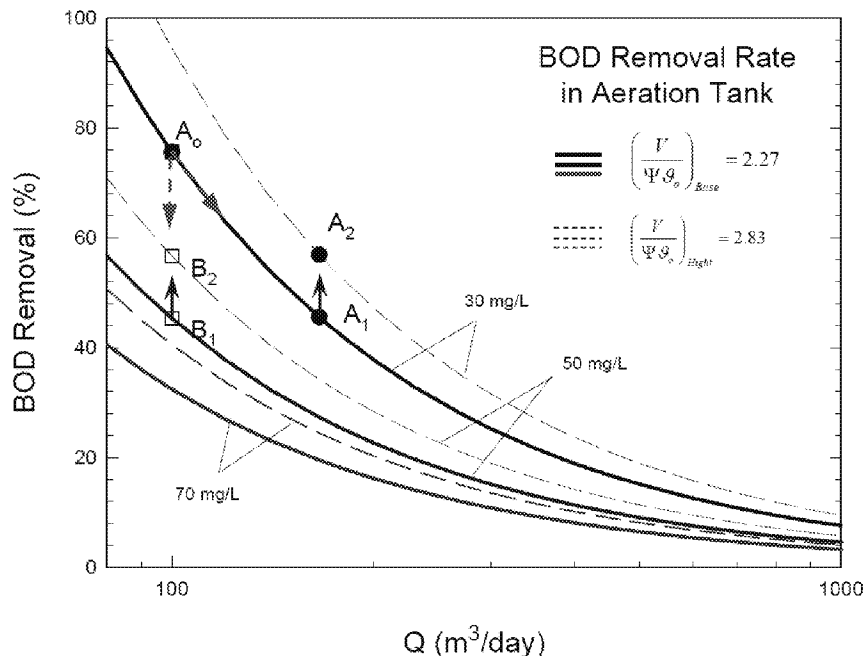


Figure 2-53 BOD removal efficiency of a wastewater activated aeration tank as a function of flow, BOD mass loading, and aeration capacity.

capacity by changing biomass cell age, aeration rate and efficiency. When cell residence age and aeration rates are adjusted for higher aeration capacity $\left(\frac{V}{\Psi g}\right)$ from 2.27 to 2.83, the BOD removal rate is increased theoretically by 56.9%, or $A_1 \rightarrow A_2$ and $B_1 \rightarrow B_2$ (Figure 2-53).

For a treatment plant of 100 m³/day design capacity, a 166% increase in flow rate can potentially decrease the BOD removal rate from 75.5% to 45.5%. The decrease is illustrated as a change from A_0 to A_1 in Figure 2-53. Similarly, treatment efficiency decreases from A_0 to B_1 as a result of increased BOD concentration and mass loading into the plant. An increase in flow and BOD mass loading reduces the BOD removal rate from starting position A_0 to A_1 and B_1 , respectively. In process adaptation, aeration capacity adjustment from 2.27 to 2.83 can partially recover the lost performance, or B_1 to B_2 and from A_1 to A_2 in Figure 2-53. Labels 30, 50, and 70 mg/L are plant inflow BOD concentrations. This is a partial recovery of the capacity loss due to the future increase in flow rate and BOD mass loading.

By a combination of using design safety factors and operational adjustments, the total realized *CR* could reach 30-80% of the design value in an activated sludge process. However, one consideration in *CR* evaluation is the performance deterioration over time for wastewater treatment facilities. Since the early study of Kincannon and Gaudy (1966), biological wastewater treatment is known for its sensitivity to both hydraulic and contaminant shock loading (Jing et al., 2009; Chen et al., 2008), leading to treatment process upset (Ray and Peters, 2008; Capodaglio, 2004) and performance deterioration (O'Reilly et al., 2009). Other causes for reduced treatment capacity include aging treatment equipment and wastewater infrastructure, poor process control, and operational inefficiencies. This portion of the treatment *CR* is recoverable by process monitoring, control and adjustment, or by using advanced engineering techniques such as fuzzy logic control (e.g., Müller et al., 1997; Peng et al., 2007). The analysis here assumes that the performance reduction is minimized through process adjustment and optimization. The realized *CR* of 30-80% design value is a reasonable estimate.

5.2.3.3. *The CR efficacy in current system design*

Based on the generalized analysis in Sections 5.2.1.-5.2.3., the range of percent infrastructure *CR* installed in current engineering practice is shown in Figure 2-54. One can approximately evaluate the adaptation need by comparing the installed *CR* against the rates of precipitation change in the contiguous U.S. The change in precipitation can result in changes in watershed hydrology, including both stream flow and water quality. It is approximated here that the rate of precipitation change in the next 50 years are proportionally translated into hydraulic design parameters (e.g., runoff).

The likely precipitation changes are determined from long-term historical measurements (Rajagopalan, and Lall, 1998; and IPCC, 2013). For approximately 1100 weather stations over the contiguous U.S., the average (U.S. Mean), the 90% and 10% percentiles (PCT), the maximum and minimum, and their associated uncertainties are shown in Figure 2-54. In comparison, the infrastructure *CR* installed by current engineering practice is a magnitude of order larger than the national average rate of precipitation changes in the next 50 years (Figure 2-54).

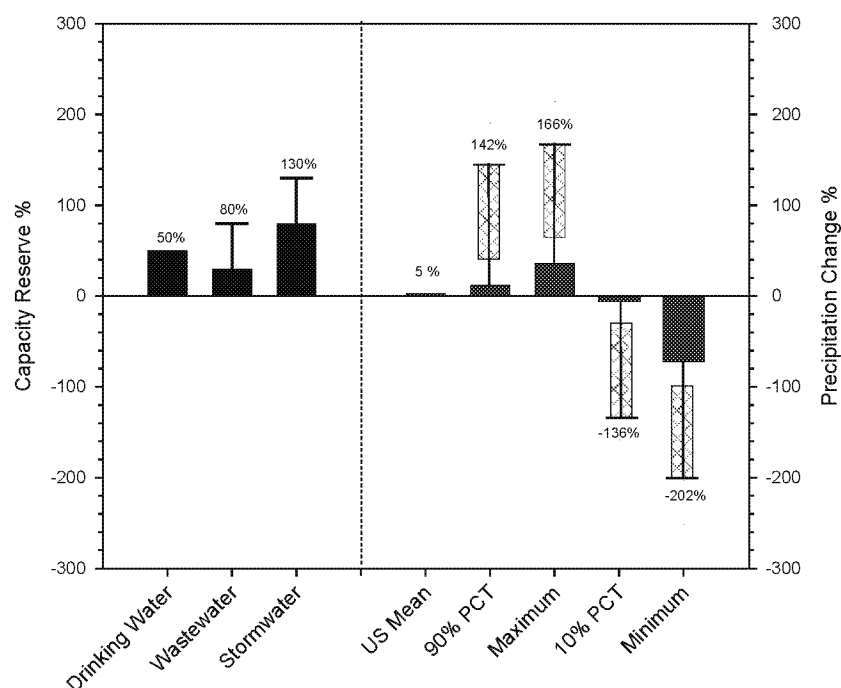


Figure 2-54 Relative magnitude of infrastructure CR installed in current engineering practice (left) in comparison with the relative precipitation change (solid bar) and its uncertainty (pattern and solid line with whisker) by 2060. PCT – percentile.

This difference of an order of magnitude is significant. In the integrated watershed simulation of future climate and land use change, the three watersheds in Ohio and Nevada showed similar degrees of change in stream flow and water quality compared to precipitation (Tong et al., 2012). For example, in the Little Miami River watershed, 20% precipitation increase or decrease in 2050 would result in a 43.83% increase and 53.08% decrease in stream flow, respectively. The total phosphorus increases in both cases by 21.35% and 6.73%. Total nitrogen concentrations change by a smaller amount <11.55% and 3.97% respectively. Thus, the hydroclimatic impacts on watershed hydrology would likely be in the same order of magnitude as precipitation changes. This generalization is also reported by a number of climate model simulations.

This relatively simple evaluation has two noteworthy implications. As a national average, the future precipitation changes of ~5% by 2060 can likely be managed by the installed CR in existing infrastructure. This generalized conclusion supports current engineering practice that has been applied worldwide for decades.

The second implication is important to water infrastructure adaptation at the local watershed level. It is noteworthy that the national average cannot represent all local conditions. This is because the precipitation change is uneven across the contiguous U.S. In many regions, it is certain that the installed CR will be inadequate, making adaptation necessary. Therefore, it is important to observe large spatial variability in future changes in hydroclimate across the U.S. (IPCC, 2007; Rajagopalan and Lall, 1989; and this study). In a significant fraction of the hydroclimatic provinces, the largest rates of precipitation change in the 90% and 10% percentiles

are comparable in magnitude with greater variability. Climate stations with precipitation increase in the 90% percentile are spatially clustered in many regions such as eastern Texas-Oklahoma region. For areas in Arizona and New Mexico, precipitation decrease in the <10% percentile is compounded by the high rate of population growth. The combined effect makes water availability the dominant adaptation factor for these regions.

Secondly, the generalized envelope analysis must be re-examined to evaluate the resilience of individual infrastructure at a specific water utility. The national general conclusions need to be “downscaled” to each urban watershed. As the water infrastructure ages and deteriorates, the degree of *CR* loss is location-specific. The degree of such vulnerability is a focus of bottom-up infrastructure assessments. One of the resilience and vulnerability analysis tools will be described subsequently in Section 5.3.2.

5.3. Water infrastructure vulnerability analysis for adaptation

5.3.1. *The resilience assessment and two approaches*

In a bottom-up approach, climate vulnerability of a water infrastructure is assessed to determine the *CR* threshold. Below the threshold, water infrastructure service function is impaired either in the short- or long-term. The result is a basis to determine infrastructure resilience against specific hydroclimatic impacts.

The U.S. water utilities have taken both top-down and bottom-up approaches in the threshold analyses (e.g., Miller and Yates, 2006; Freas et al., 2008; Stratus Consulting and MWH Global, 2009). Most utility water managers who are engaged in climate vulnerability analyses have a strong technical understanding of their water systems, including local hydrology, historical operating conditions, and standard operational practices, but have less access to climate model projections tailored to their specific regions. Their approaches tend to focus on the “bottom-up” analysis. In 2010, the U.S. EPA conducted a review of 50 water utilities nationwide on their analysis methodology. Among them, eight utilities had conducted their climate vulnerability analysis, and only two followed the bottom-up approach (Table 2-23).

The bottom-up approach generally includes a component to quantify the likely vulnerability and identify the most vulnerable critical assets in its water systems. For example, the East Bay Municipal Utility District (EBMUD), a water and wastewater utility in the Greater Oakland, CA area, used an approach adopted from the AwwaRF (now the Water Research Foundation) publication “*Climate Change and Water Resources: A Primer for Municipal Water Providers*” (Miller and Yates, 2006). The EBMUD analysis consists of several steps:

- Identify the vulnerability of potential portfolio components (e.g., new reservoirs, expanded reservoir storage, increased conservation, conjunctive use, water reclamation, desalination, interbasin transfers) and screen those components for technical, environmental, and economic feasibility;
- Develop alternate portfolios of multiple components that could meet projected demands (e.g., increased conservation and conjunctive use, or water reclamation and interbasin transfers).
- Conduct a preliminary portfolio analysis using a combination of the Water Evaluation and Planning (WEAP) system model and the District’s EBMUDsim model – known collectively as the “W-E model.” Portfolios that performed poorly under current

hydrological conditions were eliminated. The remaining portfolios were subjected to detailed analyses under anticipated climate conditions using the W-E model.

- Identify portfolios with adaptation potentials and use sensitivity analysis to evaluate critical vulnerabilities and ways to address the vulnerabilities.

Table 2-23 Types and approaches of eight water utilities in climate vulnerability assessment.

Utility	Service Provided			Vulnerability Assessment
	Type	Population	State	
East Bay Municipal Utility District (EBMUD)	Water, Wastewater	1.3 million	CA	Bottom-up
City of Boulder Utilities Division	Water, Wastewater	113,000	CO	Top-down
Denver Water	Water	1.3 million	CO	Top-down
Massachusetts Water Resources Authority	Water, Wastewater	2.2 million	MA	Top-down
New York City Department of Environmental Protection (NYCDEP)	Water, Wastewater	9.2 million	NY	Top-down
Portland Water Bureau	Water	860,000	OR	Top-down
San Antonio Water System (SAWS)	Water, Wastewater	1 million	TX	Bottom-up
Seattle Public Utilities	Water	1.35 million	WA	Top-down

The San Antonio Water System (SAWS) in western Texas, serving a population similar in size to EBMUD, also used a bottom-up approach. “This threshold approach identifies system components that are dependent on the status of climate variables (precipitation, temperature, etc.) and the overall system risk under the future hydroclimatic conditions, resulting in a preliminary risk assessment based on the professional judgment of experts who know the system and the planning area” (CH2M Hill, 2008, p. 3-2). The qualitative or semi-quantitative analysis consisted of:

- identifying the climate variables of importance and exploring the sensitivity of SAWS to these variables;
- determining water system responses to a range of potential future climate conditions;
- assessing the vulnerability of SAWS to hydroclimatic impacts;
- assessing system performance according to the uncertainty associated with hydroclimatic factors driving SAWS vulnerability; and
- evaluating overall system risk and identifying areas in need of further analysis.

5.3.2. Water resilience evaluation and resilience tool – CREAT

Systematic examination is considered a necessary process in evaluating the threshold for adaptation. While many utilities take various approaches according to their own needs, a systematic process for vulnerability analysis has emerged from the U.S. EPA's Climate Ready Water Utilities (CRWU) program¹⁴. The program conducted case studies and vulnerability analysis at participating facilities. These actions led to the establishment of an adaptive response framework (U.S. EPA, 2012b), and the publication of Climate Resilience Evaluation and Awareness Tool (CREAT) Version 2.0.

CREAT is a software tool that guides users through a series of investigative steps (Figure 2-55). As a stand-alone risk assessment product, CREAT allows users to assess potential impacts of future climate on their utility and to evaluate adaptation options to address those impacts. It follows a structured approach with the threat analysis leading to the adaptation actions. Major features are:

- A library of drinking water and wastewater utility assets (e.g., water resources, treatment plants, reservoirs, distribution system components, pump stations) for one-by-one evaluation of hydroclimatic impacts
- A list of hydroclimatic impacts (e.g., sea-level rise, precipitation changes, reduced snow pack) covering a broad range of future conditions that potentially affect water utilities
- Adaptation suggestions that can be implemented to adapt to the hydroclimatic impacts that can be customized by the user
- A series of risk-reduction cost reports that will allow the user to evaluate various adaptation options

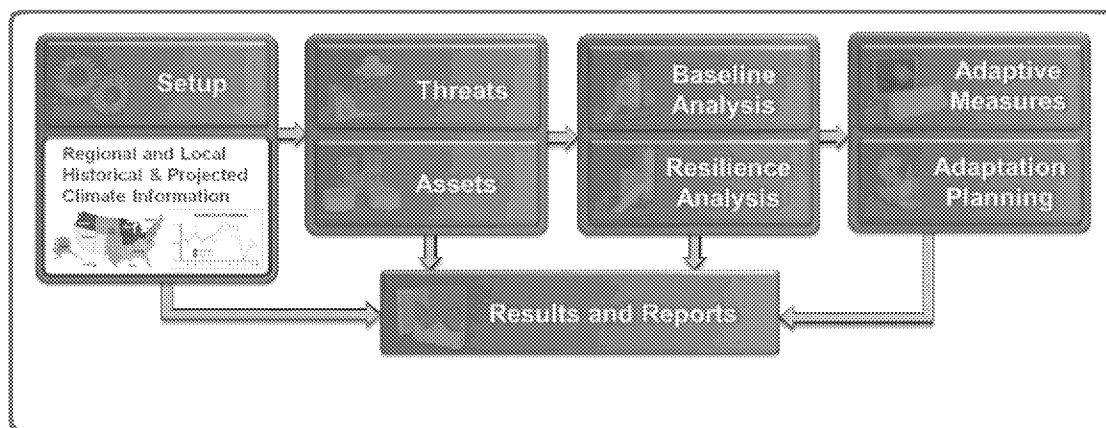


Figure 2-55 The process of climate change vulnerability analysis using EPA tool CREAT. Adopted from EPA CRWU website.

Water sector utility owners and operators can use information about their utility in CREAT to identify climate and hydrological threats, assess potential consequences, and evaluate

¹⁴ <http://water.epa.gov/infrastructure/watersecurity/climate/index.cfm>

adaptation options. This approach allows utilities to assess impacts and identify the thresholds where asset or mission failure could occur. Users can also consider existing climate science data to evaluate the plausibility of climate-related impacts and how soon these impacts may affect the utility. CREAT has been applied to a number of case studies in contiguous U.S. A few examples of the case studies conducted by the EPA CRWU program include:

New York City Department of Environmental Protection (NYCDEP)

In 2010-2011, a CREAT pilot study was conducted for the NYCDEP water and wastewater systems. The pilot site is located in Corona, New York. Through the study, CREAT was used to assist utilities in making risk management and planning decisions, and to identify areas of potential refinement for the tool before it is finalized for broader use in the Water Sector. Climate information embedded in CREAT was used to assess the risk and likelihood of climate threats. Through a desk-top exercise and technical data analysis using CREAT, the vulnerability to future hydroclimatic conditions, particularly sea level rise and storm surge, was identified for the District's water and wastewater assets. In fact, the water and wastewater transfer facilities in low-lying areas identified by CREAT later experienced operational difficulties during the Hurricane Sandy in October 2012.

New York/New Jersey Harbor

One of first CREAT pilot tests was conducted in conjunction with The New York/New Jersey (NY/NJ) Harbor Estuary Program and the North Hudson Sewerage Authority (NHSA). The receiving waters for the NHSA system are part of the NY/NJ Harbor Estuary ecosystem providing critical habitat, recreation and transportation services. The NHSA system includes 107 miles of combined sewers, 17 combined sewer overflow (CSO) regulators, 11 CSO outfalls, and 6 pump stations. This system serves many communities and is fed by a system of rivers draining five states and flowing through several metropolitan areas. It also serves as an important habitat for over 300 species of migratory birds, spawning ground for several species of fish and provides recreation and transportation services. In the pilot study, the CREAT tool was used to identify potential future impacts for water utilities and helps the utilities catalog potential actions in adaptation planning. The exercise fostered dialogue among stakeholders that share a common interest in climate resilience.

Manteo and Columbia, North Carolina

Another CREAT pilot testing was conducted with a workgroup comprised of town officials and water managers from Manteo and Columbia, North Carolina, as well as representatives from the Albemarle-Pamlico National Estuary Partnership. The towns of Manteo and Columbia are located in the Albemarle-Pamlico watershed with Manteo along the coast and Columbia on the banks of the Scuppernong River 40 miles inland to the west. Both towns have suffered damage to natural resources and water-sector infrastructure from heavy precipitation events along with coastal and inland storm surge. A major goal of this exercise was to determine how CREAT can best provide a framework and tool for small communities.

Morro Bay, California

The CREAT pilot study was located on the west coast with representatives from the Morro Bay National Estuary Program, Los Osos Water Purveyors, and contractors. The aim was to identify strategies for the Los Osos Groundwater Basin Management Plan. The Los Osos aquifer system only has one freshwater input and no interbasin transfers, and thus is very sensitive to nitrate pollution from septic systems, overdraft, and hydroclimatic impacts on precipitation. Morro Bay is located along the central coast of California. Two communities are located in the area, which only provide limited wastewater and storm water infrastructure serving approximately 25,000 residents. Through the desk-top studies, the U.S. Geological Survey's SEAWAT model was added to assess potential changes in groundwater quality due to salt water intrusion and changes in recharge dynamics.

The Ohio River basin case study

The Great Miami River watershed is located in southwestern Ohio and drains an area of 5,300 square miles including portions of fifteen Ohio counties. Principal tributaries to the Great Miami River (170.3 miles in length) include the Stillwater River, the Mad River, and Loramie Creek. The Watershed has a population of 1.5 million people and more than 75% of the population resides in the urban areas surrounding Dayton, Cincinnati, Hamilton, and Troy. Approximately 83% of the land within the watershed is used for agriculture, primarily row-crop production of corn, soybeans, and wheat. Typical livestock include swine, cattle, and poultry. Residential, commercial, and industrial lands account for approximately 12% of land use in the watershed, with the remaining area consisting of forests (4%) and water bodies or wetlands (1%). Major industries located in the watershed produce automobile parts, chemicals, household goods, paper products, and processed foods and beverages. CREAT was tested for a medium sized utility (serving approximately 20,000 people) located in the Great Miami River watershed. The results indicate the vulnerability over turbidity and water quality deterioration in flood and related events.

5.3.3. From vulnerability analysis to adaptation engineering

The vulnerability analysis on a water system, combined with climate information derived from the watershed-scale modeling-monitoring framework (Figure 2-1), may provide actionable data to support adaptation engineering. This process is represented by Steps 1, 2 or 4 in Figure 2-1 for which adaptation is designed and implemented. In the CREAT process (Figure 2-55), the vulnerability assessment is followed by adaptation planning.

An effective adaptation action may take place in urban-scale for fundamental changes of the urban system and also in water infrastructure with a purpose of improving its resilience and service functions in future climate and land use conditions. These different levels of adaptation were shown in Figure 2-2 and described in Section 1.2. In the subsequent sections 6.0-8.0, specific adaptation engineering tools and engineering methods are described and case studies are illustrated. Major components are:

- WTP-cam developed for adaptation analysis of water treatment plants;
- Water distribution adaptation methods to increased risk of elevated disinfection by-products (DBPs) in distribution system;

- Surface water management to tackle climate-induced increase of surface runoff in storm water management;
- Managed aquifer recharge and water reuse in adaptation to climate-induced water availability problems.

6. SUD Methods and Tools for Drinking Water Treatment

For existing drinking water treatment plants, adaptation engineering involves the probability-based projection of future source water changes and adaptive engineering of unit process to accommodate the changes. This section describes one major SUD component – the EPA WTP-cam computer program, and presents its application for water supply system adaptation at the GCWW Richard Miller treatment plant.

6.1. Water Treatment Plant – Climate Adaptation Model (WTP-cam)

The WTP-cam program version 1.0 is based on the climate adaptation models published by Li et al (2009; 2014) and Clark et al (2009). The computer program is developed on the basis of a Water Treatment Plant (WTP) model; WTP model was originally proposed by U.S. EPA for support of drinking water disinfection rule promulgation (U.S. EPA, 2005). The original WTP model uses empirical correlations to predict natural organic material (NOM) removal, disinfectant residual decay and disinfection by-product (DBP) formation. In 1998, the original WTP Model was updated to reflect better understanding and available plant performance data with respect to DBP formation. In addition, the 1998 WTP version incorporated several new algorithms for advanced treatment processes and alternative disinfectants.

The original WTP model was designed for single case runs with deterministic solutions. In other words, when model inputs are defined, the model outputs will be a single value for modeled water parameters. Given the uncertainties in defining hydroclimatic impacts on source water, the WTP model was upgraded in 2009 to accept stochastic inputs from source water quality through a Monte Carlo simulation. The latest model was renamed to be WTP-cam (Water Treatment Plant-Climate Adaptation Model). WTP-cam also includes features to examine the performance and associated cost of incremental adaptation to the treatment process in response to changing source water quality. At present, the model is only applicable to surface water sources subject to the hydrological impacts due to climate and land use changes. WTP-cam retains the original capability to make single case runs of a drinking water treatment plant. Major single run features include the ability to:

- Predict NOM, disinfectant residuals, and DBP concentrations.
- Predict the impact of water treatment processes on water quality parameters affecting disinfectant residual decay and DBP formation.
- Assist utilities in evaluating the possible effects of source water variation and treatment process operations on DBP formation.
- Simulate the impact of uncertainties in raw water qualities through Monte Carlo analysis.
- Design treatment process adaptation and estimate adaptation cost.
- Assist regulatory programs in evaluating adaptation design or new requirements.

6.1.1. WTP-cam functionality and approaches

This section focuses on defining and selecting new features of the WTP-cam model. These new features include Monte Carlo analysis, customization of the granular activated carbon (GAC) unit process, and a GAC optimization model. All program descriptions use the Miller plant analysis for illustration. Details of the WTP-cam program are presented in Appendix B.

6.1.1.1 Treatment processes in simulation

In WTP-cam simulation, the first step is to develop a physical model of a treatment plant for examination. Figure 2-56 shows an example using the Richard Miller water plant of the Greater Cincinnati Water Works (GCWW). The raw water from Ohio River is pumped into the plant for treatment through coagulation, sedimentation, rapid sand filtration, followed by GAC processing. The spent GAC is reactivated in two large on-site furnaces. After chlorine disinfection, the treated water is stored in a clearwell before being pumped into the distribution system. WTP-cam arranges these unit processes into a process train as shown in the sequential block diagram (Figure 2-56b).

Data input into the simulation program include physical and process information for the treatment plant. The data for conventional treatment processes – sedimentation, coagulation and flocculation, are shown in Figure 2-57a. A set of physical parameters need to be measured for specific treatment systems; for example, volume and geometry of the flocculation basins, rapid mix basin geometry, settling basin geometry, etc.

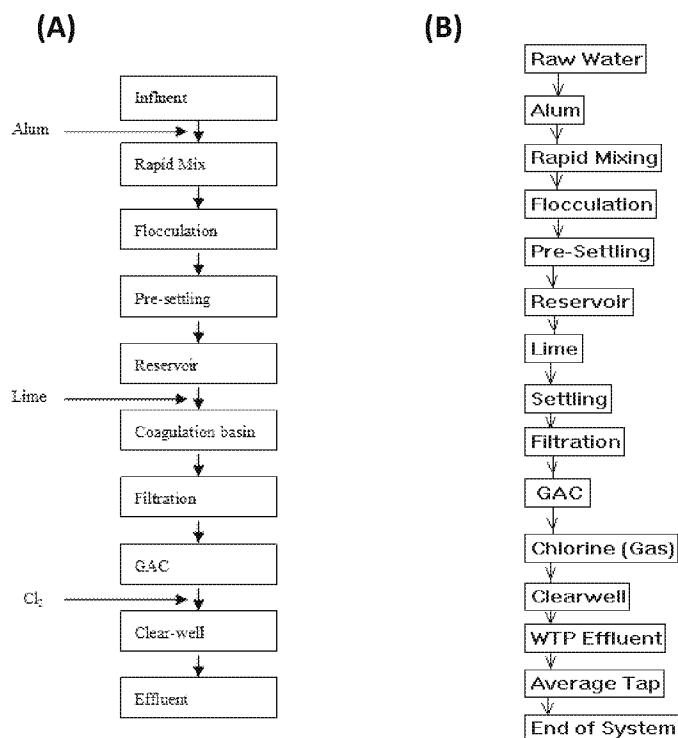


Figure 2-56 Schematic diagram for (A) treatment unit process at the GCWW Richard Miller water treatment plant, and (B) TWP-cam program flow in the example simulation.

GAC absorption is an advanced water treatment unit process effective in removing total organic carbon (TOC) and while the coagulation/sedimentation/filtration processes are good for removing turbidity. However, as carbon is exhausted by TOC and impurities in water, the treatment efficiency decreases, requiring GAC reactivation. These important processing parameters are used as model inputs in the simulation setup (Figure 2-57b).

6.1.1.2 Incorporation of hydroclimate uncertainties

■ Monte Carlo simulation for future water quality trends

Monte Carlo simulation that accounts for climate-related hydrological uncertainty is a new feature not previously available in the original WTP model. Figure 2-58 outlines key steps of the Monte Carlo analysis and the application of the new inputs (in bold). There are three key considerations that govern the Monte Carlo analysis: 1) the Quarterly Running Average, 2) Preservation of the correlation among parameters, and 3) pollutant removal targets. The Quarterly Running Average parameter is specially designed in consideration of the regulation of TOC concentrations. TOC is the target in analysis. $\text{TOC} \leq 2.0 \text{ mg/L}$ in finished water, calculated quarterly as a running annual average, is an important compliance criterion to the EPA

Influent			
pH	7.8		
Influent Temperature	18.6 (celsius)		
Minimum Temperature	2.0 (celsius)		
Total Organic Carbon	2.6 (mg/L)		
UV Absorbance at 254nm	0.096(1/cm)		
Bromide	0.069(mg/L)		
Alkalinity	72 (mg/L as CaCO3)		
Calcium Hardness	77 (mg/L as CaCO3)		
Total Hardness	141 (mg/L as CaCO3)		
Ammonia	0.21 (mg/L as N)		
Turbidity	151.0 (NTU)		
Peak Flow	220,000(MGD)		
Plant Flow	120,600(MGD)		
Surface water by SWTR	TRUE (TRUE/FALSE)		
Source Water Crypto. Concentration	0.000 (oocysts/Liter)		
LT2 Rule Watershed Control Prog. Credit?	FALSE (TRUE/FALSE)		
If GW System, Is Virus Disinfection Req'd?	FALSE (TRUE/FALSE)		
Virus Disinfection for GW, if Req'd	4.0 (logs)		
Alum			
Alum Dose	1.1 (mg/L as Al2(SO4)3*14H2O)		
Rapid Mix			
Volume of Basin	0.0084(MG)		
Ratio of T50/Detention Time	1.00 (ratio)		
Ratio of T10/Detention Time	1.00 (ratio)		
Flocculation			
Volume of Basin	1.9400(MG)		
Ratio of T50/Detention Time	1.00 (ratio)		
Ratio of T10/Detention Time	0.50 (ratio)		
Presed. Basin			
Volume of Basin	2.2300(MG)		
Ratio of T50/Detention Time	1.00 (ratio)		
Ratio of T10/Detention Time	0.44 (ratio)		
Eligible for LT2 Toolbox Crypto. Credit?	FALSE (TRUE/FALSE)		
LT2 Toolbox Crypto. Removal Credit	0.4 (logs)		
Reservoir			
Volume of Basin	373.0000(MG)		
Ratio of T50/Detention Time	1.00 (ratio)		
Ratio of T10/Detention Time	0.32 (ratio)		
Line			
Line Dose	5.0 (mg/L as Ca(OH)2)		
For pH adjustment (P) or Softening (S)	PH.ADJ.(P or S)		
Settling Basin			
Volume of Basin	26.0000(MG)		
Ratio of T50/Detention Time	1.00 (ratio)		
Ratio of T10/Detention Time	0.42 (ratio)		
Filtration			
Liquid Volume	2.4755(MG)		
Ratio of T50/Detention Time	1.00 (ratio)		
Ratio of T10/Detention Time	0.12 (ratio)		
Chlorinated Backwash water?	FALSE (TRUE/FALSE)		
Filter Media (Anthracite/Sand or GAC)	A/S (S or G)		
Giardia Removal Credit - Conv. Filters	2.5 (logs)		
Virus Removal Credit - Conv. Filters	2.0 (logs)		
Crypto. Removal Credit - Conv. Filters	3.0 (logs)		
Giardia Removal Credit - Direct Filters	2.0 (logs)		
Virus Removal Credit - Direct Filters	1.0 (logs)		
Crypto. Removal Credit - Direct Filters	3.0 (logs)		
CPE Turb. Meets LT2 Toolbox Criteria?	FALSE (TRUE/FALSE)		
IFE Turb. Meets LT2 Toolbox Criteria?	FALSE (TRUE/FALSE)		
Crypto. Credit as 2nd Stage Filt.	0.5 (logs)		
GAC			
Empty Bed Contact Time (at 'Plant Flow')	31 (minutes)		
GAC Reactivation Interval	180 (days)		
GAC Contacting System (Single/Blended)	Blended(S or B)		
TOC Breakthrough for Single Unit (Max/Avg)	Avg_TOC(M or A)		
Crypto. Removal credit as 2nd stage	0.5 (logs)		
Chlorine (Gas)			
Chlorine Dose	3.0 (mg/L as Cl2)		
Contact Tank			
Volume of Basin	25.3000(MG)		
Ratio of T50/Detention Time	1.00 (ratio)		
Ratio of T10/Detention Time	0.20 (ratio)		
WTP Effluent			
Average Tap			
Average Residence Time (For Average Flow)	1.0 (Days)		
End of System			
Maximum Residence Time (For Average Flow)	3.0 (Days)		

(A)

(B)

Figure 2-57 Original input data for the Miller example processing train. (A) inputs for plant and conventional treatment process; (B) filtration, GAC and chlorine disinfection in advanced treatment.

disinfectant/disinfection byproduct (D/DBP) rule. Furthermore, WTP-cam applies four seasons to represent the four quarters per year.

The modeling option for correlation is designed to preserve the joint correlation among raw water quality parameters when simulating stochastic raw water quality variables. In the presence of cross-correlation, concentrations of correlated reactants, are possibly high or low simultaneously. As a result, cross correlated raw water quality parameters might strongly affect the calculation of DBP formation during water treatment and distribution. A first order multivariate seasonal autoregressive model (Bras and Rodriguez-Iturbe, 1984) was applied in

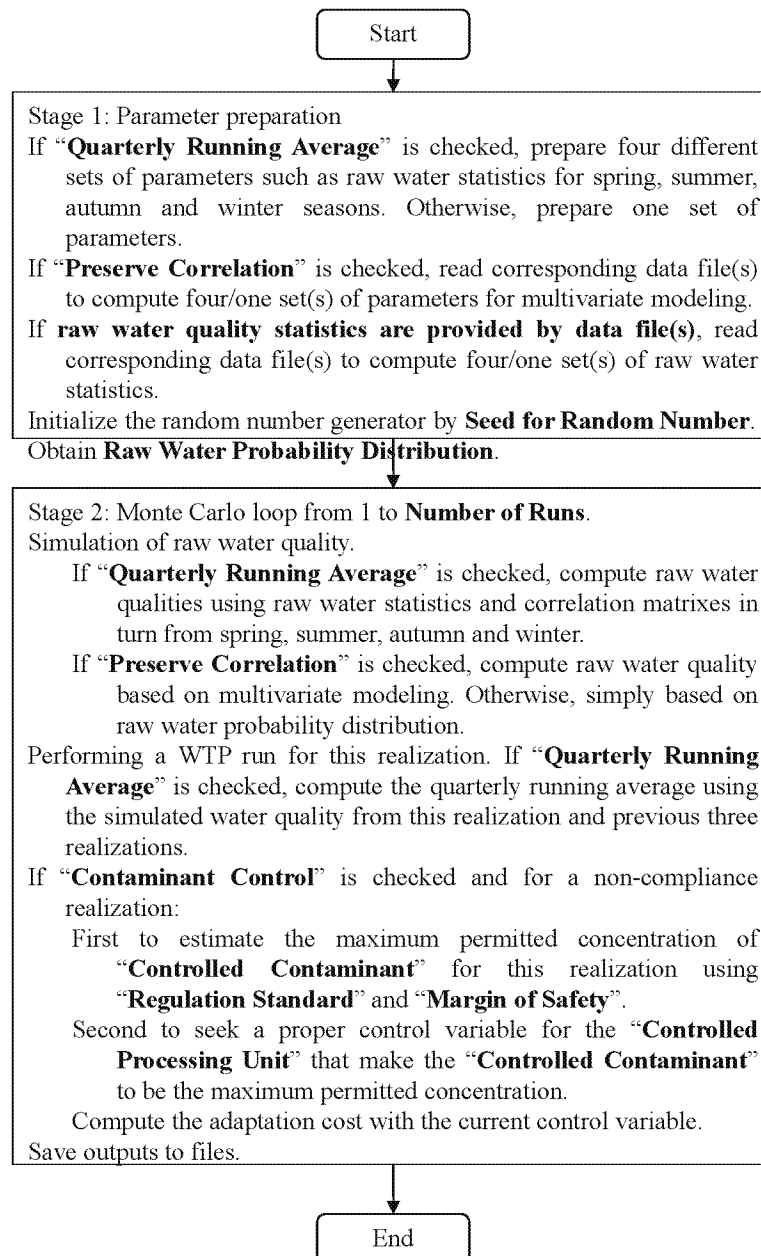


Figure 2-58 Program logic sequences in Monte Carlo simulation of future source water quality variations using the correlation matrix method (Li et al., 2014).

WTP-cam. This seasonal model preserves all seasonal means and variance for all water quality parameters, all cross correlation among all water quality parameters, and lag-one correlations between adjacent seasons and between all water quality parameters. Section 6.2 describes the theoretical basis for the applied multivariate analysis.

The pollutant option in the modeling is designed to modify the design and operation of the current processing train when a non-compliance realization is detected in simulation. For example, when a TOC non-compliance in finished water occurs, the WTP-cam program will modify operation by increasing the frequency of GAC regeneration. The adaptation measure aims to bring the TOC excursion within acceptable limits. The inputs for this option are controlled for a specified contaminant, regulation standard, margin of safety, and unit processes in a treatment plant. For the WTP-cam version 1, the engineering option for contamination component has been developed for TOC control in the GAC treatment process.

Table 2-24 Options for Monte Carlo analysis

Control	Range of value	Description
Preserve Correlation	TRUE/FALSE	Multivariate analysis will be used to simulate stochastic raw water quality if TRUE (checked).
Quarterly Running Average	TRUE/FALSE	Simulation will be based on four seasons if TRUE.
System Adaptation	TRUE/FALSE	Loading adaptation program for the non-compliance realizations if TRUE.
Controlled Contaminant	TOC/None	Determining the contaminant to be controlled by adaptation.
Controlled Unit Process	GAC/None	Determining the unit process that can be adapted for controlled contaminant.
Raw Water Probability Distribution	Normal/Lognormal	Determining the probability distribution for all raw water quality parameters

Inputs for Monte Carlo Setting

The input parameters for Monte Carlo analysis may be divided into three groups: options, control parameters, and the source of influent water quality statistics/correlation. Figure 2-59 shows a graphic user interface (GUI) for these inputs in the example processing train of Figure 2-56.

Options: options are designed to govern the flow of Monte Carlo simulation. Table 2-24 provides the name of the option, range of available values and description of the option.

Control parameters: there are four control parameters used in the Monte Carlo simulation:

- Number of Runs – a user defined integer to specify the number of runs required.
- Seed for Random Number – a positive number to initialize the random number generator

Monte Carlo Setting

Options

- ☒ Preserve Correlation
- ☒ Quarterly Running Average
- ☒ Contamination Control

Controlled Contaminant: TOC

Controlled Processing Unit: GAC

Raw WQ Probability Distrn: LogNormal

Control Parameters

Number of Runs, >1: 1000

Seed for Random Number, 1-50000: 168

Regulation Standard, mg/L: 2

Margin of Safety, mg/L: 0.05

Source of Influent WQ Statistics

Computed by Available Data File(s), Please Click Here

Or Input manually, Please Click Here

Correlation Matrix

Please Provide Data File(s) Here if Preserve Correlation is Checked

Default Example OK Cancel

Figure 2-59 Graphic user interface for inputs in Monte Carlo simulations of future water qualities.

in the program. The Monte Carlo simulation can be repeated using the same random number seed.

- Regulation standard – a value representing the compliance standard for the controlled contaminant selected in **Options**.
- Margin of Safety – refers to the difference between the compliance standard and the real controlled concentration that provides extra reliability for compliance. Margin of safety is usually within 1-10% of the regulation standard.

6.1.1.3 Source of influent water quality statistics/correlation

Influent water quality statistics are essential parameters to generate stochastic influent water quality parameters for each simulation. There are two methods provided by WTP-cam to obtain these parameters. The first is to simulate source water quality using the correlation matrix (See Section 6.2 for details). The second method is to input these parameters manually through clicking the manual input button. There will be four dialogue windows appearing one at a time for the four seasons if Quarterly Running Average is checked. Figure 2-60 shows an example of manual input window for the spring of the example processing train at the Miller plant. These datasets are saved in separate files for retrieval and simulation. See Appendix B for program details.

6.1.1.4 Customization of GAC unit process model

The performance of GAC for TOC removal is a major tool in WTP-cam to remove the climate-related or naturally occurring DBP precursors. The model is based on TOC breakthrough experiments in GAC columns under various conditions to examine different raw

water sources, GAC size, pretreatment configuration, and bed depth/empty bed contact time (EBCT). In developing the WTP model, a classic logistic function was used to represent the TOC breakthrough curve for a single GAC contactor (U.S. EPA, 2005), given by,

$$f(t) = \frac{TOC_{eff}}{TOC_{in}} = \frac{a}{1 + be^{-dt}} \quad (2.35)$$

where, $f(t)$ is TOC fraction remaining; TOC_{in} and TOC_{eff} are TOC influent and effluent concentrations at the GAC unit, respectively; t is GAC service time; a , b and d are model parameters estimated by statistical regression.

To enable accurate modeling of GAC treatment performance, WTP-cam provides a new feature to customize parameters a , b and d for specific water plant operations. One option is to use non-linear regression method for site-specific TOC treatment data when collected. The other is to choose the default statistical values, when site specific treatment data are not available. More details for the TOC breakthrough model and non-linear regression are introduced subsequently in Section 6.2.1.

The screenshot shows a window titled "Raw Water Quality Statistics Input Window". At the top right, there is a "Time Horizon:" dropdown menu set to "Spring". Below this is a table with three columns: "Parameter", "Average", and "Standard Deviation". The table contains the following data:

Parameter	Average	Standard Deviation
pH, -	7.7	0.17
Alkalinity, mg/L	55.5	18.2
Turbidity, NTU	43.4	38.0
Calcium Hardness, mg/L	63.5	23.3
Total Hardness, mg/L	110.4	18.4
TOC, mg/L	2.3	0.6
UVA, 1/cm	0.12	0.06
Bromide, mg/L	0.03	0.01
Ammonia, mg/L	0.29	0.41
Temperature, Celsius	12.4	0
Flow Rate, MGD	108.4	0

At the bottom of the window are "OK" and "Cancel" buttons.

Figure 2-60 Manual input window for influent water quality statistics

6.1.2. WPT-cam program and model simulations

After all input data are specified in the model, the WTP-cam simulation can proceed in the following sequential steps: 1) source water quality definition, 2) product water quality projection, 3) model validation, and 4) result analysis and visualization. Appendix B provides program illustrations and instructions of the WTP-cam simulation. The program is designed as a Windows-based program that can be run under a Windows 8 or newer operating system.

6.2. Principles, models and algorithms in WTP-cam

6.2.1. Monte Carlo methods in modeling source water variability

A set of source water quality parameters can affect removal of TOC and other contaminants. A newly developed modeling-monitoring platform (Figure 2-1) integrates climate and land use models for projection of future changes in major water quality parameters such as

TOC, TP, TN and turbidity. These water quality projections often have a large uncertainty in the model projections. The near real-time (daily) high-resolution satellite monitoring techniques in the platform (Figure 2-1) can generate real-time and historical reconstruction of water quality variations in surface waters of various sizes. Such data can be used to assist model calibration and validation. A number of water quality parameters relevant to drinking water treatment can be quantitatively monitored, including major nutrients, turbidity, TOC, chlorophyll-a, and microcystin. However, even with use of the integrated modeling-monitoring techniques, the full range of water quality parameters with necessary projection accuracy may not be available for water treatment operational adjustment and adaptation,

Li et al. (2014, 2012) proposed the use of Monte Carlo analysis as a practical tool to characterize the range of future source water changes. In this approach, Monte Carlo analysis is used to obtain sample solutions by repeating a simulation process for problems involving random variables with known probability distributions. As described below, the observed correlations are evident among water quality parameters in source water. This correlation is assumed to be valid in the projection period. Then it is possible to utilize these correlations to project the unknown water quality parameters based upon the known ones such as TOC and turbidity.

The new feature in Monte Carlo simulation allows one to calculate the probability distribution of the estimated source water quality parameters. For use of WTP-cam in the adaptation engineering, the analysis follows the following steps:

- Define a domain of possible inputs.
- Generate inputs randomly from the domain using a specified probability distribution.
- Perform a deterministic computation using the inputs.
- Aggregate the results of the individual computations into the final result.

6.2.1.1 Seasonal multivariate analysis

To project future water quality, it is assumed that the covariations among water quality parameters in the Ohio River source water will remain. This assumption allows one to compute all other important parameters from a target TOC level, which are modeling parameters in WTP-cam simulations. The joint correlations among raw water quality parameters are preserved when computing the stochastic raw water quality in the future. This statistics-based seasonable multivariate analysis was conducted through Monte Carlo simulations. Detailed principles and mathematical relations are contained in Section B4.1.1 of Appendix B.

In short, the first-order multivariate seasonal autoregressive model AR(1) (Bras and Rodriguez-Iturbe, 1984; Salas et al., 1980) was adopted in the WTP-cam algorithm for the simulation. For each season of a year, the observed water quality parameters involved in WTP-cam simulation are Log-transformed into variables x'_i and y'_i that are normally distributed with means $m_{x'_i}$ and $m_{y'_i}$, standard deviations $S_{x'_i}$ and $S_{y'_i}$, and the correlation coefficient among them. The sample means, standard deviations and correlations of the transformed variables x'_i and y'_i can be also obtained from the transformed historical records. The parameters of the transformed variables are then used to build the necessary auto-covariance and cross-covariance matrices (See Appendix B, Section B4.1.1.)

6.2.1.2 TOC compliance simulation

The simulation of *Quarterly Running Average* is designed for a regulatory compliance assessment for TOC in water treatment. The compliance criterion is <2.0 mg/L calculated quarterly as a running annual average.

WTP-cam takes four seasons to represent the four quarters per year. Thus, there are four computed running annual averages; one for each quarter. The running annual average is defined as the arithmetic average of TOC concentrations at current season and previous three seasons based on the U.S. EPA D/DBP rule. Table 2-25 shows the calculated running annual average for TOC in the GAC treatment effluent of the GCWW's Richard Miller water plant.

Table 2-25 Illustration of calculating running annual average for finished water TOC

Year	Season	TOC concentration	Running annual average
2009	Spring	1.3	1.7
	Summer	1.7	
	Autumn	2.2	
	Winter	1.7	
2010	Spring	1.2	1.7
	Summer	1.4	1.6
	Autumn	2.4	1.7
	Winter	1.5	1.6

The means, variances and cross correlations of raw water parameters vary with seasonal changes in most cases. Thus, four sets of input parameters for raw water qualities need to be prepared as modeling inputs (See Figure 2-58). This means four simulations each year responding to the four seasons. The TOC concentration is recomputed for each season as the running average.

6.2.1.3 GAC unit adaptation analysis

Adaptation analysis is conducted after a non-compliance event is identified in the WTP-cam simulation. Adaptation refers to necessary changes in the design and/or operation of the current water treatment plant. At this time, the adaptation module is fully developed for TOC treatment in the GAC unit process. Adaptation for other treatment unit processes has not yet been programmed in the WTP-cam software.

WTP-cam also incorporates the margin of safety in the adaptation analysis as an option. The margin of safety refers to the difference between the compliance cut-off point and the calculated concentration. For example, if margin of safety is 0.1 mg/L, the controlled TOC concentration will be 2.0 mg/L – 0.1 mg/L, namely 1.9 mg/L. In other words, the simulated running annual average of TOC concentration should be <1.9 mg/L in engineering analysis.

For example, if a TOC noncompliance event identified, one effective adaptation technique is to reduce the GAC service time by process adjustment (Li et al., 2014). In the WTP-cam simulation, the appropriate GAC service time is calculated and the process is adjusted to ensure TOC <1.9 mg/L in the process control. The computation procedure is as follows:

- Reduce current GAC service time by one day.
- Use the new service time to re-compute the TOC concentration for each of four seasons without change to the other operational conditions in each season.
- Calculate the new running annual average of TOC; and
- Compare the new calculated TOC to the controlled concentration 1.9 mg/L. The new service time is adopted if new TOC is less than 1.9 mg/L; otherwise, repeat computation from the first step until the solution is found.

6.2.1.4 Unit Process Engineering Analysis

1) Deterministic removal rate determination

WTP v2.0 utilizes empirical correlations intended for prediction of central tendencies in NOM removal, disinfection, and DBP formation. The user manual in Appendix B (U.S. EPA, 2005) and references therein describe these linear regression equations for the unit process analysis. The empirical correlations usually consist of independent variables and empirical constants. Such results are informational to national and regulatory analysis (See Figure 2-10). However, the modeling results may not provide sufficiently accurate predictions for a specific water plant.

As an improvement, WTP-cam provides an option to customize the empirical constants a , b and d of the logistic GAC model in Eq.2.35. The empirical regression is based on site-specific historical treatment data or treatability test results, and thus capture the location-specific variation in TOC removal through the GAC reactor. The improvement is essential to the use of WTP-cam in adaptation design. This feature is shown in the case study (See Section 6.3). To date, the GAC treatment unit process has been modified to allow customization of the TOC breakthrough model. Customizations for other unit processes will be incorporated in a future version of WTP-cam.

The model constants a , b and d are mostly a function of influent TOC and pH and EBCT. Based on statistical regression, these parameters can be estimated by (U.S. EPA, 2005),

$$a = 0.682 \quad (2.36)$$

$$b = 0.167\text{pH}^2 - 0.808\text{pH} + 19.086 \quad (2.37)$$

$$d = \text{TOC}_{in}[\text{pH}(-0.0000058 \cdot \text{EBCT}^2 + 0.000111\text{EBCT} + 0.00125) + 0.0001444 \cdot \text{EBCT}^2 + 0.005486\text{EBCT} + 0.06005] \quad (2.38)$$

In WTP-cam, a new feature is installed to estimate parameters a , b and d using a non-linear regression method for a given plant instead of the statistical values in Eqs.2.36-2.38. This improvement allows one to customize site-specific the model parameters. Either TOC treatment monitoring data or long-duration bench-scale studies can be used (Li et al., 2014). This modeling process is shown next.

2) Customization of GAC Unit Process

The performance of GAC for TOC removal is often characterized using TOC breakthrough experiments using GAC column experiments. This testing is normally conducted when changing GAC suppliers or in pretreatment configurations. Roberts and Summers (1982) also found that complete removal of TOC by GAC cannot be achieved under common water treatment conditions. An immediate, partial breakthrough of TOC, can be observed even with virgin GAC, indicating that a portion of the influent TOC is not amenable to removal by GAC treatment.

Furthermore, Roberts and Summers (1982) observed that the GAC effluent TOC is always lower than the influent level, even if the GAC reactor is saturated with organics. This degree of removal under the steady-state is attributed to biodegradation (U.S. EPA, 1996) similar to those in a biofilter. The ratio of TOC concentration between effluent and influent, called “fraction remaining,” generally ranges from 0.1 to 0.5 during the early stages of operation. The ratio depends on compositions of organic constituents in water and the EBCT/bed depth of a GAC contactor. For steady-state removal, the fraction remaining varies from 0.6 to 0.9 with service times from 3,000 to 14,000 bed volumes.

To obtain site-specific model parameters for design a pilot-plant or full-scale study of GAC adsorption processes is often required, which is both time-consuming and expensive. Instead, rapid small-scale column tests (RSSCT) (Crittenden et al. 1991; Zachman and Summers 2010) are widely used as a substitute. The RSSCT method is based on mass transfer models to scale down a full-size GAC contactor. Hydraulic and kinetic similarity is assured by properly selecting the GAC particle size, hydraulic loading and EBCT of the small contactor (Crittenden et al. 1991; Zachman and Summers 2010). For this purpose, U.S. EPA (1996, 2000) described the standardized guidelines for GAC treatment studies to obtain high quality TOC breakthrough data in RSSCT.

Plant-specific parameterization is the new WTP-cam feature based on the equations given below. The modeling technique was developed using the U.S. EPA’s information collection rule (ICR) treatment database for 63 treatment studies nationwide (U.S. EPA, 2000), including 44 RSSCT studies, 18 pilot studies and 1 full-scale study.

In this WTP-cam analysis, the dataset $f(t)$ versus t (Eq.2.54) were obtained from GAC treatment monitoring. The WTP-cam simulation applies a modified Gauss-Newton method to estimate model parameters a , b and d . The procedure (Li et al., 2009 and Clark et al., 2009) relies on the non-linear regression function through least square analysis based on Hartley (1961). The fitting objective function is defined as:

$$\text{Min } Q(a, b, d) = \sum_{k=1}^n (y_k - f(t_k; a, b, d))^2 \quad (2.39)$$

where, $f(t; a, b, d) = \frac{a}{1 + be^{-dt}}$; a , b and d are the model parameters to be estimated; t_k and y_k are the known field values, representing GAC service time and TOC fraction remaining respectively; n is a known number of field samples.

6.2.1.5 Adaptation cost and economics

The economic analysis function in WTP-cam allows estimating the costs of adaptation made to the design or operation of water treatment. A WTP-cam analysis considers capital, operational and management costs.

The cost for GAC processing consists of the initial GAC cost, annual GAC make-up cost, GAC contactor cost and GAC reactivation cost. The initial GAC cost is a one-time charge for GAC required to fill the contactor, equal to the product of the total volume of contactors, the density and unit cost of virgin GAC. The annual GAC make-up cost is the yearly cost of GAC lost due to reactivation. It is the product of GAC loss rate in reactivation, GAC reactivation rate and virgin GAC cost. The GAC contactor cost can be estimated from the cost model by Adams and Clark (1988):

$$y = a + b(USRT)^c d^z \quad (2.40)$$

where y is the capital, operational or maintenance cost; $USRT$ is the process design or operating variable that is the total surface area of the GAC filter for contactors (total hearth area for GAC reactivation) or the total effective volume of the GAC unit for capital cost; a , b , c and d are empirical parameters determined from nonlinear regression analysis, and z is either 0 or 1 for adjusting the cost functions for a given range of $USRT$ values. It is notable that the costs in Adam and Clark (1988) are based on the 1983 dollar value. In model computation, all costs were converted to year 2009 dollar using the Producers Price Index (US BLS, 2008). The same method can be used for other years of interest. The contactor cost can be further categorized by the costs of capital, process energy, building energy, maintenance material and operational and maintenance (O&M) labor. The computational parameters are listed in Table 2-26.

Table 2-26 GAC contactor cost estimate parameters

Type of Cost	Capital	Process energy	Building energy	Maintenance Material	O&M Labor
USRT	volume	area	area	area	area
a	93700	0	15150	540	1160
b	1999.1	12	350	23.6	0.3
c	0.712	1	0.916	0.753	1.068
d	0.958	1	1	1	1.152
z	1	1	1	1	1
Unit cost	Construction Cost 1.3y	0.08 \$/kwh (in 2009)	0.08 \$/kwh (in 2009)	--	9 \$/hr (in 1983)
Ratio of 2009 to 1983 cost	2009ENR/1983ENR= R=2.16	--	--	2009PPI/1983 PPI = 2.56	2009 PPI/1983 PPI = 2.56

The other cost variable remaining is GAC reactivation cost. It can be estimated using a similar algorithm (Eq.2.40) used to calculate GAC contactor cost. The model parameters are

different and are listed in Table 2-27. In a capital recovery analysis for a 20-year return period and a 5% annual interest rate, a cost curve can be developed to illustrate the total annual cost of the GAC system that varies with GAC service time or reactivation period. On this basis, WTP-cam simulation yields adaptation cost estimates through interpolations based on GAC service time.

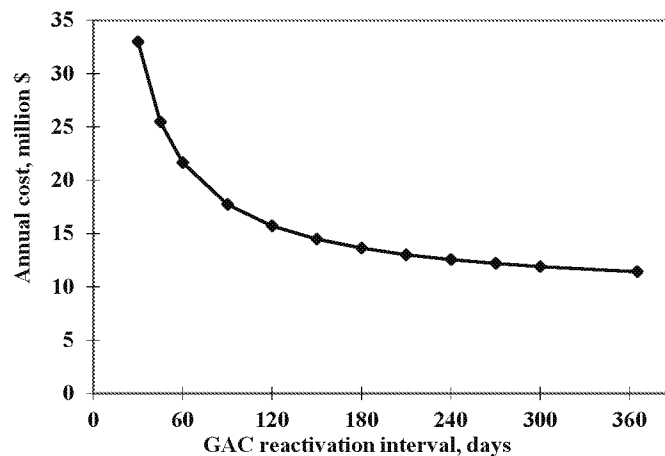


Figure 2-61. Cost curve for annual cost of GAC unit

Figure 2-61 shows an example cost curve developed for the GCWW's Miller plant. The Miller treatment plant has 12 down-flow gravity GAC contactors and two multi-hearth furnaces for onsite reactivation. Each of the Miller plant contactors has a volume of 595 m³ and a surface area of 181 m². The overall GAC loss rate through the system is about 8%. The carbon loading rate is 482 kg/day of GAC per square meter of hearth area. This cost curve is the basis for GAC adaptation analysis at the treatment plant. Details of this adaptation case study are provided in next section.

Table 2-27 GAC reactivation cost

Type of Cost	Capital	Process energy	Building energy	Maintenance Material	O&M Labor	Natural Gas
USRT	area	area	area	area	area	area
a	144000	354600	12250	0	2920	648400
b	198300.4	6387	312.1	4456.6	282	287714.9
c	0.434	0.755	0.649	0.401	0.7	0.899
d	1	1	1	1	1	1
z	1	1	1	1	1	1
Unit cost	Construction Cost 1.3y	0.08 \$/kwh (in 2009)	0.08 \$/kwh (in 2009)	--	9 \$/hr (in 1983)	\$0.0035 /scf (in 1983)
Ratio of 2009/1983 cost	2009ENR/1983ENR = R = 2.16	--	--	2009PPI/1983 PPI = 2.56	2009PPI/1983 PPI = 2.56	2009PPI/1983 PPI = 2.56

6.3. GCWW Miller plant case study using WTP-cam

GCWW provides drinking water at ~5.26 m³/s or 120 MGD to ~ 235,000 customer accounts through 5,100 km of water mains. Built in 1907, the GCWW's Richard Miller Plant

treats surface water from the Ohio River and provides 88% of the drinking water supply to the customers at a maximum summer capacity of 9.65 m³/s (220 MGD). In this adaptation case study, the WTP-cam tool was used in simulation to assess the likely hydroclimatic changes in the future on drinking water treatment at the Richard Miller water treatment plant. The investigation results have been published by Li et al (2014, 2012) and others. The technical questions for adaptation study include:

- How the climate-related risk to drinking water standard violations can be assessed,
- What adaptation limit or climate impact threshold can be established, and
- What is the probable cost associated with the adaptation scenarios?

6.3.1. Miller plant operation and performance

6.3.1.1. Treatment process and modeling

Figure 2-56 in Section 6.1.1 shows the treatment process at the water plant. Raw water is taken from the Ohio River. At the time of investigation, the treatment process consisted of coagulation, sedimentation, biologically active rapid sand filtration, GAC adsorption, and water disinfection. A new UV disinfection facility started operation shortly after this adaptation analysis. It replaced the conventional chlorination. All data acquired prior to the UV unit operation are used in this analysis based on chlorine disinfection (Figure 2-56). The intent was to examine the conventional use of chlorination as the basis for the adaptation analysis.

Table 2-28 Miller WTP Unit Process Design Parameters

Unit Process	Volume, m ³	T10, min
Rapid mixing	32	2
Flocculation basin	7343	14
Pre-settling	8441	14
Reservoir settling	1411805	1,728
Coagulation basin	98410	144
Filtration	9352	4
GAC Contactors	9311	--
Clear-well	107116	77

Note: -- data not available.

Data source: U.S. EPA ICR database.

TOC and turbidity are the subject of the adaptation study. These DBP-formation precursors or potential indicators are removed by the conventional coagulation, sedimentation, biologically active rapid sand filtration, and GAC adsorption at the plant. The Miller plant design parameters are listed in Table 2-28. In the table, T₁₀ value is the hydraulic retention time required for the effluent tracer concentration to reach 10% of the inflow tracer concentration. It is normally determined in a step-dose conservative tracer test of the treatment unit.

The plant performance and treatment efficiency of each unit process was evaluated using the U.S. EPA Information Collection Rule database. The database was designed to obtain water quality, water treatment, and occurrence information needed for the development of Safe Drinking Water Act regulations. ICR data include the detailed information on plant design,

treatment processes, and operations for all large public water utilities in the United States, each serving a population >100,000. The data collection covered an 18-month monitoring period from July 1997 through December 1998. The ICR database also provides water quality measurements at various sampling locations along water treatment train and in a water distribution system.

Table 2-29 Inflow and chemical feed levels for the Miller WTP

Parameter	Sampling period		
	10	13	16
Inflow rate, m ³ /s	4.41	5.27	5.76
Alum at RM, mg/L	0.87	1.82	0.87
Lime at COAG, mg/L	6.73	7.92	4.62
Chlorine at CLR, mg/L	1.26	1.56	1.46

Note: RM-rapid mixing; COAG-coagulation basin; CLR-clearwell.

Data source: U.S. EPA ICR database.

For the Miller plant, specific data utilized for the treatment simulation cover three sampling periods: sample period 10 (April 1998), sample period 13 (July 1998) and sample period 16 (October 1998). Raw water inflow rate and chemical feed doses during each period are listed in Table 2-29. Based on information provided by GCWW, the GAC reactivation during these periods was set at 8 months for winter-spring season and as 4 months for summer-early autumn season.

6.3.1.2. GAC absorption and TOC removal

Table 2-30 shows statistics of the performance parameters for the GAC unit based on weekly samples for the 76-month period from January 2004 to April 2010. The data includes the influent and blended effluent TOC concentrations, the number of active GAC contactors, the plant inflow rates and the GAC reactor empty bed contact time (EBCT). Influent TOC concentrations follow an annual cycle with seasonal extremes ranging from 1.01 mg/L (March 24, 2004) to 2.76 mg/L (September 22, 2004). Blended effluent TOC varied from 0.26 mg/L (July 13, 2005) to 1.44 mg/L (November 1, 2006); all concentrations were below the compliance standard of 2.00 mg/L.

Table 2-30 Statistics of full-scale field measurements.

Field Measurements (units)	Average	Standard Deviation	Coefficient of Variation	Minimum	Maximum	Sample Size
Influent TOC, (mg/L)	1.72	0.36	0.21	1.01	2.76	289 ^a
Blended effluent TOC, (mg/L)	0.85	0.26	0.31	0.26	1.44	289 ^a
Number of active GAC contactors	9	1.22	0.14	6	11	289 ^a
EBCT, (minute)	17.1	0.8	0.05	12.1	24.4	279 ^b
Plant water inflows, (m ³ /s)	5.26	0.81	0.15	3.26	7.61	279 ^b
Plant TOC mass inflow, (g/s)	9.17	2.57	0.28	4.72	16.6	279 ^b

Note: ^a 2296-day sample period from Jan 7, 2004 to April 21, 2010 (one sample every 7.94 days)

^b 2184-day sample period from Jan 7, 2004 to Dec 30, 2009 (one sample every 7.83 days)

The GAC plant flow rates averaged 5.26 m³/s (120 MGD), ranging from 3.26 m³/s (74 MGD) on December 27, 2006 to 7.61 m³/s (174 MGD) on September 5, 2007. Among the 12 available GAC contactors, 6 to 11 contactors were in operation at any given time. GCWW's operational strategy for the GAC process demands that GAC contactors be brought on-line, reactivated, and taken off-line in a staggered sequence. This operation aimed to balance a variety of operational goals including total trihalomethane (TTHM) reduction, water production, furnace operation schedules, GAC storage, and the effective removal of Spring pesticide runoff in the source water. To meet these operational goals, the monthly average EBCT was set consistently around 17 minutes

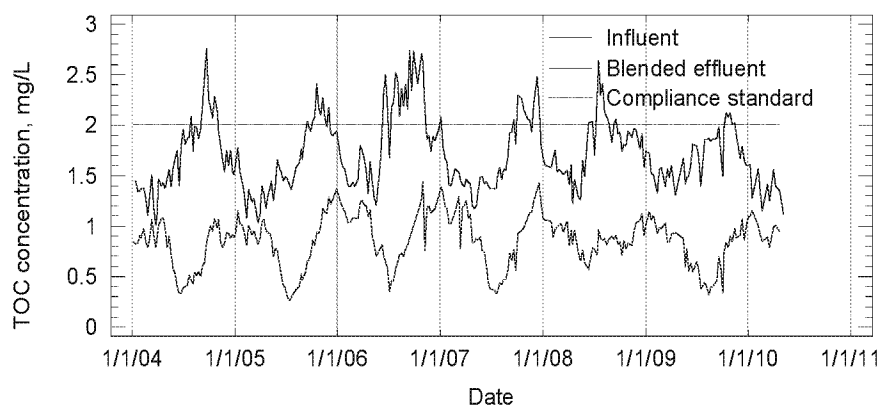


Figure 2-62 Temporal variations of influent and blended effluent TOC in the GAC unit.

Figure 2-62 shows the temporal pattern of influent TOC and blended effluent TOC concentrations at the GAC unit process during the 76-month sampling period. Seasonal changes of influent TOC to the GAC reactor are evident. Higher concentration always occurred in the second half of the year compared to the first half, and this seasonal variability is consistent with TOC levels in the Ohio River.

Furthermore, influent TOC concentrations and blended effluent TOC concentrations are not significantly correlated with each other (Figure 2-62). Pearson product-moment correlation coefficient R is only 0.08. However, as shown in Figure 2-63, the number of active GAC

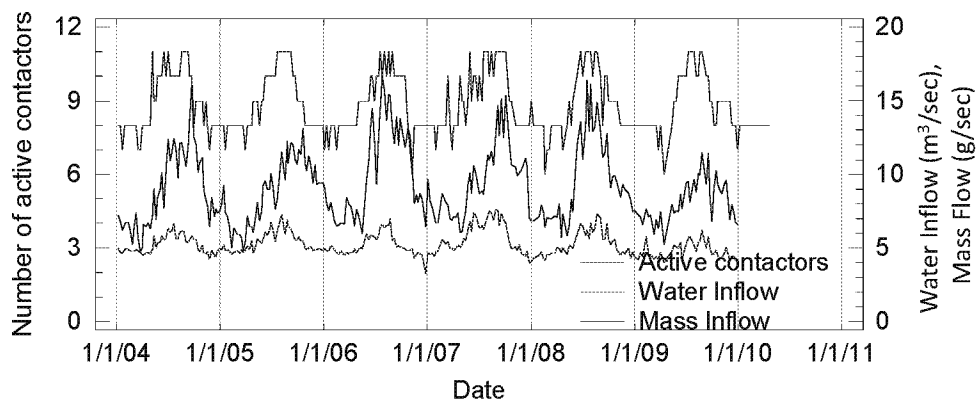


Figure 2-63 Temporal variations of inflow, mass inflow and active number of GAC contactors.

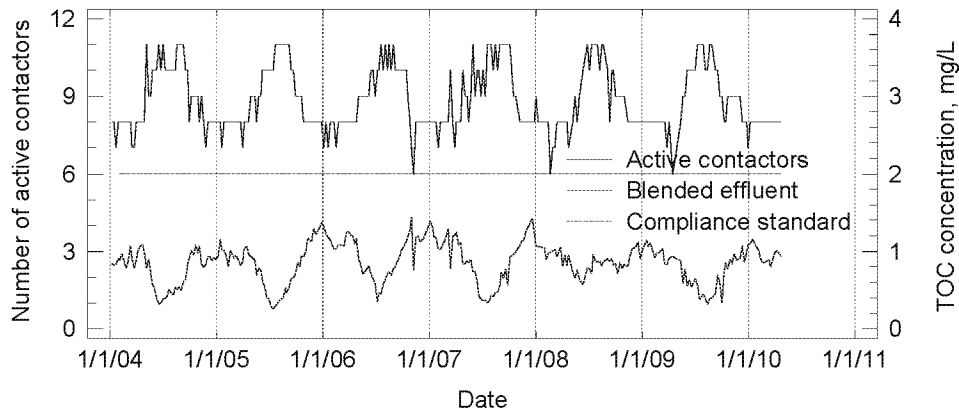


Figure 2-64 Temporal variations of active contactors and blended effluent TOC concentration.

contactors is highly correlated with plant inflow ($R=0.75$) and mass inflow ($R=0.65$). Due to increased water demands during warm weather, summer months had higher plant inflow rates than winter months, and, hence, more GAC contactors were active in the summer time. The number of active GAC contactors is negatively correlated to the blended effluent TOC concentration ($R=-0.69$). See Figure 2-64. This indicates that TOC in the finished water is controlled mainly by the number of GAC contactors in service, not TOC concentration entering the treatment unit. This result strongly shows the effectiveness of GAC operation in TOC removal.

Figure 2-65 compares temporal variations in EBCT and plant inflow. While the plant inflow rate displayed pronounced seasonality, the overall average EBCT across the bank of active GAC contactors was relatively stable. This quasi-steady EBCT is achieved during operation by adjusting the number of active GAC contactors to meet GCWW's operational goals including offsetting of the seasonal variation of the inflow.

6.3.2. WTP-cam simulation of hydroclimatic change impacts

6.3.2.1 Simulation and model assumptions

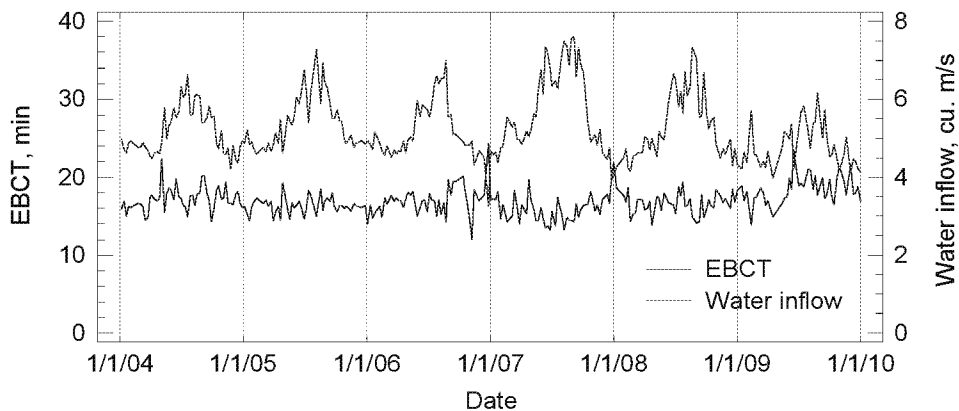


Figure 2-65 Time series of plant inflow and EBCT variations.

The changes in hydroclimatic conditions and land use may impact source water quality and thus affect water plant operations and drinking water quality at the tap. Extreme variations and associated uncertainties in source water are primary design parameters in adaptation engineering. To characterize the impact, future source water variability is calculated using the Monte Carlo simulation methods described in preceding Section 6.2.1.1.

In the Monte Carlo simulation, all source water quality parameters were assumed to be log-normally distributed. This assumption is verified in Figure 2-66 for pH and TOC using ICR data of the Ohio River collected at the Miller plant intake. The log-normal probability distribution reasonably describes the variability except for a small bias in the lower 5% probability for TOC. In the Monte Carlo simulation, the number of runs is an important criterion in a reliability analysis. Therefore, numerical tests were made to determine the minimum number of runs needed to yield a constant mean, standard deviation, and skewness using a quarterly running annual average of TOC in the finished water. The mean and standard deviation become a stable constant after 500 and 2,000 runs, respectively; the skewness become constant after 5,000 runs. Therefore, 5,000 runs were chosen for all Monte Carlo simulations.

Another assumption is that the confounding effects of population growth can be neglected for plant flow rates. This simplification allows an identification of the climate-induced water quality changes impacting water treatment performance. The design and operation conditions for the Miller plant under future scenarios were initially kept unchanged from the baseline period. In addition, it was assumed that the coefficients of variation for all water quality parameters in 2050 would remain the same as those for the baseline data. This similarity is guided by the ratios of σ_0 / μ_0 in Table 2-31.

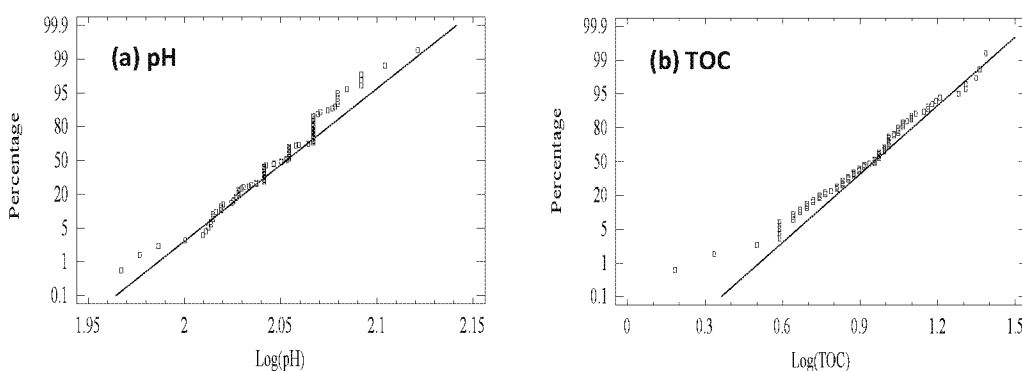


Figure 2-66 Normal probability plots for source water pH (107 samples) and TOC (93 samples) for Ohio River from the ICR database (July 1997-December 1998)

6.3.2.2 Source water characterization

Surface water quality at the plant intake from Ohio River varies significantly in response to upstream hydrological changes and watershed management. Factors affecting the water quality variation include upstream watershed management, river spills from ships, and the hydroclimatic factors such as seasonal and long-term precipitation changes.

Baseline Condition (1998)

The river water variability is characterized for a period July 1997 to December 1998 using water quality data from the ICR database. Averages and standard deviations for the baseline period are shown in Table 2-31. Because the SDWA TOC regulation require reporting of quarterly running annual average, the raw water quality at the plant is divided into the seasons of spring (March to May), summer (June to August), autumn (September to November) and winter (December to February). The source water quality exhibited statistically significant difference among the seasons.

Table 2-31 Source water inputs for the Miller water treatment plant in 1998 (Baseline)

Parameter	Unit	Spring		Summer		Autumn		Winter	
		μ_o	σ_o	μ_o	σ_o	μ_o	σ_o	μ_o	σ_o
pH	--	7.7	0.17	7.7	0.20	7.8	0.22	7.8	0.18
Alkalinity	mg/L	55.5	18.2	77.2	21.7	81.4	21.0	62.3	23.1
Turbidity	NTU	43.4	38.0	26.9	36.9	8.5	7.6	41.5	64.7
Ca hardness	mg/L	63.5	23.3	76.2	31.6	87.1	35.6	74.2	33.7
Total hardness	mg/L	110.4	18.6	140.3	26.1	161.3	31.1	133	36.5
TOC	mg/L	2.3	0.6	2.9	0.6	2.6	0.3	2.5	0.6
UVA	cm ⁻¹	0.12	0.06	0.11	0.06	0.08	0.02	0.09	0.05
Bromide	mg/L	0.03	0.01	0.05	0.02	0.10	0.04	0.07	0.04
NH ₃ _N	mg/L	0.29	0.41	0.20	0.11	0.18	0.10	0.18	0.10
Temperature	°C	12.4	NA	25.7	NA	20.8	NA	9.8	NA
Flow	m ³ /s	4.75	NA	5.01	NA	5.75	NA	5.30	NA

Note: μ_o is average and σ_o is standard deviation in the year of 1998; NA – not applicable.

Joint Correlation of Source Water Quality Parameters

For the lognormal distribution (See Figure 2-62), a Monte Carlo simulation was used in modeling source water quality parameters. The basis for the modeling, such as the joint correlation, was described in preceding section 6.2.1. Monte Carlo simulations after 5000 runs established correlations among the 9 water quality parameters for the Ohio River water. The numbers in italics (Table 2-32) illustrate that more than half of the pairs of source water quality parameters are statistically correlated; their correlation coefficient is >0.2 and the p-value is <0.1.

6.3.2.3 Projecting raw water quality in 2050

To assess future source water quality, the 1998 baseline data was modified to project possible water quality scenarios in the Ohio River in 2050. The 2050 water quality projection considered the following aspects of anticipated changes.

Table 2-32. Correlation matrix for source water quality parameters (for Ohio River during July 1997 to December 1998)

Parameter	Statistics	Alkalinity	Turbidity	Ca hardness	Total hardness	TOC	UVA	Bromide	NH ₃ _N
pH	ρ	0.63	-0.11	0.04	0.43	0.36	0.11	-0.02	-0.02
	p-value	0.00	0.27	0.67	0.00	0.00	0.32	0.87	0.83
Alkalinity	ρ	1	-0.15	0.06	0.80	0.63	0.25	0.26	-0.08
	p-value		0.13	0.51	0.00	0.00	0.02	0.02	0.45
Turbidity	ρ		1	-0.15	-0.27	0.32	0.54	-0.38	0.32
	p-value			0.11	0.01	0.00	0.00	0.00	0.00
Ca hardness	ρ			1	0.25	0.02	-0.29	0.20	-0.17
	p-value				0.01	0.85	0.01	0.06	0.14
Total hardness	ρ				1	0.36	0.10	0.59	-0.26
	p-value					0.00	0.35	0.00	0.02
TOC	ρ					1	0.65	-0.04	0.18
	p-value						0.00	0.71	0.13
UVA	ρ						1	-0.42	0.29
	p-value							0.00	0.02
Bromide	ρ							1	-0.12
	p-value								0.31

- TOC, Alkalinity, and Total Hardness

Skjelkvale et al. (2005) studied the regional trend of surface water chemistry and acidification for 12 geographic regions in Europe and North America from 1990 to 2001. As one of the 12 regions, the Appalachian Plateau includes the upstream reaches of the Ohio River. Therefore, the regional trends in their study for alkalinity, total hardness, and dissolved organic carbon (DOC) were adopted to estimate these parameters for the period 1998 to 2050. The trends for alkalinity, total hardness, and DOC are equivalent to +0.036, -0.22, and +0.03 mg/L per year, respectively. Because DOC is usually the main component of TOC, the trend for TOC is assumed the same as that for DOC.

- Ammonia

The most important sources of ammonia are from decomposed plant and animal matter, fertilizer, sewage, and industrial effluents. Whitehead et al. (2006) investigated the hydroclimatic impacts on ammonia in the River Kennet of U.K. for the period from 1961 to 2100. A 25% increase of ammonia from 1998 to 2050 can be assumed based on their study. It is believed that the 25% increase is applicable to the source water quality in this study, but the effect of ammonia on TOC in finished water is negligible (see later discussion).

- Bromides, UVA, pH, Turbidity, and Calcium Hardness

Bromides occur naturally in both surface and groundwater but are particularly high in areas of saline intrusion. Cromwell et al. (2007) pointed out that sea level rise in future climate would increase bromide levels in coastal regions. However, there is presently no evidence to indicate changes of bromide levels in inland regions because of future climate conditions. This finding was assumed to be applicable to the Miller plant in 2050.

Similarly, there is no evidence found yet to quantify changes on the levels of water quality parameters UVA, pH, turbidity, and calcium hardness under future climate conditions, these parameters in 2050 were assumed the same as the 1998 baseline values.

- Temperature

Cromwell et al. (2007) predicted increases in surface water temperatures ranging from 1.1 to 6.6°C from 1990 to 2100. The average water temperature in 2050 is estimated to be 2°C higher than the baseline values for all seasons during the 52-year period.

The analysis above generates an estimate of the key parameters for the 2050 raw water quality. Furthermore, the changes are translated to the other water quality parameters using the correlation matrix in Table 2-32. This empirical statistical analysis leads to a proposed source water quality in the Ohio River intake in 2050. The result is shown in Table 2-33.

6.3.2.4 WTP-cam model calibration and validation

Before applications to treatment process modeling was performed, the WTP-cam for the Miller plant was calibrated and validated using input data extracted from the ICR database. Model calibration and validation was based on sample period 10 (April 1998), sample period 13 (July 1998) and sample period 16 (October 1998). Plant operation data for the three periods were described in detail in preceding Section 6.3.1.

Results from the WTP-cam simulation for the field data of validation periods are shown in Table 2-34. Reasonable agreements for most water quality parameters are achieved including

pH, alkalinity, total hardness, TOC, free chlorine residual and TTHMs. The measured and simulated TOC concentrations were in good agreement in the finished water:

Table 2-33 Projected raw water quality parameters for the Miller WTP in 2050

Parameter	Unit	Spring		Summer		Autumn		Winter	
		μ_1	σ_1	μ_1	σ_1	μ_1	σ_1	μ_1	σ_1
pH	--	7.7	0.17	7.7	0.20	7.8	0.22	7.8	0.18
Alkalinity	mg/L	57.3	18.9	79.1	22.1	83.3	21.7	64.1	23.7
Turbidity	NTU	43.4	38.0	26.9	36.9	8.5	7.6	41.5	64.7
Ca Hardness	mg/L	63.5	23.3	76.2	31.6	87.1	35.6	74.2	33.7
Total Hardness	mg/L	98.8	16.8	128.9	24.5	149.9	28.5	121.5	32.8
TOC	mg/L	3.8	1.0	4.4	0.9	4.1	0.5	4.1	0.9
UVA	cm ⁻¹	0.12	0.06	0.11	0.06	0.08	0.02	0.09	0.05
Bromide	mg/L	0.03	0.01	0.05	0.02	0.10	0.04	0.07	0.04
NH ₃ _N	mg/L	0.36	0.50	0.25	0.13	0.23	0.13	0.23	0.13
Temperature	°C	14.4	--	27.7	--	22.8	--	11.8	--
Flow	m ³ /s	4.75	--	5.01	--	5.75	--	5.30	--

Note: μ_1 is average and σ_1 is standard deviation in 2050; -- Not applicable.

- The relative projection error is <10% for bulk water parameters pH, alkalinity, and total hardness. The error was 8.4±8.3% in the coagulation basin and filters, 7.5±7.4% for the GAC units and finished water, and 1.5±5.0% in the distribution system. These uncertainty assessments include all the data analyzed without excluding the period-13 data that are statistically different from the others of the calibration periods. Excluding period 13 data, the projection errors are only a half.
- For the sampling periods 10 and 16, model-simulated TOC concentrations were projected higher than measured concentrations by 26.2±2.7% in the coagulation basin and filters, but very close at the GAC units and finished water. The model estimates are >50% than the measured for the sampling period 13, when TOC concentrations were low (Table 2-34).
- The ICR data showed that UVA was removed by coagulation and GAC in the Miller plant, while the WTP-cam predicted most UVA removal by GAC. The simulated UVA agreed well in the finished water for sampling period 10.
- Excellent agreement was achieved between the simulated and the sampled chlorine residuals in the finished water.

6.3.3. Engineering analysis for water treatment adaptation

6.3.3.1. Adaptation feasibility evaluation

Tables 2-31 and 2-33 list the source water quality at the plant water intake in the 1998 base year and in the 2050 target year, respectively. For these projected source water changes, the

adaptation feasibility of the treatment plant was evaluated using the calibrated and validated WTP-cam model. In this evaluation, the plant treatment processes were assumed to remain unchanged, however adaptation took place by modifying the GAC treatment operations because GAC was projected to be the most effective process for TOC removal (See Section 6.3.1.2).

Table 2-34 Comparison of sampled and modeled water quality results

Water quality parameter	Sampling period	Data type	Influent	Coag. Basin	Filtration	GAC	Finished water	AVG1*	AVG3**
pH [--]	10	Sampled	7.7	8.7	8.6	8.0	8.5	8.6	8.6
		Modeled	7.7	9.4	9.4	9.4	9.1	9.1	9.1
	13	Sampled	7.6	7.9	7.8	7.8	8.2	8.4	8.5
		Modeled	7.6	9.2	9.2	9.2	8.9	9.0	9.0
	16	Sampled	7.7	8.3	8.1	8.0	8.4	8.3	8.6
		Modeled	7.7	8.8	8.8	8.8	8.2	8.2	8.2
Alkalinity [mg/L]	10	Sampled	56	59	58	58	58	60	60
		Modeled	56	64	64	64	62	62	62
	13	Sampled	63	56	59	58	57	64	68
		Modeled	63	72	72	72	69	69	70
	16	Sampled	75	77	80	77	81	81	82
		Modeled	75	81	81	81	78	78	78
Total Hardness [mg/L]	10	Sampled	113	128	120	119	120	121	115
		Modeled	113	122	122	122	122	122	122
	13	Sampled	98	106	107	108	106	115	120
		Modeled	98	109	109	109	109	109	109
	16	Sampled	164	162	166	164	169	164	165
		Modeled	164	170	170	170	170	170	170
TOC [mg/L]	10	Sampled	1.8	1.5	1.4	1.0	1.0	--	--
		Modeled	1.8	1.8	1.8	0.8	0.8	0.8	0.8
	13	Sampled	3.6	2.55	2.2	--	0.51	--	--
		Modeled	3.6	3.6	3.6	1.3	1.3	1.3	1.3
	16	Sampled	2.3	1.9	1.7	--	0.54	--	--
		Modeled	2.3	2.3	2.3	0.6	0.6	0.6	0.6
UVA [cm ⁻¹]	10	Sampled	0.069	0.028	0.024	0.012	0.010	--	--
		Modeled	0.069	0.061	0.061	0.009	0.006	0.006	0.006
	13	Sampled	0.178	0.068	0.054	--	--	--	--
		Modeled	0.178	0.151	0.151	0.018	0.013	0.013	0.013
	16	Sampled	0.075	--	--	--	--	--	--
		Modeled	0.075	0.067	0.067	0.004	0.003	0.003	0.003
Free chlorine residual [mg/L]	10	Sampled	--	--	--	--	1.0	0.9	0.7
		Modeled	0.0	0.0	0.0	0.0	1.0	0.7	0.5
	13	Sampled	--	--	--	--	1.2	0.8	0.7
		Modeled	0.0	0.0	0.0	0.0	1.2	0.7	0.5
	16	Sampled	--	--	--	--	1.3	1.0	0.7
		Modeled	0.0	0.0	0.0	0.0	1.2	1.0	0.9
TTHMs [µg/L]	10	Sampled	--	--	--	--	11.9	23.7	28.8
		Modeled	0.0	0.0	0.0	0.0	9	16	22
	13	Sampled	--	--	--	--	8.1	30.9	47.8
		Modeled	0.0	0.0	0.0	0.0	20	37	53
	16	Sampled	--	--	--	--	8.5	29.6	46.5
		Modeled	0.0	0.0	0.0	0.0	8	16	23

Note: *AVG1 refers to average retention time 1 day. **AVG3 refers to the maximum retention time, 3 days.
--: data not available.

Figure 2-67 compares the TOC and TTHM results between the baseline and the future scenarios. The cumulative density function (CDF) was defined by adding the probability of simulated TOC or TTHM concentrations in the finished water. The CDF curves displayed the vulnerability of potential exceedance of the drinking water standards when the treatment processes and GAC operation remain unchanged. Under the baseline conditions, the Miller plant meets the TOC compliance criteria of 2.0 mg/L (see Figure 2-67a). Under future climate conditions, however, the source water would likely have higher TOC concentrations and different water chemistry. 2765 of the 5000 Monte Carlo runs in the WTP-cam simulations show TOC concentration >2 mg/L in finished water. This result indicates a 55% probability of violating the TOC compliance criterion under the same TOC and TTHM regulation limits. If the TTHM MCL became more stringent in future, greater risk of a violation would be higher: if the TTHM MCL decreased to 60 µg/L or to 40 µg/L, the risk of an MCL violation would increase to 4% or 36% under the future scenario, respectively.

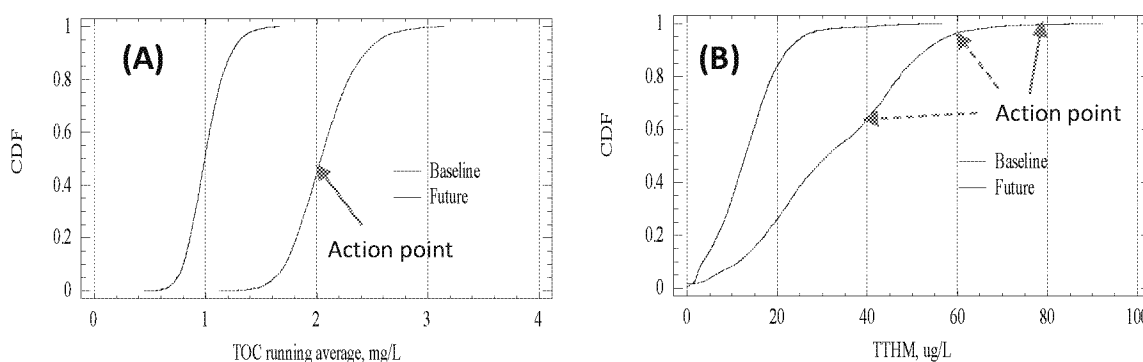


Figure 2-67 Modeled treatment performance of the Miller water plant in baseline (1998) and future (2050) scenarios. (A) TOC running average at finished water; (b) TTHM after 3 days residence in distribution system. Results based on 5000 Monte Carlo simulations.

Li et al. (2014) analyzed these model projections and discussed potential engineering options in the system-scale adaptation. They noted two potential engineering options for current plant configuration and operation:

- One option is to replace the chlorination system with the newly deployed UV disinfection treatment unit in the plant. After UV disinfection, chlorination takes places in the clear well before the product water is distributed at the Miller treatment plant. Compared to solely relying on chlorination, the modified process using UV disinfection can significantly reduce DBP generation in the treatment and in the subsequent distribution. When re-chlorination is required to satisfy the *CT* rule for biological control, the DBP formation may still become a technical challenge when TOC is not adequately removed during water treatment. Boccelli et al (2003) proposed a mathematical model to analyze the re-chlorination effects.
- The engineering feasibility also depends on water age in the distribution system. The GCWW water distribution system is a single network that supplies water to the population in a monocentric urban form. As described in Section 4.2, the Cincinnati metropolitan area started to evolve toward a multi-center configuration with increased

expansion in the northern portion of the city. How to manage the water age and system efficiency is a central subject in a detailed adaptation feasibility analysis involving both the GCWW treatment and the distribution system. Currently, for assurance of CT rule compliance in the distribution system, the post-UV product water is disinfected using chlorination at clear well at a reduced level.

- Another option is to optimize the Miller plant operation by configuration of the GAC absorption process for the current and future climate conditions. This option requires no significant capital investment, representing a practical and attractive adaptation solution. Two variables are important to the adaptation feasibility analysis. One is the adaptation threshold of current system beyond which new GAC contactors or other treatment units are required. The second is energy consumption in the GAC regeneration and its CO₂ emission in the life-cycle analysis.

6.3.3.2. Adaptation economics in TOC treatment

Treatment adaptation using the GAC process design and operational modifications is intended to reduce the likely future risk of TOC non-compliance at the Miller plant. Potential adaptation options are further evaluated with respect to cost and treatment effectiveness, in addition to the engineering feasibility described above in Section 6.3.3.1.

Technically, a reduced GAC reactivation period and operational adjustment are the feasible adaptation options. For this approach, GAC is reactivated on site, for which energy consumption is the primary adaptation cost. The adaptation cost for GAC replacement and reactor optimization was estimated using the equations with considerations described in preceding section 6.2.1.5. Currently, the Miller plant has 12 down flow gravity contactors and two multi-hearth furnaces for onsite reactivation. Each of the contactors has a volume of 595 m³ and a surface area of 181 m². The overall GAC loss rate through the system is 7-8%. The carbon loading rate is 482 kg/day of GAC per square meter of hearth area in GAC reactivation.

A capital recovery analysis assumes a return period of 20 years with an interest rate of 5%. The resulting cost curve between reactivation period and the annualized cost is shown in Figure 2-68. Annual cost of the GAC system is expected to decrease with increasing reactivation period. For a reactivation period shorter than 90 days, the annual cost increases rapidly at a shorter reactivation period.

The net annual adaptation cost is defined as the difference between annual cost calculated with Figure 2-68 and the base annual cost at the current operation. The current operation was calculated to be \$13.6 million for an average GAC reactivation period of 180 days at the Miller plant. The results are shown in Figure 2-69. The net annual cost to control

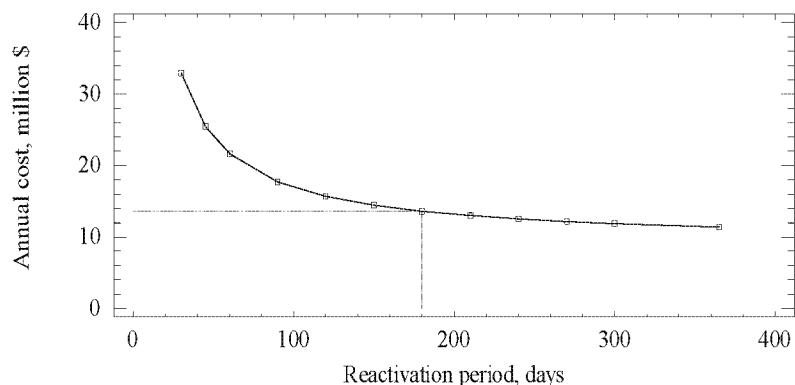


Figure 2-68 Cost curve for the GAC reactor at the Miller water treatment plant.

TOC <2.0 mg/L in the 2050 climate scenario would decrease to \$7.0 million for a 0.02 mg/L safety margin or \$7.8 million for a 0.20 mg/L safety margin. If the plant performance criterion allows a 10% risk for TOC above the 2.0 mg/L limit, the net annual cost would further reduce to \$3.4 million for a 0.02 mg/L safety margin, and \$4.4 million for 0.20mg/L safety margin (Figure 2-69).

6.3.3.3. Implication for engineering practice

The adaptation case study at the Miller plant shows an example of the engineering analysis for adaptation approaches to offset source water changes projected for year 2050. Results show a difference in adaptation reliability, cost and the ability to achieve multiple objectives in engineering economics, regulatory compliance, and climate co-benefits in energy cost and CO₂ emissions.

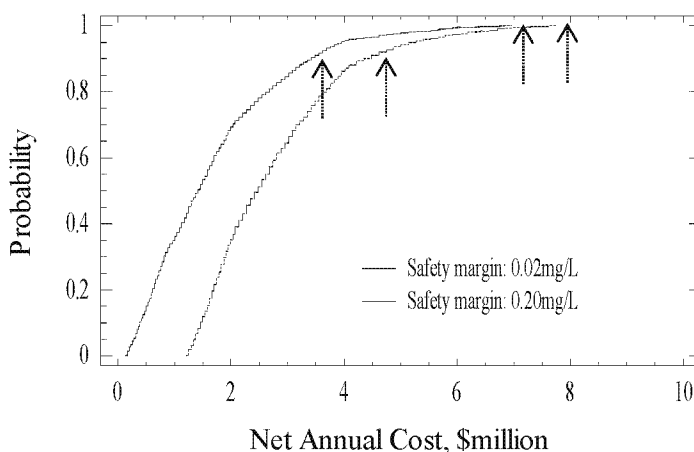


Figure 2-69 The probability distribution for net annual adaptation cost against the source water change scenario in year 2050. The energy cost can be readily converted into CO₂ emissions.

The engineering analysis using WTP-cam is quantitative in projecting the probability of compliance and adaptation costs. However, it is important to note that several assumptions were built into the analysis. These assumptions include: 1) the correlation matrix among water quality parameters used in WTP-cam modeling, which is assumed to remain unchanged in the future; 2) compliance criteria in SDWA regulations such as DBP standards in drinking water remain unchanged; and 3) the current treatment technologies in removal of TOC remain appropriate and in place. For these reasons, the adaptation analysis using WTP-cam in other applications need to rely on location-specific conditions, as well as anticipated future technological and regulatory environments.

7. Adaptation Engineering for Drinking Water Distribution

Water quality management in drinking water distribution networks is an important area of infrastructure adaptation to address the changes with climate and land use conditions. Efficient and adaptive water distribution (this section) and treatment (Sections 5.0 and 6.0) are the two essential components in the SmartWater system (Figure 2-7).

Drinking water quality at consumers' tap depends on both the water demand management in a service area and the control of water quality variations in water treatment and in the distribution system. This relationship is schematically shown in Figure 2-10. The changes in climate and land use have produced, and will likely continue to produce, impacts to surface water quality. Some examples include long-term changes, short-term extremes, and seasonal

variations of water quality parameters (e.g., TOC, turbidity), salt water intrusion, as well as the occurrence of eutrophication conditions (e.g., high temperature and nutrients) with the prevalent presence of *chlorophyll-a* and cyanobacteria. These types of source water changes challenge the planning and operation of the water treatment plant. Despite the multi-barrier approach utilized to protect public health in the U.S., perturbations or changes in source water may affect the performance of the conventional drinking water treatment plant. This is evident in the seasonal variations of TOC levels in the GAC influent in the case study of the Miller plant (See Figure 2-60).

Water demand variation, both in space and time, is the other primary variable affecting drinking water quality in municipal water supply (Figure 2-7). Water demand is a function of urban development, urban adaptation, asset management, and socioeconomic factors. These factors are often dependent upon a collection of urban management and policies, rather than a simple technical issue on the distribution network itself. For example, the urban adaptation facilitated by land use planning and transportation infrastructure can significantly affect the spatial distribution of population and business activities, and thus result in substantial changes in the location of water demands.

In addition, many water utilities are focusing on two water conservation measures (See U. S. EPA, 2015a). One is water conservation through reduction of water loss or non-revenue water in the water distribution pipelines to customers' taps. This measure is a part of the water utility asset management described extensively in literature and U.S. EPA reports (e.g., Barlett et al., 2017; EPA, 2007c). Because of the aging water infrastructure, nation-wide average rate of water loss is around 18-20%. Some utilities with old water pipes and complex pressure zones to manage may experience water loss as high as 50% in some distribution network segments. The other is water use reduction on the per capita basis. Some U.S. water utilities in water-poor regions are actively developing management and economic incentives to encourage water saving practices, such as artificial lawns. It is noted that this option may bring other implications. For example, strict per capita goals may impact water utility revenue and thus have the negative response of limiting the ability of commercial development (jobs) to grow.

For water distribution, SmartWater leverages sensor-based model-driven drinking water distribution modeling and system control based on the EPANET hydraulic model of Rossman (2002) and extensions (Uber et al., 2004; Shang et al., 2008). The control of water quality in distribution systems has been investigated since the 1990s. A wide range of technical data, models, and management methodologies have been published in the past two decades, mostly without consideration of changes in future climate conditions (e.g., Rossman, 2010; Uber et al., 2004; Shang et al., 2008; Boulos et al., 2006; Mays, 1999; and references therein).

When considering the impacts from climate and land use changes, water quality deterioration in a distribution system is the focus of adaptation. A confluence of factors can all affect the water quality management. These factors include high TOC in source water and potentially in the finished water of a treatment plant, rising water temperatures, higher ground temperatures surrounding buried water pipes, as well as changes in reactivity of organic matter in a future climate condition. There are numerous U.S. EPA guidelines on water distribution systems under the current climate conditions. Hence those will not be repeated in this report. Instead, this section is focused on surface water plant with adaptation methods and tools highlighted on flowing three topics:

- modeling DBP concentrations in water supply for vulnerability assessment;
- in-network water treatment to manage DBPs formed in the distribution system; and
- modeling of the water demand changes for policy analysis.

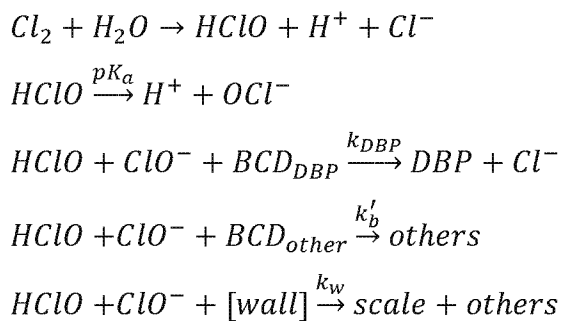
These methods are described below. At present time, computer programs for distribution such as EPANET, EPANET-MSX, and the codes for pipe junction mixing, are available for the SUD, but have not been physically incorporated.

7.1. Water age and water quality changes in distribution: Need for adaptation

Disinfection by-product (DBP) formation during drinking water distribution is an inevitable outcome due to reactions between residual disinfectants and DBP-formation precursors in the organic matter. The well-known water quality impacts are regulated under the SDWA CTR/DBP Stage-II rules (See U.S. EPA, 2015). The need for adaptation in water distribution can be assessed through compliance monitoring that is often guided by EPANET-based simulation of residual chlorine and DBP concentrations. This section is based on recent publications by Zhao et al. (2018a, 2018b, 2017) and others cited therein.

7.1.1. EPANET-based risk assessment on DBP formation

Model simulation has been widely practiced for water distribution system since its inception in the late 1980s. Chlorine as an oxidant in drinking water reacts with TOC to form DBPs, including the regulated trihalomethanes (THMs) and haloacetic acids (HAAs). At the same time, chlorine is also simultaneously transferred to pipe walls and consumed in reactions with pipe wall materials and biofilms. In the simplest terms, total free chlorine $[Cl]$ – the sum of hypochlorous acid $[HClO]$ and hypochlorite ion $[ClO^-]$ in a flowing pipe, reacts with natural organic matters $[NOM_{DBP}]$ (e.g., humic and fulvic acids) in the bulk water demand $[BCD]$ to form DBPs. A fraction of $[Cl]$ also reacts with other bulk demand $[BCD']$ without DBP formation. Bulk water demand consists of organic materials and other chlorine reactants and those forming from detachment of biofilms and pipe scales in water distribution. Chlorine also reacts with pipe wall materials and attached biofilm, with both terms lumped together as the wall demand. Generally, the multi-component chlorine reactions can be written as:



DBPs, represented by trihalomethane (THM) compounds – trichloromethane (TCM), bromodichloromethane (BDCM), dibromochloromethane (DBCM), tribromomethane (TBM), collectively as total THMs (TTHMs), form during chlorination through stepwise NOM-oxidation and hydrolysis as illustrated below. Using the model compound propanone CH_3COCH_3 and m as the Br molar fraction:

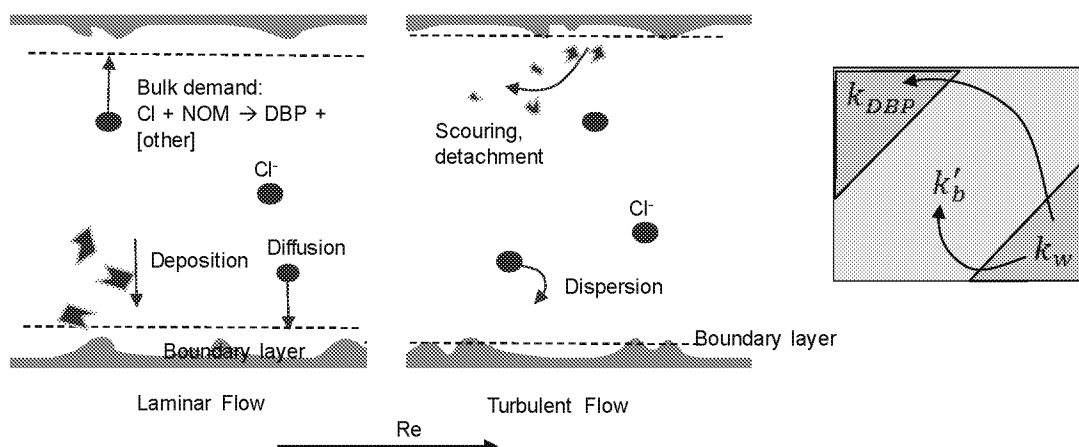
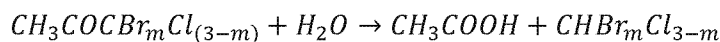
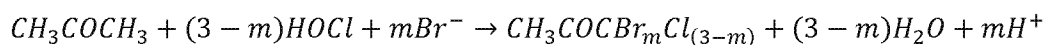


Figure 2-70. Schematic diagram showing the simultaneously occurring chlorine reactions with bulk and wall demands, mass exchange between the bulk water and pipe wall. Implications on reaction kinetics for bulk decay (k'_b), DBP formation (k_D), and wall decay (k_w) are shown on the right. From Zhao et al., (2018a).

The simultaneously occurring processes in a flowing water pipe is schematically shown in Figure 2-70. Analytical solutions for the chlorine transport and DBP formation have been published (e.g., Biswas et al., 1993; Rossman, 2002; and Clark, 1998). Clark and Haught (2005) developed a mass transfer limited chlorine model and compared it with others in Rossman et al. (1994) and Biswas et al. (1993). Clark et al (2010) further analyzed the competing chemical reactions in the modeling of chlorine decay and DBP formation. In the center of discussion are the water quality models of Clark (1998) and other subsequent publications (e.g., Clark and Sivaganesan, 2002; Boccelli et al., 2003). These models stipulate that in second order kinetics, the DBP concentration increase from initial condition ($C_B - C_{B,0}$) is proportional to the decay of chlorine concentration ($C_{A,0} - C_A$) by the proportion constant T' in the distribution pipe:

$$C_B = C_{B,0} + T'(C_{A,0} - C_A) \quad (2.41)$$

$$T' = \frac{k_D}{k_w + k'_b} \quad (2.42)$$

The proportion constant T' is simply a ratio of DBP formation kinetic rate (k_D) over the total chlorine decay ($k_E = k_w + k'_b$); k_w and k'_b are the reaction rates for wall demand and bulk demand, respectively. In this research, the analytic solution of Clark (1998) was further refined on a basis of kinetic theory and comparative experiments conducted at the U.S. EPA Test & Evaluation Facility. The study led to the proposal of new analytical models in Eqs.2.43-2.44, respectively, for chlorine decay and DBP formation (Zhao et al., 2018; Yang et al., 2008). The

DBP analytical equation can be simplified to Eq.2.45 under common conditions in water distribution when DBP-forming fractions in the bulk demand is very small or $\theta \sim 0$:

$$\frac{\Delta C_B}{C_{A,0}} \cong \frac{k_{DBP} \left(1 - \frac{C_A}{C_{A,0}}\right)}{(k'_b + k_w)} C_{E,0} - \frac{k_{DBP} \theta \cdot C_{A,0}}{2(k'_b + k_w)} \left(1 - \frac{C_A}{C_{A,0}}\right)^2 \quad (2.43)$$

$$C_A = \frac{C_{A,0}}{\left(1 + \frac{\theta}{Y} C_{A,0}\right) e^{k_E t} - \frac{\theta}{Y} C_{A,0}} \quad (2.44)$$

$$\Delta C_B \approx Y \cdot C_{A,0} - \left(\frac{k_D}{k'_b + k_w}\right) \cdot C_A \quad (2.45)$$

Among the 25 predictive models that Sadiq and Rodriguez (2004) evaluated, only three (Clark, 1998; Clark and Sivaganesan, 2002; and Gang et al., 2003) are mechanistic, relating DBP formation to chlorine consumption by kinetic laws. Others are based on empirical relations for a given water, thus limiting their applicability. The newly developed analytical models show that the DBP formation in distribution systems depends on not only initial chlorine concentration, but more importantly, the reactivity of DBP-forming precursors and their reactivity. This is expressed as the kinetic ratio $\frac{k_D}{k_w + k'_b}$ in Eq.2.45, and θ in Eq.2.43.

The findings and new models have implications on network modeling and management. The models will be further reviewed and incorporated into the EPANET for the SUD's SmartWater module. First, the simultaneous occurrence of chlorine decay and THM formation depends on the kinetic ratio $\frac{k_D}{k_w + k'_b}$ that in turn is a function of pipe flow hydrodynamics. Several common water quality parameters, including total organic carbon (TOC), residual chlorine, UV256, water pH and temperature, have been used to estimate the THM formation potential (Clark and Sivaganesan, 2002). As shown in Eqs. 2.43-2.45, the non-DBP forming bulk demand and the wall demand compete for the finite chlorine residual in water, and thus affect the THM formation potential in competitive reaction.

Second, NOM properties and specifically the chlorine-reaction fraction are the controlling variables in competitive reactions. Removal of reactive NOM fractions in treatment is the effective approach to decrease θ , T and Y in order to simultaneously maintain the required chlorine residual level and reduce the THM formation potential. For aged NOM with small θ , such as GAC-treated tap water, the hydrodynamic effects on k_E and $\frac{k_D}{(k'_b + k_w)}$ cannot be neglected. The reaction competition from Re-dependent wall demand becomes comparable with THM-forming and other bulk demand.

Finally, the kinetic constants and the time to reach a pseudo-steady state are all related to pipe flow hydrodynamics. Many parts of a distribution network may have water ages exceeding 24 hours, with re-chlorination possibly necessary to compensate for the excessive loss of chlorine residuals for biological control. Re-chlorination, however, will further increase the DBP

levels (Boccelli et al., 2003) even to the extent of violating drinking water standards. Therefore, it is of fundamental importance to reduce water age through adaptive engineering measures, such as through tank operations and better monitoring water demand in real time throughout a distribution network, and perhaps structurally by changing routing of water, pipe sizes, and other network configurations. The need for adaptation on water demand and water age management is described next.

7.1.2. *Water age variations, modeling and adaptive control*

Water age varies significantly in a distribution network. Shown in Eqs.2.44-2.45, an extended water age can result in low residual disinfectant level and elevated DBP concentrations, a phenomenon that has been widely documented. One central adaptation objective is to assess the vulnerability, as well as to plan and design corresponding adaptation measures.

For vulnerability analysis, this research recently completed real-time water demand measurements over 25% of the network nodes for 2 months for an independent distribution segment in Cincinnati, Ohio. Subsequently, a hydraulic and water age simulation was conducted using the EPANET model (Zhao et al., 2017). The ~ 38.6 km² network serves 8,485 buildings, consisting of 4,843 pipes, two elevated water tanks, four booster pumps, three control valves and one water reservoir for water supply. In the network, the north and south supply areas supplied by the two elevated tanks contain numerous local pipe loops many in “H” configurations and deadend branches of < 8-in diameter. The study results clearly showed large water age variations that can be monitored and analyzed using all-pipe and all demand (APAD) techniques (Zhao et al., 2018). In comparison, the hourly demand variation curve (HDVC) modeling widely used currently is incapable of assessing the water age variability. Two conclusions are particularly noteworthy with implications to the water age assessment and management:

- The pulse nature of water demand is prevalent among individual water users throughout the network. In the one-week 68-hr period, measured pulse demand in most network nodes is zero for approximately 70% of the time (Figure 2-71). In the analysis, the time-discontinuity in water demand starts to disappear at the level of 31-home demand aggregation. It is replaced by time-continuous variation patterns for a block of 114 homes (Figure 2-71).
- There is a large range of water ages among all network nodes (Figure 2-72). Simulated water ages during the two-week validation period average at 35.8 and 34.6 hours given by the APAD and HDVC models, respectively. Both demand models yield a large spread of simulated water ages from <15 hrs near the pump stations to over 180 hrs in dead-end branches. In all cases, the large spreads in water age and their spatial association with the network configurations (Zhao et al., 2018) point to the need of network optimization and adaptations. Some adaptation measures that were discussed in literature include reconfiguration of local pipe loops, synchronized tank operations, re-chlorination and in-network water treatment. The latter is one major technical approach as described in next Section 7.2.

7.2. In-network water treatment as adaptation measure

Except for TOC removal in water treatment plants, other adaptation approaches for effective THM management rely on water quality management in finished water distribution as

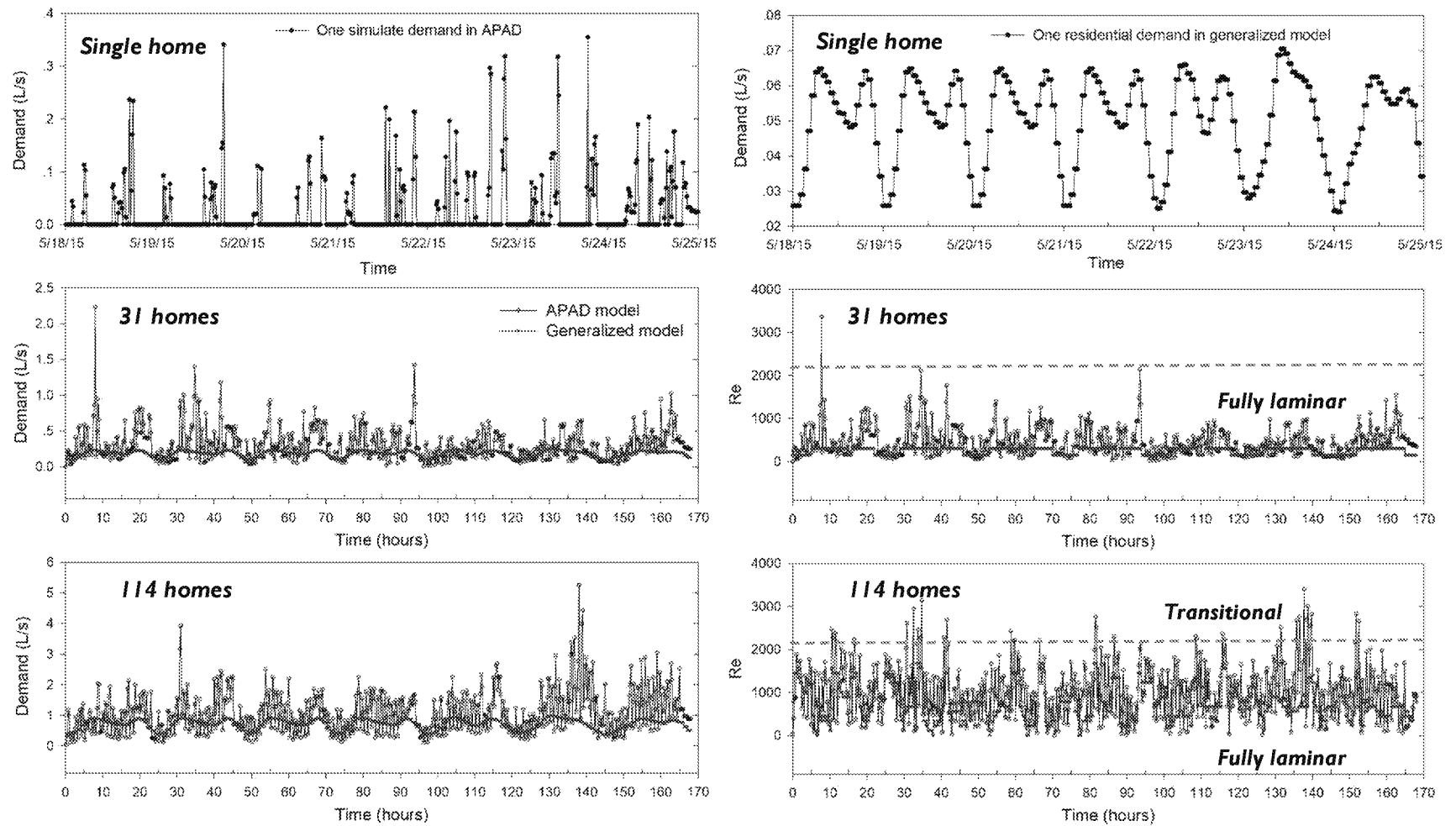


Figure 2-71 Water demand and computed Re variations in a two-week period for a single home, 31 and 114 homes of a pipe dead-end section, showing significant differences between the APAD model and the generalized water demand pattern. From Zhao et al. (2018b).

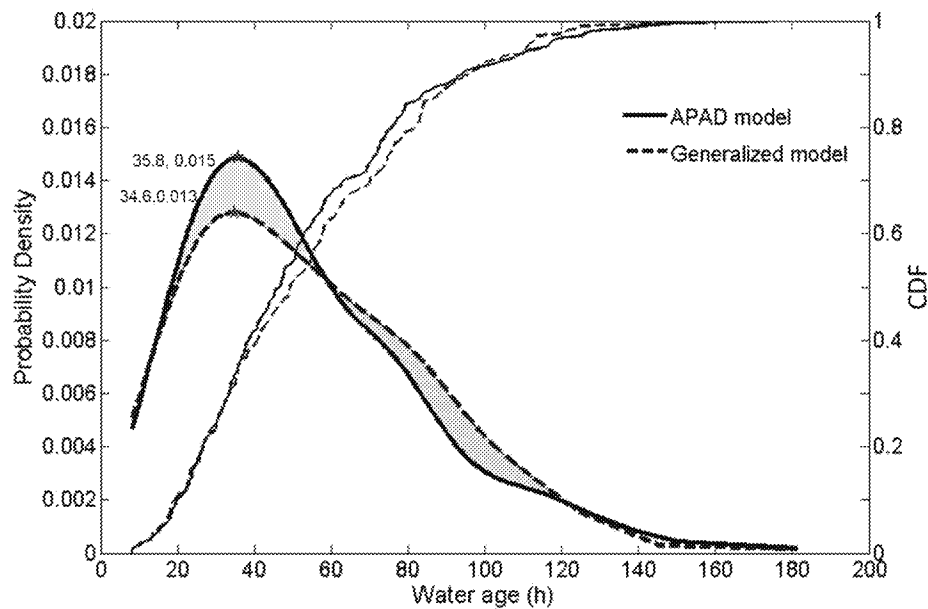


Figure 2-72 Probability distribution and corresponding CDF of simulated water age for the network. From Zhao et al. (2018b, 2017).

the last barrier to protect human health. Water quality management in distribution is not new. Decades of research and practical engineering have produced a suite of distribution system models (e.g., EPANET, EPANET-MSX, etc.¹⁵) and technological innovations in the in-network water treatment. For the latter, examples can be found in re-chlorination, in-network GAC absorption and aeration.

Unique for source water changes is the focus of adaptation measures on extreme conditions giving arise from climate and land use changes. These changes are not considered in traditional water supply engineering. For example, some water supply systems have experienced a rapid decrease of water demand due to socioeconomic changes or the loss of major employment centers, resulting in oversized distribution system. The hydroclimatic changes also can generate conditions resulting in high TOC concentrations in source water and in finished water, as well as leading to warm water temperatures in pipe lines. Higher water temperature, high-concentration and reactive NOMs in water will likely make DBP control a necessary but difficult task. It will concurrently increase biofilm formation. For these impacts, the in-network aeration and GAC treatment during distribution have been investigated to remove THM and other volatile contaminants.

In-network aeration

The use of aeration to remove volatile organic compounds, including THMs, relies on the principles of air-liquid two-film mass transport. In water distribution networks, the air stripping process is commonly used by retrofitting the existing water storage tanks and in-ground reservoirs. Such an application was being tested and investigated at the Las Vegas Valley Water

¹⁵ <http://www.epa.gov/nrmrl/wswrd/dw/epanet.html>

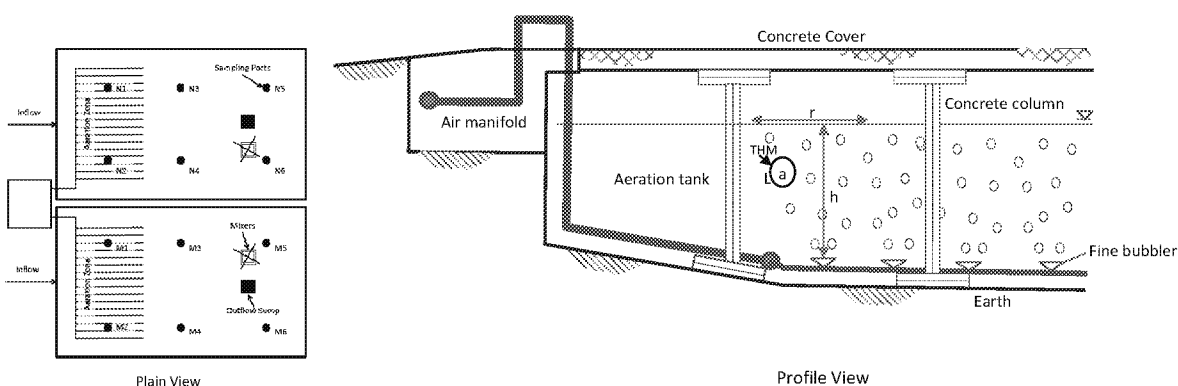


Figure 2-73 Schematic views of in-network aeration in LVVWD water distribution to remove volatile THM from drinking water in the alphas tank reservoir. Illustration after actual tank-retrofitted aeration system: left – plain view of air sparging pipes lines and tank mixers (M1-M6, and N1-N6); right – profile view showing air bubble plume geometry and the two-film transport mechanisms. h – effective water depth; r – diameter of air bubble plume.

District (LVVWD). Figure 2-73 shows a schematic illustration of the aeration system constructed at the Alphas twin tank storage basins.

In an EPA-LVVWD joint research, one retrofitted water aeration systems in the LVVWD alpha tank. The system consisted of low-profile fine bubblers, air manifold, and tank mixer (Figure 2-73). The mixer and other media (e.g., plastic cubicle) were used to improve stripping efficiency of fine bubblers. However, because of the limited water depth above the bubbler, these types of aeration systems tend to have low stripping efficiencies or use high air-to-water ratio for greater removal rates; for the latter, the improvement is at the expense of energy consumption, a major consideration in adaptation design.

In the LVVWD adaptation study, McDonnell (2012) investigated the mechanisms and modeling of in-network aeration for THM removal. The investigation included experimental testing of the THM stripping in an experimental water column, and mass transport modeling of field testing in the LVVWD's tank Alpha. The results led to the development of a THM stripping model as a program extension for the EPANET Multi Species Extension (MSX) v.1.2.0 (Shang et al., 2008). The effect of in-network aeration on water quality was further modeled using EPANET and the extension.

The aeration in the Alpha tank has significant effects on THM concentrations in the network. As shown in Figure 2-74a, pressure zone 2 receives 75% of its water from the Alpha Tank during an average day. In response, pressure zone two received the greatest reduction in average total THM concentration. The TTHM removed in nearly a half of the nodes is 90 mg/L (Figure 2-74b). This is expected since pressure zone two is heavily influenced by the Alpha tank. Water quality network modeling using EPANET 2.0 for the study is provided in McDonnell (2012).

GAC treatment and other post-formation treatment processes

GAC and other absorbents (e.g., zeolite) have been used in removal of DBP compounds from drinking water; this technology has also been applied at the point-of-use (POU) and point-

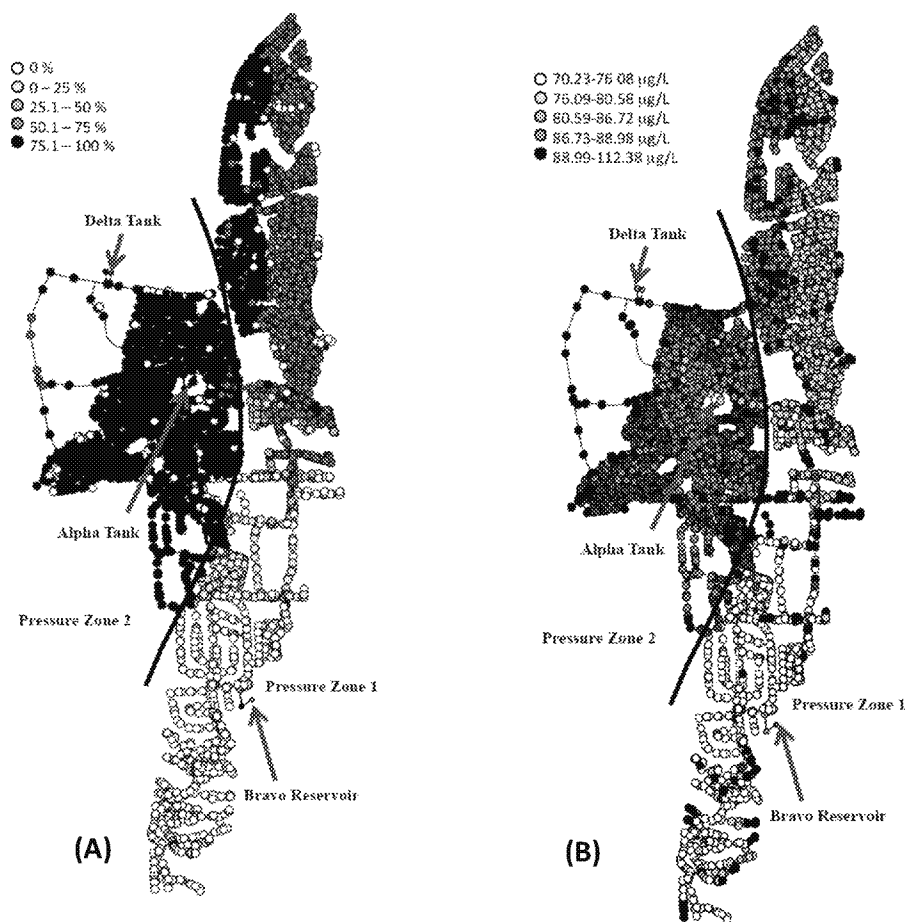


Figure 2-74 EPANET simulation of flow and THM distribution in the Western Hill portion of the LVVWD water distribution system. A). fractions of water from Alpha Tank; B). distribution of THM reduction after aeration at normal air flow rate of 2 standard cubic feet per second in the Alpha Tank. Adopted from McDonnell (2012).

of-entry (POE) (Stubbart, 2004) as a part of the small systems¹⁶. The adsorption logistic models for TOC simulation were presented in Sections 6.2-6.3. Similarly, GAC has been used to remove THMs, whereas it is less effective for mono and dihaloacetic acids (Tung et al., 2006). In addition, membrane filtration such as reverse osmosis and nanofiltration (Kimura et al., 2003; Uyak et al., 2008) have been tested and studied for removal of THM species from drinking water.

7.3. Water conservation, storage and reuse through adaptive planning

Water availability and water shortage are other characteristic impacts of the hydroclimatic and land use change. Water conservation, storage and reuse of reclaimed water are valuable practice in adaptation for many water-stressed regions. Examples can be found in Las Vegas and other cities in the U.S. southwest and in southern California. Even in water-rich

¹⁶ http://www.mae.gov.nl.ca/waterres/reports/cwws/BMPs_for_Control_of_DBPs_Apr_13_2009.pdf

regions, water conservation is often a technique for reduction in water and energy usage. These adaptation techniques to relieve hydroclimatic impacts are described in Ranatanga et al. (2014), Wang et al. (2013), Neil et al. (2012, 2014), Yang and Restivo (2010). Details of these adaptation techniques are contained in U.S. EPA (2014, 2015c, 2017).

8. SUD Applications in Coastal Regions: Water Infrastructure and Emergency Planning

Existing data and research results show that changes in precipitation patterns and overland runoff hydrographs will almost certainly impact the drainage capacity, BMPs and LID green infrastructure, as well as storm water discharges, including the long-standing CSS and CSO challenges facing many U.S. cities (U.S. EPA, 2013c; Johnson et al., 2015). Coupled with land use changes, the vulnerability of these infrastructure assets cannot be underestimated. Some specific analysis is shown in Tables 2-23 and 2-25. Impacts on unit processes are illustrated in Figure 2-50 of Section 5.2.2.2. Specific adaptive engineering solutions are location-specific, mostly related to changes in precipitation, runoff, disruptive storms such as hurricane, storm surge and sea level rise.

In this section, vulnerability and adaptation analysis for the storm water and wastewater infrastructure in coastal regions are briefly discussed. A full analysis of the coastal water resources and water infrastructure will be published separately, where case studies along the Atlantic coast and the Gulf of Mexico will be examined.

8.1. Water infrastructure vulnerability in coastal regions

The coastal zone of the United States hosts over 80% of the population, vast built infrastructure, over 90% economic outputs, and invaluable ecological resources. Nearly 39% U.S. population in 2010 lives within 50 miles (~90 km) of coastal lines¹⁷. In the low-lying Atlantic coast and the Gulf coast, the built and future infrastructure and sensitive environmental assets are vulnerable to extreme meteorological events such as Hurricane Sandy. Tropical cyclones, hurricanes, and storm surges have demonstrated the potential to compromise structural integrity and service functions of critical aboveground assets by wind damage, flooding, and the change of surface water and groundwater hydrology. The impacts and destruction of “soft” environmental assets such as coastal marshes and wetlands cannot be neglected either.

Figure 2-75 schematically shows three principle types of short-term disruptive and long-term hydroclimatic threats to the coastal infrastructure. Near the coast, sea level rise (SLR) changes the hydraulic gradient for communities in low lying areas. For example, according to the City’s Department of Environmental Protection, the City of New York has experienced the SLR effects on drainage systems and wastewater pump stations in the low-lying Queens district. Storm surge, particularly those associated with hurricanes, are shown to repeatedly result in severe inundation of the coastal areas. The combined effect of SLR and storm surge is even more disruptive. To above-ground infrastructure, wind damage associated with hurricanes can be disruptive. The electric grid damage and supply disruption are particularly important to the water infrastructure services, during and after the events.

In the inland region away from the coast line, the coastal mountains and other geophysical features induces strong atmospheric interactions with global/regional climate

¹⁷ <http://oceanservice.noaa.gov/facts/population.html>

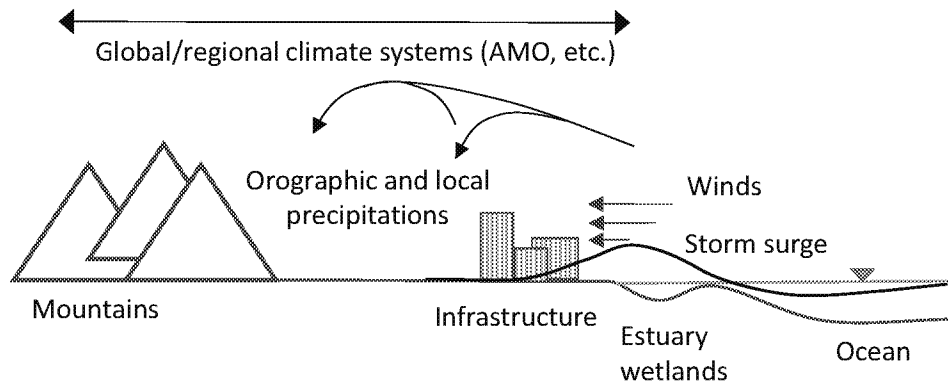


Figure 2-75 Schematic illustration of long-term climate and short-term meteorological and disruptive storm surge events in a typical coastal zone.

systems such as Atlantic Meridian Oscillation (AMO). This atmospheric interaction can introduce localized moisture circulations such as orographic precipitations and rain shadows (e.g., McKenny et al., 2006; Konrad II, 1997; Wallis et al., 2007; Changnon, 2006). These localized rainfall anomaly and changes in the future climate may not be captured in conventional hydrological design guidelines such as NOAA's Atlans-14 precipitation design tables.

Table 2-35 lists major hydrological impacts and adaptation design variables for water infrastructure and other environmental assets. These engineering considerations of intense precipitation, wind speed, and storm surge include revision to engineering parameters for wind (average speed, gust speed, and direction), precipitation (duration, depth, and intensity), and inundation level (depth and duration). Specifically:

- Design precipitation (duration, depth, and intensity). Urban infrastructure systems or components are planned and designed to assure adequate hydraulic capacities providing desired water services. The design basis is often in the form of design storm such as a 10-year 24-hour precipitation. Application examples include culvert sizing in road construction, pipe sizing and grading for drainage of urban runoff, and retention pond design for storm water management (Table 2-35). Note roadways are not exempt from this type of damage to the pavement and electrical fixtures.
- Design wind (average speed, gust speed, and direction). Design values for average wind and gust wind vary among engineering convention and often are specific to the design objective and its risk category. For example, the 25-year, 50-year, and the 100-year wind speeds are used in determining the minimum strength load requirements for Occupancy Category I, II and III infrastructure, respectively (ASCE, 2014; Simiu, 2011; Cook et al. 2011). The U.S. EPA specification requires a temporary landfill cover be designed to against a gust wind speed of 2 m/s (Table 2-35). Structures and traffic controls for roadway are vulnerable to this damage also.

Table 2-35 Selected hydrological impacts and adaptation variables in coastal area.

	Design Precipitation	Design Wind*	Design Inundation*
<u>Infrastructure assets</u>			
Roadways	<ul style="list-style-type: none"> Movement of vehicles Runoff management Pavement damage 	<ul style="list-style-type: none"> Damage to light fixtures and signs 	<ul style="list-style-type: none"> Pavement damage Base damage Damage to structures/bridges
Water supply	<ul style="list-style-type: none"> - Source water quality, - Equipment flooding 	<ul style="list-style-type: none"> - Damage to power supply - Physical damage to structures 	<ul style="list-style-type: none"> - Flooding and inundation - Salt water intrusion
Stormwater and wastewater facilities	<ul style="list-style-type: none"> - Runoff management; - Hydraulic capacity of structures (e.g., pipe, culvert, sluice gate) - Stormwater quality and discharge - Flooding 	<ul style="list-style-type: none"> - Damage to power supply - Physical damage to structures 	<ul style="list-style-type: none"> - Flooding and inundation
Solid and hazardous waste facilities	<ul style="list-style-type: none"> - Flooding - Cover design - Groundwater level and control 	<ul style="list-style-type: none"> - Cover design - Dust dispersion and control - Disruptive wind damage 	<ul style="list-style-type: none"> - Flooding and inundation
<u>Environmental assets</u>			
Estuary wetlands	<ul style="list-style-type: none"> - Nutrient flux - Changing hydraulics of flows 	<ul style="list-style-type: none"> - Disruptive wind damage 	<ul style="list-style-type: none"> - Flooding and inundation
Riverine	<ul style="list-style-type: none"> - Base flow and drought - Nutrient flux and flora ecohealth - Peak flow and erosion 	<ul style="list-style-type: none"> - Disruptive wind damage 	<ul style="list-style-type: none"> - Flooding and inundation

Note: * Refer to wind and inundation in coastal shores are related to cyclones and storm surge.

Modified from Liang et al. (2018).

- Design inundation (depth and duration). In coastal areas, the inundation level is the sum of flooding and wave action or surge. The surge actions increase the flooding level and spatial extent, and the surge-related inundation is temporary. Acute hydraulic impacts recede after the disruptive storm surge event (FEMA, 2015). The schematic in Figure 2-76 shows the concept of water action and storm surge height during a hurricane event. Thus both inundation depth and duration are two primary design parameters (Table 2-35). Road bases and pavement may be permanently damaged by inundation.

How to plan and manage these valuable assets under the current and future conditions are essential to coastal risk assessment and management. For this purpose, the SUD methods and tools are designed to analyze the hydrological and transportation impacts in coastal hydroclimatic events. Detailed analysis and technical basis for these tools will be presented in subsequent publications. Here in this report, the case study at the town of Mattapoisett in the Massachusetts southeast coast is described to show how SUD is used to develop the technical basis for wastewater adaptation and emergency evacuation planning.

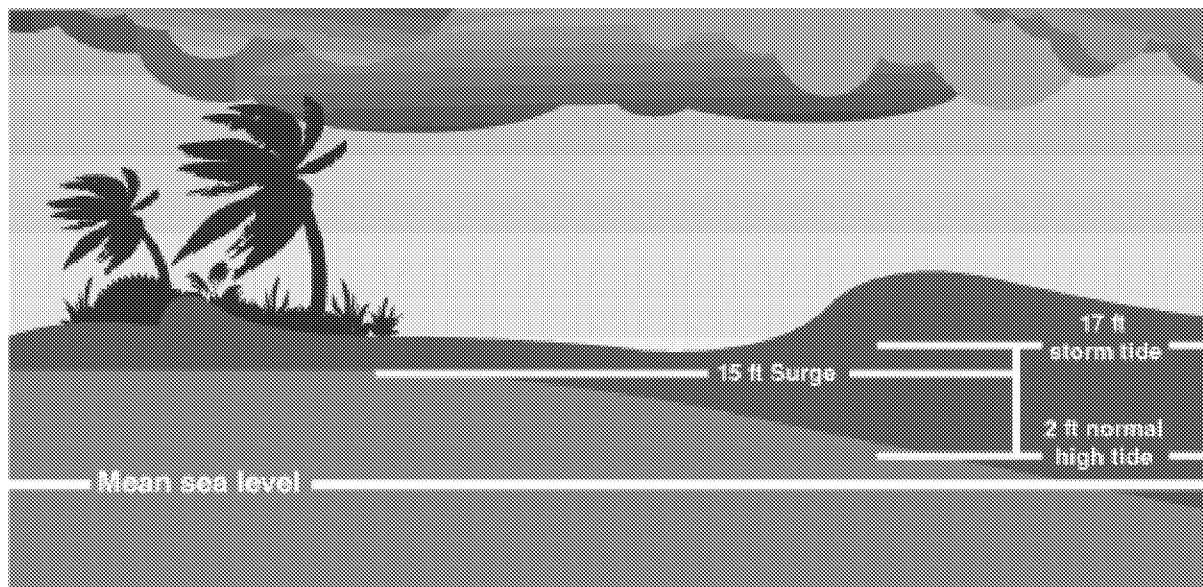


Figure 2-76 Schematic diagram showing wave action and storm surge height as a function of storm surge, tidal cycle, and sea level rise. Numbers are for illustrative purpose. From NOAA website (<https://www.nhc.noaa.gov/surge/>).

8.2. Wastewater vulnerability and adaptation in storm surge

Mattapoisett is a small fishing town at the shore of Mattapoisett Harbor. Wastewater from the residence and commercial entities is collected by a network of gravity sewer pipes, and then pumped to a regional wastewater plant using a transfer pump station at the side of harbor (Figure 2-77). One objective for the risk assessment was to quantify inundation and its impacts on wastewater system operations.

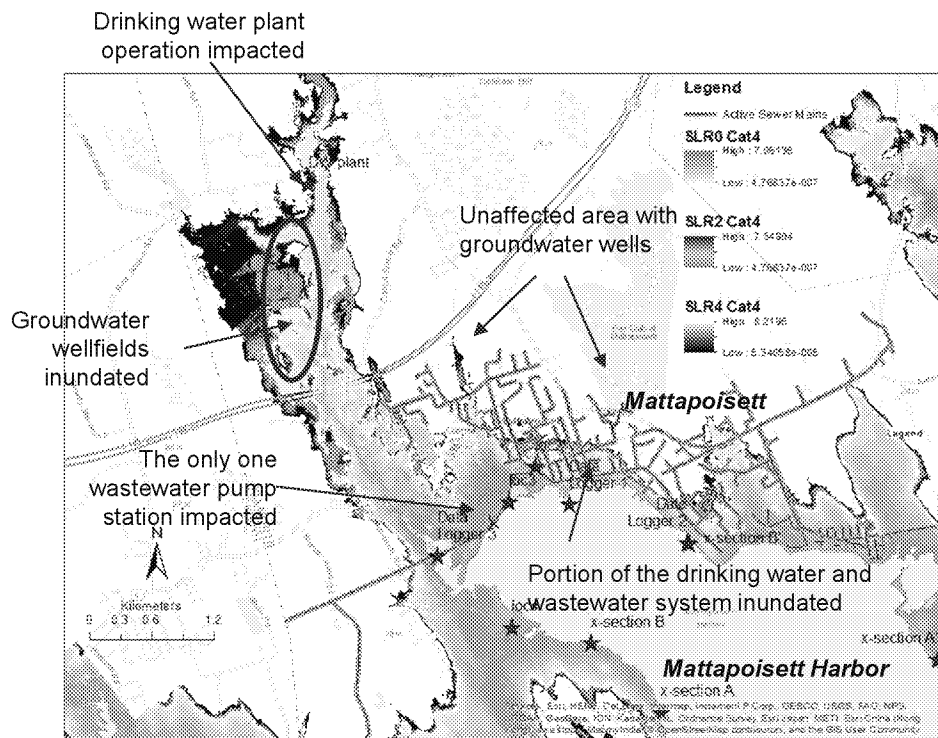


Figure 2-77. Location of the water infrastructure at the Town of Mattapoissett aside of the Mattapoissett Harbor.

In this analysis, the NOAA's Sea Land Overland Surge Height (SLOSH) model was used to simulate the storm surge height under specific local conditions including topography, Mattapoissett Harbor bathymetry, likely storm tracks in the Mattapoissett area, and atmospheric profiles at the origin of storm surge in the open sea. Table 2-36 shows the ranges of major variables, yielding to a total of 432 model runs. The modeling results give to estimates of water depth, wind speed and direction at a point of 50×200 m spatial grids. For each geographic location, the projected water depth for all model runs form an envelope of inundation depth estimates. The Maximum Envelope of Water (MEOW) provides the worst-case basin snapshot

Table 2-36. SLOSH modeling parameters for storm surge modeling at Mattapoissett, MA.

Parameters	Values	# of Variations
Landfall Location	1 (Hurricane Bob)	1
Pressure (mb)	40, 60, 80	3
Radius of Maximum Wind (mi)	25, 40, 55	3
Forward Speed (mph)	30,45,60	3
Track Direction (degree)	NNW, N, NNE, NE	4
Sea Level Rise (ft)	0, 1, 2, 4	4
Total Number of Runs		432

for a particular storm category, forward speed, trajectory, and initial tide level, incorporating uncertainty in the forecasted landfall locations. The Maximum of MEOW (MOM), on the other hand, provides the worst case snapshot for a particular storm category under "perfect" storm conditions described by a combination of forward speed, trajectory, and initial tide level. In practice, MEOW can be used for planning while MOM would be for emergency planning and evacuation.

The location-specific SLOSH modeling was calibrated against the inundation extent of historical Hurricane Bob in August 1991. During Hurricane Bob, storm surge pushed salt water over the salt-lock dam into the Mattapoissett River northwest of the town. The overtopping resulted in salt water intrusion into the River, and consequently into the unconfined aquifer and impacted groundwater at the Fairhaven Tubular well field immediately north of the dam. The aquifer is source water for the regional drinking water treatment plant, approximately 3.5 miles southwest of the town. Using the calibrated model, the inundation map based on MEOW results for a Category-4 hurricane is constructed (Figure 2-77). Major findings are:

- The vulnerable areas of Mattapoissett (the southeastern region) that are inundated by storm surge remains approximately the same under the different hurricane and sea level rise scenarios. This is due to the topographic slope towards the harbor. Storm surge and rate of inundation from a Category 4 hurricane at the current sea level could result in inundation depths over 13.4 feet in some locations in Town. The maximum inundation depth can be reached within 5 hours of the time of landfall.
- The wastewater pump station at Eel Pond in the southwestern corner of the town is also at significant risk. The pump station could be submerged under a Category 2 hurricane or above. In a Category 3 hurricane and at current seal level, the SLOSH simulation shows 5.8 feet water depth at the Eel Pond (Figure 2-78). The water depth would increase to over 13 feet under a Category 4 hurricane.

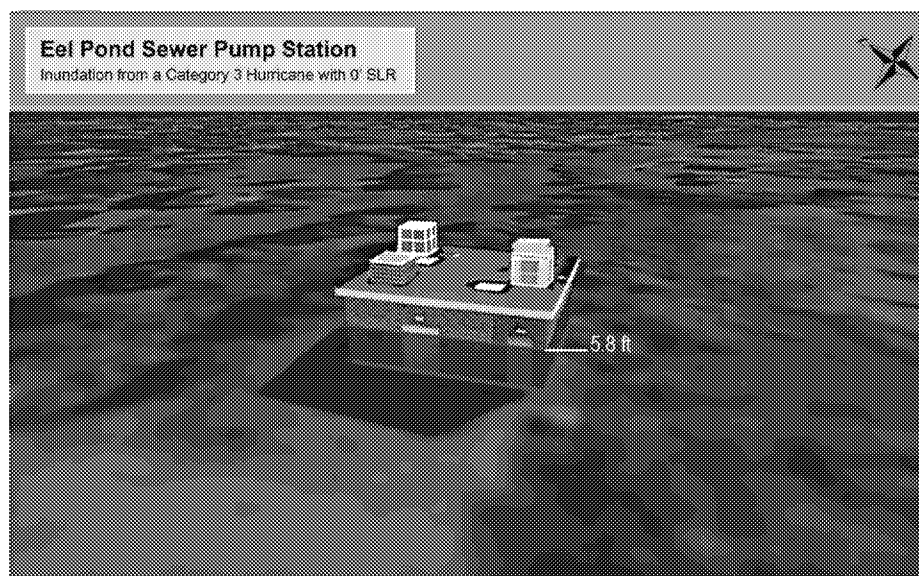


Figure 2-78. A cartoon illustration of SLOSH modeling results for likely inundation risk for the wastewater transfer station at Mattapoissett, Massachusetts.

- Such inundation and physical damage can make the critical wastewater transfer station at Eel Pond inoperable. Currently, the wastewater transfer station has no backup. Loss of service could affect the Town's residents after the hurricane during the recovery phase.

8.3. Emergency evacuation and water supplies

The AIR-SUSTAIN module of SUD system was further applied to assess the traffic conditions during hurricane evacuation, likely evacuee migration paths and bottled water supply at shelters. In this simulation, SLOSH-model generated inundation maps were used as inputs to the AIR-SUSTAIN module to estimate the inundated area, affected population, and potential evacuation routes under four categories of hurricane (Table 2-37). The population and households are based on the 2010 population census data. Overall, there would be over 2200 people and over 1500 households likely in the estimated evacuation area when a Category 4 hurricane landed directly in Mattapoissett Harbor.

Table 2-37. Population affected for evacuation under four categories of hurricane.

Sea level rise (meter)	Hurricane Category 1			Hurricane Category 2		
	Traffic analysis zones -	Affected Population	Affected Households	Traffic analysis zones -	Affected Population	Affected Household
SLR 0	121	15,995	8,429	136	28,117	14,589
SLR 1	122	16,086	8,487	136	28,235	14,675
SLR 2	122	16,196	8,561	136	28,335	14,735
SLR 4	122	16,380	8,677	136	28,514	14,845
Sea level rise (meter)	Hurricane Category 3			Hurricane Category 4		
	Traffic analysis zones -	Affected Population	Affected Households	Traffic analysis zones -	Affected Population	Affected Household
SLR 0	144	39,325	20,150	183	78,030	39,323
SLR 1	144	39,488	20,269	183	78,159	38,395
SLR 2	144	39,563	20,313	183	78,276	38,461
SLR 4	144	39,749	20,422	184	78,754	38,731

Traffic simulation using AIR-SUSTAIN considers evacuees and traffic flow from the two large cities to the west: New Bedford and Fairhaven. It is further assumed that 80% of the evacuees elect to travel to family and friends outside of the inundation zone, while the other 20% of the population travels to public shelters. In Mattapoissett, the interstate highway I-195 and the Main Street were determined to be the main evacuation routes according to the Mattapoissett transportation and police departments.

Under these assumptions, the total clearance time from the affected area is estimated for three cases of the emergency evacuation activation: slow (8 hours), moderate (6 hours), and fast (4 hours). Adding about approximately 1 hour and 20 minutes of transportation, the total time for complete clearance of the inundation area (emergency activation plus transportation) ranges from 5 hr 14 min to 9 hr 18 min (Figure 2-79). Main traffic delays were projected to occur on I-195 north of Mattapoissett due to emergency traffic from the west. Most of the traffic congestion

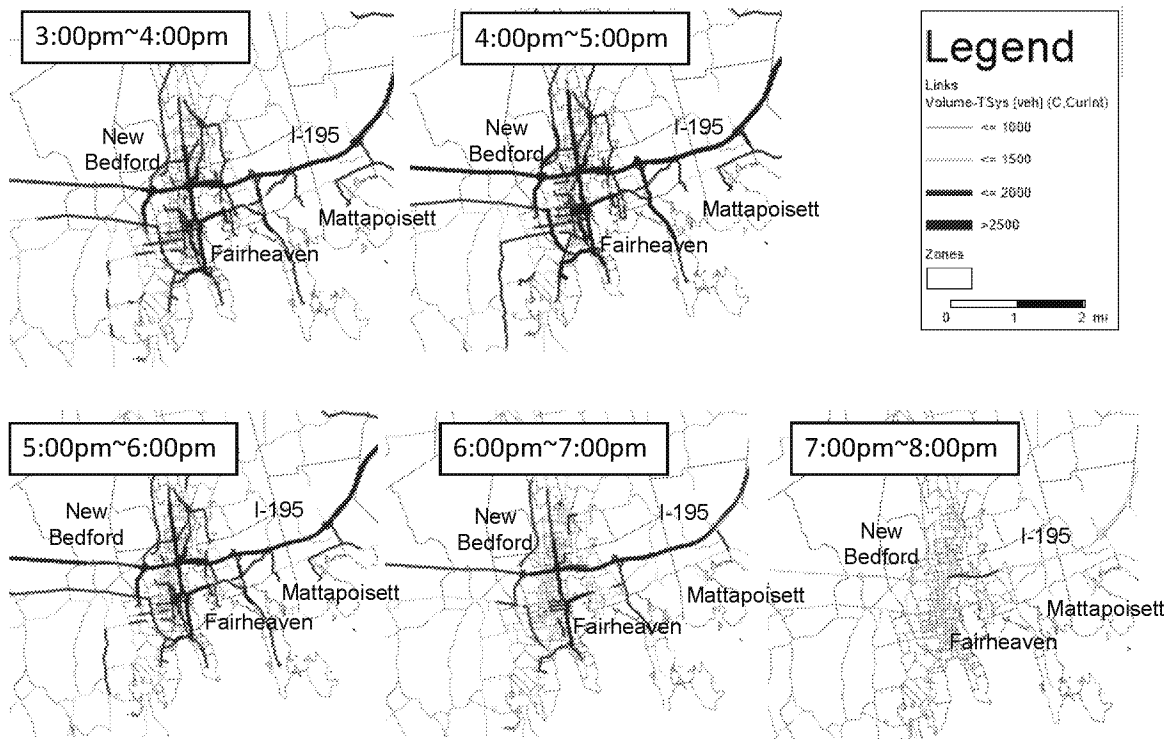


Figure 2-79. Hourly traffic map in the Mattapoisett region after evacuation order activated at noon time.

would occur on I-195 as the main regional evacuation route. For the fast 4-hr evacuation activation starting at noon, the hourly traffic maps are shown in Figure 2-79. Apparently, route traffic management is necessary to ensure a fast and smooth evacuation ending at 8 pm (Figure 2-79).

Emergency water supply would be required for evacuees in the public shelters or friends/families. Because the Mattapoisett drinking water treatment plant is likely to be adversely affected under a Category 4 hurricane, water sources for emergency supply need to be arranged in emergency preparedness planning.

9. Summary and Recommendations

This Part II infrastructure adaptation report describes methods, techniques, and case studies for adapting water infrastructure to and improving its resilience against the projected impacts of hydroclimatic and land use changes. The focus is to establish actionable science for adaptation planning and engineering at local scales.

As a part of this investigation, the relationship between climate, land use, transportation, energy, pollution and water management were shown to intersect. Urban development can lead to a substantial UHI formation, which increases energy use. Urban sprawl leads to less heat island effects, but higher use for energy in transportation, both of urban residents and material flows including water, thus adding to pollution. Development can alter rainfall and runoff characteristics, which have subsequent impacts on water supplies and water quality. The latter

changes can challenge water plant operations, requiring process engineering adaptation. This can result in increasing energy needs. Urban development patterns also impact water distribution and sewer collection. Ultimately to address the sustainability of our communities, this EPA ORD research has analyzed these inter-connectiveness and developed systematic adaptation strategy and tools to better inform decision-makers for informed decisions. Such guided decision-making can help finding optimal investments to protect their economy, property, social systems and infrastructure in anticipation of future conditions.

Water infrastructure adaptation can be planned and evaluated in three different levels: adaptation at the watershed scale, urban scale and water system scale. This spatial boundary helps define the adaptation objectives, which often requires inputs with stakeholder involvement, and also identify the adaptation parameters to investigate in planning and engineering design. Adaptation at the three-scale levels share the same iterative adaptation process (See Figure 2-2). Following defining the adaptation objective and adaptation physical boundary, the adaptation process begins with analyzing the water infrastructure vulnerability to the concurrent and future changes of hydroclimatic and land use conditions. This analysis is conducted in the context of urban developments. This first step is followed by technical and engineering analysis to define specific adaptation planning and engineering options. Upon design and implementation with consideration of the future change uncertainties, the last phase is centered at adaptation effectiveness monitoring and evaluation. For the iterative process, the monitoring-evaluation results lend a basis to revise the adaptation planning and if necessary, urban development policies and management objectives. This proposed adaptation framework is readily adopted into the current urban planning practice. Figures 2-4 and 2-6 show the current practice and the adaptive urban planning, respectively.

To support the water infrastructure adaptation in three spatial scales, the developed Smart Urban Designer (SUD) methods and tools are described in this report with case studies for illustration. At the watershed scale, the adaptation aims to protect source water quality. The developed IWM tools and methods inside of SUD can be used to project water quality in response to future climate and land use management options. In the urban scale, the SUD provides an integrated analysis of land use, transportation, and water infrastructure in scenario-based simulations that quantify basic urban functions and efficiency in transportation and water services. Specific evaluation metrics are defined to evaluate the urban development options, including air quality, water resources and utilization, and transportation access for a given urban development scenario. In the local system scale, SmartWater models and simulation tools were developed to provide specific engineering analysis of water system vulnerability and engineering options to adapt. Through case studies covering different climate regimes in the U.S. Midwest, Southwest, and coastal areas, following major findings were made:

- It is clear from the studies across the country that water infrastructure and, in a larger extent, urban adaptation can be effective in improving infrastructure resilience, and importantly, can offer potential climate-economic-compliance co-benefits. To achieve these outcomes, the adaptation must be planned and designed in a systems approach considering interactions among urban systems.
- Scenario-based adaptive monitoring and planning is essential to the urban and water infrastructure adaptation. As described earlier, the large physical footprints and inflexible infrastructure assets have created a “locked-in” condition for which alteration and changes to

the infrastructure can often be cost-prohibitive and difficult to overcome social and political barriers. Model-aided computer simulation, when conducted appropriately, can provide managers the tool to examine urban-scale adaptive planning, water infrastructure master planning, water treatment adaptation, as well as engineering options to improve water system services. The results can provide an effective venue for water professionals to communicate to stakeholders involved.

- Urban environments present one of the important potential areas for adaptation and mitigation of hydroclimatic change impacts (IPCC, 2014; Yang and Goodrich, 2014). This potential is evident in case studies described in this report. For example, multi-center transformation of the Cincinnati metropolitan area calls for a mix of automobile and mass transit framework that can reduce fuel consumption and air emission by 15.6% and average traffic delay by 25% in 2030. A large degree of carbon/energy reduction can be also achieved by selecting optimal water infrastructure expansion actions in Manatee County, Florida, when adaptation is incorporated in the master planning.
- Water supply adaptation is effective when water treatment and distribution are considered together through systems investigation. Only by this approach, future changes can be grouped into those affecting source water quality and water demand. Then, the systems analysis using the SmartWater tools can identify the most effective and economic engineering solutions to adapt the water system for better compliance at a reasonable cost. A practical example in the GCWW's Richard Miller water plant shows the feasibility by changing and optimizing GAC reactor operations under future source water conditions.
- Coastal areas host multiple dimensions of long-term hydroclimatic impacts and short-term meteorological disruptions in narrow coast zone. As a result, integrated modeling and qualitative analysis are often necessary to develop options for long-term adaptation options and emergency preparation plans against disruptive events like storm surge.

The central question for many urban managers and policy makers is as what Timmerman and White (1997) described, namely, how the urban growth can be planned adaptively to reduce the negative impacts of urban metabolism and ensure sustainable growth? This question is especially important at this stage because of the impending Nation's strategic investment on infrastructure. For this purpose, SUD methods and tools need to be developed beyond the initial stage with applications in different climate and socioeconomic settings.

10. References

- Adams, J. Q. and Clark, R. M. (1988). Development of Cost Equations for GAC Treatment Systems. *J. Environ Engineering*, 114 (3): 672-688.
- Adegoke, J.O., R. Pielke Sr., and A. M. Carleton, (2007). Observational and modeling studies of the impacts of agriculture-related land use change on planetary boundary layer processes in the central U.S. *Agricultural and Forest Meteorology*, 142:203–215.
- Alp, E., and C. S. Melching, (2009). Evaluation of the duration of storm effects on in-stream water quality. *J. Water Resour. Plng. & Mgmt.*, 135(2):107-116.

- ASCE/AWWA, (2004). *Water treatment plant design*, 4th edition. Ed., E.E. Baruth, McGraw-Hill, 896p.
- ASCE, (2014). Minimum Design Loads for Buildings and Other Structures, *Standard ASCE/SEI 7-10*. ASCE, Reston, VA.
- Asian Developmental Bank (ADB), (2012). *Green Cities*. eds, Lindfield M, Steinberg F, Manila, Phillips, adbpub@adb.org, 412p.
- Ashley, R., J. Blanksby, A. Cashman, L. Jack, G. Wright, J. Packman, L. Fewtrell, T. Poole, and C. Maksimovic, (2007). Adaptable urban drainage: Addressing change in intensity, occurrence and uncertainty of stormwater (AUDACIOUS). *Built Environment*, 33(1):70-84.
- Auch, R., Taylor, J., and Acevedo, W., (2004). Urban growth in America Cities. *USGS Circular 1252*. 52p.
- Azadi P, Inderwildi OR, Farnood R, King DA, (2013). Liquid fuels, hydrogen and chemicals from lignin: A critical review. *Renewable and Sustainable Energy Review*, 21:506-523.
- Baldauf, R., Thoma, E., Khlystov, A., Isakov, V., Bowker, G., Long, T., Snowe, R., 2008. Impacts of noise barriers on near-road air quality. *Atmospheric Environment*, 42, 7502–7507.
- Barceló, J., Codina, E., & Casas, J. (2005). Microscopic traffic simulation: A tool for the design, analysis and evaluation of intelligent transport systems. *Journal of Intelligent and Robotic Systems*, 173-203.
- Bartlett, S., Cisneros, H., Heartwell, G., McAndrew, K., Warnock, A., Nellenbach, M., Kline, S., Winkler, A., and Varn, J., (2017). *Understanding America's water and wastewater challenges*. Bipartisan Policy Center, Washington, DC., 28p.
- Baynes, T. M., (2009). Complexity in urban development and management: Historical overview and opportunities. *Journal of Industrial Ecology*, 13 (2), 214-227.
- Beck, M.B., (2005). Vulnerability of water quality in intensively developing urban watersheds. *Environmental Modelling and Software*, 20:381-400.
- Biswas, P., C. Lu, and R.M. Clark, 1993. A model for chlorine concentration decay in drinking water distribution pipes. *Water Research*, 27(12), 1715-1724.
- Black, J., and T. Endreny, (2006). Increasing stormwater outfall duration, magnitude, and volume through combined sewer separation. *J. Hydrol. Engrg.*, 11(5):472-481.
- Board of County Commissioners, (2008). *Manatee County Water Supply Facilities Work Plan*, Manatee County Administrative Center Commission Office Commission, Bradenton, Florida
- Boccelli, D.L., M.E. Tryby, J.G. Uber, and R.S. Summers, (2003). A reactive species model for chlorine decay and THM formation under rechlorination conditions. *Water Research*, 37: 2654-2666.
- Boccelli, D.L., M. J. Small, and U. M. Diwekar, (2007). Drinking water treatment plant design incorporating variability and uncertainty. *J. Envir. Engrg.* 133(3):303-312.

- Bonnin, G., D. Martin, T. Parzybok, B. Lin, D. Riley, and M. Yekta, 2006: Precipitation frequency atlas of the United States. *NOAA Atlas 14* Volume 2, Version 3.0, National Weather Service, Silver Spring, Maryland.
- Bonnin, G.M., D. Martin, B. Lin, T. Parzybok, M. Yekta, and D. Riley, (2011). Precipitation-frequency Atlas of the United States, *NOAA Atlas 14*, volume 1-9. National Weather Service, Silver Spring, Maryland.
- Boulos, P.F., Landsey, K.E., and Karney, B.W., (2006). *Comprehensive water distribution systems analysis handbook for engineers and planners*. MWH SOFT, Pasadena.
- Braganza, K., Karoly, D. J., & Arblaster, J. M. (2004). Diurnal temperature range as an index of global climate change during the twentieth century. *Geophysical Research Letters*, 31(13).
- Bras, R.L. and Rodriguez-Iturbe, I. (1984). *Random Functions and Hydrology*. Addison-Wesley Publishing Company.
- Brown, C., Ghile, Y., Lavery, M., and Li, K., (2012). Decision scaling: Linking bottom-up vulnerability analysis with climate projections in the water sector. *Water Resources Research*, 48, W09537
- Buchberger, S., R. Clark, W. Grayman, Z. Li, M. McCutcheon, and J. Yang, (2009). Needs and trends of the nation's drinking water infrastructure - The utility perspective. *EWRI 2009*, Kansas City, Kansas.
- Bull-Kamanga, L., Diagne, K., Lavell, A., Leon, E., Lerise, F., MacGregor, H., Maskrey, A., Meshack, M., Pelling, M., Reid, H., Satterthwaite, D., Songsore, J., Westgate, K., and Yitambe, A., (2003). From everyday hazards to disasters: the accumulation of risk in urban areas. *Environment & Urbanization*, 15,1, 193-203.
- Buyadi, S. N. A., Mohd, W. M. N. W., & Misni, A. (2013). Green Spaces Growth Impact on the Urban Microclimate. *Procedia-Social and Behavioral Sciences*, 105, 547-557
- Capodaglio, A.G., (2004). Improving sewage treatment plant performance in wet weather. *Nato Science Series: IV: Earth and Environmental Sciences*, 43: 175-185. DOI 10.1007/1-4020-2694-3.
- Carrico, B., and P. C. Singer, (2009). Impact of booster chlorination on chlorine decay and THM production: Simulated analysis. *J. Envir. Engrg.* 135(10): 928-935.
- Carter, T., and C. R. Jackson, (2007). Vegetated roofs for stormwater management at multiple spatial scales. *Landscape and Urban Planning*, 80:84-94
- Chang, H.-J., R. Hargrove, Y.-X. Long, and D. J. Osborne, (2006). Reconstruction after the 2004 tsunami: ecological and cultural considerations from case studies. *Landscape Ecol Eng*, 2:41-51.
- Chang, N.-B., Qi, C., and Yang, Y. J., (2012). Optimal expansion of a drinking water infrastructure system with respect to carbon footprint, cost-effectiveness and water demand. *J Environ Management*, 110:194-206.
- Changnon, D., (2006). Regional and temporal variations in heavy precipitation in south Carolina. *Int'l J. Climatology*, 14(2):165-177.

- Chen, Y., J. J. Cheng, and K. S. Creamer, (2008). Inhibition of anaerobic digestion process: A review. *Bioresource Technology*, 99:4044–4064.
- Chung, G., K. Lansey, and G. Bayraksan, (2009). Reliable water supply system design under uncertainty. *Environmental Modelling & Software*, 24:449–462.
- Clark, R.M., Y.J. Yang, C. Impellitteri, R.C. Haught, D. Schupp, S. Panguluri, and E.R. Krishnan, (2010). Controlling disinfectant residual losses in drinking water distribution systems: Results from experimental and modeling studies. *J. AWWA*. 102(4):1-21.
- Clark, R.M., Z. Li, S. G. Buchberger, and Y. J. Yang, (2009). Evaluating the Effects of Climate Change on the Operation, Design and Cost of Water Treatment. *WQTC 09*, Seattle
- Clark, R.M. (1987a). Modeling TOC Removal by GAC: The General Logistic Function. *J. AWWA*, 79(1): 33-37
- Clark, R.M. (1987b). Evaluating the cost and performance of field-scale granular activated carbon systems. *Environ. Sci. Technol.*, 21 (6), pp 573–580
- Clark, R.M, and M. Sivaganesan, (2002). Predicting chlorine residuals in drinking water: second order model, *Journal of Water Resources Planning and Management* 2002; 128(2): 152-160.
- Clark, R. M., (1998). Chlorine demand and TTHM formation kinetics: a second order model, *Journal of Environmental Engineering*; 124(1): 16-24.
- Clark, R.M., and R.C. Haught, 2005. Characterizing pipe wall demand: Implications for water quality modeling. *J. Wat. Res. Planning and Management*, 208-217.
- Clarke, J. F., (1969). Nocturnal urban boundary layer over Cincinnati, Ohio. *Mon. Weather Rev.* 97 (8), 582–589.
- Comfort, L.K., (2006). Cities at risk: Hurricane Katrina and the Drowning of New Orleans. *Urban Affairs Review*, 41,4, 501-516
- Cooley H, Fulton J, Gleick PH, (2011). *Water for energy: Future water needs for electricity in the intermountain west*. Pacific institute, ISBN 1-893790-36-3.
- Cooper, D., Leclerc, M., Archuleta, J., Coulter, R., Eichinger, W., Kao, C., & Nappo, C. (2006). Mass exchange in the stable boundary layer by coherent structures. *Agricultural and Forest Meteorology*, 136(3), 114-131.
- Crittenden, J.C., Reddy, P.S., Arora, H., Trynoski, J., Hand, D.W., Perram, D.L., and Summers, R.S. (1991). Predicting GAC performance with rapid small-scale column tests. *J. AWWA*, 83 (1): 77-87.
- Cromwell III, J.E., J.B. Smith, and R.S. Raucher, (2007). No doubt about climate change and its implications for water suppliers. *J. AWWA*, 99(9):112-117
- Crozes, G; P. White, and M. Marshall, (1995). Enhanced coagulation; its effect on NOM removal and chemical costs. *JAWWA*, 87(1):78-89.
- Dennison, F.J., Azapagic, A., Clift, R., and Colbourne, J. S. 1998. Assessing management options for wastewater treatment works in the context of life cycle assessment. *Water Science and Technology*, 38(1998), 11, 23–30.

- Diaz-Fierros, T.F., J. Puerta, J. Suarez, and F. D.-Fierros, (2002). Contaminant loads of CSOs at the wastewater treatment plant of a city in NW Spain. *Urban Water*, 4(3):291-299.
- Dietz, M.E., (2007). Low impact development practices: A review of current research and recommendations for future directions. *Water, Air, & Soil Pollution*, 186:351-363.
- Dodder, R. S., (2014). A review of water use in the U.S. electric power sector: insights from systems-level perspectives. *Current Opinion in Chemical Engineering*, 5, 7-14.
- Dodder R, Felgenhauer T, Yelverton W, King C, (2011). Water and greenhouse gas tradeoffs associated with a transition to a low carbon transportation system. In *ASME 2011 International Mechanical Engineering Congress and Exposition*, 2011, pp. 531-547.
- Dodman D, (2009). Blaming cities for climate change? An analysis of urban greenhouse gas emissions inventories. *Environ. Urbanization*, 2009, 21, 185-201.
- Dominguez, D., and Gujer, W., (2006). Evolution of a wastewater treatment plant challenges traditional design concepts. *Water Research* 40, 1389-1396.
- Donofrio, J., Y. Kuhn, K. McWalter, and M. Winsor, (2009). Water-sensitive urban design: An emerging model in sustainable design and comprehensive water-cycle management. *Environmental Practice*, 11(3):179-189.
- Eastman, J. R. (2009). *IDRISI Help System*. IDRISI Taiga. Worcester, MA, USA: Clark University.
- EBMUD (2009). *WSMP 2040: Water Supply Management Program 2040 Plan*. East Bay Municipal Utility District. October.
- Ewing, R., H. 2008. *Characteristics, causes, and effects of sprawl: A literature review*. In *Urban Ecology*, edited by John M. Marzluff, Eric Shulenberg, Wilfried Endlicher, Marina Alberti, Gordon Bradley, Clare Ryan, Ute Simon and Craig ZumBrunnen, 519-535. Springer US.
- Faiers, G.E., J. M. Grymes, B. D. Keim, and R. A. Muller, (1994). A reexamination of extreme 24-hour rainfall in Louisiana, USA. *Climate Research*, 4:25-31.
- Farge, M. (1992). *Wavelet transformations and their applications to turbulence*. Annual Reviews, Inc.
- Federal Highway Administration (FHWA). (2012). *Project-level Conformity and Hot-spot Analysis*. Retrieved 10 1, 2014, from Air Quality: http://www.fhwa.dot.gov/environment/air_quality/conformity/guide/guide09.cfm
- Felgenhauer, T., and Webster, M., (2013). Modeling adaptation as a flow and stock decision with mitigation. *Climatic Change*, 122,4, 665-679.
- Felgenhauer, T., and Bruin K.C., (2009). The optimal paths of climate change mitigation and adaptation under certainty and uncertainty. *Int'l J. Global Warming*, 1, 66-88.
- FHWA. (1990). *Calibration and Adjustment of System Planning Models*. Washington D.C.: FHWA.

- FHWA. (2002). *An Introduction to Urban Travel Demand Forecasting - A Self Instructional Text*. Retrieved December 23, 2013, from U.S. Department of Transportation: <http://ntl.bts.gov/DOCS/UT.html>
- FHWA. (2012). *Scenario Planning Guidebook*. Washington D.C.
- Felgenhauer, T. and M. Webster (2013a). Multiple Adaptation Types with Mitigation: A Framework for Policy Analysis. *Global Environmental Change* 23(6): 1556-1565.
- Felgenhauer, T, Webster M., (2013b). Modeling adaptation as a flow and stock decision with mitigation. *Climatic Change*, DOI:10.1007/s10584-013-1016-9.
- Feng, Y., Liu, M., Liu, Y., Tong, X., & Deng, S. (2011). Modeling dynamic urban growth using cellular automata and particle swarm optimization rules. *Landscape and Urban Planning*, 102, 188-196.
- Fernando, H. J. S. (2010). Fluid dynamics of urban atmospheres in complex terrain. *Annual Review of Fluid Mechanics*, 42, 365-389.
- Flanders, F., Yang, J., Dodder, R., Furie, G., Baldauf, R., Bachle, L., Bostrom, A., Berry, L., Walters, C., Bare, J., Barzyk, T., Bruins, R., Cooter, E., DiCosmo, F., Eason, T., Fontaine, T., Jackson, L., Schumaker, N., and Weaver, J., (2014). Synthesis paper on sustainable transportation. *EPA Program Briefing Paper*. 126p. RTP, North Carolina.
- Freas, K., B. Bailey, A. Munevar, and S. Butler. (2008). Incorporating climate change in water planning. *J.AWWA*, 100:6. June
- Fu, X., Wang, X., and Yang, Y.J., (2018). Deriving suitability factors for CA-Markov land use simulation model based on local historical data. *J. Environ Management*, 206: 10-19.
- Gang, D.C., Clevenger, T.E., and Banerji, S.K., 2003. Modeling chlorine decay in surface water. *J. Environ. Inform.*, 1(1), 21-27.
- Garcia-López, M.-À., 2012. Urban spatial structure, suburbanization and transportation in Barcelona. *Journal of Urban Economics*, 72 (2–3):176-190.
- Gesch, D., (2005). *Topography-based analysis of Hurricane Katrina inundation of New Orleans*. U.S. Geological Survey, Sioux Falls, SD.
- Gettman, D., & Head, L. (2003). *Surrogate Safety Measures From Traffic Simulation Models*, Final Report. Federal Highway Administration.
- Giaimo, G. (2001). *Travel Demand Forecasting Manual 1 – Traffic Assignment Procedures*. Columbus: Ohio Department of Transportation.
- Gim, T. T., 2012. A meta-analysis of the relationship between density and travel behavior. *Transportation* 39 (3):491-519.
- Gikas, P., and G. Tchobanoglous, (2009). The role of satellite and decentralized strategies in water resources management. *J. Environ Management*, 90:144-152.
- Gilroy, K.L., and R. H. McCuen, (2009). Spatio-temporal effects of low impact development practices. *J. Hydrology*, 367:228–236.

- Girard, M., and M. Mortimer, (2006). *The Role of standards in adapting Canada's infrastructure to the impacts of climate change*. <http://www.csa.ca/climatechange>, Canadian Standards Association. 71p.
- Gleick, P.H., (2000). The changing water paradigm, a look at twenty-first century water resources management. *International Water Resources Association*. 25,1, 127-138.
- Gordon, P., H. W. Richardson, and H. L. Wong. 1986. The distribution of population and employment in a polycentric city: The case of Los Angeles. *Environment & Planning A* 18 (2):161-173.
- Godschalk, D. (2003). Urban Hazard Mitigation: Creating Resilient Cities. *Nat. Hazards Rev.*, 4(3), 136–143.
- Guan, D., Li, H., Inohae, T., Su, W., Nagaie, T., & Hokao, K. (2011). Modeling urban land use change by the integration of cellular automaton and Markov model. *Ecological Modelling*, 222, 3761-3772.
- Guhathakurta, S., and Gober, P., (2007). The impact of the Phoenix urban heat island on residential water use. *J. Am. Plann. Assoc.*, 73, 3, 317-329.
- Guo, J. C.Y., and K. Hargadin, (2009). Conservative design rainfall distribution. *J. Hydrologic Engrg*, 14(5):528-530
- Gupta, A.K., and R. K. Shrivastava, (2006). Uncertainty analysis of conventional water treatment plant design for suspended solids removal. *J. Envir. Engrg.*, 132(11):1413-1421
- Guzmán-Torres, D., Eiguren-Fernández, A., Cicero-Fernández, P., Maubert-Franco, M., Retama-Hernández, A., Ramos Villegas, R., & Miguel, A. H. (2009). Effects of meteorology on diurnal and nocturnal levels of priority polycyclic aromatic hydrocarbons and elemental and organic carbon in PM₁₀ at a source and a receptor area in Mexico City. *Atmospheric Environment*, 43(17), 2693-2699.
- Han, J., Hayashi, Y., Gao, X., & Imura, H. (2009). Application of an integrated system dynamics and cellular automata model for urban growth assessment: a case study of Shanghai, China. *Landscape and Urban Planning*, 91, 133-141.
- Harrington, J. J. and Gidley, J. S., 1985. Variability of alternative decisions in a water resources planning problem. *Water Resources Research*, 21, 12, 1831-1840.
- Hartley, H.O. (1961). The modified Gauss Newton method for the fitting of nonlinear regression functions by least squares. *Technometrics* 3 (2): 269-280.
- Heikkila, E., Gordon, P., Kim, J. I., Peiser, R. B., Richardson, H. W., and Dale-Johnson, D., (1989). What happened to the CBD-distance gradient?: Land values in a policentric city. *Environment and Planning A*, 21 (2):221-232.
- Hering JG, Waite TD, Luthy RG, Dewes JE, Sedlak DL., (2013). A changing framework for urban water systems. *Environ. Sci. Technol.*, 47, 10721-10726.
- Hershfield, D.M., (1961). Rainfall frequency atlas of the United States for durations from 30 minutes to 24 hours and return periods from 1 to 100 years. *Weather Bureau, Technical Paper No.40.*, Washington, DC.

- Hidalgo, J., Masson, V., & Gimeno, L. (2010). Scaling the daytime urban heat island and urban-breeze circulation. *Journal of Applied Meteorology and Climatology*, 49(5), 889-901.
- Horowitz. (1979). The Accuracy of the Multinomial Logit Model as an Approximation to the Multinomial Probit Model of Travel Demand. *Transport Reseach Part B*, 148, 331-341.
- Hummel, D., and A. Lux, (2006). Population decline and infrastructure: The case of the German water supply system. *Vienna Yearbook of Population Research* 2007, pp. 167-191.
- Ibrahim H, Ilinca A, Perron J., (2008). Energy storage systems – Characteristics and comparisons. *Renew. Sustain. Energy Rev.*, 12, 1221-1250.
- Imhoff, M. L., Zhang, P., Wolfe, R. E., & Bounoua, L. (2010). Remote sensing of the urban heat island effect across biomes in the continental USA. *Remote Sensing of Environment*, 114(3), 504-513.
- International Energy Agency, (2013a). *World Energy Outlook 2013*. www.iea.org. 9 rue de la Fédération 75739 Paris Cedex 15, France. 2013a, 232p.
- International Energy Agency, (2013b). *Redrawing the energy-climate map*. www.iea.org. 9 rue de la Fédération 75739 Paris Cedex 15, France. 2013b, 126p.
- Intergovernmental Panel on Climate Change (IPCC), (2014). *Climate Change 2014: Mitigation of Climate Change*. Draft. 2014, <http://www.ipcc.ch/>
- Intergovernmental Panel on Climate Change (IPCC), (2007). *Climate change 2007: The Physical Science Basis*. Cambridge University Press.
- Iziomon, M. G., Mayer, H., & Matzarakis, A. (2003). Downward atmospheric longwave irradiance under clear and cloudy skies: Measurement and parameterization. *Journal of Atmospheric and Solar-Terrestrial Physics*, 65(10), 1107-1116.
- Kheshgi, H.S., Prince, R.C., Marland, G., (2000). The potential of biomass fuels in the context of global climate change: Focus on transportation fuels. *Annu. Rev. Energy Environ.*, 25:199-244
- Kumar, M. S., Anandan, V. K., Rao, T. N., & Reddy, P. N. (2012). A climatological study of the nocturnal boundary layer over a complex-terrain station. *Journal of Applied Meteorology and Climatology*, 51(4), 813-825.
- Järvinen, A.V.O., M.T. Pelkonen, and T. Vartiainen, (1991). *Upgrading the removal of humic substances and mutagen precursors in water treatment*. In B. Allard, H. BorOn, A. Grimvall (Eds), *Humic Substances in the Aquatic and Terrestrial Environment*, Springer Berlin / Heidelberg, 225-231
- Jiang, G., Zhang, F., & Kong, X. (2009). Determining conversion direction of the rural residential land consolidation in Beijing mountainous areas. *Transactions of the CSAE*, 25(2), 214-221.
- Johnson, T., Butcher, J., Deb, D., Faizullabhoy, M., Hummel, P., Kittle, J., McGinnis, S., Mearns, L.O., Nover, D., Parker, A., Sarkar, S., Srinivasan, R., Tuppad, P., Warren, M., Weaver, C., and Witt, J., (2015). Modeling Streamflow and Water Quality Sensitivity to Climate Change and Urban Development in 20 U.S. Watersheds. *J. AWWA*, 50(5), 1321-1341.

- Jones, P., Koppelman, F., & Orfueil, J. (1990). *Activity analysis: State-of-the-art and Future Directions. New developments in dynamic and activity-based approaches to travel analysis* (pp. 34-55). Aldershot, England: Gower Publishing.
- Kenworthy JR., (2006). The eco-city: ten key transport and planning dimensions for sustainable city development. *Environment & Urbanization*, 18(1), 67–85.
- Kim, Y-I, and B.-U. Bae, (2007). Design and evaluation of hydraulic baffled-channel PAC contactor for taste and odor removal from drinking water supplies. *Water Research*, 41:2256–2264.
- Kimura, K., Amy, G.L., Drewes, J.E., and Herberer, T. (2003). Rejection of organic micropollutants (disinfection by-products, endocrine disrupting compounds, and pharmaceutically active compounds) by NF/RO membranes. *Journal of Membrane Science*, Vol. 227, pp. 113-121.
- Kincannon, D.F., and A. F. Gaudy, Jr., (1966). Some effects of high salt concentrations on activated sludge. *J. Water Pollution Control Federation*, 38(7):1148-1159.
- Konrad II, C.E., (1997). Synoptic-scale features associated with warm season heavy rainfall over the interior southeastern United States. *J. Climate*, 12:557-571.
- Lai, F.-S., (2008). Review of sewer design criteria and RDII prediction methods. *EPA/600/R-08/010*, USEPA, Office of Research and Development, Cincinnati, Ohio.
- Larson, William, Feng Liu, and Anthony Yezer. 2012. Energy footprint of the city: Effects of urban land use and transportation policies. *Journal of Urban Economics*, 72 (2–3):147-159.
- Lee, E.J., Criddle, C.S., Bobel, P., Freyberg, D. L, (2013). Assessing the scale of resource recovery for centralized and satellite wastewater treatment. *Environ. Sci. Technol*, 47, 10762-10770.
- Levin, R.B., P. R. Epstein, T. E. Ford, W. Harrington, E. Olson, and E. G. Reichard, (2002). U.S. drinking water challenges in the twenty-first century. *Environmental Health Perspectives*, 110 (S.1): 43-52.
- Li, Z., R. Clark, S. Buchberger, and J. Yang, (2009). Assessing the impact of climate change on drinking water treatment plant design and operation. *EWRI 2009*, Kansas City.
- Li, Z., R.M. Clark, S.G. Buchberger, and Y.J. Yang, (2012). Evaluation of Logistic Model for GAC Performance in Water Treatment, *JAWWA*, doi.org/10.5942/jawwa.2012.104.0120
- Li Z, Clark RM, Buchberger SG, Yang YJ, (2014). Evaluation of Climate Change Impact on Drinking Water Treatment Plant Operation. *J Environ Engrg.*, 140(9), Special Issue: Drinking Water Safety, Security, and Sustainability, A4014005.
- Liang, M.S., (2014). *Quantitative analysis of major factors affecting black carbon transport and concentrations in the unique atmospheric structure of urban environment*. Ph.D. Dissertation, University of Cincinnati.
- Liang, M. S., Keener, T. C., Birch, M. E., Baldauf, R., Neal, J., & Yang, Y. J. (2013). Low-wind and other microclimatic factors in near-road black carbon variability: A case study and assessment implications. *Atmospheric Environment*, 80, 204-215.

- Liang, M.S., and Julius, S., (2017). On the coastal topography and storm surge for infrastructure risk assessment and adaptation. *EWRI 2017*, Sacramento, California
- Liang, M.S., and Keener, T.C., (2015). Atmospheric Feedback of Urban Boundary Layer with Implications for Climate Adaptation. *Environmental Science & Technology*, 49 (17), 10598-10606
- Lin, S.D., (2001). *Water and wastewater calculations manual*. McGraw-Hill, New York. 854p.
- Liu, Y., Shintaro, G., Zhuang, D., & Kuang, W. (2012). Urban surface heat fluxes infrared remote sensing inversion and their relationship with land use types. *Journal of Geographical Sciences*, 22(4), 699-715.
- Lundie, S., Peters, G.M., and Beavis, P.C., 2004. Life cycle assessment for sustainable metropolitan water systems planning, *Enviorn. Sci. Technol.*, 38, 3465-3473.
- Lundin, M., Bengtsson, M., and Molander, S. 2000. Life cycle assessment of wastewater systems: influence of system boundaries and scale on calculated environmental loads. *Enviorn. Sci. Technol*, 34, 180–186.
- Luther RG, (2013). Design options for a more sustainable urban water environment. *Enviorn. Sci. Technol*, 47, 10719 -10720.
- Mailhot, A., S. Duchesne, D. Caya, and G. Talbot, (2007). Assessment of future change in intensity-duration-frequency (IDF) curves for southern Quebec using the Canadian Regional Climate Model (CRCM). *J. Hydrology*, 347: 197-210.
- Marsalek, J., and B. Chocat, (2002). International report: Stormwater management. *Water Science and Technology*, 46(6–7): 1–17.
- Marshall, J.D., Toffel, M.W., (2005). Framing the elusive concept of sustainability: A sustainability hierarchy. *Enviorn. Sci. Technol*, 39, 3, 673-682.
- Martilli, A. (2002). Numerical study of urban impact on boundary layer structure: Sensitivity to wind speed, urban morphology, and rural soil moisture. *Journal of Applied Meteorology*, 41(12), 1247-1266.
- Martuzevicius, D.; Luo, J.; Reponen, T.; Shukla, R.; Kelley, A. L.; Clair, H. S.; Grinshpun, S. A., (2005). Evaluation and optimization of an urban PM 2.5 monitoring network. *J. Environ. Monit.*, 7(1), 67–77
- Matos, J.C., Valente, I.B., Cruz, P.J.S., and Neves, L.C., (2013). An advanced probabilistic updating algorithm for life-cycle analysis of civil structures. In Strauss, Frangopol & Bergmeister eds., “*Life-Cycle and Sustainability of Civil Infrastructure Systems*”. Taylor & Francis Group, London, ISBN 978-0-415-62126-7
- Mays, L.W., (1999). *Water distribution systems handbook*. McGraw-Hill, New York.,
- McCorquodale, J A., (2007). Storm-water jets and plumes in rivers and estuaries. *Canadian J. Civil Engineering*, 34(6): 691-702
- McDaniels, T., S. Chang, D. Cole, J. Mikawoz, and H. Longstaff, (2008). Fostering resilience to extreme events within infrastructure systems: Characterizing decision contexts for mitigation and adaptation. *Global Environmental Change*, 18:310–318

- McDonnell, B.E., (2012). *Controlling disinfection by-products within a distribution system by implementing bubble aeration within storage tanks*. Master Thesis, University of Cincinnati, 206p.
- McNally, M. (2007). *The four step model*. (D. a. Hensher, Ed.) Oxford, UK: Elsevier Science.
- McNally, M. (1996). *An Activity-Based Microsimulation Model for Travel Demand Forecasting*. UC Irvine: Center for Activity Systems Analysis.
- Miller, G.R., D. D. Baldocchi, B. E. Law, and T. Meyers, (2007). An analysis of soil moisture dynamics using multi-year data from a network of micrometeorological observation sites. *Advances in Water Resources*, 30:1065–1081.
- Miller, K. and D. Yates. (2006). *Climate Change and Water Resources: A Primer for Municipal Water Providers*. Jointly sponsored by Awwa Research Foundation, Denver, CO and University Corporation for Atmospheric Research, Boulder, CO. Awwa Research Foundation, American Water Works Association, and IWA Publishing.
- Milman, A., and A. Short, (2008). Incorporating resilience into sustainability indicators: An example for the urban water sector. *Global Environmental Change*, 18:758–767.
- Mitsova, D., Shuster, W., & Wang, X. (2011). cellular automata model of land cover change to integrate urban growth with open space conservation. *Landscape and Urban Planning*, 99, 141-153.
- Montalto, F., C. Behr, K. Alfredo, M. Wolf, M. Arye, and M. Walsh, (2007). Rapid assessment of the cost-effectiveness of low impact development for CSO control. *Landscape and Urban Planning*, 82:117–131.
- Müller, A., S. Marsili-Libelli, A. Aivasidis, T. Lloyd, S. Kroner, and C. Wandrey, (1997). Fuzzy control of disturbances in a wastewater treatment process. *Water Research*, 31(12):3157-3167.
- Mulvihill, M. E. and Dracup, J. A. 1974. Optimal timing and sizing of a conjunctive urban water supply and waste water system with nonlinear programming. *Water Resources Research*, 10(2), 170-175.
- National Oceanic and Atmospheric Administration (NOAA), (2007). *Rainfall Atlas 14*, National Climatic Center, Asheville, NC, <http://hdsc.nws.noaa.gov>.
- Neuman, M., (2009). Spatial planning leadership by infrastructure: An American view. *International Planning Studies*, 14(2):201–217.
- Neil C., Yang YJ, Schupp D, Jun Y-S, (2014). Water chemistry impacts on arsenic mobilization from arsenopyrite dissolution and secondary mineral precipitation: Implication for managed aquifer recharge. *Environ. Sci. Technol*, 48(8), 4395-4405.
- Neil, C.W., Y.J. Yang, and Y-S. Jun, (2012). A critical review of the potential impact of managed aquifer recharge on mineral-water interactions responsible for arsenic mobilization in groundwater. *J. Environ. Monit.*, 14: 1772-1788.
- Novotny, V., and J.W. Witte, (1997). Ascertaining aquatic ecological risks of urban stormwater discharges. *Water Research*, 31(10): 2573-2585.

- Novotny V., (2013). Water–energy nexus: retrofitting urban areas to achieve zero pollution. *Building. Research & Information*, 41(5), 589-604.
- Perrone D, Murphy J, Hornberger GM, (2011). Gaining perspective on the water-energy nexus at the community scale. *Enviorn. Sci. Technol.*, 45, 4228-4234
- Oh, K., Jeong, Y., Lee, D., Lee, W., and Choi, J., (2005). Determining development density using the urban carrying capacity assessment system. *Landscape and Urban Planning*, 73, 1-5.
- Oke, T. R. (1976). The distinction between canopy and boundary-layer urban heat islands. *Atmosphere*, 14(4), 268-277.
- Oke, T.R. (2006). Initial guidance to obtain representative meteorological observations at urban sites. *World Meteorological Organization, TD-No.1250*, 47p.
- O’Neal, M.R., M.A. Nearing, R. C. Vining, J. Southworth, and R. A. Pfeifer, (2005). Climate change impacts on soil erosion in Midwest United States with changes in crop management. *Catena*, 61:165-184.
- Ong, S. L. and Adams, B. J. 1990. Capacity expansion for regional wastewater systems. *Journal of Environmental Engineering*, 116(3), 542-560.
- O’Reilly, J., C. Lee, G. Collins, F. Chinalia, T. Mahony, and V. O’Flaherty, (2009). Quantitative and qualitative analysis of methanogenic communities in mesophilically and psychrophilically cultivated anaerobic granular biofilms. *Water Research*, 43:3365 – 3374.
- Oron, G., L. Gillerman, A. Bick, Y. Mnaor, N. Buriakovsky, and J. Hagin, (2007). Advanced low quality waters treatment for unrestricted use purposes: imminent challenges. *Desalination*, 213:189–198.
- Ostrom, E., (2010). Beyond markets and states: Polycentric governance of complex economic systems. *American Economic Review*, 100 (3):641-672.
- Oulman, C.S. (1980). The logistic curve as a model for carbon bed design. *J. AWWA*. 75 (1): 51.
- Pacific Northwest National Laboratory (PNNL), (2012) Climate and energy-water-land system interactions – Technical report to the U.S. Department of Energy in support of the national climate assessment. *PNNL-21185*. <http://www.ntis.gov>.
- Pahl-Wostl, C., (2007). Transitions towards adaptive management of water facing climate and global change. *Water Resour Manage*, 21:49–62.
- Parshall L, Gurney K, Hammer SA, Mendoza D, Zhou Y, Geethakumar S, (2010). Modeling energy consumption and CO₂ emissions at the urban scale: Methodological challenges and insight from the United States. *Energy Policy*, 38, 4765-4782.
- Pedersen, N., & Sandahl, D. (1982). Highway Traffic Data for Urbanized Area Project Planning and Design. *NCHRP Report 255*. . Washington D.C.: Transportation Research Board.
- Peng, Y., W. Zeng, and S. Wang, (2007). DO concentration as a fuzzy control parameter for organic substrate removal in SBR Processes. *Environmental Engineering Science*, 21(5): 606-616.

- Pires, M., (2003). Watershed protection for a world city: the case of New York. *Land Use Policy*, 21:161-175.
- Peters, G. M. and Lundie, S. 2001. Life-cycle assessment of biosolids processing options. *Journal of Industrial Ecology*, 5(2), 1088-1980.
- Pielke Sr., R.A., J. O. Adegoke, T. N. Chase, C. H. Marshall, T. Matsui, D. Niyogi, (2007). A new paradigm for assessing the role of agriculture in the climate system and in climate change. *Agricultural and Forest Meteorology*, 142:234–254
- Prasad, T.D., G. A. Walters, and D. A. Savic, (2004). Booster disinfection of water supply networks: Multiobjective approach. *J. Water Resour. Plng. and Mgmt.*, 130(5):367-376.
- Qi, C, Chang, N.B. and Yang, Y.J., 2010. Life cycle assessment and carbon footprint in a drinking water infrastructure system for screening expansion alternatives, *International Journal of Live Cycle Assessment*, in review.
- Rajagopalan, B., and U. Lall, (1998). Interannual variability in western US precipitation. *J. Hydrology*, 210: 51-69.
- Ranatunga T., Tong S. T.Y., Sun Y., Yang J.Y., (2014). A comprehensive approach to total water management: A case study of the Las Vegas wash watershed, Nevada. *Physical Geography*, 35(3), 220-244
- Rao, K. D. (2005). Multi-criteria spatial decision analysis for forecasting urban water requirements: a case study of Dehradun city, *India. Landscape and Urban Planning*, 71, 163-174.
- Ray, S., and C. A. Peters, (2008). Changes in microbiological metabolism under chemical stress. *Chemosphere*, 71:474–483.
- Rebetez, M. (2001). Changes in daily and nightly day-to-day temperature variability during the twentieth century for two stations in Switzerland. *Theoretical and Applied Climatology*, 69(1-2), 13-21.
- Rendón, A. M., Salazar, J. F., Palacio, C. A., Wirth, V., & Brötz, B. (2014). Effects of Urbanization on the Temperature Inversion Breakup in a Mountain Valley with Implications for Air Quality. *Journal of Applied Meteorology and Climatology*, 53(4), 840-858.
- Roberts, P.V. and Summers R.S. (1982). Granular Activated Carbon Performance for Organic Carbon Removal. *J. AWWA*, 74:113-118
- Rosenzweig, C., Major, D.C., Demong, K., Stantion, C., Horton, R., and Stults, M., (2007). Managing climate change risks in New York City's water system: Assessment and adaption planning. *Mitigation and adaptation Strategies for Global Change*, 12(8), 1391-1409.
- Rossman, L.A., (2002). *EPANET Version 2 Users Manual*, USEPA, Cincinnati.
- Rossman, L.A., R.M. Clark, and W.M. Grayman, 1994. Modeling chlorine residuals in drinking-water distribution systems. *J Env. Engng.*, 120(4), 803-820.

- Rotach, M. W., Vogt, R., Bernhofer, C., Batchvarova, E., Christen, A., Clappier, A., ... & Voogt, J. A. (2005). BUBBLE—an urban boundary layer meteorology project. *Theoretical and Applied Climatology*, 81(3-4), 231-261.
- Rothausen SGSA, Conway D, (2011). Greenhouse-gas emissions from energy use in the water sector. *Nature Climate Change*, 1:210-218.
- Saaty, T. (1980). How to make a decision: the analytic hierarchy process. *Interfaces*, 24(6), 19-43.
- Sadiq, R., Rodriguez, M.J., 2004. Disinfection by-products (DBPs) in drinking water and the predictive models for their occurrence: a review. *Science of the Total Environment*, 321, 21-4.
- Salas, J. D., Delleur, J. W., Yevjevich, V. and Lane, W. L. (1980). *Applied Modeling of Hydrologic Time Series*. Water Resources Publications, Littleton, CO, 484 pages
- Salvato, J.A., N. L. Nemerow, F. J. Agardy, (2008). *Environmental Engineering*, 8th edition. Wiley & Sons, New York. 1544p.
- Sang, L., Zhang, C., Yang, J., Zhu, D., & Yun, W. (2011). Simulation of land use spatial pattern of towns and villages based on CA–Markov model. *Mathematical and Computer Modelling*, 54, 938-943.
- Santé, I., S., A. M. García, D. Miranda, and R. Crecente, (2012). Cellular automata models for the simulation of real-world urban processes: A review and analysis. *Landscape and Urban Planning*, 96, 108-122.
- Schaad, D.E., J. Farley, and C. Haynes, (2009). Design and routing of storm flows in an urbanized watershed without surface streams. *J. Hydrology*, 375(3-4):334-344
- Schrank, D., and Lomax, T., (2009). 2009 *Urban Mobility Report*. Reports by Texas Transportation Institute, The Texas A&M University
- Semadeni-Davies, A., C. Hernebring, G. Svensson, L.-G. Gustafsson, (2008). The impacts of climate change and urbanization on drainage in Helsingborg, Sweden: Suburban stormwater. *J. Hydrology*, 350:114-125.
- Shang, F., Uber, J., and Rossman, L. (2008). EPANET Multi-species Extension Users Manual. *EPA/600/S-07/021*. Cincinnati, Ohio
- Silva, E. A., & Clarke, K. C. (2002). Calibration of the SLEUTH urban growth model for Lisbon and Porto, Portugal. *Comput. Environ. Urban Syst*, 26, 525-552.
- Simiu, E. (2011). Design of Buildings for Wind: *A Guide for ASCE 7-10 Standard Users and Designers of Special Structures*. Second edition. John Wiley & Sons, Inc., Hoboken, NJ.
- Skjelkvale, B.L., Stoddard, J.L., Jeffries, D.S., Torseth, K., Hogasen, T., Bowman, J., Mannio, J., Monteith, D.T. (2005). Regional scale evidence for improvements in surface water chemistry 1990–2001. *Environ. Pollut.* 137: 165–176.
- Slowinski, R., Urbaniak, A. and Weglarz, J. 1985. Multicriteria capacity expansion planning of a water supply and wastewater treatment system. *International Journal of Modelling and Simulation*, 5(4), 124-127.

- Small, K. A., and Song, S., (1994). Population and employment densities: Structure and change. *Journal of Urban Economics*, 36:292-313.
- Stratus Consulting and MWH Global. (2009). Implications of Climate Change for Adaptation by Wastewater and Stormwater Agencies. *Water Environment Research Foundation Report No. CC2R08*.
- Stubbart, J., (2004). How do we treat to prevent DBPs. *Opflow*, 30(9): 8-9.
- Sudhira, H. S., T. V. Ramachandra, Andreas Wytzisk, and C. Jeganathan. 2005. *Framework for Integration of Agent-based and Cellular Automata Models for Dynamic Geospatial Simulations*. Bangalore: Indian Institute of Science, Centre for Ecological Sciences.
- Sukkoo, Kim. 2007. Changes in the nature of urban spatial structure in the United States, 1890–2000. *Journal of Regional Science*, 47 (2):273-287.
- Sun, Y., S.T.Y. Tong, M. Fang, & Y.J. Yang, (2013). Exploring the effects of population growth on future land use change in the Las Vegas Wash Watershed: An integrated approach of geospatial modeling and analytics. *Environment, Development and Sustainability*, 15, 1495-1515.
- Tafari, A.T., and A. Selvakumar, (2002). Wastewater collection system infrastructure research needs in the USA. *Urban Water*, 4(1):21-29.
- Theobald, D.M., (2005). Landscape patterns of exurban growth in the USA from 1980 to 2020. *Ecology and Society*, 10(1), 32
- Tillman, A. M., H. Lundertroem, and M. Svingby, (1998). Life cycle assessment of municipal waste water systems. *International Journal of LCA*, 3, 145–157.
- Tillman, D.E., T.A. Larsen, C. Pahl-Wostlm, and W. Gujer, (2005). Simulating development strategies for water supply systems. *J. Hydroinformatics*, 7, 41-51.
- Timmerman, P., and R. White, (1997). Megahydropolis: Coastal cities in the context of global environmental change. *Global Environmental Change*, 7(3):205-234.
- Tong, S.T.Y, Sun, Y., and Y.J. Yang, (2012). Generating a future land use change scenario with a modified population-coupled Markov Cellular Automata Model. *Journal of Environmental Informatics*, 19(2): 108-119.
- Torrence, C., and G. P. Compo, (1998). *A Practical Guide to Wavelet Analysis*. Boulder, CO: American Meteorological Society.
- Trompetter, W. J., S. K. Grange, P. K. Davy, and T. Ancelet, (2013). Vertical and temporal variations of black carbon in New Zealand urban areas during winter. *Atmospheric Environment*, 75, 179-187.
- Tung, H., R.F. Unz, and Y.F. Xie, (2006). HAA removal by GAC adsorption. *J. AWWA*, 98:6, 107-112.
- Turnipseed, D. P., K. Van Wilson, J. Stoker, Jr., and D. Tylor, (2007). Mapping hurricane Katrina peak storm surge in Alabama, Mississippi, and Louisiana. *37th Annual Mississippi Water Resources Conference*, Jackson, MS.

- Uber, J., Shang, F., and Rossman, L. (2004) Extensions to EPANET for fate and transport of multiple interacting chemical or biological components. *Critical Transitions in Water and Environmental Resources Management*. doi: 10.1061/40737(2004)486
- Uno, I., H. Ueda, and S. Wakamatsu, (1989). Numerical modeling of the nocturnal urban boundary layer. *Boundary-Layer Meteorology*, 49(1-2), 77-98.
- Uno, I., S. Wakamatsu, H. Ueda, and A. Nakamura, (1988). An observational study of the structure of the nocturnal urban boundary layer. *Boundary-Layer Meteorology*, 45(1-2), 59-82.
- Urbaniak, A. (1988). Multicriteria capacity expansion planning for an urban water system with random data. *Civil Engineering Systems*, 5, 129-136.
- U.S. BLS (Bureau of Labor Statistics), (2008). *BLS Handbook of Methods, Chapter 14 Producer Prices-Background*. http://www.bls.gov/pub/hom/homch14_a.htm.
- US EPA (2017). Decision support system for aquifer recharge (AR) and aquifer Recovery (ASR) planning, design, and evaluation: Principles and technical basis. *EPA/600/R-16/222*.
- U.S. EPA (2015a). National water infrastructure adaptation assessment. Part I: Climate change adaptation readiness analysis. *EPA/600/R-15/141*.
- U.S. EPA (2015b). *BASINS 4.1 (Better Assessment Science Integrating point & Non-point Sources) Modeling Framework*. National Exposure Research Laboratory, RTP, North Carolina. <https://www.epa.gov/exposure-assessment-models/basins>.
- U.S. EPA (2015c). The impact of traditional and alternative energy production on water resources: Assessment and adaptation studies. *EPA 600/R-14/272*
- U.S. EPA, (2014). National stormwater calculator - Version 1.1 (Model). Washington, DC, *EPA/600/C-13/106b*.
- U.S. EPA, (2013a). *Preferred/Recommended Regulatory Atmospheric Models*. Retrieved December 28 , 2013, from U.S. EPA Office of Air and Radiation: http://www.epa.gov/scram001/dispersion_prefrec.htm
- U.S. EPA, (2013b). Our built and natural environments. *EPA231K13001*. Washington, DC., 139p.
- U.S. EPA, (2013c). *Watershed modeling to assess the sensitivity of streamflow, nutrient, and sediment loads to potential climate change and urban development in 20 U.S. watersheds*. Draft in review. <http://cfpub.epa.gov/ncea/global/recordisplay.cfm?deid=247495>
- U.S. EPA. (2012a). A framework for sustainability indicators at EPA. *EPA/600/R/12/687*. Cincinnati.
- U.S. EPA. (2012b). *Adaptive response framework for drinking water and wastewater utilities*. Office of Water. Washington, D.C., <http://water.epa.gov/infrastructure/watersecurity/climate/upload/epa817f12009.pdf>
- U.S. EPA. (2011). *Transportation Control Measures: An Information Document for Developing and Implementing Emissions Reduction Programs*. U.S. EPA.

- U.S. EPA. (2010a). *Motor Vehicle Emission Simulator (MOVES) user guide for MOVES 2010a*. U.S. Environmental Protection Agency.
- U.S. EPA, (2010b). Integrated climate and land-use scenarios (ICLUS) v1.3 User's manual: ArcGIS tools and datasets for modeling US housing density growth. *EPA/600/R-09/143F*. 19p.
- U.S. EPA, (2009a). A Screening assessment of the potential impacts of climate change on combined sewer overflow (CSO) mitigation in the Great Lakes and New England regions (External Review Draft). *EPA/600/R-07/033A*, U.S. Environmental Protection Agency, Washington, DC.
- U.S. EPA, (2009b). Land-use scenarios: National-scale housing-density scenarios consistent with climate change storylines. *EPA/600/R-08/076F*, Washington, DC.
- U.S. EPA, (2008). A screening assessment of the potential impacts of climate change on combined sewer overflow (CSO) mitigation in the Great Lakes and New England regions. *EPA/600/R-07/033F*, Global Change Research Program, National Center for Environmental Assessment, Washington, DC, p.39.
- U.S. EPA, (2007a). An approach for using load duration curves in the development of TMDLs. *EPA 841-B-07-006*, Washington DC., 68p.
- U.S. EPA. (2007b). *Moving Toward Sustainability*. Retrieved July 12, 2011, from <http://water.epa.gov/infrastructure/sustain/index.cfm>
- U.S. EPA, (2007c). Aging water infrastructure research program: Addressing the challenge through innovation. Washington, DC, *EPA/600/F-07/015*
- U.S. EPA. (2006). Growing Toward More Efficient Water Use: Linking Development, Infrastructure, and Drinking Water Policies. *EPA 230-R-06-001*. Washington, DC
- U.S. EPA, (2005). *Water Treatment Plant Model Version 2.2 User's Manual*. Office of Ground Water and Drinking Water, U.S. Environmental Protection Agency, Cincinnati, Ohio.
- U.S. EPA, (2004a). Stormwater best management practice design guide: Volume 3 basin best management practices. *EPA/600/R-04/121B*.
- U.S. EPA, (2004b). *AERMOD Description of Model Formulation*. Ann Arbor: USEPA.
- U.S. EPA, (2004c). Stormwater best management practice design guide: Volume 3 Basin best management practices. *EPA/600/R-04/121B*.
- U.S. EPA, (2002). Onsite wastewater treatment systems manual. *EPA/625/R-00/008*. Cincinnati, Ohio.
- U.S. EPA, (2001). Report to Congress: Implementation and Enforcement of the CSO Control Policy. *EPA 833-R-01-003*, Washington, DC.
- U.S. EPA (2000). ICR treatment study database, version 1.0. *EPA 815-C-00-003*, Office of Water, Washington, D.C.
- U.S. EPA. (1998). *Transportation Control Measures: Traffic Flow Improvements*. Transportation Air Quality Center.

- U.S. EPA, (1996). ICR manual for bench and pilot-scale treatment studies. *EPA 814-B-96-003*, Office of Water, Washington, D.C.
- U.S. EPA, (1994). Combined sewer overflow control policy. *Federal Register [FRL-4732-7]*, Part VII, April 19, 1994. 16p.
- Uyak, V., K. Ozdemir, and I. Toroz, (2008). Seasonal variations of disinfection by-product precursors profile and their removal through surface water treatment plants. *Science of the Total Environment*, 390: 417-424.
- Voivontas, D., G. Arampatzis, E. Manoli, C. Karavitis, and D. Assimacopoulos, (2003). Water supply modeling towards sustainable environmental management in small islands: the case of Paros, Greece. *Desalination*, 156, 127-135.
- Wallis, J.R., M.G. Schaefer, B.L. Barker, and G.H. Taylor, (2007). Regional precipitation-frequency analysis and spatial mapping for 24-hour and 2-hour durations for Washington State. *Hydrol. Earth Syst. Sci.*, 11(a):415-442.
- Wang, K., H. Ye, F. Chen, Y. Xiong, and C. Wang, (2012). Urbanization effect on the diurnal temperature range: different roles under solar dimming and brightening. *J. Climate*, 25(3), 1022-1027.
- Wang X., A. Burguess, and Y.J. Yang, (2013). A scenario-based water conservation planning support system (SB-WCPSS). *Stochastic Environmental Research and Risk Assessment*, 27(3), 629-641.
- Ward, D. P., A. T. Murray, and S. R. Phinn, (2000). A stochastically constrained cellular model of urban growth. *Comput. Environ. Urban Syst*, 24, 539-558.
- Webster, M., P. Donohoo, and B. Palmintier, (2013). Water-CO₂ trade-offs in electricity generation planning. *Nature Climate Change*, 3, 1029-1032.
- Wei, H., T. Zuo, H. Liu, and J.Y. Yang, (2017). Integrating land use and socioeconomic factors into scenario-based travel demand and carbon emission impact study. *Urban Rail Transit*, doi:10.1007/s40864-017-0056-2.
- Wei, H., X. Wang, Z. Yao, H. Liu, S. Liang, and Y. Yang, (2012). Framework for Integrating Traffic-Source Emission Estimates into Sustainability Analysis. *CICTP 2012*: 3612-3619. doi: 10.1061/9780784412442.364
- Weinstein, N., (2009). Decentralized stormwater controls for urban retrofit and combined sewer overflow reduction, Phase 2. *WERF Report 03-SW-3A*. ISBN: 9781843393535
- Weng, Q., D. Lu, and J. Schubring, (2004). Estimation of land surface temperature–vegetation abundance relationship for urban heat island studies. *Remote sensing of Environment*, 89(4), 467-483.
- Whitehead, P. G., R. L. Wilby, D. Butterfield, and A. J. Wade, (2006). Impacts of climate change on in-stream nitrogen in a lowland chalk stream: An appraisal of adaptation strategies. *Science of the Total Environment*, 365: 260–273
- Whitehead, P.G., R.L. Wilby, R.W. Battarbee, M. Kernan, and A.J. Wade, (2009). A review of the potential impacts of climate change on surface water quality. *Hydrological Sciences Journal / Journal des Sciences Hydrologiques*, 54(1), 101-123.

- Wing, S., S. Freedman, and L. Band, (2002). The potential impact of flooding on confined animal feeding operations in Eastern North Carolina. *Environ. Health Persp.*, 110(4), 387-391.
- Wilby, R.L., (2007). A review of climate change impacts on the built environment. *Built Environment*, 33(1):31-45.
- Yamout, G. and M. El-fadel, (2005). An optimization approach for multi-sectoral water supply management in the Grater Beirut Area. *Water Resources Management*, 19, 791-812.
- Yang, J., & Lee, H. (1997). An AHP decision model for facility location selection. *Facilities*, 15(9), 241-254.
- Yang, Y. J., M. S. Liang, Y. Zhao1, and J. Neal, (2017). Establishing design storm values from climate models in coastal regions: Challenges and opportunities. *EWRI 2017*, Sacramento, CA.
- Yang Y.J., and J.A. Goodrich, (2014). Toward quantitative analysis of water-energy-urban-climate nexus for urban adaptation planning. *Current Opinion in Chem Engrng*, 5, 22-28.
- Yang, Y. J., N-B. Chang, J. Neal, H. Wei, M.S. Liang, and T.C. Keener, (2013). Water and carbon footprints for sustainability analysis of urban infrastructure. *EWRI 2013*, Cincinnati, Ohio
- Yang, J. Y., (2010). Re-define adaptation of water resource infrastructure to a non-stationary climate (Editorial). *J. Water Resour. Plng. & Mgmt.* 136(3):297-298
- Yang, Y. J., C. A. Impellitteri, R. M. Clark, R. C. Haught, D.A. Schupp, S. Panguluri, and E. R. Krishnan, (2008). Chlorine decay and DBP formation under different flow regions in PVC and ductile iron pipes: Preliminary results on the role of flow velocity and radial mass transfer. *EWRI 2008*, Atlanta.
- Yang, Y.J., R. C. Haught, J. Neal, K. Carlton-Perkins, T. C. Keener, J.-Y. Lee, (2008b). Variations in high-intensity precipitation under climate changes in the LMRB and implications for drinking water supply security. *EWRI 2008*, Hawaii.
- Yang, Y.J., J. A. Goodrich, S.Y. Li, and R.C. Haught, (2007). AST/R-based water reuse as a part of the total water solution for water-stressed regions: An overview of engineering practice and regulatory prospective. *EWRI 2007*, Tampa, Florida.
- Yang, Y.J., and A. Restivo, (2010). ASR application in climate change adaptation: The need, issues and research focus. *Water & Energy in Changing Climate*, Ground Water Protection Council, Pittsburgh, PA. September 2010.
- Yang, Y. J., A. Hale, D. Chapman, and D. Keith, (2002). Water quality and biological response to water aeration of glycol-contaminated streams in cold temperatures. Proc. of the Water Environment Federation, *Industrial Wastes 2002*, 962-978(17).
- Yao, Z., Wei, H., Wang, X., Liu, H., Yang, J., (2014). Scenario-based carbon footprint inventory tool for urban sustainable development decision support: The Cincinnati case study. *Transportation Research Board Annual Meeting 2014 Paper #14-3242*
- Zachman, B. A. and Summers, R.S. (2010). Modeling TOC breakthrough in granular activated carbon adsorbers. *J. Environmental Engineering*, 136(2), 204-210.

- Zeleny, M. 1973. Compromise programming, in: *Multiple Criteria Decision Making*, eds: J. L. Cochrane and M. Zeleny, University of South Carolina Press, Columbia, SC, pp. 262-301.
- Zhao, Y., Yang, Y.J., Shao, Y., Neal, J., and Zhang, T., (2018a). The dependence of chlorine decay and DBP formation kinetics on pipe flow properties in drinking water distribution. *Water Research*, 141:32-45.
- Zhao, Y., Yang, Y.J., Shao, Y., Lee, Y., and Zhang, T., (2018b). Demand-driven spatiotemporal variations of flow hydraulics and water age by comparative modeling analysis of distribution network. *J. Wat. Resour. Plann. & Manag.*, in print.
- Zhao, Y., Yang, Y.J., Lee, Y., Panguluri, S., and Shao, Y., (2017). Better water demand and Pipe description improve the distribution network modeling results. *EWRI 2017*, Sacramento, California.
- Zhou, J., Lin, J., Cui, S., Qiu, Q., and Zhao, Q., (2013). Exploring the relationship between urban transportation energy consumption and transition of settlement morphology: A case study on Xiamen Island, China. *Habitat International*, 37, 70-79.
- Zmud, J. P., Barabba, V. P., Bradley, M., Kuzmyak, J. R., Zmud, M., & Orrell, D. (2014). Strategic Issues Facing Transportation, Volume 6: The Effects of Socio-Demographic on Future Travel Demand. *TRB's National Cooperative Highway Research Program (NCHRP) Report 750*. Transportation Research Board, Washington, DC

Appendix A

AIR-SUSTAIN program input and output structures

Table of Content

A I.1	AIR-SUSTAIN Program and Operations	189
A I.1.1	Program Interfaces.....	189
1	Scenario Information Specification.....	189
2.	Regional Level Analysis.....	195
3.	Project Level Analysis.....	198
4.	Results Comparison.....	200
A I.1.2	Inputs and outputs.....	202
A I.2	Database In AIR-SUSTAIN	213
A I.2.1	Database Structure.....	213
A I.2.2	MOVES Emission Lookup Tables	221
A I.3	Transportation Analysis Examples Using the AIR-SUSTAIN tool	227

List of Tables

Table A1-1	Sample of Population Change	194
Table A1-2	Sample of Employment Change	194
Table A1-3	Sample of University Enrollment Change	194
Table A1-4	Sample of High School Enrollment Change	194
Table A1-5	Inputs for the AIR-SUSTAIN	202
Table A1-6	Outputs from the AIR-SUSTAIN	203
Table A1-7	Inputs for the Scenario Development.....	203
Table A1-8	Land Use Inputs	205
Table A1-9	List of Outputs from the Scenario Development	206
Table A1-10	Inputs for the Regional Level Analysis	207
Table A1-11	Description of a VISUM File.....	209
Table A1-12	Outputs from the Regional Level Analysis	210
Table A1-13	Inputs for the Project Level Analysis	211
Table A1-14	Outputs from the Project Level Analysis	212
Table A2-1	Tables and fields of AIR-SUSTAIN Scenario Database	213
Table A2-2	Tables and Items of the MOVES Input Database	215
Table A2-3	Tables and Items of the MOVES Output Database	217
Table A2-4	Geodatabase	218
Table A2-5	The MOVES Source Types	221
Table A2-6	The MOVES Road Type	221
Table A2-7	MOVES Age Distribution Categories	222
Table A2-8	MOVES Operating Modes.....	222
Table A3-1	Sample of Population Change	228
Table A3-2	The MOVES Road Type	232
Table A3-3	Sample of Employment Fraction	233
Table A3-4	Sample of Vehicle Composition	233
Table A3-5	Sample of Age Distribution	234
Table A3-6	Sample of Fuel Formulation	235
Table A3-7	Sample of Fuel Supply	235
Table A3-8	Sample of Meteorology	235
Table A3-9	Sample of State and County	235
Table A3-10	Sample of Selected Hot-spot Links for Corridor Level Impact Analysis	238
Table A3-11	Vehicle Volume	240
Table A3-12	Vehicle Type Class and Category	240
Table A3-13	Car Following Behavior Parameters	241
Table A3-14	Lane Change Parameters	241
Table A3-15	Ramp metering design criteria of FHWA	242
Table A3-16	Signal Control Parameters	242
Table A3-17	VISSIM Calibration Final Parameter Values	242
Table A3-18	VISSIM Validation Results	243
Table A3-19	Microscopic Simulation Link ID (Sheet1).....	244
Table A3-20	Microscopic Simulation Link ID (Sheet2)	244
Table A3-21	Microscopic Simulation Results (Sheet1)	244

Table A3-22	Microscopic Simulation Results (Sheet2).....	245
Table A3-23	An Example of Hotspots Emissions by Different Scenarios	246

List of Figures

Figure A1-1	Scenario Information	189
Figure A1-2	Interface for (a) New Scenario; (b) and Load Scenario	190
Figure A1-3	“Save Scenario As” Interface	191
Figure A1-4	Scenario Development Interface	192
Figure A1-5	Load Base Year Data	192
Figure A1-6	Assumed Changes in Demographic and Socioeconomic Factors	193
Figure A1-7	Population and Employment Changes	193
Figure A1-8	Land use projection	194
Figure A1-9	Socioeconomic Data Update Based on Assumed Changes	195
Figure A1-10	Regional Level Analysis Interface	196
Figure A1-11	Travel Demand Forecasting Panel	196
Figure A1-12	Emission Estimation Panel	197
Figure A1-13	Hotspots Identification	198
Figure A1-14	Project Level Analysis Interface	199
Figure A1-15	Microscopic Simulation Results Import	199
Figure A1-16	Hotspots Emission Estimation	200
Figure A1-17	Updating hotspot identification results to regional analysis panel	200
Figure A1-18	Results Comparison Interface	201
Figure A3-1	Import Base Year Data in Example	227
Figure A3-2	Program interface for A) importing the Base Year data; B) assigning population change; and C) assigning employment changes at TAZ levels	228
Figure A3-3	Target Year Land Use in Example	229
Figure A3-4	Target Year Land Use in Example	229
Figure A3-5	VISUM Demand Set Up	230
Figure A3-6	Example of road network from the input function	231
Figure A3-7	Example of VISUM Matrix.....	231
Figure A3-8	VISUM Procedure Set Up	232
Figure A3-9	Example of Trip Distribution Result from VISUM (Trips between Two Centers)	234
Figure A3-10	Emission Results Displayed in ArcGIS	236
Figure A3-11	Hotspots Identification Criteria	236
Figure A3-12	Identified Hotspots in Traffic Emission	237
Figure A3-13	VISSIM Links over the Base Map	238
Figure A3-14	Schematic for Hotspot Microscopic Analysis	239
Figure A3-15	An Example of Desired Speed Distribution for Cars and Trucks...	240

AIR-SUSTAIN is a major component of the Smart Urban Designer (SUD) program. The principles and functionalities are described in the main report Sections 3.0-4.0. This Appendix describes program inputs, outputs, and major program interfaces for program use and project simulation.

A I.1 AIR-SUSTAIN Program and Operations

A I.1.1 Program Interfaces

The execution of each analysis function within the AIR-SUSTAIN is achieved through interfaces embedded in a GIS environment. Main functions and interfaces of the AIR-SUSTAIN are:

- Scenario Information Specification;
- Scenario Development;
- Regional Level Analysis;
- Project Level Analysis; and
- Results Comparison.

1. Scenario Information Specification

The AIR-SUSTAIN provides a Scenario Information interface (Figure A1-1). Before performing a scenario analysis, the scenario information must be set up first in the either by creating a scenario (via the **New Scenario** button on the menu bar) or loading an existing scenario (via the **Load Scenario** button on the menu).

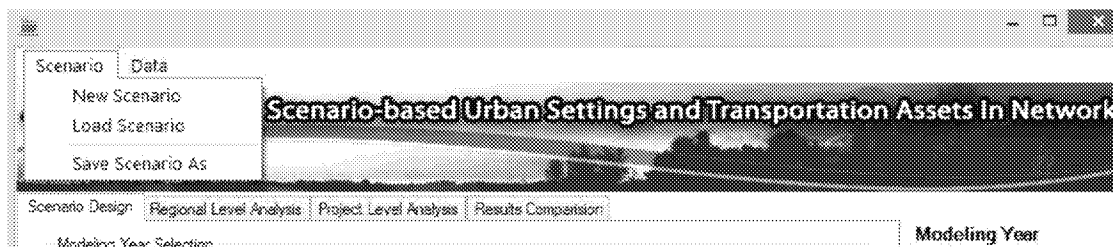


Figure A1-1 Scenario Information

Scenario information in the **New Scenario** and **Load Scenario** windows (as shown in Figure A1-2) includes:

- 1) **Scenario Name** (required): the name of a scenario analysis specified by user;
- 2) **Project Directory** (required): the route where user place the scenario folder;
- 3) **Modeling Year** (required): Base Year and Target Year;

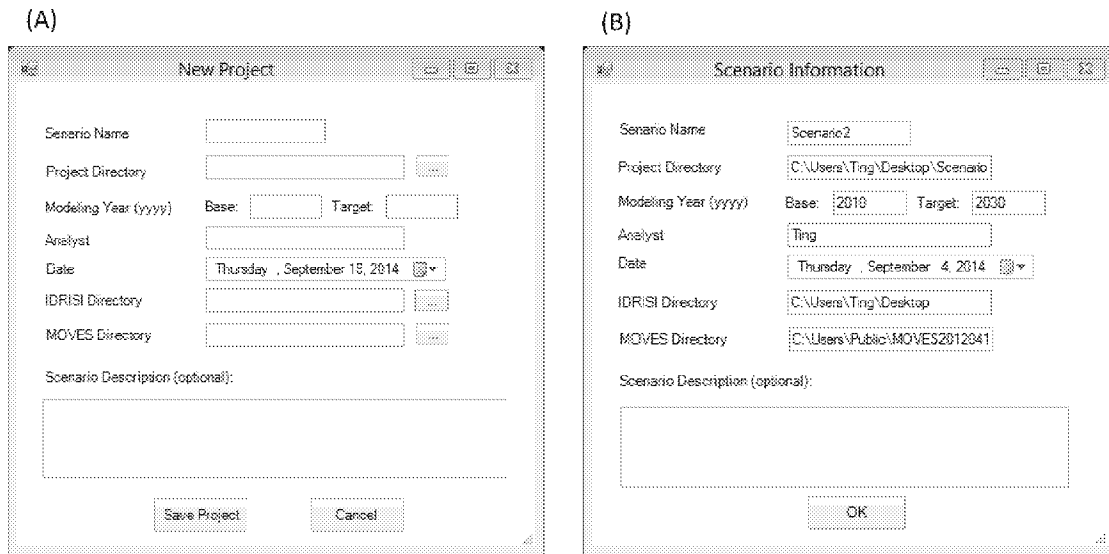


Figure A1-2 Interface for (a) New Scenario; (b) and Load Scenario

- 4) **Analyst** (required);
- 5) **Date** (required);
- 6) **IDRISI Directory** (required): where IDRISI is installed;
- 7) **MOVES Directory** (required): where MOVES is installed; and
- 8) **Scenario Description** (optional).

After setting up all required data, in the **New Scenario** tab, by clicking the **Save Project** button, a scenario folder and five MySQL databases are created. A scenario folder contains:

- GIS.gdb: a geodatabase store feature classes such as TAZ, road network, incentive boundary, and scenario analysis results;
- IDRISI: a subfolder to store inputs and outputs for the land use projection;
- MOVES: a subfolder to store inputs and outputs for the emission estimation;
- VISSIM: a subfolder to store microscopic traffic simulation input and output files.
- VISUM: a subfolder to store the TDF model inputs and outputs;
- ScenarioName_map: an ArcGIS map file that contains input maps and analysis result maps.

The MySQL database (See details later) includes:

- AIR-SUSTAIN_ScenarioName database, including projectInfo, IDRISIInfor, employmentGrowth, emplymentTripRate, populationGrowth, householdTripRate, increasePercentage, unversityEnrollment, HighSchoolEnrollment, baseYearResults, targetYearResults;

- ScenarioName_In database: used as the MOVES input database in the regional level analysis;
- ScenarioName_Out database: used as the MOVES output database in the regional level analysis;
- ScenarioName_Project_In database: used as the MOVES input database in the project level analysis;
- ScenarioName_Project_Out database: used as the MOVES output database in the project level analysis.

If a scenario is created, the user can load the scenario information by clicking the **Load Scenario** on the menu bar. Afterwards, the scenario information is displayed in a pop-up window shown as Figure A1-2b.

The **Save Scenario As** (as shown as in Figure A1-3) window provides a function to save a new scenario based on current scenario data by specifying a new scenario name and a new scenario directory in the **SaveASForm** window.

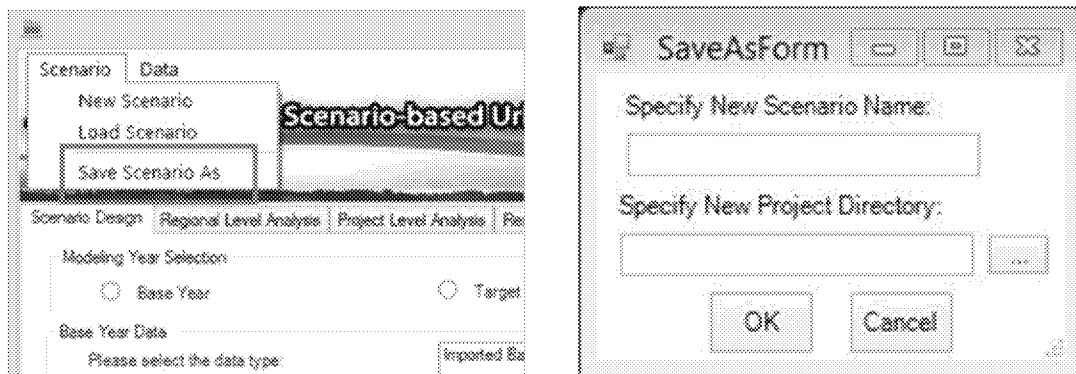


Figure A1-3. “Save Scenario As” Interface

There are three main panels in the **Scenario Development** tab (Figure A1-4): **Modeling Year Selection**, **Base Year Data**, and **Target Year Scenario Development**.

- The **Modeling Year Selection** panel is applied to select scenario analysis year by checking either the **Base Year** or **Target Year**.
- The **Base Year Data** panel provides the function (shown as Figure A1-5a) to import base year feature classes (i.e., *TAZ*, *RoadNetwork*, and *Incentiveboundary*). As illustrated by Figure A1-5, users can select the data type (i.e. *TAZ* shown as Figure A1-5b) from the dropdown list and import data by clicking the **Import** button (as Figure A1-5c). The imported data will be listed in the right box (as Figure A1-5d). Users can also remove the

imported data by selecting the data name in the box and then clicking the **Remove** button in Figure A1-5c.

The screenshot shows the 'Scenario Development' interface with the following components:

- Scenario Development** (selected tab) | Regional Level Analysis | Project Level Analysis | Results Comparison
- Modeling Year Selection**
 - ☐ Base Year
 - ☐ Target Year
- Base Year Data**
 - Please select the data type: [dropdown menu]
 - Import** | **Remove**
 - Imported Base Data:** [empty box]
- Target Year Scenario Design**
 - 1. Assumed Changes in Demographic and Socioeconomic Factors
 - a. Population Change: ☐ Edit | ☐ Load File
 - b. Employment Change: ☐ Edit | ☐ Load File
 - c. University Enrollment Change: ☐ Load File
 - d. High School Enrollments Change: ☐ Load File
 - View**
 - 2. Land Use Projection
 - a. Initial Year (yyyy): [text box]
 - b. Land Use Inputs Directory: [text box] **Run**
 - c. IDRIS: **Run**
 - d. Target Year Land Use: **View Results**
 - 3. Demographic and Socioeconomic Data Update Based on Assumed Changes
 - a. Allowable Population Density: [text box]
 - b. Linkage Model: **Run**
 - c. Target Year Demographic and Socioeconomic Data: [dropdown menu] **View**
- Modeling Year**
 - yyy
- Process Status**
 - Project Information
 - Modeling Year Selection
 - Base Year Data
 - Target Year Scenario Design
 - Travel Demand Forecasting
 - Emission Estimation
 - Hubzone Identification
 - Microscopic Simulation Results
 - Hubzone Emission Estimation
 - Regional Emissions Update

Figure A1-4. Scenario Development Interface

The diagram illustrates the process of loading base year data in four steps:

- Base Year Data**
 - Please select the data type: [dropdown menu]
 - 1. TAZ
 - 2. Road Network
 - 3. Incentive Boundary
- Base Year Data**
 - Please select the data type: [dropdown menu]
 - Import** | **Remove**
- Base Year Data**
 - Please select the data type: [dropdown menu]
 - 1. TAZ
 - 2. Road Network
 - 3. Incentive Boundary
- Imported Base Data:**
 - TAZ
 - RoadNetwork
 - Incentiveboundary

Figure A1-5 Load Base Year Data

The **Target Year Scenario Design** panel provides functions to set up assumed changes in demographic and socioeconomic factors, including population change, employment change, university enrollment change, and high school enrollment change. There are two ways to set up population change and employment change: 1) clicking the **Edit** button to set up the change percentages in incentive area and non-incentive area separately (left window of Figure A1-6), and 2) clicking the **Load File** button to import an excel file including population change in each TAZ (right window of Figure A1-6). University enrollment change and high school enrollment change can be imported to AIR-SUSTAIN by clicking the **Load File** buttons at right side of item c and d (shown as Figure A1-7). The sample input files are shown in Figure A1-7 and Tables A1-1 through 1-4.

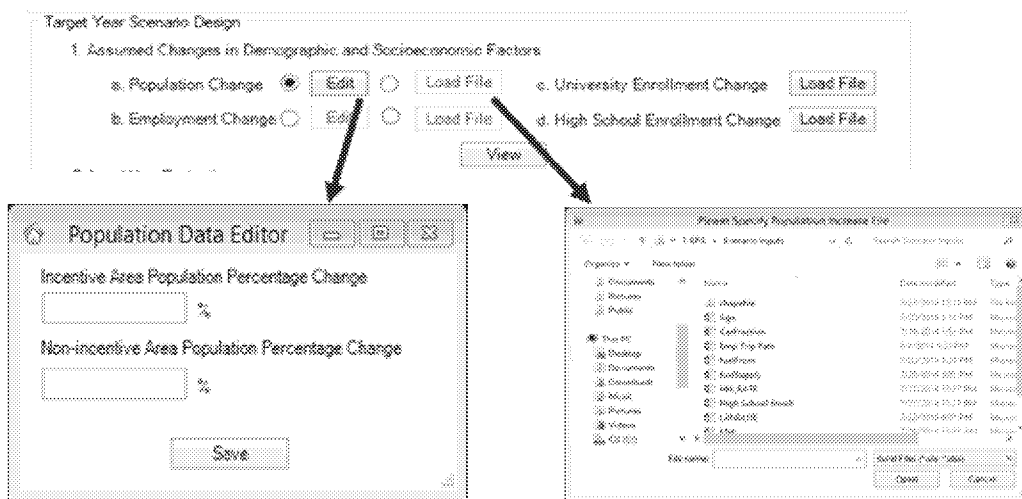


Figure A1-6 Assumed Changes in Demographic and Socioeconomic Factors

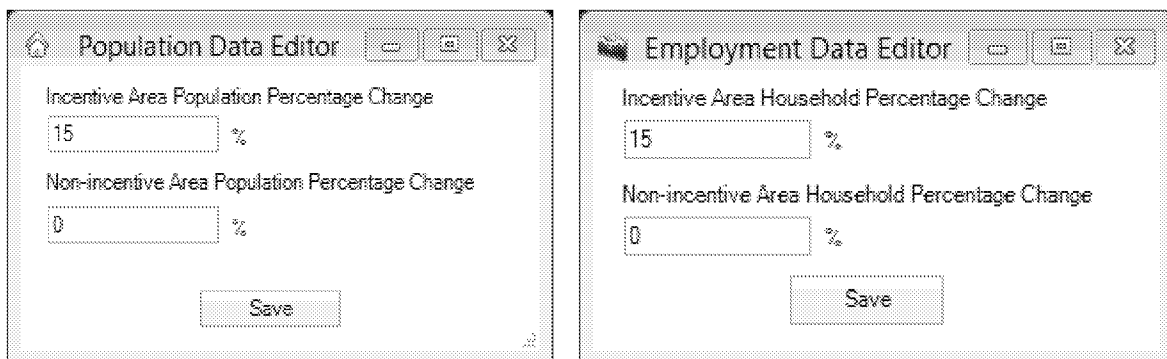


Figure A1-7 Population and Employment Changes

Table A1-1 Sample of Population Change

TAZ	Population
330	156
338	191
318	268

Table A1-2 Sample of Employment Change

TAZ	Employment
330	156
338	191
318	268

Table A1-3 Sample of University Enrollment Change

TAZ	Enrollment	Name
330	156	Hebrew Union College
338	191	Institute of Technical Careers
318	268	God's Bible College

Table A1-4 Sample of High School Enrollment Change

TAZ	Enrollment	Name
210	2556	Walnut Hills High School
244	613	Merry Middle School
251	584	Creative & Performing Arts Hi School

In the **Target Year Scenario Design** panel, target year land use is projected in the **Land Use Projection** (see Figure A1-8). Before performing land use projection, the **Initial Year** needs to be specified by the user. Other land use inputs are loaded by specifying the route of a folder that

2. Land Use Projection

a. Initial Year (yyyy)

b. Land Use Inputs Directory

c. IDRISI

d. Target Year Land Use

Figure A1-8. Land use projection

contains files listed in Table A1-4. Then by executing IDRISI, target year land use is projected, and land use projection results can be displayed in the ArcMap main window by clicking the **View Results** button.

Figure A1-9 shows the **Socioeconomic Data Update Based on Assumed Data** panel. In the **Target Year Scenario Design**, target year demographic and socioeconomic data are generated by base year demographic and socioeconomic data, assumed changed in demographic and socioeconomic factors, base year land use, and target year land use by linkage model. Before running the linkage model, the allowable population density should be set up. The maximum population density is used as the maximum unit area population capacity in a TAZ. In this panel,

3. Demographic and Socioeconomic Data Update Based on Assumed Changes

a. Allowable Population Density

b. Linkage Model

c. Target Year Demographic and Socioeconomic Data

Figure A1-9. Socioeconomic Data Update Based on Assumed Changes

target year socioeconomic data can be viewed by specifying the data type in the drop list and clicking the **View Results** button.

2. Regional Level Analysis

The Regional Level Analysis module is used to estimate the base and target year travel demand and on-road emissions for the study area. The **Travel Demand Forecasting** and **Emission Estimation** panels are highlighted by red boxes in Figure A1-10. When performing the regional level analysis, a TDF model first simulates trips on roadway links for the entire study area based on demographic and social economic data, as well as transportation infrastructure, i.e. road network, TAZs. Afterwards, the forecasted traffic data are utilized to generate inputs for a traffic emission model which is adopted to estimate road link based vehicle emissions. Particularly in the emission analysis, CO₂ equivalent and energy consumption for individual road links in the study area are estimated by the user selected emission model.

There are five components in the **Travel Demand Forecasting** panel (Figure A1-11). In Component 1, the user needs to specify the TDF model. Among the popular TDF tools such as VISUM, Cube, and TransCAD, the current version of the AIR-SUSTAIN supports VISUM 13.0. Other models will be included in the software in the future. When the VISUM label is selected by the user, the VISUM panel is activated. In the VISUM model, a *VISUM file*, *Household Faction and Trip Rate*, and *Employment Fraction* need to be loaded by Component 2, 3, 4 respectively (Figure A1-11). Component 5 provides functions to execute VISUM and view TDF results in VISUM.

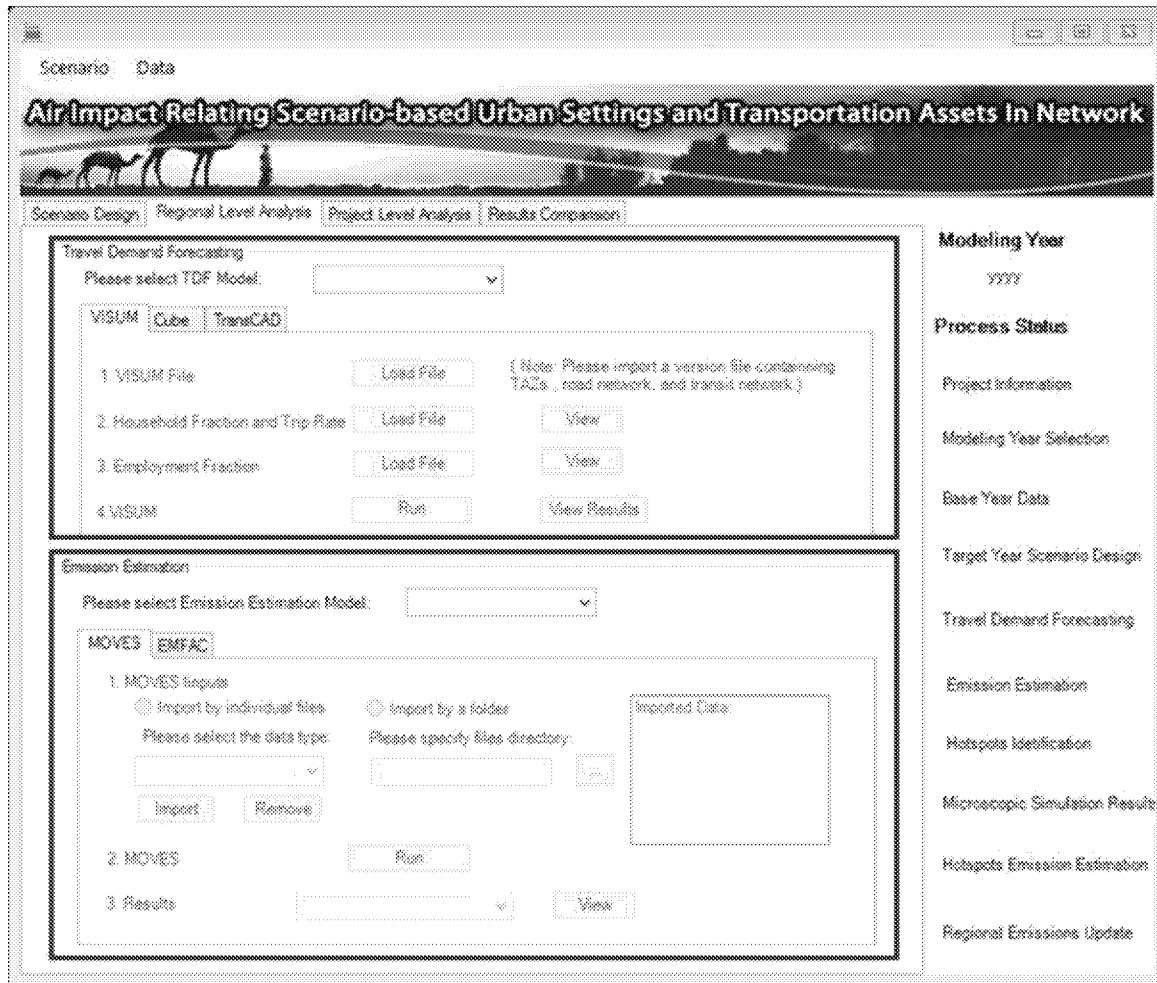


Figure A1-10 Regional Level Analysis Interface

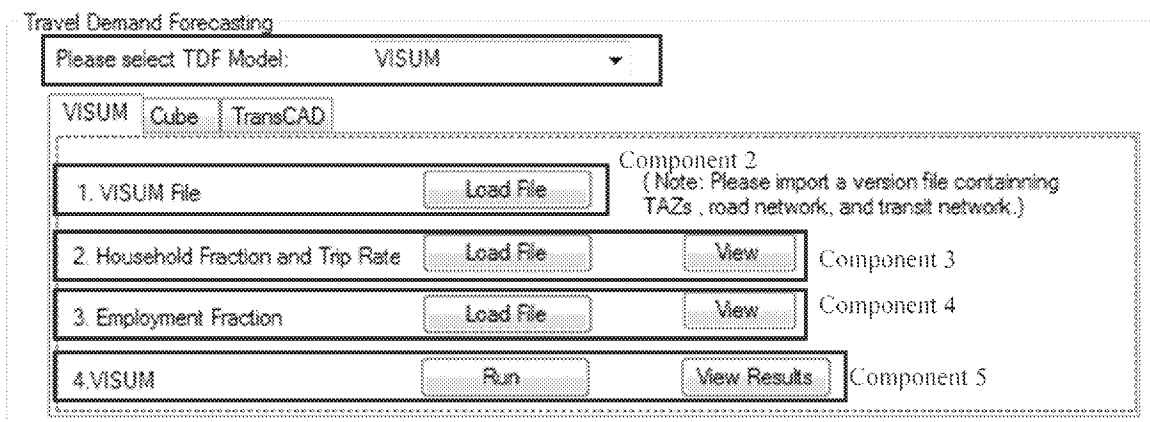


Figure A1-11. Travel Demand Forecasting Panel

Figure A1-12 shows the **Emission Estimation** panel which contains five components. Similar to travel demand forecasting, the user is allowed to specify the emission model in Component 1. For the current version of AIR-SUSTAIN, the regional level transportation emission estimation will be conducted by using the MOVES model. The functions for supporting EMFAC model will be developed in the future. Two methods of loading MOVES inputs are provided in Component 2. When the **Import by individual files** is checked, MOVES input files can be imported individually. Alternatively, if the **Import by a folder** is checked, all files in the specified folder are imported as MOVES inputs. The steps in the two methods of loading MOVES inputs are:

The screenshot shows the 'Emission Estimation' window with the following components:

- Component 1:** A dropdown menu labeled 'Please select Emission Estimation Model:'.
- Component 2:** A section titled 'MOVES Inputs' containing two radio buttons: 'Import by individual files' and 'Import by a folder'. Below the first radio button is a dropdown for 'Please select the data type:' and an 'Import' button. Below the second radio button is a text field for 'Please specify files directory:' and a 'Browse' button. A 'Remove' button is also present.
- Component 3:** A box titled 'Imported Data:' containing a list of imported files.
- Component 4:** A button labeled 'Run'.
- Component 5:** A button labeled 'View'.

Figure A1-12 Emission Estimation Panel

When the **Import by individual files** is checked, the user should specify the input data type, (i.e. meteorology, age distribution, fuel formulation, fuel supply and State and County), and import the corresponding file by clicking Import button. The imported file can be deleted by clicking the **Remove** button.

- When the **Import by a folder** is checked, the user only need to specify the directory where all required files (listed in Table A1-1 and Table A1-4) are placed. The user needs to prepare each file in the folder according to specifications listed in Table A1-1.

Component 3 in Figure A2-12 is for displaying imported data. The user can select individual data files in Component 3 and click the **Remove** button to delete it. When all data files are imported, the user can run the MOVES by using Component 4. When MOVES simulation is finished, the user can visualize the results in Component 5.

Component 3 in Figure A2-12 is for displaying imported data. When all inputs are imported, the user can run the MOVES by using Component 4. When MOVES is finished, the user can choose to view the results in Component 5 by clicking the **View** button.

3. Project Level Analysis

In the **Hotspots Identification** panel (as shown in Figure A1-13), the user can identify hotspot links by clicking **Run** button. This panel and function resides in the **Project Level Analysis** shown in Figure A1-14. Then the **Hotspots Identification** window will be displayed. The window contains default and optional criteria for identifying hotspots. Default criteria include the **Daily Link Volume** (equal to or larger than 125,000 passenger cars) and **Truck Fraction** (equal or larger than 8%). Optional criteria include the **Average speed**, **Delay**, **Queue length**, **D/C ratio**, **CO₂ equivalent**, and **Energy consumption**.

In current version of the AIR-SUSTAIN system, only the default criteria are used. When criteria are set up, the hotspots identification function is performed by clicking **OK** button.



Figure A1-13 Hotspots Identification

In Component 1 of the **Microscopic Simulation Results Import** panel (as shown in Figure A1-15), the user needs to first import the **Microscopic Simulation Link ID** profile, which records a map between links in microscopic simulation network and links in VISUM. Then the micro-simulation results can be imported through Component 2. To this end, the user needs to set up names of traffic control measures in item *a* and load simulation results in item *b*. This process in Component 2 can be repeated if there are multiple files of simulations results to import. Imported files are listed on Component 3. A function of removing imported data is also provided in Component 4. Those simulation results by different traffic control measures can be compared and displayed by clicking the **View Results** button in Component 5.

Scenario
Data

Air Impact Relating Scenario-based Urban Settings and Transportation Assets In Network

Scenario Design
Regional Level Analysis
Project Level Analysis
Results Comparison

Hotspots Identification

Hot Spot Identification
Run
View

Microscopic Simulation Results Import

1. High Resolution Link ID
Load File
Imported Data:

2. Traffic Control Management

a. Management Strategy
Load File

b. Load Files
Load File

3. Comparison
View Results
Remove Data

Hotspots Emission Estimation

Please select Emission Estimation Model:

MOVES
EMFAC

1. MOVES
Run

2. Results
View

Regional Emissions Update

1. Traffic Control Management Strategy Name
Update

2. Strategy Results
View

Modeling Year
YYYY

Process Status

Project Information

Modeling Year Selection

Base Year Data

Target Year Scenario Design

Travel Demand Forecasting

Emission Estimation

Hotspots Identification

Microscopic Simulation Results

Hotspots Emission Estimation

Regional Emissions Update

Figure A1-14 Project Level Analysis Interface

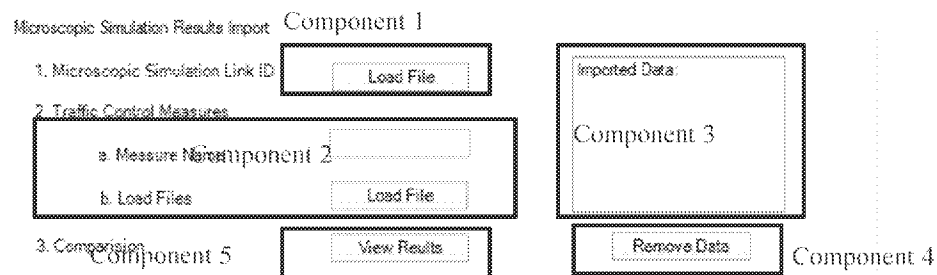


Figure A1-15 Microscopic Simulation Results Import

With those imported results, hotspots' emission is recalculated by emission estimation model which is similar to the functions of emission estimation in the regional level analysis. The emission model can be directly executed without requiring users to import extra data. In fact, the traffic inputs of the emission model are automatically prepared based on the micro-simulation results and the non-traffic inputs are retrieved from regional analysis database. Figure A1-16 shows the panel of **Hotspots Emission Estimation**.

Figure A1-16 Hotspots Emission Estimation

The **Project Level Analysis** panel provides a function to feed back the effects of different traffic control measures to the regional level results database. This is achieved by updating traffic and emission results of hotspot links to corresponding regional links. Figure A1-17 shows the panel of this function. To perform this function, the emission results by which traffic control measure should be chosen first in the drop list of the **Traffic Control Measure Name**. Then the emission results are exported to the regional database by clicking on Update button. The results can be displayed by clicking the **View** button after selecting emission type in the drop list of the **Results**.

Figure A1-17 Updating hotspot identification results to regional analysis panel

4. Results Comparison

After performing the scenario design, regional level analysis and project level analysis, results from the base year and target year can be compared and visualized in ArcGIS by the **Results Comparison** tab (Figure A1-18). Those visualized results include:

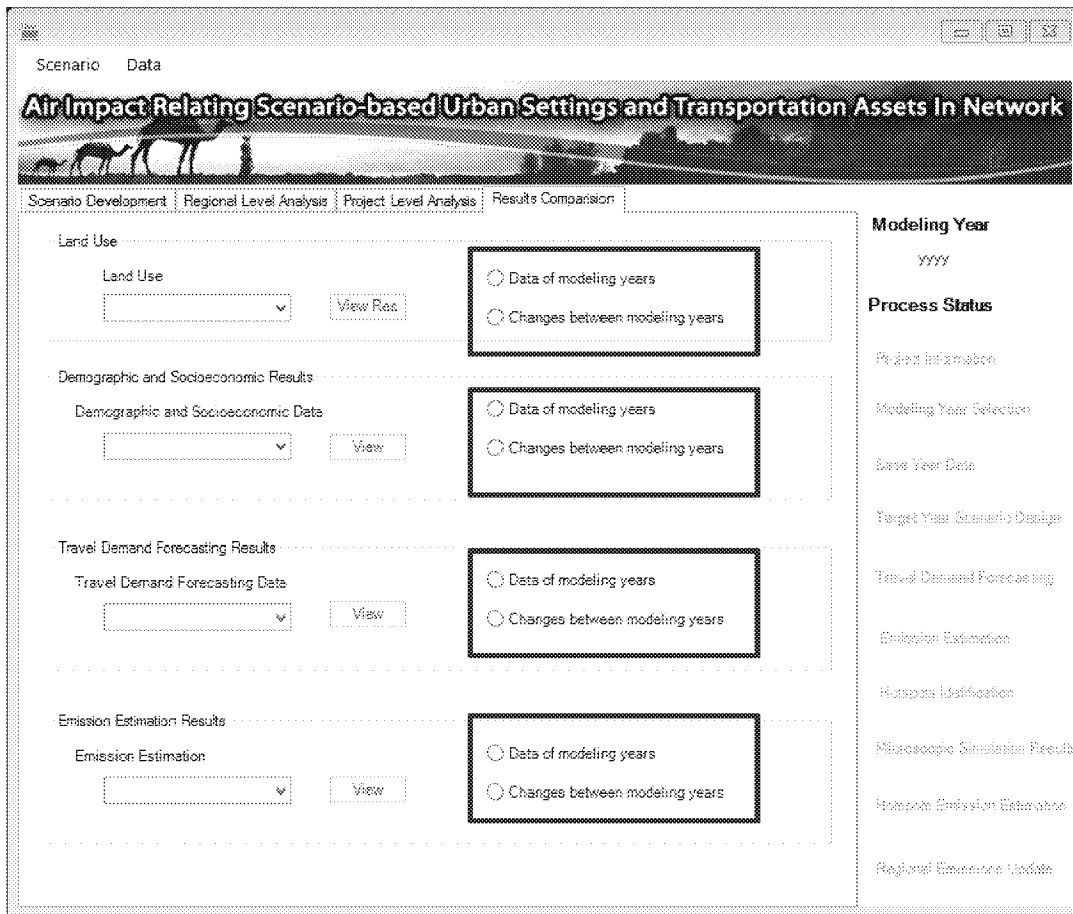


Figure A1-18 Results Comparison Interface

- Land Use, contains land use in the base year and target year;
- Demographic and Socioeconomic Data, including population, household, employment, university enrollment, high school enrollment.
- Travel Demand Forecasting Results, is to view link traffic information including volume, average speed, D/C ratio, delay, and queue length; and
- Emission Estimation, includes CO2 Equivalent and energy consumption.

By clicking the **View Results** button in the **Land Use** panel, base year and target year land uses are displayed in ArcGIS. In the **Demographic and Socioeconomic Results** panel, demographic and socioeconomic data are displayed in ArcGIS by clicking the **View** button when either the **Data of modeling year** or **Changes between modeling years** is checked. The **Travel Demand Forecasting Results** panel provides options to view the results of base year and target year or the difference between base year and target year by checking the **Data of modeling year** or **Changes between modeling years**. Similar functions are also provided in the **Emission Estimation Results** panel.

A1.1.2 Inputs and outputs

The summarized data items of the inputs and outputs for the AIR-SUSTAIN are listed in Tables A1-5 and A1-6, respectively.

Table A1-5 Inputs for the AIR-SUSTAIN

Module	Function	Data Item	Format
Scenario Development	Base Year Data	TAZ	Feature Class
		RoadNetwork	Feature Class
		Incentiveboundary	Feature Class
	Assumed Changes in Demographic and Socioeconomic Factors	Population Change	Numbers or Excel
		Employment Change	Numbers or Excel
		University Enrollment Change	Excel
		High School Enrollment Change	Excel
	Land Use Projection	Land Use Inputs Directory	Folder
Regional Level Analysis	Travel Demand Forecasting	VISUM File	Version File
		Household Faction and Trip Rate	Excel
		Employment Faction	Excel
	Emission Estimation	Age Distribution	Excel
		Fuel Supply	Excel
		Fuel Formulation	Excel
		Meteorology	Excel
		County and State	Excel
Project Level Analysis	Microscopic Simulation Results Import	Microscopic Simulation Link ID	Excel
		Microscopic Simulation Results	Excel

Table A1-6 Outputs from the AIR-SUSTAIN

Data Item	Description	Data Source	Format
Landuse_Target	Target year land use	Land use projection	Feature class
TargetYearTAZ	Target year population, household, employment, university enrollment, high school enrollment, residential area, employment area	Linkage model	Feature class
BaseTDF/ TargetTDF	Base/Target year travel demand forecasting results from trip generation, trip distribution, mode split, and traffic assignment	TDF	Version file
RoadNetwork	Base year traffic information including volume, average speed, D/C ratio, delay, and queue length	TDF	Feature class
	Target year traffic information including volume, average speed, D/C ratio delay, and queue length	TDF	Feature class
	Base year emission results including CO2 equivalent and energy consumption	Emission estimation	Feature class
	Target year emission results including CO2 equivalent and energy consumption	Emission estimation	Feature class
	Target year emission results including CO2 equivalent and energy consumption updated with project level emission results	Regional emission Update	Feature class
Hotspots	Links meet hotspots identification criteria	Hotspots identification	Feature class

Inputs and Outputs for the Scenario Development

Inputs for the scenario development are summarized in Table A1-7. Details of land use inputs are listed in Table A1-8. Outputs for the development are listed in Table A1-9.

Table A1-7 Inputs for the Scenario Development

Date Item	Field	Description	Type
TAZ	TAZ	TAZ name, the format is TAZ_TAZ Number, i.e. TAZ_151	String
	TAZ_N	TAZ number	Integer
	TAZ_Order	The field to link TAZs in ArcGIS and TAZs in VISUM	Integer

Date Item	Field	Description	Type
	POP	Target year population	Integer
	HH	Target year household	Integer
	EMP	Target year employment	Integer
	HI	Target year high school enrollment	Integer
	UN	Target year university enrollment	Integer
	AREA_TYPE	1=CBD&Urban ; 2=suburban; 3= rural	Integer
	GEOCODE_Base_1	Base year residential area (ft ²)	Double
	GEOCODE_Base_2	Base year employment area (ft ²)	Double
	GEOCODE_Base_3	Base year institutional area (ft ²)	Double
	GEOCODE_Base_4	Base year undeveloped area (ft ²)	Double
	GEOCODE_Base_5	Base year other area (ft ²)	Double
	GEOCODE_1	Target year residential area (ft ²)	Double
	GEOCODE_2	Target year employment area (ft ²)	Double
	GEOCODE_3	Target year institutional area (ft ²)	Double
	GEOCODE_4	Target year undeveloped area (ft ²)	Double
	GEOCODE_5	Target year other area (ft ²)	Double
RoadNetwork	NO	Link number	Integer
	Length	Link length (mile)	Double
	t0	Free flow travel time (s)	Double
Incentiveboundary	Name	Incentive area name	String
	Shape_Area	Area (mile ²)	Double
Population Change	TAZ	TAZ number	Integer
	Population Change	Population change	Integer
Employment Change	TAZ	TAZ number	Integer
	Employment Change	Employment change	Integer
University Enrollment Change	TAZ	TAZ number	Integer
	University Enrollment Change	University enrollment change	Integer
	Name	University name(s)	String
High School Enrollment Change	TAZ	TAZ	Integer
	High School Change	High school enrollment change	Integer
	Name	High school name(s)	String
Land Use Inputs	See details in Table 3.4	See details in Table 3.4	N/A

Table A1-8 Land Use Inputs

Name	Description	Format
21_natural_restrictions	Base year natural restricted areas	Raster
22_administrative_restrictions	Base year administrative restricted areas	Raster
231_residential_zoning	Residential zoning	Raster
234_employment_zoning	Employment zoning	Raster
30_incentive	User specified incentive layer	Raster
111_population_change	Suitability of Average Annual Percentage Change (AAPC) of population from initial year to base year	Table
112_employment_change	Suitability of Average Annual Percentage Change (AAPC) of employment from initial year to initial year	Table
113_median_income	Base year median income suitability	Table
114_distance_to_freeway	Base year Distance to Freeway exits suitability	Table
115_distance_to_transit	Base year walkable distance to transit stops suitability	Raster
116_VCratio	Base year D/C ratio suitability	Table
117_CarbonEmission	Base year carbon emission suitability	Table
118_slope	Slope suitability	Table
119_distance_to_employment	Base year distance to employment land suitability	Raster
120_distance_to_residential	Base year distance to residential land suitability	Raster
121_distance_to_vacant	Base year distance to vacant land suitability	Raster
01_ilu	Initial year land use	Raster
02_blu	Base year land use	Raster
Residential suitability image	Base year residential land use suitability score image	Raster
Employment suitability image	Base year employment land use suitability score image	Raster
Institution suitability image	Base year institution land use suitability image	Raster
Undeveloped suitability image	Base year undeveloped land use suitability score image	Raster
Others suitability image	Base year other land use suitability score image	Raster

Table A1-9 List of Outputs from the Scenario Development

Name	Field	Description	Type
TargetYearTAZ	TAZ	TAZ name, the format is TAZ_TAZ Number, i.e. TAZ_151	String
	TAZ_N	TAZ number	Integer
	TAZ_Order	The field to link TAZs in ArcGIS and TAZs in VISUM	Integer
	POP	Target year population	Integer
	HH	Target year household	Integer
	EMP	Target year employment (employee)	Integer
	HI	Target year high school enrollment	Integer
	UN	Target year university enrollment	Integer
	AREA_TYPE	CBD&Urban or suburban or rural	Integer
	GEOCODE_Base_1	Base year residential area (ft ²)	Double
	GEOCODE_Base_2	Base year employment area (ft ²)	Double
	GEOCODE_Base_3	Base year institutional area (ft ²)	Double
	GEOCODE_Base_4	Base year undeveloped area (ft ²)	Double
	GEOCODE_Base_5	Base year other area (ft ²)	Double
	GEOCODE_1	Target year residential area (ft ²)	Double
	GEOCODE_2	Target year employment area (ft ²)	Double
	GEOCODE_3	Target year institutional area (ft ²)	Double
	GEOCODE_4	Target year undeveloped area (ft ²)	Double
	GEOCODE_5	Target year other area (ft ²)	Double
Landuse_Target	GEOCODE	Land use type, 1=residential, 2=employment, 3=institutional, 4=undeveloped, 5=other	Integer
	Shape_Area	Area (ft ²)	Double

1) Inputs and Outputs for the Regional Level Analysis

Inputs for the regional level analysis include the *Household Fraction and Trip Rate*, *Employment Fraction*, *VISUM File* for travel demand forecasting, *Age Distribution*, *Fuel Supply*, *Fuel Formulation*, *Meteorology*, *County and State* for emission estimation. Fields and data type of those input files are listed in Table A1-10, and details about a VISUM file are provided in Table A1-11. Output files for the regional level analysis are listed in Table A1-12.

Table A1-10 Inputs for the Regional Level Analysis

Name	Field	Description	Type
Household Faction and Trip Rate	HH_ID	Household ID	Integer
	Fraction	The portion of households whose ID=HH_ID to the total number of households	Double
	HBO_Rate	The trip generation rate by trip purpose HBO	Double
	HBW_Rate	The trip generation rate by trip purpose HBW	Double
	HBSC_Rate	The trip generation rate by trip purpose HBSC	Double
	HBU_Rate	The trip generation rate by trip purpose HBU	Double
Employment Faction	TAZ_N	TAZ number	Integer
	LEMP	The rate of low trip rate employment in TAZ_N	Double
	MEMP	The rate of medium trip rate employment in TAZ_N	Double
	HEMP	The rate of high trip rate employment in TAZ_N	Double
VISUM File	See details in Table 4-7	See details in Table 4-7	See details in Table 4-7
Age Distribution	SourceType	11=Motorcycle; 21= Passenger Car; 31= Passenger Truck; 32=Light Commercial Truck; 41=Intercity Bus; 42=Transit Bus; 43=School Bus; 51=Refuse Truck; 52=Single Unit Short-haul Truck; 53=Single Unit Long-haul Truck; 54 Motor Home; 61=Combination Short-haul Truck; 62=Combination Long-haul Truck	Integer
	YearID	Calendar year	Integer
	AgeID	Age	Integer
	AgeFraction	Distribution of AgeIDs	Double
	countyID	County	Integer
Fuel Supply	fuelYearID	Fuel year	Integer
	monthGroupID	Fuel month	Integer

Name	Field	Description	Type
	fuelFormulationID	Fuel formulation identification number. Must be greater than 100 and less than 25000	Integer
	marketShare	Market share	Double
	marketShareCV	Null	Double
Fuel Formulation	fuelFormulationID	Fuel formulation identification number. Must be greater than 100 and less than 25000	Integer
	fuelSubtypeID	Fuel Sub-type coding	Integer
	RVP	Reid vapor pressure in psi	Integer
	sulfurLevel	Fuel sulfur level in ppm Sulfur	Integer
	ETOHVolume	Ethanol Volume (% vol)	Double
	MTBEVolume	MTBE Volume (% vol)	Double
	ETBEVolume	ETBE Volume (% vol)	Double
	TAMEVolume	TAME Volume (% vol)	Double
	aromaticContent	Aromatic content (% wt)	Double
	olefinContent	Olefin content (% wt)	Double
	benzeneContent	Benzene content (% wt)	Double
	e200	Lower volatility percentage (%)	Integer
	e300	Upper volatility percentage (%)	Integer
	volToWtPercentOxy	Constant based on oxygenate type	Double
	BioDieselEsterVolume	BioDiesel Ester Volume (%)	Double
	CetaneIndex	NULL	NULL
	PAHContent	NULL	NULL
	T50	Temperature (F) where 50% of the fuel is vapor	Integer
	T90	Temperature (F) where 90% of the fuel is vapor	Integer
Meteorology	monthID	Calendar month	Integer
	zoneID	Zone	Integer
	hourID	Hour	Integer
	temperature	Temperature	Double
	relHumidity	Humidity	Double
County and State	State Name	State Name	Integer
	County Name	County Name	Integer

Table A1-11 Description of a VISUM File

Data	Description	Format
TAZ	A shapefile of traffic analysis zones. Attributes which need to be created by users include TAZ_Num, HH_ID_1, HH_ID_2, HH_ID_3, HH_ID_4, HH, EMP, LEMP, MEMP, HEMP, HIEN, and UNEN.	Polygon
Road Network	A shapefile of street center lines. Attributes which need to be specified by users are Cap (capacity), V0 (free flow speed).	Line
Transit Network	A shapefile of transit lines and transit stops.	
Matrixes	Matrixes store number of trips, and travel times between TAZs	Table
Four Step Model Parameters	<p><i>a. Trip Generation</i></p> <p>The trip generation in VISUM is implemented by connecting the socioeconomic data to its corresponding trip production and attraction rates. Trip production rates and attraction rates including $NHBPRATE_{at(i)}^{mx}$, $LEMPRATE_i$, $MEMPRATE_i$, $HEMPRATE_i$, $HHRATE_i$, $URATE_i$, and $HRATE_i$ (in Eq. 3.17 and Eq. 3.18 in Section 3.3) are required.</p> <p><i>b. Trip Distribution</i></p> <p>The trip distribution in VISUM is implemented by assigning an appropriate distribution model in VISUM. An iterative procedure is employed to refine trip interchange estimates until convergence is met, i.e., the estimated zonal trip ends attracted to each zone closely match the desired zonal trip attractions calculated in the trip generation phase. To implement this, the parameter α in Eq. 3.19 needs to be set up, and k_{ij} is automatically estimated by balancing the trip generations and attractions.</p> <p><i>c. Mode Split</i></p> <p>The trip mode choice in VISUM is implemented by assigning an appropriate mode split model. The mode split model adapts the Logit utility function with parameters of β in Eq. 3.20.</p> <p><i>d. Trip Assignment</i></p> <p>The equilibrium traffic assignment utilizes the Wardrop's first principle and breaks the OD demand matrix into the proportions per iteration step. The traffic assignment procedure is an iterative step where a proportion of traffic will be assigned in each iteration until convergence criteria meets.</p>	N/A

Table A1-12 Outputs from the Regional Level Analysis

Name	Field	Description	Type
TargetYearTAZ	TAZ	TAZ name, the format is TAZ_TAZ Number, i.e. TAZ_151	String
	TAZ_N	TAZ number	Integer
	TAZ_Order	The key field to link TAZs in ArcGIS and TAZs in VISUM	Integer
	POP	Target year population	Integer
	HH	Target year household	Integer
	EMP	Target year employment	Integer
	HI	Target year high school enrollment	Integer
	UN	Target year university enrollment	Integer
	AREA_TYPE	1=CBD&Urban; 2= suburban; 3= rural	Integer
	GEOCODE_Base_1	Base year residential area (ft ²)	Double
	GEOCODE_Base_2	Base year employment area (ft ²)	Double
	GEOCODE_Base_3	Base year institutional area (ft ²)	Double
	GEOCODE_Base_4	Base year undeveloped area (ft ²)	Double
	GEOCODE_Base_5	Base year other area (ft ²)	Double
	GEOCODE_1	Target year residential area (ft ²)	Double
	GEOCODE_2	Target year employment area (ft ²)	Double
	GEOCODE_3	Target year institutional area (ft ²)	Double
	GEOCODE_4	Target year undeveloped area (ft ²)	Double
	GEOCODE_5	Target year other area (ft ²)	Double
	GEOCODE	Land use type, 1=residential, 2=employment, 3=institutional, 4=undeveloped, 5=other	Double
	Shape_Area	Area (ft ²)	Double
RoadNetwork	Volume_Base/ Volume_Target	Base/ Target year volume (veh)	Double
	Speed_Base/ Speed_Target	Base/ Target year speed (mile/h)	Double
	DCRatio_Base/ DCRatio_Target	Base/ Target year demand/capacity ratio (%)	Double
	Delay_Base/ Delay_Target	Base/ Target year delay (min/veh/mile)	Double
	QueueLength_Base/ QueueLength_Target	Base/ Target year queue length (veh/mile)	Double
	CO2_Equivalent_Base/ CO2_Equivalent_Target	Base/ Target year CO2 equivalent (kg)	Double

Name	Field	Description	Type
	Energy_Consumption_Base/ Energy_Consumption _Target	Base/ Target year energy consumption (kJ)	Double
Vehicle Composition	LINKID	Link number	Integer
	Car fraction	The fraction of cars to the total number of vehicles on a link	Double

2) Inputs and Outputs for the Project Level Analysis

Details about inputs and outputs for the project level analysis are listed in Table A1-13 and Table A1-14, respectively.

Table A1-13 Inputs for the Project Level Analysis

Name	Sheet	Field	Description	Type
Microscopic Simulation Links	Sheet1	GISLinkID	Link ID in RoadNetwork	Integer
	Sheet1	MicroscopicLinkID	Link ID in microscopic simulation	Integer
	Sheet2	GISLinkID	Link ID in RoadNetwork	Integer
	Sheet2	RoadType	(1=Off-Network; 2=Rural Restricted Access; 3=Rural Unrestricted Access; 4=Urban Restricted Access; 5=Urban Unrestricted Access)	Integer
	Sheet2	LinkLength	Link length (mile)	Double
	Sheet2	LinkGrade	Link grade	Double
Microscopic Simulation Results VISUM File	Sheet1	MicroscopicLinkID	Link ID in microscopic simulation	Integer
	Sheet1	time (sim sec)	Time stamp	Integer
	Sheet1	Car #	Car number	Integer
	Sheet1	Car v	Car speed (mile/sec)	Double
	Sheet1	Car a	Car acceleration (mile/sec ²)	Double
	Sheet1	Truck #	Truck number	Integer
	Sheet1	Truck v	Truck speed (mile/sec)	Double
	Sheet1	Truck a	Truck acceleration (mile/sec ²)	Double
	Sheet2	MicroscopicLinkID	Link ID in microscopic simulation	Double
	Sheet2	AverageSpeed	Average speed (mile/h)	Double
	Sheet2	Delay	Delay (min/vehile)	Double
	Sheet2	QueueLength	Queue length (veh)	Double

Table A1-14 Outputs from the Project Level Analysis

Name	Field	Description	Type
	TAZ	TAZ name, the format is TAZ_TAZ Number, i.e. TAZ_151	String
	TAZ_N	TAZ number	Integer
	TAZ_Order	The field to link TAZs in ArcGIS and TAZs in VISUM	Integer
	POP	Target year population	Integer
	HH	Target year household	Integer
	EMP	Target year employment	Integer
	HI	Target year high school enrollment	Integer
	UN	Target year university enrollment	Integer
	AREA_TYPE	1=CBD&Urban; 2= suburban; 3= rural	Integer
	GEOCODE_Base_1	Base year residential area (ft ²)	Double
	GEOCODE_Base_2	Base year employment area (ft ²)	Double
	GEOCODE_Base_3	Base year institutional area (ft ²)	Double
	GEOCODE_Base_4	Base year undeveloped area (ft ²)	Double
	GEOCODE_Base_5	Base year other area (ft ²)	Double
	GEOCODE_1	Target year residential area (ft ²)	Double
	GEOCODE_2	Target year employment area (ft ²)	Double
	GEOCODE_3	Target year institutional area (ft ²)	Double
	GEOCODE_4	Target year undeveloped area (ft ²)	Double
	GEOCODE_5	Target year other area (ft ²)	Double
Landuse_Target	GEOCODE	Land use type, 1=residential, 2=employment, 3=institutional, 4=undeveloped, 5=other	Integer
	Shape_Area	Area (ft ²)	Double
RoadNetwork	CO2_Equivalent_Updated	CO2 equivalent (kg)	Double
	Energy_Consumption_Updated	Energy consumption (kJ)	Double

A I.2 Database In AIR-SUSTAIN

A I.2.1 Database Structure

All model outputs and intermediate data are stored in five (5) MySQL databases and an ArcGIS Geodatabase. The five MySQL databases are automatically generated for each AIR-SUSTAIN scenario. They are AIR-SUSTAIN scenario database, regional MOVES input database, regional MOVES output database, project-level MOVES input database, and project-level MOVES output database. The fields and data sources of data tables in the MySQL databases are listed in Table A2-1.

Table A2-1 Tables and fields of AIR-SUSTAIN Scenario Database

Table Name	Fields	Data Source
projectInfo	scenarioID	Specified by the user in the AIR-SUSTAIN GUI
	baseYear	Specified by the user in the AIR
	targetYear	Specified by the user in the AIR
	analyst	Specified by the user in the AIR
	date	Specified by the user in the AIR
	projectDir	Specified by the user in the AIR
	idrisiDir	Specified by the user in the AIR
	movesDir	Specified by the user in the AIR
	projectDescription	Specified by the user in the AIR
Increase Percentage	PopIncrease	Specified by the user in the AIR
	EmplIncrease	Specified by the user in the AIR
PopulationGrowth	TAZ	Imported from Population Change
	Population	Imported from Population Change
EmploymentGrowth	TAZ	Imported from Employment Change
	Employment	Imported from Employment Change
UniversityEnrollment	TAZ	Imported from University Enrollment Change
	Enrollment	Imported from University Enrollment Change
	Name	Imported from University Enrollment Change
HighSchoolEnrollment	TAZ	Imported from High School Enrollment Change
	Enrollment	Imported from High School Enrollment Change
	Name	Imported from High School Enrollment Change
HouseholdTripRate	TAZ	Imported from Household Fraction and Trip Rate
	Fraction	Imported from Household Fraction and Trip Rate

Table Name	Fields	Data Source
	HBO	Imported from Household Fraction and Trip Rate
	HBW	Imported from Household Fraction and Trip Rate
	HBSC	Imported from Household Fraction and Trip Rate
	HBU	Imported from Household Fraction and Trip Rate
EmploymentTripRate	TAZ	Imported from Employment Fraction
	LowRate	Imported from Employment Fraction
	MediumRate	Imported from Employment Fraction
	HighRate	Imported from Employment Fraction
BaseYearResults	LinkID	Output from TDF
	Volume	Output from TDF
	FunctionClass	Output from TDF
	AvgSpeed	Output from TDF
	DCRatio	Output from TDF
	Delay	Output from TDF
	QueueLength	Output from TDF
	TruckFraction	Output from TDF
	CO2 Equivalent	Output from emission estimation
	EnergyConsumption	Output from emission estimation
BaseYearResults	LinkID	Outputted from TDF
	Volume	Outputted from TDF
	FunctionClass	Outputted from TDF (1=Off-Network; 2=Rural Restricted Access; 3=Rural Unrestricted Access; 4=Urban Restricted Access; 5=Urban Unrestricted Access)
	AvgSpeed	Output from TDF
	DCRatio	Output from TDF
	Delay	Output from TDF
	QueueLength	Output from TDF
	TruckFraction	Output from TDF
	CO2 Equivalent	Output from emission estimation
	EnergyConsumption	Output from emission estimation
IDIRSIInfo	InitialYear	Specified by the user in AIR-SUSTAIN GUI

Table Name	Fields	Data Source
	Folderpath	Specified by the user in AIR-SUSTAIN GUI

The data tables for the regional and project-level MOVES inputs in the databases are the same. In addition, the data tables of regional and project-level MOVES outputs in the databases are also the same. The data tables and fields of MOVES input database are listed in Table A2-2. The data table and included items of the MOVES output database are illustrated in Table A2-3.

Table A2-2 Tables and Items of the MOVES Input Database

Table Name	Items	Data Source
link	linkID	TDF
	countyID	Specified by the user
	zoneID	MOVES database
	roadTypeID	TDF
	linkLength	TDF based on geometry input
	linkVolume	TDF or microscopic simulation data source
	linkAvgSpeed	TDF or microscopic simulation data source
	linkDescription	N/A
	linkAvgGrade	Calculated by AIR-SUSTAIN based on geometry input
linksource-typehour	linkID	TDF
	sourceTypeID	TDF
	sourceTypeHourFraction	TDF or microscopic simulation data source
opmode-distribution	sourceTypeID	MOVES database
	hourDayID	TDF or micro-simulation data source
	linkID	TDF
	polProcessID	MOVES database
	opModeID	MOVES database
	opModeFraction	Calculated by AIR-SUSTIAN based on traffic input
	opModeFractionCV	Null
	isUserInput	Null
County	countyID	From State and County
	stateID	From State and County
	CountyName	From State and County
	altitude	MOVES database

Table Name	Items	Data Source
	GPAFract	MOVES database
	barometricPressure	MOVES database
	barometricPressureCV	Null
sourcetypeage-distribution	sourceTypeID	MOVES database
	yearID	Specified by user
	ageID	From Age Distribution
	ageFraction	Non-traffic input
state	stateID	From State and County
	stateName	From State and County
	stateAbbr	From State and County
year	yearID	From input base year or target year
	isBaseYear	Calculated by AIR-SUSTAIN based on traffic input
	fuelYearID	From file Fuel Supply
zone	zoneID	MOVES database
	countyID	From State and County
	startAllocFactor	1
	idleAllocFactor	1
	SHPAllocFactor	1
zone-monthhour	monthID	Specified by the user
	zoneID	MOVES database
	hourID	TDF
	temperature	From Meteorology
	temperatureCV	Null
	relHumidity	From Meteorology
	heatIndex	Null
	specificHumidity	Null
	relativeHumidityCV	Null
zoneroadtype	zoneID	MOVES database
	roadTypeID	TDF
	SHOAllocFactor	1
fuel-formulation	fuelFormulationID, fuelSubTypeID, RVP, sulfurLevel, ETOHVolume, MTBEVolume, TAMEVolume, aromaticContnet, olefinContent, benzeneContent, e200, 2300, volToWtPercentOxy, BioDieselEsterVolume, CetaneIndex, PAHContent, T50, T90	From Fuel Formulation
fuelsupply	countyID, fuelYearID, monthGroupID, fuelFormulationID, marketShare, marketShareCV	From Fuel Supply

Table A2-3 Tables and Items of the MOVES Output Database

Table Name	Items	Description
activitytype	activityTypeID, activityType, activityTypeDesc,	This table lists the activity types that can be reported in the movesactivityoutput table and provides their activitytypeid (1= distance traveled; 2=source hours; 3= source hour idling; 4= source hours operating; 5= source hours parked; 6= population; 7= starts).
bundletracking	hostType, MOVESRunID, loopableClassName, workerVersion, workerComputerID, workerID, bundleNumber, isCleanUp, iterationID, processID, roadTypeID, linkID, zoneID, countyID, stateID, yearID, monthID, dayID, HourID, executionGranularity	This table contains information about data that is processed by the MOVES master and workers.
movesactivityoutput	MOVESRunID, iterationID, yearID, monthID, dayID, hourID, stateID, countyID, zoneID, linkID, sourceTypeID, fuelTypeID, modelYearID, roadTypeID, SCC	This table provides information on the vehicle activity generated and run.
moveserror	MOVESError, MOVESRunID, yearID, monthID, dayID, hourID, stateID, zoneID, linkID, pollutantID, processID, errorMessage	This table contains any error messages or diagnostic information that might be generated if the MOVES run is unsuccessful.
moveeventlog	EventRecordID, MOVESRunID, EventName, WhenStarted, WhenStoped, Duration	This table stores diagnostic results.
movesoutput	MOVESRunID, iterationID, yearID, monthID, dayID, hourID, stateID, countyID, zoneID, linkID, pollutantID, processID, sourceTypeID, fuelTypeID, modelYearID, roadTypeID, SCC	This table contains the inventory emission results of the run disaggregated by parameters, such as Year, Month, etc.
movesrun	MOVESRunID, outputTimePeriod, timeUnits, distanceUnits, massUnits, energyUnits, runSpecFileName, runSpecDescription, runSpecFileDateTime, runDataTime, scale, minutesDuration, defaultDatabaseUsed, masterVersionDate, masterComputerID, masterIDNumber, domain, domainCountyID, domainCountyName, domainDatabaseServer, domainDatabaseName, expectedDONEFiles, retrivedDONEFiles	The table contains information about the date and time of the run, information about the run specifications, and the name of the units in which MOVES outputs are represented.
movestableused	MOVESRunID, databaseServer, databaseName, tableName, dataFileSize, dataFileModificationDate, tableUseSequence	This table stores a list of the tables used when executing MOVES.
movesworkerused	MOVESRunID, wokerverversion, wokerComputerID, workerrID, bundleCount, failedBundleCount	This table contains information as to which copy of the MOVES Worker Program processed portions of the run.
rateperdistance	MOVESScenarioID, MOVESRunID, yearID, monthID, dayID, hourID, linkID, pollutantID, processID, sourceTypeID, SCC, fuelTypeID,	This table stores emissions as rates per distance with the units

	modelYearID, riadTypeID, avgSpeedBinID, temperature, relHumidity, ratePerDistance	depending on those selected on run specification.
rateperprofile	MOVESScenarioID, MOVESRunID, temperatureProfile, yearID, dayID, hourID, pollutantID, processID, sourceTypeID, SCC, fuelTypeID, modelYearID, temperature, rateperVehicle	This table stores vapor venting emissions from parked vehicles as rates per vehicle.
ratepervehicle	MOVESScenarioID, MOVESRunID, yearID, dayID, hourID, pollutantID, processID, sourceTypeID, SCC, fuelTypeID, modelYearID, temperature, rateperVehicle	This table stores vapor venting emissions from starts and extended idle, and some evaporative emissions from parked vehicle as rates per vehicle.

All feature classes, including TAZ, TargetYearTAZ, RoadNetwork, Incentiveboundary, Hotspots, and Landuse_Target, are stored in a Geodatabase. The feature class names and items of each feature class are illustrated in Table A2-4.

Table A2-4 Geodatabase

Feature class	Item	Source
TAZ	FID	Generated by ArcGIS automatically
	TAZ	Specified by the user
	TAZ_N	Specified by the user
	TAZ_Order	The key to link TAZs in feature class and TAZs in VISUM
	POP	Specified by the user
	HH	Specified by the user
	EMP	Specified by the user
	HI	Specified by the user
	UN	Specified by the user
	AREA_TYPE	Specified by the user
	GEOCODE_1	Specified by the user
	GEOCODE_2	Specified by the user
	GEOCODE_3	Specified by the user
	GEOCODE_4	Specified by the user
	GEOCODE_5	Specified by the user
Incentiveboundary	FID	Generated by ArcGIS automatically
	Shape_Area	Generated by ArcGIS after the user specify the boundary
TargetYearTAZ	FID	Generated by ArcGIS automatically
	TAZ	Specified by the user

Feature class	Item	Source
	TAZ_N	Specified by the user
	TAZ_Order	The key to link TAZs in feature class and VISUM
	POP	From linkage model
	HH	From linkage model
	EMP	From linkage model
	HI	From linkage model
	UN	From linkage model
	AREA_TYPE	From linkage model
	GEOCODE_1	From land use projection
	GEOCODE_2	From land use projection
	GEOCODE_3	From land use projection
	GEOCODE_4	From land use projection
	GEOCODE_5	From land use projection
Landuse_Target	FID	Generated by ArcGIS automatically
	GEOCODE	From survey data
	Shape_Area	From survey data
RoadNetwork	FID	Generated by ArcGIS automatically
	NO	Specified by users
	Length	Specified by the user
	Volume_Base	Output from TDF
	Speed_Base	Output from TDF
	DCRatio_Base	Output from TDF
	Delay_Base	Output from TDF
	QueueLength_Base	Output from TDF
	CO2_Equivalent_Base	Output from emission estimation
	Energy_Consumption_Base	Output from emission estimation
	Volume_Target	Output from TDF
	Speed_Target	Output from TDF
	DCRatio_Target	Output from TDF
	Delay_Target	Output from TDF
	QueueLength_Target	Output from TDF
	CO2_Equivalent_Target	Output from emission estimation
	Energy_Consumption_Target	Output from emission estimation
	CO2_Equivalent_Update	Output from TDF

Feature class	Item	Source
	Energy_Consumption_Update	Output from TDF
Hotspots	FID	Generated in ArGIS
	NO	From RoadNetwork
	Length	From RoadNetwork
	Volume_Base	From RoadNetwork
	Speed_Base	From RoadNetwork
	DCRatio_Base	From RoadNetwork
	Delay_Base	From RoadNetwork
	QueueLength_Base	From RoadNetwork
	CO2_Equivalent_Base	From RoadNetwork
	Energy_Consumption_Base	From RoadNetwork
	Volume_Target	From RoadNetwork
	Speed_Target	From RoadNetwork
	DCRatio_Target	From RoadNetwork
	Delay_Target	From RoadNetwork
	QueueLength_Target	From RoadNetwork
	CO2_Equivalent_Target	From RoadNetwork
	Energy_Consumption_Target	From RoadNetwork

A I.2.2 MOVES Emission Lookup Tables

The MOVES model incorporates similar regression based equations for mean and variance model for braking/deceleration and uses similar approach of heavy-duty vehicles (U.S. EPA, 2012). The vehicle activity mix is determined by the emission source type, age group, road type and operating mode distribution. The lookup tables for emission source type, road type, and vehicle age distribution are presented in Table A2-5 to A2-8.

Emission Source Type

Table A2-5 The MOVES Source Types

Source Type ID	Source Type Name	HPMS Vehicle Type ID	HPMS Vehicle Type Name
11	Motorcycle	10	Motorcycles
21	Passenger Car	20	Passenger Cars
31	Passenger Truck	30	Other 2 axle-4 tire vehicles
32	Light Commercial Truck	30	Other 2 axle-4 tire vehicles
41	Intercity Bus	40	Buses
42	Transit Bus	40	Buses
43	School Bus	40	Buses
51	Refuse Truck	50	Single Unit Trucks
52	Single Unit Short-haul Truck	50	Single Unit Trucks
53	Single Unit Long-haul Truck	50	Single Unit Trucks
54	Motor Home	50	Single Unit Trucks
61	Combination Short-haul Truck	60	Combination Trucks
62	Combination Long-haul Truck	60	Combination Trucks

Road Type

Table A2-6 The MOVES Road Type

Road Type ID	Road Type Description
1	Off-Network
2	Rural Restricted Access
3	Rural Unrestricted Access
4	Urban Restricted Access
5	Urban Unrestricted Access

Vehicle Age Distribution

Table A2-7 MOVES Age Distribution Categories

ageID	ageCategoryName	ageID	ageCategoryName
0	new	21	21 years old
1	one year old	22	22 years old
2	two years old	23	23 years old
3	three years old	24	24 years old
4	four years old	25	25 years old
5	five years old	26	26 years old
6	six years old	27	27 years old
7	seven years old	28	28 years old
8	eight years old	29	29 years old
9	nine years old	30	30 or more years old
10	ten years old		
11	eleven years old		
12	twelve years old		
13	13 years old		
14	14 years old		
15	15 years old		
16	16 years old		
17	17 years old		
18	18 years old		
19	19 years old		
20	20 years old		

Operating Mode

Table A2-8 MOVES Operating Modes

opModel D	opModeName	VSP Lower	VSP Upper	Speed Lower	Speed Upper
0	Braking	0	0	0	0
1	Idling	0	0	-1	1
11	Low Speed Coasting; VSP < 0; 1 ≤ Speed < 25	0	0	1	25

opModel D	opModeName	VSP Lower	VSP Upper	Speed Lower	Speed Upper
12	Cruise/Acceleration; 0<=VSP< 3; 1<= Speed<25	0	3	1	25
13	Cruise/Acceleration; 3<=VSP< 6; 1<=Speed<25	3	6	1	25
14	Cruise/Acceleration; 6<=VSP< 9; 1<=Speed<25	6	9	1	25
15	Cruise/Acceleration; 9<=VSP<12; 1<=Speed<25	9	12	1	25
16	Cruise/Acceleration; 12<=VSP; 1<=Speed<25	12	0	1	25
21	Moderate Speed Coasting; VSP< 0; 25<=Speed<50	0	0	25	50
22	Cruise/Acceleration; 0<=VSP< 3; 25<=Speed<50	0	3	25	50
23	Cruise/Acceleration; 3<=VSP< 6; 25<=Speed<50	3	6	25	50
24	Cruise/Acceleration; 6<=VSP< 9; 25<=Speed<50	6	9	25	50
25	Cruise/Acceleration; 9<=VSP<12; 25<=Speed<50	9	12	25	50
26	Cruise/Acceleration; 12<=VSP; 25<=Speed<50	12	0	25	50
27	Cruise/Acceleration; 12<=VSP<18; 25<=Speed<50	12	18	25	50
28	Cruise/Acceleration; 18<=VSP<24; 25<=Speed<50	18	24	25	50
29	Cruise/Acceleration; 24<=VSP<30; 25<=Speed<50	24	30	25	50
30	Cruise/Acceleration; 30<=VSP; 25<=Speed<50	30	0	25	50
33	Cruise/Acceleration; VSP< 6; 50<=Speed	0	6	50	0
35	Cruise/Acceleration; 6<=VSP<12; 50<=Speed	6	12	50	0
36	Cruise/Acceleration; 12 <= VSP; 50<=Speed	12	0	50	0
37	Cruise/Acceleration; 12<=VSP<18; 50<=Speed	12	18	50	0
38	Cruise/Acceleration; 18<=VSP<24; 50<=Speed	18	24	50	0

opModel D	opModeName	VSP Lower	VSP Upper	Speed Lower	Speed Upper
39	Cruise/Acceleration; 24<=VSP<30; 50<=Speed	24	30	50	0
40	Cruise/Acceleration; 30<=VSP; 50<=Speed	30	0	50	0
100	Starting (Used for all starts)	0	0	0	0
101	Soak Time < 6 minutes	0	0	0	0
102	6 minutes <= Soak Time < 30 minutes	0	0	0	0
103	30 minutes <= Soak Time < 60 minutes	0	0	0	0
104	60 minutes <= Soak Time < 90 minutes	0	0	0	0
105	90 minutes <= Soak Time < 120 minutes	0	0	0	0
106	120 minutes <= Soak Time < 360 minutes	0	0	0	0
107	360 minutes <= Soak Time < 720 minutes	0	0	0	0
108	720 minutes <= Soak Time	0	0	0	0
150	Hot Soaking	0	0	0	0
151	Cold Soaking	0	0	0	0
200	Extended Idling	0	0	0	0
201	Hotelling Diesel Aux	0	0	0	0
202	Hotelling Fuel Operated Heater	0	0	0	0
203	Hotelling Battery AC	0	0	0	0
204	Hotelling APU Off	0	0	0	0
300	All Running	0	0	0	0
301	running; speed < 2.5mph	0	0	0	2.5
302	running; 2.5mph <= speed < 7.5mph	0	0	2.5	7.5
303	running; 7.5mph <= speed < 12.5mph	0	0	7.5	12.5
304	running; 12.5mph <= speed < 17.5mph	0	0	12.5	17.5
305	running; 17.5mph <= speed <22.5mph	0	0	17.5	22.5
306	running; 22.5mph <= speed < 27.5mph	0	0	22.5	27.5

opModel D	opModeName	VSP Lower	VSP Upper	Speed Lower	Speed Upper
307	running; 27.5mph <= speed < 32.5mph	0	0	27.5	32.5
308	running; 32.5mph <= speed < 37.5mph	0	0	32.5	37.5
309	running; 37.5mph <= speed < 42.5mph	0	0	37.5	42.5
310	running; 42.5mph <= speed < 47.5mph	0	0	42.5	47.5
311	running; 47.5mph <= speed < 52.5mph	0	0	47.5	52.5
312	running; 52.5mph <= speed < 57.5mph	0	0	52.5	57.5
313	running; 57.5mph <= speed < 62.5mph	0	0	57.5	62.5
314	running; 62.5mph <= speed < 67.5mph	0	0	62.5	67.5
315	running; 67.5mph <= speed < 72.5mph	0	0	67.5	72.5
316	running; 72.5mph <= speed	0	0	72.5	0
400	tirewear; idle	0	0	0	0
401	tirewear; speed < 2.5mph	0	0	0	2.5
402	tirewear; 2.5mph <= speed < 7.5mph	0	0	2.5	7.5
403	tirewear; 7.5mph <= speed < 12.5mph	0	0	7.5	12.5
404	tirewear; 12.5mph <= speed < 17.5mph	0	0	12.5	17.5
405	tirewear; 17.5mph <= speed < 22.5mph	0	0	17.5	22.5
406	tirewear; 22.5mph <= speed < 27.5mph	0	0	22.5	27.5
407	tirewear; 27.5mph <= speed < 32.5mph	0	0	27.5	32.5
408	tirewear; 32.5mph <= speed < 37.5mph	0	0	32.5	37.5
409	tirewear; 37.5mph <= speed < 42.5mph	0	0	37.5	42.5
410	tirewear; 42.5mph <= speed < 47.5mph	0	0	42.5	47.5

opModel D	opModeName	VSP Lower	VSP Upper	Speed Lower	Speed Upper
411	tirewear; 47.5mph <= speed < 52.5mph	0	0	47.5	52.5
412	tirewear; 52.5mph <= speed < 57.5mph	0	0	52.5	57.5
413	tirewear; 57.5mph <= speed < 62.5mph	0	0	57.5	62.5
414	tirewear; 62.5mph <= speed < 67.5mph	0	0	62.5	67.5
415	tirewear; 67.5mph <= speed < 72.5mph	0	0	67.5	72.5
416	tirewear; 72.5mph <= speed	0	0	72.5	0
500	Existing	0	0	0	0
501	brakewear; stopped	0	0	0	0

A I.3 Transportation Analysis Examples Using the AIR-SUSTAIN tool

To evaluating the three competing scenarios for Cincinnati metropolitan area, a 15% increase of population and employment is assumed to occur from the base year 2010 to the target year 2030. All increase of population and employment is allocated and distributed around the center(s). The process for a scenario analysis is taken in Steps 1 through 18, as described below. Finally the analysis results of those three scenarios are compared at Step 19.

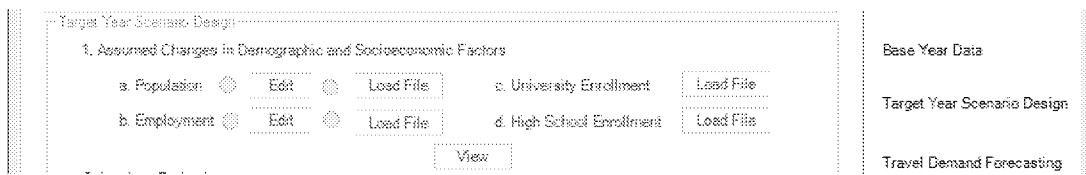
- Step 1:** Create a new scenario by clicking the **Scenario** button followed by clicking **New Scenario** button on the menu bar, and then, input the **Scenario Name** (e.g. “Example”) and other required information (as shown in Figure A3-1) in the **New Scenario** tab. Then, click on the **Save Scenario** button to save scenario files in the specified scenario folder, and create the AIR-SUSTAIN database in MySQL and ArcGIS. Then, go to step 2.
- Step 2:** Select the **Base Year** first, or the **Target Year** in the **Modeling Year** panel if the Base Year data is already created.
- Step 3:** Import three feature classes: *TAZ*, *RoadNetwork*, and *Incentiveboundary* in the **Base Year Data** panel. The data import panel and the sample feature classes are shown in Figure 3.44. If in Step 2, the **Base Year** is selected, go to step 7 to perform regional level analysis; if the **Target Year** is checked, go to step 4.
- Step 4:** Define the assumed **Population Change**, **Employment Change**, **University Enrollment Change** and **High School Enrollment Change** in **Assumed Changes in Demographic and Socioeconomic Factors** panel (as shown in Figure A3-2). *Population Change* and *Employment Change* can be specified within and without incentive boundaries separately. They can also be specified for individual TAZs and imported from excel files as shown in Tables A3-1. Then, go to step 5.

Base Year Data

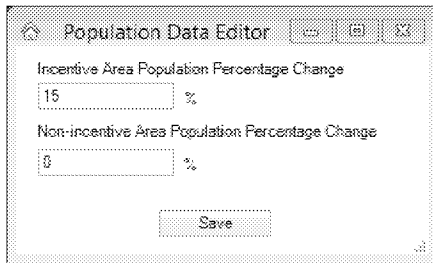
Please select the data type:

Imported Base Data:
TAZ
RoadNetwork
Incentiveboundary

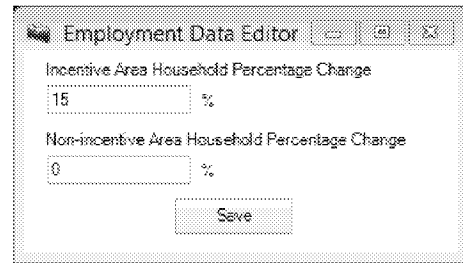
Figure A3-1 Import Base Year Data in Example



(A)



(B)



(C)

Figure A3-2 Program interface for A) importing the Base Year data; B) assigning population change; and C) assigning employment changes at TAZ levels.

Table A3-1 Sample of Population Change

TAZ	Population
330	156
338	191
318	268
249	274
261	383
336	822
337	1249
349	3571
208	7980
332	36784

Step 5: Specify the **Initial Year**, i.e. 2000, and load *Land Use Inputs*, and then project the target year land use by clicking the **Run** button on the **Land Use Projection** panel. The target year land use (shown as Figure A3-3) can be visualized in ArcGIS by clicking **View Results** in the **Land Use Projection** panel. Go to Step 6.

Step 6: Set up the **Maximum Population Density** in the incentive area, i.e 15000 (person/mile²), then generate target year demographic and socioeconomic data by the linkage model based on base year data and assumed demographic and socioeconomic changes. Results can be viewed by the user by selecting the corresponding data type and displaying it (as shown in Figure A3-4). Then, go to Step 7.

Step 7: Select a *TDF Model* (only VISUM is supported by the current version of AIR-

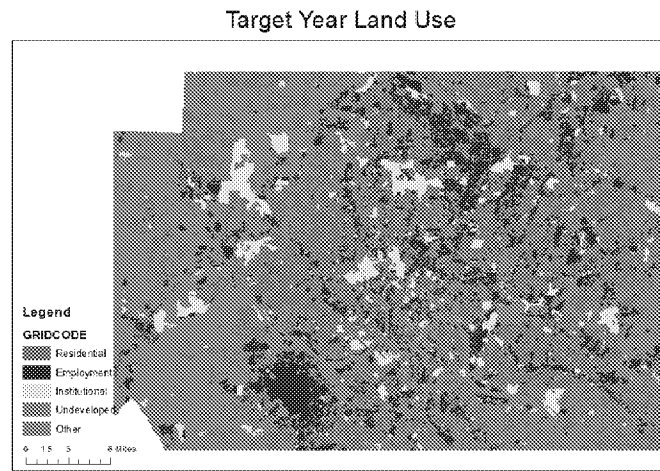


Figure A3-3 Target Year Land Use in Example



Figure A3-4 Target Year Land Use in Example

SUSTAIN) and activate the **Travel Demand Forecasting** panel, then go to step 8.

Step 8: Import a *VISUM File* containing TAZs, road network, and transit network, and four step model parameters (the steps in create a *VISUM file* are briefly introduced by Step 8.1 through 8.6, and details can be found in VISUM user manual (PTV VISUM, 2013)). When it's finished, then go to step 9.

Step 8.1: Set up the travel demand model and travel demand segment in VISUM (shown as Figure A3-5). Go to step 8.2.

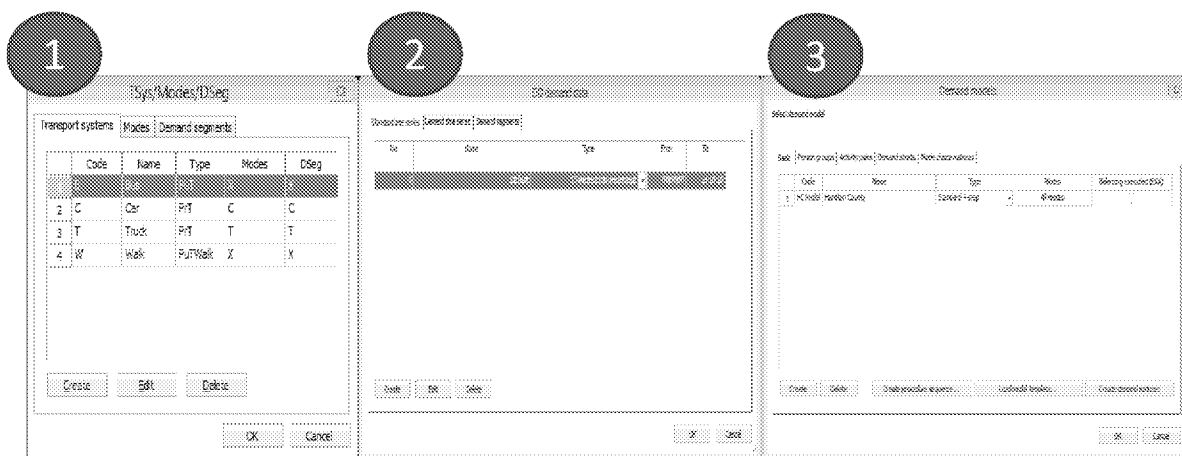


Figure A3-5 VISUM Demand Set Up

Step 8.2: Load TAZ and road network shapefiles, or draw them in VISUM directly (shown as Figure A3-6). For transit lines and stops, the user can only set them up manually in VISUM. Go to step 8.3.

Step 8.3: Generate connectors to connect TAZs with road network, then go to step 8.4.

Step 8.4: Create the required fields in zonelist and linklist in VISUM (see in Table 3.7 in Section 3.2), then go to step 8.5.

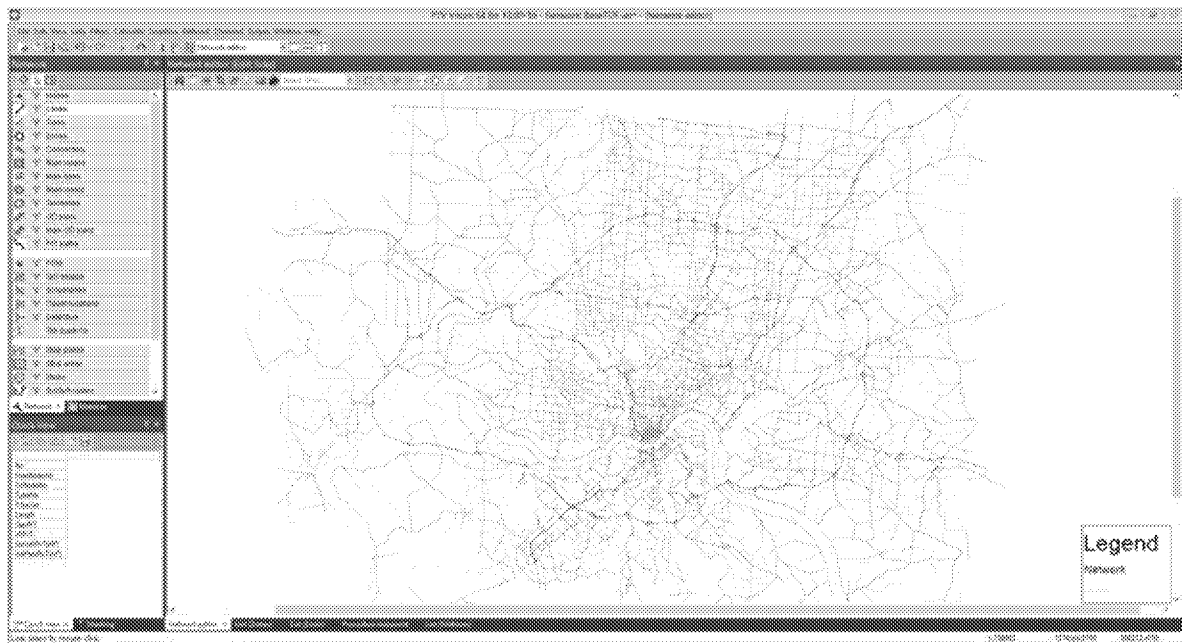


Figure A3-6 Example of road network from the input function

Step 8.5: Build zone matrix (to store demand) and skim matrix (to store impedance) for each traffic mode (shown as Figure A3-7), then go to step 8.5.

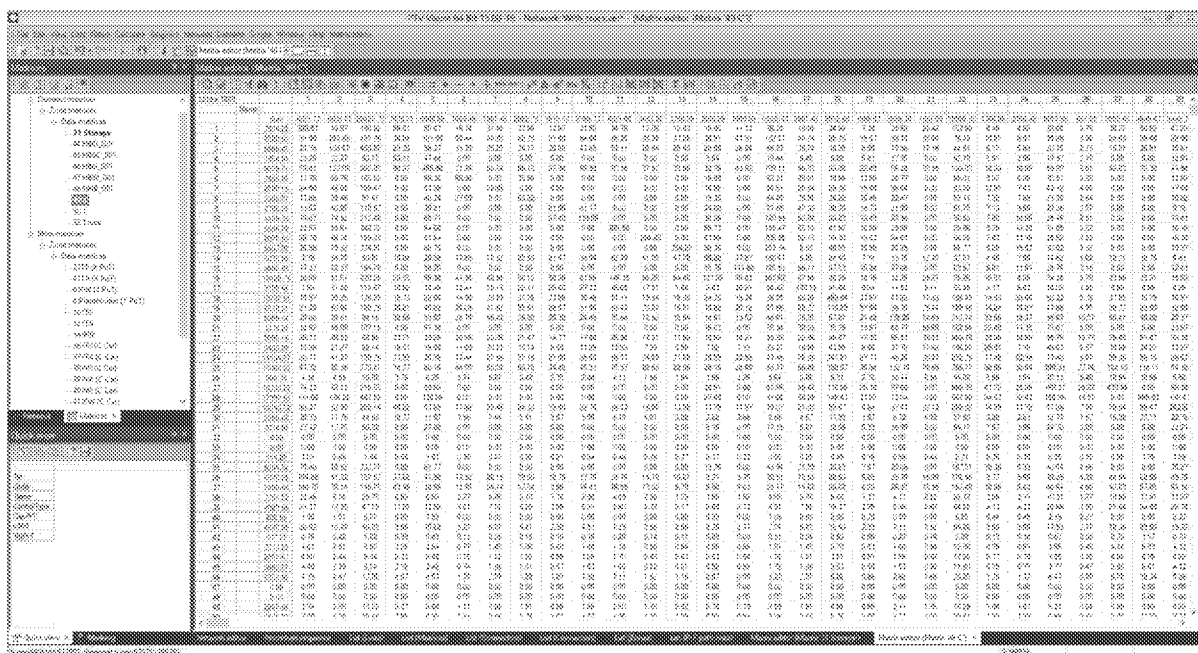


Figure A3-7 Example of VISUM Matrix

Step 8.6: Set up the calculation procedure, and parameters for each step (as shown in Figure A3-8), then stop.

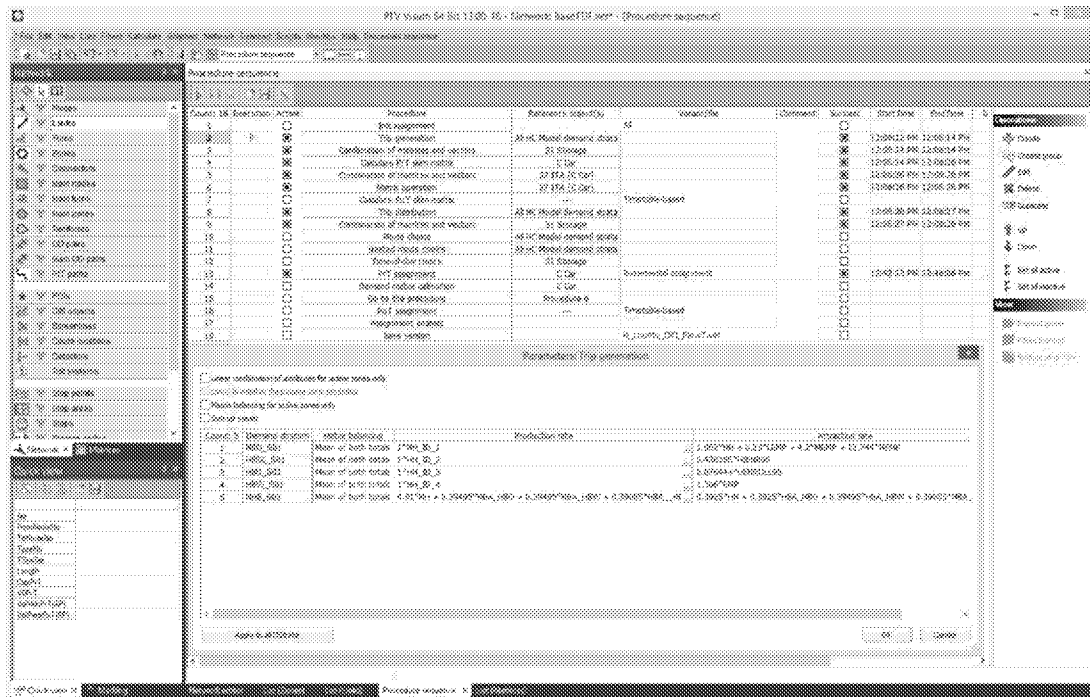


Figure A3-8 VISUM Procedure Set Up

Step 9: Import *Household Fraction and Trip Rate* (Excel file, as shown in Table A3-2), and *Employment Fraction* (Excel file, as shown in Table A3-3), and then, go to Step 10.

Table A3-2 Sample of Household Fraction and Trip Rate

HH_ID	Fraction	HBO	HBSC	HBU	HBW
47	0.014699	0.0122	0.0122	0.0278	0.8797
48	0.009301	0.0122	0.0122	0.0278	0.8797
49	0.004951	0.0122	0.0122	0.0278	0.8797
50	0.002039	0.0122	0.0122	0.0278	0.8797
51	0.002277	0.0011	0.0011	0.0278	0.8797
52	0.197834	0.0011	0.0011	0.0278	0.8797
53	0.030421	0.0011	0.0011	0.0762	1.2348
54	0.007077	0.0011	0.0011	0.0762	1.2348
55	0.007276	0.0049	0.0049	0.0762	1.2348
56	0.008519	0.0049	0.0049	0.0762	1.2348
57	0.003471	0.0049	0.0049	0.0762	1.2348
58	0.019597	0.0049	0.0049	0.0762	1.2348

Table A3-3 Sample of Employment Fraction

TAZ	Low Trip Rate Employment	Medium Trip Rate Employment	High Trip Rate Employment
151	0.18	0.55	0.27
162	0	0.94	0.06
163	0.13	0.37	0.5
156	0.06	0.44	0.5
155	0.03	0.67	0.29
161	0.14	0.79	0.07
159	0.36	0.49	0.16
160	0.01	0.86	0.13
165	0.14	0.5	0.37
164	0.05	0.42	0.53
168	0.15	0.52	0.34
170	0.04	0.66	0.3
171	0.06	0.74	0.2

Step 10: Run VISUM model, and go to Step 11 when VISUM model is finished. TDF outputs contain VISUM from four-step model which can be viewed in VISUM (shown as Figure A3-9), and vehicle composition (Excel file, as shown as Table A3-4) which will be used as an input for emission estimation.

Table A3-4 Sample of Vehicle Composition

LinkID	Car Fraction
3	0.82
4	0.96
6	0.85
8	0.94
10	0.93
12	0.98
14	0.87
16	0.99

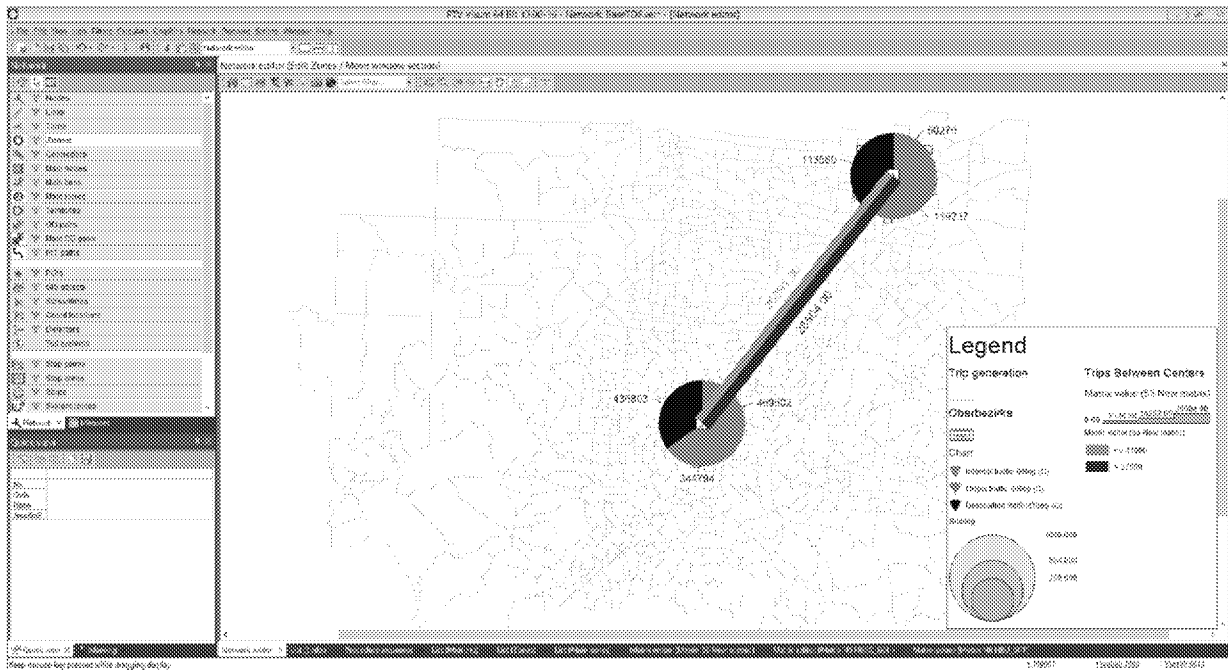


Figure A3-9 Example of Trip Distribution Result from VISUM (Trips between Two Centers)

Step 11: Select the **Emission Estimation Model**. In current version of the AIR-SUSTAIN, only MOVES is currently available. Go to step 12.

Step 12: Import MOVES Inputs including *Age Distribution* (Excel file), *Fuel Formulation* (Excel file), *Fuel Supply* (Excel file), *Meteorology* (Excel file), and *State and County* (Excel file). Samples of those files are shown in Tables A3-5 through A3-9. And then, go to step 13.

Table A3-5 Sample of Age Distribution

sourceTypeID	yearID	ageID	ageFraction
21	2000	0	0.0798
21	2000	1	0.0847
21	2000	2	0.0749
21	2000	3	0.0799
21	2000	4	0.0735
21	2000	5	0.0754

Table A3-6 Sample of Fuel Formulation

fuelFormulationID	fuelSubtypeID	RVP	sulfurLevel	ETOHVolume	MTBEVolume	ETBEVolume	TAMEVolume	aromaticContent	olefinContent	benzeneContent	o200	o300	isoToMonoDiEsterVolume	CetaneIndex	PAHContent	T50	T90
10	10	0	0	0	0	0	0	0	0	0	0	0	0	0	0	0	219.345
97	10	6.6	190	0	11.7581	0	0	24	11	0.8	52	94	0	0	0	0	219.345
4979	10	6.7	22.71	0	11.7581	0	0	33.17	6.47	1.36	40.1	81.11	0	0	0	0	219.345
4980	10	6.7	22.71	0	11.7581	0	0	33.17	6.47	1.36	40.1	81.11	0	0	0	0	219.345
8807	10	6.7	22.71	0	0	0	0	33.17	6.47	1.36	40.1	81.11	0	0	0	0	219.345
8808	10	6.7	22.71	0	0	0	0	33.17	6.47	1.36	40.1	81.11	0	0	0	0	219.345
8879	10	6.7	50.71	0	0	0	0	21.56	8	0.71	40.42	85.08	0	0	0	0	219.345
4532	10	6.7	76.305	0	1.42319	0	0	32.085	7.635	1.08	39.8	80.705	0	0	0	0	219.345
6637	10	6.7	76.305	0	0	0	0	32.085	7.635	1.08	39.8	80.705	0	0	0	0	219.345
5022	10	6.7	92.29	0	0.6895	0	0	25.43	12.51	1.04	45.21	80.89	0	0	0	0	219.345
5043	10	6.7	92.29	0	0.6895	0	0	24.91	12.54	1.04	46.25	80.95	0	0	0	0	219.345
6157	10	6.7	92.29	0	0	0	0.609	25.43	12.51	1.04	45.21	80.89	0	0	0	0	219.345
6170	10	6.7	92.29	0	0	0	0.8885	24.91	12.54	1.04	46.25	80.95	0	0	0	0	219.345
6819	10	6.7	92.29	0	0	0	0	25.43	12.51	1.04	45.21	80.89	0	0	0	0	219.345
4988	10	6.7	106.26	0	0.3314	0	0	25	11.18	1.25	49.87	82	0	0	0	0	219.345
6131	10	6.7	106.26	0	0	0	0.3314	25	11.18	1.25	49.87	82	0	0	0	0	219.345
4298	10	6.7	129.9	0	0.8	0	0	31	8.8	0.8	39.5	80.3	0	0	0	0	219.345
4537	10	6.7	131.505	0	2.64826	0	0	32.335	8.595	1.18	41.25	79.955	0	0	0	0	219.345
6642	10	6.7	131.505	0	0	0	0	32.335	8.595	1.18	41.25	79.955	0	0	0	0	219.345
4533	10	6.7	137.655	0	1.16693	0	0	31.035	9.335	1.08	42	80.955	0	0	0	0	219.345
6638	10	6.7	137.655	0	0	0	0	31.035	9.335	1.08	42	80.955	0	0	0	0	219.345
4538	10	6.7	142.41	0	2.11612	0	0	31.385	8.595	1.18	42.9	80.455	0	0	0	0	219.345
6643	10	6.7	142.41	0	0	0	0	31.385	8.595	1.18	42.9	80.455	0	0	0	0	219.345
8814	10	6.7	143.2	0	0	0	0	30.7	7.88	1.54	37.59	81.65	0	0	0	0	219.345
4885	10	6.7	165.945	0	1.46265	0	0	28.205	11.62	1.02	44.275	79.875	0	0	0	0	219.345
6669	10	6.7	165.945	0	0	0	0	28.205	11.62	1.02	44.275	79.875	0	0	0	0	219.345
4886	10	6.7	176.785	0	1.18842	0	0	27.255	11.62	1.02	45.975	80.375	0	0	0	0	219.345
6670	10	6.7	176.785	0	0	0	0	27.255	11.62	1.02	45.975	80.375	0	0	0	0	219.345

Table A3-7 Sample of Fuel Supply

countyID	fuelYearID	monthGroupID	fuelFormulationID	marketShare	marketShareCV
39061	2010	7	9309	1	0
39061	2010	7	20011	1	0

Table A3-8 Sample of Meteorology

monthID	zoneID	hourID	temperature	relHumidity
7	390610	10	63.93	41.42

Table A3-9 Sample of State and County

State Name	County Name
Ohio	Hamilton

Step 13: Run MOVES model. Sample result is shown by Figure A3-10. Then, go to Step 14.

Step 14: Set up criteria in **Hot Spot Identification** window (Figure A3-11), and identify hotspots links by clicking **OK** button (as shown in Figure A3-12). And then, go to Step15.

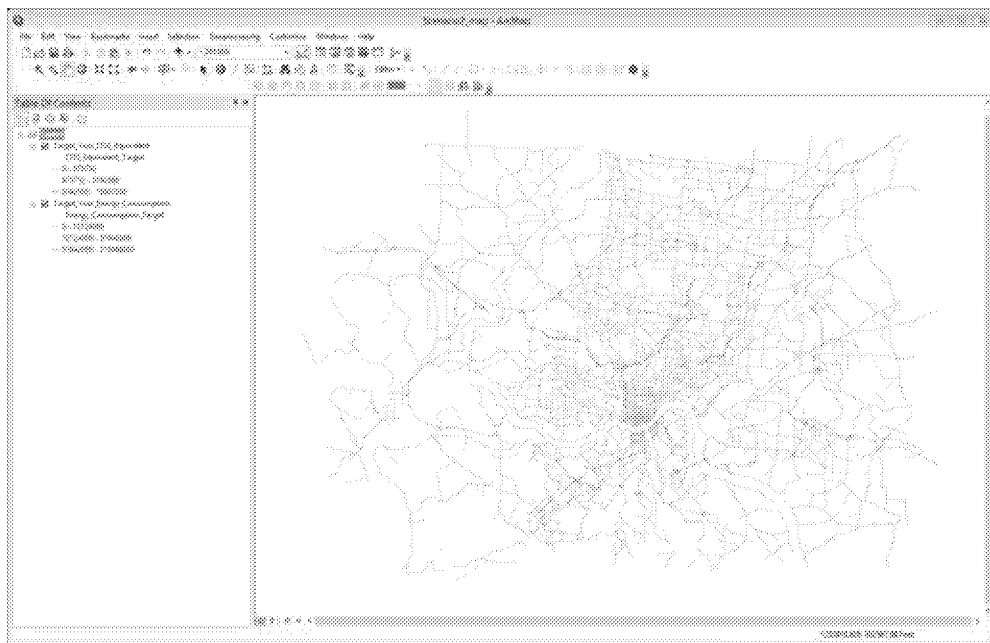


Figure A3-10 Emission Results Displayed in ArcGIS

Hotspots Identification

Please specify hotspot identification criteria:

Default:

☒ Daily link volume >= 125000

☒ Truck fraction >= 0.08

Optional:

☐ Average speed <=

☐ Delay >=

☐ Queue length >=

☐ O/C ratio >=

☐ CO2 equivalent >=

☐ Energy consumption >=

OK Cancel

Figure A3-11 Hotspots Identification Criteria

Hotspots

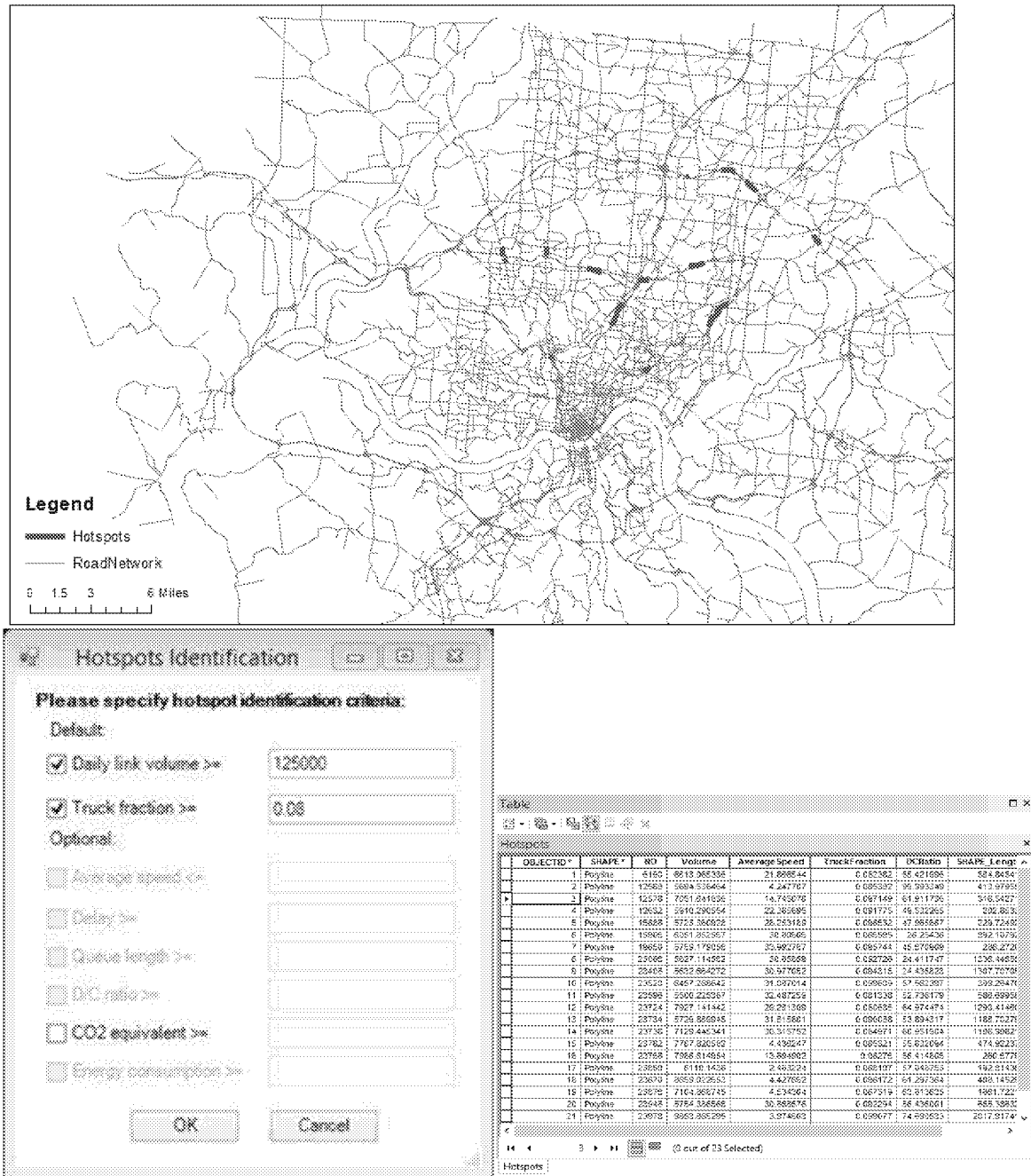


Figure A3-12 Identified Hotspots in Traffic Emission

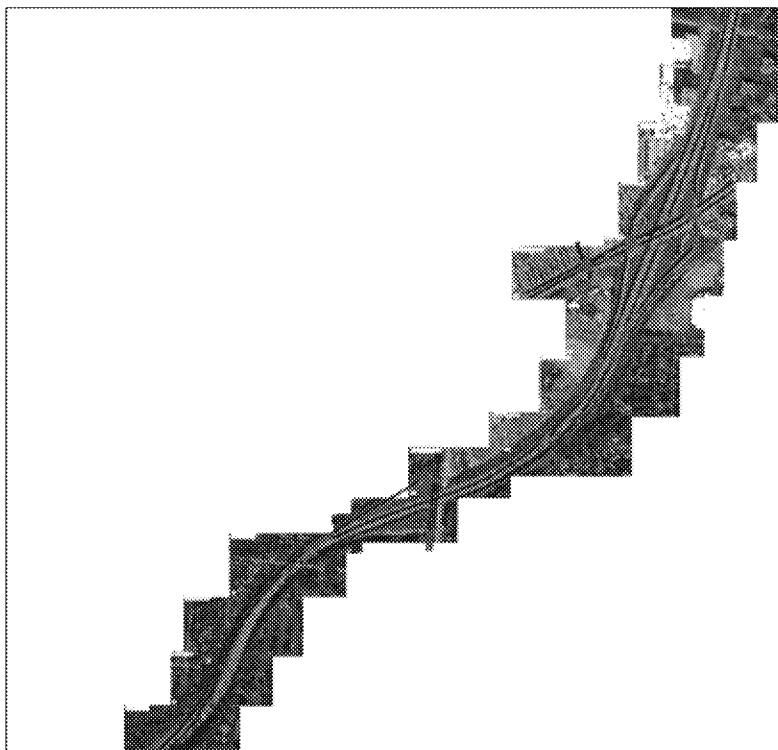
Step 15: Based on Hot Spot Identification results, select study road links and apply TCMs in the microscopic simulation model (note: this step is processed in the VISSIM model).

Step 15.1: Select hotspots links (an example is shown in Table A3-10) from identified hotspots (seen Figure 3-12). Go to Step 15.2.

Table A3-10 Sample of Selected Hot-spot Links for Corridor Level Impact Analysis

LinkNO	Length (Mile)	Car Volume	Truck Volume
23540	0.477	5055	457
23523	0.385	5489	497
26830	0.316	5489	497
23876	0.991	6125	554
17830	0.193	435	39
16938	0.341	636	58

Step 15.2: Load a base map to the VISSIM model. Then the VISSIM links are drawn on top of the base map. In this example, ramp metering is selected as a traffic control measure with the purpose of analyzing its impact on hotspot traffic operations and emissions.



Selected hotspot road network is built up in the VISSIM environment as shown in Figure A3-13 (where the base map with VISSIM links is superimposed). Figure A3-14 shows the sketch of the hotspot area to be divided into 6 segments for scenario comparison. The segment in the red box is the hotspot study area, and red dash line illustrates the locations of data collection points for model calibration and validation.

Figure A3-13 VISSIM Links over the Base Map

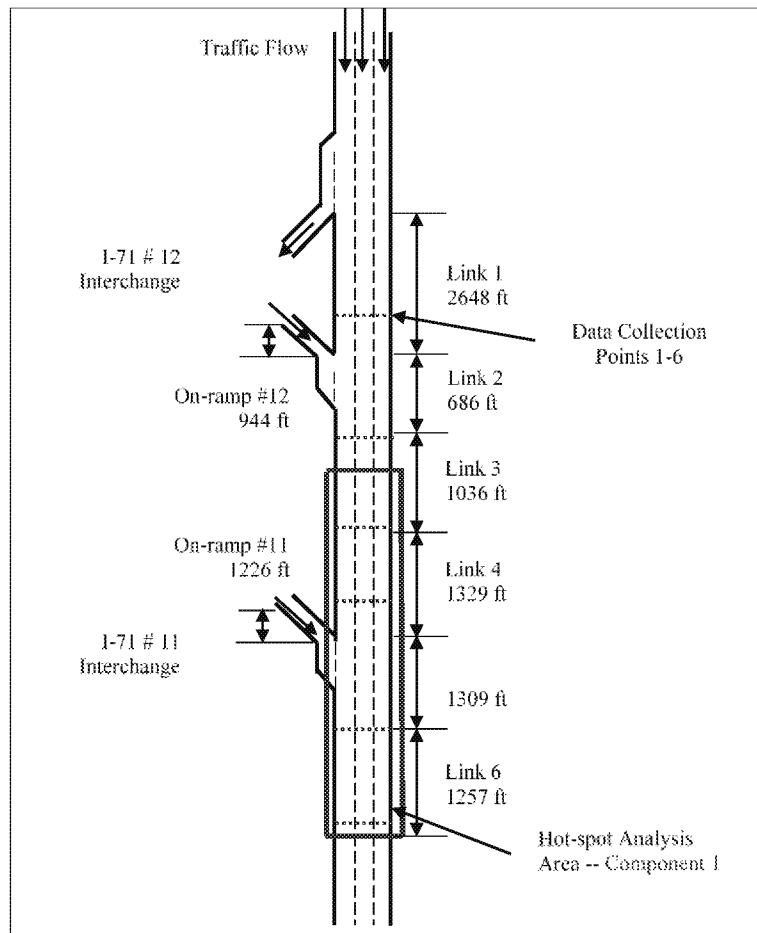


Figure A3-14 Schematic for Hotspot Microscopic Analysis

Step 15.3: Prepare real vehicle volume input and truck percentage for microscopic simulation analysis. Table A3-11 shows a sample of the traffic volume and truck percentage for all links in the hotspot analysis corridor. Then, go to Step 15.4.

Step 15.4: Set up the *Desired Speed Distribution*. They are used to model the changes of traffic flow speed within VISSIM network. The desired speed changes are determined based on the study site specifications and speed limits. An example is shown by Figure A3-15. Then, go to Step 15.5.

Table A3-11 Vehicle Volume

Link Number in VISSIM	Peak Hour Traffic Volume	Truck Percentage
1	4791	8%
2	5344	8%
3	5344	8%
4	5344	8%
5	6130	8%
6	6130	8%
On-ramp #12	553	8%
On-ramp #11	782	8%

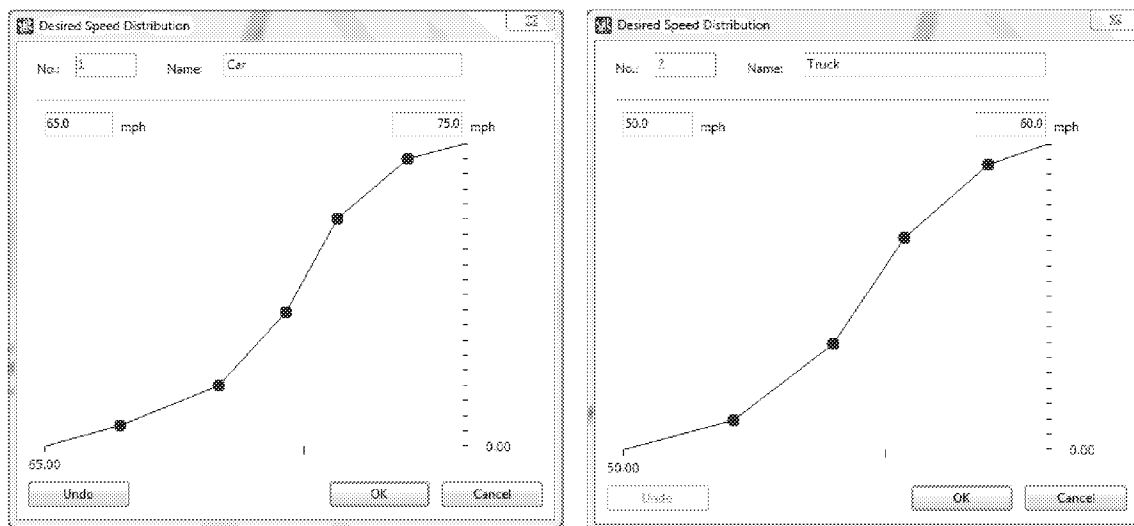


Figure A3-15 An Example of Desired Speed Distribution for Cars and Trucks

Step 15.5: Specify vehicle type, class and category. Example is shown in Table A3-12. Then go to Step 15.6.

Table A3-12 Vehicle Type Class and Category

No.	Name	Width (m)	Relative Flow	Desired Speed Range (mph)
100	Car	1.5	0.917	65, 75
200	HGV	2.5	0.083	50, 60

Step 15.6: Specify driving behavior. Car following and lane change are two main aspects of driving behavior. Tables A3-13 and A3-14 illustrate the car following and lane change parameters respectively in the VISSIM model for highway. Then, go to Step 15.7.

Table A3-13 Car Following Behavior Parameters

Parameters		Value	Unit
CC0	Standstill Distance	4.99	ft
CC1	Headway Time	0.91	s
CC2	'Following' Variation	13.12	ft
CC3	Threshold for Entering 'Following'	-8	-
CC4	Negative 'Following' Threshold	-0.35	-
CC5	Positive 'Following' Threshold	0.35	-
CC6	Speed Dependency of Oscillation	11.44	-
CC7	Oscillation Acceleration	0.82	ft/s ²
CC8	Standstill Acceleration	11.48	ft/s ²
CC9	Acceleration at 50 mph	4.92	ft/s ²

Table A3-14 Lane Change Parameters

General Behavior	Freeway		Unit
	Free Lane Selection	Trailing Vehicle	
Maximum deceleration	-4	-3	ft/s ²
-1 ft/s ² per distance	200	200	ft
Accepted deceleration	-1	-0.5	ft/s ²
Waiting time before diffusion	N/A	60	s
Min. headway (front/rear)	N/A	0.5	ft
To slower lane if collision time above	N/A	0	s
Safety distance reduction factor	N/A	0.6	N/A
Maximum deceleration for cooperative braking	N/A	-3	ft/s ²
Overtake reduced speed areas	N/A	Leave box unchecked	N/A

Step 15.7: Set up the signal control at the metered ramps. Table A3-15 is the design criteria for metering rate and signal cycle of Federal Highway Administration (FHWA). An example of fixed time signal is shown in Table A3-16 as the type of ramp metering for on-ramps. Then, go to Step 15.8.

Table A3-15 Ramp metering design criteria of FHWA

Flow Control Scheme	No. of Lanes	Cycle Length	Approximate Range of Metering Rates (veh/h)
One vehicle Per Green	1	4-4.5 sec.	240-900
Three Vehicles Per Green (Bulk)	1	6-6.5 sec.	240-1200
Dual-lane	2	6-6.5 sec.	400-1700

Table A3-16 Signal Control Parameters

Signal Group	Type	Cycle (s)	Green Time (s)	Metering Rate	Reference
1	Fixed time	4	2	240-900	FHWA

Step 15.8: Calibrate and validate microscopic model (more details are provided in Section 3.3.5). Tables A3-17 and Table A3-18 show an example of VISSIM calibration and validation results, respectively. Then go to Step 15.9.

Table A3-17 VISSIM Calibration Final Parameter Values

Parameters		Value	Unit
CC0	Standstill Distance	4.99	ft
CC1	Headway Time	0.91	s
CC2	'Following' Variation	13.12	ft
CC3	Threshold for Entering 'Following'	-8	-
CC4	Negative 'Following' Threshold	-0.35	-
CC5	Positive 'Following' Threshold	0.35	-
CC6	Speed Dependency of Oscillation	11.44	-
CC7	Oscillation Acceleration	0.82	ft/s ²
CC8	Standstill Acceleration	11.48	ft/s ²
CC9	Acceleration at 50 mph	4.92	ft/s ²

Table A3-18 VISSIM Validation Results

Traffic Volume					
LinkID	Real volume	Simulated volume	Difference	Criteria (Oregon)	Result
1	4791	4832	0.35	GEH<5	pass
2	5344	5431	1.40	GEH<5	pass
3	5344	5423	1.16	GEH<5	pass
4	5344	5425	1.22	GEH<5	pass
5	6130	6157	0.12	GEH<5	pass
6	6130	6154	0.09	GEH<5	pass
Travel Time					
Range	Real travel time (s)	Simulated travel time (s)	Difference	Criteria (<10%)	Result
Link 1-6	124.5	130	5.5	12.45	pass
Spot Speed					
Data collectionID	Real speed (mph)	Simulated speed (mph)	Difference	Criteria (10% real speed)	Result
1	59.08	64	4.92	5.908	pass
2	58	60.2	2.2	5.8	pass
3	58.73	63.1	4.37	5.873	pass
4	61.2	63.4	2.2	6.12	pass
5	56.08	56.6	0.52	5.608	pass
6	60.64	62.9	2.26	6.064	pass

Step 15.9: After using real site traffic volume, spot speed and travel time to calibration and validation the model, *Traffic Volume* and *truck percentage* (8.0% for all links) from the regional-level results of VISUM for each link are applied for two project-level analysis scenarios:

- Scenario 1 without any traffic control measure; and
- Scenario 2 with 4-sec cycle length ramp metering.

Then, run VISSIM and export VISSIM outputs. Then, go to Step 16.

Step 16: Import *Microscopic Simulation Link ID* in sheets 1 and 2 (Excel file; an example is shown in Tables A3-19 and A3-20) which are constructed in microscopic simulation software like VISSIM. The VISSIM model simulates traffic for one hour and finally produces second-by-second vehicle speed, queue length, and delay (as shown in Tables

A3-21 and A3-22). Load *Microscopic Simulation Results* in sheets 1 and 2 (Excel file; examples are shown in Tables A3-21 and A3-22) under different scenarios, separately. Compare those imported results, and then go to step 17.

Table A3-19 Microscopic Simulation Link ID (Sheet1)

GISLinkID	VissimLinkID
23540	1
23523	2
23523	3
26830	4
23876	5
23876	6
17830	12
16938	11

Table A3-20 Microscopic Simulation Link ID (Sheet2)

GISLinkID	RoadType	LinkLength	LinkGrade
23540	4	0.477	0
23523	4	0.385	0
26830	4	0.316	0
23876	4	0.991	0
17830	4	0.193	0
16938	4	0.341	0

Table A3-21 Microscopic Simulation Results (Sheet1)

VissimLinkID	Time (sim sec)	Car #	Car v (m/s)	Car a (m/s ²)	Truck #	Truck v (m/s)	Truck a (m/s ²)
1	1	0	0	0	0	0	0
2	1	1	22.6	0	0	0	0
3	1	0	0	0	0	0	0
4	1	0	0	0	0	0	0
5	1	3	29.7	-0.2	0	0	0
6	1	3	30.5	0.1	0	0	0

7	1	3	30	0	0	0	0
8	1	0	0	0	1	27.2	0.8
1	2	2	26.3	1.5	1	25.4	0
2	2	2	29	0	0	0	0
3	2	0	0	0	0	0	0
4	2	0	0	0	0	0	0
5	2	1	32.6	0	0	0	0
6	2	0	0	0	0	0	0
7	2	0	0	0	0	0	0
8	2	3	29.7	-0.2	0	0	0
1	3	3	30.5	0.1	0	0	0
2	3	3	30	0	0	0	0
3	3	0	0	0	0	0	0

Table A3-22 Microscopic Simulation Results (Sheet2)

Link	Scenario 1			Scenario 2		
	Average Speed (mph)	Delay (s/veh)	Average Queue Length (vehs)	Average Speed (mph)	Delay (s/veh)	Average Queue Length (vehs)
1	63.72	1.8	0	63.79	1.7	0
2	59.21	1.5	0	60.07	1.4	0
3	59.41	3.2	3	59.61	2	0
4	46.01	13.6	31	59.65	2.5	2
5	46.93	11.7	28	56.21	3.3	3
6	56.92	2.2	0	57.03	2.2	0
12	46.28	0.6	0	46.38	0.6	0
11	49.92	0.4	0	17.17	5.1	8

Step 17: Select the **Emission Estimation Model** (only MOVES is currently available in the current version of AIR-SUSTAIN and will be added with more options in the future), then run MOVES (an example is shown in Table A3-23). After it's finished, go to Step 18.

Table A3-23 An Example of Hotspots Emissions by Different Scenarios

LinkID	S1_CO2 (kg)	S1_Energy (kJ)	S2_CO2 (kg)	S2_Energy (kJ)
23532	1406.47	19,409,200	1406.46	19,409,190
23540	1073.49	14,812,350	1056.59	14,579,600
23876	944.21	13,029,600	811.57	11,198,300
26830	1933.76	26681,300	1778.17	24,535,100
17830	31.95	441,704	31.92	440,866
16938	58.43	808,036	80.97	1,120,090

Note: S1 and S2 represent Scenario 1 and Scenario 2, respectively.

Step 18: Update regional emission results by project level analysis emission results. If both target year and base year have been analyzed, then go to step 19; else go back to Step 2.

Step 19: Compare results between base year and target year. Then, stop.

Appendix B

WTP-CAM User's Manual

Table of Content

B 1.0 Program Overview	254
B 1.1 WTP-CAM setup	254
B 1.2 WTP-CAM workspaces.....	255
B 1.2.1 Main menu bar	255
B 1.2.2 Tool bar	257
B 1.2.3 Status bar	259
B 1.2.4 Cursor bar	259
B 1.2.5 Processing train window.....	259
B 1.2.6 Property editor.....	259
B 1.3 Setting up a processing train.....	260
B 1.3.1 Building a physical processing train.....	260
B 1.3.2 Editing a non-physical settings.....	261
B 1.4 Saving and opening projects	261
B 1.5 Running WTP-CAM	261
B 2.0 Understanding the Input File	262
B 2.1 Introduction to the example processing train	262
B 2.2 Inputs for Monte Carlo simulation.....	262
B 2.2.1 Overview.....	262
B 2.2.2 Inputs for Monte Carlo simulation	266
B 2.3 Customization of GAC unit process model	269
B 2.3.1 Overview	269
B 2.3.2 Inputs for GAC model customization	270
B 3.0 Understanding the Output Data	271
B 3.1 Standard output tables for a one-time run	271
B 3.2 Tabular outputs for Monte Carlo simulation	278
B 3.2.1 Samples/statistics of raw water qualities	278
B 3.2.2 Samples/statistics of effluent water qualities	278
B 3.2.3 Samples/statistics of adaptation costs	279
B 3.2.4 Samples/statistics for compliance/non-compliance realizations	279
B 3.2.5 Running log	280
B 3.3 Graphic outputs for Monte Carlo simulation	280
B 3.3.1 Samples chart	280
B 3.3.2 Frequency chart	280
B 3.3.3 Cumulative frequency chart	281
B 4.0 Models and Algorithms in WTP-CAM	281
B 4.1 Monte Carlo methods	281
B 4.1.1 Seasonal multivariate analysis	282

B 4.1.2	Simulation of quarterly running average (TOC compliance)	284
B 4.1.3	Adaptation of unit process	285
B 4.2	Customization of unit process	286
B 4.2.1	Customization of GAC unit process	286
B 4.3	Economics	289
B 4.3.1	Adaptation Costs for GAC Processing	289
B 5.0	References	291

Attachment

A.	Confirmation Tests	293
A-1	Seasonal multivariate analysis.....	293
A-2	Customization of GAC model.....	295
B.	Error and Warning Messages	300

List of Tables

Table B1-1 List of Standard Toolbars	258
Table B1-2 List of Unit Processes Toolbars	258
Table B2-1 Options for Monte Carlo analysis	267
Table B4-1 Illustration of calculating running annual average for finished water TOC	285
Table B4-2 GAC contactor cost	290
Table B4-3 GAC reactivation cost	290

Attachments

Table A-1 Comparison of the mean and standard deviation in summer.....	294
Table A-2 Comparison of cross correlation matrix in summer.....	294
Table A-3 Comparison of the mean and standard deviation in winter.....	295
Table A-4 Comparison of cross correlation matrix in winter.....	295
Table A-5 Parameters estimated for TOC breakthrough model.....	296
Table A-6 Summary of field data sets and estimated parameters.....	298
Table A-7 Comparison of sum of least square for customized GAC models.....	298
Table B-1 Error message.....	300
Table B-2 Warning message.....	300

List of Figures

Figure B1-1 WTP-CAM workspace	255
Figure B1-2 Three edit functions for unit process menu	259
Figure B1-3 The property editor	260
Figure B1-4 Setting dialogue box for Monte Carlo analysis	261
Figure B2-1 Schematic diagram for treatment unit process at the GCWW Richard Miller water treatment plant	263
Figure B2-2 Schematic diagram TWP-cam program flow in the example simulations	263
Figure B2-3 Original input data for the GCWW example processing train	264
Figure B2-4 Illustration diagram for Monte Carlo analysis	265
Figure B2-5 Monte Carlo inputs for the example processing train	267
Figure B2-6 Manual input window for influent water quality statistics	268
Figure B2-7 Dialogue window for name of data files	268
Figure B2-8 Example format of influent water quality data file	269
Figure B2-9 GAC unit process property window	270
Figure B2-10 Dialogue window for TOC breakthrough customization	270
Figure B2-11 Example format for TOC breakthrough data file	271
Figure B3-1 Standard output “Table 1” for the example processing train	272
Figure B3-2 Standard output “Table 2” for the example processing train	273
Figure B3-3 Standard output “Table 3” for the example processing train	274
Figure B3-4 Standard output “Table 4” for the example processing train	274
Figure B3-5 Standard output “Table 5” for the example processing train	275
Figure B3-6 Standard output “Table 6” for the example processing train	275
Figure B3-7 Standard output “Table 7” for the example processing train	276
Figure B3-8 Standard output “Table 8” for the example processing train	276
Figure B3-9 Standard output “Table 9” for the example processing train	277
Figure B3-10 Standard output “Table 10” for the example processing train	277
Figure B3-11 Sample outputs of raw water qualities	278
Figure B3-12 Selected sample outputs of effluent water qualities at finished water	278
Figure B3-13 Sample outputs for adaptation costs	279
Figure B3-14 Sample outputs of raw water quality and adaptation cost for non-compliance events	279
Figure B3-15 Example format of the log file	280
Figure B3-16 Example sample chart for raw water TOC	280
Figure B3-17 Example frequency chart for raw water TOC	281
Figure B3-18 Example cumulative frequency chart for effluent TOC at finished water.....	281
Figure B4-1 Cost curve for annual cost of GAC unit process	291
 <i>Attachments</i>	
Figure A-1 Comparison of GAC models with RSSCT dataset 1.....	296
Figure A-2 Comparison of GAC models with RSSCT dataset 2.....	297
Figure A-3 Comparison of sum of error square for GAC models.....	297

List of Abbreviations and Notation

Abbreviations

Alk	alkalinity
AR(1)	autoregressive model of order one
BLS	Bureau of Labor Statistics
Bro	bromide
Ca-H	calcium hardness
Cl ₂	chlorine
CCAM	climate change adaptation model
DBP	disinfection by-products
GAC	granular activated carbon
GCWW	Greater Cincinnati Water Works
HAAs	haloacetic acids (nine individual species and the total of five (HAA ₅), six (HAA ₆) and nine (HAA ₉) species)
ICR	information collection rule
ID	identification
MC	Monte Carlo
NH ₃	ammonia
NOM	natural organic material
O&M	operation and maintenance
PPI	Producers Price Index
Q _{in}	influent flow rate
RSSCT	rapid small-scale column test
Temp	temperature
TOC	total organic carbons
Tt-H	total hardness
TTHM	sum of four individual species of trihalomethanes
Turb	turbidity
USEPA	U.S. Environmental Protection Agency
UV	ultra violet
UVA	ultraviolet absorbance at 254 nm
WRAP	USEPA Water Resources Adaptation Program
WTP	water treatment plant

Notation

θ	a vector of parameters to be estimated
θ_0	initial parameter vector

θ_1	corrected parameter vector
v	a variable between 0 and 1
ε_j	a (9×1) vector of standard normal deviates for season j
a	GAC model parameter, [-]
A	the Gauss-Newton coefficient matrix
A_j	(9×9) parameter matrix for season j
b	GAC model parameter, [-]
B_j	(9×9) parameter matrix for season j
c	GAC model parameter
d	GAC model parameter, [1/day]
D	a positive definite matrix, defined by $D = B_j B_j^T$
EBCT	empty bed contact time, [min]
$E[Y]$	mean of random variable Y
$f(t)$	TOC fraction remaining, defined by $f(t) = \frac{TOC_{eff}}{TOC_{in}}$, [-]
m_j	a known vector of the means for the nine parameters for season j
m_{x_i}	a mean of variable x_i
${}_j M_0$	a lag-zero covariance matrix of $(X_j - m_j)$ for season j
${}_j M_1$	a lag-one covariance matrix of $(X_j - m_j)$ for season j
n	sample size, [-]
$r_{x_i x_j}$	the lag-zero correlation between x_i and x_j , [-]
$r_{y_i x_j}$	the lag-one correlation between variables y_i and x_j , [-]
R	a right-hand-side vector of Gauss-Newton equation
S_{x_i}	standard deviation of variable x_i
S_{xx}	covariance matrix, defined by $S_{xx} = E[XX^T]$
t	GAC service time, [day]
t_k	field measurement of GAC service time, [day]
TOC_{eff}	effluent TOC concentrations at the GAC unit, [mg/L]
TOC_{in}	influent TOC concentrations at the GAC unit, [mg/L]
USRT	process design or operating variable
x'_i	log-normal distributed variable, defined by, $x'_i = \ln(x_i)$
X	defined by, $X = X_{j-1} - m_{j-1}$
X_j	a (9×1) vector of nine raw water quality parameters for season j
y	the capital, operational or maintenance cost, [US \$]
y_k	a field measurement of TOC fraction remaining, [-]
Y	defined by, $Y = X_j - m_j$
z	a parameter is either 0 or 1 for adjusting cost functions for a range of USRT values, [-]

The WTP-CAM program was developed from the climate adaptation models (CAMs) published in Li et al (2009; 2013; 2014), Clark et al (2013; 2012) and Yang et al. (2012; 2011). The computer program is developed on the basis of Water Treatment Plant (WTP) model that was proposed originally for the USEPA in 1992 (USEPA, 2005). WTP software exists in two versions. the Version WTP v2.2 is further improved from original 1992 WTP v.1.0. Appendix C contains a copy of the WTP v2.2 user manual.

This manual is intended to provide guidance to the WTP-CAM user with the new features:

- Utilizing the WTP-CAM program - navigating the user interface.
- Selecting inputs and interpreting outputs related to Monte Carlo analysis and adaptation.
- Understanding the algorithms applied in WTP-CAM relating multivariate analysis, customization of processing units, and cost analysis.

In addition to this introductory Section, this User's Manual contains four other Sections:

- Section 2 explains menu components and describes how to set up and run WTP-CAM.
- Section 3 describes how to input the required data for the new features. A model of a typical treatment plant is developed as an example; data input options are outlined.
- Section 4 provides guidance for interpretation of the output from the WTP-CAM based on the example developed in Section 3.
- Section 5 describes the new algorithms used in the WTP-CAM program.

The user manual also contains two appendices. Appendix A shows confirmation tests to verify the new algorithms introduced in WTP-CAM, including seasonal multivariate analysis, and GAC model customization. Appendix B provides tables of error and warning messages, including error or warning message ID, their meanings, and recommended actions for error correction.

B1.0 Program Overview

B1.1 WTP-CAM Setup

WTP-CAM Version 1.0 is designed as a Windows-based program that can be run under the Window 7 or newer operating system. It tested successfully on an Intel CPU 1.90 GHz computer with 2 GB memory. The disk space requirement is mainly used to save simulation results; 500Mb minimal disk space is recommend. The program also allows users to use either free or professional version of the SQL database. The file formats and designations remain the same as the those in the folder.

In order to run and use the WTP-CAM program, the user should setup a single folder in which to place three files:

- *WTP-CAM1.exe* - the main executable file.
- *WTP-CAM User Manual* - this support document.
- *WQ example input.txt* - a sample input file to illustrate the format of raw water quality parameters.

When the executable file has been placed in a single directory, the user simply needs to double-click on the *WTP-CAM.exe* icon to launch the program. To remove WTP-CAM from your computer, simply delete the file folder.

B1.2 WTP-CAM Workspace

The basic workspace for WTP-CAM consists of the following user interface elements: main Menu Bar, Cursor Menu, Tool Bars, Status Bars, Property Editor, and Processing Train window as shown in Figure B1.1.

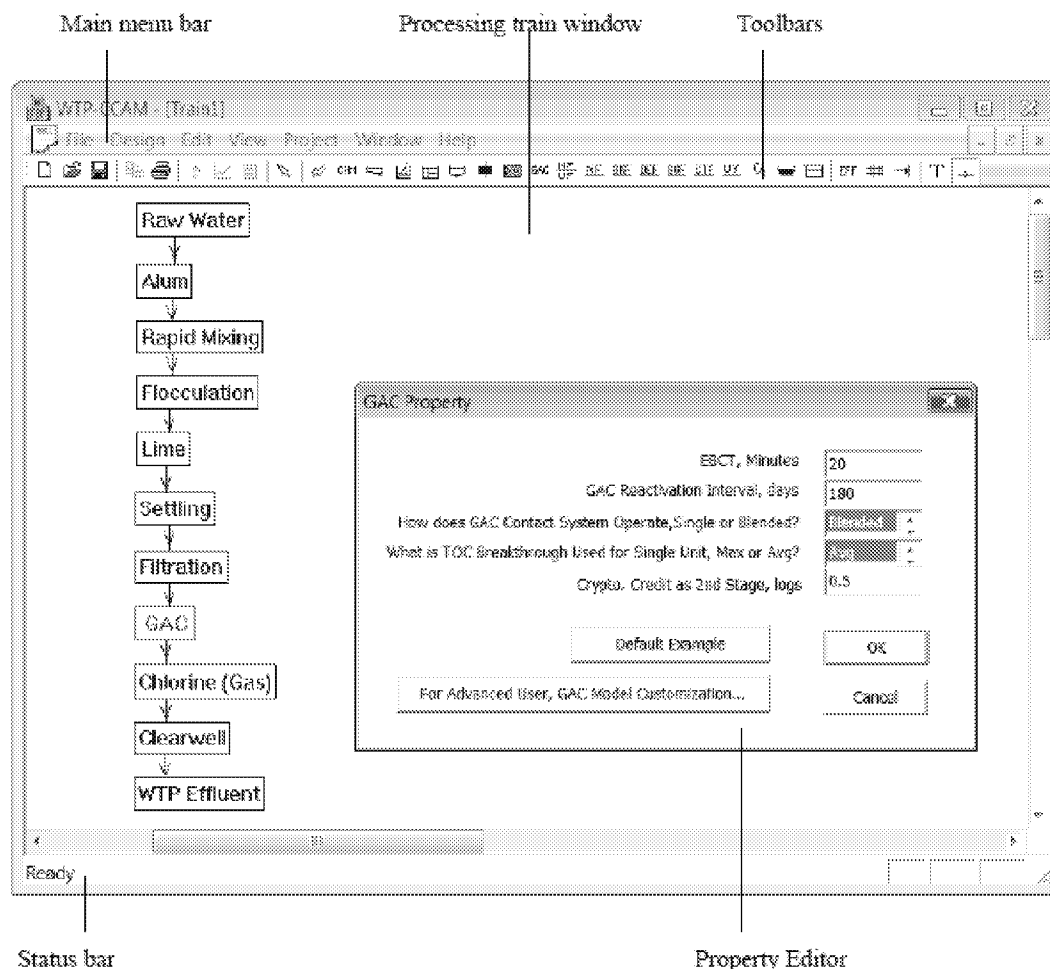


Figure B1-1 WTP-CAM workspace

B1.2.1 Main Menu Bar

The Menu Bar located across the top of the WTP-CAM workspace contains a collection of menus used to control the program, including: File Menu, Design Menu, Edit Menu, View Menu, Project Menu, Window Menu, and Help Menu.

File Menu: Contains commands for opening and saving data files and for printing.

Command	Description
New	Creates a new WTP project
Open	Opens an existing project
Save	Saves the current project
Save As	Saves the current project under a different name
Print	Prints the current view
Print Preview	Previews a printout of the current view
Print Setup	Sets page margins, headers, and footers for printing
Exit	Exits WTP-CAM

Design Menu: Contains commands to select unit processes, chemical feeds, and sampling points.

Unit Processes	Chemical Feeds	Sampling Points
Raw Water	Alum	WTP Effluent
Pre-settling Basin	Ammonia Sulfate	Average Tap
Rapid Mix	Ammonia	End of System
Flocculation	Carbon Dioxide	
Settling Basin	Chlorine (Gas)	
Filtration	Chlorine Dioxide	
GAC	Iron	
MF/UF	Lime	
Nano-filtration	Ozone	
Slow Sand Filtration	Permanganate	
UV Disinfection	Sodium Hydroxide	
Ozone Chamber	Sodium Hypochlorite	
Contact Tank	Soda Ash	
Reservoir	Sulfur Dioxide	
Bank Filtration	Sulfuric Acid	
D.E. Filtration		
Bag Filtration		
Cartridge Filtration		

Edit Menu: Contains a control for copying.

Command	Description
Copy To	Copies the currently active view (processing train, graph or table) to clipboard.

View Menu: Contains controls for the user interface and commands for reporting results in different formats.

Command	Description
Tool Bar	Toggles the tool bars on/off.
Status Bar	Toggles the status bars on/off.
Graph	Creates frequency/cumulative frequency chart of selected parameters.
Table	Creates a tabular display of selected parameters.
Options	Controls the display style of a graph, or table.

Window Menu: Contains commands for displaying opened windows.

Command	Description
New Window	Open another window for the active document.
Cascade	Arrange windows so they overlap.
Window List	Lists all open windows; selected window currently with highlight.

Project Menu: Contains commands to define modeling conditions and to set up simulations for the current project being analyzed.

Command	Description
Monte Carlo Setting	Define conditions and inputs for Monte Carlo analysis.
Cost Analysis	Define the conditions for cost analysis.
Optimization Analysis	Define the conditions for unit process optimization analysis.
One Time Run	Simulate water treatment at a defined condition.
Multiple Runs	Make Monte Carlo simulations.

Help Menu: Contains commands for identifying problems and solutions during simulation.

Command	Description
Error Message	Identifies problems and suggested solutions during simulation.
About	Lists information about current version of WTP-CAM.

B1.2.2 Tool Bars

Toolbars provide shortcuts to commonly used operations. These operations are also available at the main menu bar. The toolbars can be docked underneath the Main Menu bar or

dragged to any location on the WTP-CAM workspace. The toolbars can be made visible or invisible by selecting *View >> Toolbar*. There are two types of toolbars:

- Standard Toolbars: contains speed buttons for commonly used commands (see Table B1-1).
- Unit Processes Toolbars: contains buttons for working with processing train (see Table B1-2).

Table B1-1 List of Standard Toolbars























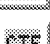


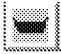
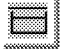

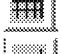



Toolbar Icon	Equivalent command at the main menu bar
	File >> New
	File >> Open
	File >> Save
	File >> Print
	Edit >> Copy to
	Project >> MC Simulation
	View >> Graph
	View >> Table

Table B1-2 List of Unit Process Toolbars

Toolbar Icon	Equivalent command at the main menu bar
	Design >> Pointer (Deactivate selection)
	Design >> Raw Water
	Design >> Presettling Basin
	Design >> Rapid Mixing
	Design >> Flocculation
	Design >> Sedimentation
	Design >> Filtration
	Design >> Slow Sand Filter
	Design >> GAC
	Design >> Micro/Ultra Filter
	Design >> Nano-Filter
	Design >> Bank Filtration
	Design >> D.E. Filtration
	Design >> Bag Filtration
	Design >> Cartridge Filtration
	Design >> UV Disinfection
	Design >> Ozone Chamber

Toolbar Icon	Equivalent command at the main menu bar
	Design >> Reservoir
	Design >> Contact Tank
	Design >> Effluent
	Design >> Average Tap
	Design >> End of System
	Design >> Chemical Feed
	Design >> Connection

B1.2.3 Status Bar

The Status Bar appears at the bottom of the WTP-CAM workspace to show information explaining the selected command in the main menu bar or the Tool Bars.

B1.2.4 Cursor Menu

There are two status options for the Cursor Menu in the processing train window. When the mouse cursor does not point to any unit process in the processing train window, clicking the right key of the mouse will show exactly the same Design Menu in the main menu bar (refer to the introduction to the Design Menu in Section B1.2.1). When the mouse cursor points to a unit process in the processing train window, clicking the right key of mouse leads to a new cursor menu with three commands (Figure B1-2) as following:

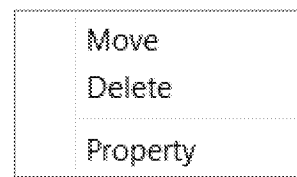


Figure B1-2. Three edit functions for unit process menu

- Move – move the selected unit process box to any user desired location in the train window.
- Delete – delete the selected unit process from the processing train.
- Property – show the Property Editor for the selected unit process.

B1.2.5 Processing Train Window

The Processing Train Window is the interface for users to build their own water treatment processing train and input parameters for unit processes or Monte Carlo analysis. Section B1.3 describes how to build a processing train in this window.

B.1.2.6 Property Editor

The Property Editor (Figure B1-3) is used to edit the properties of a unit process. It is invoked when a unit process in the Processing Train Window is selected and double-clicked or the property in the Cursor Menu is clicked. Following is an example Property Editor for flocculation.

The following points help explain how to use the Property Editor.

- The Editor usually consists of two columns (one for the property's name and the other for its value), an “OK” button, a “Cancel” button and a “WTP Example” button.
- The property value is initialized with zero or the first element in the dropdown list. Pressing the “WTP Example” button will provide user example values for all properties in this opened Editor.
- Depending on the property, the value field can be entered either by typing in a value for a text edit box or by selecting from a list of choices in a dropdown list box.
- You can use both the mouse and the tab key on the keyboard to move between properties.
- To have WTP-CAM accept what you have entered, press the “OK” button; to cancel, press the “Cancel” button.
- The Editor window can be moved via the normal Windows procedures.

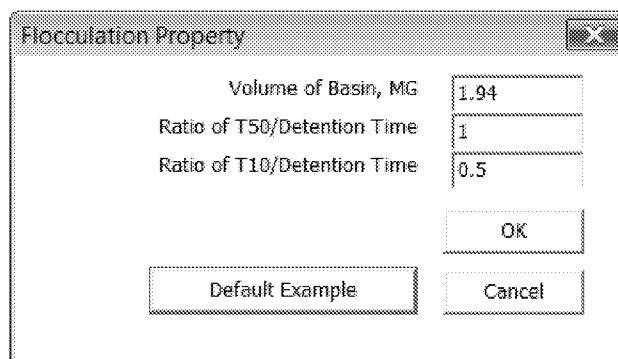


Figure B1-3 The property editor

B1.3 Setting up a Processing Train

A processing train includes both physical objects that can appear on the Train Window, and non-physical settings that encompass design and operational information as well as simulation controls. The physical objects include water treatment unit processes, chemicals and connection lines. Non-physical settings cover the properties of unit processes and settings for Monte Carlo simulation, cost analysis, and optimization analysis.

B1.3.1 Building a Physical Processing Train

To add a unit process to a processing train, the first step is to select the object unit process from one of three methods (Design Menu, Cursor Menu or Toolbars), and then move the mouse to a desired location on the Train Window, and click to finalize.

To add a chemical to the train, select the “Chemical” first from either Design Menu/Cursor Menu, or the “Chemical” button in the Toolbars and then move the mouse to a desired location on the Train Window and click. A dialogue box will appear, select the desired chemical from the dropdown list and click “OK” button.

To add a connection line to the train, the first step is to select the “Connection” from either Design Menu/Cursor Menu, or the Connection button in the Toolbars. The second step is to move the mouse to the starting unit process and click; without releasing, continue to move the mouse to the ending unit process and then release.

An object in the processing train can be deleted or moved using the Cursor Menu. To delete or move an object, click on the object first, then click the right mouse key to invoke the Cursor Menu, finally click Delete or Move from the Cursor Menu. For moving an object, move

the object to a desired location in the Train Window and click left mouse key to finish the moving action.

B1.3.2 Editing a Non-physical Settings

The Property Editor (see Section B1.2.6) is used to edit the properties of objects that can appear in the Train Window. To edit one of these objects, select the object in the processing train, then click the Property in the Cursor Menu or simply double-click the selected object. The properties of objects usually consist of design and operational parameters for unit processes or chemical feeds. A detailed explanation of such parameters can be found in Chapter C3 of the WTP manual in Appendix C (USEPA, 2005).

Settings for Monte Carlo analysis are illustrated in Figure B1-4, which includes control parameters for computer simulation, data source for raw water quality statistics and cross correlation matrix, and options available for the Monte Carlo simulation. Section 3 provides a detailed explanation of the settings for a Monte Carlo analysis.

Figure B1-4 Setting dialogue box for Monte Carlo analysis

B1.4 Saving and Opening Projects

Having completed the initial design and sequence of a processing train, it is a good idea to save the project to a file.

- From the File menu, select the Save As option.
- In the Save As dialog that appears, select a folder and file name under which to save this project. An extension of .wtp will be added to the file name.
- Click OK to save the project to file.

To open the project at some later time, select the Open command from the File menu.

B1.5 Running WTP-CAM

The WTP-CAM is designed to run under two modes:

- Single Case Run: make one-time run of the WTP analysis based on the deterministic influent water quality entered from the Property Editor of Raw Water without use of Monte Carlo

setting.

- Monte Carlo Simulation: make multiple runs of the WTP analysis based on stochastic influent water quality simulated with Monte Carlo setting.

When design of a processing train is complete, the WTP-CAM can be run by selecting either **Project>>Single Case Run** or **Project>>MC Simulation**. If the run is successful, a notice window will appear indicating end of simulation. The demonstrations and explanations of the outputs from WTP-CAM are described in Section 6.0 of the main report.

B2.0 Understanding the Input Data

As introduced in Section B1.0, input data for WTP-CAM can be categorized into original inputs and new inputs. The original inputs, including the design and operational parameters for unit processes and information for chemical feeds, are used to make a traditional single case simulation for a processing train and are introduced in detail in Chapter C3.0 of the original WTP manual (USEPA, 2005). This WTP-CAM manual will not replicate the description for the original inputs again. Instead, this manual focuses on definition and selection of the new inputs added for the new features such as Monte Carlo analysis or customization of the GAC unit process model. The description of the new inputs is illustrated through an example processing train at Greater Cincinnati Water Works' (GCWW) Richard Miller drinking water treatment plant.

B.2.1. Introduction to the Example Processing Train

As shown in Figure B2-1, the Miller plant treats the raw water through coagulation, sedimentation, rapid sand filtration, followed by granular activated carbon (GAC) processing. The spent GAC is reactivated in two large on-site furnaces. After chlorination disinfection, the treated water is stored temporarily in a clearwell and then pumped into the distribution system. WTP-CAM arranges the unit process components of the process train in a sequential block diagram, as illustrated in Figure B2-2. Figure B2-3 summarizes the original input data for the processing train.

B 2.2 Inputs for Monte Carlo Simulation

B 2.2.1 Overview

The ability to make Monte Carlo simulation is an important new feature not previously available in the original WTP model. To understand the inputs for Monte Carlo analysis, it is helpful to introduce the procedures involved in the analysis. Figure B2-4 outlines key steps of the Monte Carlo analysis and the application of the new inputs (in bold). It can be seen that there are three key options that govern the Monte Carlo analysis: Quarterly Running Average, Preserving Correlation and Contamination Control.

1
2
3

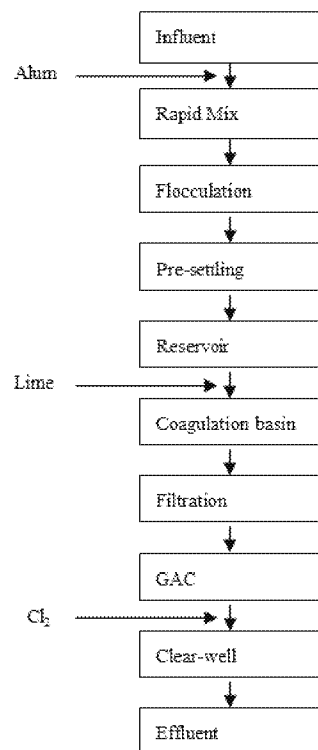


Figure B2-1 Schematic diagram for treatment unit process at the GCWW Richard Miller water treatment plant

4

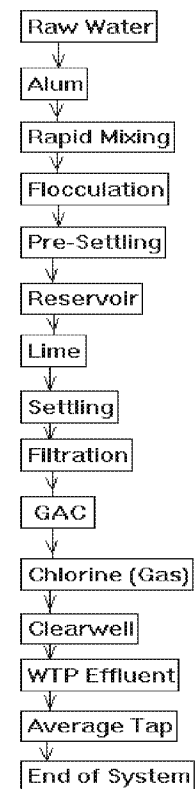


Figure B2-2 Schematic diagram TWP-cam program flow in the example simulation

Influent		
pH	7.8	
Influent Temperature	18.6	(Celsius)
Minimum Temperature	2.0	(Celsius)
Total Organic Carbon	2.6	(mg/L)
UV Absorbance at 254nm	0.096	(L/cm)
Bromide	0.069	(mg/L)
Alkalinity	72	(mg/L as CaCO3)
Calcium Hardness	77	(mg/L as CaCO3)
Total Hardness	141	(mg/L as CaCO3)
Ammonia	0.21	(mg/L as N)
Turbidity	151.0	(NTU)
Peak Flow	220.000	(MGD)
Plant Flow	120.600	(MGD)
Surface water by SWTR	TRUE	(TRUE/FALSE)
Source water Crypto. Concentration	0.000	(oocysts/Liter)
LT2 Rule watershed Control Prog. Credit?	FALSE	(TRUE/FALSE)
If GW System, Is Virus Disinfection Req'd?	FALSE	(TRUE/FALSE)
Virus Disinfection for GW, if Req'd	4.0	(logs)
Alum		
Alum Dose	1.1	(mg/L as Al2(SO4)3*14H2O)
Rapid Mix		
Volume of Basin	0.0084	(MG)
Ratio of T50/Detention Time	1.00	(ratio)
Ratio of T10/Detention Time	1.00	(ratio)
Flocculation		
Volume of Basin	1.9400	(MG)
Ratio of T50/Detention Time	1.00	(ratio)
Ratio of T10/Detention Time	0.50	(ratio)
Presed. Basin		
Volume of Basin	2.2300	(MG)
Ratio of T50/Detention Time	1.00	(ratio)
Ratio of T10/Detention Time	0.44	(ratio)
Eligible for LT2 Toolbox Crypto. Credit?	FALSE	(TRUE/FALSE)
LT2 Toolbox crypto. Removal Credit	0.4	(logs)
Reservoir		
Volume of Basin	373.0000	(MG)
Ratio of T50/Detention Time	1.00	(ratio)
Ratio of T10/Detention Time	0.32	(ratio)
Lime		
Lime Dose	5.0	(mg/L as Ca(OH)2)
For pH adjustment (P) or Softening (S)	PH_ADJ.(P or S)	
Settling Basin		
Volume of Basin	26.0000	(MG)
Ratio of T50/Detention Time	1.00	(ratio)
Ratio of T10/Detention Time	0.42	(ratio)
Filtration		
Liquid Volume	2.4708	(MG)
Ratio of T50/Detention Time	1.00	(ratio)
Ratio of T10/Detention Time	0.12	(ratio)
Chlorinated Backwash water?	FALSE	(TRUE/FALSE)
Filter Media (Anthracite/sand or GAC)	A/S	(S or G)
Giardia Removal Credit - Conv. Filters	2.5	(logs)
Virus Removal Credit - Conv. Filters	2.0	(logs)
Crypto. Removal Credit - Conv. Filters	3.0	(logs)
Giardia Removal Credit - Direct Filters	2.0	(logs)
Virus Removal Credit - Direct Filters	1.0	(logs)
Crypto. Removal Credit - Direct Filters	3.0	(logs)
CFF Turb. Meets LT2 Toolbox Criteria?	FALSE	(TRUE/FALSE)
IFE Turb. Meets LT2 Toolbox Criteria?	FALSE	(TRUE/FALSE)
Crypto. Credit as 2nd Stage Filtr.	0.5	(logs)
GAC		
Empty Bed Contact Time (at 'Plant Flow')	31	(minutes)
GAC Reactivation Interval	180	(days)
GAC Contacting System (Single/Blended)	Blended	(S or B)
TOC Breakthrough for Single Unit (Max/Avg)	Avg_TOC	(M or A)
Crypto. Removal Credit as 2nd Stage	0.5	(logs)
Chlorine (Gas)		
Chlorine Dose	3.0	(mg/L as Cl2)
Contact Tank		
Volume of Basin	28.3000	(MG)
Ratio of T50/Detention Time	1.00	(ratio)
Ratio of T10/Detention Time	0.20	(ratio)
WTP Effluent		
Average Tap		
Average Residence Time (For Average Flow)	1.0	(Days)
End of System		
Maximum Residence Time (For Average Flow)	3.0	(Days)

Figure B2-3 Original input data for the GCWW example processing train.

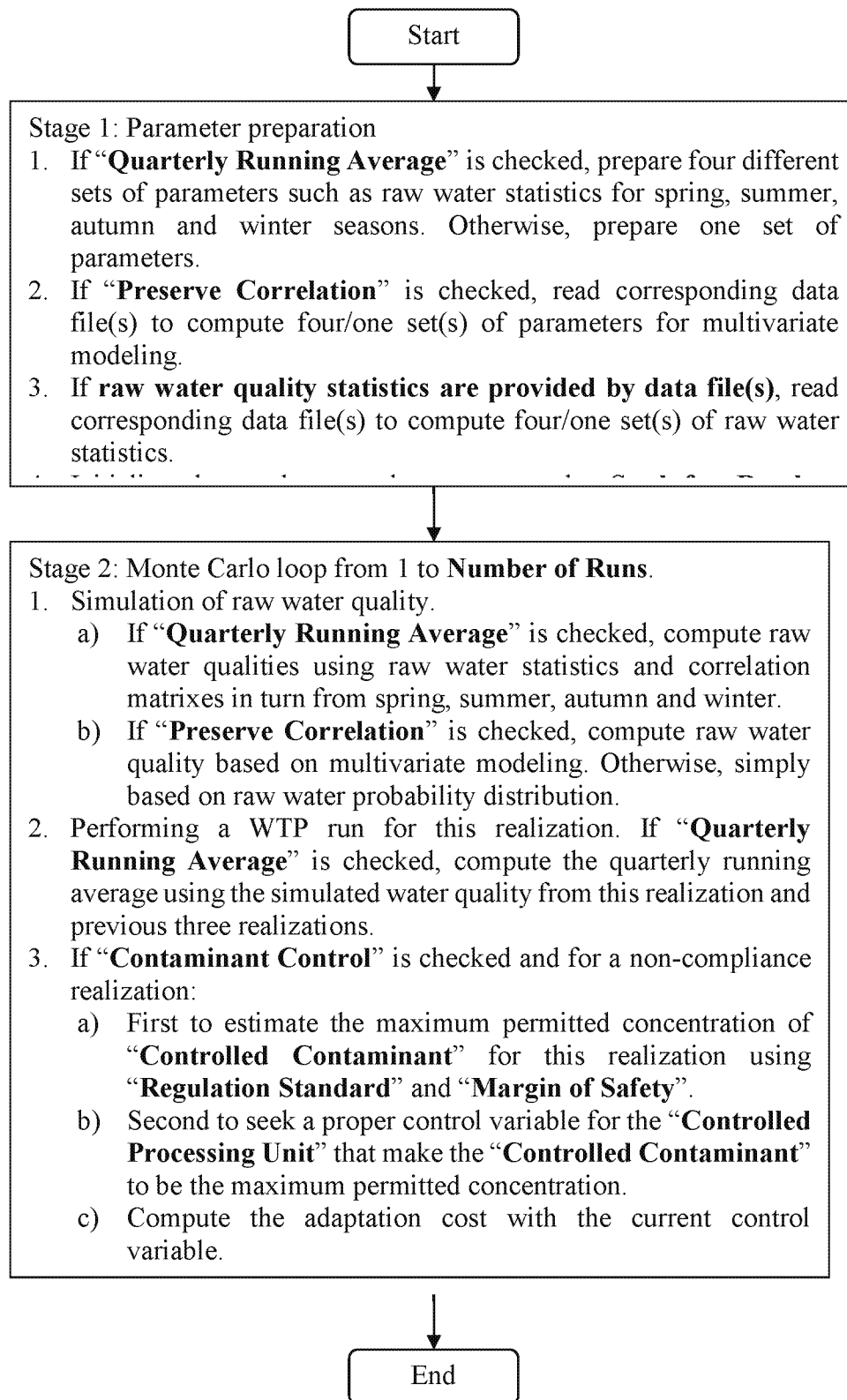


Figure B2-4 Illustration diagram for Monte Carlo analysis

The simulation option for Quarterly Running Average is specially designed for regulation of contaminant TOC. According to the USEPA disinfectant/disinfection byproduct (D/DBP) rule, an important compliance criterion for TOC treatment of surface water sources is that the treated water TOC level does not exceed 2.0 mg/L, calculated quarterly as a running annual average. WTP-CAM applies four seasons to represent the four quarters per year. As a result, this option affects the inputs of raw water quality (both statistics and correlation) and simulation procedure for pursuing the quarterly running average. More details for simulation related to Quarterly Running Average are introduced in Section B4.0.

The option for correlation is designed to preserve the joint correlation among raw water quality parameters when simulating stochastic raw water quality variables in each realization. In the presence of cross-correlation, concentrations of correlated reactants are possibly high or low simultaneously. As a result, cross correlated raw water quality parameters might exert a strong influence on DBP formation during water treatment and distribution. A multivariate seasonal autoregressive model of order one (Bras and Rodriguez-Iturbe, 1984) was applied in WTP-CAM. This seasonal model preserves all seasonal means and variance for all water quality parameters, all cross correlation among all water quality parameters, and lag-one correlations between adjacent seasons and between all water quality parameters. Section B5.0 describes the theoretical basis for the multivariate analysis applied.

Contamination option is designed to modify the design and operation of the current processing train when a non-compliance realization is simulated. For example, if a TOC violation is detected, the WTP-CAM program will modify operation by increasing the frequency of GAC regeneration in order to bring the TOC excursion within acceptable limits. The inputs for this option are controlled contaminant, regulation standard, margin of safety, and unit process to be controlled. So far, the option for contamination component has been developed only for TOC contaminant and GAC unit process. More details are available in Section B5.0.

B 2.2.2 Inputs for Monte Carlo Setting

The input parameters for Monte Carlo analysis may be divided into three groups: options, control parameters and source of influent water quality statistics/correlation. Figure B2-5 demonstrates these inputs for the example processing train shown in Figure B2-1.

Options: options are designed to govern the flow of Monte Carlo simulation. Table B2-1 provides the name of option, range of available values and description. Additional controlled contaminant and controlled unit processes will be added with further development of WTP-CAM.

Table B2-1 Options for Monte Carlo analysis

Control	Range of value	Description
Preserve Correlation	TRUE/FALSE	Multivariate analysis will be used to simulate stochastic raw water quality if TRUE (checked).
Quarterly Running Average	TRUE/FALSE	Simulation will be based on four seasons if TRUE.
System Adaptation	TRUE/FALSE	Loading adaptation program for the non-compliance realizations if TRUE.
Controlled Contaminant	TOC/None	Determining the contaminant to be controlled by adaptation.
Controlled Unit Process	GAC/None	Determining the unit process that can be adapted for controlled contaminant.
Raw Water Probability Distribution	Normal/Lognormal	Determining the probability distribution for all raw water quality parameters

Monte Carlo Setting

Options

- ☒ Preserve Correlation
- ☒ Quarterly Running Average
- ☒ Contamination Control

Controlled Contaminant

TOC

Controlled Processing Unit

GAC

Raw WQ Probability Distrn

LogNormal

Control Parameters

Number of Runs, >1: 1000

Seed for Random Number, 1-50000: 168

Regulation Standard, mg/L: 2

Margin of Safety, mg/L: 0.05

Source of Influent WQ Statistics

Computed by Available Data File(s), Please Click Here

Or Input manually, Please Click Here

Correlation Matrix

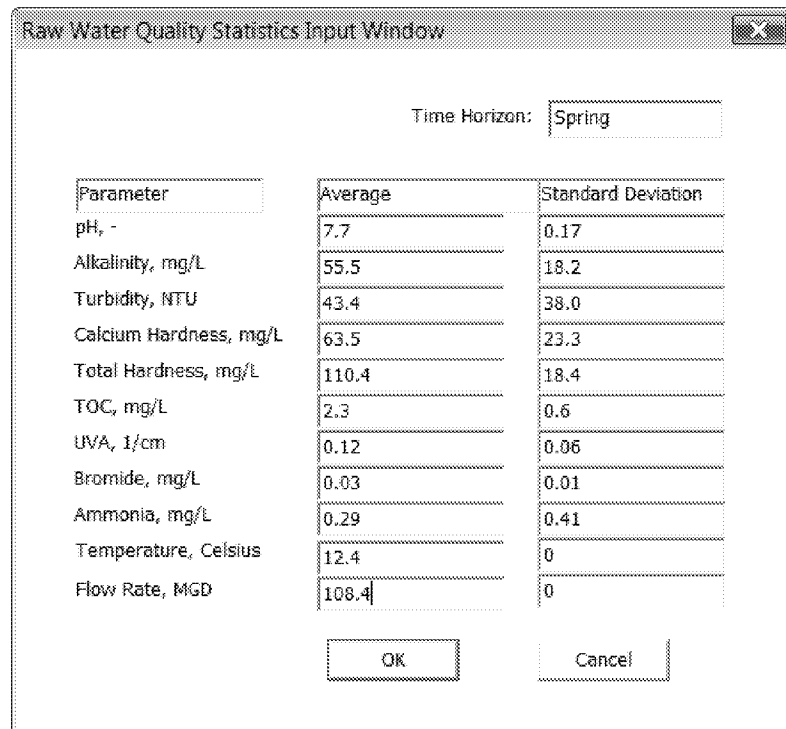
Please Provide Data File(s) Here if Preserve Correlation is Checked

Default Example OK Cancel

Figure B2-5 Monte Carlo inputs for the example processing train

Control parameters: there are four control parameters used in the Monte Carlo simulation:

- Number of Runs – a user defined integer to specify the number of runs required.
- Seed for Random Number – a positive number to initialize the random number generator in the program. Monte Carlo simulation can be repeated using the same random number seed.
- Regulation standard – a value representing the compliance standard for the controlled contaminant selected in **Options**.
- Margin of Safety – refers to the difference between the compliance standard and the real controlled concentration that provides extra reliability for compliance. Margin of safety is usually within 1-10% of the regulation standard.



Raw Water Quality Statistics Input Window

Time Horizon: Spring

Parameter	Average	Standard Deviation
pH, -	7.7	0.17
Alkalinity, mg/L	55.5	18.2
Turbidity, NTU	43.4	38.0
Calcium Hardness, mg/L	63.5	23.3
Total Hardness, mg/L	110.4	18.4
TOC, mg/L	2.3	0.6
UVA, 1/cm	0.12	0.06
Bromide, mg/L	0.03	0.01
Ammonia, mg/L	0.29	0.41
Temperature, Celsius	12.4	0
Flow Rate, MGD	108.4	0

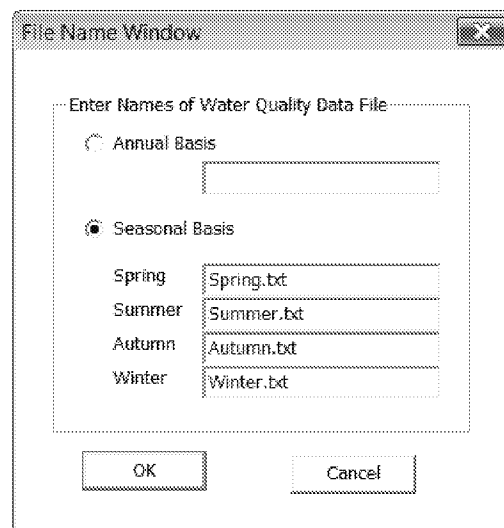
OK Cancel

Figure B2-6 Manual input window for influent water quality statistics

Source of influent

water quality statistics/correlation: influent water quality statistics are essential parameters to generate stochastic influent water quality parameters for each realization. There are two methods provided by WTP-CAM to obtain these parameters. One method is to input these parameters manually through clicking the manual input button. There will be four dialogue windows appearing one at a time for the four seasons if Quarterly Running Average is checked. Figure B2-6 illustrates an example of manual input window for the spring of the example processing train.

The other method is to compute the statistics using data file(s) provided by a user through clicking the button of “Computed by Available Data file”.



File Name Window

Enter Names of Water Quality Data File

☐ Annual Basis

☒ Seasonal Basis

Spring	Spring.txt
Summer	Summer.txt
Autumn	Autumn.txt
Winter	Winter.txt

OK Cancel

Figure B2-7 Dialogue window for name of data files

Figure B2-7 demonstrates the input window for the name (including the extension name) of data files prepared by user. The following points are important:

- Location of file(s): the data file must reside in the same folder as WTP-CAM executive file.
- Format of data: as illustrated in Figure B2-8, the data file consists of 11 columns. The columns are pH, alkalinity, turbidity, calcium hardness, total hardness, TOC, UVA, bromide, ammonia, temperature, and inflow rate. The first two rows are used to indicate the title and unit for each column. There is no limit for the number of data points. Each column needs to be assigned a digit for correct reading of the input file. Empty columns are not allowed. If the value in a column is not available, fill the column with -100.

pH	Alk	Turb	Ca-H	Tt_H	TOC	UVA	Bro	NH3	Temp	Qin
--	mg/l	NTU	mg/l	mg/l	mg/l	l/cm	mg/l	mg/l	Celsius	MGD
7.72	62.5	22.51	99.43	106.72	2.77	0.0924	0.028	0.253	14.4	108.4
7.57	68.2	56.74	57.08	111.41	4.91	0.2106	0.024	0.231	14.4	108.4
7.7	60.94	26.72	77.51	128.73	3.04	0.0768	0.039	0.199	14.4	108.4
7.25	19.12	19.96	53.73	62.22	1.82	0.0376	0.027	0.077	14.4	108.4
7.74	70.12	58.77	56.11	105.38	5.02	0.1991	0.028	0.091	14.4	108.4
7.55	36.65	64	70.74	75.75	2.82	0.061	0.028	0.291	14.4	108.4
7.83	53.49	26.97	54.36	103.91	3.7	0.1178	0.028	0.256	14.4	108.4
7.85	72.55	33.61	75.43	106.96	4.02	0.1536	0.028	0.065	14.4	108.4
7.7	84.91	24.4	53.93	136.28	4.25	0.2098	0.03	0.035	14.4	108.4
7.65	42.93	37.82	38.34	81.68	3.3	0.0848	0.026	0.375	14.4	108.4
7.78	89.18	91.96	36.55	96.79	5.7	0.267	0.023	0.351	14.4	108.4
7.71	49.82	39.61	28.41	80.11	4.21	0.1457	0.029	0.071	14.4	108.4
7.82	67.18	11.59	55.91	117.06	3.13	0.1153	0.026	0.064	14.4	108.4
7.98	73.69	26.57	113.48	124.85	3.79	0.0863	0.036	0.127	14.4	108.4
7.63	37.58	38.38	58.76	89.53	2.14	0.0655	0.026	0.232	14.4	108.4
7.81	49.56	12.52	58.76	97.8	2.95	0.081	0.028	0.158	14.4	108.4
7.74	68.48	27.88	31.01	103.98	3.82	0.2052	0.027	0.089	14.4	108.4
7.72	40.19	35.25	76.38	80.51	3.96	0.0561	0.033	0.376	14.4	108.4
7.97	89.01	4.31	77.95	128.13	3.53	0.0493	0.046	0.23	14.4	108.4
7.8	52.82	12.94	84.92	96.78	2.89	0.0748	0.027	0.083	14.4	108.4
7.82	56.56	36.99	73.16	94.35	4.41	0.0943	0.027	0.662	14.4	108.4

Figure B2-8 Example format of influent water quality data file

If “Preserve Correlation” is checked, users are required to provide the raw water data file(s) for multivariate analysis through clicking the button in Correlation Matrix. The requirements for location of file(s), the format of file and the file name input window are the same as those for compute influent water quality statistics by file as described above.

B2.3 Customization of GAC Unit Process Model

B2.3.1 Overview

The performance of GAC for TOC removal has been studied using TOC breakthrough experiments in GAC columns under various conditions to examine different raw water sources, GAC size, pretreatment configuration, and bed depth/empty bed contact time (EBCT). In developing the WTP model, a classic logistic function was used to represent the TOC breakthrough curve for a single GAC contactor (USEPA, 2005), given by,

$$f(t) = \frac{TOC_{eff}}{TOC_{in}} = \frac{a}{1 + be^{-d \cdot t}} \quad (B3.1)$$

Where, $f(t)$ is TOC fraction remaining; TOC_{in} and TOC_{eff} are TOC influent and effluent concentrations at the GAC unit; t is GAC service time; a , b and d are model parameters estimated by statistical regression.

To improve the accuracy of GAC treatment modeling, WTP-CAM provides a new feature to customize parameters a , b and d using non-linear regression method if users can provide site-specific TOC treatment study data instead of the default statistical values. More details for the TOC breakthrough model and non-linear regression are introduced in Section B4.0.

B2.3.2 Inputs for GAC Model Customization

The GAC model customization is invoked by clicking the GAC model customization button located at bottom of the GAC property window as shown in Figure B2-9. A dialogue window for TOC breakthrough customization will appear as shown in Figure B2-10. There are five edit boxes for user's input.

- File name for TOC breakthrough data: provide the file name including the extension name in the edit box and keep the data file in the same folder as WTP-CAM program. The format of data is illustrated in Figure B2-11. The data file consists of three columns: GAC service time, influent and effluent TOC concentration to the GAC processing unit. The first two rows are used to indicate the title and unit for each column. There is no limit for the number of data points. Empty columns are not allowed.

Figure B2-9 GAC unit process property window

Parameter:	a [-]	b [-]	d [1/day]
Initial value:	0.5	5	0.035
Estimated:	0.604	9.444	0.036

Buttons: OK, Cancel, Click to estimate the parameters

Figure B2-10 Dialogue window for TOC breakthrough customization

- Number of data points: number of valid data points in the data file.
- Initial value for parameter a : a value between 0.6-0.9 (Roberts and Summers, 1982).
- Initial value for parameter b : a value between 3-30 (Based on USEPA, 2005 and initial studies).
- Initial value for parameter d : a value between 0.01-0.1 (Based on USEPA, 2005 and initial studies).

RunTime	TOCin	TOCout
day	mg/l	mg/l
1.5	1.8452	0.1034
5	1.8452	0.1268
9	1.8452	0.084
13	1.8452	0.1103
17	1.8452	0.0812
21	1.8452	0.0772
25	1.8452	0.1372
29	1.8452	0.1223
33	1.8452	0.1867
.....		

Figure B2-11 Example format for TOC breakthrough data file

B3.0 Understanding the Output Data

This Section provides a brief overview of the outputs generated by the WTP-CAM Model. Section B4.1 briefly describes the various output tables for a one-time run. Section B4.2 presents tabular outputs for Monte Carlo analysis. Section B4.3 introduces the graphic outputs based on Monte Carlo simulation. All outputs are based on the example processing train introduced in Section B3.0 for various inputs.

The output module for WTP-CAM is still in development. Therefore, some results in this Section are used for illustrative purposes to show program outputs expected in future.

B3.1 Standard Output Tables for a One-time Run

Based on the example process train shown in Figure B2-2, and input parameters summarized in Figure B2-3, the WTP-CAM will generate full standard outputs contained in 10 output tables and save temporarily in a text file named "WTP-CAM stdout.txt" in the working folder after "One Time Run" command. These 10 output tables are in fact replicated from the outputs of original WTP model. The Tables 1-9 in WTP-CAM outputs are associated with the (typical average) "Plant Flow" and "Influent Temperature" inputs. Outputs for "Table 10" are associated with worst-case disinfection input parameters of "Peak Flow" and "Minimum Temperature." Figure B3-1 through B3-10 demonstrated the standard outputs by one-time run. For a detailed interpretation of these tables please refer to Chapter 4 of the WTP User Manual in USEPA (2005).

Table 1 Water Quality Summary for Raw, Finished, and Distributed water At Plant Flow (120.6 MGD) and Influent Temperature (18.6 C)					
Parameter	Units	Raw water	Effluent	Avg. Tap	End of Sys
pH	(-)	7.8	8.1	8.2	8.2
Alkalinity	(mg/L as CaCO3)	72	74	74	74
TOC	(mg/L)	2.6	1.2	1.2	1.2
UV	(1/cm)	0.096	0.010	0.010	0.010
(T)SUVA	(1/cm)	3.7	0.9	0.9	0.9
Ca Hardness	(mg/L as CaCO3)	77	84	84	84
Mg Hardness	(mg/L as CaCO3)	64	64	64	64
Ammonia-N	(mg/L)	0.21	0.00	0.00	0.00
Bromide	(ug/L)	69	59	50	41
Free Cl2 Res.	(mg/L as Cl2)	0.0	1.0	0.6	0.4
Chloramine Res.	(mg/L as Cl2)	0.0	0.0	0.0	0.0
TTHMs	(ug/L)	0	14	26	37
HAA5	(ug/L)	0	5	8	10
HAA6	(ug/L)	0	6	10	13
HAA9	(ug/L)	0	6	12	17
TOX	(ug/L)	0	33	49	62
Bromate	(ug/L)	0	0	0	0
Chlorite	(mg/L)	0.0	0.0	0.0	0.0
TOC Removal	(percent)		55		
E.C. not required - raw TOC, raw SUVA, and/or finished TOC <= 2					
E.C. Step 1 TOC removal requirement ACHIEVED					
CT Ratios					
Virus	(-)	0.0	33.7	33.7	33.7
Giardia	(-)	0.0	4.2	4.2	4.2
Cryptosporidium*	(-)	1.0	1.0	1.0	1.0
*Crypto. Disinfection Calcs. Based on Proposed LT2 Rule					
Crypto. CT Ratio = 1 because other credits met full disinfection requirements					

Figure B3-1 Standard output "Table 1" for the example processing train

Table 2 Selected Input Parameters			
Parameter	value	Units	
TEMPERATURES			
Average	18.6	(deg. C)	
Minimum	2.0	(deg. C)	
PLANT FLOW RATES			
Average	120.600	(mgd)	
Peak Hourly	220.000	(mgd)	
DISINFECTION INPUTS/CALCULATED VALUES			
Surface Water Plant?	TRUE		
Giardia: Total Disinfection Credit Required	3.0	(logs)	
Giardia: Credit Achieved (other than by CT)	2.5	(logs)	
Giardia: Inactivation Credit by CT Required	0.5	(logs)	
Virus: Total Disinfection Credit Required	4.0	(logs)	
Virus: Credit Achieved (other than by CT)	2.0	(logs)	
Virus: Inactivation Credit by CT Required	2.0	(logs)	
Crypto.: Total Disinfection Credit Required	3.0	(logs)	
Crypto.: Credit Achieved (other than by CT)	3.5	(logs)	
Crypto.: Inactivation Credit by CT Required	0.0	(logs)	
DISINFECT. CREDITS (not incl. CT): Giardia Virus Crypto			
(in order of appearance)			
Filtration	2.5	2.0	3.0
GAC -2nd stage filt.	0.0	0.0	0.5
CHEMICAL DOSES			
(in order of appearance)			
Alum	1.1	(mg/L as Al2(SO4)3*14H2O)	
Lime	5.0	(mg/L as Ca(OH)2)	
Chlorine (Gas)	3.0	(mg/L as Cl2)	
PROCESS HYDRAULIC PARAMETERS: T10/Tth T50/Tth VOL. (MG)			
(in order of appearance)			
Rapid Mix	1.0	1.0	0.0084
Flocculation	0.5	1.0	1.9400
Presed. Basin	0.4	1.0	2.2300
Reservoir	0.3	1.0	373.0000
Settling Basin	0.4	1.0	26.0000
Filtration	0.1	1.0	2.4708
Contact Tank	0.2	1.0	28.3000
GAC OPERATION INPUTS			
Empty Bed Contact Time	31.0	(minutes)	
Reactivation Frequency	180.0	(days)	
Sys. Config. ('S'= Single, 'B'= Blended)	B		

Figure B3-2 Standard output "Table 2" for the example processing train

Table 3 Predicted water Quality Profile At Plant Flow (120.6 MGD) and Influent Temperature (18.6 C)								
Location	pH (-)	TOC (mg/L)	UVA (1/cm)	(T)SUVA (L/mg-m)	Cl2 (mg/L)	NH2Cl (mg/L)	Residence Time Process (hrs)	Cum. (hrs)
Influent	7.8	2.6	0.096	3.7	0.0	0.0	0.00	0.00
Alum	7.7	2.6	0.096	3.7	0.0	0.0	0.00	0.00
Rapid Mix	7.7	2.6	0.084	3.3	0.0	0.0	0.00	0.00
Flocculation	7.7	2.6	0.084	3.3	0.0	0.0	0.39	0.39
Presed. Basin	7.7	2.6	0.084	3.3	0.0	0.0	0.00	0.39
Reservoir	7.7	2.6	0.084	3.3	0.0	0.0	74.23	74.62
Lime	9.0	2.6	0.084	3.3	0.0	0.0	0.00	74.62
Settling Basin	9.0	2.6	0.084	3.3	0.0	0.0	5.17	79.79
Filtration	9.0	2.6	0.084	3.3	0.0	0.0	0.49	80.28
GAC	9.0	1.2	0.015	1.3	0.0	0.0	0.52	80.80
Chlorine (Gas)	8.1	1.2	0.010	0.9	1.4	0.0	0.00	80.80
Contact Tank	8.1	1.2	0.010	0.9	1.0	0.0	5.63	86.43
WTP Effluent	8.1	1.2	0.010	0.9	1.0	0.0	0.00	86.43
Additional Point	8.2	1.2	0.010	0.9	0.8	0.0	12.00	98.43
Average Tap	8.2	1.2	0.010	0.9	0.6	0.0	24.00	110.43
Additional Point	8.2	1.2	0.010	0.9	0.5	0.0	48.00	134.43
End of System	8.2	1.2	0.010	0.9	0.4	0.0	72.00	158.43
TOC Removal (percent): 55 E.C. not required - raw TOC, raw SUVA, and/or finished TOC <= 2 E.C. Step 1 TOC removal requirement ACHIEVED								

Figure B3-3 Standard output "Table 3" for the example processing train

Table 4 Predicted water Quality Profile At Plant Flow (120.6 MGD) and Influent Temperature (18.6 C)							
Location	pH (-)	Alk (mg/L)	Calcium Hardness (mg/L)	Magnesium Hardness (mg/L)	Solids (mg/L)	NH3-N (mg/L)	Bromide (ug/L)
Influent	7.8	72	77	64	0.0	0.2	69
Alum	7.7	71	77	64	0.0	0.2	69
Rapid Mix	7.7	71	77	64	0.0	0.2	69
Flocculation	7.7	71	77	64	0.0	0.2	69
Presed. Basin	7.7	71	77	64	211.9	0.2	69
Reservoir	7.7	71	77	64	211.9	0.2	69
Lime	9.0	78	84	64	211.9	0.2	69
Settling Basin	9.0	78	84	64	211.9	0.2	69
Filtration	9.0	78	84	64	211.9	0.2	69
GAC	9.0	78	84	64	211.9	0.2	69
Chlorine (Gas)	8.1	73	84	64	211.9	0.0	69
Contact Tank	8.1	74	84	64	211.9	0.0	59
WTP Effluent	8.1	74	84	64	211.9	0.0	59
Additional Point	8.2	74	84	64	211.9	0.0	53
Average Tap	8.2	74	84	64	211.9	0.0	50
Additional Point	8.2	74	84	64	211.9	0.0	45
End of System	8.2	74	84	64	211.9	0.0	41

Figure B3-4 Standard output "Table 4" for the example processing train

Table 5 Predicted Trihalomethanes and other DBPs At Average Flow (120.6 MGD) and Temperature (18.6 C)								
Location	BrO3- (ug/L)	ClO2- (mg/L)	TOX (ug/L)	CHCl3 (ug/L)	BDCM (ug/L)	DBCM (ug/L)	CHBr3 (ug/L)	TTHMs (ug/L)
Influent	0	0.0	0	0	0	0	0	0
Alum	0	0.0	0	0	0	0	0	0
Rapid Mix	0	0.0	0	0	0	0	0	0
Flocculation	0	0.0	0	0	0	0	0	0
Presed. Basin	0	0.0	0	0	0	0	0	0
Reservoir	0	0.0	0	0	0	0	0	0
Lime	0	0.0	0	0	0	0	0	0
Settling Basin	0	0.0	0	0	0	0	0	0
Filtration	0	0.0	0	0	0	0	0	0
GAC	0	0.0	0	0	0	0	0	0
Chlorine (Gas)	0	0.0	0	0	0	0	0	0
Contact Tank	0	0.0	33	3	4	4	3	14
WTP Effluent	0	0.0	33	3	4	4	3	14
Additional Point	0	0.0	43	4	6	7	5	22
Average Tap	0	0.0	49	5	7	8	6	26
Additional Point	0	0.0	57	7	8	10	7	33
End of System	0	0.0	62	8	9	12	8	37

Figure B3-5 Standard output "Table 5" for the example processing train

Table 6 Predicted Haloacetic Acids - through HAA5 At Average Flow (120.6 MGD) and Temperature (18.6 C)						
Location	MCAA (ug/L)	DCAA (ug/L)	TCAA (ug/L)	MBAA (ug/L)	DBAA (ug/L)	HAA5 (ug/L)
Influent	0	0	0	0	0	0
Alum	0	0	0	0	0	0
Rapid Mix	0	0	0	0	0	0
Flocculation	0	0	0	0	0	0
Presed. Basin	0	0	0	0	0	0
Reservoir	0	0	0	0	0	0
Lime	0	0	0	0	0	0
Settling Basin	0	0	0	0	0	0
Filtration	0	0	0	0	0	0
GAC	0	0	0	0	0	0
Chlorine (Gas)	0	0	0	0	0	0
Contact Tank	1	2	1	0	1	5
WTP Effluent	1	2	1	0	1	5
Additional Point	1	2	1	0	2	7
Average Tap	1	3	1	1	2	8
Additional Point	1	3	1	1	3	9
End of System	1	4	2	1	3	10

Figure B3-6 Standard output "Table 6" for the example processing train

Table 7 Predicted Haloacetic Acids (HAA6 through HAA9) At Average Flow (120.6 MGD) and Influent Temperature (18.6 C)						
Location	BCAA (ug/L)	BDCAA (ug/L)	DBCAA (ug/L)	TBAA (ug/L)	HAA6 (ug/L)	HAA9 (ug/L)
Influent	0	0	0	0	0	0
Alum	0	0	0	0	0	0
Rapid Mix	0	0	0	0	0	0
Flocculation	0	0	0	0	0	0
Presed. Basin	0	0	0	0	0	0
Reservoir	0	0	0	0	0	0
Lime	0	0	0	0	0	0
Settling Basin	0	0	0	0	0	0
Filtration	0	0	0	0	0	0
GAC	0	0	0	0	0	0
Chlorine (Gas)	0	0	0	0	0	0
Contact Tank	1	0	0	0	6	6
WTP Effluent	1	0	0	0	6	6
Additional Point	2	0	0	0	8	10
Average Tap	2	1	1	1	10	12
Additional Point	3	1	1	1	11	15
End of System	3	1	2	1	13	17

Figure B3-7 Standard output "Table 7" for the example processing train

Table 8 Predicted Disinfection Parameters - Residuals and CT Ratios At Plant Flow (120.6 MGD) and Influent Temperature (18.6 C)									
Location	Temp (C)	pH (-)	Cl2 (mg/L)	NH2Cl (mg/L)	Ozone (mg/L)	ClO2 (mg/L)	CT Ratios		
							Giardia	virus	Crypto
Influent	18.6	7.8	0.0	0.0	0.00	0.00	0.0	0.0	1.0
Alum	18.6	7.7	0.0	0.0	0.00	0.00	0.0	0.0	1.0
Rapid Mix	18.6	7.7	0.0	0.0	0.00	0.00	0.0	0.0	1.0
Flocculation	18.6	7.7	0.0	0.0	0.00	0.00	0.0	0.0	1.0
Presed. Basin	18.6	7.7	0.0	0.0	0.00	0.00	0.0	0.0	1.0
Reservoir	18.6	7.7	0.0	0.0	0.00	0.00	0.0	0.0	1.0
Lime	18.6	9.0	0.0	0.0	0.00	0.00	0.0	0.0	1.0
Settling Basin	18.6	9.0	0.0	0.0	0.00	0.00	0.0	0.0	1.0
Filtration	18.6	9.0	0.0	0.0	0.00	0.00	0.0	0.0	1.0
GAC	18.6	9.0	0.0	0.0	0.00	0.00	0.0	0.0	1.0
Chlorine (Gas)	18.6	8.1	1.4	0.0	0.00	0.00	0.0	0.0	1.0
Contact Tank	18.6	8.1	1.0	0.0	0.00	0.00	4.2	33.7	1.0
WTP Effluent	18.6	8.1	1.0	0.0	0.00	0.00	4.2	33.7	1.0
Additional Point	18.6	8.2	0.8	0.0	0.00	0.00	4.2	33.7	1.0
Average Tap	18.6	8.2	0.6	0.0	0.00	0.00	4.2	33.7	1.0
Additional Point	18.6	8.2	0.5	0.0	0.00	0.00	4.2	33.7	1.0
End of System	18.6	8.2	0.4	0.0	0.00	0.00	4.2	33.7	1.0

Crypto. CT Ratio = 1 because other credits met full disinfection requirements

Figure B3-8 Standard output "Table 8" for the example processing train

Number	Qin MGD	Alk mg/L	Bro mg/L	Ca-H mg/L	Tt-H mg/L	NH3 mg/L	Turb mg/L	PH	Temp C	TOC mg/L	UVA 1/cm
1	120.6	55.52	0.035	49.4	100.8	0.061	12.0	7.60	18.6	3.06	0.061
2	120.6	63.23	0.033	44.4	107.3	0.124	19.5	7.80	18.6	3.76	0.109
3	120.6	61.30	0.033	71.0	104.9	0.191	28.5	7.57	18.6	4.74	0.110
4	120.6	30.96	0.027	62.6	83.5	0.141	26.8	7.72	18.6	1.99	0.095
5	120.6	82.32	0.035	54.8	117.0	0.171	21.1	7.77	18.6	4.99	0.147
6	120.6	59.12	0.031	95.9	108.1	0.063	15.9	7.93	18.6	2.77	0.061
7	120.6	100.52	0.026	89.0	120.5	0.268	281.7	7.87	18.6	5.81	0.406
8	120.6	45.33	0.036	45.6	94.3	0.291	32.3	7.39	18.6	3.14	0.100
~											
996	120.6	47.58	0.028	44.5	90.5	0.236	11.9	7.71	18.6	2.85	0.042
997	120.6	51.37	0.031	56.6	93.3	0.246	44.9	7.57	18.6	3.96	0.106
998	120.6	41.62	0.030	89.7	90.9	0.249	12.5	7.44	18.6	3.17	0.058
999	120.6	58.67	0.027	82.0	101.6	1.558	146.5	7.80	18.6	5.09	0.147
1000	120.6	40.39	0.031	72.4	94.3	0.351	18.1	7.60	18.6	2.14	0.041
Samples	1000	1000	1000	1000	1000	1000	1000	1000	1000	1000	1000
Mean	120.6	58.18	0.030	62.6	98.9	0.359	43.7	7.71	18.6	3.83	0.113
St. dev	0.0	22.36	0.006	23.2	18.0	0.446	40.5	0.16	0.0	1.11	0.056
Min	120.6	15.48	0.014	23.8	49.5	0.003	2.1	7.14	18.6	1.36	0.024
Max	120.6	232.32	0.053	183.3	219.6	4.178	506.9	8.13	18.6	8.82	0.406

Figure B3-11 Sample outputs of raw water quality.

B3.2 Tabular Outputs for Monte Carlo Simulation

Tabular outputs are saved in text format with extension name “txt” in the working folder to allow viewing with any text editor. The tabular outputs will be managed through the main menu “View”-> “Table...” (To be developed). The tabular outputs for Monte Carlo simulations may be classified into five types as described in the following sections.

B3.2.1 Samples/statistics of Raw Water Qualities

The samples of influent water qualities plus inflow rate and temperature for all realizations can be collected as outputs to provide to users. At the bottom of results, the basic statistics, including sample number, mean, standard deviation, minimum and maximum, are also provided. Figure B3-11 illustrates a sample of influent water quality output.

B3.2.2 Samples/Statistics of Effluent Water Quality

Similar to the sample outputs of raw water quality, the sample and basic statistics of effluent water qualities for all realizations can also be outputted. The difference is each unit process has effluent water. Therefore, a location has to be designated for the sample outputs. In addition, it may not be necessary to output all water quality parameters. Thus, an optional list will be provided to users to select output parameters (to be developed). Figure B3-12 demonstrates an example output for selected water quality parameters, pH, TOC,

Number	pH	TOC mg/L	Cl2 mg/L	TTHM ug/L	HAA5 ug/L
--	--				
1	8.34	0.67	1.76	7.90	3.72
2	8.35	1.07	1.08	14.27	6.69
3	8.20	1.75	0.39	22.84	10.87
4	7.86	0.22	1.52	1.64	0.94
5	8.37	1.90	0.43	26.90	12.08
6	8.22	0.55	1.86	5.06	2.58
7	8.23	2.04	0.00	27.86	0.00
8	7.94	0.74	0.32	6.78	2.92
~					
996	8.08	0.55	0.77	4.31	2.06
997	8.10	1.21	0.34	13.63	6.40
998	7.94	0.75	0.55	7.00	3.45
999	8.12	1.97	0.00	8.20	5.52
1000	7.79	0.28	0.19	1.38	0.55
Samples	1000	1000	1000	1000	1000
Mean	8.14	1.12	0.66	10.93	4.08
St. Dev	0.21	0.57	0.67	9.82	3.82
Min	7.25	0.09	0.00	0.00	0.00
Max	8.70	2.05	2.27	41.41	15.62

Figure B3-12 Selected sample outputs of effluent water qualities at finished water.

chlorine, TTHM and HAA₅, at finished water

B3.2.3 Samples/Statistics of Adaptation Costs

Similarly, the sample and basic statistics of adaptation variable and adaptation costs for all realizations can be outputted. Figure B3-13 demonstrates an example output for the adaptation variable, GAC reactivation period, and adaptation cost.

B3.2.4 Samples/Statistics for Compliance/Non-compliance Realizations

In certain sampling-based sensitivity analysis techniques used to identify important dynamic input variables, each vector of input variables is classified behaviorally into two sample sets: those that created simulation outputs above a threshold (regulated standard) as “non-compliance” sample set and those that created outputs below the threshold as “compliance” sample set. WTP-CAM provides similar outputs and their basic statistics for the compliance or the non-compliance sample set for selected parameters from optional list (To be developed). Figure B3-14 demonstrates an example for non-compliance samples to regulated TOC at finished water with selected parameters: the raw water quality parameters and the adaptation cost.

Number --	React days	cost M\$
1	180	13.622
2	180	13.622
3	93	17.511
4	180	13.622
5	82	18.760
6	180	13.622
7	56	22.663
8	180	13.622
~		
996	180	13.622
997	177	13.706
998	180	13.622
999	78	19.284
1000	180	13.622
~		
Samples	1000	1000
Mean	146	15.480
St. Dev	46	3.142
Min	24	13.622
Max	180	32.481

Figure B3-13
Sample outputs for
adaptation costs

Number --	pH --	Alk mg/l	Turb NTU	Ca-H mg/l	Tt_H mg/l	TOC mg/l	UVA 1/cm	Bro mg/l	NH3 mg/l	Cost M\$
2	7.68	53.8	146.9	56.0	79.2	7.84	0.191	0.020	0.59	32.48
5	7.77	48.3	34.7	57.9	88.0	4.18	0.093	0.032	0.81	15.41
8	7.58	58.6	21.9	51.1	96.8	4.65	0.122	0.037	0.50	17.58
10	8.01	63.0	88.7	40.0	90.5	5.27	0.268	0.023	0.21	20.46
14	7.57	61.3	28.5	70.9	104.8	4.74	0.110	0.033	0.19	18.24
16	7.77	82.3	21.1	54.8	117.0	4.99	0.147	0.035	0.17	19.55
18	7.87	100.5	281.7	89.0	120.5	5.81	0.406	0.026	0.27	23.43
20	7.73	84.6	13.6	59.9	123.8	4.66	0.146	0.035	0.18	17.71
~										
981	7.67	78.1	39.2	57.9	109.5	6.19	0.147	0.026	0.36	24.96
982	7.64	79.3	42.8	70.8	114.0	4.47	0.115	0.030	0.93	16.97
983	7.99	101.9	26.8	43.3	114.3	4.87	0.227	0.027	0.01	18.89
989	8.01	85.8	45.5	104.5	120.7	5.13	0.102	0.033	0.45	20.46
998	7.97	112.5	21.3	136.9	128.2	8.82	0.136	0.035	0.32	13.62
999	7.83	76.2	111.3	159.2	120.5	4.57	0.169	0.030	0.10	17.58
~										
Samples	451	451	451	451	451	451	451	451	451	451
Mean	7.75	71.1	48.3	63.5	104.6	4.83	0.145	0.030	0.36	18.47
St. Dev	0.16	23.5	41.0	25.0	19.1	0.81	0.060	0.006	0.43	3.62
Min	7.28	27.8	5.3	25.9	66.9	3.85	0.047	0.017	0.01	13.62
Max	8.13	232.3	326.1	183.3	219.6	8.82	0.406	0.053	3.06	32.98

Figure B3-14 Sample outputs of raw water quality and adaptation cost for non-compliance events

B3.2.5 Running Log

Running log (To be developed) will be generated automatically when WTP-CAM is executed. The log file provides the status of execution and messages of error or warning occurred, which will assist the user to diagnose problems.

Appendix A provides further information concerning the error ID and warning ID.

Figure B3-15 shows the format of the log file.

```
WTP-CCAM Version 1.0
Latest Update: August 12, 2010
Developed for USEPA by the University of Cincinnati
Name of project: Sample Processing Train
Date of running: Fri Aug 13 13:03:56 2010
-----
Reading input file... successfully
Monte Carlo simulation... successfully
simulation is completed, thank you.
```

Figure B3-15 Example format of the log file

B3.3. Graphic Outputs for Monte Carlo Simulation

The tabular results, after data processing, can be viewed using graphs. The graphs can be further printed or saved as a data file. The results of Monte Carlo analysis can be illustrated either with a sample versus realization chart, frequency chart, cumulative frequency chart or sensitivity chart for the sample-based data.

B3.3.1. Sample Chart (To be developed)

A sample chart is used to illustrate directly how a sampled random variable changes with realization. The realization may represent the time sequence or spatial sequence depending on the circumstance studied. Figure B3-16 demonstrates a sample chart for raw water TOC. The realization may present daily, weekly, or monthly time horizon.

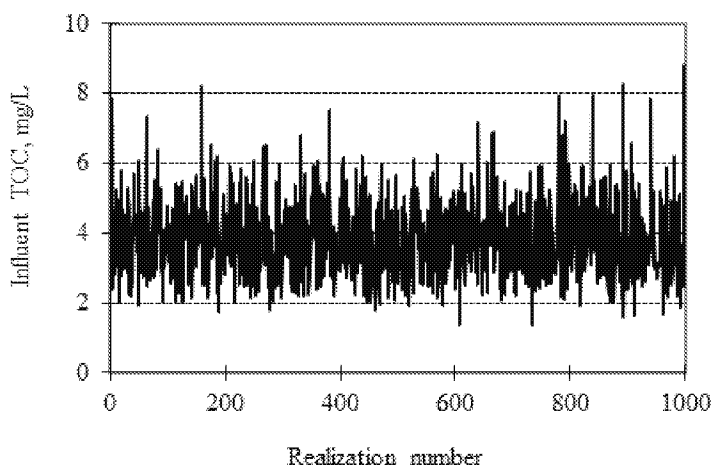


Figure B3-16 Example sample chart for raw water TOC

B3.3.2. Frequency Chart (To be developed)

The frequency chart, a graphical display of tabular frequencies, is used to plot density of data and show the degree of uncertainty for a selected parameter. In other words, a frequency chart illustrates how often they occur in the range of the selected parameter values. Figure B3-17 shows an example frequency chart for raw water TOC.

B3.3.3. Cumulative Frequency Chart (To be developed)

The cumulative frequency chart provides another way to explain the results from Monte Carlo simulation and is often preferred. This chart presents the probability that a value falls within, above or below a given range. Figure B3-18 illustrates an example cumulative frequency chart for effluent TOC at finished water. It can be seen that only 62% of the effluent TOC concentration is less than 2 mg/L, the regulation compliance. Conversely, the TOC compliance standard is violated in 38 percent of the samples.

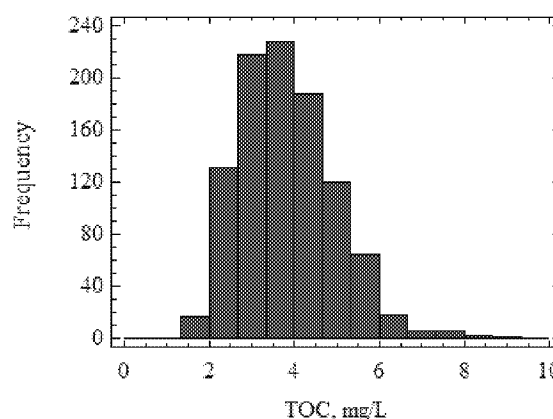


Figure B3-17 Example frequency chart for raw water TOC

B4.0 Models and Algorithms in WTP-CAM

B4.1 Monte Carlo Methods

Monte Carlo analysis is a practical tool that is widely used to obtain sample solutions by repeating a simulation process for problems involving random variables with known probability distributions. Monte Carlo methods are useful for modeling phenomena with significant uncertainty in inputs such as climate change induced raw water qualities. Because Monte Carlo simulation considers random sampling of probability distribution functions as model inputs to produce hundreds or thousands of possible outcomes instead of a few discrete scenarios, the results provide probabilities of different outcomes occurring. Monte Carlo methods usually follow a particular procedure below:

- Define a domain of possible inputs.
- Generate inputs randomly from the domain using a specified probability distribution.
- Perform a deterministic computation using the inputs.
- Aggregate the results of the individual computations into the final result.

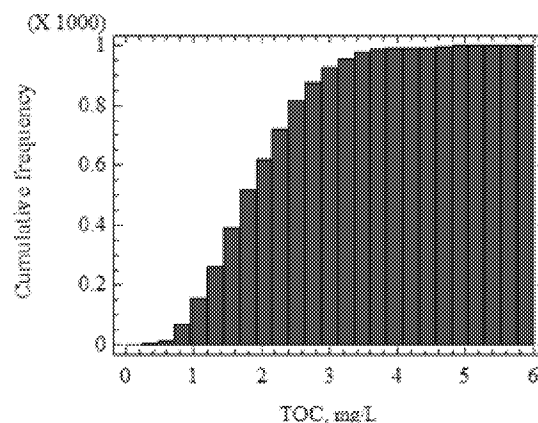


Figure B3-18 Example cumulative frequency chart for effluent TOC at finished water

As briefly introduced in Section B3.1, the ability to conduct Monte Carlo simulation is an important new feature of WTP-CAM. Three key options govern the Monte Carlo analysis: Preserving Correlation, Quarterly Running Average and Contamination Control/Adaptation of Unit Process. Sections B5.1.1 to B5.1.3 provide descriptions of these controls.

B4.1.1 Seasonal Multivariate Analysis

The control for preserving correlation is designed to preserve the joint correlation among raw water quality parameters when simulating stochastic raw water quality inputs in each realization. A multivariate seasonal autoregressive model of order one, AR(1), (Bras and Rodriguez-Iturbe, 1984; Salas *et al.*, 1980) was applied in WTP-CAM to simulate the raw water quality since this seasonal model preserves all seasonal means and variance for all water quality parameters, all cross correlation among all water quality parameters, and lag-one correlations between adjacent seasons and between all water quality parameters. According to Bras and Rodriguez-Iturbe (1980), the lag-one multivariate seasonal autoregressive model is,

$$(X_j - m_j) = A_j (X_{j-1} - m_{j-1}) + B_j \varepsilon_j \quad (B5.1)$$

Where, X_j is the (9×1) vector of nine raw water quality parameters for season j . m_j is the known vector of the means for the nine parameters for season j . ε_j is an (9×1) vector of standard normal deviates for season j . A_j and B_j are (9×9) parameter matrices for season j . A_j and B_j can be estimated by the covariance matrices (Bras and Rodriguez-Iturbe, 1984),

$$A_j = {}_jM_{1j-1} M_0^{-1} \quad (B5.2)$$

$$B_j B_j^T = {}_jM_0 - {}_jM_{1j-1} M_0^{-1} {}_jM_1^T \quad (B5.3)$$

where, ${}_jM_0$ is the lag-zero covariance matrix of $(X_j - m_j)$ for season j ; ${}_jM_1$ is the lag-one covariance matrix of $(X_j - m_j)$ for season j ; superscript (-1) refers to the invertible matrix; superscript (T) refers to the transpose matrix.

Let $Y = X_j - m_j$ and $X = X_{j-1} - m_{j-1}$, Equation B5.1 becomes,

$$Y = A_j X + B_j \varepsilon_j \quad (B5.1a)$$

The covariance matrices are defined by,

$${}_jM_0 = S_{yy} = E[YY^T] \quad (B5.4)$$

$${}_jM_1 = S_{yx} = E[YX^T] \quad (B5.5)$$

$${}_{j-1}M_0 = S_{xx} = E[XX^T] \quad (B5.6)$$

Matrices S_{xx} , S_{yy} and S_{yx} can be represented in terms of variances, standard deviations and correlations as,

$$\mathbf{S}_{xx} = \begin{pmatrix} S_{x_1}^2 & r_{x_1 x_2} S_{x_1} S_{x_2} & L & r_{x_1 x_9} S_{x_1} S_{x_9} \\ r_{x_2 x_1} S_{x_2} S_{x_1} & S_{x_2}^2 & L & r_{x_2 x_9} S_{x_2} S_{x_9} \\ M & M & O & M \\ r_{x_9 x_1} S_{x_9} S_{x_1} & r_{x_9 x_2} S_{x_9} S_{x_2} & L & S_{x_9}^2 \end{pmatrix} \quad (5.7)$$

$$\mathbf{S}_{yy} = \begin{pmatrix} S_{y_1}^2 & r_{y_1 y_2} S_{y_1} S_{y_2} & L & r_{y_1 y_9} S_{y_1} S_{y_9} \\ r_{y_2 y_1} S_{y_2} S_{y_1} & S_{y_2}^2 & L & r_{y_2 y_9} S_{y_2} S_{y_9} \\ M & M & O & M \\ r_{y_9 y_1} S_{y_9} S_{y_1} & r_{y_9 y_2} S_{y_9} S_{y_2} & L & S_{y_9}^2 \end{pmatrix} \quad (5.8)$$

$$\mathbf{S}_{yx} = \begin{pmatrix} r_{y_1 x_1} S_{y_1} S_{x_1} & r_{y_2 x_1} S_{y_2} S_{x_1} & L & r_{y_9 x_1} S_{y_9} S_{x_1} \\ r_{y_1 x_2} S_{y_1} S_{x_2} & r_{y_2 x_2} S_{y_2} S_{x_2} & L & r_{y_9 x_2} S_{y_9} S_{x_2} \\ M & M & O & M \\ r_{y_1 x_9} S_{y_1} S_{x_9} & r_{y_2 x_9} S_{y_2} S_{x_9} & L & r_{y_9 x_9} S_{y_9} S_{x_9} \end{pmatrix} \quad (B5.9)$$

where, S_{x_i} is the standard deviation of variable x_i , $r_{x_i x_j}$ is the lag-zero correlation between x_i and x_j , $r_{y_i x_j}$ is the lag-one correlation between variables y_i and x_j . The sample means, standard deviations and correlations are known parameters obtained from historical records.

Therefore, the matrix \mathbf{A}_j can be computed directly with Equation B5.2. Matrix \mathbf{B}_j can be obtained by decomposition of $\mathbf{B}_j \mathbf{B}_j^T$ through taking matrix \mathbf{B}_j as a lower triangular form,

$$\mathbf{B}_j = \begin{pmatrix} b_{11} & 0 & L & 0 \\ b_{21} & b_{22} & L & 0 \\ M & M & O & M \\ b_{91} & b_{92} & L & b_{99} \end{pmatrix} \quad (B5.10)$$

$$\text{Let } \mathbf{D} = \begin{pmatrix} d_{11} & d_{12} & L & d_{19} \\ d_{21} & d_{22} & L & d_{29} \\ M & M & O & M \\ d_{91} & d_{92} & L & d_{99} \end{pmatrix} = \mathbf{B}_j \mathbf{B}_j^T \quad (B5.11)$$

According to Salas *et al* (1980), if \mathbf{D} is a positive definite matrix, a unique solution for \mathbf{B}_j can be obtained when \mathbf{B}_j is a lower triangular matrix. The non-zero elements of \mathbf{B}_j are calculated by,

$$\text{For } j=1, \quad b_{ij} = d_{ij} / b_{jj} \quad i=1, \dots, 9 \quad (B5.12)$$

$$\text{For } j=2, 3, \dots, 9 \text{ and } i=j, b_{ij} = \sqrt{d_{ij} - \sum_{k=1}^{j-1} b_{jk}^2} \quad (\text{B5.13})$$

$$\text{For } j=2, 3, \dots, 8 \text{ and } i=j+1, \dots, 9, b_{ij} = \left(d_{ij} - \sum_{k=1}^{j-1} b_{jk} b_{ik} \right) / b_{ij} \quad (\text{B5.14})$$

When matrices A_j and B_j are computed and vector ε_j is simulated, the normally distributed stochastic water quality parameters with preserved correlation, X_j , can be calculated with Equation B5.1.

If the elements of vector X and Y , x_i and y_i , are random variables following a two-parameter log-normal distribution, define the new variables, x'_i and y'_i , as following,

$$x'_i = \ln(x_i) \quad (\text{B5.15})$$

$$y'_i = \ln(y_i) \quad (\text{B5.16})$$

Thus, the transformed variables x'_i and y'_i are normally distributed with means $m_{x'_i}$ and $m_{y'_i}$, standard deviations $s_{x'_i}$ and $s_{y'_i}$, and the correlation coefficient among them given by $r_{x'_i y'_i}$. The sample means, standard deviations and correlations of the transformed variables x'_i and y'_i can be also obtained from the transformed historical records through Equation B5.15 and B1.16.

The parameters of the transformed variables are then used to build the necessary auto-covariance and cross-covariance matrices using the equations B5.7 to B5.9. Matrices A_j and B_j can be obtained from the previous introduced Equations.

In order to get the original variables from results based on the transformed computation, the inverse transformation must be performed as following,

$$x_i = \exp(x'_i + m_{x'_i}) \quad (\text{B5.17})$$

$$y_i = \exp(y'_i + m_{y'_i}) \quad (\text{B5.18})$$

B4.1.2 Simulation of quarterly running average (TOC compliance).

The simulation of Quarterly Running Average is specially designed for regulation of contaminant TOC. According to the USEPA disinfectant/disinfection byproduct (D/DBP) rule, an important compliance criterion for TOC treatment for surface water as source is that the treated water TOC concentration does not exceed 2.0 mg/L, calculated quarterly as a running annual average. WTP-CAM applies four seasons to represent the four quarters per year. Therefore, there are four running annual averages computed for each year. The running annual average is defined as the arithmetic average of TOC concentrations at current season and previous three seasons based on the USEPA D/DBP rule. Table B4-1 illustrates calculations of running annual average for TOC in finished water.

Since the means, variances and cross correlations of raw water parameters vary with seasonal changes in most circumstances, it is necessary to prepare four sets of input parameters for raw water qualities as shown in Figure 2-4. Therefore, there are four simulations each year, corresponding to the four seasons. The TOC concentration is recomputed each season with TOC values defined above.

Table B4-1 Illustration of calculating running annual average for finished water TOC

Year	Season	TOC concentration	Running annual average
2009	Spring	1.3	--
	Summer	1.7	--
	Autumn	2.2	--
	Winter	1.7	1.7
2010	Spring	1.2	1.7
	Summer	1.4	1.6
	Autumn	2.4	1.7
	Winter	1.5	1.6

B4.1.3 Adaptation of Unit Process

Adaptation refers to necessary changes of design and/or operation of the current water treatment train when a non-compliance event is simulated. So far, the only adaptation module that has been developed is for TOC treatment in the GAC unit process. More contaminant controls and unit processes will be added with further development of WTP-CAM.

There are four parameters required from users: controlled contaminant, regulation standard, margin of safety, and unit process to be adapted. For example, if TOC is selected as the controlled contaminant, the regulation standard is 2.0 mg/L. In order to better ensure the compliance, a margin of safety may be applied to adaptation. Margin of safety refers to the difference between the compliance standard and the real controlled concentration that provides extra reliability for compliance. For instance, if margin of safety is 0.1mg/L, the controlled the TOC concentration will be $2.0 \text{ mg/L} - 0.1 \text{ mg/L} = 1.9 \text{ mg/L}$. In other words, the simulated running annual average of TOC concentration will be less than 1.9 mg/L after adaptation. The unit process to be adapted is where a change of a design or operation parameter happens. For example, if a noncompliance event happens for TOC in finished water and GAC unit process is available in the process train, an effective way to enhance TOC removal is to reduce the GAC service time in GAC contactors (see Section 5.2.1 for detail). WTP-CAM will seek a GAC service time so that the TOC concentration is right below the controlled concentration 1.9 mg/L.

The specific procedure of computation is as follows. The first step is to reduce current GAC service time by one day. The second step is to use the new service time to re-compute the TOC concentration for each of four seasons without change of other conditions in each season. The third step is to calculate the new running annual average of TOC. The final step is compare the new calculated TOC to the controlled concentration 1.9mg/L; if new TOC is less than 1.9 mg/L, the new service time is adopted; otherwise, go back to the first step and repeat computation again.

B4.2 Customization of Unit Process

Chapter 5 of original WTP model user manual (USEPA, 2005) in Appendix C provides a detail description of equations used to model various unit processes. The WTP Model primarily uses empirical correlations to predict central tendencies of NOM removal, disinfection, and DBP formation in a treatment plant. The algorithms were generally developed using multiple linear regression techniques. As a result, the empirical correlations usually consist of independent variables and empirical constants. These statistical models generally work well for providing the central tendencies. However, they may not provide sufficiently accurate predictions for a specific utility. As a new feature, therefore, WTP-CAM provides options to customize the empirical constants in regression equations using site-specific treatment study data. To date, only the GAC treatment unit process has modified to allow customization of the TOC breakthrough model. Customizations for other unit processes will be added with the development of WTP-CAM.

B4.2.1 Customization of GAC Unit Process

GAC treatment has been used as an alternative for reducing organic contamination in water supplies since early 1970's (Roberts and Summers, 1982). The performance of GAC for TOC removal has been studied using TOC breakthrough experiments in GAC columns under different conditions, such as GAC sources or pretreatment configurations. Roberts and Summers (1982) found that complete removal of TOC by GAC cannot be achieved under water treatment conditions. An immediate, partial breakthrough of TOC can be observed, even using a column filled with fresh GAC, which indicates that a portion of the influent TOC is not amenable to removal by GAC treatment. With increased service time, the effluent TOC concentration rises and eventually reaches a steady state value, which indicates that the GAC becomes saturated with organics. They also observed that the effluent TOC seldom reaches the influent concentration but is lower than the influent level. This constant steady-state removal usually is attributed to biodegradation (USEPA, 1996). During early stages of operation, the ratio of effluent to influent TOC concentration (called "fraction remaining") generally ranges from 0.1 to 0.5, depending on composition of the organic constituents and EBCT/bed depth. For steady-state removal, the fraction remaining varies from 0.6 to 0.9 with corresponding range of service times from 3,000 to 14,000 measured in bed volumes.

The TOC breakthrough curve in a single GAC contactor is often described mathematically by a logistic functions (Oulman, 1980; Clark, 1987a, 1987b; USEPA, 2005). According to USEPA (2005), the classic logistic function used by the WTP model is given by,

$$f(t) = \frac{TOC_{eff}}{TOC_{in}} = \frac{a}{1 + be^{-d \cdot t}} \quad (B3.1)$$

Where, a , b and d are model parameters developed to reflect the impact of influent TOC and pH and EBCT. Based on statistical regression, these parameters can be estimated by (USEPA, 2005),

$$a = 0.682 \quad (\text{B5.19})$$

$$b = 0.167 pH^2 - 0.808 pH + 19.086 \quad (5.20)$$

$$d = TOC_m \left\{ pH \left[-0.0000058 EBCT^2 + 0.000111 EBCT + 0.00125 \right] + 0.0001444 EBCT^2 + 0.005486 EBCT + 0.06005 \right\} \quad (\text{B5.21})$$

To improve the accuracy of GAC treatment modeling, WTP-CAM provides a new feature to estimate parameters a , b and d using a non-linear regression method if site-specific TOC treatment study data are available instead of the statistical values estimated by Equations B5.19-B5.21.

It may be time-consuming and expensive to obtain site-specific data from a pilot-plant or full-scale study of GAC adsorption processes. Instead, the rapid small-scale column test (RSSCT) may be used to generate the data required (Crittenden *et al.* 1991; Zachman and Summers 2010). An RSSCT is a scaled-down version of a pilot or full-scale GAC column contactor. The RSSCT method use mass transfer models to scale down the full-scale contactor to a small column. Similarity of operation to that of large-scale contactors is assured by properly selecting the GAC size, hydraulic loading and EBCT of the small contactor (Crittenden *et al.* 1991; Zachman and Summers 2010). USEPA (1996, 2000) provides standardized guidelines for GAC treatment studies that help obtain quality assurance data of TOC breakthrough in a GAC column. The USEPA's information collection rule (ICR) treatment studies database also provide GAC treatment study data from 63 treatment studies nationwide (USEPA, 2000), including 44 RSSCT studies, 18 pilot studies and 1 full-scale study.

When $f(t)$ versus t dataset are obtained from GAC treatment studies, WTP-CAM applies a modified Gauss-Newton method to estimate model parameters a , b and d by fitting the non-linear regression function (Equation B3.1) through least square analysis based on Hartley (1961). The objective function is defined as,

$$\text{Min } Q(a, b, d) = \sum_{k=1}^n (y_k - f(t_k; a, b, d))^2 \quad (\text{B5.22})$$

Where, $f(t; a, b, d) = \frac{a}{1 + be^{-d \cdot t}}$; a , b and d are the model parameters to be estimated; t_k and y_k are the known field values representing GAC service time and TOC fraction remaining; n is a known number of field samples.

As a widely used method, Gauss-Newton method seeks solutions through iteration. Therefore, an important step is to correct model parameters during iteration using equation,

$$\theta_i = \theta_0 + vD \quad (\text{B5.23})$$

Where, θ is a vector of parameters to be estimated, $\theta = \begin{pmatrix} a \\ b \\ d \end{pmatrix}$, θ_0 represent the initial parameter vector and θ_i represent the corrected parameter vector; D is a correction vector to the initial parameters as a solution from the Gauss-Newton equations, $D = \begin{pmatrix} D_1 \\ D_2 \\ D_3 \end{pmatrix}$; ν is a value from 0 to 1 to minimize $Q(a,b,d)$ during each iteration.

The Gauss-Newton equation is given by,

$$AD = R \quad (B5.24)$$

Where, A is the Gauss-Newton coefficient matrix, defined by,

$$A = \begin{pmatrix} 2\sum_{k=1}^n \left(\frac{\partial f}{\partial a}\right)^2 & 2\sum_{k=1}^n \frac{\partial f}{\partial a} \frac{\partial f}{\partial b} & 2\sum_{k=1}^n \frac{\partial f}{\partial a} \frac{\partial f}{\partial d} \\ 2\sum_{k=1}^n \frac{\partial f}{\partial b} \frac{\partial f}{\partial a} & 2\sum_{k=1}^n \left(\frac{\partial f}{\partial b}\right)^2 & 2\sum_{k=1}^n \frac{\partial f}{\partial b} \frac{\partial f}{\partial d} \\ 2\sum_{k=1}^n \frac{\partial f}{\partial d} \frac{\partial f}{\partial a} & 2\sum_{k=1}^n \frac{\partial f}{\partial d} \frac{\partial f}{\partial b} & 2\sum_{k=1}^n \left(\frac{\partial f}{\partial d}\right)^2 \end{pmatrix} \quad (\text{Herein, } f = f(t, a, b, d)) \quad (B5.25)$$

R is a right-hand-side vector of Gauss-Newton equation, defined by,

$$R = \begin{pmatrix} -\frac{\partial Q}{\partial a} \\ -\frac{\partial Q}{\partial b} \\ -\frac{\partial Q}{\partial d} \end{pmatrix} \quad (\text{Herein, } Q = Q(a, b, d)) \quad (B5.26)$$

Vector D can then be solved by,

$$D = A^{-1}R \quad (B5.27)$$

Where, A^{-1} is inverse of matrix A .

In order to find an approximate minimum of $Q(a,b,d)$, ν value is estimated by the parabola through $Q(\nu=0)$, $Q\left(\nu=\frac{1}{2}\right)$, and $Q(\nu=1)$, given by,

$$\nu = \frac{1}{2} + \frac{1}{4} \frac{[Q(\nu=0) - Q(\nu=1)]}{\left[Q(\nu=1) - 2Q\left(\nu=\frac{1}{2}\right) + Q(\nu=0)\right]} \quad (B5.28)$$

Where, $Q(\nu=0)$, $Q(\nu=\frac{1}{2})$, and $Q(\nu=1)$ represent the $Q(a_1, b_1, d_1)$ values evaluated with $\nu=0$, $\nu=\frac{1}{2}$ and $\nu=1$ through Equation B5.23.

The specific procedure can be summarized by the following steps. Step 1 is to provide initial vector for θ_0 . Step 2 is to solve for the vector D using Equation B5.27. Step 3 is to solve for ν value with Equation 5.28. Step 4 is to check whether $Q(a_1, b_1, d_1)$ value meets the precision requirement. If the answer is “no”, the initial parameters are replaced by the values calculated with equation B5.23 and iterated from step 2.

B4.3 Economics

WTP-CAM provides an economic analysis to estimate the costs associated with adaptation made to design or operation of water treatment in order to provide a metric to assess impact of climate change. The total costs considered in WTP-CAM include capital, operational and management costs. To date, only the GAC treatment unit process has a cost analysis model. Cost models for other unit processes will be added with the development of WTP-CAM.

B4.3.1 Adaptation Costs for GAC Processing

The costs for GAC processing consist of four types of costs: initial GAC cost, annual GAC make-up cost, GAC contactor cost and GAC reactivation cost. The initial GAC cost is one-time charge for GAC required to fill the contactors, which is calculated by the product of the total volume of contactors, the density and unit cost of new GAC. The annual GAC make-up cost is yearly cost for GAC loss during reactivation, which is calculated by the product of GAC loss rate for reactivation, GAC reactivation rate and unit cost. The GAC contactor cost can be estimated with a general form of the cost models by Adams and Clark (1988),

$$y = a + b(USRT)^c d^z \quad (B5.29)$$

where, y is the capital, operational or maintenance cost; $USRT$ is the process design or operating variable, which is usually the total surface area of the GAC filter for contactors (total hearth area for GAC reactivation) or the total effective volume of the GAC unit for capital cost; a , b , c and d are empirical parameters determined from nonlinear regression analysis, and z is either 0 or 1 for adjusting the cost functions for a range of $USRT$ values. The model parameters can be found from Adams and Clark (1988), which was obtained based on the costs in 1983. For consistence of comparison, all costs were converted to 2009 currency using the Producers Price Index (US BLS, 2008). The contactor cost can be further categorized by the costs of capital, process energy, building energy, maintenance material and operational and maintenance (O&M) labor. The computational parameters for contactors are listed in Table B5-2.

The GAC reactivation cost can be estimated using a similar algorithm used to calculate GAC contactor cost based on Equation B5.29. However, the model parameters are different from those for contactor cost. Table B5-3 lists the parameters used to estimate GAC reactivation cost.

Table B4-2 GAC contactor cost

Type of Cost	Capital	Process energy	Building energy	Maintenance Material	O&M Labor
USRT	volume	area	area	area	area
a	93700	0	15150	540	1160
b	1999.1	12	350	23.6	0.3
c	0.712	1	0.916	0.753	1.068
d	0.958	1	1	1	1.152
z	1	1	1	1	1
Unit cost	Construction Cost 1.3y	0.08 \$/kwh (in 2009)	0.08 \$/kwh (in 2009)	--	9 \$/hr (in 1983)
Ratio of 2009 to 1983 cost	2009ENR/1983ENR R=2.16	--	--	2009PPI/1983 PPI = 2.56	2009 PPI/1983 PPI = 2.56

If the capital recovery analysis is assumed a return period of 20 years with an interest rate of 5%, a cost curve can be developed to illustrate the total annual cost of the GAC system varies with GAC service time (reactivation period). WTP-CAM takes the cost curve and uses the curve to estimate the adaptation cost through interpolations based on GAC service time.

Table B4-3 GAC reactivation cost

Type of Cost	Capital	Process energy	Building energy	Maintenance Material	O&M Labor	Natural Gas
USRT	area	area	area	area	area	area
a	144000	354600	12250	0	2920	648400
b	198300.4	6387	312.1	4456.6	282	287714.9
c	0.434	0.755	0.649	0.401	0.7	0.899
d	1	1	1	1	1	1
z	1	1	1	1	1	1
Unit cost	Construction Cost 1.3y	0.08 \$/kwh (in 2009)	0.08 \$/kwh (in 2009)	--	9 \$/hr (in 1983)	\$0.0035 /scf (in 1983)
Ratio of 2009 to 1983 cost	2009ENR/1983ENR = R = 2.16	--	--	2009 PPI/1983PPI = 2.56	2009PPI/1983 PPI = 2.56	2009PPI/1983 PPI = 2.56

Figure B4-1 demonstrate an example cost curve developed for GCWW's Miller plant. The Miller treatment plant has 12 down flow gravity contactors and two multi-hearth furnaces for onsite reactivation. Each of the Miller plant contactors has a volume of 595 m³ and a surface area of 181 m². The overall GAC loss rate through the system is about eight percent. The carbon loading rate is 482 kg/day of GAC per square meter of hearth area.

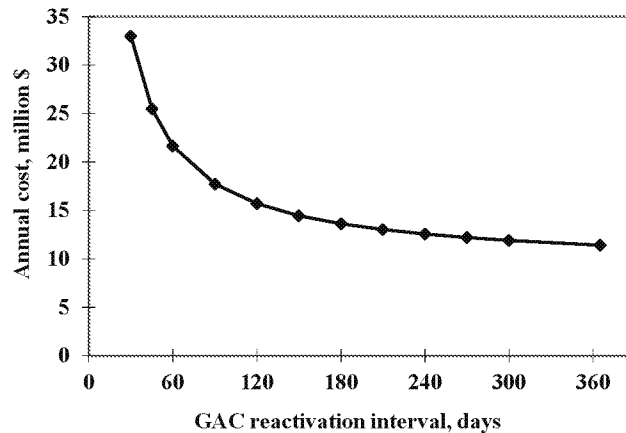


Figure B4-1 Cost curve for annual cost of GAC unit process

B5.0 References

- Adams, J. Q. and Clark, R. M. (1988). "Development of Cost Equations for GAC Treatment Systems." *Journal of Environmental Engineering*, 114 (3): 672-688.
- Bras, R.L. and Rodriguez-Iturbe, I. (1984). "Random Functions and Hydrology." *Addison-Wesley Publishing Company*.
- Clark, R.M. (1987a). "Modeling TOC Removal by GAC: The General Logistic Function." *J. AWWA*, 79(1): 33-37
- Clark, R.M. (1987b). "Evaluating the cost and performance of field-scale granular activated carbon systems." *Environmental Science and Technology*. 21 (6): 573-580.
- Crittenden, J.C., Reddy, P.S., Arora, H., Trynoski, J., Hand, D.W., Perram, D.L., and Summers, R.S. (1991). "Predicting GAC performance with rapid small-scale column tests." *J. AWWA*, 83 (1): 77-87.
- Hartley, H.O. (1961). The modified Gauss Newton method for the fitting of nonlinear regression functions by least squares. *Technometrics* 3 (2): 269-280.
- Interlandi, S. J., and Crockett C. S. (2003). "Recent water quality trends in the Schuylkill River, Pennsylvania, USA: a preliminary assessment of the relative influences of climate, river discharge and suburban development." *Water Resources*, 37: 1737-1748.
- Jacobs, K., Adams, D. B., and Gleick, P. (2001). "Chapter 14, Potential Consequences of Climate Variability and Change for the Water Resources of the United States", in *Climate Change Impacts On the United States –the Potential Consequences of Climate Variability and Change* edited by Jerry Meilillo, Anthony Janetos and Thomas Karl, Cambridge University Press, New York.
- Oulman, C.S. (1980). "The logistic curve as a model for carbon bed design." *J. AWWA*. 75 (1): 51.

- Roberts, P. V. and Summers R.S. (1982). "Granular Activated Carbon Performance for Organic Carbon Removal." *J. AWWA*, 74:113-118
- Salas, J. D., Delleur, J. W., Yevjevich, V. and Lane, W. L. (1980). "Applied Modeling of Hydrologic Time Series." *Water Resources Publications*, Littleton, CO, 484 pages.
- US BLS (Bureau of Labor Statistics) (2008). BLS Handbook of Methods, Chapter 14 Producer Prices-Background. http://www.bls.gov/opub/hom/homch14_a.htm.
- U.S. Environmental Protection Agency (2010). Water Resource Adaptation Program (WRAP). <http://www.epa.gov/nrmrl/wswrd/wqm/wrap/index.html>.
- U.S. Environmental Protection Agency (2005). "Water Treatment Plant Model Version 2.2 User's Manual." Office of Ground Water and Drinking Water, U.S. Environmental Protection Agency, Cincinnati, Ohio.
- U.S. Environmental Protection Agency (2000). "ICR treatment study database, version 1.0." Rep. No. EPA 815-C-00-003, Office of Water, Washington, D.C.
- U.S. Environmental Protection Agency (1996). "ICR manual for bench and pilot-scale treatment studies." Rep. No. EPA 814-B-96-003, Office of Water, Washington, D.C.
- Whitehead, P. G., Wilby, R. L., Battarbee, R. W., Kernan, M. and Wade, A. J. (2009). "A review of the potential impacts of climate change on surface water quality". *Hydrological Sciences*. 54 (1): 101-123.
- Zachman, B. A. and Summers, R.S. (2010). "Modeling TOC breakthrough in granular activated carbon adsorbers." *J. Environmental Engineering* (ASCE). Pp 204-210. (February 2010)

Attachment A

Confirmation Tests

Confirmation tests are designed to verify that the algorithms applied in WTP-CAM are correctly coded and the modeling results with these algorithms are consistent to the corresponding evaluation criteria. The confirmation tests validate the following two algorithms in WTP-CAM: seasonal multivariate analysis, customization of GAC model.

A-1 Seasonal multivariate analysis

The algorithm of seasonal multivariate analysis is described in section B5.1.1.1. The purpose of incorporation of seasonal multivariate analysis is to preserve the means, variances, and cross correlations of the raw water quality parameters. For this purpose, the sample means, variances and cross correlations of raw water quality series from the Monte Carlo simulations are compared to the corresponding given means, variances and cross correlations of the inputted raw water quality parameters.

The comparisons are made in two seasons: summer and winter. The given means, standard deviations, and cross correlation matrix of raw water parameters are calculated from the input data files “summer_example_data.txt”, and “winter_example_data.txt”, which will be provided with this user manual as sample input files. There are 500 rows (sample size) in each of the input files. The sample means, standard deviation and cross correlation matrix of raw water quality are computed from 1000 Monte Carlo simulations.

Table A-1 compares the sample means and standard deviation in summer, it can be seen that the multivariate analysis algorithm well replicate the given mean since the maximum of the relative error between the simulated means and the given means is 6.3%. Reasonably good agreements are also achieved between the modeled standard deviation and given standard deviation as the maximum of relative error is 34.2%. Similar results are also obtained in winter as shown in Table A-3 since the maximum relative errors of means and standard deviations are 7.7% and 39.8%. The simulation of turbidity has much larger relative errors in sample mean and standard deviation than other water quality parameters owing to its large coefficient of variation (1.21 for summer and 1.34 for winter). Increase of number of Monte Carlo runs may reduce these relative errors.

Table A-2 compares the cross correlations between the given and modeled correlation matrix in summer. It can be observed that reasonably good agreements are achieved. Among the 36 pairs of correlation coefficients, the errors of 32 pairs are less than 0.1, errors of 3 pairs are greater than 0.1 but less than 0.2, and only 1 pair's errors are greater than 0.2. Reasonably good agreements are also achieved for the comparisons in winter as shown in Table a.4. Among the 36 pairs of correlation coefficients, the errors of 30 pairs are less than 0.1, errors of the rest 6 pairs are greater than 0.1 but less than 0.2.

Table A-1 Comparison of the mean and standard deviation in summer

Parameter Unit	pH	Alkalinity mg/L	Turbidity NTU	Calcium hardness mg/L	Total hardness mg/L	TOC mg/L	UVA cm ⁻¹	Bromide mg/L	NH ₃ -N mg/L
μ_0	7.71	79.08	25.85	74.43	128.54	4.43	0.111	0.053	0.25
μ_m	7.71	79.96	27.48	75.01	129.05	4.42	0.110	0.054	0.25
Relative Error (%)	0.0	1.1	6.3	0.8	0.4	0.3	1.0	0.7	0.1
σ_0	0.24	22.19	31.17	27.92	24.96	0.91	0.056	0.022	0.128
σ_m	0.24	26.04	41.83	31.04	26.82	0.94	0.053	0.024	0.133
Relative Error (%)	0.0	17.3	34.2	11.2	7.5	3.5	4.8	9.4	4.0

Note: Subscript "0" representing given values from input data.
Subscript "m" representing results from Monte Carlo analysis

Table A-2 Comparison of cross correlation matrix in summer

Parameter	pH	Alkalinity	Turbidity	Calcium hardness	Total hardness	TOC	UVA	Bromide	NH ₃ -N
pH ₀	1	0.568	-0.145	0.104	0.432	0.367	0.203	0.102	-0.171
pH _m	1	0.473	-0.131	0.087	0.397	0.308	0.222	0.108	-0.187
Error		0.096	0.014	0.017	0.035	0.060	0.019	0.006	0.017
Alkalinity ₀		1	-0.114	0.136	0.798	0.737	0.515	0.304	-0.207
Alkalinity _m		1	-0.138	0.180	0.883	0.643	0.467	0.364	-0.300
Error			0.024	0.044	0.085	0.094	0.049	0.060	0.093
Turbidity ₀			1	-0.120	-0.256	0.131	0.387	-0.429	0.138
Turbidity _m			1	-0.110	-0.265	0.103	0.359	-0.362	0.154
Error				0.011	0.009	0.028	0.028	0.067	0.016
Ca hardness ₀				1	0.381	0.040	-0.155	0.296	-0.100
Ca hardness _m				1	0.419	0.019	-0.215	0.421	-0.134
Error					0.038	0.022	0.061	0.125	0.034
Total hardness ₀					1	0.496	0.296	0.565	-0.276
Total hardness _m					1	0.337	0.175	0.639	-0.334
Error						0.159	0.121	0.074	0.058
TOC ₀						1	0.698	0.128	0.020
TOC _m						1	0.654	-0.076	0.029
Error							0.044	0.204	0.009
UVA ₀							1	-0.335	-0.223
UVA _m							1	-0.335	-0.178
Error								0.000	0.045
Bromide ₀								1	-0.053
Bromide _m								1	-0.033
Error									0.020

Note: Subscript "0" representing given values from input data.
Subscript "m" representing results from Monte Carlo analysis

The comparison results in the confirmation tests indicate that the multivariate analysis algorithm in the WTP-CAM works reasonably well and is confirmed for further application.

Table A-3 Comparison of the mean and standard deviation in winter

Parameter Unit	pH --	Alkalinity mg/L	Turbidity NTU	Calcium hardness mg/L	Total hardness mg/L	TOC mg/L	UVA cm ⁻¹	Bromide mg/L	NH ₃ -N mg/L
μ_0	7.78	64.14	39.64	72.19	121.14	4.06	0.089	0.071	0.23
μ_m	7.78	65.38	42.71	72.87	121.99	4.05	0.088	0.072	0.23
Relative Error (%)	0.0	1.9	7.7	1.0	0.7	0.3	1.2	1.7	0.1
σ_0	0.16	23.64	53.14	29.67	33.73	0.96	0.054	0.041	0.124
σ_m	0.16	28.56	74.28	33.19	36.65	0.99	0.051	0.046	0.129
Relative Error (%)	0.0	20.8	39.8	11.9	8.7	3.1	6.2	10.1	4.0

Note: Subscript "0" representing given values from input data.
Subscript "m" representing results from Monte Carlo analysis

Table A-4 Comparison of cross correlation matrix in winter

Parameter	pH	Alkalinity	Turbidity	Calcium hardness	Total hardness	TOC	UVA	Bromide	NH ₃ -N
pH ₀	1	0.562	-0.140	0.103	0.426	0.365	0.199	0.099	-0.171
pH _m	1	0.459	-0.128	0.086	0.390	0.305	0.219	0.106	-0.189
Absolute Error		0.103	0.013	0.016	0.036	0.060	0.020	0.006	0.018
Alkalinity ₀		1	-0.108	0.138	0.793	0.735	0.512	0.299	-0.205
Alkalinity _m		1	-0.125	0.184	0.885	0.627	0.451	0.365	-0.290
Absolute Error			0.017	0.046	0.093	0.109	0.061	0.066	0.086
Turbidity ₀			1	-0.119	-0.243	0.121	0.363	-0.377	0.133
Turbidity _m			1	-0.105	-0.240	0.096	0.343	-0.309	0.144
Absolute Error				0.014	0.003	0.025	0.020	0.068	0.012
Ca hardness ₀				1	0.377	0.039	-0.151	0.286	-0.101
Ca hardness _m				1	0.417	0.020	-0.208	0.415	-0.132
Absolute Error					0.040	0.019	0.057	0.129	0.031
Total hardness ₀					1	0.490	0.286	0.558	-0.272
Total hardness _m					1	0.332	0.168	0.630	-0.325
Absolute Error						0.158	0.117	0.072	0.052
TOC ₀						1	0.694	0.127	0.020
TOC _m						1	0.646	-0.072	0.027
Absolute Error							0.048	0.199	0.006
UVA ₀							1	-0.304	-0.215
UVA _m							1	-0.309	-0.174
Absolute Error								0.005	0.042
Bromide ₀								1	-0.054
Bromide _m								1	-0.038
Absolute Error									0.016

Note: Subscript "0" representing given values from input data.
Subscript "m" representing results from Monte Carlo analysis

A-2 Customization of GAC model

Section B5.2.1 introduces the algorithm of GAC model customization, which is used to provide users options to refine the empirical constants in GAC model using site-specific treatment study data so that better prediction can be obtained in a specific utility. There are two tasks in this confirmation tests for GAC model customization: one is to verify the improved performance of the customized GAC model over the original GAC model in the WTP model; the other is to validate the customized GAC model using field data from the GCWW's Richard Miller treatment plant.

To compare the performance between the customized GAC model and original model in the WTP model, two sets of RSSCT data from the Richard Miller plant were used to estimate the customized GAC model parameters in Equation B3.1 using the non-linear regression algorithm given by Equations B5.22-B5.28. The original GAC model parameters were calculated using Equations B5.19-B5.21 when pH is 7.8, EBCT is 20 minutes and inflow TOC concentration is

2.25 mg/L. Table A-5 summarized the model parameters for the two RSSCT datasets. Then, the customized and original models were used to simulate the GAC logistic curve and are compared to the corresponding RSSCT data sets. Obvious improvements can be observed with the customized GAC model over the original model as shown in Figures A-1 to A-2. Figure A-3 quantifies the improvements by comparison the sum of error squares given by Equation B5.22. It can be seen that the sum of error squares by the customized model is only 10.4% of that by the original model for RSSCT dataset 1 and 37.4% for the RSSCT dataset 2.

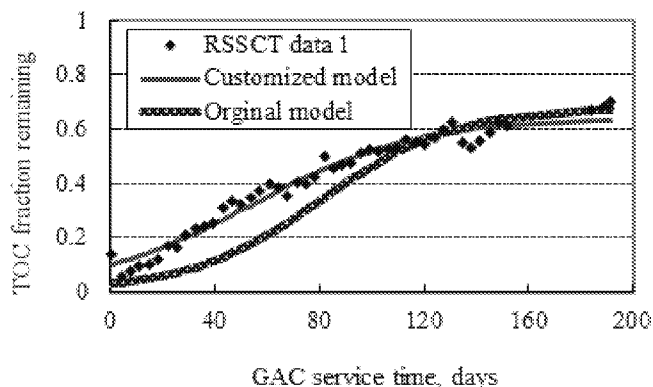
Table A-5 Parameters estimated for TOC breakthrough model

Data source	GAC model	Parameter a	Parameter b	Parameter d [day ⁻¹]
RSSCT data 1	Customized	0.644	5.448	0.0314
	Original	0.682	22.94	0.0388
RSSCT data 2	Customized	0.604	9.445	0.0359
	Original	0.682	22.94	0.0388

Customized GAC model can be further validated with field data at the Miller treatment plant. There are eight episodes identified from field measurements for one of 12 contactors at the Miller plant during January 2004 to May 2010. The TOC fraction remaining is obtained by calculation of the ratio of the contactor effluent TOC concentration over inflow TOC concentration. Each of the eight datasets were used to estimate the GAC model parameters the using the non-linear regression algorithm given by Equations B5.22-B5.28. Table A-6 summarizes the minimum and maximum TOC fraction remaining, GAC service period, and estimated parameters.

Figure A-4 exhibits the TOC breakthrough field measurements for the 8 datasets. TOC breakthrough field curves in Figures A-4a, A-4d, A-4e, and A-4h do not achieve steady state of a logistic curve. As a result, model parameters estimated with these datasets present great fluctuation as parameter a varies from 0.53 to 3.05 or parameter d changes from 0.016 to 0.046. Obviously, GAC models with parameters estimated with these datasets are not amenable to represent the TOC breakthrough in the Miller plant because of the incomplete data. Thus, these incomplete datasets should be ignored. The averages of the parameters estimated from the rest four “complete” data sets are used for the customized GAC model, given by,

Figure A-1 Comparison of GAC models with RSSCT dataset 1



$$f(t) = \frac{0.759}{1 + 8.124e^{-0.029 \cdot t}} \quad (\text{A.1})$$

In addition to Equation A.1 (represented with “average-based” in Figure A-4), a customized GAC model using averages of parameters estimated with RSSCT data listed in Table A-5 is also validated against the field data (represented with “RSSCT-based” in Figure A.4), given by,

$$f(t) = \frac{0.624}{1 + 7.447e^{-0.034 \cdot t}} \quad (\text{A.2})$$

For reference, customized GAC models with parameters estimated for individual datasets as listed in Table A-6 are provide as well, represented with “self-based” in Figure A.4.

Table A-7 provides the sums of error square (defined by Equation 5.22) of “self-based”, “RSSCT-based” and “average-based” customized GAC model for all 8 data sets. As expected, the self-based models provide the best fitting for individual datasets. Similar performances are achieved for both RSST-based and average-based models when GAC service time is less than 100 days (incomplete datasets).

However, the average-based model presents much better simulation than the RSSCT-based model when service time is over 200 days. The bias results of the RSSCT-based model is probably owing to the breakthrough curves are not well developed.

In sum, the average-based customized GAC model is validated to provide better simulation of TOC breakthrough than those by the original GAC model in the WTP model.

Figure A-2 Comparison of GAC models with RSSCT dataset 2

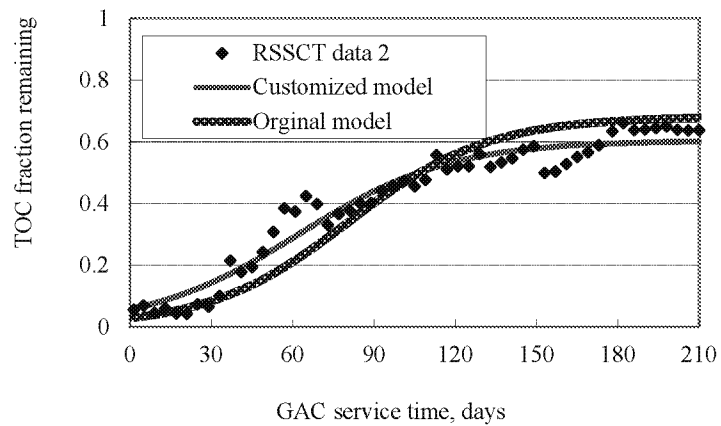


Figure A-3 Comparison of sum of error square for GAC models

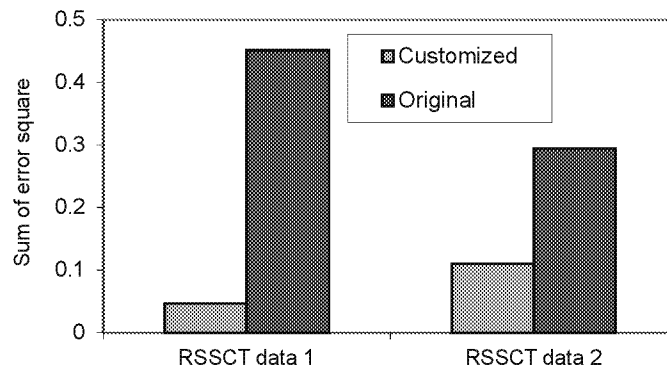


Table A-6 Summary of field data sets and estimated parameters

Data set #	Min. of observed $f(t)$	Max. of observed $f(t)$	GAC service period, day	Parameter a	Parameter b	Parameter $d \text{ day}^{-1}$	Comment
1	0.110	0.519	88	0.809	11.271	0.035	Incomplete
2	0.088	0.808	256	0.767	11.134	0.035	Complete
3	0.127	0.841	312	0.783	8.391	0.025	Complete
4	0.080	0.500	102	0.527	7.322	0.046	Incomplete
5	0.134	0.452	116	0.732	6.065	0.021	Incomplete
6	0.097	0.844	291	0.725	8.210	0.035	Complete
7	0.083	0.849	275	0.760	4.762	0.022	Complete
8	0.110	0.477	109	3.048	35.221	0.016	Incomplete
Average for "Complete" datasets	0.099	0.836	284	0.759	8.124	0.029	

Table A-7 Comparison of sum of least square for customized GAC models

Data set #	1	2	3	4	5	6	7	8
Self-based GAC model ¹	0.019	0.036	0.036	0.040	0.021	0.082	0.072	0.029
RSSCT-based GAC model ²	0.037	0.434	0.417	0.052	0.054	0.300	0.232	0.107
Average-based GAC model ³	0.034	0.068	0.078	0.054	0.080	0.112	0.106	0.125

Note: ¹ Self-based GAC model refers to the model using parameters estimated for individual datasets given in Table A.6;

² RSSCT-based GAC model refers to the model using parameters estimated by RSSCT tests given by Equation A.2;

³ Average-based GAC model refers to the model using average of parameters based on "complete datasets" given by Equation A.1.

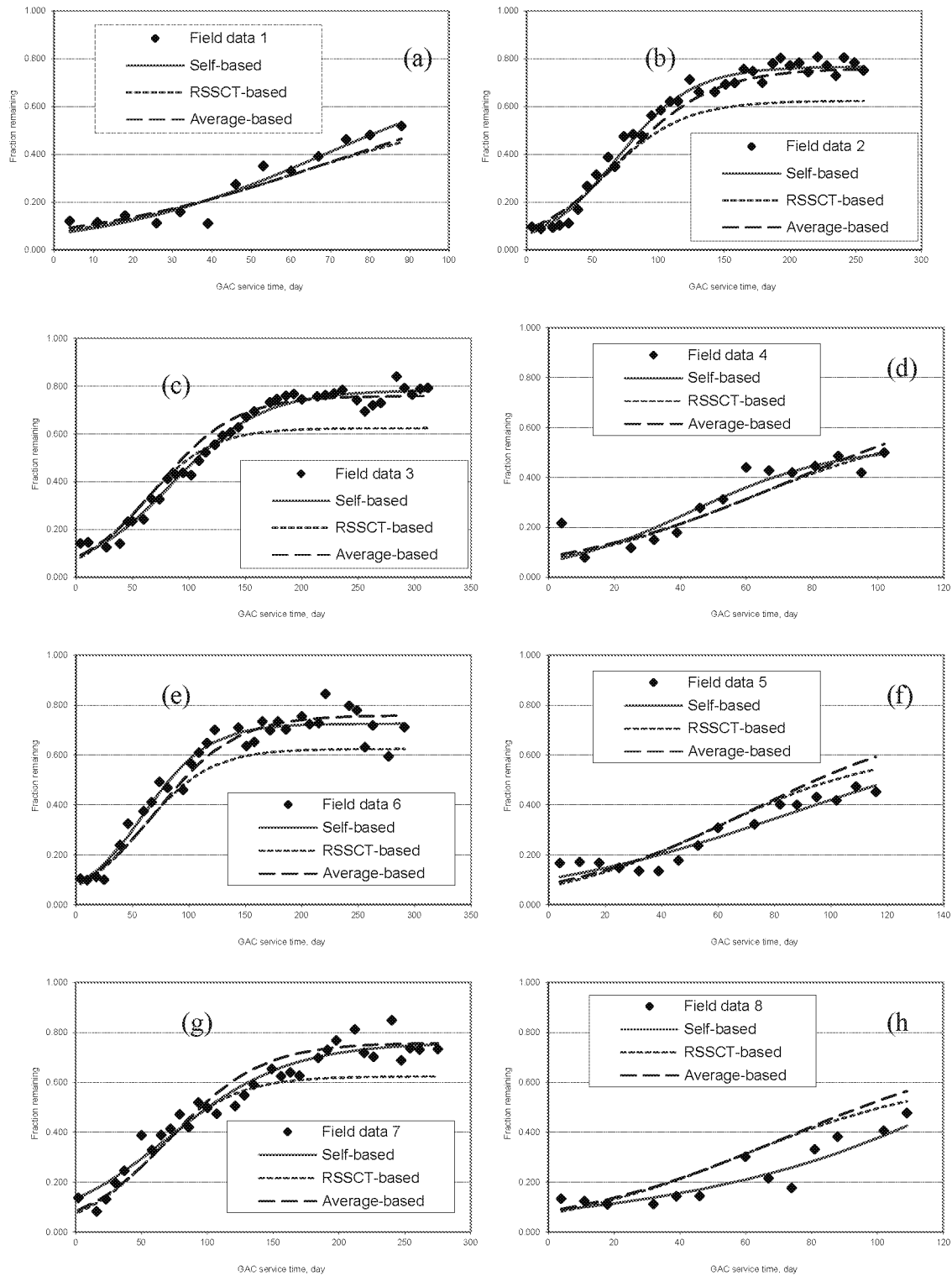


Figure A-4 Validation of GAC model with field data

Attachment B

Error and Warning Messages

There are two types of messages in WTP-CAM: error message and warning message. The error message is a fatal error and has to be corrected before the WTP-CAM can be executed successfully. The warning message is either caused by uncommon parameters user specified or used to provide user information for unusual running conditions of WTP-CAM. The warning messages do not affect execution of WTP-CAM. The error and warning message will be developed in subsequence refinement of WTP-CAM and summarized in Tables B-1 and B-2.

Table B-1 Error message (to be developed)

ID	Explanation	Correction
1	Can't open file " <i>File name</i> "	Check the existence of file

Table B-2 Warning message (to be developed)

ID	Explanation	Recommendation
1	User-defined parameter is out of range	Stay within recommend range